THE POKAI AND CHIMP IGNIMBRITES

OF

NW TAUPO VOLCANIC ZONE

A thesis

submitted in fulfillment

of the requirements for the Degree

of

Doctor of Philosophy in Geology

in the

University of Canterbury

by

RITVA ANNIKKI KARHUNEN

University of Canterbury

1993

with 2 separate maps in back pocket.

To my parents with all my love

CONTENTS

ABSTRACT

Taupo Volcanic Zone (TVZ) is the largest active volcanic belt in New Zealand, and has erupted >10.000 km^3 of dominantly rhyolitic magma during the last 1.6 m.y. This study concerns the field relations, volcanology and petrology of two post-Whakamaru (330 ka) - pre-Mamaku (140 ka) ignimbrites, informally named as the Pokai and Chimp ignimbrites, occurring in a ca. 360 km^2 area SW and W from Rotorua in the northwestern TVZ.

The Pokai Ignimbrite has a minimum volume of ca. 33 km^3 DRE, whereas the older Chimp Ignimbrite has a minimum volume of only ca. 5 km^3 DRE. Of the two ignimbrites the younger Pokai Ignimbrite is better preserved and is thus the main emphasis in this thesis.

The Chimp Ignimbrite is relatively pumice- and crystal-poor (1-2 vol.% phenocrysts), and the exposed flow units are relatively thin (4-6 m). A short plinian phase preceded the Chimp Ignimbrite, whereas the Pokai Ignimbrite is marked by a number of pre-ignimbrite air-fall pumice and ash layers. The Pokai Ignimbrite represents a multiple flow unit ignimbrite, with single flow units usually ranging from 6-30 m. Thick deposits (>20 m thick) are usually welded in the upper middle part of the deposit. Ground deposits, i.e. layer 1 deposits, are rare. Field evidence suggest that the Pokai Ignimbrite originated from the Kapenga Volcanic Centre, a multiple caldera structure in the northern central TVZ.

Two pumice types occur in the Pokai Ignimbrite; a crystal-poor type (2-3 % phenocrysts) and a crystal-rich type (6-12 % phenocrysts). Plagioclase is the dominant phenocryst throughout, with minor amounts of orthopyroxene, Fe-Ti oxides and quartz, which occurs in ca. 30 % of the pumices. Hornblende and clinopyroxene are present occasionally. The Pokai Ignimbrite ranges from mildly to strongly peraluminous, whereas the Chimp Ignimbrite is mildly peraluminous, both coinciding with other TVZ rhyolitic ignimbrites, but clearly differing from the rhyolitic lavas which are usually metaluminous to only mildly peraluminous.

Whereas most TVZ rhyolitic eruptives have been regarded as relatively homogeneous, the Pokai Ignimbrite shows significant geochemical variation. The magma chamber was compositionally zoned from crystal-poor, high silica, low Sr (77 % SiO_2, 50 ppm Sr) rhyolitic top to more crystal-rich, low silica, high Sr (70 % SiO_2, 130 ppm Sr) rhyolite at the deeper levels. Prior to the eruption vigorous mixing of magma from different levels occurred, producing different pumice types in the air-fall deposits, and multiple phenocryst populations in single pumice clasts. As the eruption progressed successively deeper levels of the magma chamber were tapped, the last eruption products representing the less evolved, crystal-rich magma. Least squares and Rayleigh fractionation models indicate that the Pokai, and the Chimp magmas most probably generated by AFC from TVZ andesitic magmas contaminated by Mesozoic basement sediments.

1. INTRODUCTION

1.1. General outline of the Taupo Volcanic Zone

Volcanism has played a major role in the geological development of New Zealand particularly during late Cenozoic times and in a general way the different volcanic provinces can be related to Cenozoic tectonic processes (Smith, 1986). The boundary between the Pacific and Indo-Australian plates passes along the eastern margin of the North Island, at the Hikurangi Trough (Fig.1.1, inset), where the relative motion of the Pacific plate westwards beneath the Indo-Australian plate is 50 mm/year (Walcott, 1978). It is this convergence of the Pacific and Indo-Australian plates that is responsible for the currently active Taupo Volcanic Zone (TVZ), which forms a part of an older volcanic zone, the Central Volcanic Region (CVR, Fig.1.1.).

The plate boundary then passes through the South Island along the Alpine Fault. TVZ has been interpreted by Cole (1990) as a back-arc basin of the Taupo-Hikurangi subduction system, and forms the southward extension of the Tonga-Kermadec arc system (Cole & Lewis, 1981). The Central Volcanic Region (CVR) forms a wedge-shaped area extending from Mount Ruapehu northwards to the Bay of Plenty (Fig.1.1). Adjoining the outer margins both in the E and W are northward-diverging, mainly Mesozoic greywacke ranges forming natural boundaries to the CVR. The volcanic rocks range approximately from Miocene to Pliocene.

TVZ is the largest active volcanic belt in New Zealand. It extends over 300 km from Mount Ruapehu to White Island in the north (Fig.1.1). It is about 50 km wide in the central part

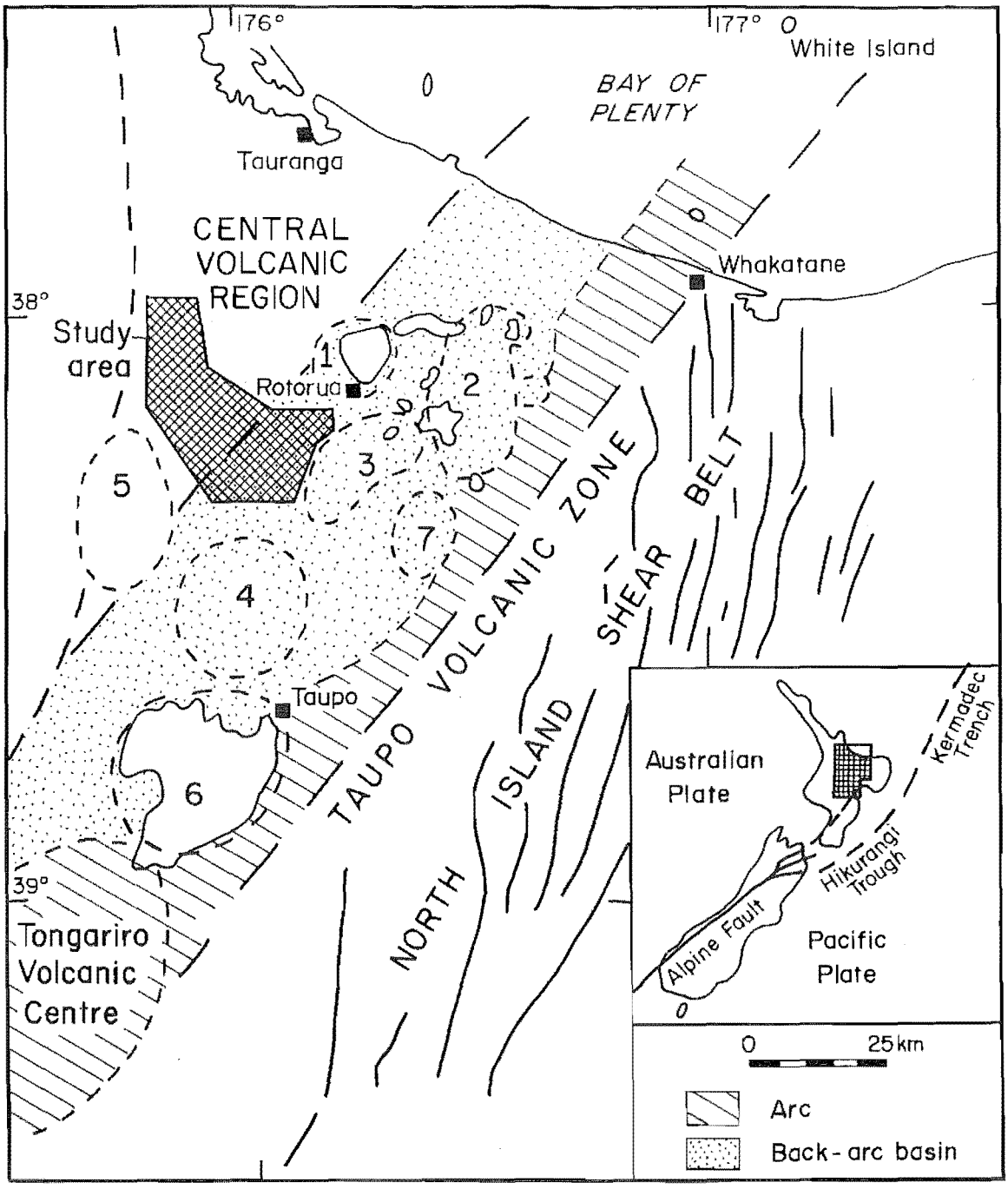

Figure 1.1. The Taupo Volcanic Zone (TVZ) and surrounding structural features. Rhyolitic volcanic centres are as follows: 1, Rotorua; 2, Okataina; 3, Kapenga; 4, Maroa; 5, Mangakino; and 6, Taupo. 7, Reporoa Caldera (possibly a seventh rhyolite centre).

but narrows both south- and northwards. CVR and TVZ share a common eastern boundary. The western boundary of TVZ has a strong topographical expression in that it separates rhyolite domes to the east from the broad ignimbrite covered plateaux to the west. It is therefore roughly defined by the area of Upper Quaternary rhyolite domes and pyroclastics. Over 10,000 km^3 DRE of mainly rhyolitic lava and pyroclastics have been erupted along the TVZ since late Pliocene times (Cole, 1981).

Rhyolitic volcanic centres are found in all volcano-tectonic settings. Typically they lack a topographically impressive cone, and often form a large, broad volcano-tectonic depression; such as Lake Taupo in New Zealand, formed during the ultraplinian and ignimbrite-forming Taupo 186 AD eruption (Wilson et al., 1980; Walker, 1981e). The primary eruptive products of these volcanic centres are rhyolitic plinian fall deposits, voluminous ignimbrites and small volume rhyolitic lavas.

TVZ can be divided into three parts; a northern and a southern region, which are andesite-dominated, and a central region which is predominantly rhyolitic. In the central region six major rhyolitic volcanic centres have been identified (Wilson et al., 1984). Each of them has a central collapse caldera formed after large amounts of pyroclastic material were erupted. Vast ignimbrite (ash-flow tuff) sheets now cover both the E and W sides and the central part of TVZ. The major volcanic centres include Rotorua, Okataina, Kapenga, Maroa, Mangakino and Taupo (Fig.1.1). The Rotorua Volcanic Centre (Fig.1.2) is a rounded physiographic feature expressed by a basin of 20 km in diameter (containing Lake Rotorua), and thought to be associated with the eruption of the Mamaku

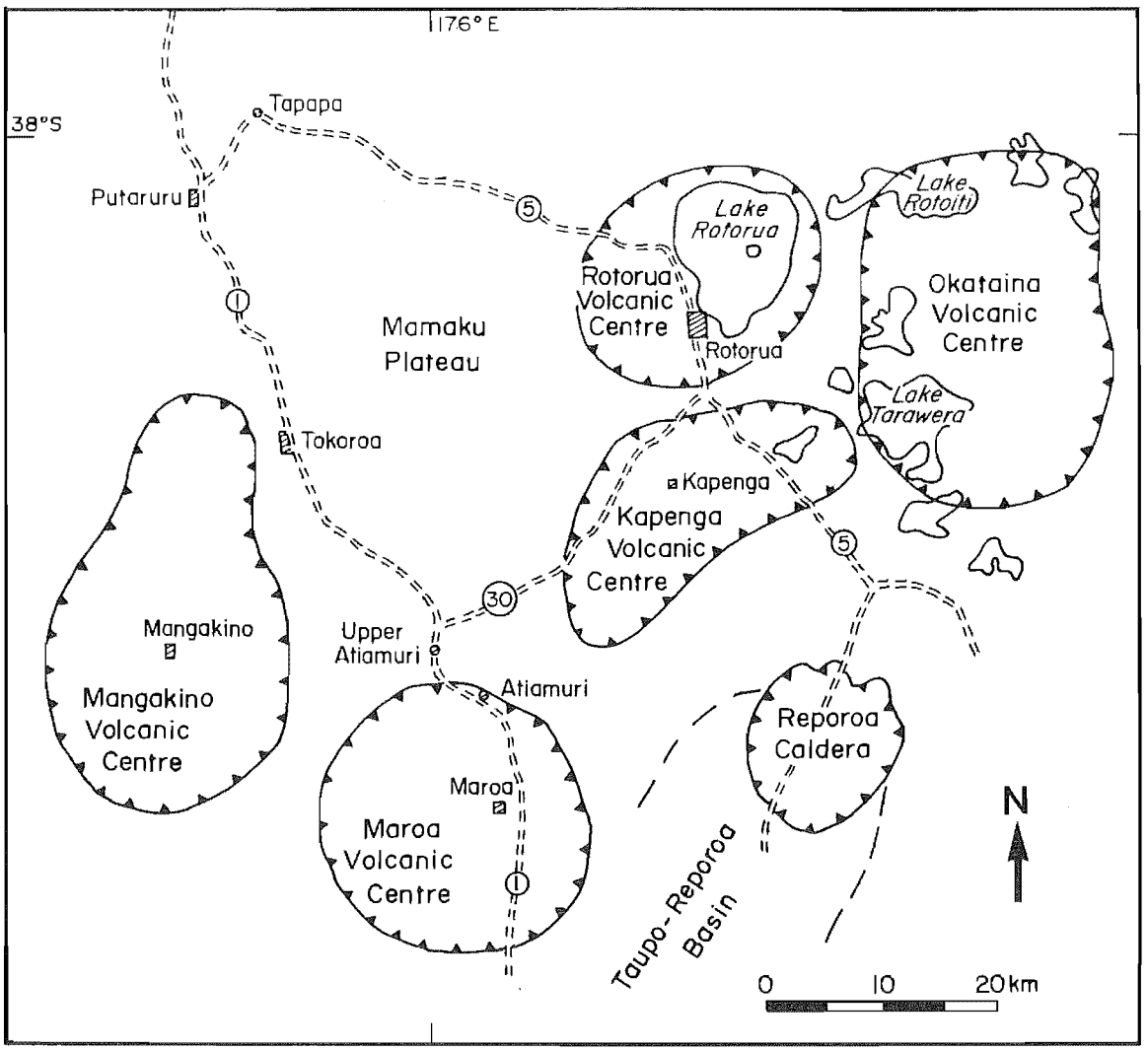

Figure 1.2. Rhyolitic volcanic centres in the northern TVZ.

Ignimbrite, ca. 140,000 years ago (Murphy & Seward, 1981; Houghton, 1982; Wilson et al., 1984).

The Kapenga Volcanic Centre (Fig.1.2) is outlined by a broad negative gravity anomaly (Rogan, 1982). The centre is composed of at least two distinct collapse structures of different ages, a smaller basin to the northeast, and a larger one in the southern part, referred to as the northeast and southern centres, respectively (Wilson et al., 1984). Recent studies of Nairn et al. (1993) have revealed a new caldera structure (referred to as the Reporoa Caldera) at the northern end of the Taupo-Reporoa Basin (Fig.1.2).

A topographic depression of ca. 20 km in diameter, lying 200-400 m below the surrounding ignimbrite plateaux, forms the centre of the Mangakino Volcanic Centre (Fig.1.2). The exposed eruptive products are almost entirely rhyolitic pyroclastics, deposited mainly on the western margin of TVZ (Wilson et al. 1984).

Tongariro volcanic centre, in the southern TVZ (Fig.1.1), is part of a young (< 250 ka) andesite-dacite volcanic arc and has no associated rhyolitic volcanism (Cole & Lewis, 1981). In the western part of the central region, vast ignimbrite sheets form two plateaux, the West Taupo Plateau at the southern end, and the Patetere or Mamaku Plateau, which extends from near Upper Atiamuri NNE to Tauranga at the north end.

The study area, situated around the southern extension of Mamaku Plateau (Fig.1.3) is primarily composed of rhyolitic volcanic rocks ranging from over 1.1 Ma years to 1800 B.P. The oldest rocks, the Pukerimu Ignimbrites (>1.1 Ma), are found in the Matahana Basin, on the SE part of the study area.

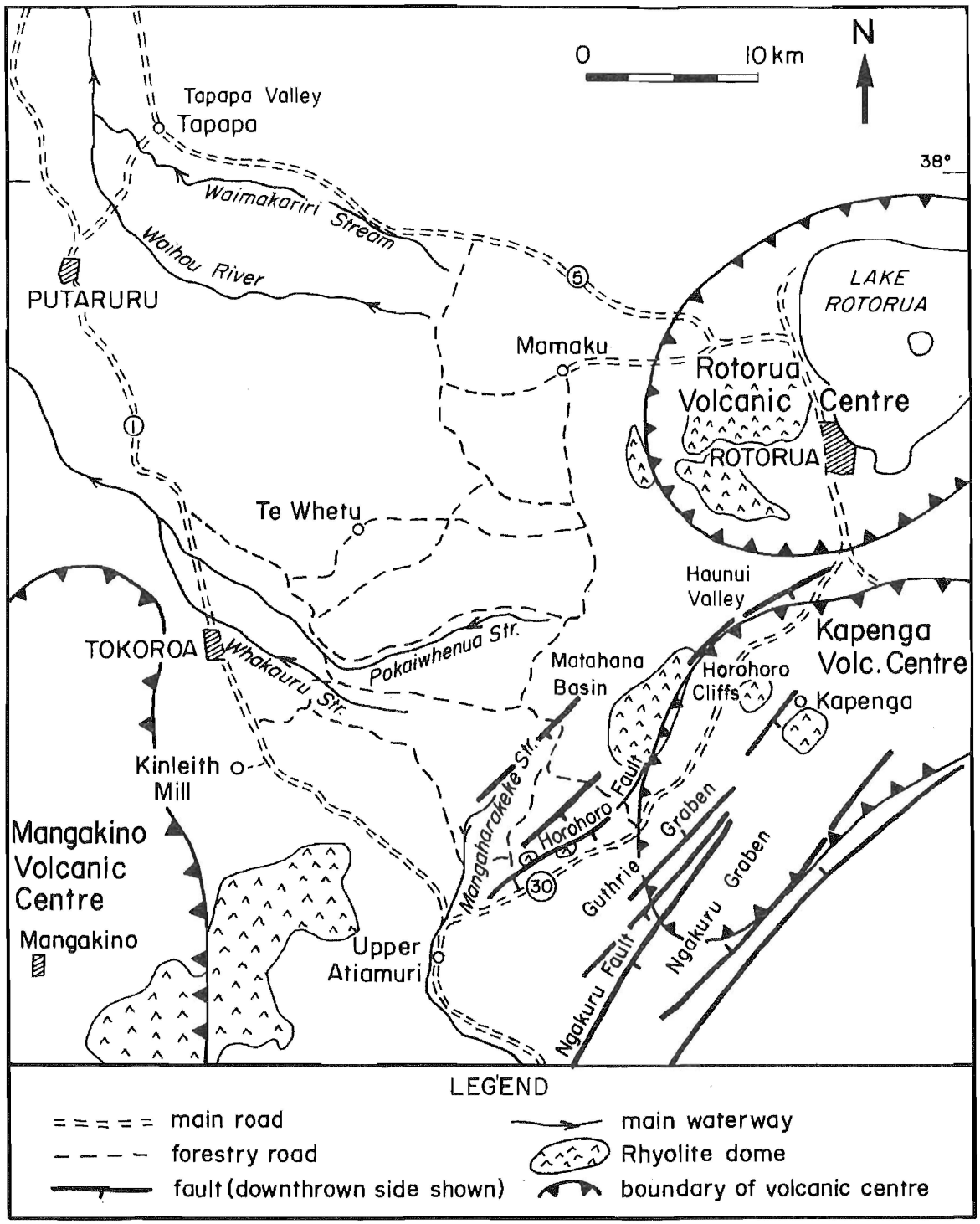

Figure 1.3. Location map for the study area.

The youngest formations consist of the 1800 BP Taupo pumice and air-fall deposits, found in the southern corner of the area. Conspicuous rhyolite domes, belonging to the older Haparangi Group (middle Pleistocene; Healy et al., 1964) occur along the southeastern and south-southwestern margin of Mamaku Plateau (Fig.1.3). The most impressive is exposed along the Horohoro Cliffs, 15 km southwest of Rotorua and forms the western side of the Horohoro fault scarp.

The surface deposits along the southeastern Mamaku Plateau and in the Kapenga Volcanic Centre are cut by several faults. Most surface faulting in TVZ is normal, the strikes between 040 and 080, and are steeply dipping (>40)(Cole, 1990). The structure in the Kapenga Volcanic Centre is a typical 'graben' with central axis flanked by faults that are downthrown towards the axis. The axis is not a single line through the depression but is 'en echelon' (Cole, 1986). In the southern Kapenga area there are two major graben structures, Guthrie Graben and Ngakuru Graben (Fig.1.3), each filled with lake sediments of the Huka Group (Grindley, 1959). The Huka Group Formation is a series of widespread freshwater sediments and interbedded tuffs which occur between Lake Taupo and Bay of Plenty. Their age extends from middle to late Pleistocene (Healy et al., 1964).

1.2. Access and physiography

Much of the study area is in Kinleith Forests - owned by NZ Forest Products Limited - between the townships of Rotorua in the east and Putaruru in the west and is bounded by State Highways 1 and 5 in the south (Fig.1.3 and Map A). Within the

forest is a network of private roads, which allow access by car to most of the forest. The best exposures are located in the southwestern Kinleith Forests, east of Tokoroa, where road-cutting operations have exposed sections through the ignimbrite stratigraphy. Access to many of the higher vertical section is only possible with a rope (see Fig.2.2). A number of sub-vertical sections could be partially reached from the sides of the adjoining slopes. Both Haunui Valley and the areas around Putaruru are composed of mixed farming land with a few private farm tracks.

The area is dominated by the Mamaku Plateau (Fig.1.4), a broad fan-shaped structure at an elevation of 400-600 m.a.s.l. extending NNE from near Atiamuri to Tauranga at the north end. The surface of the plateau is largely controlled by ignimbrites which when eroded tend to preserve a flat upper surface surrounded by steep, often columnar-jointed walls. The plateau is cut by several NE-SW trending faults especially numerous in SE near the Matahana Basin (Fig.1.3). In the central Kinleith Forests the Mamaku Plateau is cut by several waterways which give the area a canyon-like appearance (Fig.1.5). In the southwest of the area, the canyon-like appearance of the plateau diminishes with broader valleys found between somewhat less steep hill slopes (Fig.1.6).

The plateau descends in the west and northwest towards State Highway 1, where the valleys are separated by gently sloping hills. Along the eastern margin at the boundary with the Rotorua basin and along the southern margin, the Mamaku Plateau ends in steep cliffs. The plateau at the top of the Horohoro Cliffs is the highest point in the area, 817 m.a.s.l.. South and southeast from Horohoro the altitude

Figure 1.4. Mamaku Plateau, looking NE from Tikorangi lookout (GR 776222).

Figure 1.5. An uneven upper surface of Pokai Ignimbrite exposed along a narrow river canyon, 3 km N from Te Whetu (GR 688373).

Figure 1.6. A broad erosional valley along Mangaharakeke Stream in the southern margin of Mamaku Plateau. Columnar-jointed Pokai Ignimbrite cliffs are seen in the background on right.

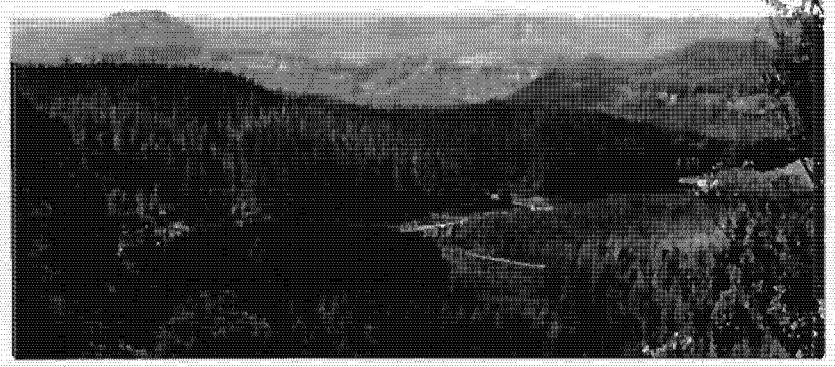

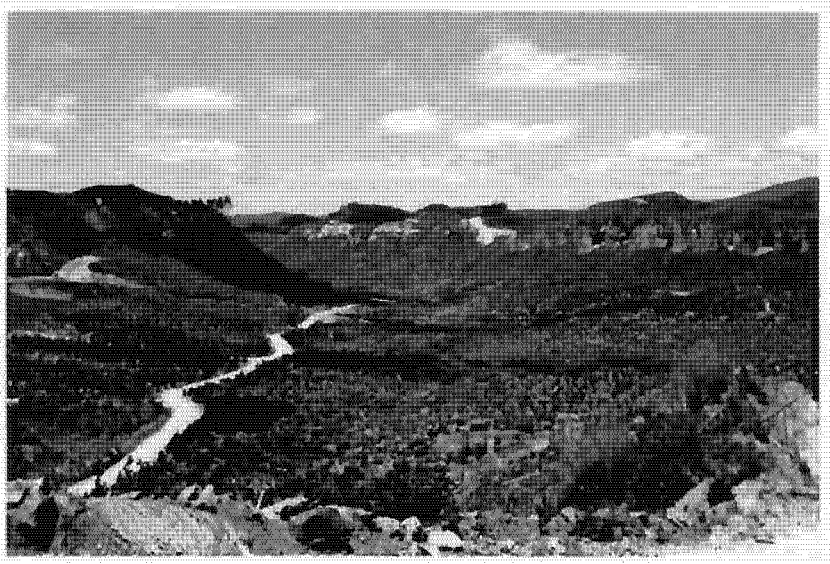

decreases rapidly towards a subcircular lowland area occupied by the Kapenga caldera. Major rivers in the study area are the Mangaharakere Stream in south, the Whakauru and Pokaiwhenua Streams in west and the Waihou River and Waimakariri Stream in northwest (Fig.1.3).

1.3. Ignimbrites

Ignimbrite-forming eruptions are generally associated with caldera collapse. Studies of ignimbrite stratigraphy indicate the following sequence of activity:

a) an early plinian phase producing a pumice-fall deposit,

b) pyroclastic surges and a pyroclastic flow phase forming the ignimbrite, and

c) an effusive phase producing lava.

Many of the most voluminous ignimbrites, such as those of western North America, are compositionally zoned, indicating in some cases the tapping of large zoned magma chambers (Smith, 1979). The ash-fall and ash-flow sheets of the Bishop Tuff represent a well known example of zoned rhyolitic magma emplaced during the collapse of the Long Valley caldera, California, USA (Hildreth, 1979).

Several types of source vents for ignimbrites have been proposed. The most voluminous ignimbrites are generally associated with either linear or fissure eruptions or with continuous ring-fissure eruptions. An example of the first model is described by Nairn (1981) from the Okataina rhyolitic centre, New Zealand. All of the post caldera-forming eruptions (< 20 ka), producing plinian deposits and pumice flows, are thought to have been from multiple vents along fissures.

A popular model for an ignimbrite source vent is thought to be an eruption along a ring fracture, around which caldera collapse may occur during the eruption (Smith & Bailey, 1968; Cas & Wright, 1987). An excellent example of this type of eruption is the Crater Lake ignimbrite in Oregon, USA (Bacon, 1983). Other examples include the lower Bandelier Tuff associated with the Toledo Caldera, New Mexico, USA (Self et al., 1986) and the Cerro Galan ignimbrite and caldera in northwestern Argentina (Francis et al., 1983).

Quaternary ignimbrites with associated caldera formation have also been related to central vents. The Rio Caliente ignimbrite in Mexico (Wright, 1981) and the Taupo 186 AD ultraplinian pumice-fall and ignimbrite in New Zealand (Wilson & Walker, 1982) were probably erupted through central vents.

1.4. Classification and terminology of ignimbrites

A 'formation' is the primary unit in lithostratigraphy consisting of a succession of strata useful for mapping or description (ISSC: Hedberg, 1976). An ignimbrite produced during a course of one eruption may consist of one or many individual flow units. An ignimbrite formation covers all the flow units as well as the air-fall and surge deposits produced during the same eruptive event. Ignimbrite formations are separated from each other by soils, reworked or in situ, pyroclastic or epiclastic materials and/or erosion surfaces. In places where the stratigraphic position is not exposed the separate ignimbrites can be distinguished from one another by means of their mineralogy, petrology, colour, grain-size, pumice content and/or style of welding.

Two quite different classification systems have been adopted for pyroclastic rocks (Wright et al., 1981). A genetic classification interprets the genesis of a deposit while a lithological classification, which is primarily descriptive, gives the major characteristics (such as grain-size), the type of constituent fragments and the degree of welding of a deposit. A genetic classification may rely on information forming the basis of a lithological classification. In this thesis a genetic classification is used to describe the deposits for which origins can be clearly established.

In pyroclastic deposits formed by fragmentation of magma and rock by explosive volcanic activity, three main genetic types of deposits have been identified (Sparks & Walker, 1973): 1) pyroclastic fall 2) pyroclastic flow and 3) pyroclastic surge. Pyroclasts fall through the air from the eruption plume and accumulate as pyroclastic fall deposits. The movement and deposition of the pyroclasts is influenced by gravity, wind drifting, expansion of the plume and by initial lateral velocity imparted at the vent. In pyroclastic flows, pyroclasts move over the ground as a gravity-controlled, hot and highly concentrated particulate flow, while in surges, pyroclasts are carried laterally as expanding, turbulent gas/solid dispersion with a low particle:gas ratio (Wright et al., 1980; Walker, 1981).

Three main types of pyroclastic flow deposits are now recognised in volcanic successions (Wright et al., 1980): 1) block- and ash-flow deposits, 2) scoria-flow deposits, and 3) pumice-flow deposits or ignimbrites. The term 'ignimbrite' was first introduced by Marshall (1935) and used both in a lithological and genetic sense. As a result there has always

been some confusion as to the precise meaning of the word. The geological features of ignimbrites were summarised in more detail in the beginning of 1960s by Smith (1960) and Ross & Smith (1961), and followed by Sparks et al. (1973), Sparks (1975, 1976), Sparks and Walker (1977), Wilson and Walker (1982) and Wilson (1986) among others. An ignimbrite is here defined after Sparks et al. (1973) as "a rock or deposit formed from pumiceous pyroclastic flow irrespective of the degree of welding or volume".

Ignimbrites are typically poorly sorted, massive deposits containing mostly ash and lapilli pumice or blocks with variable amounts of loose crystals and lithic fragments. Within an ignimbrite flow unit, larger pumice clasts can show reverse grading, whereas lithic clasts can be normally graded. Sometimes one or more welded zones are present. Some features by which non-welded ignimbrites may be identified are their usual pink colour, the occasional presence of carbonised wood and gas segregation pipes.

Modern pyroclastic flows have been observed to have a characteristic nature. During emplacement of a flow, three features are recognised (Wilson 1986): (a) a dense underflow (the pyroclastic flow proper), often preceded by (b) smaller pyroclastic surges, and (c) an overlying ash cloud. As the pyroclastic flow is emplaced these features generate a particular sequence of deposits. Sparks et al. (1973) first constructed an idealised depositional flow-unit model showing the main phases of a pyroclastic flow. The ignimbrite flow-unit model has been expanded by Fisher (1979) and later by Wilson & Walker (1982). An idealised sequence consists of a 'ground surge' deposit (layer 1), a pyroclastic flow-unit

(layer 2), an ash cloud surge unit (layer 3), and a fine-grained air-fall ash unit or a co-ignimbrite ash-fall (Fig.1.7).

Wilson and Walker (1982) proposed that a pyroclastic flow can be divided into head, body and tail. The most fluidised part of the flow will be the flow-head (Wilson, 1980), with large quantities of ingested air. Deposits emplaced from the flow head are bound to be more fines-depleted and enriched in crystals and lithic clasts than the deposits generated from the remaining portions of the flow. Most pyroclastic flow deposits studied so far do not show well developed head deposits. An exception is the Taupo ignimbrite in New Zealand (Wilson & Walker, 1982; Walker & Wilson, 1983), which comprises about 20% fines-depleted layer 1 deposits (Wilson, 1981).

Based on the studies on Taupo ignimbrite, New Zealand, Wilson and Walker (1982) and Wilson (1986) further divided the individual units into subunits (Fig.1.7). Layer 1 may consist of layer 1(P), predominantly containing pumiceous material, and/or of layer 1(H), predominantly made of lithics and crystals, and if present, overlying layer 1(P). Layer 1(P) forms the fines-depleted ignimbrite and layer 1(H) the ground layer.

The body and tail of a pyroclastic flow build up the layer 2 deposits. Layer 2 can be divided to a fine-grained basal layer, 2a, and to the overlying pyroclastic flow itself, layer 2b. A pumice concentration zone (PCZ) towards the top of layer 2b is not uncommon. Sometimes an upper fine-grained segregation layer can be found on the top of layer(s) 2a/2b.

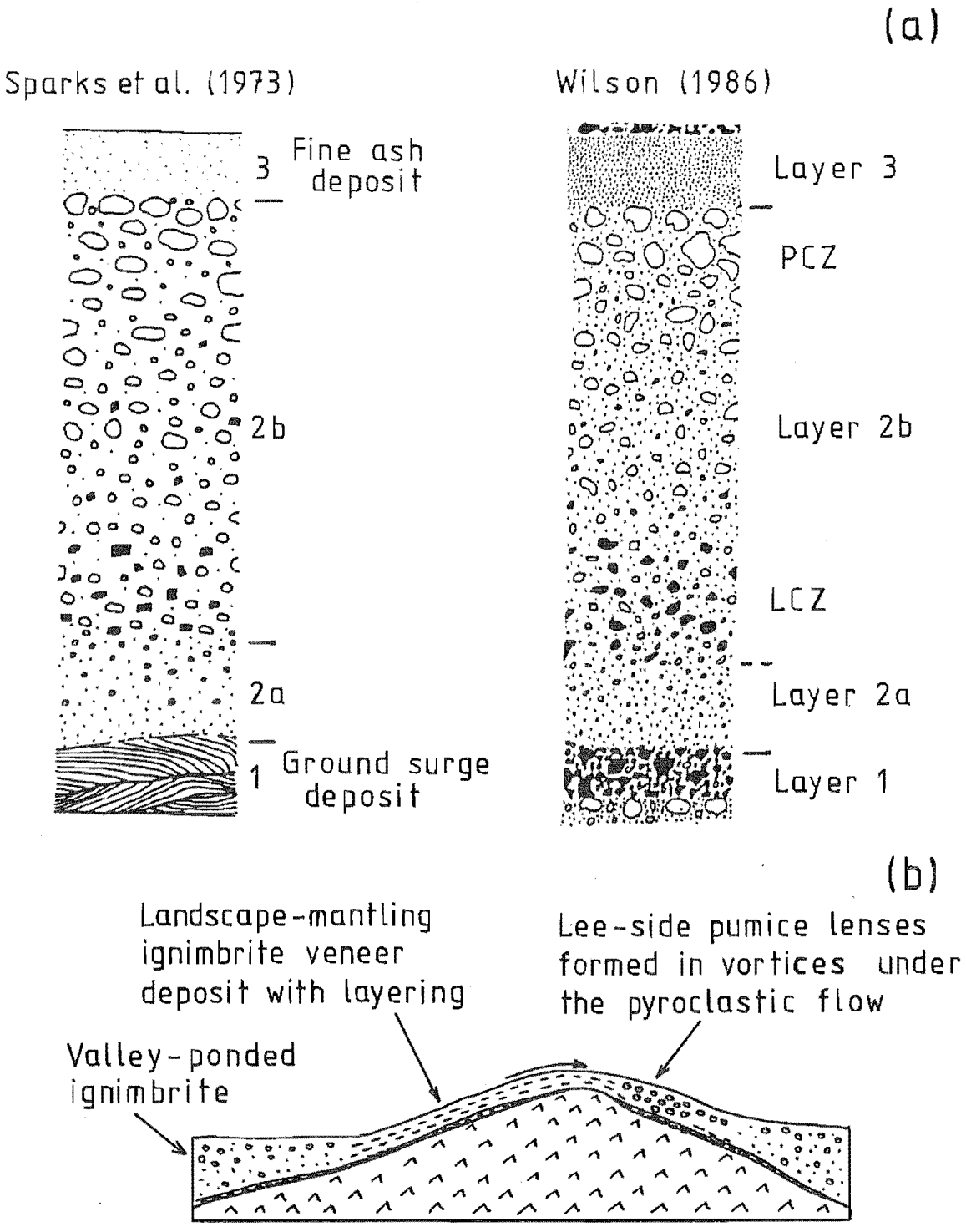

Figure 1.7. (a) Relationship between the layering scheme of Sparks et al. (1973) and Wilson (1986), showing grain size and grading variation within a single ignimbrite flow unit. (b) Schematic cross section showing the two different facies of layer 2 deposit, the valley-ponded ignimbrite (VPI), deposited by the flow body, and ignimbrite veneer deposit (IVD), deposited by the flow tail (Walker 1981d).

PCZ and LCZ are well developed pumice and lithic concentration zones, respectively. Open shapes denote pumice, filled shapes lithics, and stippling the fine matrix.

The body-tail material of a pyroclastic flow usually represents the bulk of the erupted material. Most pyroclastic flows are gravity-controlled filling topographic depressions with poorly-sorted material. They typically have a sub-horizontal flat top and are termed 'valley-ponded ignimbrites', or VPI (Walker et al., 1980b; Wilson & Walker, 1982).

Studies of Taupo ignimbrite, New Zealand, have revealed another type of layer 2 deposit, an 'ignimbrite veneer deposit', or IVD (Fig.1.7; Walker et al., 1980b; Wilson & Walker, 1982; Walker & Wilson, 1983). Structurally, the IVD is very different from VPI, as it mantles the landscape, is stratified and occasionally shows bedforms. The IVD has been interpreted to represent the 'tail' deposit of a pyroclastic flow, consisting the lowest part of the flow. Because of the proximity to the ground surface it was moving less rapidly and was thus left behind (Wilson & Walker, 1982; Wilson, 1986).

1.5. Previous work on TVZ ignimbrites

The volcanic rocks of the Taupo-Rotorua subdivision were mapped and described over 50 years ago by Grange (1937), who described the areas around Matahana Basin, as well as the Haunui Valley area NE of Horohoro Cliffs where the major rock units are fine-grained, flat-lying rhyolitic sheets which he named Patetere Ignimbrite and Breccia. Marshall (1935) had named such rhyolite sheets 'ignimbrites' inferring that these rocks had been deposited from laterally moving hot ash clouds. In 1930s scientists in the USA and (also) elsewhere had described similar rhyolitic volcanic deposits. In the USA

these widespread pyroclastic flow deposits were given the name 'ash-flow tuffs'.

Grindley (1959) mapped the geology of Sheet N85 at a scale of 1:63360 and stated that the rocks in the area belong either to the Waiotapu Ignimbrite formation or to the Ohakuri Formation, which consists mainly of reworked pumice tuffs and breccias. He dated the Waiotapu Ignimbrite as lower Castlecliffian (>700 ka) and the Ohakuri deposits as Waitotaran or upper Pliocene. A more detailed ignimbrite stratigraphy of TVZ was published by Martin (1961) and a detailed map (Sheet 5 - Rotorua) produced by Healy et al. (1964) at a scale 1:250,000. In Healy et al's map, largely based on Martin's (1961) ignimbrite stratigraphy, there are four ignimbrite formations in the Kinleith Forests area which are from the oldest to the youngest: Marshall, Waiotapu, Whakamaru and Mamaku. A summary of differences between previous stratigraphic interpretations and this study is shown in Table 1.1.

Healy et al's (1964) Marshall Ignimbrite, underlying both the Waiotapu and Whakamaru ignimbrites, has been found in the SW part of Kinleith Forests, but exposures NE of Kinleith, mapped by Healy et al. (1964) as Marshall Ignimbrite lie stratigraphically above both the Waiotapu and Whakamaru ignimbrites and thus cannot represent the Marshall Ignimbrite.

Detailed studies of smaller areas in and around Kinleith Forests have been completed during the past 20 years. Briggs (1973) described several outcrops of the Whakamaru-group ignimbrites in the area around Kinleith Mill and established a stratigraphy immediately E from Kinleith, while R.Murphy (1977) mapped the geology of Matahana Basin at a scale 1:15840

Grange, 1937		Healy et al., 1964	Murphy, 1977; Murphy & Seward, 1981	Houghton et al., 1986 (drillhole data, Sutton Rd)	This study	Published age
PLEISTOCENE	Haparangi Rhyolite	Mamaku Ign.	Mamaku Ign.	Mamaku Ign. (surface exp.)	Mamaku Ign.	140 ka (1)
		Haparangi Rhyolite	Unit D	Unnamed ign. (surface exp.)	Pokai Ign.	
			Haparangi Rhyolite	Unnamed ign. (surface exp.)	Chimp Ign.	
		Whakamaru Ign.		Whakamaru Ign.	Whakamaru Ign.	330 ± 2 ka (2)
		Waiotapu Ign.	Waiotapu Ign.	Waiotapu Ign.	Waiotapu Ign.	
		Marshall Ign.	Marshall Ign.	Marshall Ign.		520 ka (3) 630 ka (4)
		Pakaumanu Group: Rocky Hill Ign. Ahuroa Ign. Ongatiti Ign.	Unit C	Rocky Hill Ign.		
			Unit B			
			Rahopaka Ign.			720 ka (3)
						954 ± 25 ka (2)
			Unit A			
			Tikorangi Ign.	Ongatiti Ign. — (end of drillhole at -457 m)		1030 ka (3)
PLIOCENE	Patetere Rhyolite flows Patetere Ign. and Breccia		Pukerimu Ign.			1251 ± 60 ka (2)

Table 1.1. Comparison of the stratigraphy on the northwestern TVZ.

Source references for dates:
(1) Murphy & Seward (1981) and Healy (1982)
(2) Pringle et al. (1992)
(3) Murphy & Seward (1981)
(4) Kohn (1973)

and recorded several exposures of 'Marshall Ignimbrite' in that area (Table 1.1). The Marshall Ignimbrite was dated at 520 ka (Murphy & Seward, 1981), but this does not fit the known field stratigraphy as the ignimbrite is stratigraphically between the Waiotapu/Whakamaru and Mamaku ignimbrites.

The confusion between the Marshall Ignimbrite found southwest of Kinleith and the ignimbrite deposits around Matahana Basin, is probably due to their similar lithological characteristics. The Marshall Ignimbrite has orange pumice in a dark grey matrix at its base, while the unit at Matahana Basin grades from pale pink pumice and matrix at the base to orange pumice in a dark grey or brown matrix on the top.

During reconnaissance mapping of the geology of Sheet U16 in 1980 B.F.Houghton and E.F.Lloyd (DSIR, Geology & Geophysics, Rotorua) identified two previously unnamed ignimbrites in the Kinleith Forests, stratigraphically lying between the Whakamaru and Mamaku ignimbrites. The younger one was correlated with Murphy's 'Marshall Ignimbrite' mapped in the Matahana Basin area.

In 1982 Franzen mapped an area NE of Putaruru. He concentrated on the Mamaku Ignimbrite but also briefly described two ignimbrites found between Whakamaru and Mamaku ignimbrites. The older unit he named the 'Waihou ignimbrite' and the younger one the 'Waimakariri ignimbrite'. L.Murphy (1983) mapped the geology around Haunui Valley, 10 kilometres SW from Rotorua. She recorded a thick ignimbrite unit situated between the Waiotapu and Mamaku ignimbrites and called it 'Korokoro ignimbrite', but didn't correlate this ignimbrite to any other

ignimbrite outside Haunui Valley.

A 457 metre deep hole, drilled by DSIR Geophysics Division in 1986 at Sutton Road, 5 km east-northeast of Tokoroa, shows a succession through the major deposits on the western margin of TVZ (Houghton et al., 1986). The major stratigraphy of the data is shown in Table 1.1. The data reveals two unknown ignimbrites between the Whakamaru and Mamaku ignimbrites, which stratigraphically seem to correlate with the 'Waihou' and 'Waimakariri' ignimbrites mapped by Fransen (1982).

Keiller (1987) mapped an area on the western part of Kinleith Forests especially concentrating on the younger one of the two preciously unnamed ignimbrites between the Whakamaru and Mamaku ignimbrites. He first used the informal names Chimp and Pokai ignimbrite in literature (Keiller, 1987). No formal names have yet been given to these two ignimbrites (Houghton, pers.comm., 1992).

1.6. Purpose of the study

This study is a detailed examination of the Chimp and Pokai ignimbrites in the NW Taupo Volcanic Zone. Stratigraphically, the ignimbrites studied postdate the Whakamaru-group ignimbrites, which were erupted approximately at 330 ka (Pringle et al., 1992) from northern Lake Taupo area, and are overlain by Mamaku Ignimbrite, erupted from Rotorua caldera (Healy, 1982; Wilson et al., 1986). The Mamaku Ignimbrite has been dated at 140 ka (Murphy & Seward, 1981). The Chimp and Pokai ignimbrites are separated by two paleosols, several thick air-fall tephra units and a number of thinner epiclastic beds. Of the two ignimbrites the younger one, the Pokai

Ignimbrite, is better preserved and is hence the primary object of this study.

This research was initiated to investigate the stratigraphy and nature of the Chimp and Pokai ignimbrites, and to provide constraints on the most probable source area for the ignimbrites and thus their association with established caldera centres. Depositional models and eruption mechanisms of ignimbrites described elsewhere are discussed.

One of the main objectives of this thesis was to investigate a possible chemical variation in the ignimbrites, suggested by the occurrence of different pumice types (crystal-poor and crystal-rich). Detailed petrochemical and mineralogical work has been undertaken to investigate geochemical relationships between the two ignimbrites, and their relationship to other TVZ volcanic rocks. In the light of this work, the possible origin of the rhyolitic ignimbrites is discussed.

2. POKAI IGNIMBRITE

2.1. Field relationships

The Pokai Ignimbrite is a widespread and voluminous unit exposed along the southern and southwestern margin of Mamaku Plateau. Outcrop pattern, estimated distribution and outcrop elevations are shown on Figure 2.1. The northernmost outcrops, having a thickness of 20-25 m are in Tapapa Valley, 35 km NW of Rotorua; the most eastern outcrops (>40 m thick) in Haunui Valley, between Rotorua and Kapenga caldera margins, and the southernmost outcrops (8-20 m thick), 4-5 km S of Kinleith.

The ignimbrite occurs as a multiple-flow, simple cooling unit with single flow units ranging from 6-30 m in thickness. The maximum observed thickness is over 80 m (along Chamois and Harry Johnson Roads southwest of Horohoro, GR 801188, Map A and Fig.2.2), but the basement is not exposed. There are three lower (>4, 11 and 20 m) and two upper flow units (26 and 20 m, respectively) exposed with interbedded stratified deposits and thin (<1 m) ignimbrite flow units.

An informal type locality has been designated for Pokai Ignimbrite (Keiller, 1987; Houghton and Lloyd, pers.comm., 1989), at Pokai Road (GR 682268; field nos. 33 & R.[1].), a forestry road 6 km east of Tokoroa (Map A). Here the ignimbrite is 30 m thick and composed of a pre-ignimbrite plinian fall deposit (33 cm), a basal layer (2a), and at least two ignimbrite flow units (2b). The ignimbrite rests conformably on a 60 cm thick paleosol. At this locality the

[1] A list of all field localities with the rock type information is given in Appendix A.

Figure 2.1.

(a) Distribution and approximate thicknesses (in metres) of the Pokai Ignimbrite. Thick dashed lines mark the recorded Pokai Ignimbrite outcrop areas, dash-dot line is the approximate minimum distribution of the Pokai Ignimbrite. ● = recorded minimum thickness; o = estimated minimum thickness. The circular cross-hatch areas in E, SE and S mark the volcanic centres of Rotorua, Kapenga and Maroa, respectively.

(b) Elevations (in m.a.s.l.) of the Pokai Ignimbrite outcrops. Solid lines in the SE corner mark Quaternary faults (after Healy et al., 1964).

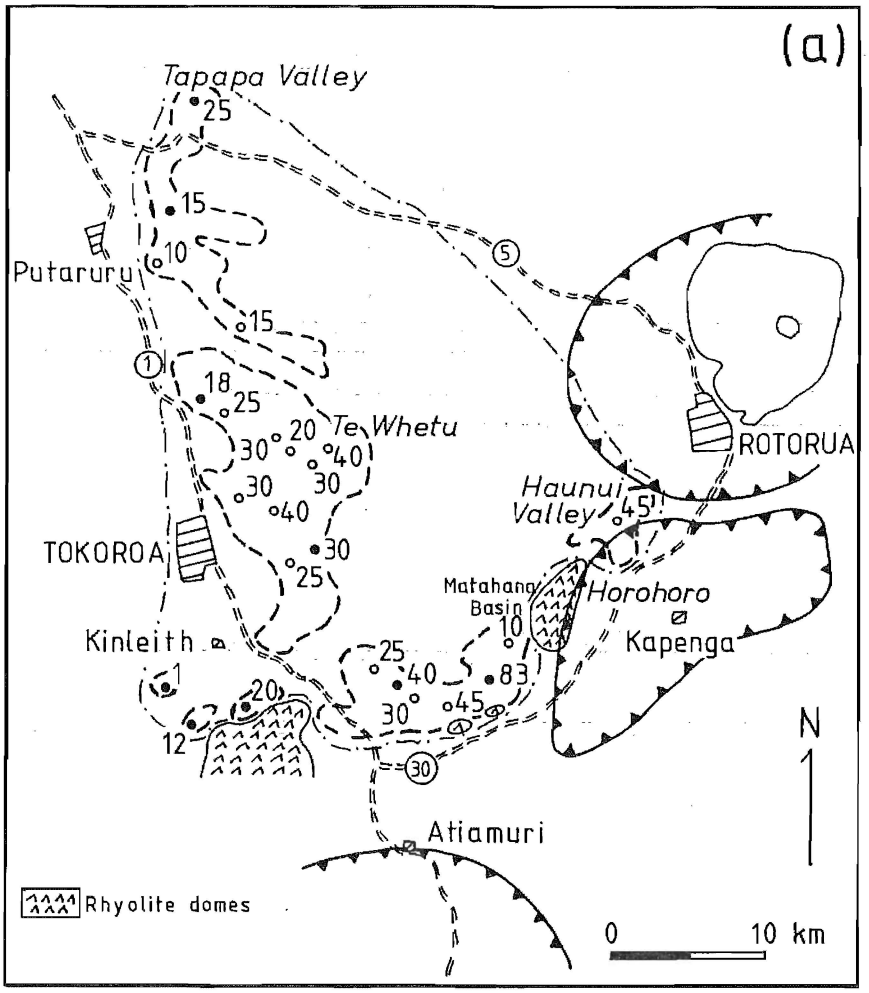
(a)
Tapapa Valley
25
15
10
Putaruru
15
18
25
20
Te Whetu
30
40
30
30
40
TOKOROA
30
25
Haunui Valley
45
ROTORUA
Matahana Basin
Horohoro
10
Kapenga
Kinleith
25
40
83
20
30
45
12
30
Atiamuri
N
Rhyolite domes
0
10 km

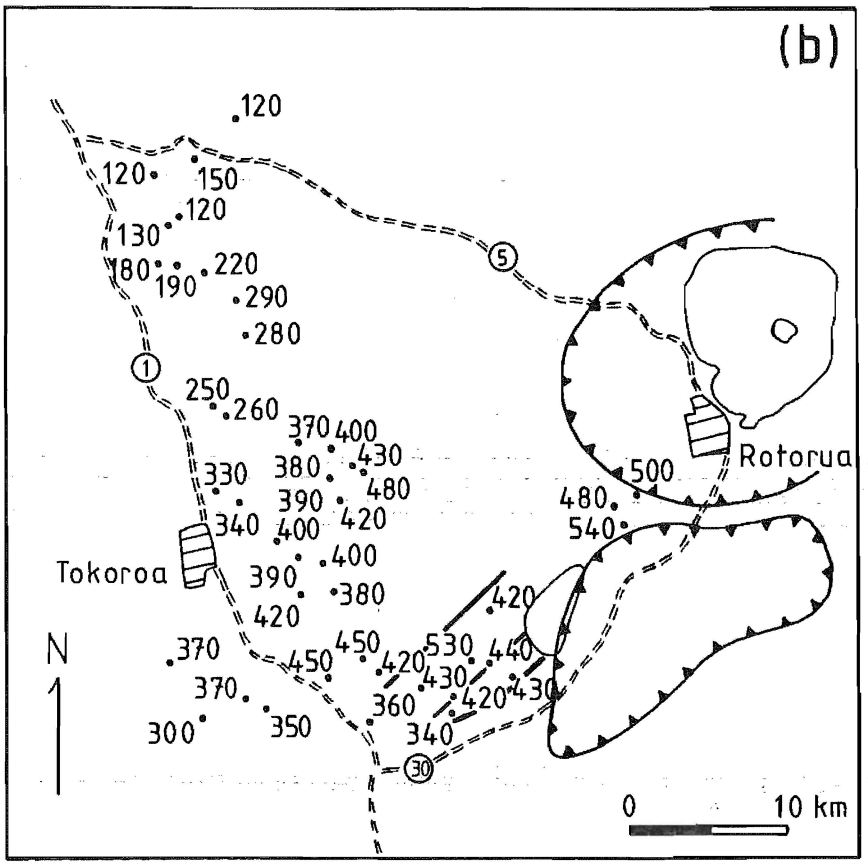
(b)
120
120
150
120
130
180
190
220
290
280
250
260
370
400
430
330
380
480
390
340
400
420
Tokoroa
400
390
380
420
420
N
370
450
450
420
530
440
430
370
420
430
360
300
350
340
Rotorua
500
480
540
0
10 km

Figure 2.2. Chamois Road section (GR 801188), displaying 80 m of Pokai Ignimbrite. Note the stratified succession in the middle of the section.

Figure 2.3. Densely welded Pokai Ignimbrite outcrop (GR 794194) ca. 1 km W from the Chamois Road section.

Pokai Ignimbrite is separated by two paleosols and a number ofthin air-fall tephra units from the underlying Chimp Ignimbrite. Other localities where the base of the Pokai Ignimbrite is exposed are at Galaxy Road (GR 673264; field no. 70), Puriri Road (GR 660294; field nos. 1 & 129) and McDowall Road at Te Whetu (GR 689335; field no. 12).

The Pokai Ignimbrite is usually very pumice-rich though normally matrix-supported. Localities where clast-supported pumice-concentration zones (PCZ) are exposed have been found at Moorhouse Road (GR 625358; field no. 91) and Te Rere Road (GR 609363; field no. 144). Pumice fragments are rounded to sub-rounded and often elongated parallel to vesicle tubes, with completely rounded pumice clasts found occasionally near the base of the ignimbrite. Lithic clasts are abundant and, with a few exceptions, evenly dispersed in the matrix. In its lower part the Pokai ignimbrite is composed of creamy-white or pale pink rhyolitic pumice in a pale yellow-brown to pale pink fine-grained shard-rich matrix. Upwards the colour darkens, until, at the top of the ignimbrite, dark orange-coloured pumices occur in a dark grey or brown matrix. The pumice size ranges from fine lapilli (>0.2 cm) to blocks 40 cm in diameter.

The base of the ignimbrite is non-welded; thicker flow units (>10 m) usually pass upwards into an indurated and then a moderately welded zone. The very top is normally non-welded. The welding is most intense in the upper third of a flow unit. In thick ignimbrite units (30-40 m) the upper part may be densely welded with strongly flattened pumices sometimes displaying black glassy fiamme. Here the flattened pumice and groundmass glass shards define a horizontal or sub-horizontal

foliation (eutaxitic texture), along the flow unit (Fig.2.3). A streaky appearance is partly due to the colour contrast between dark brown to black, collapsed pumice fragments and lighter brown or grey groundmass. The mean flattening ratios of the pumice clasts (calculated by the method of Peterson, 1979) range from 2 in the compacted and slightly welded zones up to 12 in the most densely welded zones (Fig.2.3). Columnar joints are common and usually well developed even in moderately welded parts of a flow unit (Fig.2.4).

The ignimbrite is generally crystal-poor, with 2-3 vol.% phenocrysts in pumice clasts. Crystals are predominantly plagioclase and clinopyroxene with lesser amounts of quartz, magnetite, ilmenite and titanite. In the northwestern part of the study area and in limited areas in the southwest and in Haunui Valley flow units with higher crystal content occur, up to 8 vol.% phenocrysts in pumice clasts (Chapter 4). The matrix contains lithics from <1 mm up to 8 cm in diameter; the median lithic content is between 2-3 vol.%. Lithics are generally angular to sub-angular and composed predominantly of flow-banded and spherulitic rhyolite and minor greywacke.

2.2. Pre-ignimbrite fall deposits

Air-fall pumice and ash deposits form the base of the Pokai eruptive units. The pre-ignimbrite air-fall tephra fell on to a strongly developed soil covered with at least some vegetation. There is no weathering evident between the air-fall deposits and the overlying ignimbrite indicating no significant time break in the eruptive activity. However, due to the erosive effect of the later ignimbrite, some of the

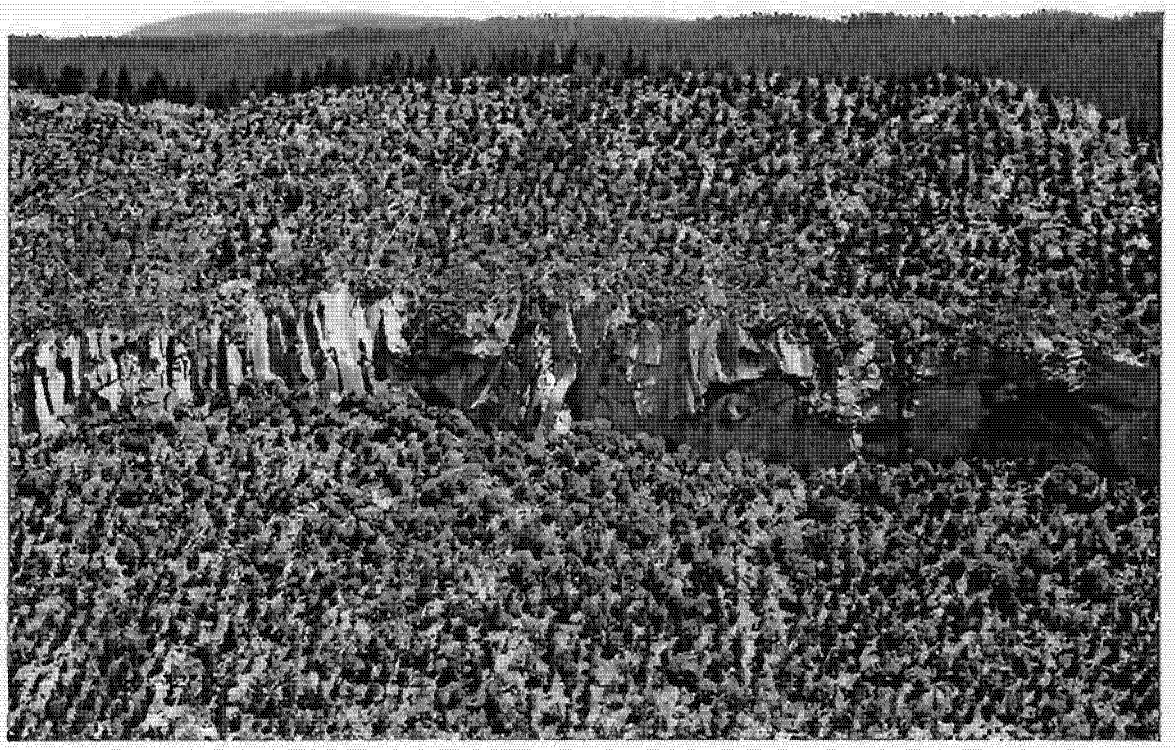

Figure 2.4. Columnar joints in the Pokai ignimbrite below Shrew Road (GR 696251).

air-fall units are only partly preserved and the true nature of the contact is not discernible. At Pokai Road, for example, only part of the pre-ignimbrite fall deposit is present while 30 m east all the Pokai air-fall units are missing and the ignimbrite rests directly on the underlying paleosol. The distal stratigraphy of the pre-ignimbrite fall deposits have been divided into pumice- and ash-fall units. Interbedded with the fall deposits are a few, thin flow units, which are referred to as distal flow units I, II and IIIa/b. Emplaced between the pre-ignimbrite fall deposits, the early pyroclastic flows are termed intraplinian ignimbrites.

There are only ten (10) outcrops displaying pre-ignimbrite fall deposits and no proximal air-fall deposits with ballistic lithics have been found. The best preserved Pokai air-fall deposits are in the SW Kinleith Forests, between 15 and 20 km ENE from Horohoro.[2]. The pre-ignimbrite air-fall deposits have a maximum thickness of about 3 m found in Matahana Basin, at Glass Road (field no. 57), located 12 km SW and 6 km W of the present day Rotorua and Kapenga caldera rims, respectively (Fig.2.5). Here the basement is not exposed, nor is the ignimbrite.[3]. The section begins with an approximately 1.8 m thick reversely graded pumice fall deposit, ranging from

---

[2] In the following descriptions MP = maximum pumice, the average diameter, in cm, of the three largest pumice clasts; ML = maximum lithic, the average diameter, in cm, of the three largest lithic clasts; MdØ = median diameter (from sieving data).

[3] The lack of any reference deposits nearby brings up a question about the origin of this deposit. Though no ballistic clasts have been found, the MP (7.7) and ML (4.8) data indicate proximity to the source. This air-fall deposit could be part of the younger Mamaku Ignimbrite Formation. There is a several metres thick air-fall pumice deposit (MP=3.5, ML=1.1) overlying the Pokai Ignimbrite and underlying the Mamaku Ignimbrite at Pukerimu Road (GR 786205), less than 2.5 km SSW from Glass Road. If both of these air-fall deposits were erupted from the Rotorua Volcanic Centre during the Mamaku eruption, a more homogeneous grain-size distribution between these two deposits would be expected. Moreover, the geochemical data of the basal Mamaku Ignimbrite from the Pukerimu Road location (Houghton & Weaver, unpubl. data, Appendix D, Table D.6) are different to the Glass Road data (Appendix D, Table D.3, samples 57/1-3, ref.nos. 124-126).

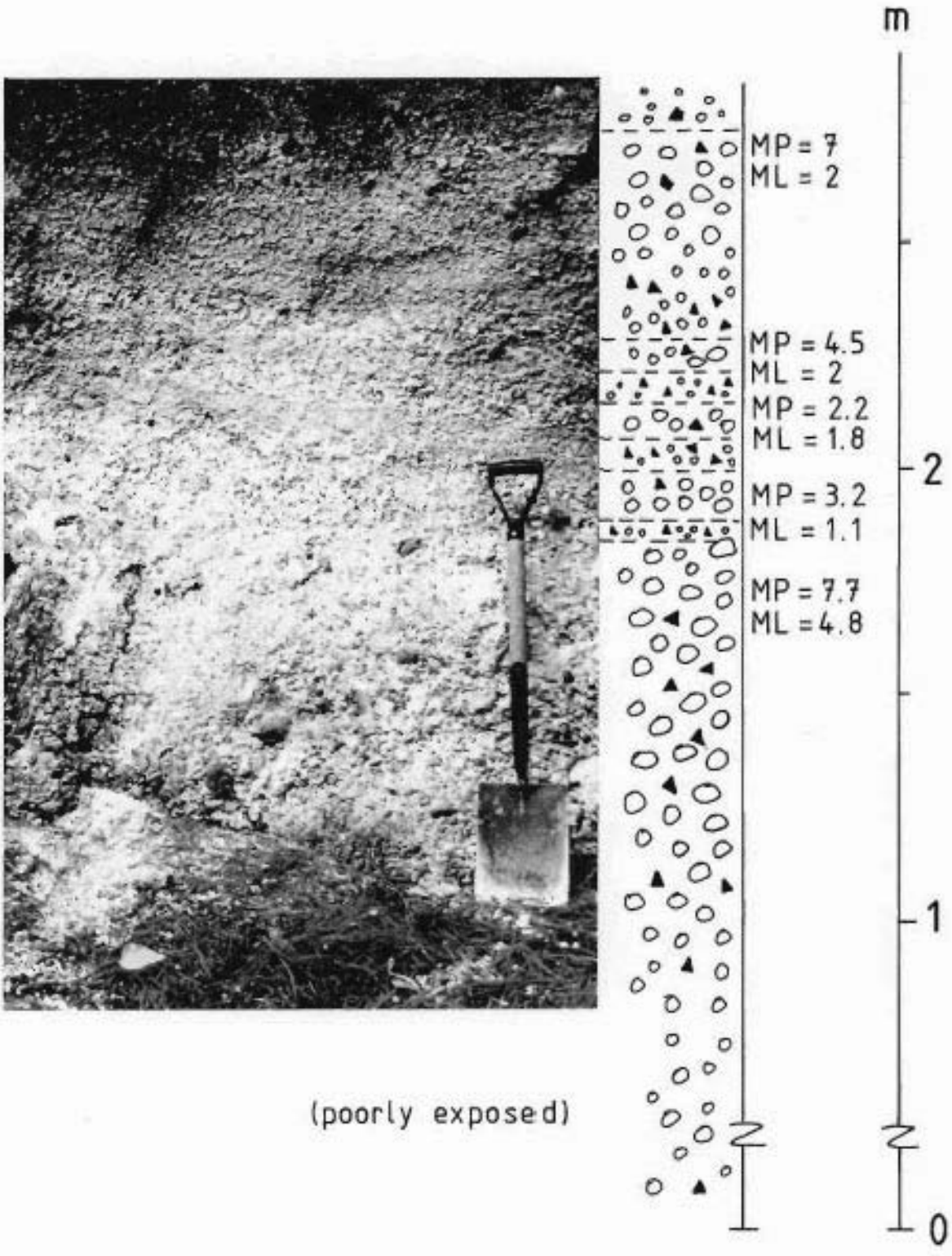

Figure 2.5. Pre-ignimbrite plinian air-fall (unit A) at Glass Road (GR 795224; field no. 57; for location, see also Fig.2.6, inset).

medium-sized to coarse lapilli and pumice blocks (MP=7.7). Lithic fragments (ML=4.8) are abundant and comprise about 38 weight % of the deposit. No ballistic clasts have been found. Fragments of obsidian are common and some phenocrysts of plagioclase, quartz and clinopyroxene occur, comprising only about 0.5 weight % of the deposit (analysed for the ½ mm fraction and coarser). The upper part of the section is composed of somewhat poorly defined stratification defined by several coarser and finer plinian-style layers. The finer-grained layers are always very lithic-rich, approximately up to 50 vol.% lithics.

The reversely graded coarse pumice layer is followed by four thin (6-20 cm), fine-grained, lithic-rich lapilli beds interbedded with slightly reversely graded medium lapilli beds (8-15 cm thick). The lowermost lithic-rich bed is relatively poorly defined and partly mixed up with both the underlying and overlying coarser pumice. The uppermost fine-grained bed passes gradually upward into more pumice-rich, reversely graded coarse lapilli (MP=7). A fifth, somewhat poorly defined, finer-grained bed (ca. 20 cm thick) can be seen on the top of this section.

Finer beds intercalated with coarser pumice can be produced in different ways. The abundance of lithic fragments in the finer beds suggest these beds may have formed after a temporary break in the eruption due to vent closure by wall collapse. The overlying deposits would be enriched in lithic fragments as a result from explosive re-opening of the vent (Walker, 1980). Further up in the stratigraphy the deposit becomes coarser and poorer in lithics. This kind of fluctuation can take place several times during the course of eruption, and

will be seen as a succession of coarser, pumice-rich and lithic-poor, and finer, lithic-rich layers. Many plinian deposits show an overall reverse grading, usually due to a progressive widening of the vent during the eruption.

Further west (for example at Galaxy, Pokai and Puriri Road sections) the pre-ignimbrite air-fall deposits are composed of several clearly defined units, both of plinian air-falls and phreatoplinian ash-falls with associated accretionary lapilli. It is possible that the changes seen at Glass Road are equivalent to the separate units found at other localities. However, the lack of fine material (ash-size) and accretionary lapilli, and the lack of interbedded flow units, which cut the lowermost pumice fall unit at Galaxy Road (Fig.2.6 and chapter 2.3) suggest that the Glass Road deposits represent only the lowermost initial pumice fall (air-fall unit A).

A detailed description of the Galaxy Road section (GR 673264, Map B; field nos. 70 & 128) is given with reference to other key localities to show some of the lateral variation of the deposits. Only the lowermost air-fall unit is preserved well enough to give any indication of the possible source area. However, all the air-fall units found in the study area will be described to give an idea of the style of the early plinian phase. The stratigraphy and correlation of a number of key localities is illustrated in Figure 2.6. The Galaxy Road locality (Fig.2.7), with data combined from two outcrops 100 m apart, was selected in favour of the previous informal type locality (Pokai Road) because the air-fall units are much more completely preserved along Galaxy Road (Fig.2.8). The Galaxy Road section also displays interbedded distal flow units (I, II and III) not found in Pokai Road.

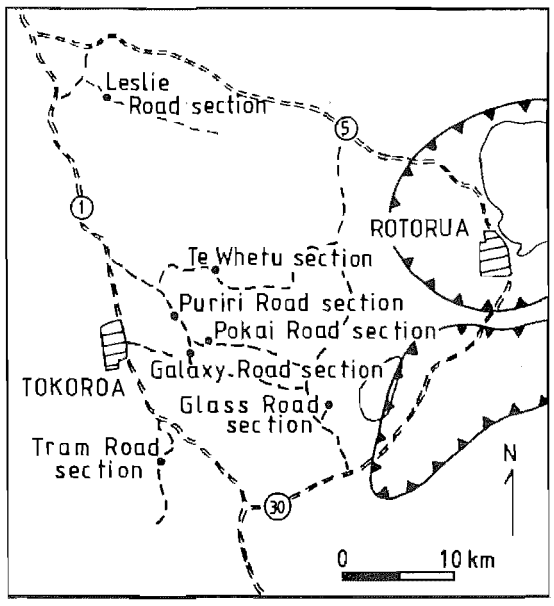

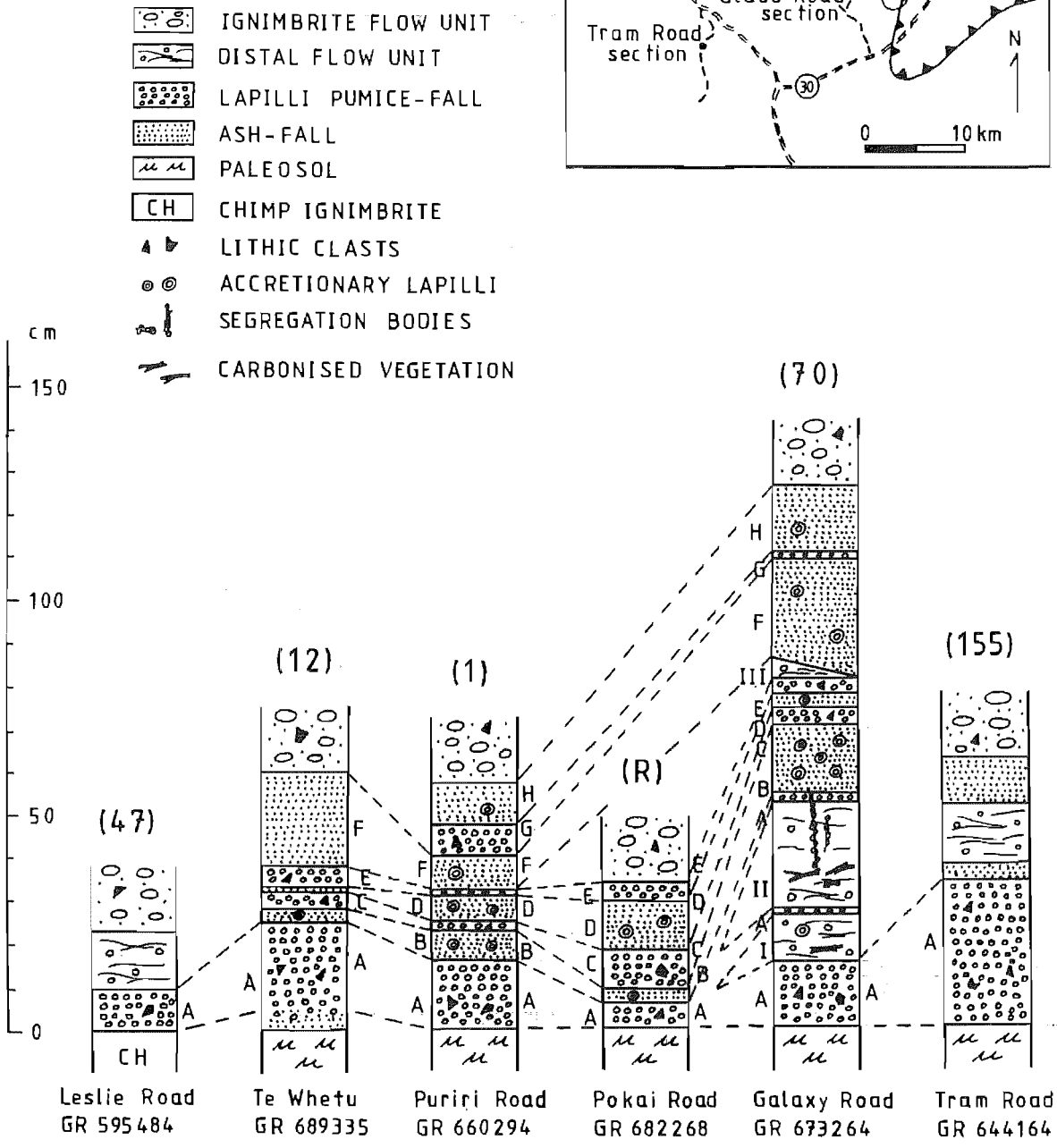

Figure 2.6. Stratigraphy and correlation of the Pokai air-fall units and early intra-plinian flow units. The numbers in parenthesis are the field numbers. The circular cross-hatch lines in the inset figure mark the volcanic centres of Rotorua (E) and Kapenga (SE), respectively.

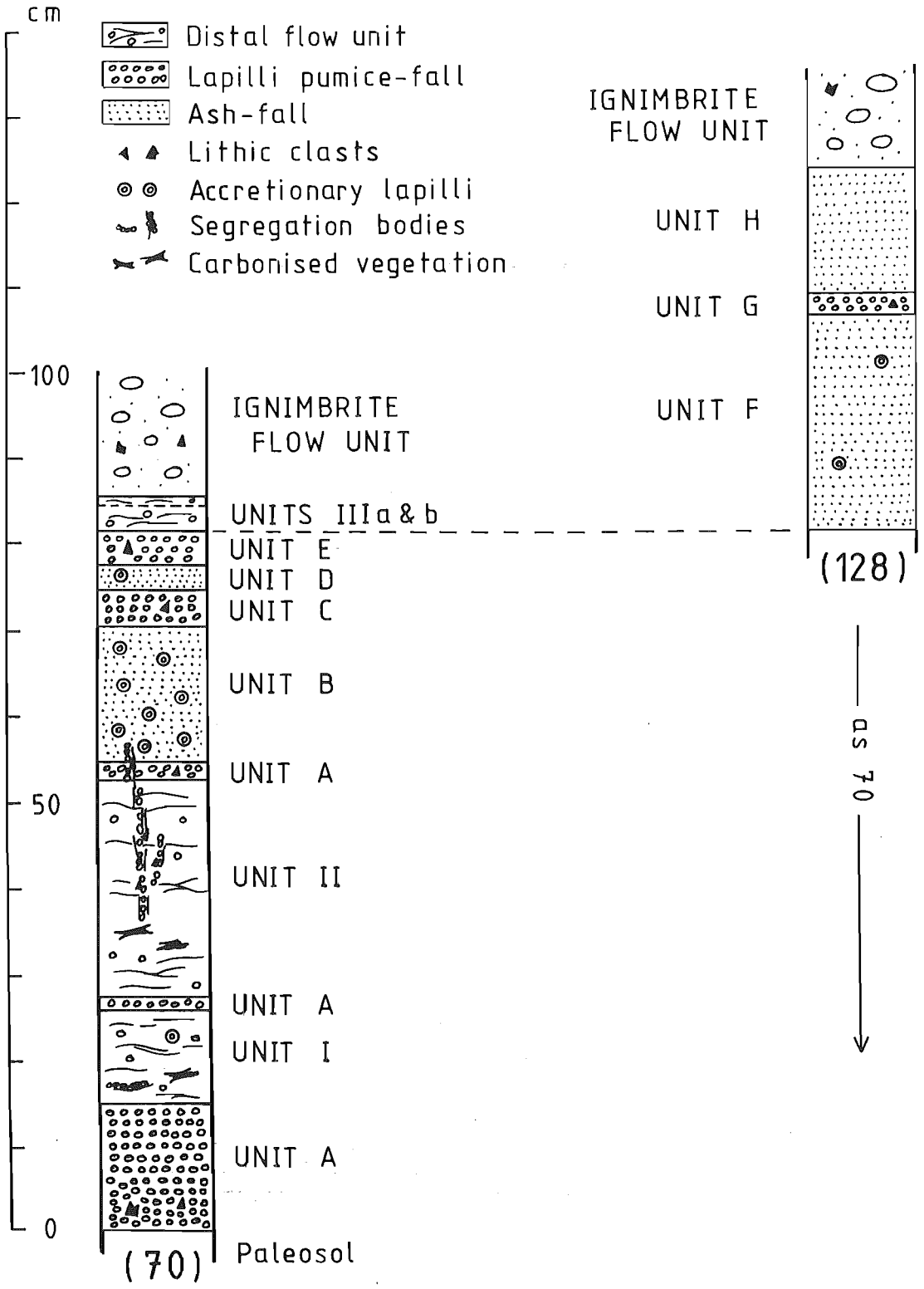

Figure 2.7. Stratigraphy of the Pokai air-fall units and early intra-plinian flow units at Galaxy Road (GR 673264, see also Fig.2.8, for location, see Fig.2.6, inset.); data combined from two sections 100 m apart (field nos. 70 & 128, respectively). The sections are identical up to air-fall unit E.

Figure 2.8. Galaxy Road (field no. 70) Pokai air-fall units A-E and distal, intra-plinian flow units I-III, also shown schematically in Fig.2.7.

(a) Air-fall unit A. This is a poorly sorted plinian pumice fall at the base of the section and is composed of grey-white, fine to coarse pumice lapilli and blocks up to 7 cm in diameter. Broken pieces of obsidian are relatively abundant. Phenocrysts of plagioclase, quartz, clinopyroxene and some Fe-Ti-oxides occur, comprising about 6.5 weight.% of the deposit (for the ½ mm fraction and coarser). The equivalent figures for the Glass (field no. 57) and Leslie Road (field no. 47) localities are 0.5 and 32 weight.%, respectively. Lithic clasts are common (ML=2.7) and comprise about 10 weight.% of the unit (at Glass Road about 38 wt.% and at Leslie Road about 2 wt.%). The lithics are composed mostly of fragments of rhyolite, and minor greywacke. The pumices show a slight reverse grading whereas the lithics are normally graded. At Galaxy Road fall unit A is 19 cm thick, and the upper part is interbedded with distal flow units.

Ash-sized material is rare. At one locality (Te Whetu section, GR 689335, field no. 12) a thin bed of coarse ash (3-5 cm) conformably underlies the plinian pumice. Upwards this ash bed quickly coarsens to lapilli and becomes indistinguishable from the rest of the pumice-fall. Maps showing the thickness, MP, ML and Mdø of the air-fall unit A are given in Figure 2.9.

(b) Air-fall unit B. This unit is pale pink - pale brown and composed of very fine-grained glassy ash with only a few quartz grains. Accretionary lapilli, with a maximum diameter of 1.6 cm, comprise approx. 30 vol.% of unit B. The water may have come from the vent, as accretionary lapilli are highly abundant in phreatomagmatic pyroclastics (Self & Sparks, 1978), or from accompanying rain (Walker, 1981a; Cas & Wright, 1987).

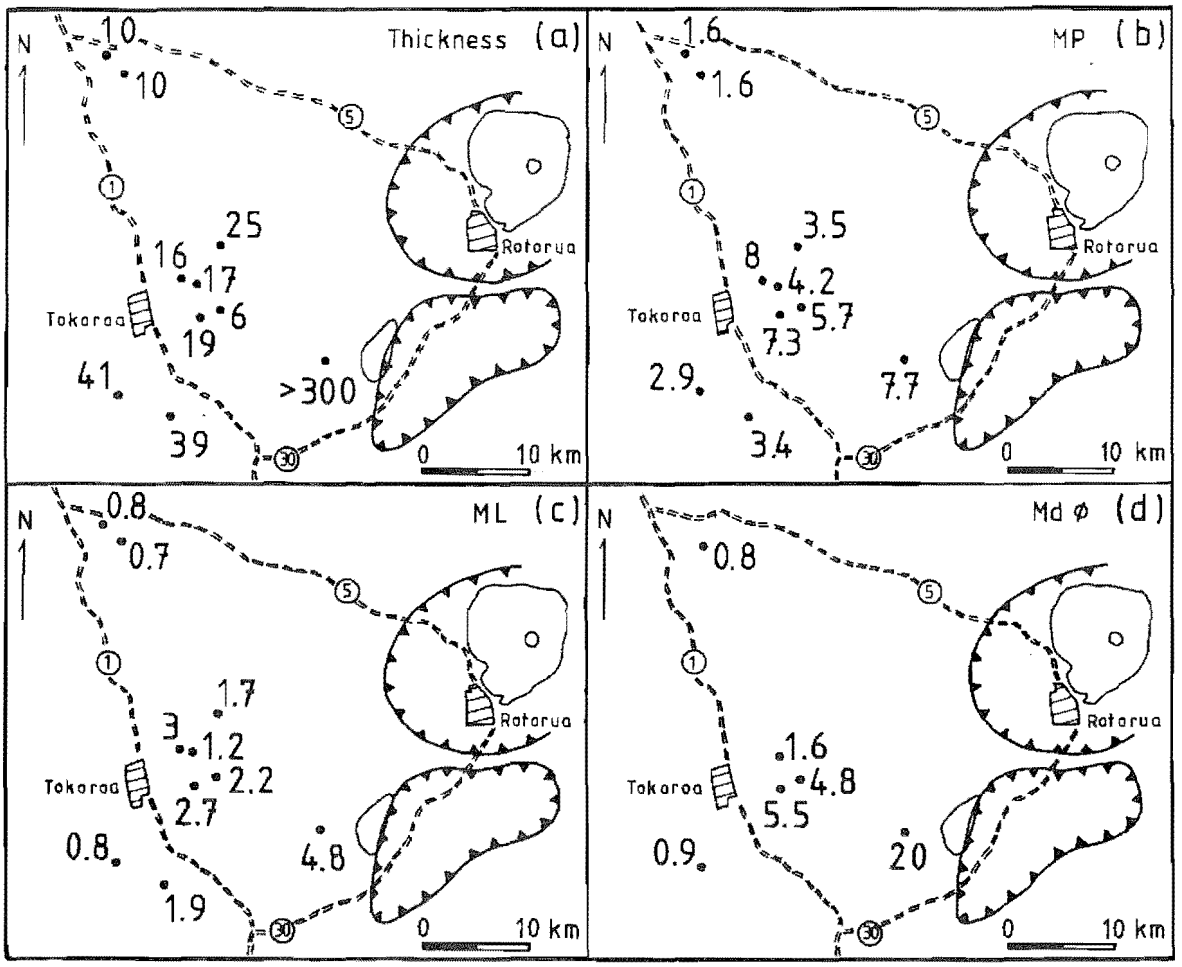

Figure 2.9. Maps showing (a) the measured thickness, (b) MP, (c) ML, and (d) Mdø in the air-fall unit A (pumice-fall). Values for the thickness, MP and ML are in cm, for the Mdø in mm. The circular cross-hatch lines mark the volcanic centres of Rotorua (E) and Kapenga (SE), respectively.

The thickness of unit B ranges between 3-16 cm at localities where it is preserved (Fig.2.10). The high abundance of accretionary lapilli and the thickness variation indicate that the material was deposited from a wet phreatoplinian eruption column. Water-splash laminations have not been found, suggesting that the effect of possible rain-flushing was small.

(c) Air-fall unit C. This is a plinian pumice-fall deposit composed of grey-white, predominantly medium and coarse lapilli pumice (MP=5.8). Lithic clasts, broken fragments of rhyolite and greywacke, are relatively abundant, but small (ca. 0.5 cm). Free crystals include quartz and plagioclase. The thickness, MP and ML data are shown in Figure 2.11.

(d) Air-fall unit D. D is a grey, fine ash-fall deposit with some accretionary lapilli (maximum diameter 0.8 cm). Microlithics and a few quartz and plagioclase crystals occur in this unit. At Galaxy Road unit D is only 4 cm thick and reaches a maximum thickness of 11 cm in Pokai Road (Fig.2.12).

(e) Air-fall unit E. This unit is a thin (4 cm thick) plinian pumice-fall, composed of grey-white, fine to medium lapilli pumice (MP=3). Lithic clasts occur, but are small (ML=0.5). The thickness, MP and ML data are given in Figure 2.13. At Galaxy Road unit E is overlain by two thin distal flow units (IIIa and IIIb).

(f) Air-fall unit F. This grey, fine ash-fall deposit is found only at three localities; at Galaxy Road (128), at Puriri Road and at Te Whetu (Fig.2.6). At Galaxy Road (128) unit F directly overlies pumice-fall E, the distal flow units IIIa and IIIb are missing. The thickness of unit F ranges from 8-24

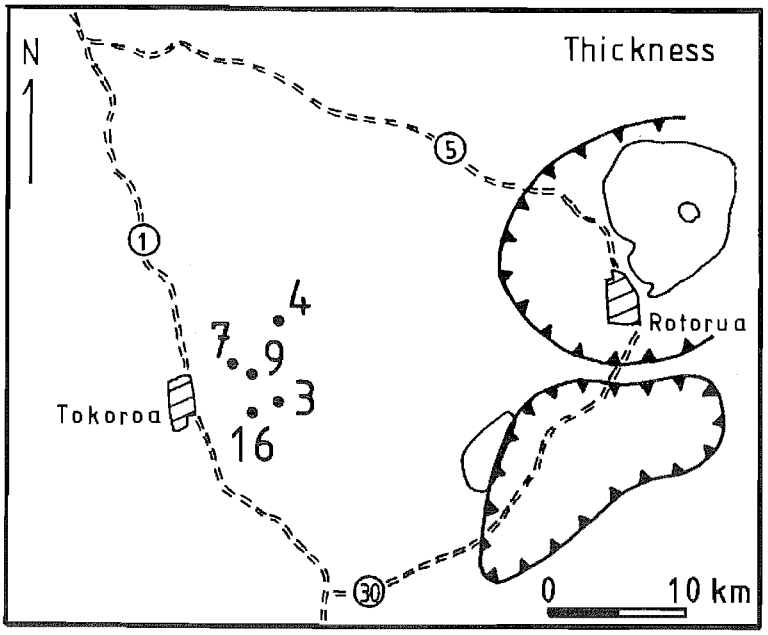

Figure 2.10. Map showing the measured thickness, in cm, of the air-fall unit B (ash-fall). The circular cross-hatch lines mark the volcanic centres of Rotorua (E) and Kapenga (SE), respectively.

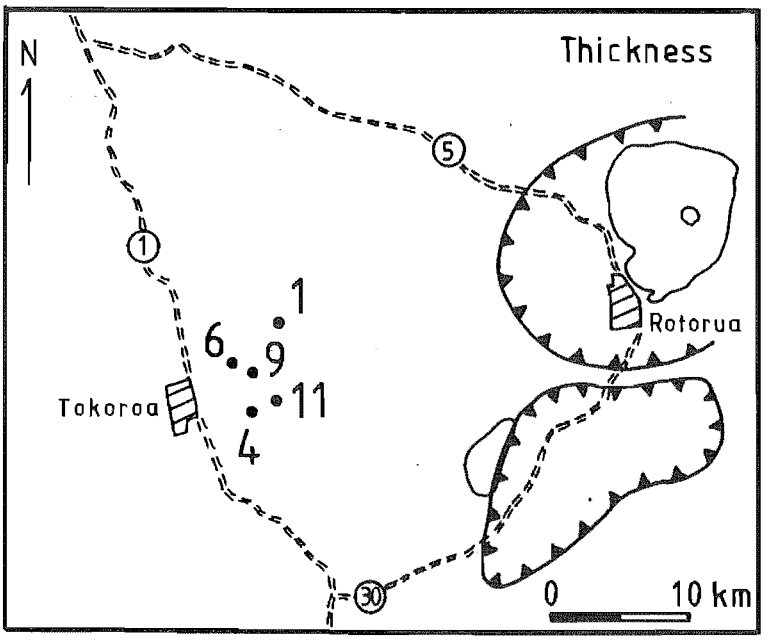

Figure 2.12. Map showing the measured thickness, in cm, of the air-fall unit D (ash-fall). The circular cross-hatch lines mark the volcanic centres of Rotorua (E) and Kapenga (SE), respectively.

Figure 2.11. Maps showing (a) the measured thickness, (b) MP, and (c) ML in the air-fall unit C (pumice-fall). All values are in cm. The circular cross-hatch lines mark the volcanic centres of Rotorua (E) and Kapenga (SE), respectively.

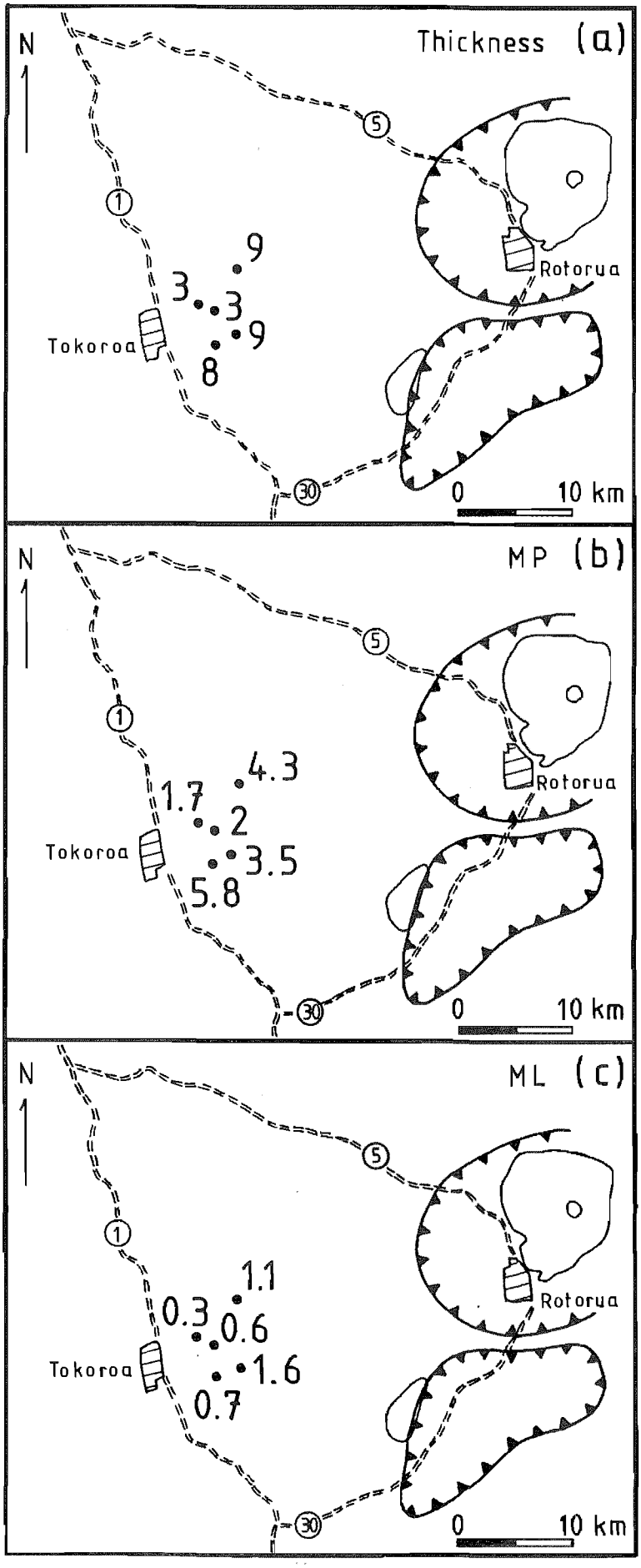
N
Thickness (a)
5
1
9
3
3
9
8
Tokoroa
Rotorua
30
0
10 km
N
MP (b)
5
1
4.3
1.7
2
3.5
5.8
Tokoroa
Rotorua
30
0
10 km
N
ML (c)
5
1
1.1
0.3
0.6
1.6
0.7
Tokoroa
Rotorua
30
0
10 km

Figure 2.13. Maps showing (a) the measured thickness, (b) MP, and (c) ML in the air-fall unit E (pumice-fall). All values are in cm. The circular cross-hatch lines mark the volcanic centres of Rotorua (E) and Kapenga (SE), respectively.

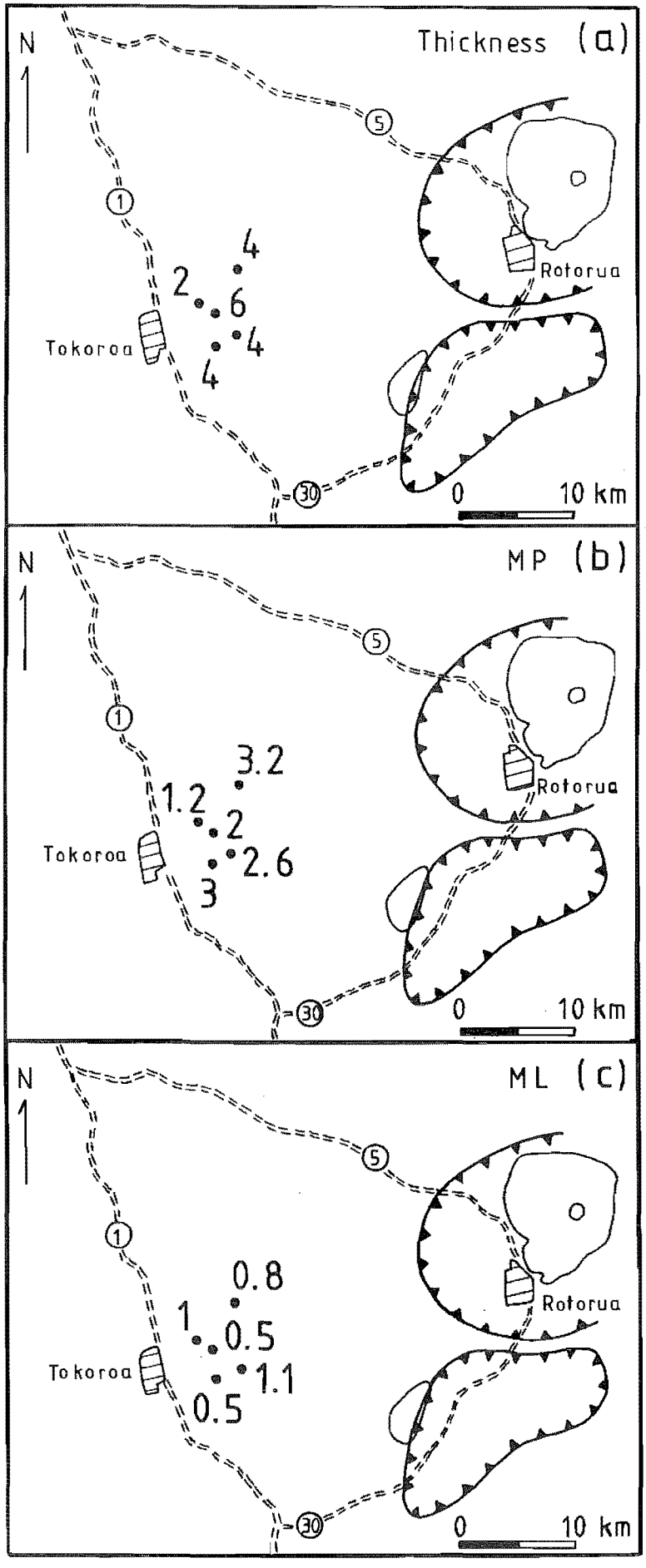
N
Thickness (a)
5
1
4
2
6
4
4
Tokoroa
Rotorua
30
0
10 km
N
MP (b)
5
1
3.2
1.2
2
2.6
3
Tokoroa
Rotorua
30
0
10 km
N
ML (c)
5
1
0.8
1
0.5
1.1
0.5
Tokoroa
Rotorua
30
0
10 km

cm. Accretionary lapilli are rare.

(g) Air-fall unit G. This plinian lapilli pumice deposit has been recorded only at Galaxy Road (128), where it is 2 cm thick, and at Puriri Road, where it is 7 cm thick. Unit G is composed of grey-white, mostly fine lapilli pumice (MP=1.8). Small lithics (ML=0.3) and some free crystals (quartz and plagioclase) occur.

(h) Air-fall unit H. This is a light grey, fine ash deposit found only at Galaxy Road (128), where it is 15 cm thick, and at Puriri Road, where the deposit measures nearly 20 cm. Accretionary lapilli are missing at Galaxy Road (128), although some are present at Puriri Road. The low abundance of accretionary lapilli in units F and H suggests that they were deposited from relatively dry phreatoplinian columns and the occasional accretionary lapilli may be due to rain-flushing.

At Tram Road (GR 644164, field no. 155) a 4 cm thick fine ash-fall deposit overlies air-fall unit A (pumice-fall). No accretionary lapilli were found in this pinkish-brown ash indicating it could represent a more distal part of ash-fall units F or H rather than of units B or D. It may also represent a co-ignimbrite ash-fall deposit associated with some of the early flow units.

For plinian deposits, the thickness distribution (isopach) map and maximum grain size (isopleth) map are generally useful indicators of source vent(s) as both MP and ML increase consistently towards source (Walker & Croasdale, 1971; Self et al., 1986). However, plinian deposits are not always thickest at the vent, for example the Taupo and Waimihia plinian deposits have maximum thickness isopaches that close around an

area downwind from vent (Walker, 1981). The distribution maps for the other air-fall units than unit A proved to be less informative as an indicator of source direction, especially because the upper units are missing from both the southernmost and northernmost localities, and much of the ash was so unevenly accumulated as mud rains. A thickness isopach combining all pre-ignimbrite air-fall deposits is shown in Fig.2.14.

Histograms showing the grain size and component analysis for the Pokai Ignimbrite air-fall unit A are illustrated in Figure 2.15. The median grain sizes (Mdø) have been plotted against distance from different possible source areas, namely the Rotorua, Kapenga and Maroa Volcanic Centres and Matahana Basin (Fig.2.16.a). The Mdø increases eastward and a linear correlation of the Mdø against distance from both Rotorua and Kapenga centres, and from Matahana Basin are evident. The data also indicates that the air-fall unit A could not have come from the Maroa Volcanic Centre.

Isopleths of average maximum lithic size are of particular use, because the larger lithics would be less affected by prevailing winds than the lighter pumice clasts. Larger ballistic lithics, exceeding 10 cm, usually extend out to 3-5 km from the vent (Booth et al., 1978; Walker, 1981d). The largest lithics found in the Pokai Ignimbrite air-fall deposits are 5-5.5 cm (at Glass Road). This size of lithics are though unlikely to be carried several tens of kilometres away from the vent. The ML and the weight percentages of the lithics ½ mm and coarser for the air-fall unit A plotted against distance from Rotorua, Kapenga, Maroa and Matahana Basin are shown in Figure 2.16.a&b, respectively. There is a

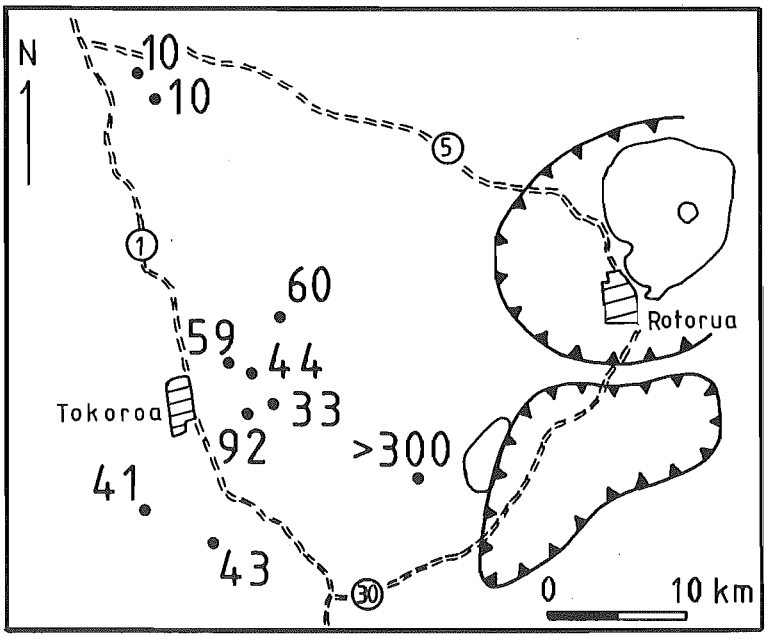

Figure 2.14. Total thickness, in cm, of all pre-ignimbrite air-fall deposits. The circular cross-hatch lines mark the volcanic centres of Rotorua (E) and Kapenga (SE), respectively.

Figure 2.15. Grain size histograms of the Pokai Ignimbrite air-fall unit A. The bars for ½ mm (1 phi) and coarser classes are subdivided to show the proportions of components.

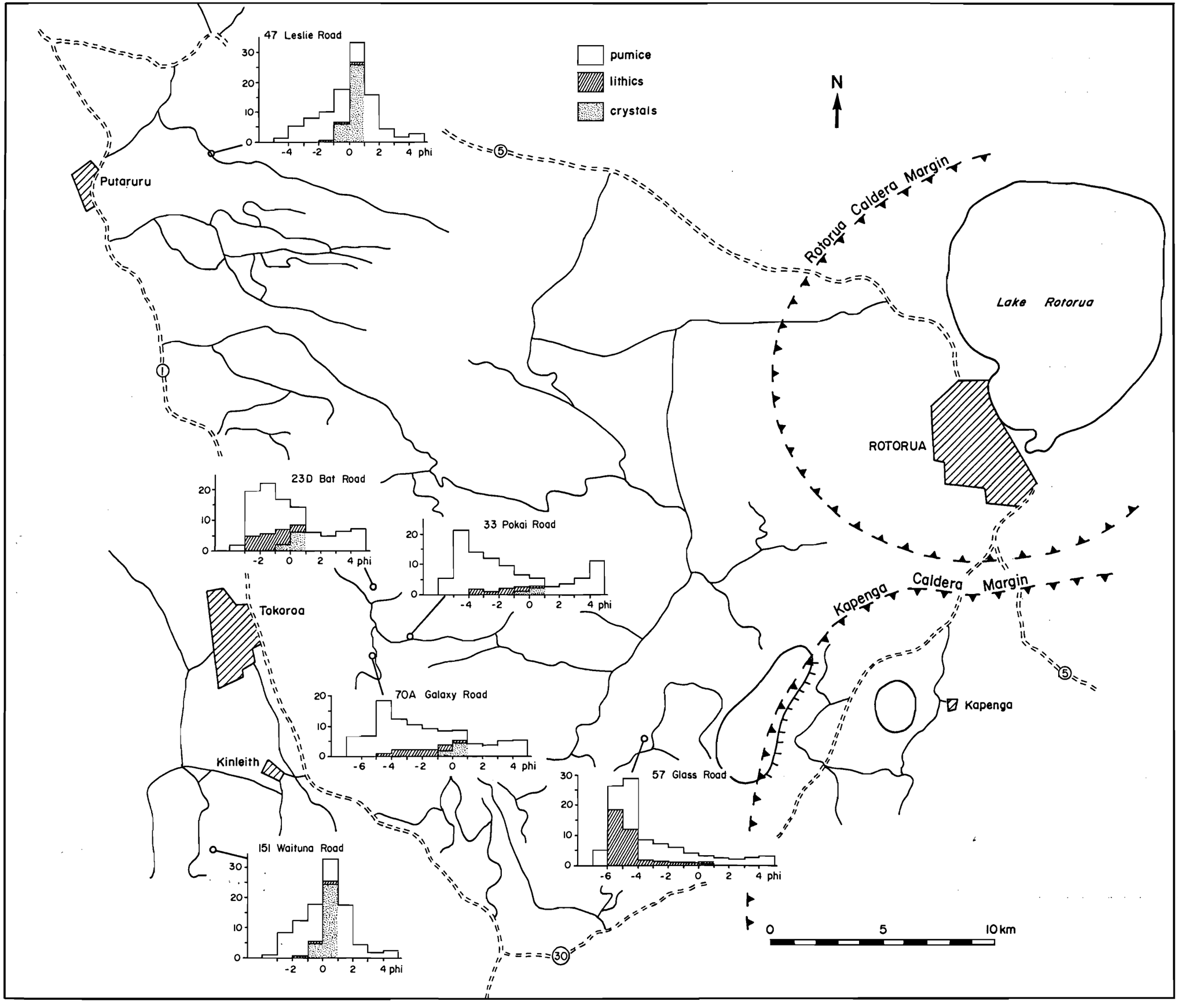
pumice
lithics
crystals
N
47 Leslie Road
30
20
10
0
-4 -2 0 2 4 phi
Putaruru
Rotorua Caldera Margin
Lake Rotorua
ROTORUA
23D Bat Road
20
10
0
-2 0 2 4 phi
33 Pokai Road
20
10
0
-4 -2 0 2 4 phi
Tokoroa
70A Galaxy Road
20
10
0
-6 -4 -2 0 2 4 phi
Kapenga Caldera Margin
Kapenga
Kinleith
57 Glass Road
30
20
10
0
-6 -4 -2 0 2 4 phi
151 Waituna Road
30
20
10
0
-2 0 2 4 phi
0 5 10 km

Figure 2.16. (a) Mdø, (b) ML, and (c) weight percentages (wt.%) of lithics for the fraction ½ mm (1 phi) and coarser, expressed as percentage of the whole sample, in the Pokai Ignimbrite air-fall unit A plotted against distance from the Rotorua, Kapenga and Maroa Volcanic Centres and Matahana Basin.

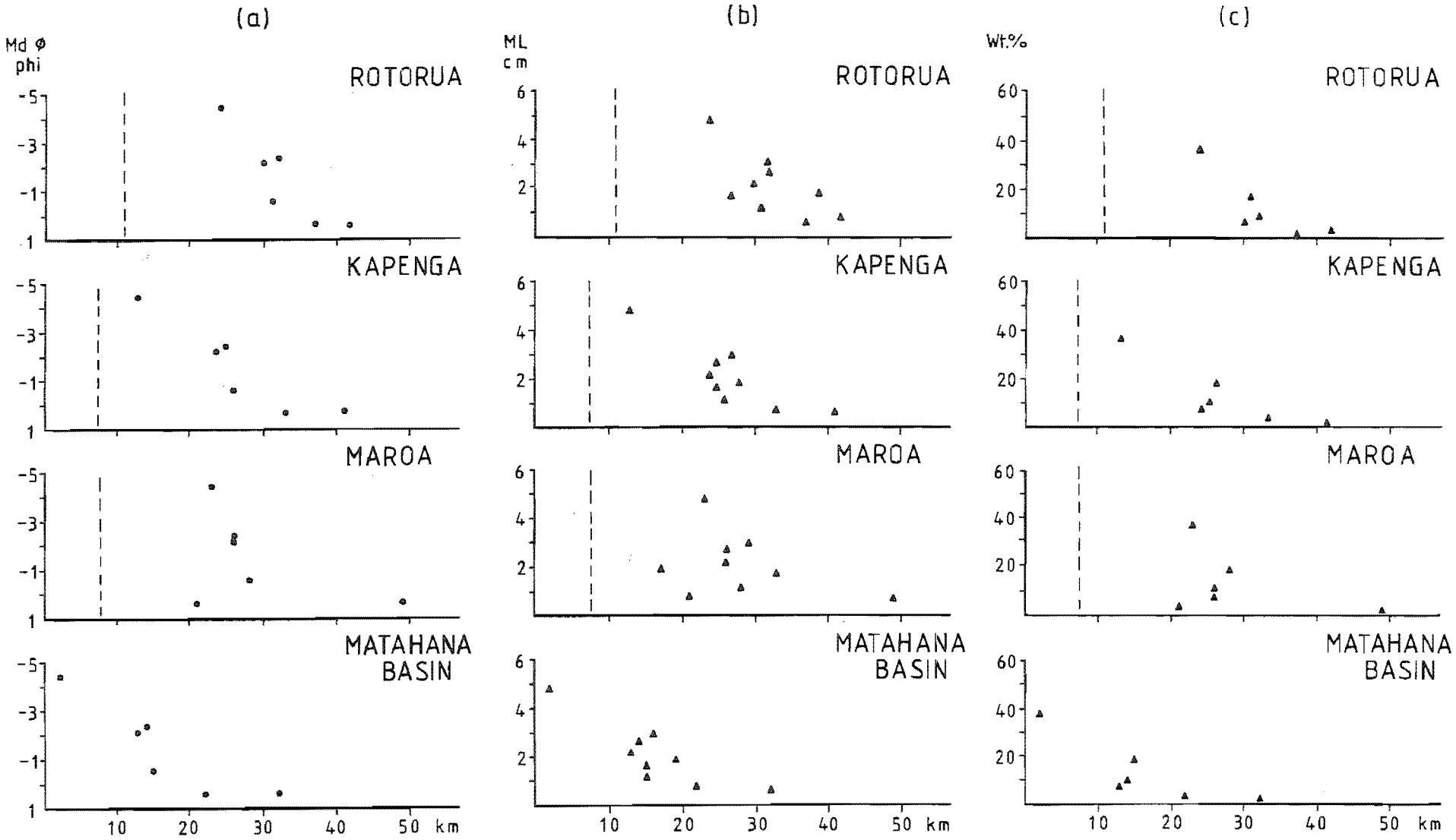
(a)
Md ϕ
phi
ROTORUA
KAPENGA
MAROA
MATAHANA
BASIN
-5
-3
-1
1
10
20
30
40
50 km
(b)
ML
cm
ROTORUA
KAPENGA
MAROA
MATAHANA
BASIN
6
4
2
10
20
30
40
50 km
(c)
Wt.%
ROTORUA
KAPENGA
MAROA
MATAHANA
BASIN
60
40
20
10
20
30
40
50 km

linear correlation between the weight percentages and the distance from Rotorua, Kapenga and Matahana Basin, but again the correlation with Maroa is poor.

The weight percentage of lithics (½ mm and coarser) is highest at the Glass Road locality; nearly 40 % of the whole sample. The distance to the centre of the Rotorua caldera is over 20 km, and the present day caldera rim is about 13 km towards northeast. It is questionable if such a high amount of lithics could stay airborne for such distances, if the unit was sourced from Rotorua caldera. Kapenga centre is situated 12 km east from Glass Road, and the present day caldera margin is only about 6 km away, and thus seems a more likely source area. The Glass Road locality lies only 2 km south from the central Matahana Basin; however, no ballistic lithics was found (thus indicating that the vent was situated further away).

2.3. Distal early flow units.

At Galaxy Road (Figs.2.7 and 2.8) the initial air-fall unit A is sharply overlain by an uneven, 7-11 cm thick, fine-grained tephra unit (distal flow unit I). It is pale pinkish-brown and composed of very fine ash with some accretionary lapilli. Broken pieces of obsidian, a few microlithics and rare fine-grained lapilli pumices are evenly distributed in the matrix, together with pieces of carbonized vegetation, lying horizontally along the bed. Some 'drawn-out' lenses of fine-grained lapilli pumice and small lithics occur along the base. The uneven thickness, elongated segregation pods and carbonized vegetation suggest deposition from a pyroclastic

flow.

Another distal flow unit (unit II), 20-25 cm thick, overlies the basal pumice-fall A (Figs.2.7 and 2.8). It is composed of grey, fine to coarse ash with abundant white, fine-grained lapilli pumice (MP=1.6). Small lithics (<0.5 cm) and free crystals (plagioclase and quartz) are present. Fragments of carbonized vegetation and gas segregation pipes are relatively abundant.

Overlying air-fall ash unit E there are two thin (3.5 and 1 cm), pale brown, irregular ash layers (Figs.2.7 and 2.8). Some white, fine-grained lapilli pumice (MP=1.1), a few free crystals (plagioclase and quartz) and microlithics are present. These layers have also been interpreted to represent the most distal parts of early flow units, and are referred to as distal flow units IIIa and IIIb.

In the central and western Kinleith Forests distal intraplinian flow units have been found only at the Galaxy Road locality. All units are relatively poorly sorted, rich in fine material, contain carbonized vegetation (except unit III) and unit I has occasionally eroded the top of the underlying plinian deposit; features typical of distal pyroclastic flow units (Wilson & Walker, 1985). All are features consistent with a distal facies, where, even though volume has been reduced, the velocity remains (Wilson & Walker, 1982). Both in the southern- and northernmost outcrops (Tram Road and Leslie Road sections, respectively) thin distal flow units (<25 cm) have been recorded between the air-fall units and the Pokai ignimbrite (Fig.2.6).

2.4. Ignimbrite flow units

An idealised ignimbrite flow unit consists of layer 1, the ground deposits, layer 2, which forms the bulk of the deposit and layer 3, the co-ignimbrite ash-fall deposit (see Fig.1.7). Layer 1 deposits are rare in the Pokai ignimbrite. This could be due either to non-deposition or to penecontemporaneous erosion. Traces of layer 1(P)-type material have been found at the Pokai Road section, as small pumice concentration lenses at the base of layer 2a.

At the corner of Harry Johnson and Tikorangi Roads (GR 802192) a small Pokai Ignimbrite outcrop is exposed (2x4 m). It is composed of coarse, though matrix-supported, well rounded lapilli pumice and blocks (MP=17). The outcrop is located at the side of a rounded topographic depression at 420 m.a.s.l. All the other Pokai Ignimbrite outcrops in that area are situated at higher elevations, for example the base of the >80 m thick Chamois Road section, only 0.4 km away, is situated approximately at 430-440 m.a.s.l. The coarse pumice deposit may be an upper pumice-rich zone of a flow unit or it may represent a 'pumice dune', sometimes found at the base of an ignimbrite. This type of fines-depleted ignimbrite deposit (FDI) is considered to be a part of layer 1 deposits and is usually best developed at the base of the lowermost flow unit due to ingestion of cold air at the ignimbrite flow head. Layer 1(H) deposits have not been recorded.

The bulk of the Pokai ignimbrite forms a valley-ponded (VPI) layer 2 deposit. Pokai VPI can be divided into two layers: layer 2a, which represents the boundary layer to the flow as it was moving into place, and layer 2b, the bulk of the flow.

Layer 2a, the basal layer, differs from the main portion of the flow unit in that it lacks the largest pumice and lithic clasts. MP and ML seldom exceed 4 and 1.5 cm, respectively. The thickness of the basal layer ranges from 15 cm to 1.2 m with no correlation between the thickness of the basal layer and the thickness of the overlying flow unit.

Most of the exposed ignimbrite is layer 2b. The base of layer 2b is usually pale pink - pale yellow-brown with relatively abundant pale pink to creamy-white fine to coarse pumice lapilli and blocks. Lithics are present but small (ML=1.5). At 1-2 m above the base of layer 2b the pumice size and concentration increases. A slight lithic concentration zone (ML=3.9 at Galaxy Road, GR 673264) has also been recorded at this level. Otherwise the lithic clasts are relatively evenly scattered throughout unit 2b until at the top of the flow units, which are systematically poorer in lithics and have a smaller lithic size. Lithic clasts (rhyolite and minor greywacke) commonly range from 1.5 to 4 cm in diameter.

Detailed studies of ignimbrites (Walker, 1981d; Walker & Wilson, 1983) have revealed that they generally show systematic lateral variations in grain size and composition, so that at the distal end an ignimbrite trends towards a composition of 100 % of vitric fine ash and dust. The main mass, layer 2 deposit, shows a slight progressive decrease in grain size to the west (Fig.2.17). Average MP in layer 2b varies from 27 cm at localities in Haunui Valley to 7 and 5 cm, at localities 5 km south from Kinleith Mill and at Tapapa in northwest, respectively. Average ML at the same localities are 5.3, 0.3 and 1 cm, respectively.

Figure 2.17. Isopleth maps of MP and ML in the Pokai Ignimbrite layer 2b (VPI). Shaded patches in the MP map mark the areas with well developed coarse-tail grading (flow type 3 of Wilson, 1980); MP in parenthesis. The open triangle in both maps represents data from a lithic breccia deposit (see section 2.7). Both the isopleth and location values are in cm. The circular cross-hatch lines mark the volcanic centres of Rotorua (E) and Kapenga (SE), respectively.

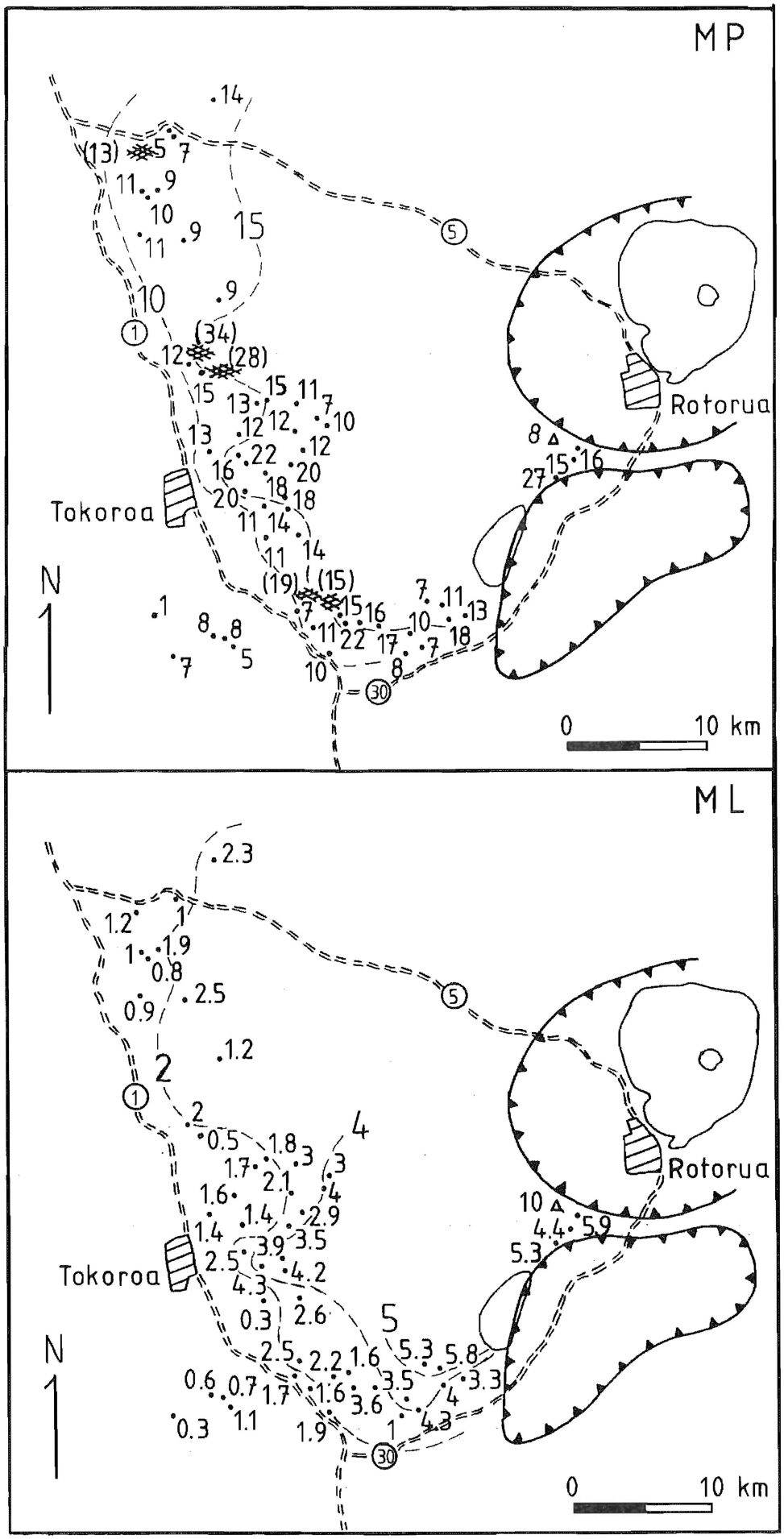
MP
Rotorua
Tokoroa
N
0
10 km
ML
Rotorua
Tokoroa
N
0
10 km

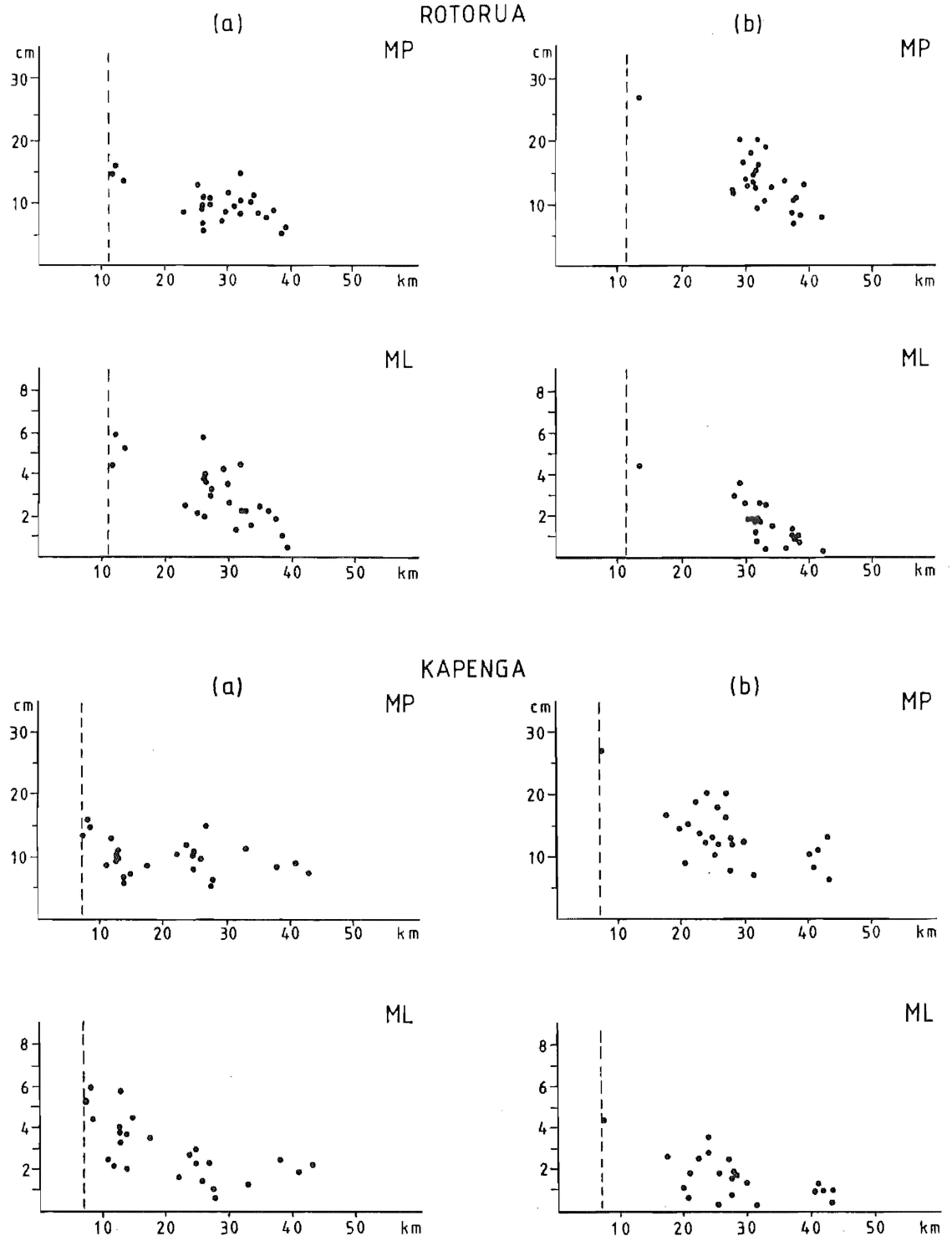

Figure 2.18. MP and ML (a) in the lower part (2-6 m above the base), and (b) at the top of the valley-ponded Pokai Ignimbrite plotted against distance from the Rotorua and Kapenga Volcanic Centres. Dashed lines mark the approximate present day caldera margins for both volcanic centres.

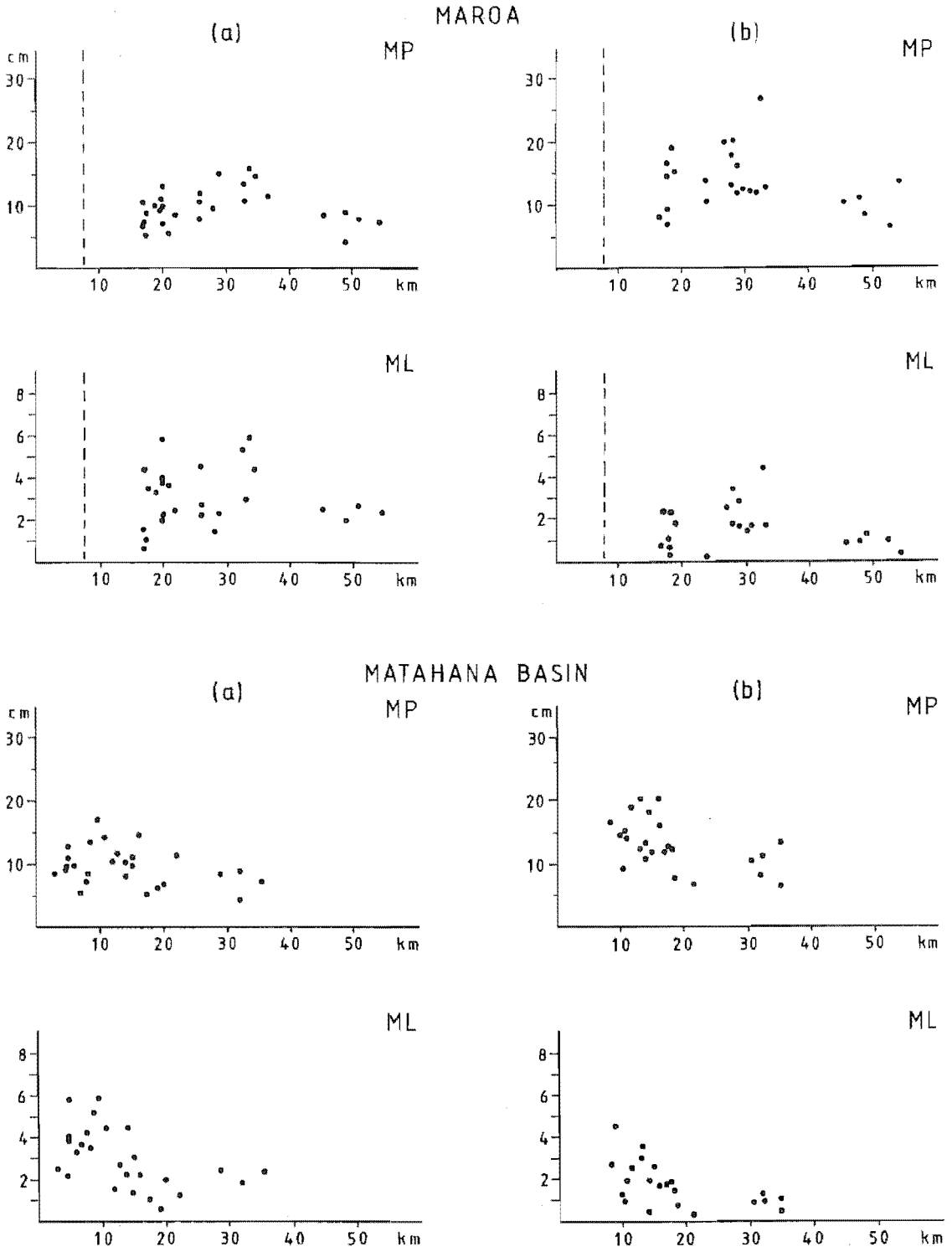

Figure 2.19. MP and ML (a) in the lower part (2-6 m above the base), and (b) at the top of the valley-ponded Pokai Ignimbrite plotted against distance from the Maroa Volcanic Centre and Matahana Basin. Dashed lines mark the approximate present day caldera margin for the Maroa Volcanic Centre.

Relation of MP and ML against distance from Rotorua, Kapenga, Maroa and Matahana Basin are given in Figures 2.18 and 2.19. Two diagrams for each possible source areas are given, one (a) showing the MP and ML for the lower part of a flow unit, where a slight lithic concentration was usually detected, and the other diagram (b) shows the data for the top part of a flowunit with a moderately developed coarse-tail grading (increased pumice size and concentration, decreased lithic size). A linear correlation of MP and ML against distance from Rotorua, Kapenga and Matahana Basin is seen, the correlation between the grain sizes and the distance from the Kapenga Volcanic Centre suggest an origin from east rather than from northeast of the study area (Fig.2.18). No linear correlation is evident between the grain sizes and the distance from the Maroa Volcanic Centre (Fig.2.19).

MP usually varies less consistently than ML. The reason might be that pyroclastic flows have a capacity to carry large quantities of lighter pumice, but only a limited capacity to carry lithics, which tend to drop out (Walker & Wilson 1983). The flow 'lobes' showing coarse zones may represent loci of the main pyroclastic flow routes, largely controlled by the paleotopography.

Histograms showing the grain size and component analysis from 13 ignimbrite matrix samples are illustrated in Figure 2.20. Eleven of the samples represent material from a non-welded lower part (2-6 m above the base) of crystal-poor flow units with a moderate pumice content. One sample (field no. 98) is from the PCZ (still matrix-supported) of the crystal-rich southeastern flows. The Leslie Road sample (field no. 47) comes from a crystal-rich northwestern flow unit with a

Figure 2.20. Grain size histograms of the Pokai Ignimbrite matrix (≤16 mm). The bars for ½ mm (1 phi) and coarser classes are subdivided to show the proportions of components.

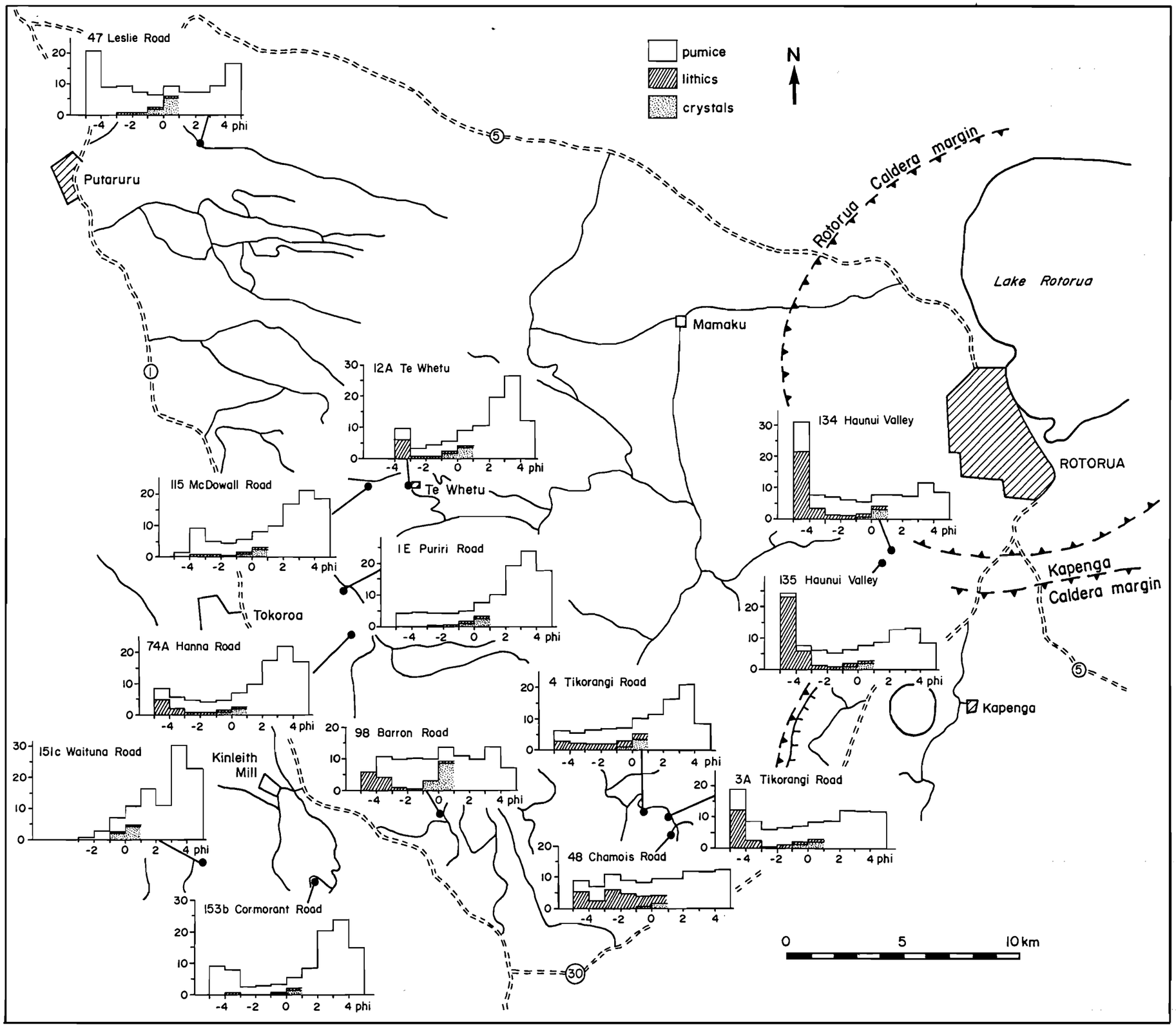
pumice
lithics
crystals
N
47 Leslie Road
Putaruru
Rotorua Caldera margin
Lake Rotorua
Mamaku
12A Te Whetu
Te Whetu
134 Haunui Valley
ROTORUA
115 McDowall Road
1E Puriri Road
Tokoroa
135 Haunui Valley
Kapenga Caldera margin
74A Hanna Road
4 Tikorangi Road
Kapenga
98 Barron Road
151c Waituna Road
Kinleith Mill
3A Tikorangi Road
48 Chamois Road
153b Cormorant Road
0 5 10 km
-4 -2 0 2 4 phi

somewhat higher pumice content than the normal Pokai Ignimbrite.

To examine the ignimbrite matrix material only grain-size fractions 16 mm and finer were used. After removal of the coarser material all the data was recalculated to 100 % and is here referred to as the ignimbrite matrix. The Pokai Ignimbrite matrix shows a linear decrease in Mdø outwards from both the Rotorua and Kapenga centres (Fig.2.21.a). No trend is seen in the Mdø plotted against the Maroa Volcanic Centre and the correlation to the Matahana Basin is also poor (Fig.2.21.a). Matrices from the PCZ have a somewhat greater Mdø than normal ignimbrite at the same distance from the possible source areas. The exceptionally high Mdø in the Leslie Road sample is probably due to the high overall pumice content in the northwestern flow units.

In layer 2 deposits, the content of fine material is bound to show a general increase from near source to distal outcrops (Walker & Wilson, 1983). Weight percentages for the ½ mm and finer fractions in the ignimbrite matrix plotted against distance from Rotorua, Kapenga, Maroa and Matahana Basin are shown in Figure 2.21.b. The weight percentages of fine material (≤½ mm) in the ignimbrite matrix varies from about 40 wt% up to 90 wt%, the lowest values are in the Haunui Valley samples and the highest one in the Waituna Road sample, from southeast of Kinleith Mill. The PCZ samples and the pumice-rich Leslie Road sample again differ from the normal ignimbrite data.

The overall lithic content in the ignimbrite matrix decreases more or less systematically with distance from both the Rotorua and Kapenga centres (Fig.2.21.c), the Kapenga Volcanic

Figure 2.21. (a) Mdo, (b) weight percentages (wt.%) of the fractions ½ mm (1 phi) and finer, and (c) weight percentages (wt.%) of lithics for the fraction ½ mm (1 phi) and coarser, in the Pokai Ignimbrite matrix (<16 mm) plotted against distance from the Rotorua, Kapenga and Maroa Volcanic Centres and from Matahana Basin. Open □/Δ = data from the PCZ; closed □/♦ = data from crystal- and pumice-rich Leslie Road sample. Dashed lines mark the approximate present day caldera margins for each volcanic centre.

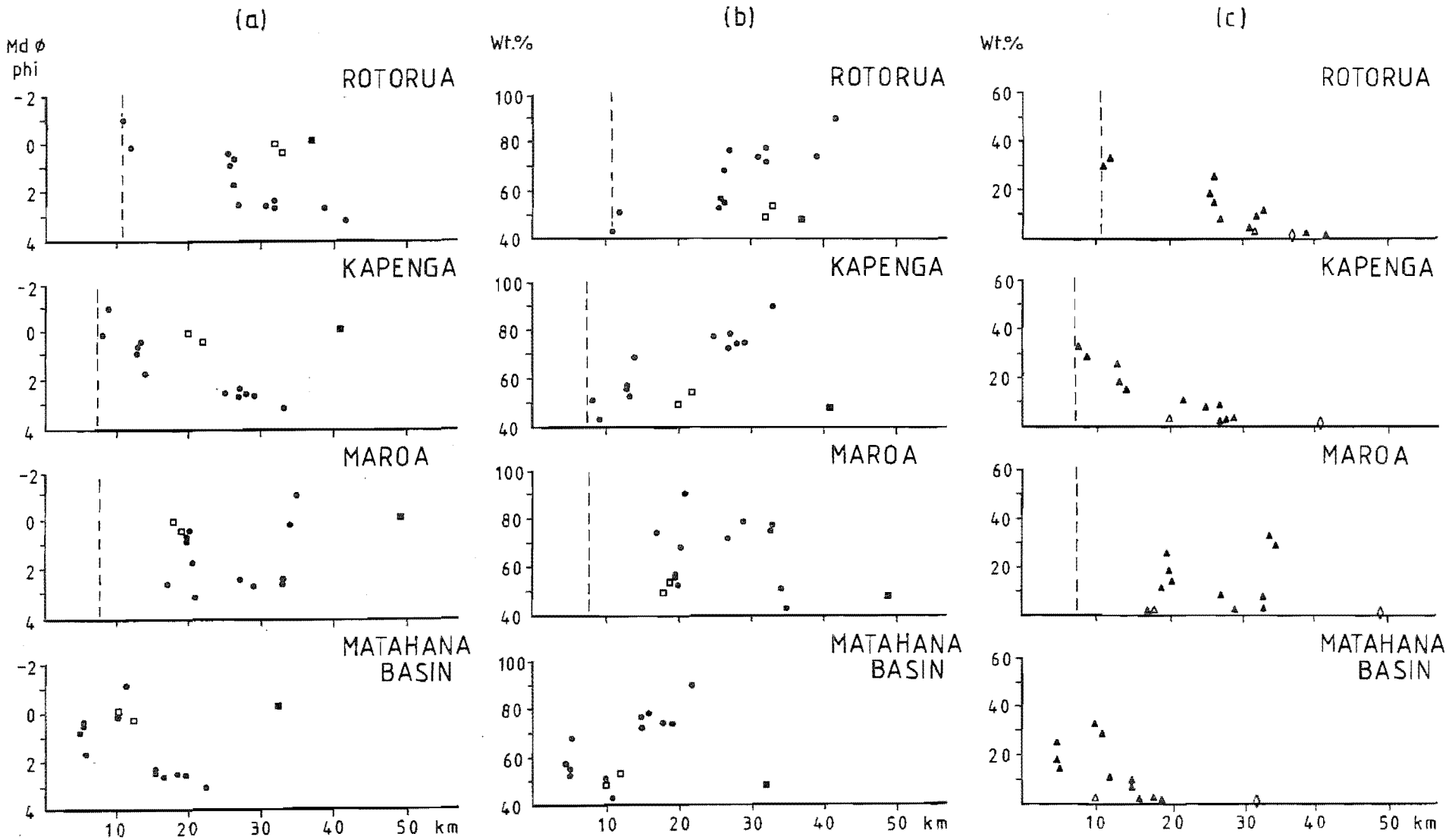
(a)
(b)
(c)
Md ø
phi
Wt.%
Wt.%
ROTORUA
KAPENGA
MAROA
MATAHANA
BASIN
-2
0
2
4
100
80
60
40
60
40
20
10
20
30
40
50 km

Centre showing a slightly better linear correlation. No clear correlations with the Maroa Volcanic Centre and Matahana Basin are evident (Fig.2.21.c).

The upward enrichment in both pumice size and concentration ranges from vaguely defined increase in MP sizes to a relatively sharply defined pumice-concentration zone (PCZ). Most of the sections show a slight or moderately developed coarse-tail grading - flow type 2 of Wilson (1980) - indicating that the flows were expanded, but not highly fluidised. At a number of measured vertical sections (22-40 m thick) two zones with moderately developed coarse-tail grading often occur; the lower zone 8-10 m above the base and the upper one on the top of the flow. This strongly indicates that the Pokai Ignimbrite is a multiple flow unit.

The best developed coarse-tail grading - flow type 3 of Wilson (1980) - is found on the hill sides of a relatively narrow, east-west valley 2 km east from Highway 1 on the western side of the study area (Ngutuwera Stream valley, see Fig.1.3). Te Rere Road section (GR 609363; field no. 144) on the northern side of the valley is composed of two sharply defined pumice concentration zones (PCZ), each resting on fine-grained layers of 2b (Figs.2.22 and 2.23). The PCZ's contain the coarsest pumices in the ignimbrite (MP=34); the largest individual pumice found has a diameter of 43 cm. The PCZ's are usually just matrix-supported, but in some cases the coarsest blocks are in contact (Fig.2.24). Lithics are rare and no segregation bodies were found.

Coarse-tail grading in pyroclastic flows generally originate by gravitational, or buoyant, rise of low-density pumice through the flow, or by shear (Sparks, 1976; Wilson & Walker,

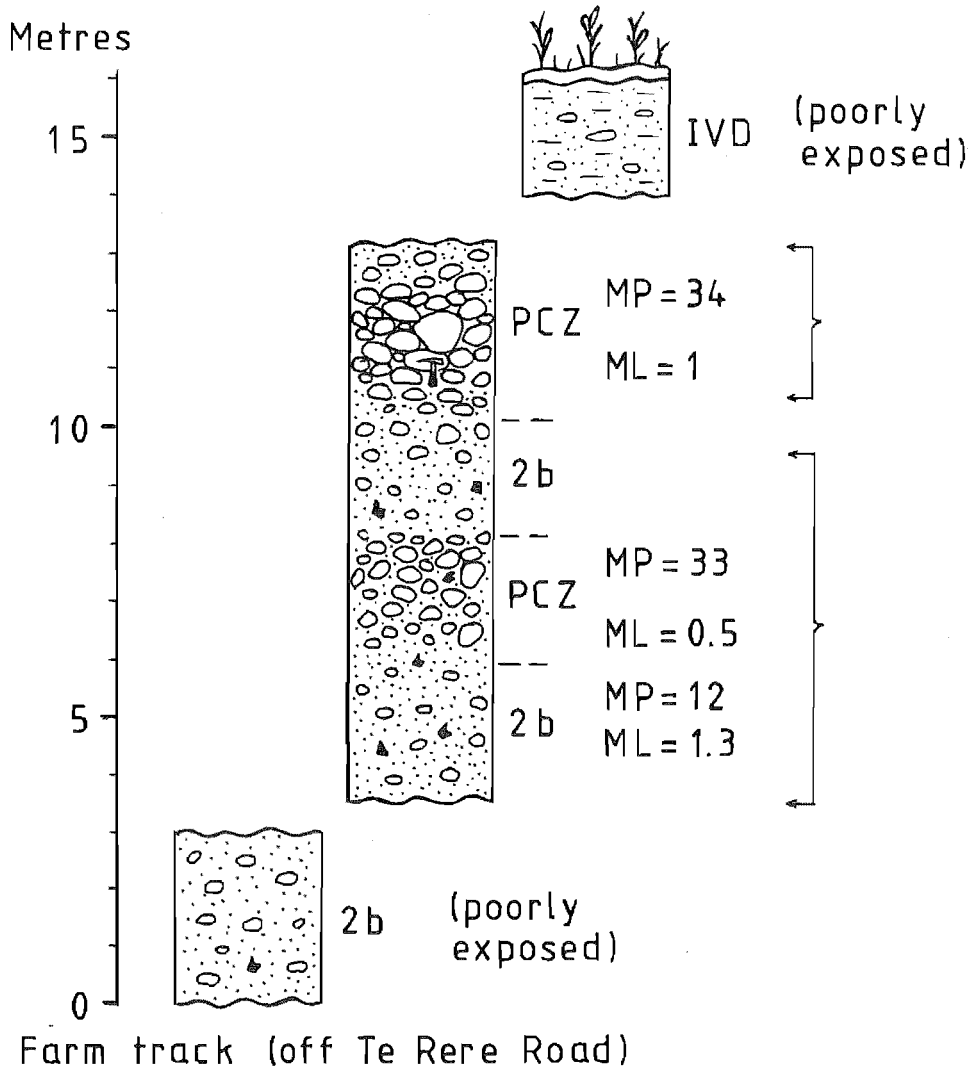

Figure 2.22. Schematic section showing the outcrop nature at Te Rere Road, exposed diagonally along a hill side (GR 650440; field no. 143 & 144; see also Figs.2.23 and 2.24).

Figure 2.23. Te Rere Road section (GR 609363) with the lower PCZ, also shown schematically in Fig.2.22.

Figure 2.24. Te Rere Road section (GR 609363) with the upper PCZ, also shown schematically in Fig.2.22.

1982; Cas & Wright, 1987). Sharply defined PCZ, produced by the buoyant rise of pumice in greatly expanded, highly fluidised flows normally contain numerous segregation bodies due to the entrapped air in the fast moving flow (Wilson, 1985). There are no segregation bodies in the Pokai PCZ's. Most of the Pokai ignimbrite flows were only moderately expanded, relatively slow moving flows with low internal gas flow rates.

The clast-supported PCZ's probably represent local disturbances in the flow pattern. By the time of the Pokai ignimbrite eruption there may well have been a corresponding paleovalley in the place of the present day Ngutuwera Stream valley, since the same drainage system tends to persist throughout the history of a volcanic centre (Sparks, 1975). On entering a narrow, deep valley the sides of the flows would be affected by strong shear. The upper parts of the moving flow already carried a layer of larger pumices and due to an additional strong shear the upper parts were further enriched in coarse pumice and depleted in fine material.

Segregation bodies have been found locally near the base of layer 2b deposits. Gas segregation pipes vary in size from 1 cm up to 25-30 cm in diameter (Fig.2.25); segregation pods, ranging usually from 5-25 cm, occur more rarely. Segregation pipes and pods can be produced internally when gas is released from juvenile clasts, or externally, which include gas trapped during initial flow, i.e. air trapped beneath the flow front, gas released from combusting vegetation and steam from heated surface water (Walker, 1972; Wilson, 1980). Gas segregation bodies found near the base of the flow units are interpreted to have come from external sources rather than from intraflow

Figure 2.25. Segregation pipes in the Pokai Ignimbrite at Harry Johnson Road (GR 810193).

gas sources.

A high concentration of segregation pipes and pods is present in the lower flow units south of Matahana Basin. Here the total thickness of the ignimbrite is over 80 m. As the deposits lie between steep hills composed of older rocks, it is suggested that the ignimbrite flows cascaded over steepcliffs into deep paleovalleys trapping air beneath them. The bottom of the ancient valleys may also have been water-saturated at the time of emplacement and the pipes could represent local steam vents.

Pokai Ignimbrite also occurs as thin (0.3-3 m thick), landscape mantling ignimbrite veneer deposit (IVD). These have been found locally in the area south and southwest of Te Whetu and occasionally in some other parts in the study area. The veneer deposits show crude layering, are lithic-rich and often lack coarse pumice. Maps showing the MP and ML data for the IVD are given in Figure 2.26, and their relationships plotted against distance from Rotorua, Kapenga, Maroa and Matahana Basin are shown in Figure 2.27. Layering together with imbricated pumice fragments define a measurable flow lineation (Fig.2.28). The lineation tend to follow the topography and hence do not necessarily give an absolute movement direction.

If both VPI and IVD are present, the veneer deposits are always sitting on top of the conventional flow units. This location together with crude layering and the relatively high lithic concentration indicates that the veneer deposit represents the trailing parts of an ignimbrite flow.

Ignimbrites with little or no veneer deposits are interpreted to have been emplaced fairly gently so that the flow merely

Figure 2.26. Isopleth maps of MP and ML in the Pokai IVD. Both the isopleth and location values are in cm. The circular cross-hatch lines mark the volcanic centres of Rotorua (E) and Kapenga (SE), respectively.

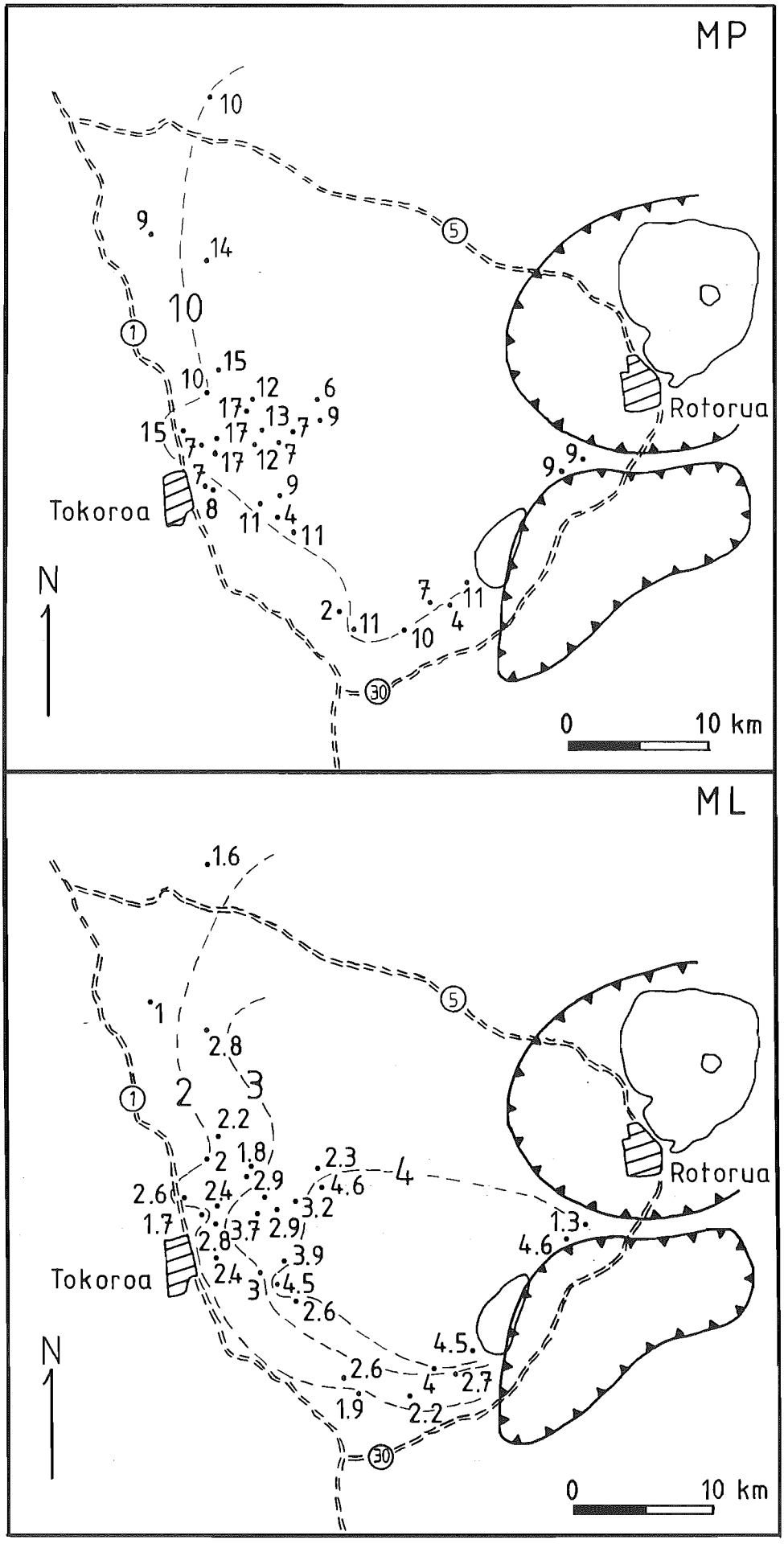
MP
Rotorua
Tokoroa
N
0
10 km
ML
Rotorua
Tokoroa
N
0
10 km

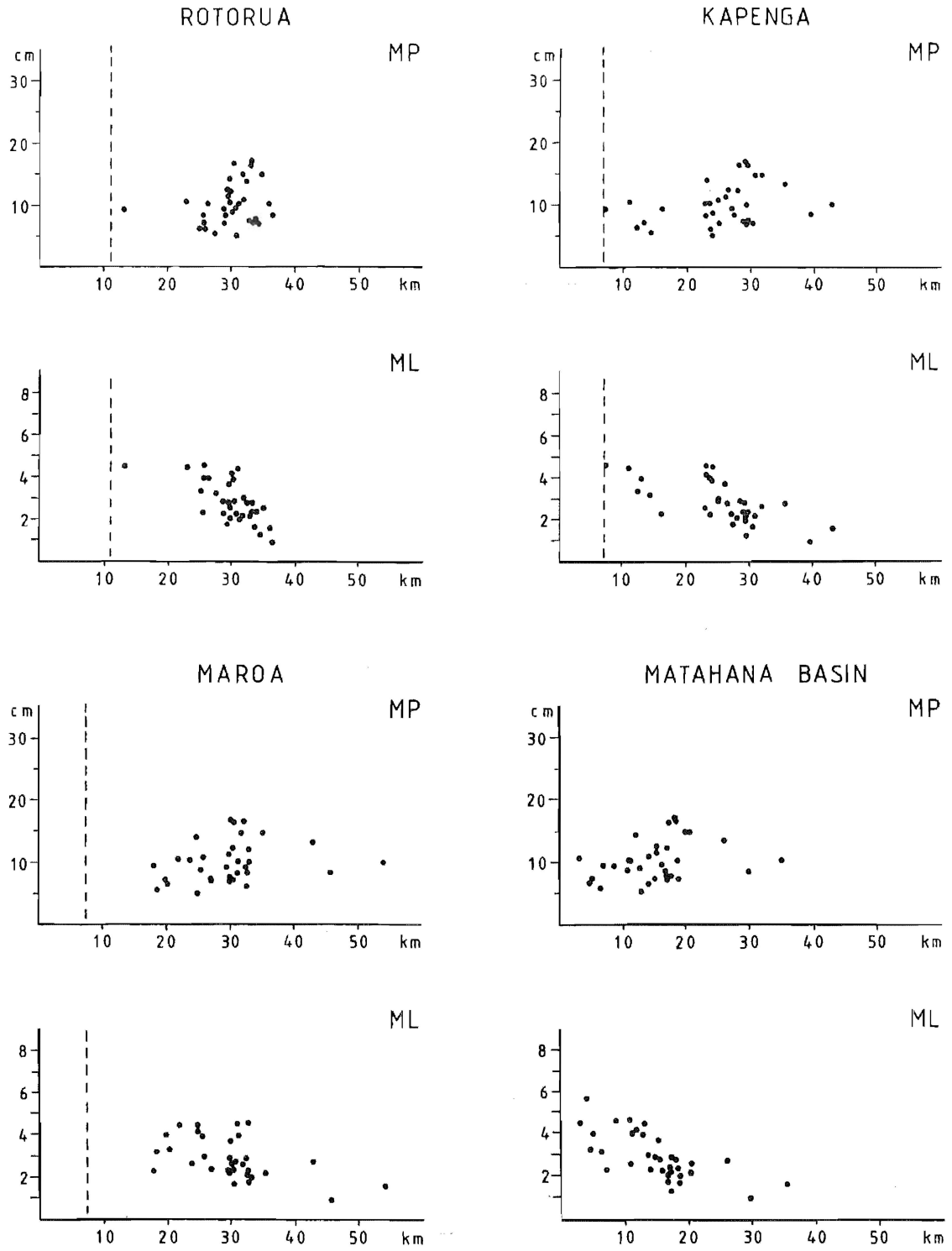

Figure 2.27. MP and ML in the Pokai IVD plotted against distance from the Rotorua, Kapenga and Maroa Volcanic Centres and from Matahana Basin. Dashed lines mark the approximate present day caldera margins for each volcanic centre.

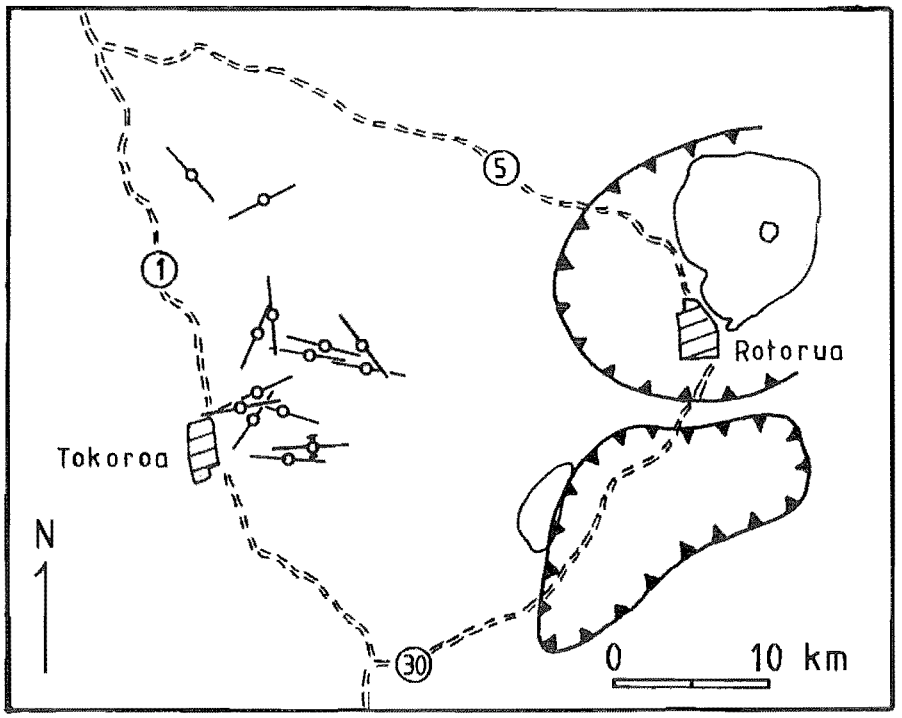

Figure 2.28. Flow lineation -o- and imbrication of pumice -Φ- in the Pokai IVD. The circular cross-hatch lines mark the volcanic centres of Rotorua (E) and Kapenga (SE), respectively.

lapped up against the topography rather than surmounting it (Wilson, 1986). Violently emplaced, low-aspect ratio ignimbrites have much higher proportion of veneer deposits included in layer 2 (Taupo ignimbrite includes 40% veneer and 60% valley ponds; Wilson, 1986). The scarcity of veneer deposits in Pokai ignimbrite suggests the ignimbrite was emplaced gently (i.e. as a high aspect ratio deposits), although it is possible that some of the IVD have been eroded.

Low aspect ratio ignimbrites, emplaced at very high velocities, like the Taupo Ignimbrite, often have highly expanded flow heads and build up well developed head deposits. The lack of coarse-grained head deposits in Pokai ignimbrite is additional support for the interpretation of emplacement from a relatively slow moving, moderately fluidised flow.

2.5. Proximal ? deposits

Ignimbrites are commonly thickest and have the largest number of flow units close to their source. However, thickness alone is not a reliable indication of vent location, because it is partly dependant on the local topography. Few ignimbrites with a thickness <1 m have been documented, but a succession of thin flows, often associated with surge deposits seem to be fairly common in near vent exposures (Wilson & Walker, 1982; Fisher et al., 1983).

Throughout most of its extent in the study area the Pokai Ignimbrite seems to be made up of two to three flow units ranging from 6-30 m. A succession of different types of pyroclastic flow facies is found in an area south and southwest of Matahana Basin, along Chamois Road and at Bob

Road (GR 801188 and 747177; field nos. HJ & 48 and 112, respectively). The Chamois Road section (Fig.2.2) is of particular interest since it displays a several meters thick series of thin ignimbrite flow units interbedded with fine-grained stratified units and fine ash found in the middle of a 78 m thick ignimbrite section. The following description is partly based on unpublished mapping by M. Cook, and on grain-size analyses made by the author. A schematic section showing the stratigraphy at the Chamois Road section with associated grain-size histograms is given in Figure 2.29.

At the lower part of the Chamois Road locality there is a >4 m thick, non-welded, pink ignimbrite flow unit with medium to coarse, reversely graded, creamy white to pink lapilli pumice and blocks (MP=9.7 and 20, at the base and top, respectively). Lithic clasts are abundant and the largest clasts are found in the numerous segregation pipes and pods at the base of the section. This flow unit is overlain by a ca. 0.5 m thick, fine-grained stratified deposit, which may represent a series of thin flow or surge units. Above this are two thick (11 and 20 m, respectively) ignimbrite flow units (Figs.2.2. and 2.29), both showing coarse-tail grading. The lower flow unit has a marked fine-grained base (MP=2.1, ML=0.4); the grain-sizes indicating that it is a layer 2a deposit.

The flow units are overlain by a 1.2 m, relatively fine-grained, pumice-poor and lithic-rich unit (HJ11h), above which is 2½ m of thin, stratified, low-angle cross-bedded units (17-50 cm thick) intercalated with three fine-grained, accretionary lapilli-rich ash beds (HJ11a-g). Two thin, reversely graded pyroclastic flow units (0.7 and 1 m) overlie the stratified deposits. The upper part of the section is

Figure 2.29. Stratigraphy of the Pokai Ignimbrite at Chamois Road (GR 801188; field nos. HJ & 48) with grain size histograms of representative flow/surge unit matrices (≤16 mm). The bars for ½ mm (1 phi) and coarser classes are subdivided to show the proportions of components.

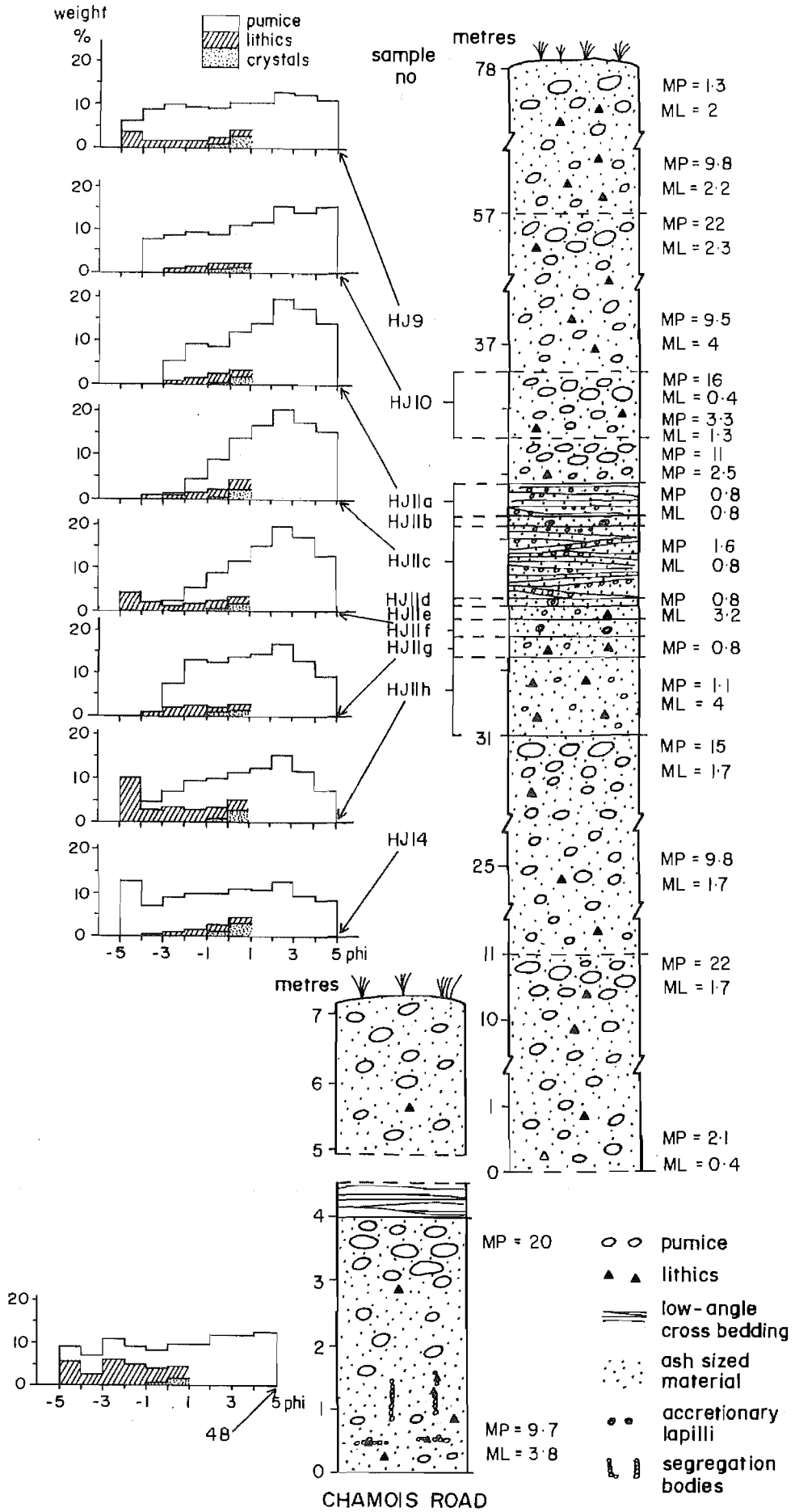
weight %
pumice
lithics
crystals
sample no
metres
HJ9
HJ10
HJ11a
HJ11b
HJ11c
HJ11d
HJ11e
HJ11f
HJ11g
HJ11h
HJ14
-5 -3 -1 1 3 5 phi
MP = 1·3
ML = 2
MP = 9·8
ML = 2·2
MP = 22
ML = 2·3
MP = 9·5
ML = 4
MP = 16
ML = 0·4
MP = 3·3
ML = 1·3
MP = 11
MP = 2·5
MP 0·8
ML 0·8
MP 1·6
ML 0·8
MP 0·8
ML 3·2
MP = 0·8
MP = 1·1
ML = 4
MP = 15
ML = 1·7
MP = 9·8
ML = 1·7
MP = 22
ML = 1·7
MP = 2·1
ML = 0·4
78
57
37
31
25
11
10
1
0
7
6
5
4
3
2
1
0
MP = 20
MP = 9·7
ML = 3·8
48
pumice
lithics
low-angle cross bedding
ash sized material
accretionary lapilli
segregation bodies
CHAMOIS ROAD

Figure 2.30. (A) Mdø/δø plot and (B) grain size characteristics of weight percentage $<_{1/16}$ mm vs weight percentage <1 mm, for the Pokai Ignimbrite. Solid lines labelled 1 and 4 are contours for the field of pyroclastic flow deposits and within these 99 and 96 %, respectively, of sieve analyses of flow deposits occur; broken lines are similar contours for the pyroclastic surge analyses (after Walker, 1983).

● = Pokai Ignimbrite flow units; * = Pokai Ignimbrite flow units at the Chamois Road section (Fig.2.29 nos. HJ9, HJ10, HJ14 and 48); x = intra-ignimbrite surge/thin flow units at the Chamois Road section (the small letters a, c, e, g and h refer to the sample numbers HJ11 -a, -c, -e, -g and -h in Fig.2.29, respectively).

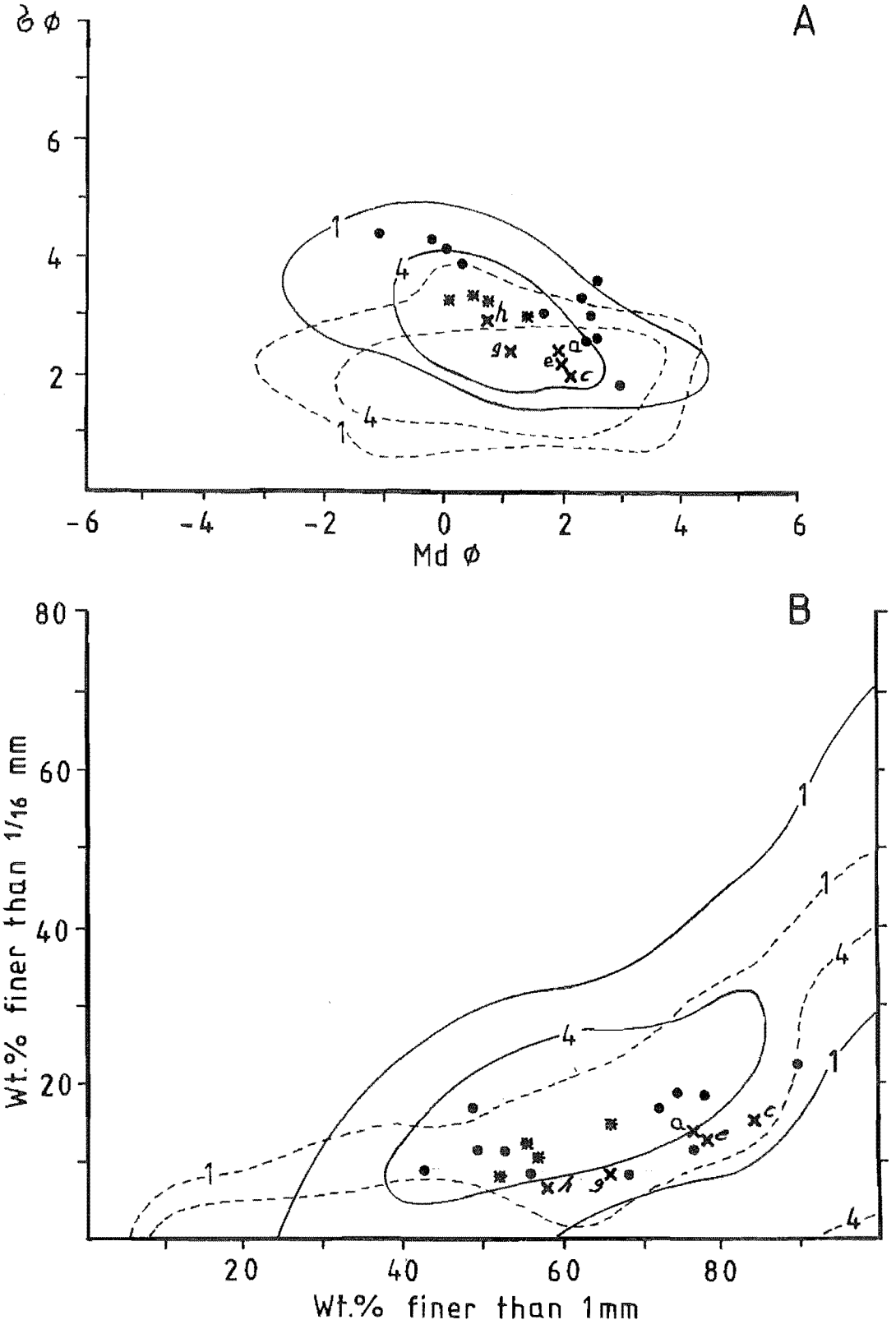
A
σ φ
6
4
2
-6
-4
-2
0
2
4
6
Md φ
1
4
h
g
a
e
c
B
80
60
40
20
Wt.% finer than 1/16 mm
20
40
60
80
Wt.% finer than 1mm

composed of two thick ignimbrite flow units (26 and 20 m, respectively).

Grain-size characteristics of the stratified units and of selected flow units are shown in the histograms in Figure 2.29 and in Figure 2.30 as Mdø/δø and weight % <1 mm/weight % <1/16 mm. The ignimbrite flow units (48, HJ9 and HJ14) show rather similar grain-size characteristics. The high lithic content in sample 48 is probably due to the abundance of segregation bodies and indicates proximity to the flow base. Unit HJ10 has a somewhat lower Mdø, but a marked PCZ on top, and most probably represents a thin ignimbrite flow unit.

Units HJ11a, HJ11c and HJ11e have sandy, relatively lithic-rich, pumiceous matrices (MP=1-2), a low-angle cross-stratified nature often with lensoid pumice concentration marking the top of an individual layer. On Mdø/δø diagram they differ from the ignimbrite flow units by having a smaller Mdø and a slight depletion of fine ash material (<1/16 mm). They are also better sorted (δø=2-2.4) than the ignimbrite flow units (δø=3-3.3). Weight percentages of lithics and crystals in units HJ11a, c and e (Fig.2.31) do not differ markedly from those in the flow units (except 48), however, units HJ11a, c and e have a high percentage of less vesicular, high density pumice. All the characteristics of units HJ11a, c, and e suggest their origin as pyroclastic surges.

Units HJ11g and HJ11h have grain-size characteristics between the ignimbrite flows and surge deposits with Mdø=0.8-1.2 and δø=2.3-3. Unit HJ11h, with a high lithic content (24 wt.% and ML=4) may represent an IVD, a trailing part of the underlying flow unit (HJ14). An origin as a surge deposit cannot be

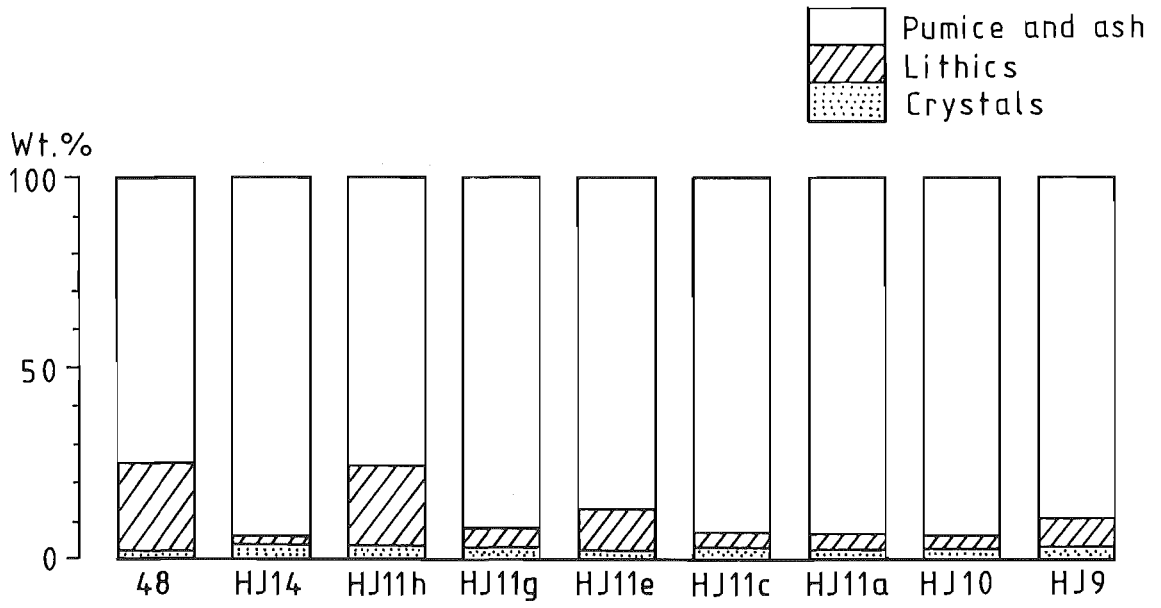

Figure 2.31. Weight percentages of lithics and crystals from representative Pokai Ignimbrite samples for the fractions ½ mm (1 phi) and coarser. The sample numbers refer to the Chamois Road section shown in Fig.2.29. Only matrix material (≤16 mm fractions) was used.

excluded, as surges, though usually fine-grained, may include coarse fragments due to the turbulent nature of their flow (Cas & Wright, 1987). The grain-size of surge deposits may also vary due to fragmentation at the time of eruption. Unit HJ11g may represent either a thin ignimbrite flow unit or a surge deposit.

Stratified deposits are often found associated with pyroclastic flow deposits. Ground surges usually occur at the base of pyroclastic flow units and are interpreted as precursors to pyroclastic flows, preceding their flow fronts (Wright et al., 1980; Wilson, 1980, 1984). Generated out of the head of a moving pyroclastic flow the ground surges may extend almost as far as the flow unit itself. Base surges commonly develop from phreatomagmatic blasts in the vent and will often be wet. Being a vent related facies, they will rapidly thin out and are usually not found further than about 10 km from the vent (Cas & Wright, 1987). Base surge deposits are nearly always composed of multiple layers, as seem to be the case at the Chamois Road section, thus representing multiple surge events.

In wet surges fine ash and water droplets readily begin to adhere to each other, producing clumps. As a result surges do segregate into a lower concentrated layer and a more diluted suspension cloud (Cas & Wright, 1987). Some deposits may thus contain a separate, lower surge unit and an associated upper, accretionary lapilli-rich 'co-surge' ash-fall deposit. Units HJ11b, d and f (Fig.2.29), composed of fine ash with accretionary lapilli have been interpreted to represent 'co-surge' ash-falls associated with the underlying surge deposits. Unit HJ11g (Fig.2.30), with characteristics between

a flow and a surge deposit, would thus represent a surge deposit.

The thickness of the individual surge beds (usually <50 cm) and the alternation of the deposits with interbedded accretionary lapilli-rich ash beds indicate their origin as a series of base surges. The occurrence of base surges and the abundance of ignimbrite flow units (at least seven, compared to 2-3 further west) are indicative of proximity to the vent.

At Bob Road, ca. 5 km southwest from the Chamois Road locality, a similar kind of succession is present (Fig.2.32), though it seems to be much thinner. At Bob Road there is a lower (>10 m thick) ignimbrite flow unit overlain by a ca. 0.5 m thick stratified deposit. Above the stratified unit there is about 0.5 m thick fine-grained, accretionary lapilli-rich ash bed. This sequence may represent base surge deposit(s) with an associated 'co-surge' ash-fall. The sequence is directly overlain by a 10-12 m thick ignimbrite flow unit, with a 0.5 m thick fine-grained basal layer, layer 2a (MP=1.9, ML=1.6), and a reversely graded layer 2b (MP=16.7, ML=2.6). The stratified sequence (1-1.2 m thick) in the middle of the thick flow units may be equivalent to the 2.5 m thick surge- and thin flow unit-sequence found at Chamois Road. Many of the thinner units at Chamois Road would probably not have reached the Bob Road area explaining the difference in total thickness.

No stratified units or intra-ignimbrite air-fall deposits have been found further southwest, west or northwest. At Pokai Road, the ignimbrite is composed of an initial air-fall deposit and of at least two flow units. The lowermost flow unit is about 11 m thick and has a clear PCZ on the top

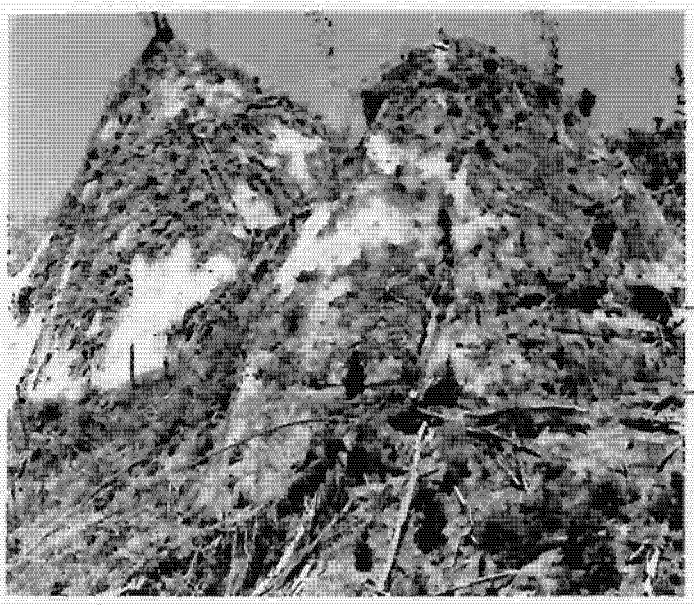

Figure 2.32. Bob Road section (GR 747177, field no. 112) with a stratified succession between two ignimbrite flow units.

(MP=22). The upper flow unit has a relatively pumice-poor (MP=7.8) and lithic-rich (ML=3.9) base. The abundance of lithics is possibly due to vent wall collapse during the eruption. The break between the first and second flow units may be equivalent to the major break in the eruption, seen as the series of surge units at Chamois Road.

2.6. Layer 3 deposits

Co-ignimbrite ash-fall deposits occur only in a few outcrops. In most places the co-ignimbrite ash has probably been rapidly removed or buried by younger deposits. Where present, the layer 3 deposit is 20-40 cm thick, pale brown and composed of fine, vitric ash. The upper contact is usually gradational and the ash is mixed with overlying pyroclastics or reworked material, or it grades to a younger soil formation.

Near Waituna Road, 4 km southwest of Kinleith (GR 598182; field no. 151) a 10 cm thick, creamy-white, fine ash layer occurs between a pre-ignimbrite pumice-fall (presumably unit A) and a thin Pokai ignimbrite flow unit (Fig.2.33). This fine, vitric ash may represent a co-ignimbrite ash-fall associated with some of the early flow units.

2.7. Lithic breccia deposit

In Haunui Valley, 1.2 km southwest from the Rotorua caldera margin (GR 885305, field no. 131), there is a small, isolated Pokai ignimbrite outcrop of special interest. The exposed section (Fig.2.34) is about 4 m high and about 3 m wide; no

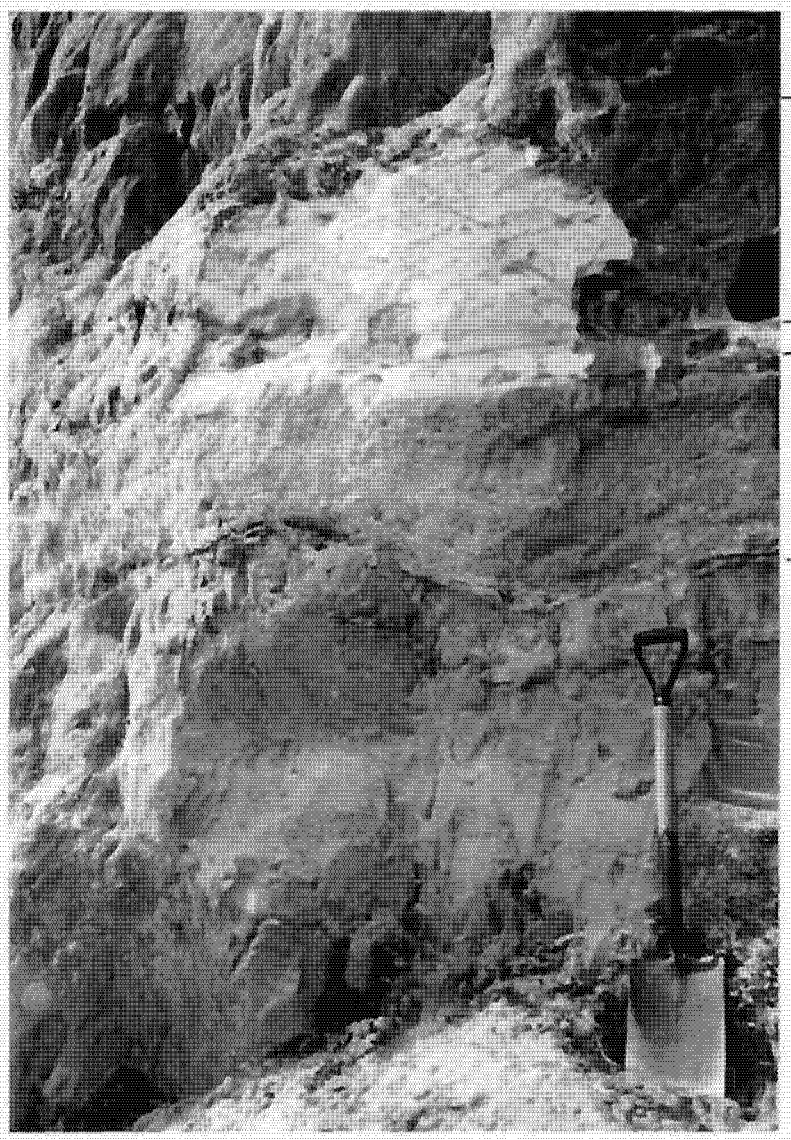

Figure 2.33. Waituna Road section (GR 598182, field 151). Pokai air-fall unit A, a thin, fine ash bed and an ignimbrite flow unit, ca 1.2 m thick, exposed above 1.5 m thick paleosol and Whakamaru Ignimbrite.

Figure 2.34. Pokai Ignimbrite lithic breccia exposed in Haunui Valley (GR 885305). Note the ignimbrite lithics (harder, more resistant to weathering) 'sticking out' from the vertical outcrop.

other outcrops occur in the nearby area.[4].

The unit has a brown, case-hardened matrix of coarse ash, is relatively rich in orange-yellow, fine to coarse pumice lapilli (MP=7.5) and has a high abundance of coarse lithics; between 8-10 vol.%. Some of the lithic clasts are of the same type that has been found throughout the Pokai ignimbrite, i.e. mostly rhyolite (ML=4). The dominant lithics are, however, angular and sub-angular, fragments of an unknown, lithic-rich ignimbrite. These clasts are very uniform in size and noticeably larger (ML=10) than any of the pumice clasts in this unit. The ignimbrite clasts have a moderate vesicularity but are case-hardened and relatively dense. They also show higher resistivity to weathering and thus 'stick out' from the vertical outcrop (Fig.2.34).

These ignimbrite 'lithics' have similar characteristics to the Pokai Ignimbrite, they have orange-brown, lithic-rich matrix with abundant medium-sized, fibrous, orange pumice, some with abundant black, glassy fiammes. It seems likely that these lithic clasts represent blocks of welded Pokai Ignimbrite deposited at an early stage around the vent and during a vent wall, or possibly a caldera collapse were then mixed with the erupting magma.

The deposit is non-stratified, poorly sorted and the coarse ignimbrite lithics lack any impact structures, suggesting that some lateral transport of the material may have been taken place. It is a lithic breccia and is interpreted to be part of a pyroclastic flow as it shows characteristics of flow unit rather than of air-fall unit. It is suggested that the Pokai

[4] The pumice chemistry has confirmed that this deposit represents the Pokai Ignimbrite (see Appendix D, Table D.3., samples 131C1 and 131C2, ref.nos. 174 and 175).

lithic breccia originated by segregation of the heavy ignimbrite lithics through a fluidised pyroclastic flow, probably near the site where eruption column collapse occurred.

Such co-ignimbrite lithic breccias are indicators of proximity to the source (Wright et al., 1979; Wright & Walker, 1981; Druitt & Sparks, 1982) and are commonly found on the edges of calderas. Walker (1985) has recently summarised these deposits, suggesting that they occur within the "deflation zone", at sites near the collapsing eruption column and is inferred to vary from 0.5 km to as much as 20 km at sites of eruptive column collapse. The "co-ignimbrite lag breccias" (Walker, 1985) are usually characterised by their coarseness, fines depletion, and the presence of internal stratification.

The lithic breccia could be considered as a thick equivalent of layer 2b lithic concentration zone, sometimes seen in the distal parts of the Pokai Ignimbrite. A relatively small size of the lithics compared to other known lithic breccias (clasts >1 m in size), the lack of internal stratification and the presence of fine-grained matrix may be explained by the fact that only the upper part of a much thicker breccia is exposed. The small size of lithics could also mean that the deposit is situated at some distance from the vent.

2.8. Eruption sequence

The stratigraphy of the recorded basal units, together with field characteristics and the grain-size distributions of the pyroclastic deposits enables a model of the early eruption sequence to be put forward. The event began with eruption and

deposition of coarse (phreato)plinian ash. The finer grain-size at the base could imply that some water had access to the vesiculating magma early in the eruption, but as the eruption continued less water reached the magma. The assemblage of grain-sizes ejected from the vent(s) quickly coarsened as the pyroclastic fall deposition continued, producing the reversely graded, lithic-rich lapilli pumice-fall, unit A. The lithic-rich bands at the Glass Road section indicate fluctuations during the course of eruption, possibly due to vent wall collapses following explosive re-opening of the vent.

After a period of plinian activity, the eruption column or columns collapsed and pyroclastic flows swept out from the source. Probably the area now occupying the central Kinleith Forests was covered by the early flow units and their most distal parts are seen as the thin intraplinian flow units I and II exposed at Galaxy Road.

There are two possibilities how the eruption continued. Water may have had access to the erupting magma so that a period of phreatoplinian activity occurred producing a fine-grained ash deposit, or perhaps the activity temporarily ceased, caused for instance by collapse of the vent wall(s) which blocked the conduit. During such a break, fine ash may be deposited from the previous column as it breaks down, forming a fine ash-fall unit. If a break in activity was due to collapse of the vent wall(s), the next fall unit would at first be rich in accidental lithics, as the lithics that blocked the conduit reamed out (Cas & Wright, 1987). However, no increase in lithic abundance occurs in the following air-fall units.

The abundance of accretionary lapilli and the very fine grain-

size of the ashy beds indicate that they originate from a wet, fine-grained eruption column and were deposited mainly as mud rains and aggregates (ash-fall B). The source of most of the water is assumed to have been steam-generated at the vent by the interaction of magma and sub-surface and/or surface water (from a ground-water reservoir or from a pre-eruption lake and/or river system). Possibly the deposition was further influenced by local rains, contributing to the uneven distribution of the ash-fall beds.

The eruption then went into a plinian phase and a thin deposit of lapilli accumulated (air-fall unit C). Deposition of units D-H mark a period involving relatively rapid alternations in the eruptive style, reflecting fluctuations in the amount of water entering the vent. Most probably, water from a nearby lake or river from time to time penetrated into the vent, and fragmentation of the magma took place together with evaporation of the water causing phreatoplinian outbursts of wet, fine-grained ejecta. While the vent was cleared of water the nature of the eruption changed abruptly to a 'dry' phase and less fragmented, coarser-grained material was ejected.

Another possibility is a dual-source origin for the interbedded pumice and fine ash. While phreatomagmatic activity was proceeding from one part of the fissure, the coarser pumice may have erupted from another part of the fissure. The decrease in abundance of accretionary lapilli upwards in units D-H stratigraphy suggests that at the beginning of each successive phreatoplinian eruption progressively less water reached the vent; either the pre-eruption lake drained out and/or the drainage system in the area changed as the volcanic activity continued.

It is very likely that simultaneous collapse of some part of the plinian column(s) took place and a new group (batch) of early flow units were emplaced. The distal flow units IIIa and IIIb exposed at Galaxy Road may represent the distal part of these flows. Thin, distal flow units underlying the ignimbrite flow proper have also been recorded in Leslie and Tram Roads.

The air-fall deposits, and the intra-plinian flow units, are overlain by the main ignimbrite flow units with no evidence for any significant time interval between their formation. A widespread eruption column collapse producing the thick, main flow units could have been due either to a vent widening beyond a certain critical radius to be able to maintain the eruption column (Self et al., 1986), or alternatively a decrease in magmatic gas content (Sparks et al., 1978).

Interbedded with the main flow units several ground surge deposits occur in the area south of Matahana Basin, probably generated by phreatomagmatic blasts in the vent. This suggests that small amounts of ground water may have had access to the vent in the early stages of the large scale column collapse event.

Topography largely controlled the thickness of the main flow units, thus also contributing the generation of the VPI and IVD. It is likely, that some major structural changes with a caldera collapse took place during the later phases of the eruption. A transition to multiple vent phase (possibly ring fracture) may have taken place as the roof zone of the magma chamber foundered.

3. CHIMP IGNIMBRITE

3.1. Field relationships

The Chimp Ignimbrite is exposed on the southwestern and western margin of Mamaku Plateau, east of Tokoroa and Putaruru, respectively (Fig.3.1, Maps A and B), outcropping along the forestry roads. In the western Kinleith Forests the total thickness of the ignimbrite is up to 20 m, decreasing to a total thickness of only 1.5 m (Fig.3.1.a) in the southernmost exposures (4 km east-southeast from Kinleith), and to ca. 4-5 m in the northernmost exposures. One poorly exposed outcrop (>2 m thick) with features characteristic of Chimp Ignimbrite was found in Matahana Basin.[5].

The best outcrops are situated along Puriri Road (Road J, GR 665290; field nos. 8 & 76) and at Te Whetu (GR 688338; field no. 11), where the ignimbrite is overlain by the Pokai Ignimbrite. Near Putaruru the ignimbrite outcrops at lower elevations (at 120 m, in Leslie Road, GR 595484, field no 47) than towards the east and southeast where it is exposed at 230-350 m (Fig.3.1.b). Southeast of Te Whetu (GR 688231) and at Boundary Road (GR 703328) the ignimbrite is exposed at 400 and 440 m, respectively. Because ignimbrites have a tendency to flow into topographic depressions (Walker et al., 1980a), these elevations suggests that the source of the Chimp Ignimbrite might have been to the east or south rather than to the north of the outcrop areas.

[5] Due to the relatively limited outcrop area as well as small outcrops the Chimp Ignimbrite will be described only briefly.

Figure 3.1.

(a) Distribution and approximate thicknesses (in metres) of the Chimp Ignimbrite. Thick dashed lines mark the recorded outcrop areas. ● = recorded minimum thickness; o = estimated minimum thickness. Stipples denote the areas where welded Chimp Ignimbrite occurs. The circular cross-hatch areas in NE, E, S and W mark the volcanic centres of Rotorua, Kapenga, Maroa and Mangakino, respectively.

(b) Elevations (in m.a.s.l.) of the Chimp Ignimbrite outcrops. Solid lines in the SE corner mark Quaternary faults (after Healy et al., 1964).

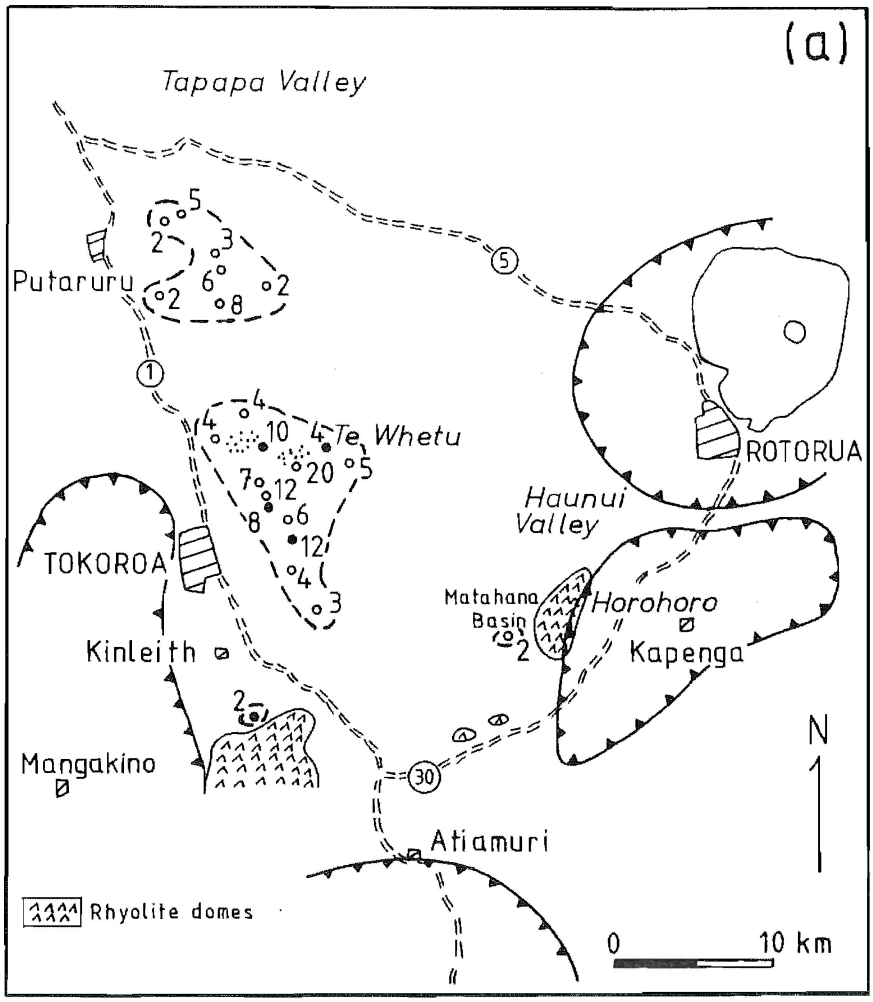
(a)
Tapapa Valley
Putaruru
Te Whetu
ROTORUA
Haunui Valley
TOKOROA
Matahana Basin
Horohoro
Kapenga
Kinleith
Mangakino
Atiamuri
Rhyolite domes
N
0
10 km

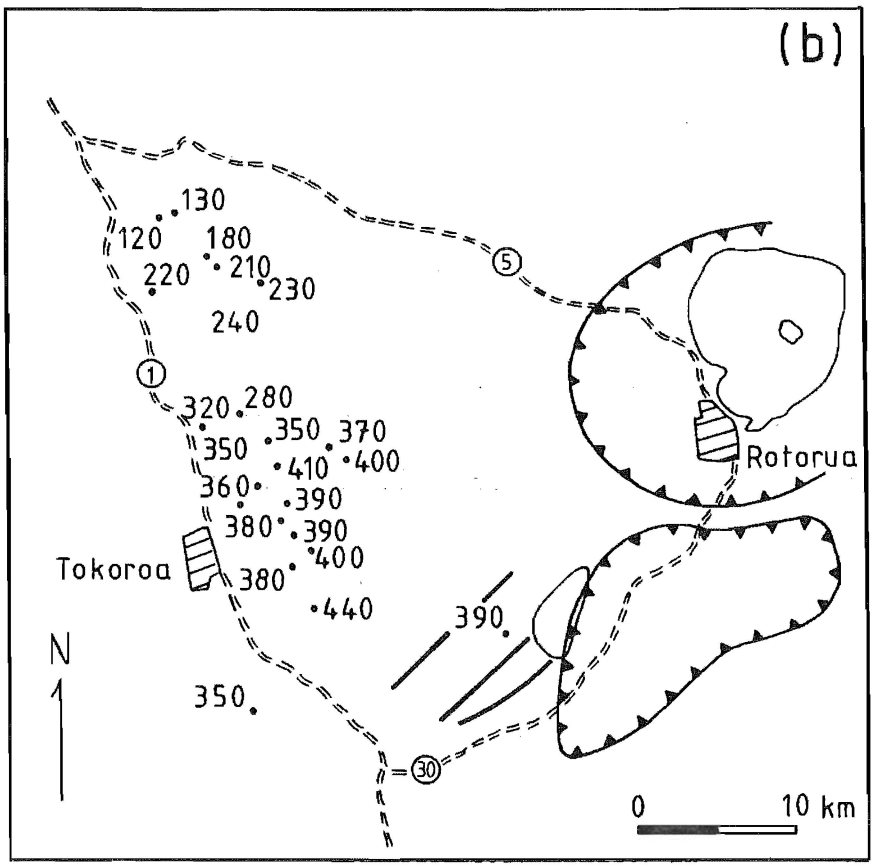
(b)
Rotorua
Tokoroa
N
0
10 km

At Road J the Chimp ignimbrite rests on eroded Whakamaru Ignimbrite separated only by 80 cm of reworked Whakamaru epiclastics and by a 40 cm thick paleosol (Fig.3.2). At Te Whetu and at Tunnel Road (GR 650440, field no. 140) it is separated from the Whakamaru Ignimbrite by >3 m of alternating thin units (5-30 cm) of air-fall tephra, their reworked derivatives and paleosols.

The Chimp Ignimbrite is a multiple-flow, simple cooling unit with relatively thin flow units, ranging from 2-10 m in thickness. It is relatively pumice- and crystal-poor, has a fine-grained, creamy-white to pale pink groundmass with two types of rhyolitic pumice (types A and B). Type A pumice is white or creamy white to pale pink, occasionally with orange bands, and has a delicate fibrous or wispy (silky) structure. The pumice is extremely crystal-poor (<1 vol.% phenocrysts).

Type B pumice is white to silver-grey, more vesicular than type A and has a higher crystal content (up to 8 vol.% phenocrysts). In most outcrops type A pumice is dominant. There are a few localities where type B pumice predominate; these are found in the northwestern study area (Leslie Road, GR 595484; field no. 47, and an area around Waihou River, GR = 594478). At two localities in the central study area (at Moorhouse Road, GR 637353, field no. 93, and at Panda Road, GR 673277, field no. 37) both type A and B pumice occur, approximately at equal proportions. Where type B pumice predominate the ignimbrite matrix is also more crystal-rich than the matrix hosting predominantly type A pumice.

Pumice clasts are usually rounded or sub-rounded and range from fine lapilli to blocks up to 20 cm in diameter. Lithic

Figure 3.2. The relationship between the Whakamaru Ignimbrite and the Chimp Ignimbrite at the Road J locality (GR 665290, field nos. 8 & 76). The Chimp Ignimbrite main flow unit is underlain by three thin pyroclastic flow units, 76s1-3, and a pre-ignimbrite air-fall pumice unit, 76a (see also sections 3.2 and 3.3). Note the large Whakamaru Ignimbrite block (Wh) on the left cutting the air-fall and the thin flow units.

content varies considerably in different localities and also in different parts of a flow unit. The lithic clasts are composed predominantly of angular to sub-rounded, flow-banded or porphyritic rhyolite, and fragments of Whakamaru Ignimbrite occur commonly; greywacke fragments are rare.

The ignimbrite is usually non-welded with a 'sandy' matrix. West and southwest of Te Whetu (Fig.3.1), where the ignimbrite is 10-20 m thick, moderately welded zones occur. The welded zones are composed of fine- to medium-grained (1-4 cm), dark purple or grey lapilli pumice in purple-grey or yellow-brown matrix. The welded ignimbrite seems to be more devitrified than the non-welded ignimbrite. The pumice clasts are slightly flattened with a mean flattening ratio of 4 (calculated by the method of Peterson, 1979). No flow boundaries are evident in the welded zones.

No co-ignimbrite ash deposits have been found. In the few places where the top of the ignimbrite is exposed it is unconformably overlain either by younger tephras or reworked pyroclastics.

3.2. Air-fall deposit

An initial pumice-fall deposit underlies the ignimbrite flow units at Road J, Te Whetu and Tunnel Road sections. The stratigraphy of the basal Chimp Ignimbrite is illustrated in Figure 3.3 with histograms showing the grain size and component analysis. Grain size characteristics are shown in Figure 3.6. The air-fall tephra fell on to a strongly weathered soil (20-40 cm thick), probably covered with abundant vegetation, and has a maximum thickness of 20 cm

Figure 3.3. The basal stratigraphy of the Chimp Ignimbrite with grain size histograms of the air-fall pumice and early flow units. The bars for the ½ mm and coarser classes are subdivided to show the proportion of components. The circular cross-hatch lines in the inset figure mark the volcanic centres of Rotorua (E) and Kapenga (SE), respectively.

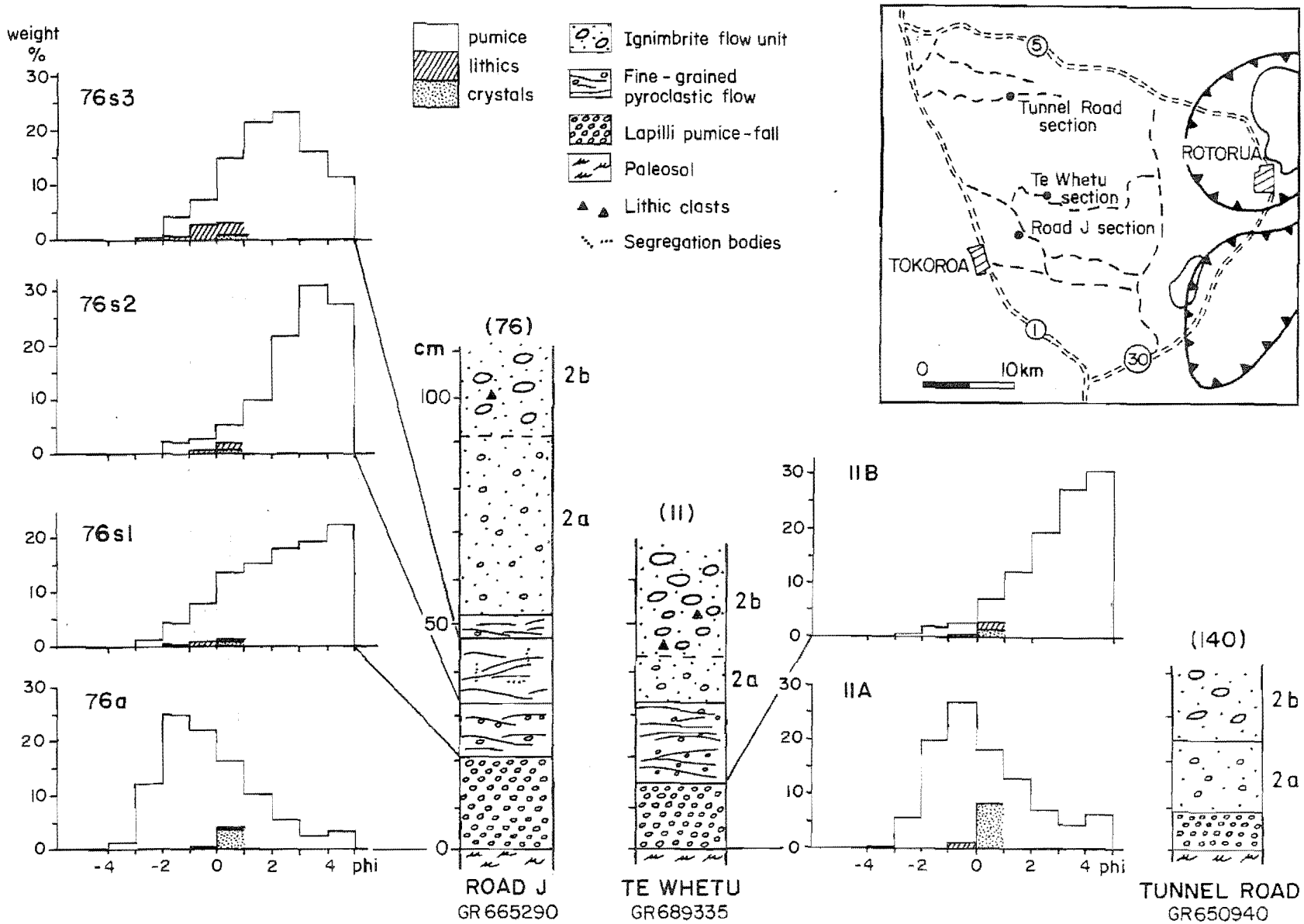
weight %
pumice
lithics
crystals
Ignimbrite flow unit
Fine-grained pyroclastic flow
Lapilli pumice-fall
Paleosol
Lithic clasts
Segregation bodies
76s3
76s2
76s1
76a
30
20
10
0
-4
-2
0
2
4
phi
(76)
cm
100
50
0
2b
2a
ROAD J
GR 665290
(11)
TE WHETU
GR689335
IIB
IIA
(140)
TUNNEL ROAD
GR650940
Tunnel Road section
Te Whetu section
Road J section
ROTORUA
TOKOROA
5
1
30
0
10km

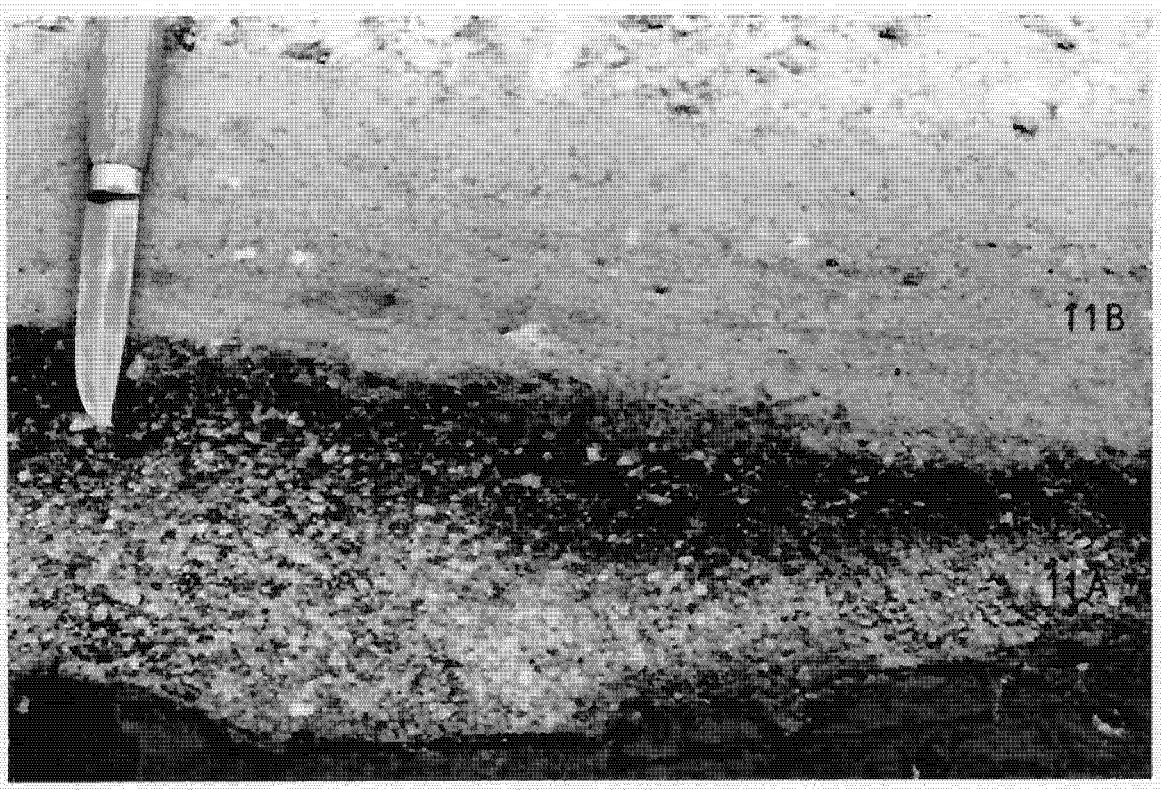

Figure 3.4 Chimp air-fall pumice at Te Whetu (GR 688338, field no. 11), overlain by a thin, low-angle cross-stratified flow unit (11B, see also Fig.3.3).

(Fig.3.2). It is poorly sorted, slightly reversely graded and composed of white, fine- to medium-grained lapilli pumice with an occasional coarse lapilli (MP=4.4; Fig.3.4). Small lithics (ML=0.6) and some plagioclase crystals are present. MT, MP, ML and Mdø data for the three localities are given in Figure 3.5.

3.3. Distal flow units

At Road J and at Te Whetu the basal air-fall deposit is overlain by thin, uneven, 12-18 cm thick, fine-grained pyroclastic flow units (Figs.3.3, 3.4 and 3.6). The lowermost unit at Road J, 76s1, is a 12-18 cm thick, creamy-white, fine-grained unit with only a few lapilli pumice (MP=1.2) and lithics (ML=0.4). It is overlain by another uneven, 4-14 cm thick, creamy-white tephra unit, 76s2, composed of coarse ash with moderate abundance of fine lapilli pumice (MP=0.5). Plagioclase and pyroxene crystals and small lithics (<0.3 cm) are present. Small segregation pods and pipes are abundant and tiny fragments of carbonized vegetation occur. The Te Whetu thin flow unit, 11B (Figs.3.4 and 3.6), has very similar grain size characteristics to unit 76s2 and may represent a part of the same unit. Poorly developed low-angle cross-stratification is seen at the Te Whetu section (Fig.3.4).

All these units are poorly sorted, fine-ash dominant, and unit 76s2 contains carbonized vegetation. These features are consistent with an interpretation as fine-grained distal facies of early pyroclastic flow units.

A third tephra unit (<5 cm thick) occurs at Road J. This unit, 76s3, is pale orange-brown and composed of fine ash with some fine lapilli pumice (MP=0.6) and a few plagioclase and

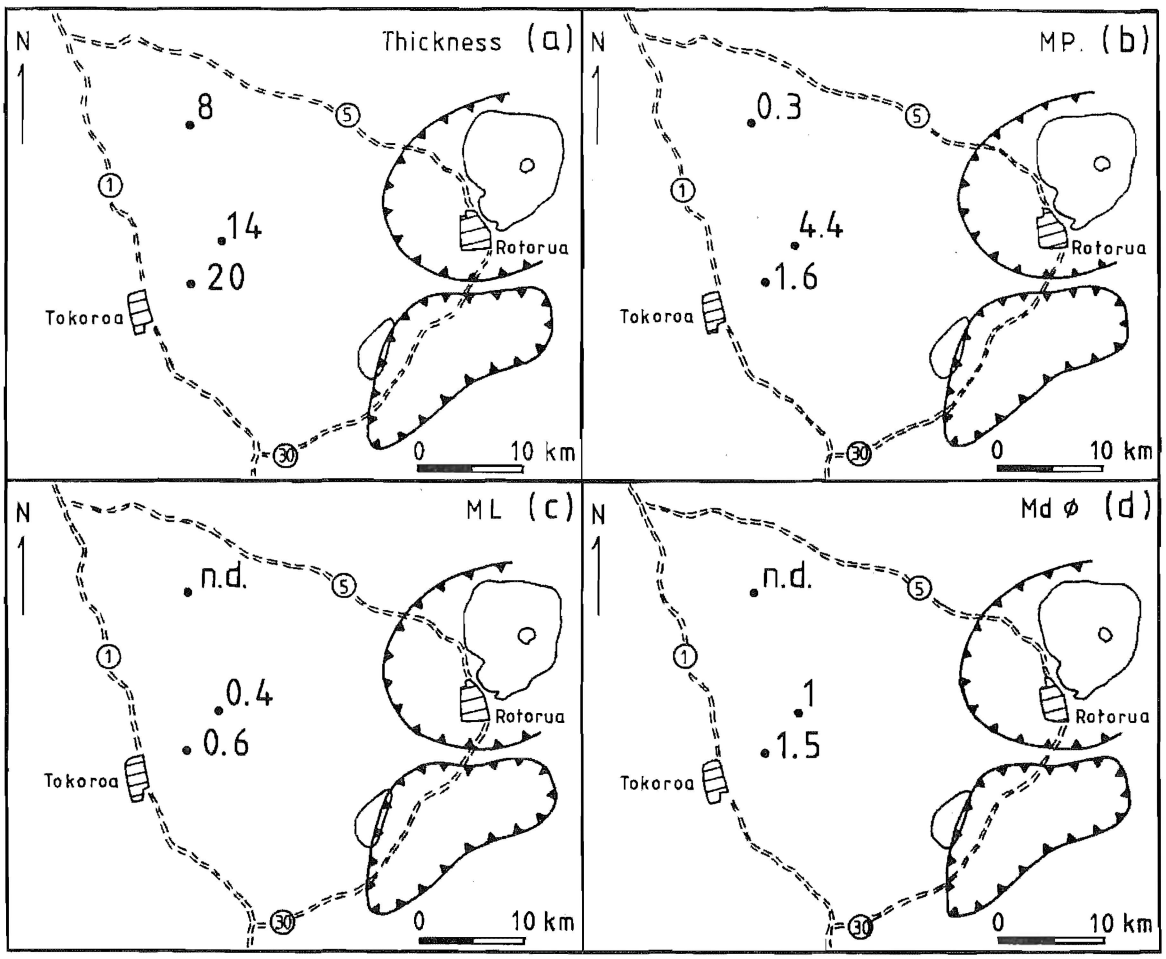

Figure 3.5. Maps showing (a) the measured thickness, (b) MP, (c) ML, and (d) Mdø for the Chimp Ignimbrite air-fall pumice. Values for the thickness, MP and ML are in cm, for the Mdø in mm. The circular cross-hatch lines mark the volcanic centres of Rotorua (E) and Kapenga (SE).

Figure 3.6. (A) Mdø/δø plot and (B) grain size characteristics of weight percentage $<_{1/16}$ mm vs weight percentage <1 mm, for the Chimp Ignimbrite. Solid lines labelled 1 and 4 are contours for the field of pyroclastic flow deposits and within these 99 and 96 %, respectively, of sieve analyses of flow deposits occur; dashed lines are similar contours for the pyroclastic surge analyses (after Walker, 1983).

● = Chimp Ignimbrite flow units; x = thin flow units at the Road J (76s1-3) and Te Whetu (11B) sections (the numbers refer to the sample numbers shown in the stratigraphic sections in Fig.3.3).

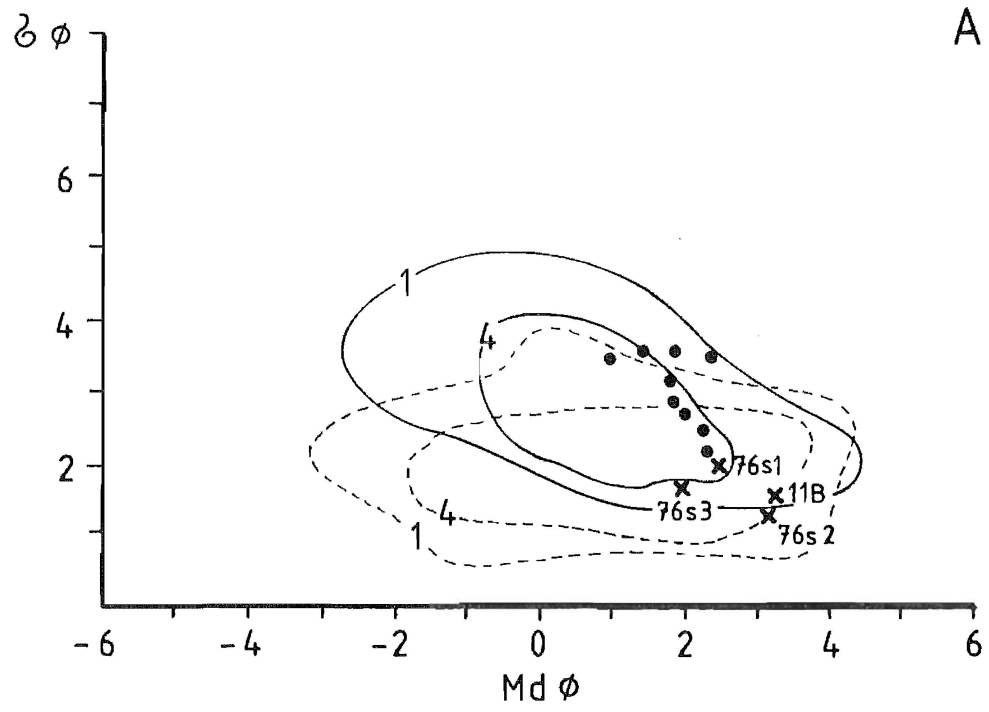
A
δ φ
6
4
2
-6
-4
-2
0
2
4
6
Md φ
1
4
76s1
11B
76s3
76s2

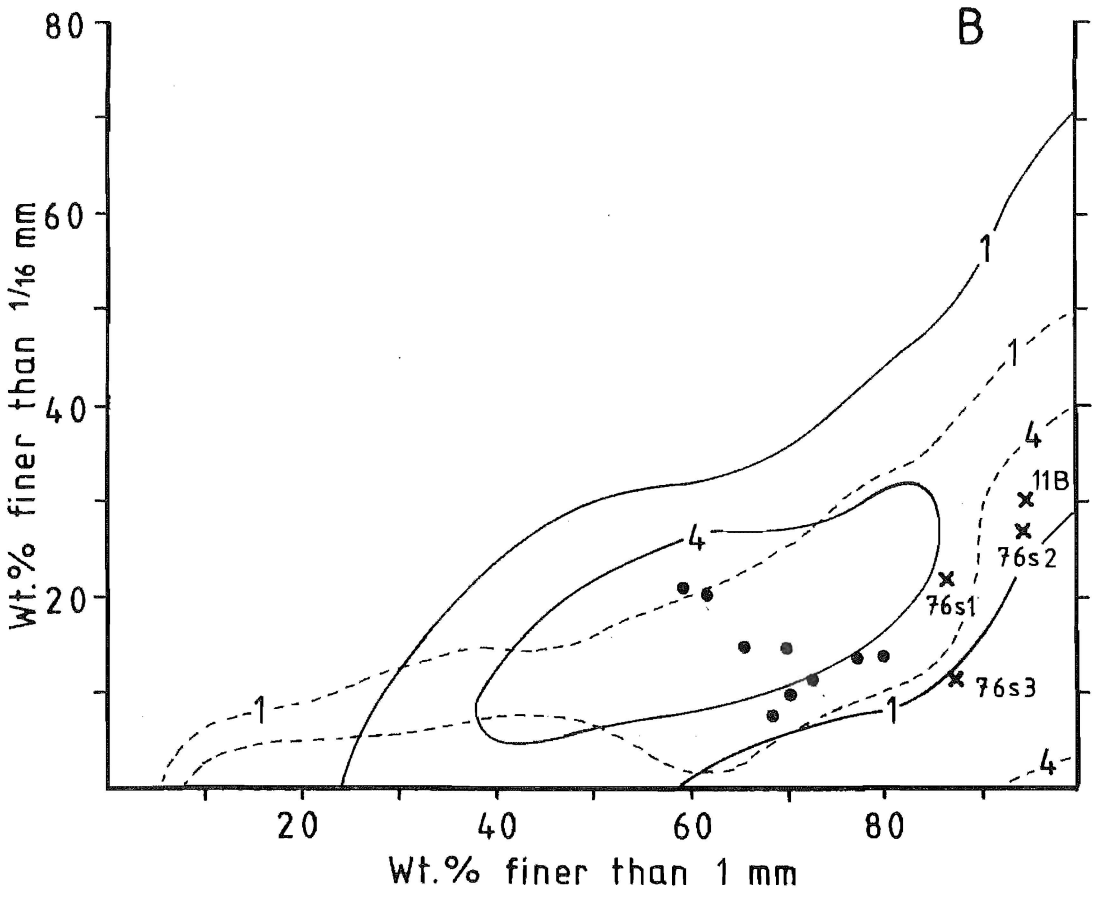
B
80
60
40
20
Wt.% finer than 1/16 mm
20
40
60
80
Wt.% finer than 1 mm
1
4
11B
76s2
76s1
76s3

pyroxene crystals. Small lithics (<0.3 cm) are relatively abundant. Grain-size analysis show that this unit has a higherlithic content than the underlying distal flow units and is also depleted in fine material (Figs.3.3 and 3.6). These features suggest that unit 76s3 may represent a surge deposit, possible associated with the overlying ignimbrite flow unit.

3.4. Ignimbrite flow units

A typical Chimp Ignimbrite flow unit is 4-8 m thick, relatively pumice-poor but may have a thin (0.4-0.7 m) upper zone with moderately- to well-developed coarse-tail grading; equivalent to flow type 2-3 of Wilson (1980). At most outcrops, only one flow unit is exposed, but in some areas 2-3 flow units are definable, eg. Waihou River and Te Whetu section. At these outcrops the resulting ignimbrite lacks clear flow unit boundaries, but shows variations in grain size characteristics that are inconsistent with it being composed of a single flow unit (see below).

All the outcrops are of valley pond ignimbrite (VPI); no ignimbrite veneer deposit (IVD) have been recorded. Either the IVD facies was never emplaced or it has been eroded. No layer 1 deposits have been found. Layer 2a, the boundary layer, is present though rather poorly defined, and its thickness ranges usually from 10-40 cm (Fig.3.3). At Downer Road (GR 646334, field no. 117) a 80-90 cm thick layer 2a occurs, with an 8-10 m layer 2b, directly overlying a pre-Chimp paleosol and Whakamaru epiclastics. Layer 2a is rich in fine material and lacks coarse pumice and lithic clasts. MP and ML are ca. 5 and <1 cm, respectively.

Layer 2b forms the main mass of the ignimbrite. While the base of layer 2b is usually very pumice- and lithic-poor, there is an upward increase in pumice size and concentration. In some flow units an enrichment of both pumice and lithics seemed to occur throughout the flow unit, which then have a concentration of both large pumice and lithics on the top. The concentration of large pumice may be due to fluidisation causing coarse-tail grading; the origin of the lithics is somewhat unclear. The uneven occurrence of lithics suggest that they may be predominantly locally derived, perhaps picked up from scree material.

The best developed coarse-tail grading is found at Te Whetu. The section has a total thickness of about 4 m and has three sets of thin flow units, each with an upward coarsening top (MP=18.5). These are flow types 3 of Wilson (1980). The flow unit contacts are irregular, suggesting that the lower unit was still inflated when the upper unit was emplaced. A slight enrichment of lithic clasts (ML=3.3) occurs at the base of the lowermost flow unit. No such enrichments is seen in the two overlying units.

The set of multiple thin flow units at Te Whetu may represent deposits from the trailing tail of successive pyroclastic flows, the bulk of which travelled further before coming to rest. Three km west the total thickness of the ignimbrite is over 15 m (Fig.3.1). IVD are usually generated from slower moving basal parts of a flow unit, left behind because of ground friction (Wilson, 1986). However, a small proportion of layer 2 consisting of PCZ material on the top of the flow may be stranded by the onward movement of the flow to form thin, pumice-rich drapes over the landscape (Wilson & Walker, 1982),

which probably accounts for the three thin (1-1.5 thick) flow units at Te Whetu.

Segregation bodies are abundant throughout layer 2b. Two distinct morphological types occur; (I) segregation pipes (Fig.3.7) form sub-vertical features from 3-5 mm to 8-10 cm wide and up to 50-70 cm high, and (II) segregation pods, which form lenses and irregular masses from ca 1 to 25 cm across. The latter seem to be concentrated towards the base of the flow and usually contain the coarsest lithics (ML=6.6, at McDowall Road, GR 703328, field nos. 45 & 106, between 1-2.5 m above the base). Fluidisation experiments (Wilson 1980, 1984) indicate that segregation pods and pipes form in 'fluid' and 'stiff' flows, respectively.

Gas segregation bodies are most abundant in the central part of the study area, from south Galaxy Road to Te Whetu, but are found occasionally in the northwestern area. Carbonized vegetation is common, ranging from tiny fragments to small logs with a diameter of 10-12 cm. At Te Whetu sub-horisontal carbonized logs have a ca. E-W orientation (from 80°E to 105°SE).

Distribution of the MP and ML data have been constructed (Fig. 3.8) and MP and ML data plotted against distance from Rotorua, Kapenga, Maroa and Mangakino Volcanic Centres are shown in Figure 3.9. Two diagrams are given, one (a) showing the MP and ML for the lower part of a flow unit, and the other (b) shows the data for the top part of a flow unit, estimated on the basis of increased pumice size and concentration. It should be noted that some of the flow units lack lithics. For reasons mentioned above it seems clear that the ML data is not very

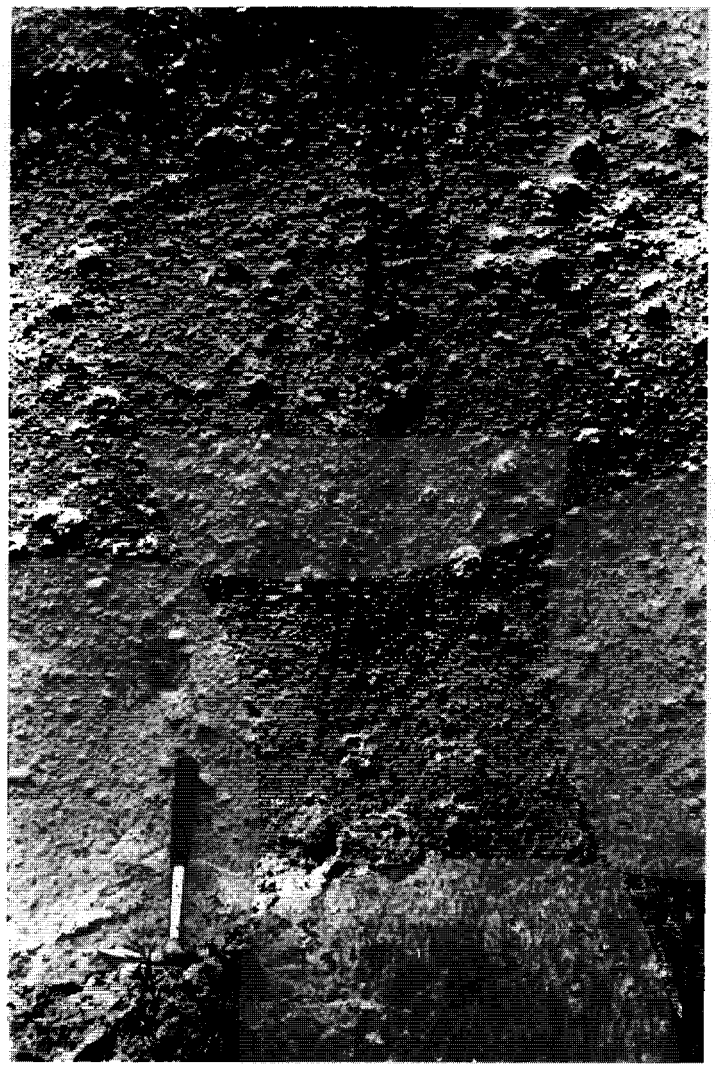

Figure 3.7. Gas segregation pipes in the upper part of the Chimp Ignimbrite at Pokai Road (GR 683368, field no. 33).

Figure 3.8. Distribution maps of MP and ML in the Chimp Ignimbrite. The shaded patch in the MP map marks the area of well developed coarse-tail grading (flow type 3 of Wilson, 1980); MP in parenthesis. All the values are in cm. The circular cross-hatch lines mark the volcanic centres of Rotorua (E) and Kapenga (SE), respectively.

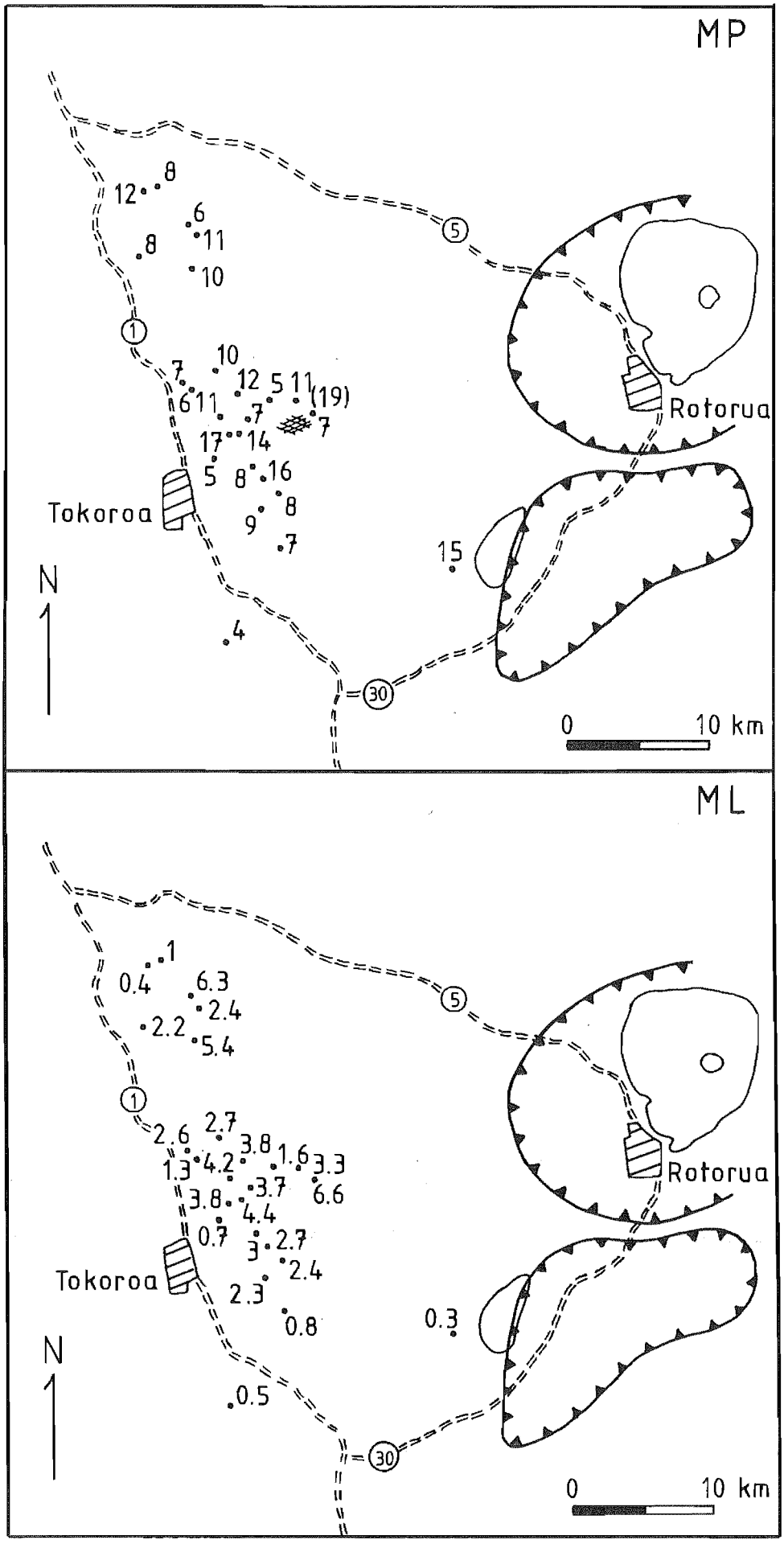
MP
12
8
6
11
8
10
10
7
12
5
11
(19)
6
11
7
7
17
14
5
8
16
8
9
7
15
4
Tokoroa
Rotorua
N
0
10 km
ML
1
0.4
6.3
2.4
2.2
5.4
2.7
2.6
3.8
1.6
3.3
1.3
4.2
3.7
6.6
3.8
4.4
0.7
3
2.7
2.4
2.3
0.8
0.3
0.5
Tokoroa
Rotorua
N
0
10 km

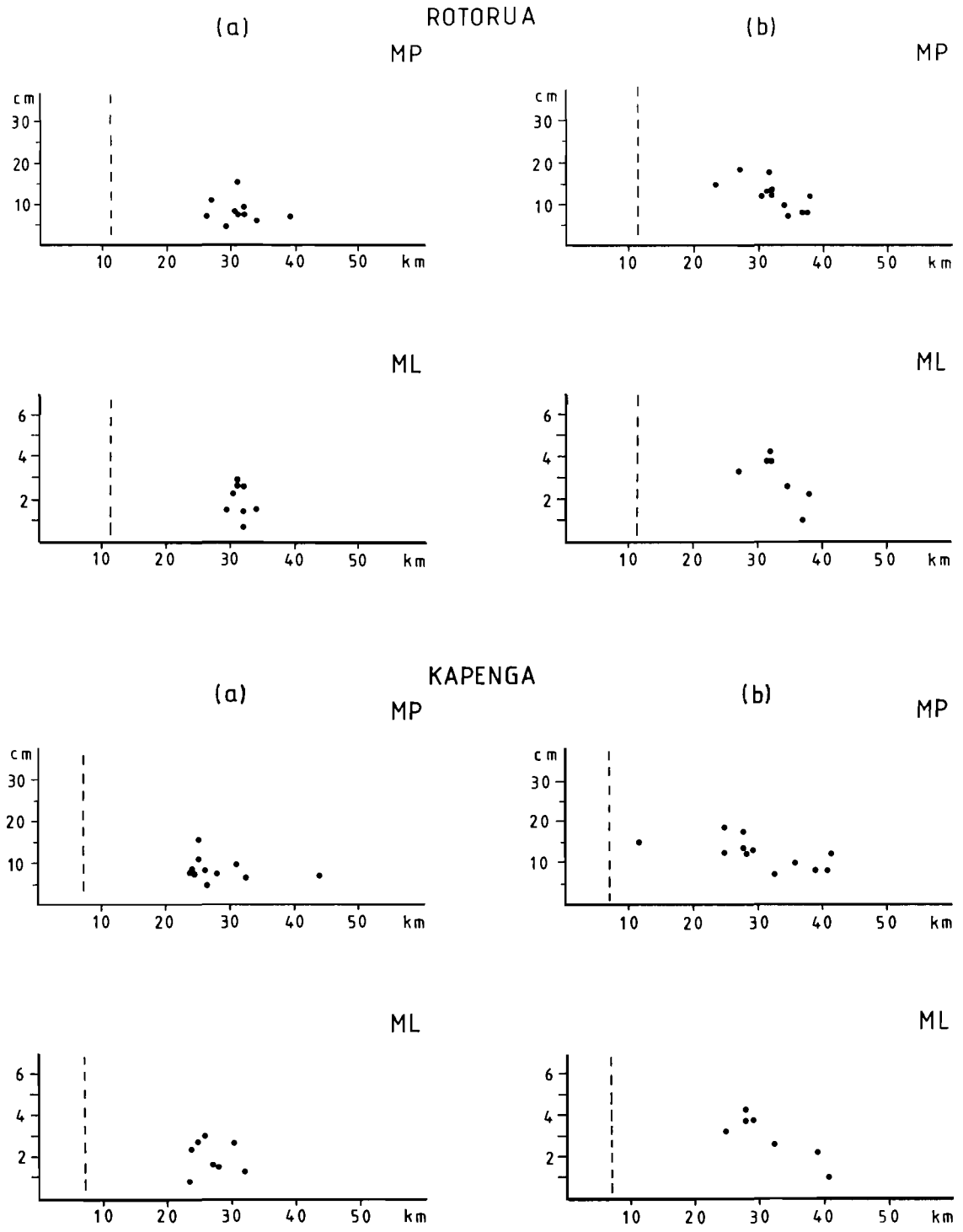

Figure 3.9. MP and ML (a) in the lower part, and (b) at the top of the Chimp Ignimbrite plotted against distance from the Rotorua and Kapenga Volcanic Centres. Dashed lines mark the approximate present day caldera margins for both volcanic centres.

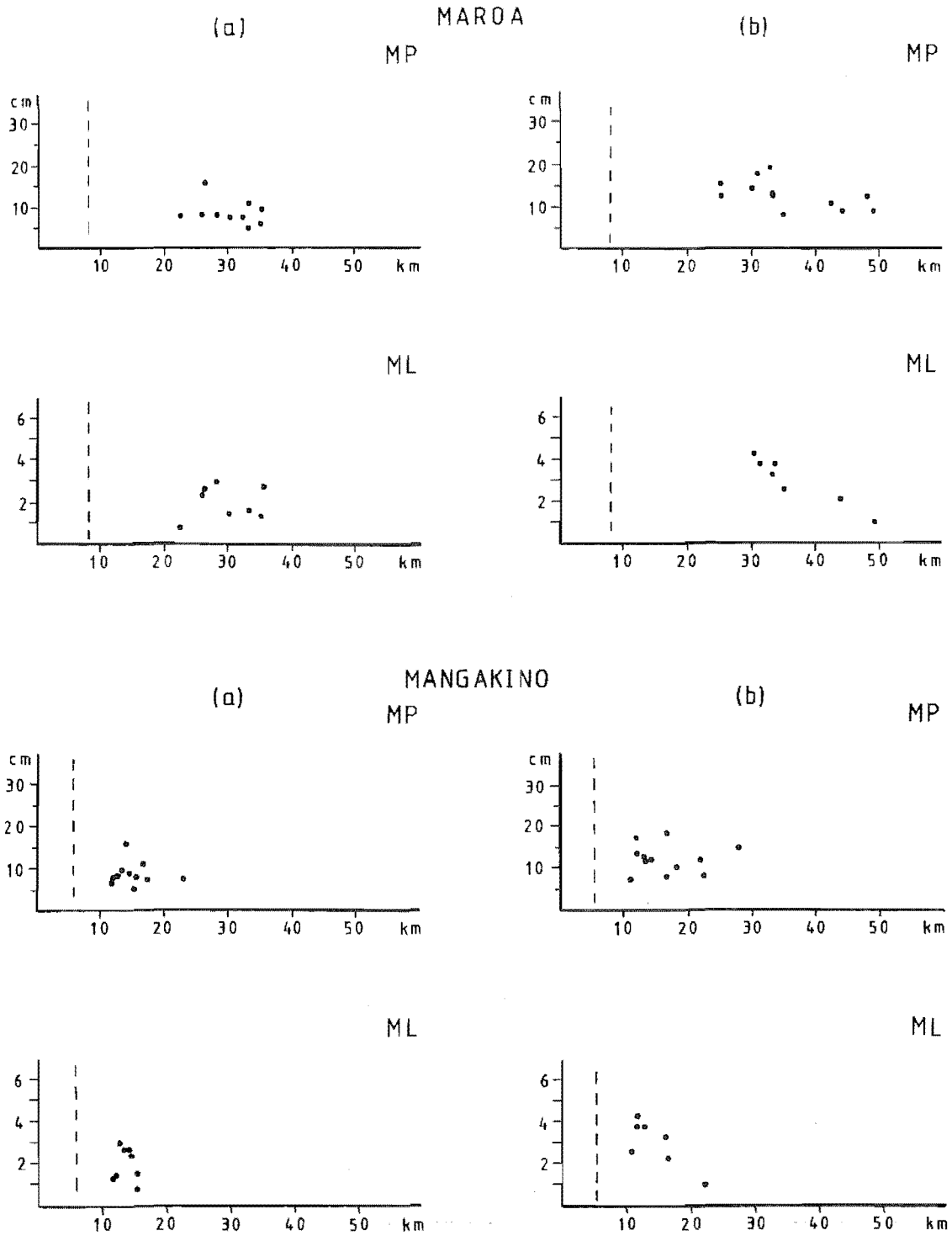

Figure 3.10. MP and ML (a) in the lower part, and (b) at the top of the Chimp Ignimbrite plotted against distance from the Maroa and Mangakino Volcanic Centres. Dashed lines mark the approximate present day caldera margins for both volcanic centres.

reliable as an indicator for a possible source area.

MP data shows a slight decrease against distance from both the Kapenga and Maroa centres and also a slight correlation with distance from the Rotorua Volcanic Centre for the upper flow units. This data is not, however, significant enough to point any definite source area for the Chimp Ignimbrite.

MP and ML data plotted against distance from possible source areas have relatively narrow distribution fields (15-20 km for the Rotorua and Mangakino Volcanic Centres and 20-40 km for the Kapenga and Maroa centres) and a wide grain-size distribution could be expected. For example, the Taupo Ignimbrite, with a distribution of 80 km radially around the source vent, also shows wide grain-size variation 30-50 km from source, and even a slight increase in MP between 25-50 km from the source vent (Wilson 1986).

Histograms showing the grain size and component analysis from nine ignimbrite matrix samples are illustrated in Figure 3.11. Most of the samples represent approximately a lower middle part of a flow unit. The Leslie Road sample, in the north, comes from a pumice-rich and lithic-poor top of a crystal-rich flow unit, the Te Whetu sample represents layer 2a and the Tram Road sample, in south, comes from a thin, 1.5 m thick, lithic-poor flow unit.

The median diameter, Mdø, for the ignimbrite matrix (≤16 mm fraction) plotted against distance from several possible source areas (Fig.3.12.a) does not show any linear correlation to the proposed source areas. To exclude the effect of the possible locally derived lithics, all lithics >¼ mm were separated from the matrix and the material was recalculated to

Figure 3.11. Grain size histograms for the Chimp Ignimbrite matrix (≤16 mm). The bars for ½ mm (1 phi) and coarser classes are subdivided to show the proportions of components.

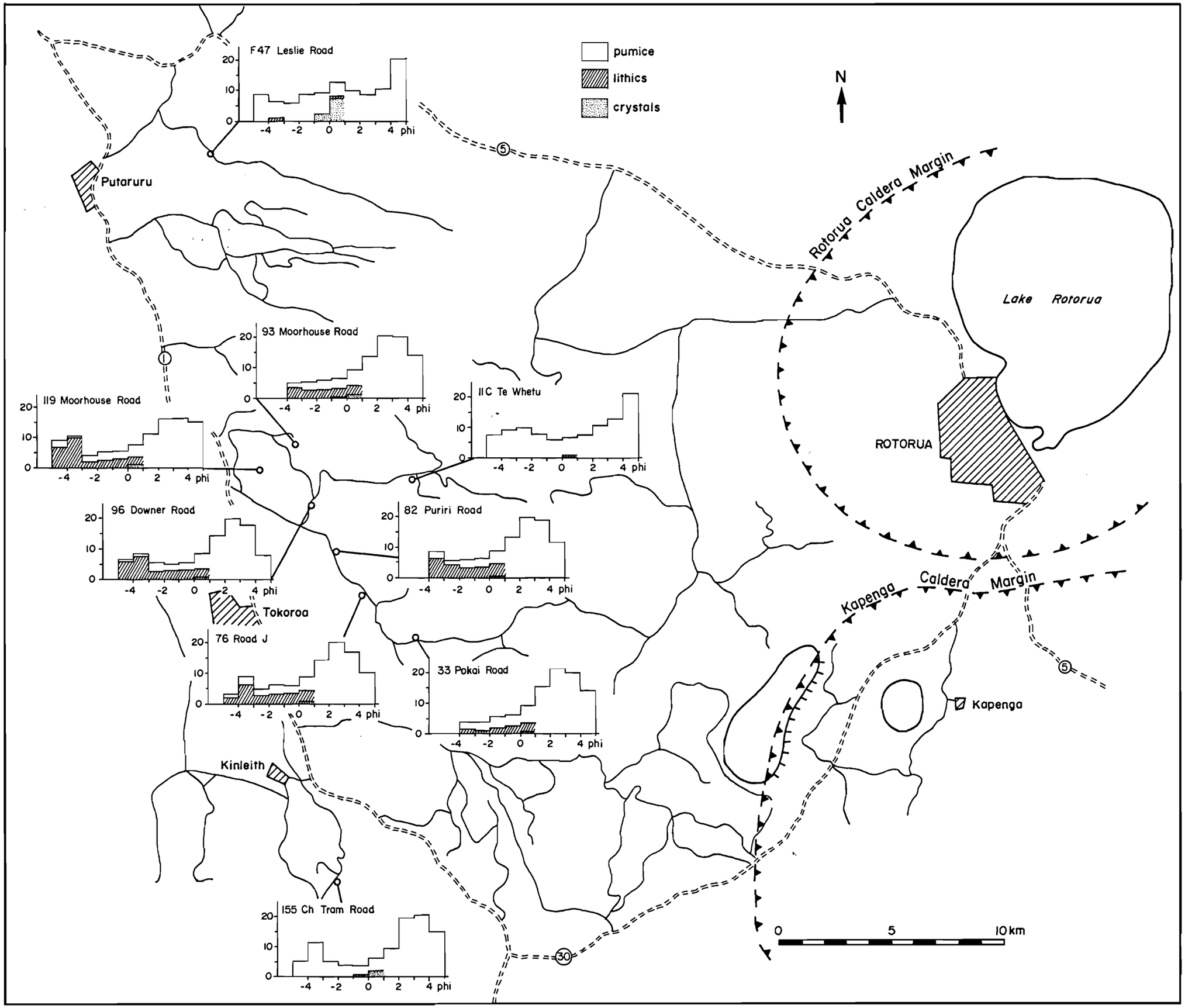
pumice
lithics
crystals
N
F47 Leslie Road
Putaruru
93 Moorhouse Road
119 Moorhouse Road
11C Te Whetu
96 Downer Road
82 Puriri Road
Tokoroa
76 Road J
33 Pokai Road
Kinleith
155 Ch Tram Road
Rotorua Caldera Margin
Lake Rotorua
ROTORUA
Kapenga Caldera Margin
Kapenga
0 5 10km
20
10
0
-4 -2 0 2 4 phi

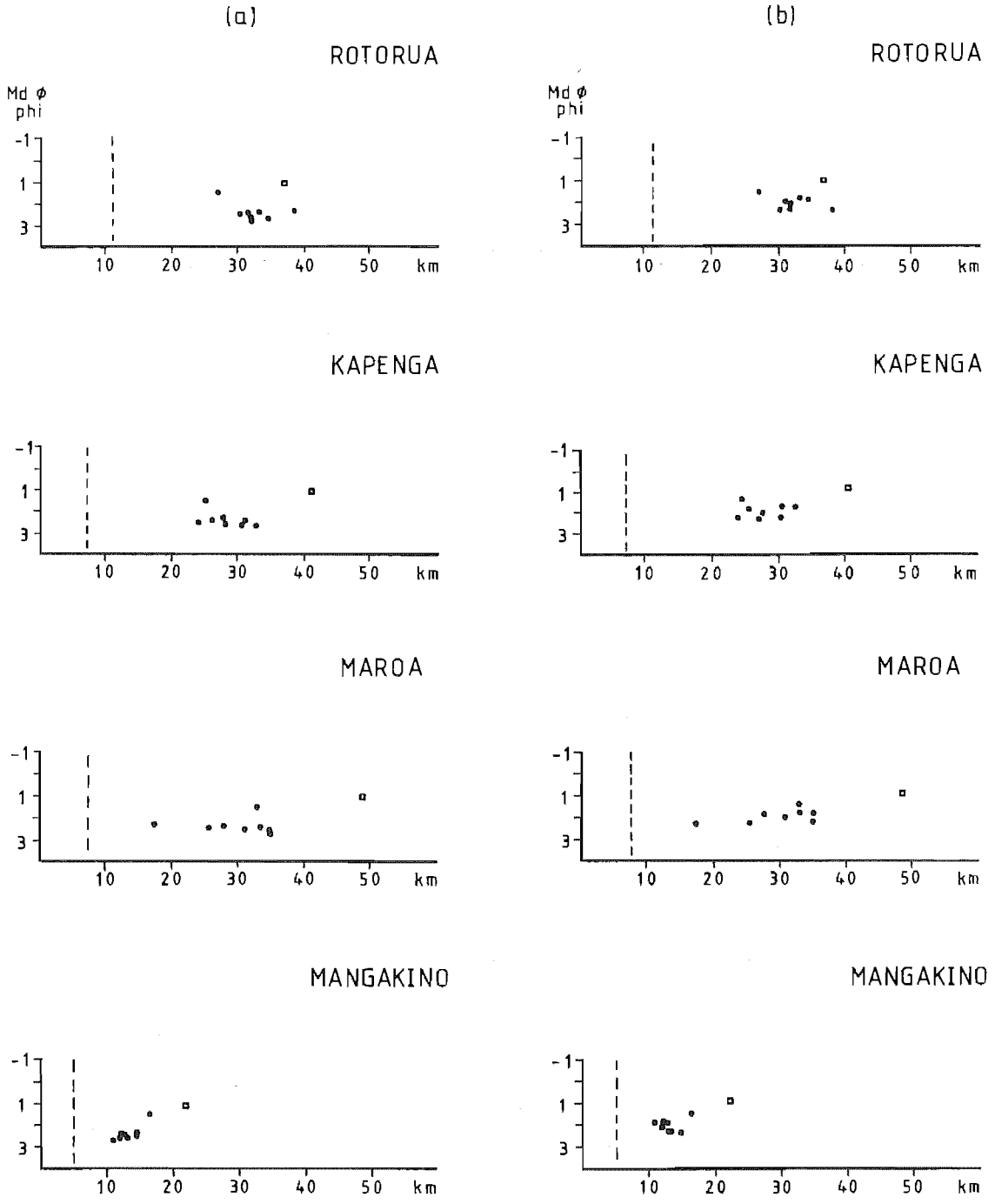

Figure 3.12. (a) Mdø in the Chimp Ignimbrite matrix, and (b) Mdø in the recalculated lithic-free Chimp Ignimbrite matrix plotted against distance from the Rotorua, Kapenga, Maroa and Mangakino Volcanic Centres. Dashed lines mark the approximate present day caldera margins for each volcanic centre. □ = pumice-rich top of a crystal-rich northern flow unit.

100%. Mdø for the lithic-free matrices is shown in Figure 3.12.b. A very slight linear correlation outward from the Rotorua, Kapenga and possibly from the Maroa Volcanic Centres is seen. The content of material ≤½ mm (Fig.3.13.a) in the ignimbrite matrix varies from 60-80% but does not show any general increase away from the possible source areas. The content of material finer than 1/16 mm (Fig.3.13.b) is between 8-21 % and possible a slight increase away from Kapenga and Maroa/Mangakino areas towards northwest and north, respectively, occurs.

The content of free crystals in the sum of the sub-1 mm and sub-½ mm classes are shown (Fig.3.14), since most of the crystals belong to these sub-classes. The crystal contents show some decrease away from the Maroa Volcanic Centre, however, the data is not sufficient to point out any definite source area.

3.5. Eruption sequence

A brief eruption model is here interpreted largely on the basis of the two best preserved outcrops near Puriri Road and Te Whetu, respectively (section 3.1). The eruption began with a plinian phase producing a pumice-fall deposit, which commonly ranges from fine to medium lapilli with an occasional coarse lapilli. No interbedded ash units occur, indicating a single air-fall pumice eruption from a single vent. After a short (?) plinian phase the eruption column became unstable with minor collapse of the column margins generating a series of early, thin flow units. The occurrence of units 11B and 76s1-3 at Te Whetu and Puriri Road, respectively, represent

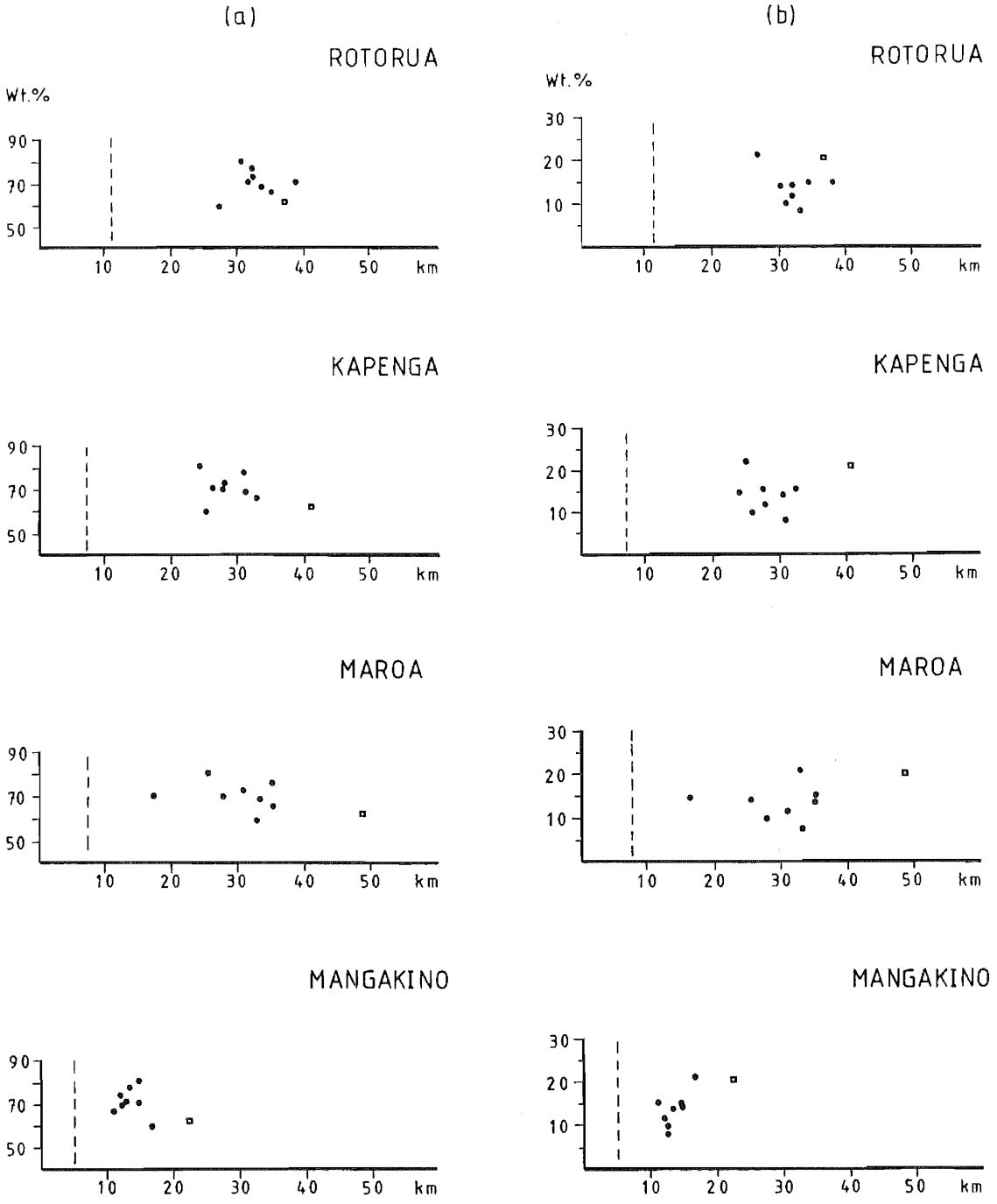

Figure 3.13. (a) Weight percentages of the fractions ≤½ mm, and (b) <1/16 mm in the Chimp Ignimbrite matrix (≤16 mm) plotted against distance from the Rotorua, Kapenga, Maroa and Mangakino Volcanic Centres. Dashed lines mark the approximate present day caldera margins for each volcanic centre. □ = pumice-rich top of a crystal-rich northern flow unit.

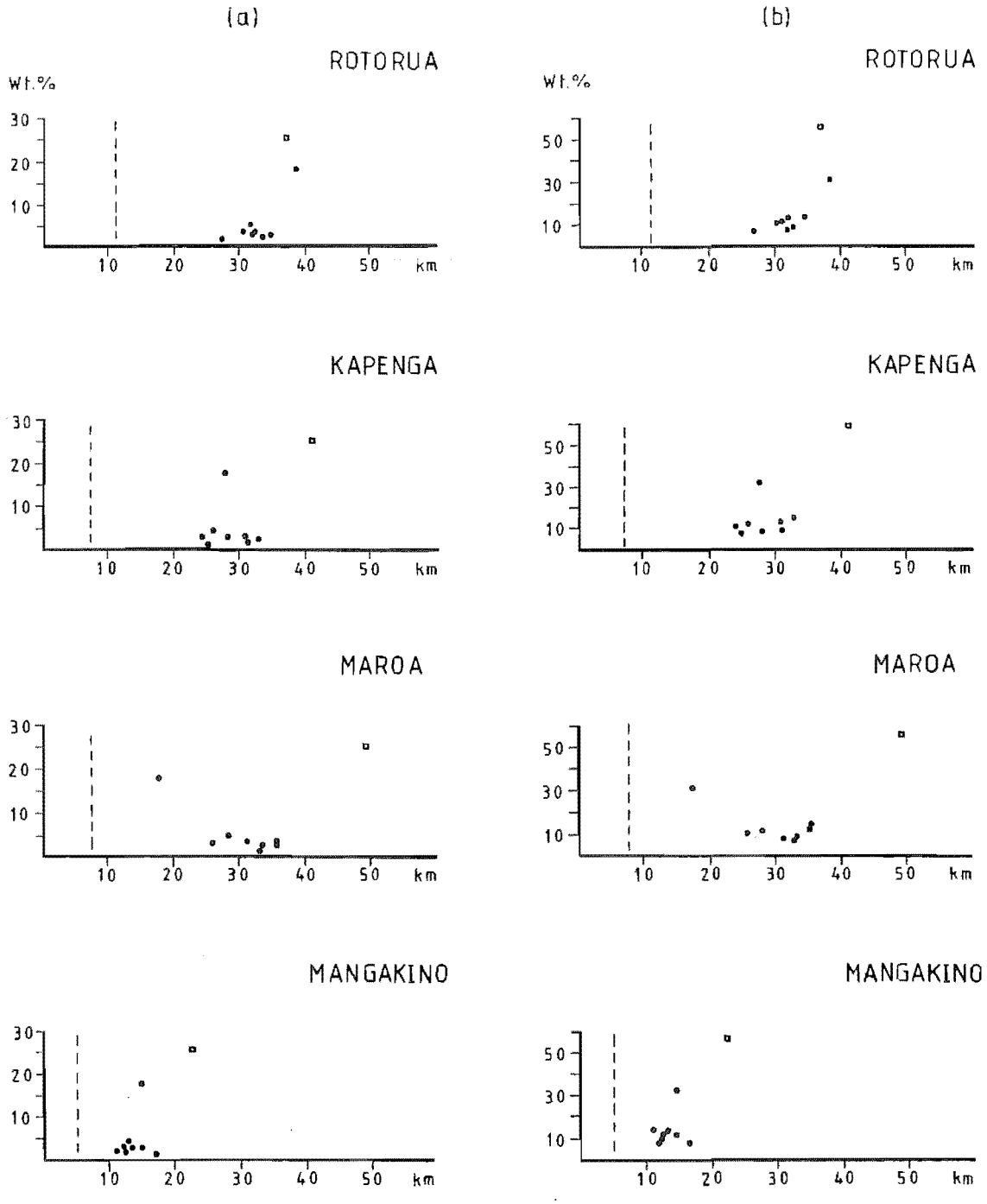

Figure 3.14. Weight percentages of free crystals in the (a) sub-1 mm, and (b) sub-½ mm fractions in the Chimp Ignimbrite matrix plotted against distance from the Rotorua, Kapenga, Maroa and Mangakino Volcanic Centres. Dashed lines mark the approximate present day caldera margins for each volcanic centre. □ = pumice-rich top of a crystal-rich northern flow unit.

those units. Probably immediately following the plinian and the early column collapse phases, a more widespread column collapse took place, and the main ignimbrite flow units were deposited.

4. PETROGRAPHY AND MINERALOGY

4.1. Introduction

In this chapter the petrography and mineralogy of the Pokai and Chimp Ignimbrites are presented. Fifty seven (57) Pokai and fourteen (14) Chimp ignimbrite samples from the non-welded ignimbrite and pre-ignimbrite air-fall units were studied under a binocular microscope. Petrographic descriptions and modal analyses of thin sections are given in Appendix B. Modal analyses of selected samples from the Pokai and Chimp ignimbrites are given in Tables 4.1-4.4 and 4.11-4.14, respectively.

Of the pumice samples used for whole rock analysis, 22 were selected for microprobe analysis (18 from the Pokai and 4 from the Chimp ignimbrite). The pumices were crushed and the crystals separated from the lighter pumice glass by washing in distilled water. Probe sections were also used to estimate phenocryst proportions. The mineral and pumice glass analyses were made using a JEOL 8600 Superprobe at the Department of Geology, University of Otago, Dunedin; a description of microprobe analytical techniques is presented in Appendix C.

Representative analyses of plagioclase, pyroxenes, titanomagnetite and ilmenite with equilibrium temperature estimates from the Pokai and Chimp ignimbrites are given in Tables 4.5-4.9 and 4.15-4.20, respectively. Unless otherwise stated all mineral and glass analyses presented in this chapter have been recalculated to 100 % anhydrous. A list of all microprobe analyses is presented in Appendix C. Only mineral analyses with totals between 98.5-101 % for major

elements were accepted.[6].

4.2. Pokai Ignimbrite

4.2.1. Petrography

Matrix.

In hand specimen the Pokai Ignimbrite is a fine-grained, non-welded to densely welded, pumice-rich ignimbrite with a relatively low crystal and lithic contents. Plagioclase and orthopyroxene are the dominant phenocryst phases in both the groundmass and pumices.

Under the microscope the ignimbrite displays a chaotic mixture of transparent and/or orange-yellow glass shards and vitric dust, pumice, phenocrysts and lithic fragments (Fig.4.1). Glass shards and vitric dust make up between 40-70 vol.% (Table 4.1). Pumice content varies between 20-50 vol.%. Phenocrysts make up 3-8 vol.% of the ignimbrite whereas lithic contents range from trace amounts in the pumice concentration zone (PCZ) to 8 vol.% in the most lithic-rich parts of the ignimbrite.

Near the base and top of the ignimbrite, pumice clasts, free crystals and lithics occur in a loose matrix in which the glass shards are well preserved with cuspate, branched, platelike or fibrous forms with a large proportion of tubular pore space. In the slightly to moderately welded zones somewhat flattened pumice, free crystals and lithic fragments are set in a deformed matrix composed of compressed and distorted glass shards (Fig.4.2). In the more densely welded

[6] Except for one clinopyroxene analysis of Chimp Ignimbrite (chapter 4.3.2, Table 4.19).

Figure 4.1. Slightly welded Pokai Ignimbrite displaying orange-yellow glassy matrix (mtx) with pumice clasts (pum), phenocrysts (Pl = plagioclase) and lithics (Li). Magnification 10x. Plane polarized light.

Figure 4.2. Moderately welded Pokai Ignimbrite showing slightly distorted and compressed glassy matrix. Mt = magnetite/ilmenite. Magnification 16x. Plane polarized light.

Figure 4.3. Densely welded Pokai Ignimbrite with strongly distorted and compressed glassy matrix. The glass shards show evidence of plasticity during welding, the glass material has been squeezed into the embayments between the plagioclase phenocrysts. Pl = plagioclase; Opx = orthopyroxene. Magnification 16x. Plane polarized light.

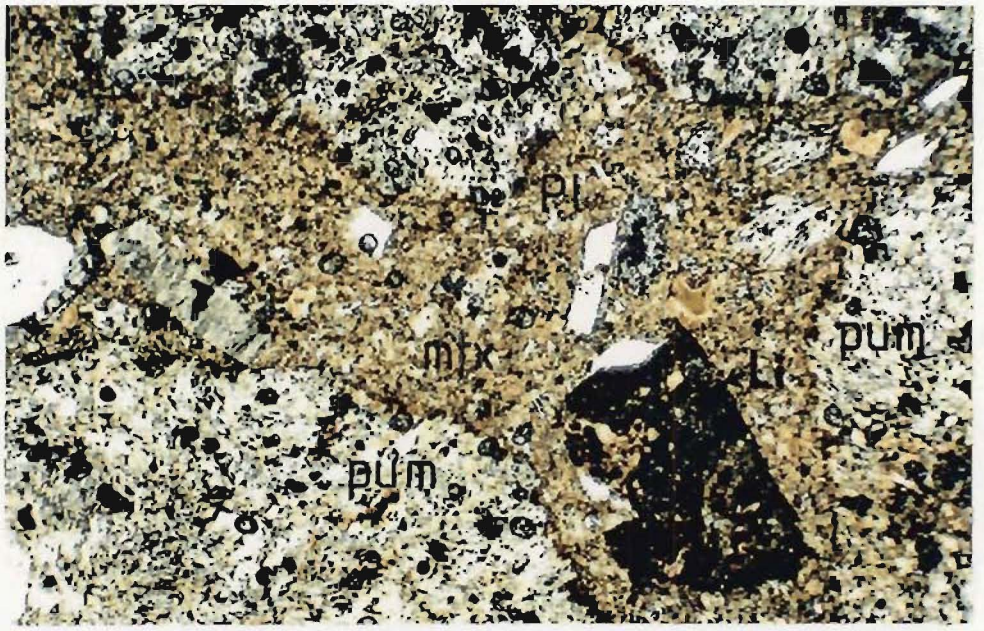
Pl
mtx
pum
Lt
pum

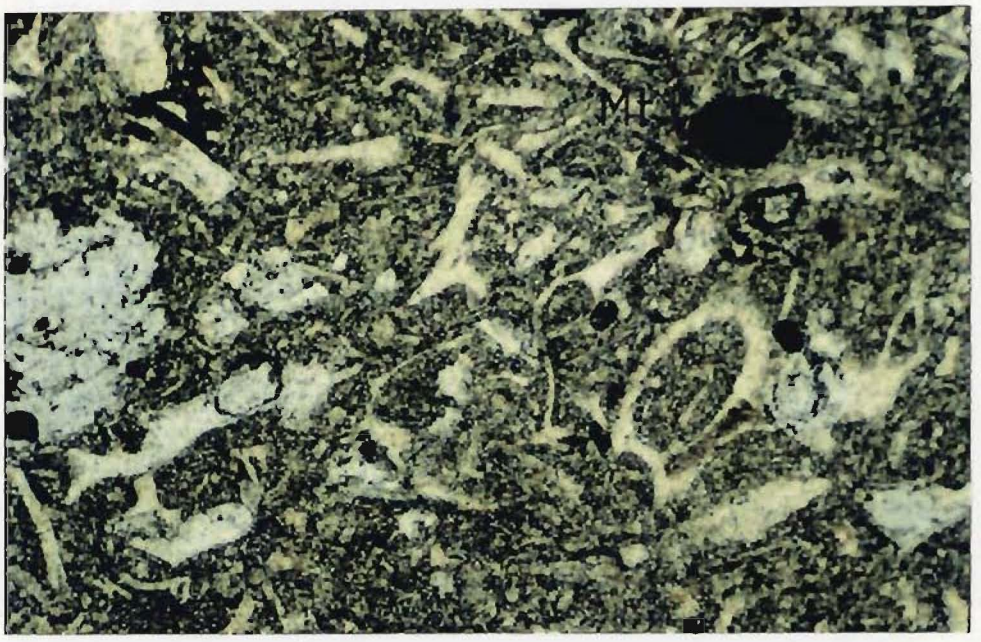
Mt

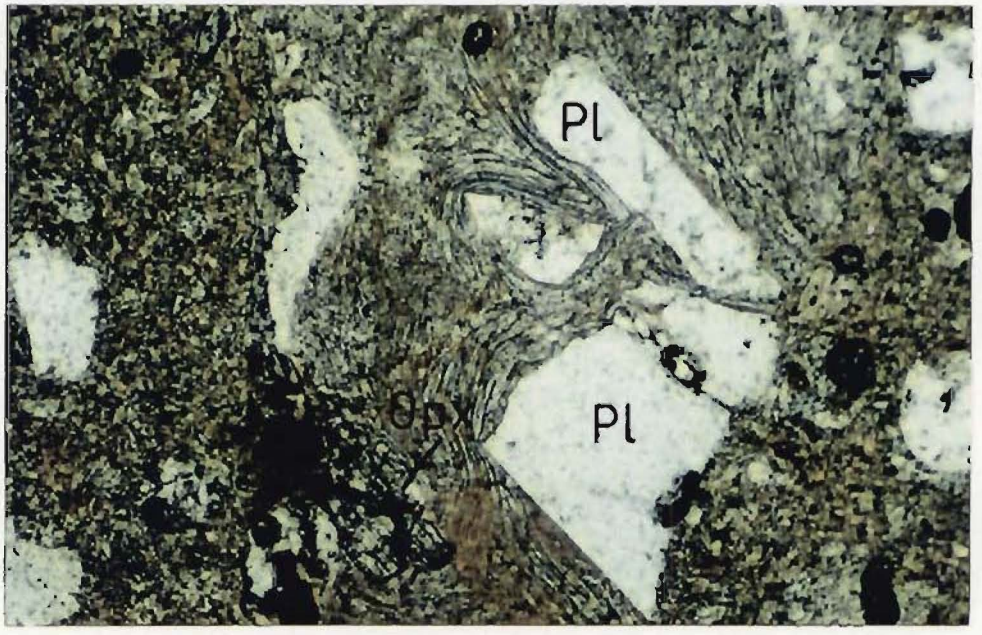
Pl
Opx
Pl

Table 4.1. Modal proportions of the Pokai Ignimbrite constituents from selected flow unit samples as vol.%. Point-counted from thin sections to approx. 1200 points. S = sample number.

S	Mtx glass	Pumice	Lithics	Phenocrysts
P1i	42.8	52.2	1.1	3.9
P4i	68.6	22.6	3.3	5.5
P5i	65.7	23.8	6.9	3.6
63	65.5	28.2	1.2	5.1
133	44.4	46.3	1.0	8.3
131A	65.9	19.0	10.5	4.6

Table 4.2. Modal proportions of phenocrysts in the Pokai Ignimbrite matrix. S = sample number.

S	Plag	Prx	Fe-Ti	Qz	Zr
P1/1	78.9	7.0	3.5	8.8	1.8
P1/4	87.3	7.6	2.5	2.5	-
P1/5	83.3	2.8	5.6	8.3	tr
63	94.0	0.6	2.4	3.0	-
133	92.9	1.6	5.5	-	-
131A	85.6	3.6	4.5	6.3	-

Plag = plagioclase
Prx = ortho/clinopyroxene
Fe-Ti = Fe-Ti oxide
Qz = quartz
Zr = zircon

tr = trace amounts

P1i = Rauna Road, top of >30 m ignimbrite exposure, basement not exposed, moderately welded
P4i = Rauna Road, 8 m below top, welded
P5i = Rauna Road, 11 m below top, welded
63 = an unnamed road near Tikorangi Road, welded
133 = Haunui Valley, welded, crystal-rich unit
131A = Haunui Valley, lag breccia

parts, with higher compression and marked distortion, the glass shards have been strongly moulded against the pumice, phenocrysts and lithics in a eutaxitic texture which resembles flow texture (Fig.4.3). In the most welded parts of the ignimbrite the matrix is slightly devitrified. The devitrification appears to be in the early stages of development as the original vitroclastic nature is still visible in most samples examined (Figs.4.2 & 4.3). In the welded samples vesicularity is low (usually <2 vol.%).

Plagioclase is the dominant phenocryst constituent in the matrix with 80-90 vol.% of all crystals (Table 4.2). The proportion of orthopyroxene varies greatly from 0.6-8 vol.%, and Fe-Ti oxides 2-4 vol.%. Quartz occurs between trace amounts and 9 vol.%, reaching up to 22 vol.% in one sample. Amphibole and clinopyroxene are rare. Zircon, apatite and titanite occur in trace amounts.

Pumice.

Pumices range from mm-sized particles to large pumice blocks. The pumice clasts are composed of vesicular glass with 2-8 vol.% phenocrysts. The pumice clasts are best preserved near the base and top of the ignimbrite showing nearly spherical vesicles with unbroken, glassy vesicle walls (Fig.4.4). Vesicularity (pore space) varies from nearly 60 vol.% in the non-welded pumice to less than 10 vol.% in the welded types (Table 4.3). The slightly welded pumice (from 6-10 m above the base) is composed of ellipsoidal vesicles with some distortion of the glass shards (Fig.4.5). Still higher in the flow unit (between 12-20 m), in the moderately and densely welded zone, the vesicularity of the pumices decreases and the vesicles

Figure 4.4. Highly vesicular pumice from non-welded Pokai Ignimbrite with spherical, unbroken glassy vesicle walls. Pl = plagioclase; Opx = orthopyroxene. Magnification 10x. Plane polarized light.

Figure 4.5. Slightly welded Pokai Ignimbrite pumice with somewhat flattened (ellipsoidal) vesicles. Opx = orthopyroxene; Mt = magnetite/ilmenite. Magnification 16x. Plane polarized light.

Figure 4.6. Densely welded Pokai Ignimbrite pumice with strongly flattened and elongated vesicles and deformed glass shards. Pl = plagioclase. Magnification 12.5x. Plane polarized light.

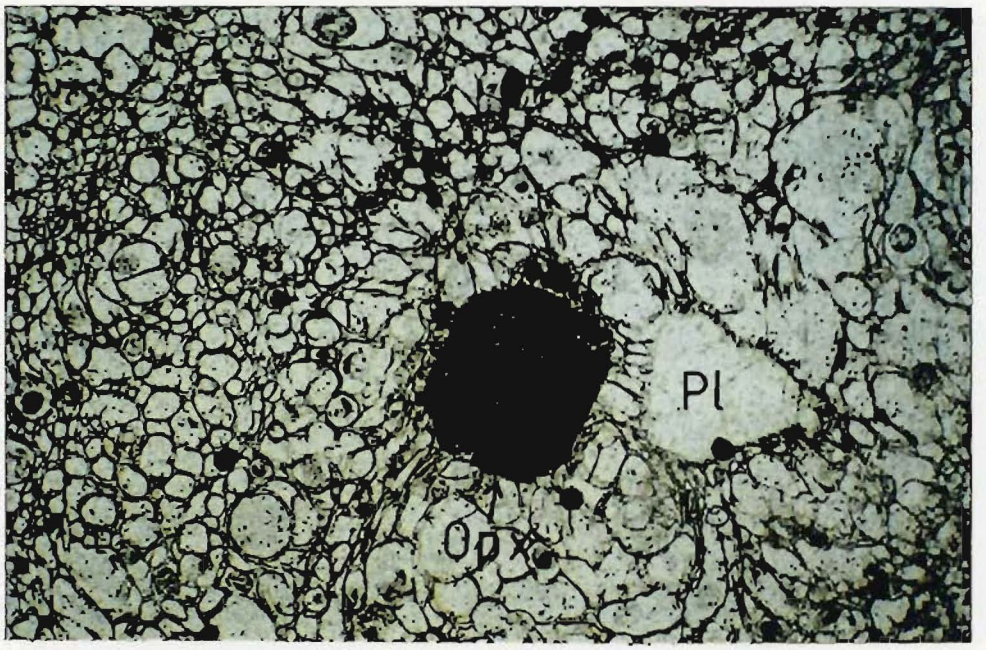
Pl
Op

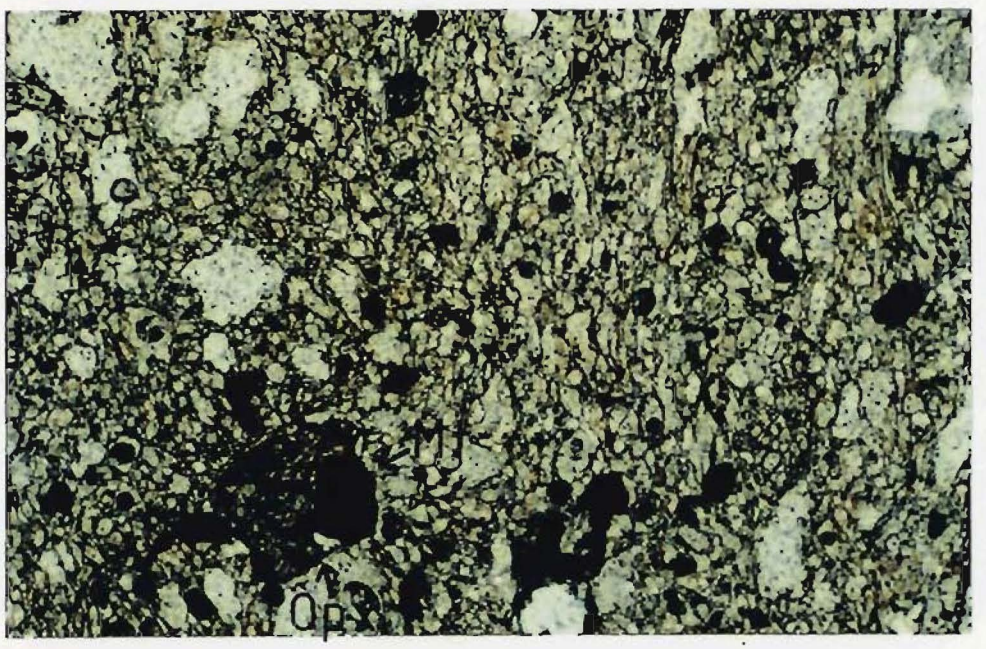
Op

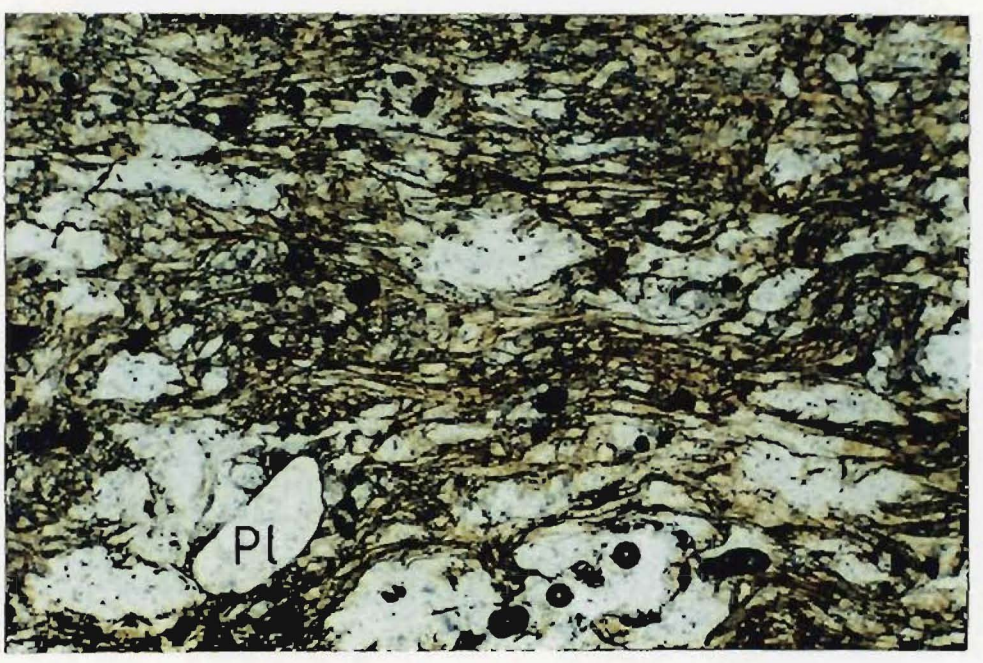
Pl

Table 4.3. Modal analyses of the Pokai Ignimbrite pumice constituents (glass & phenocrysts). Vesicularity is given separately for each sample. Values as vol.%. Rno = reference number for samples analysed by XRF (listed in Appendix D, Table D.2); S = sample number; T = pumice type: A = crystal-poor, B = crystal-rich.

Rno	S	T	Glass	Phenocrysts	Vesicularity
-	**R12**	A	98.8	1.2	45.8
-	**R6**	A	97.6	2.4	21.8
128	**66/1**	A	95.7	4.3	14.2
95	**HJ2/2**	A	99.1	0.9	9.7
-	**P5**	A	95.2	4.8	23.0
-	**132**	A	96.4	3.6	16.5
-	**133a**	B	90.9	9.1	32.0
231	**T24/1**	B	87.8	12.2	17.4
-	**47B**	B	94.0	6.0	52.0

R12 = Pokai Road, 2 m above the base, non-welded
R6 = Pokai Road, 18.5 m above the base, welded
66/1 = Chamois Road, total thickness unknown, moderately welded
HJ2/2 = Harry Johnson Road, ca. 72 m above the base, welded
P5 = Rauna Road, 11 m below top, welded
132 = Haunui Valley, Pylon line, approx. 20 below top, basement not exposed, welded
133a = Haunui Valley, total thickness unknown, welded
T24/1 = Tapapa Valley, top of an approx. 25 m thick ignimbrite exposure, welded
47B = Leslie Road, base of an approx. 10 m thick exposure, non-welded

become increasingly elongated and flattened. Many of the vesicles have collapsed and the majority of glass shards are highly deformed (Fig.4.6). Tiny aggregates of vapour-phase crystallised quartz and alkali feldspar occur around some of the pore spaces. Slight devitrification also occurs, although vitroclastic texture can still be recognised in most Pokai Ignimbrite pumices examined (Figs.4.5 & 4.6).

Two pumice types (see chapter 2.2) occur in the Pokai Ignimbrite, crystal-poor and crystal-rich, referred to as Type A and Type B pumices, respectively. Modal analyses of the crystal-poor, Type A pumices give a mean phenocryst content of 2.2 vol.% (vesicle pore-space not included). The crystal-rich pumices, Type B, have a phenocryst content of about 8 vol.%. A list of representative modal analyses is given in Table 4.3. Pumices also contain rare (usually <1 vol.%) microxenoliths (1-2 mm) of devitrified rhyolite.

Plagioclase is the most abundant phenocryst in the pumice (80-95 vol.%, Table 4.4). Orthopyroxene (0.5-9 vol.%) and Fe-Ti oxides (0.5-7 vol.%) also occur in all pumice samples. Quartz (2-16 vol.%) is present in about half of the samples examined, but does not appear to correlate with any individual flow unit or location. Zircon, apatite and titanite occur as trace amounts, and tiny grains (≤0.8 mm) of black amphibole and brownish-green clinopyroxene have been found occasionally. The crystal-rich, Type B pumices - and the pumices in the early air-fall units - seem to have a somewhat higher mafic phenocryst contents (6-15 vol.%) than the crystal-poor, Type A pumices (1-10 vol.%). Phenocryst proportions roughly correlate with those of the ignimbrite matrix.

Table 4.4. Modal proportions of phenocrysts in the Pokai Ignimbrite pumice as vol.%. Rno = reference number for samples analysed by XRF (listed in Appendix D, Table D.2); S = sample number; T = pumice type.

Rno	S	T	Plag	Prx	FeTi	Qz	Am	Zr	Ap	Tit
135	70e/1	A	84.7	7.9	7.1	-	-	0.3	tr	-
38	26A/1	A	95.3	3.6	1.1	tr	-	-	-	-
39	26A/2	A	91.2	5.1	1.1	2.6	tr	tr	-	-
179	132/1	A	93.0	5.3	1.7	tr	-	tr	-	-
180	132/2	A	92.5	4.4	0.5	2.6	-	tr	-	-
218	T2/1	A	92.7	0.9	6.4	-	-	-	-	-
219	T2/2	A	80.2	6.7	3.4	9.7	tr	-	tr	-
229	T19/3	A	86.9	4.8	2.3	5.9	tr	0.1	-	-
227	T19/1	B	88.5	9.2	2.0	tr	-	0.3	tr	-
147	97/3	B	85.1	8.3	4.1	2.1	-	tr	0.2	0.2

Plag = plagioclase
Prx = ortho- and/or clinopyroxene (clinopyroxene however rare)
FeTi = Fe-Ti oxides (magnetite and ilmenite)
Qz = quartz
Am = amphibole
Zr = zircon
Ap = apatite
Tit = titanite

tr = trace amounts

70e/1 = Galaxy Road, air-fall unit C
26A/1 & 2 = Harry Johnson Road
132/1 & 2 = Haunui Valley
T2/1 & 2 = Tapapa Valley, near base
T19/3 = Tapapa Valley, near top
T19/1 = Tapapa Valley, near top
97/3 = Barron Road

The crystal content in the pumice clasts is usually lower than that in the ignimbrite matrix suggesting that some elutriation of shards as fine ash occurred during the emplacement of the ignimbrite. A notable feature is that at any particular horizon or flow unit pumice blocks of either Type A or Type B predominate, there are usually a few clasts of the other type present as well.

4.2.2. Mineralogy and glass chemistry

Plagioclase

Plagioclase occurs as euhedral to subhedral, often fractured phenocrysts, sometimes containing inclusions of glass, Fe-Ti oxides and apatite needles (Fig.4.7). Glomeroporphyritic aggregates with orthopyroxene and Fe-Ti oxides are common. Most of the plagioclase crystals are 0.5-2 mm long, are often strongly zoned and show varying degrees of resorption, i.e. rounded crystal corners. Most of these crystals have relatively homogeneous cores. Tiny sub- to anhedral, resorbed plagioclase microphenocrysts commonly appear in the ignimbrite matrix and occasionally in the pumice.

The composition of plagioclase phenocrysts ranges from oligoclase to andesine (An_{22}-An_{44}). Microprobe analyses of plagioclase from representative samples are given in Table 4.5 and are plotted on the system An-Ab-Or in Figure 4.8. Both normally and reversely zoned crystals occur.

Geothermometric calculations have been made to estimate the range of temperatures over which plagioclase crystallised from the melt. The plagioclase liquidus geothermometer developed by Kudo and Weill (1970), with improvements by Mathez (1973), was

Figure 4.7. Pokai Ignimbrite showing an euhedral plagioclase phenocryst with slightly rounded, resorbed crystal corners and mineral/glass inclusions. Pl = plagioclase; Mt = magnetite/ilmenite; Gl = glass inclusions. Magnification 16x. Plane polarized light.

Figure 4.9. Pokai Ignimbrite showing two strongly resorbed orthopyroxene phenocrysts. Opx = orthopyroxene; Mt = magnetite/ilmenite; Pl = plagioclase. Magnification 12x. Plane polarized light.

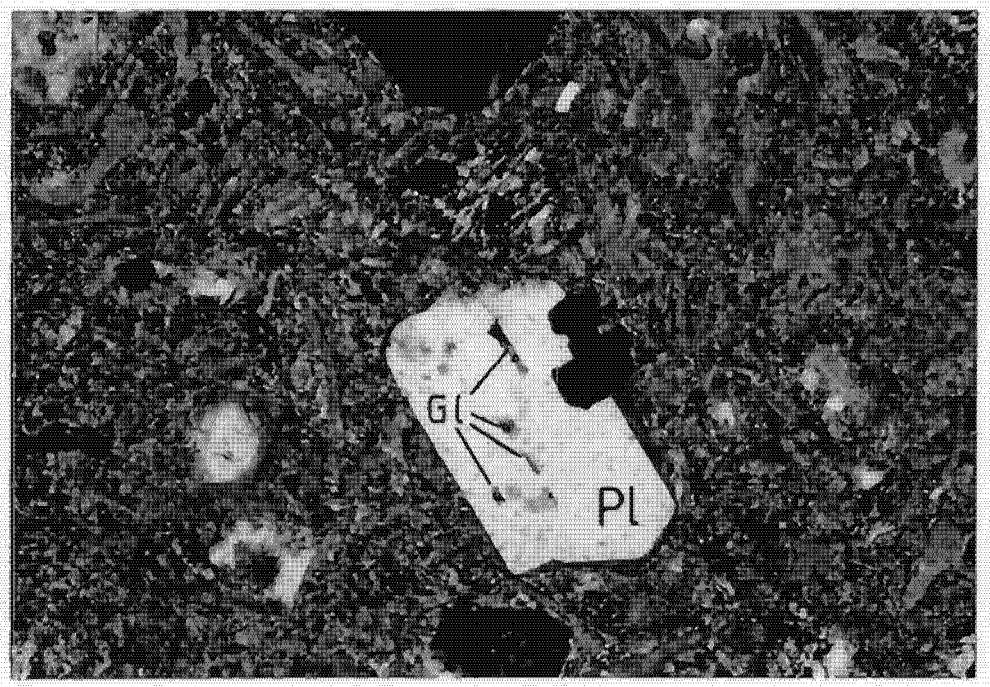
Gl
Pl

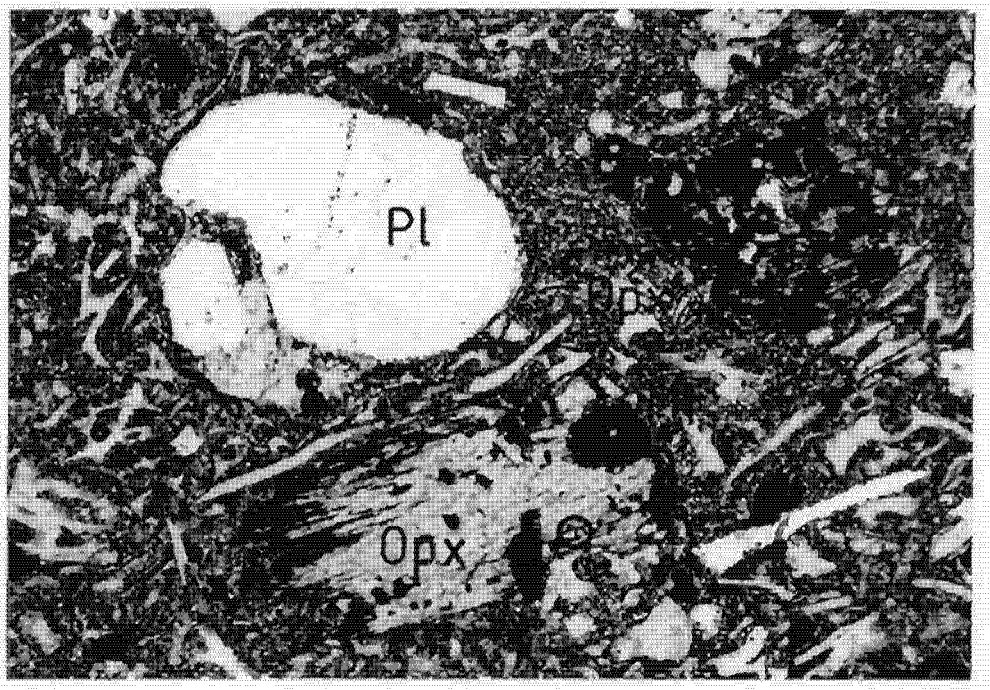
Pl
Opx
Opx

Table 4.5. Representative microprobe analyses of plagioclase phenocrysts from Pokai Ignimbrite pumice. Analysis # = analysis numbers for plagioclase microprobe analyses, listed in Appendix C, Table C.1. r = plagioclase rim, c = core. Total iron as FeO_t.

Analysis #	15 (r)	14 (c)	82 (r)	83 (c)	122 (r)
SiO_2	62.19	59.11	62.78	64.29	63.23
TiO_2	-	-	-	-	-
Al_2O_3	22.97	25.01	22.77	22.08	22.24
FeO_t	0.24	0.29	0.18	0.20	0.21
MnO	-	-	-	-	-
MgO	-	-	-	-	-
CaO	6.13	8.45	5.64	4.82	5.10
Na_2O	7.98	6.85	8.05	7.91	8.69
K_2O	0.49	0.30	0.58	0.70	0.54
Ab	68.3	58.5	69.7	71.7	73.3
An	29.0	39.8	27.0	24.2	23.7
Or	2.8	1.7	3.3	4.2	3.0

Analysis #	123 (c)	43	60 (r)	59 (c)	27
SiO_2	62.85	61.69	62.01	60.54	63.64
TiO_2	-	0.03	-	-	-
Al_2O_3	22.42	23.47	23.48	24.03	22.40
FeO_t	0.26	0.21	0.20	0.29	0.14
MnO	-	-	-	-	-
MgO	-	-	-	-	-
CaO	5.45	7.08	6.01	7.34	5.27
Na_2O	7.49	7.12	7.87	7.45	7.95
K_2O	0.53	0.39	0.44	0.33	0.60
Ab	71.7	63.1	68.6	63.5	70.6
An	25.4	34.7	28.9	34.6	25.8
Or	2.9	2.3	2.5	1.9	3.5

15 & 14: host pumice 26A/2 (Type A, ref.no. 39)
82 & 83: host pumice 132/2 (Type A, ref.no. 180)
122 & 123: host pumice T19/1 (Type B, ref.no. 227)
43: host pumice 70e/1 (Type A, ref.no. 135), air-fall unit C
60 & 59: host pumice 108/1 (Type B, ref.no. 153)
27: host pumice 66/1 (Type A, ref.no. 128)

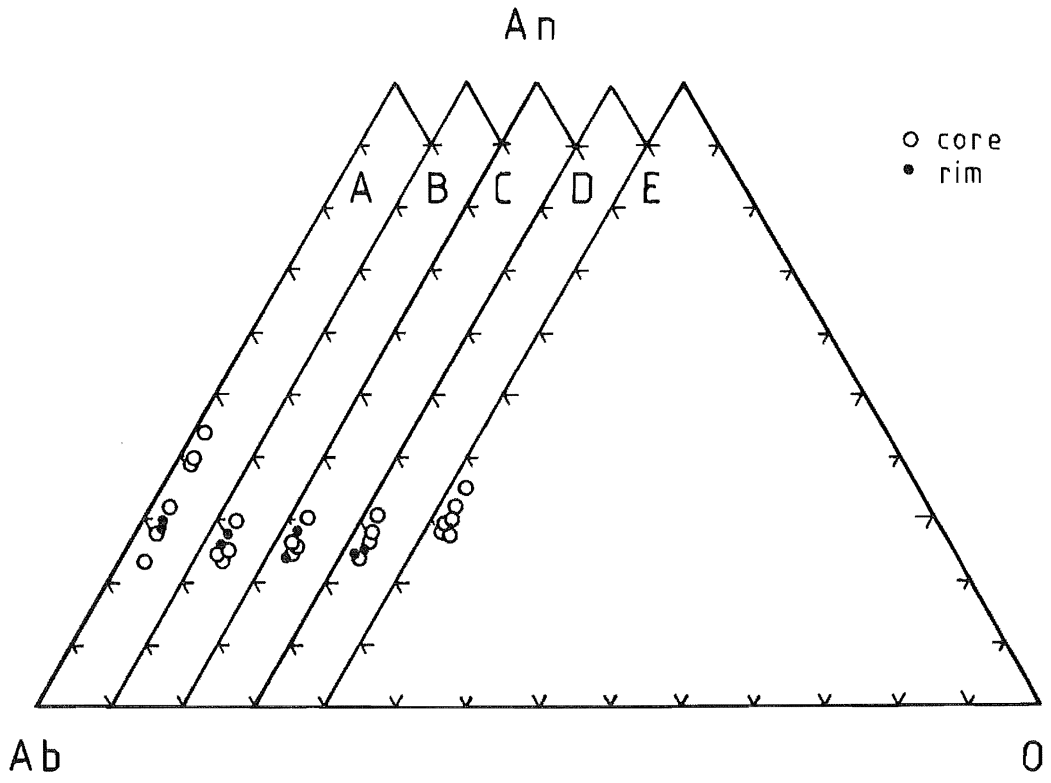

Figure 4.8. Representative plagioclase compositions from the Pokai Ignimbrite pumices from microprobe data plotted on the Ab-An-Or system.

A. Plagioclase phenocryst cores and rims, 26A/2 (ref.no. 39), Harry Johnson Road.

B. Plagioclase phenocryst cores and rims, 132/2 (ref.no. 180), Haunui Valley.

C. Plagioclase phenocryst cores and rims, T19/1 (ref.no. 227), Tapapa Valley.

D. Plagioclase phenocryst cores and rims, 85/1 (ref.no. 136), Mohina Road.

E. Plagioclase phenocryst cores, 70e/1 (ref.no. 135), air-fall unit C, Galaxy Road.

Table 4.6. Whole rock analyses (recalculated to 100 % anhydrous) for Table 4.5 plagioclase host pumices and corresponding temperature estimates at 0, 0.5 and 1 kb total pressures using plagioclase liquidus geothermometer (based on the method of Kudo & Weill 1971, with refinements by Mathez 1973). Total iron as FeO_t.

	1	2	3	4	5	6
SiO_2	74.90	75.58	72.04	75.58	73.58	76.23
TiO_2	0.18	0.11	0.34	0.22	0.29	0.16
Al_2O_3	14.51	14.15	15.78	13.48	13.62	12.89
FeO_t	1.81	1.64	2.48	2.08	2.31	1.80
MnO	0.05	0.04	0.08	0.07	0.07	0.05
MgO	0.17	0.12	0.24	0.17	0.41	0.17
CaO	0.99	0.78	1.51	1.10	1.50	1.09
Na_2O	4.00	3.86	4.25	3.83	4.78	3.76
K_2O	3.39	3.69	3.21	3.47	3.41	3.83
P_2O_5	0.01	0.02	0.07	0.01	0.03	0.01

P H_2O	15 (r)	14 (c)	82 (r)	83 (c)	122 (r)
0 kb	715°C	830°C	708°C	649°C	652°C
0.5 kb	784°C	794°C	800°C	830°C	782°C
1 kb	910°C	1024°C	912°C	868°C	828°C

P H_2O	123 (c)	43	60 (r)	59 (c)	27
0 kb	682°C	696°C	634°C	699°C	740°C
0.5 kb	765°C	815°C	850°C	805°C	908°C
1 kb	855°C	906°C	814°C	900°C	772°C

1 = 26A/2 (Type A; ref.no. 39) for plagioclase analyses 15 and 14
2 = 132/2 (Type A; ref.no. 180) for plagioclase analyses 82 and 83
3 = T19/1 (Type B; ref.no. 227) for plagioclase analyses 122 and 123
4 = 70e/1 (Type A; ref.no. 135), air-fall unit C, for plagioclase analysis 43
5 = 108/1 (Type B; ref.no. 153) for plagioclase analyses 60 and 59
6 = 66/1 (Type A; ref.no. 128) for plagioclase analysis 27

used at a range of P H_2O values of 0, 0.5 and 1 kb. Results for representative samples are shown in Table 4.6, and for all samples in Appendix C, Table C.6.

Calculations give a wide range of crystallisation temperatures from different samples (765-908°C at 0.5 kb), but vary also between different plagioclase crystals within the same pumice (758-931°C at 0.5 kb; analyses 119 and 117, Table C.6). Table 4.7. shows the mean plagioclase An-content and crystallisation temperatures with standard deviations from different localities. There is no clear trend between the stratigraphy and the crystallisation temperatures; the plagioclase composition does not vary regularly from site to site. This together with the strong zoning and resorbed features indicates a plagioclase-melt disequilibrium. The occurrence of reversely zoned plagioclase phenocrysts suggests that the crystals may have circulated within the magma chamber.

Orthopyroxene

Bright green orthopyroxene is found in all samples examined. It occurs as euhedral, 0.4-1.2 mm long prisms, commonly with inclusions of Fe-Ti oxides, apatite needles and sometimes zircon. Glass inclusions are occasionally found. Many of the crystals are broken or fractured and resorption is common (Fig.4.9).

All pyroxene crystals for which probe data are available are low-Ca orthopyroxenes (enstatite-ferrosilite using the nomenclature of Morimoto et al. 1988). Most of the pyroxenes are ferrosilites, ranging from En_{30}-En_{49}. A few pyroxenes with enstatite composition were found in the Pokai Ignimbrite fall deposits, En_{59}-En_{63}, and in the crystal-rich, Type B pumices,

Table 4.7. Mean An compositions and equilibrium temperatures of plagioclase phenocrysts analysed from Pokai pumices. Rno = reference number for samples analysed by XRF (listed in Appendix D, Tables D.2 and D.3); S = sample number; T = pumice type; Locality = sample locality; No = number of plagioclase analyses included in mean; An = mean An composition; STD = standard deviation; 0, 0.5 & 1 kb = mean equilibrium temperatures at 0, 0.5 & 1 kb, respectively.

Rno	S	T	Locality	No	An	STD
38	**26A/1**	A	Harry Johnson Road	10	33.2	7.3
39	**26A/2**	A	Harry Johnson Road	9	32.6	6.9
100	**HJ7/1**	A	Chamois Road	3	26.3	3.4
128	**66/1**	A	Chamois Road	10	30.5	2.9
132	**70/3**	A	Galaxy Road air-fall unit A	5	25.9	2.3
135	**70e/1**	A	Galaxy Road air-fall unit C	6	30.6	2.5
136	**85/1**	A	Mohina Road	8	25.9	2.1
162	**126/1**	A	Harry Johnson Road	7	24.3	2.4
179	**132/1**	A	Haunui Valley	7	30.4	2.2
180	**132/2**	A	Haunui Valley	6	26.1	1.8
181	**132/3**	A	Haunui Valley	8	29.2	3.2
210	**153/1**	A	Cormorant Road	3	28.9	1.2
218	**T2/1**	A	Tapapa Valley	17	32.0	3.7
219	**T2/2**	A	Tapapa Valley	6	26.4	8.2
229	**T19/3**	A	Tapapa Valley	5	18.8	1.3
147	**97/3**	B	Barron Road	7	28.1	6.0
153	**108/1**	B	McCracken Road	7	30.0	3.0
227	**T19/1**	B	Tapapa Valley	8	26.4	1.9

Table 4.7. cont.

Rno	S	0 kb	STD	0.5 kb	STD	1 kb	STD
38	**26A/1**	755°C	80	789°C	33	942°C	79
39	**26A/2**	751°C	75	795°C	33	943°C	79
100	**HJ7/1**	680°C	49	878°C	23	815°C	53
128	**66/1**	687°	37	880°C	18	794°C	57
132	**70/3**	696°C	36	784°C	29	889°C	31
135	**70e/1**	654°C	30	847°C	19	843°C	41
136	**85/1**	842°C	18	822°C	28	1012°C	20
162	**126/1**	674°C	23	834°C	22	867°C	47
179	**132/1**	746°C	25	740°C	21	931°C	25
180	**132/2**	688°C	33	809°C	21	897°C	26
181	**132/3**	659°C	44	839°C	25	860°C	58
210	**153/1**	738°C	15	754°C	17	928°C	15
218	**T2/1**	662°C	41	845°C	32	840°C	59
219	**T2/2**	758°C	34	889°C	65	816°C	110
229	**T19/3**	709°C	16	884°C	9	744°C	26
147	**97/3**	655°C	77	787°C	72	825°C	86
153	**108/1**	661°C	21	841°C	22	827°C	51
227	**T19/1**	695°C	26	752°C	25	868°C	25

En_{50}-En_{55}. The air-fall pumice (70e/1, ref.no. 135) shows the widest compositional variation (En_{33}-En_{63}).

Microprobe analyses of orthopyroxenes from representative samples are given in Table 4.8 and are plotted on the pyroxene quadrilateral in Figure 4.10. Mg number ranges from 32-63 (Table 4.8). Compositions of the rim and core of six unbroken orthopyroxene grains were determined to detect any possible zoning. The compositions of the rim and core vary greatly, from 3-13 % En, cores always having higher En-contents than the rims (Fig.4.10).

Some of the individual pumice samples show a wide variation in their pyroxene compositions, and bimodal phenocryst populations are not uncommon. Figure 4.11 shows the variation of Fe# (Fe+Mn)/Fe+Mn+Mg) (atomic) for all of the samples; note the especially large variation in the air-fall pumice sample 70e/1 (ref.no. 135). The compositions from phenocryst rims always have a higher Fe# number than that of the cores, indicating a removal of the crystals to more basic compositions or a change of the liquid composition to more basic in composition.

Clinopyroxene.

Small (<0.4 mm) brown-green pyroxene grains have been detected in some pumice samples. The colour, form, cleavage and the oblique extinction angle suggest these mineral to be clinopyroxenes (possibly augites), rather than orthopyroxenes. No microprobe analyses could be made because of the small size and very low abundance of these minerals.

Table 4.8. Representative microprobe analyses of orthopyroxene phenocrysts from Pokai Ignimbrite pumice. Analysis # = analysis numbers for orthopyroxene microprobe analyses, listed in Appendix C, Table C.2. r = orthopyroxene rim, c = core. Total iron as FeO_t.

Analysis #	6 (r)	5 (c)	50 (r)	51 (c)	75 (r)
SiO_2	48.90	50.27	48.29	48.86	50.91
TiO_2	0.14	0.11	0.09	0.07	0.26
Al_2O_3	0.22	0.32	0.19	0.25	0.97
FeO_t	37.22	30.16	37.99	36.63	27.72
MnO	1.66	2.22	1.96	1.62	1.63
MgO	10.73	15.78	10.26	11.36	17.09
CaO	1.14	1.13	1.21	1.21	1.33
Na_2O	-	-	-	-	0.09
K_2O	-	-	-	-	-
Mg #	34.0	48.3	32.5	35.6	52.4

Analysis #	74 (c)	40 (r)	39 (c)	19	22
SiO_2	51.33	50.25	50.34	51.05	53.54
TiO_2	0.11	0.10	0.11	0.15	0.17
Al_2O_3	0.39	0.25	0.37	0.42	1.03
FeO_t	27.21	31.32	30.41	31.60	21.92
MnO	1.49	1.95	1.78	1.59	0.50
MgO	18.40	15.01	15.74	13.84	21.21
CaO	0.98	1.12	1.26	1.31	1.58
Na_2O	0.09	-	-	0.04	0.06
K_2O	-	-	-	-	-
Mg #	54.6	46.1	48.0	43.9	63.3

6 & 5: host pumice 26A/2 (Type A; ref.no. 39)
50 & 51: host pumice 132/2 (Type A; ref.no. 180)
75 & 74: host pumice T19/1 (Type B; ref.no. 227)
40 & 39: host pumice 108/1 (Type B; ref.no. 153)
19 & 22: host pumice 70e/1 (Type A; ref.no. 135), air-fall unit C

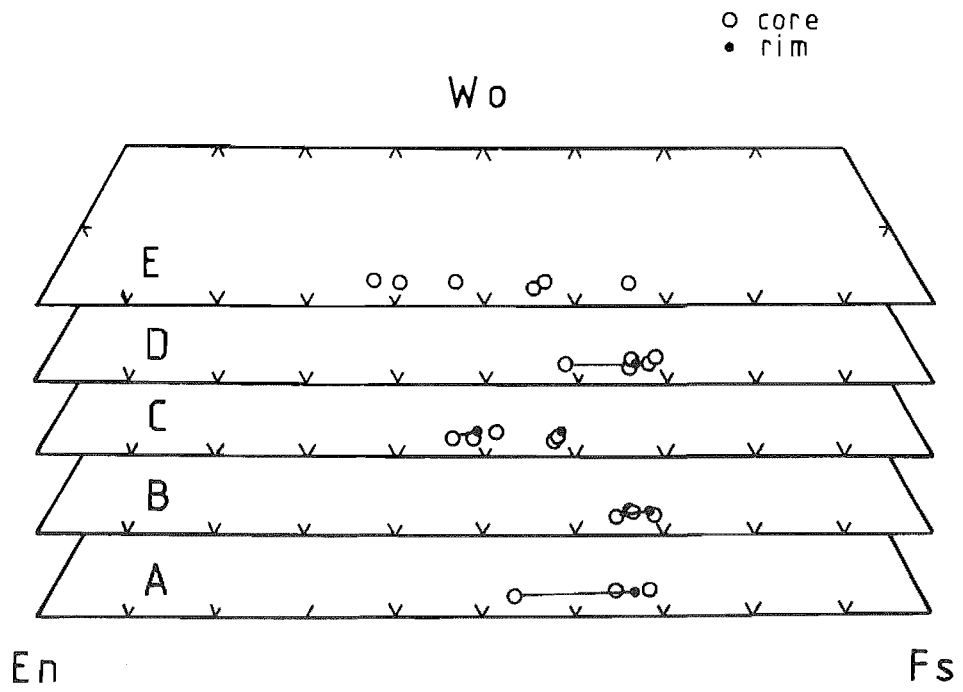

Figure 4.10. Representative orthopyroxene compositions from the Pokai Ignibmrite pumices from microprobe data plotted on the pyroxene quadrilateral.

A. Orthopyroxene phenocryst cores and rim, 26A/2 (ref.no. 39), Harry Johnson Road.

B. Orthopyroxene phenocryst cores and rim, 132/2 (ref.no.180), Haunui Valley.

C. Orthopyroxene phenocryst cores and rims, T19/1 (ref.no. 227), Tapapa Valley.

D. Orthopyroxene phenocryst cores and rim, 85/1 (ref.no. 136), Mohina Road.

E. Orthopyroxene phenocryst cores, 70e/1 (ref.no. 135), air-fall unit C, Galaxy Road.

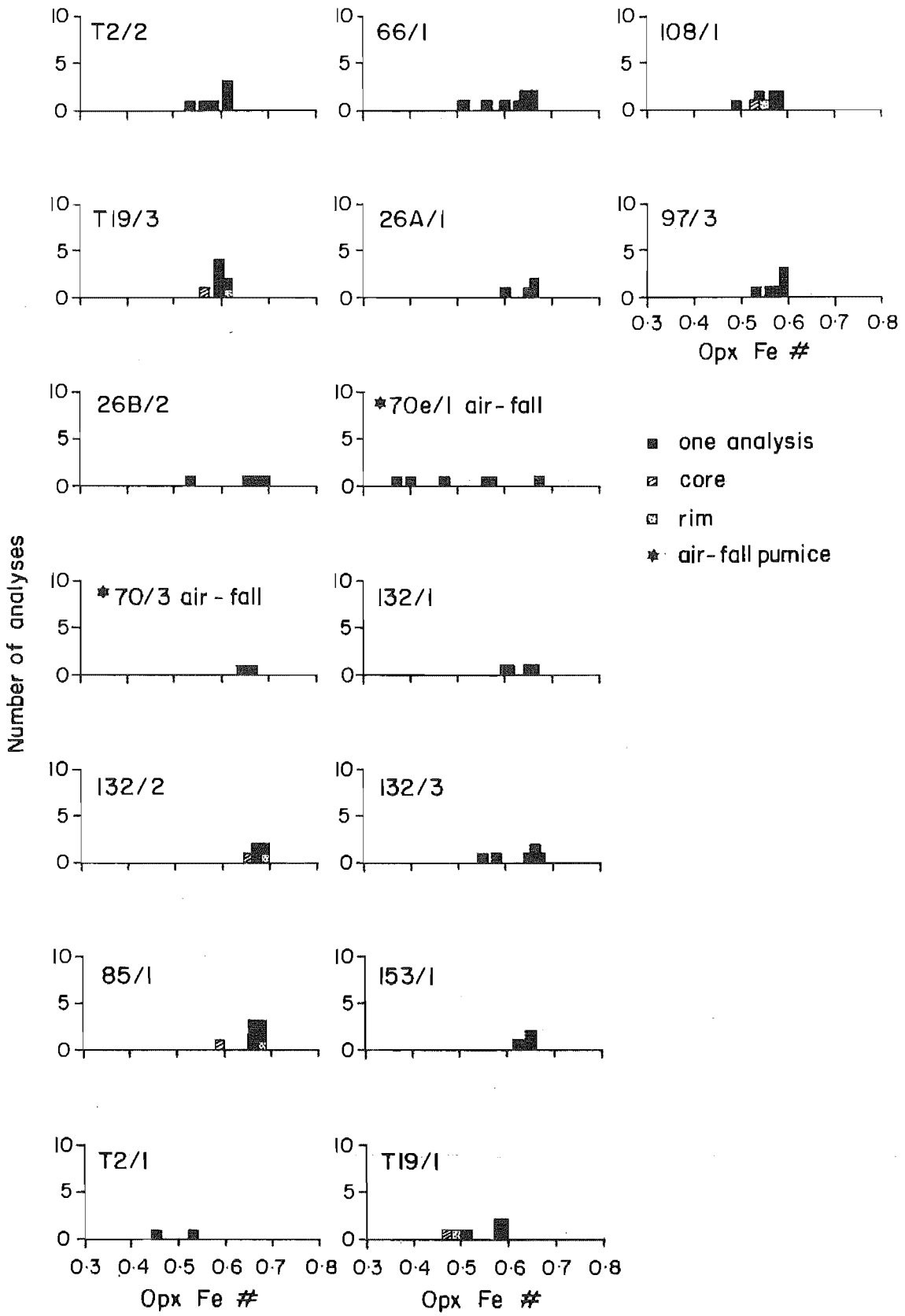

Figure 4.11. Frequency distributions of the compositions of orthopyroxene phenocrysts plotted as Fe# (Fe+Mn)/(Fe+Mn+Mg) (atomic) from Pokai Ignimbrite pumices. Numbers on each histogram are sample numbers.

Fe-Ti oxides

Titanomagnetite, which usually occurs as 0.1-0.2 mm octahedral grains, is the predominant opaque mineral. It commonly occurs as discrete phenocrysts, and as inclusions in pyroxene and occasionally plagioclase (see Figs.4.7 & 4.9). Titanomagnetite inclusions always display perfect octahedral form. Rare inclusions of titanite have been found in some titanomagnetite grains.

Ilmenite is present in 15 of the 18 analysed Pokai Ignimbrite probe samples and is much less abundant than titanomagnetite. Ilmenite occurs as stubby, usually euhedral 0.1 mm grains often as inclusions or attached to the orthopyroxenes. Microprobe analyses of titanomagnetite and ilmenite from representative samples are given in Table 4.9.

In most cases mineral textures (euhedral grain boundaries, no exsolution features) indicate that titanomagnetite and ilmenite were in equilibrium with the liquid. Titanomagnetite-ilmenite pairs were used to estimate Fe-Ti oxide crystallisation temperatures [based on the geothermometer of Buddington and Lindsley (1964) with refinements by Andersen and Lindsley (1985)]. Representative values are given in Table 4.9 and all data is plotted on a Fe-Ti oxide temperature versus fO_2 diagram in Figure 4.12. The temperature estimates range between 740-1030°C with corresponding oxygen fugacity, log(10) fO_2 from -14.4 to -10.6 (Fig.4.12). Several samples contain polymodal phenocryst populations - giving a temperature range within one sample of 240°C. This indicates that some of these phenocrysts were not in equilibrium with their surrounding liquid at the time of

Table 4.9. Representative microprobe analyses of titanomagnetites and ilmenites from the Pokai Ignimbrite pumice and temperature estimates using titanomagnetite-ilmenite pairs (based on the method of Buddington and Lindsley 1964, with refinements by Andersen and Lindsley 1985). An.# = analysis numbers for titanomagnetite (tm) and ilmenite (il) microprobe analyses, listed in Appendix C, Tables C.3 and C.4, respectively. Total iron as FeO_t.

An.#	tm 10	il 1	tm 42	il 15	tm 50	il 24
SiO_2	0.11	0.02	0.09	0.03	0.07	-
TiO_2	13.79	49.24	11.78	48.79	7.16	48.21
Al_2O_3	1.06	0.08	1.11	0.07	1.07	0.06
FeO_t	83.80	48.64	85.80	49.29	90.72	49.25
MnO	0.87	1.15	0.92	1.17	0.63	1.53
MgO	0.34	0.86	0.28	0.65	0.34	0.94
CaO	0.03	0.01	-	-	-	-
Na_2O	-	-	-	-	-	-
K_2O	-	-	-	-	-	-
Temp.	792°C		780°C		740°C	
Log(10)fO_2	-14.4		-14.4		-14.5	

An. #	tm 56	il 26	tm 21	il 5	tm 46	il 18
SiO_2	0.05	-	0.05	0.03	0.03	0.09
TiO_2	19.72	47.48	16.05	48.86	23.42	48.55
Al_2O_3	0.86	0.06	1.15	0.07	0.91	0.05
FeO_t	77.48	49.98	81.46	49.02	74.13	49.26
MnO	1.20	1.34	0.87	1.18	0.95	1.22
MgO	0.55	1.02	0.37	0.79	0.56	0.80
CaO	-	-	0.02	-	-	0.03
Na_2O	0.14	0.11	0.03	0.05	-	-
K_2O	-	-	-	-	-	-
Temp	979°C		839°C		1030°C	
Log(10)fO_2	-10.8		-13.5		-10.6	

10 & 1: host pumice 26A/2 (Type A, ref.no. 39)
42 & 15: host pumice 132/2 (Type A, ref.no. 180)
50 & 24: host pumice T2/2 (Type A, ref.no. 219)
56 & 26: host pumice T19/1 (Type B, ref.no. 227)
21 & 5: host pumice 70e/1 (Type A, ref.no. 153), air-fall unit C
46 & 18: host pumice 132/3 (Type A, ref.no. 181)

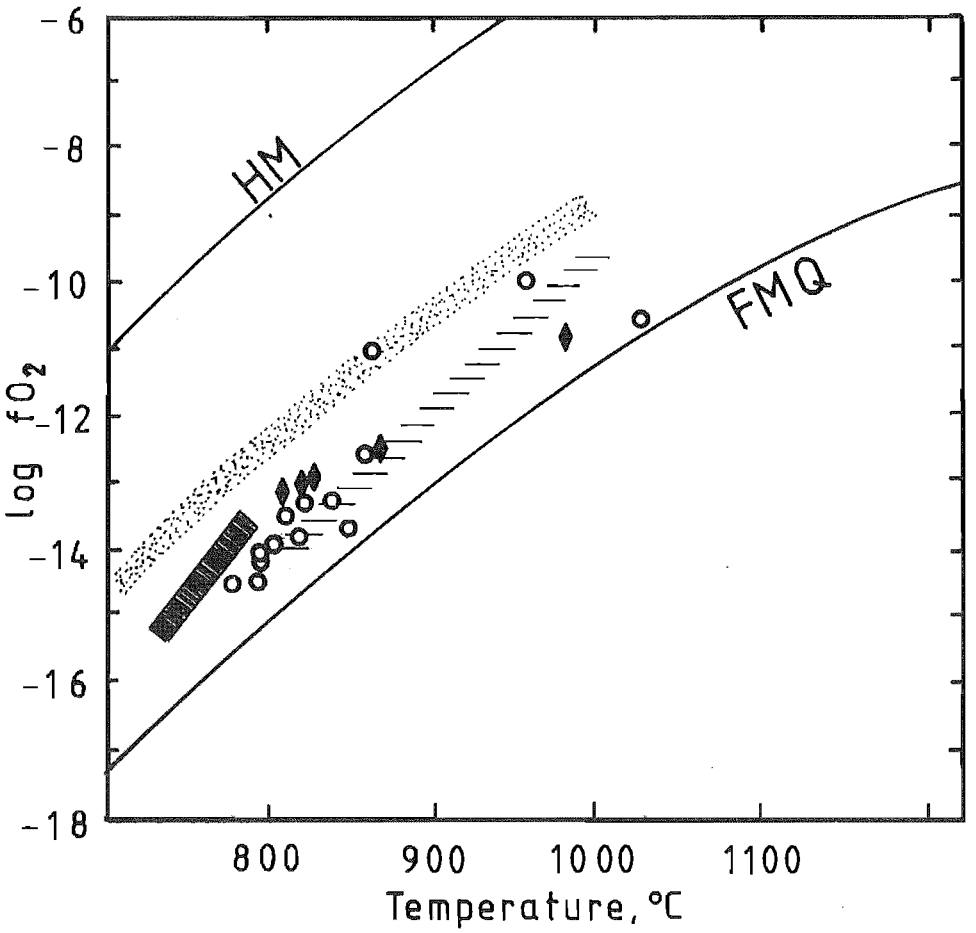

Figure 4.12. Fe-Ti oxide equilibrium temperatures and oxygen fugacities (log fO_2) from coexisting titanomagnetite-ilmenite analyses of Pokai Ignimbrite pumices (calculated by the method of Buddington and Lindsley, 1964, with refinements by Andersen and Lindsley, 1985). Stippled line = temperature and fO_2 trend in biotite- and/or amphibole-bearing silicic lavas; thick line = temperature and fO_2 trend in amphibole- and orthopyroxene-bearing silicic lavas; dashed line = temperature and fO_2 trend in orthopyroxene-bearing silicic lavas; HM = Hæmatite-Magnetite buffer line; FMQ = Fayalite-Magnetite-Quartz buffer line (Carmichael et al., 1974).

o = data from Type A pumices
♦ = data from Type B pumices

the eruption. fO_2 is slightly greater in the crystal-rich, Type B samples.

The calculated average equilibrium temperature (850°C) is higher than the average for most TVZ acid magmas (760°C, Ewart et al. 1971; note that most of Ewart et al.'s data represent analyses of rhyolitic lavas). However, the range of temperatures and fO_2 of the Pokai ignimbrite data coincide with that of other orthopyroxene-bearing silicic volcanic rocks (dashed line in Fig.4.12), above the FMQ buffer curve indicating that the solid phases buffered fO_2. The modal mineralogy also shows that orthopyroxene is the dominant mafic mineral. Two analyses which lie at the biotite and/or amphibole buffer line contain occasional amphibole phenocrysts.

Carmichael et al. (1974) have used a geothermometer to compare the respective temperatures determined from plagioclase and Fe-Ti oxides. Because zoning is commonly found in plagioclase and is usually absent in the Fe-Ti oxides, the response time to changing temperature of the plagioclase thermometer is likely to be much longer than that of the Fe-Ti oxides (Carmichael et al. 1974). Since the plagioclases are often zoned, temperatures of both the cores and rims of the plagioclase crystals have been calculated. Comparative values are shown in Figure 4.13. The best fit correlation between the Fe-Ti oxide and the plagioclase temperatures is seen at conditions indicating 0.5 kb water pressure. This suggests that the crystallisation started at water pressures below 1 kb but not under completely dry conditions.

Figure 4.13. Plagioclase geothermometer temperatures for the cores (●) and rims (o) of plagioclase phenocrysts plotted against the coexisting Fe-Ti oxide equilibration temperatures. The plagioclase results have been calculated assuming three sets of conditions: dry, 0.5 and 1 kb water pressure. The dashed line in each diagram indicates the locus of correspondence between the two methods of temperature estimates (Carmichael et al., 1974).

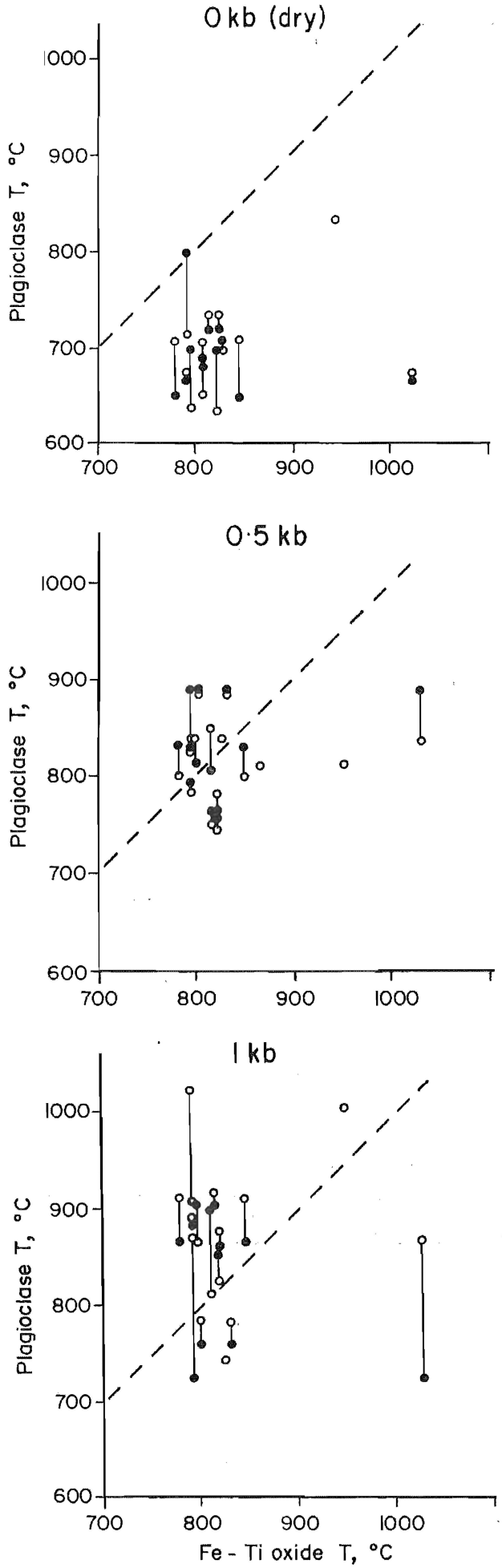
0 kb (dry)
0·5 kb
1 kb
Plagioclase T, °C
Fe - Ti oxide T, °C
600
700
800
900
1000

Quartz

Quartz occurs as euhedral, bipyramidal grains up to 2.2 mm long. Many quartz crystals are broken, and often slightly resorbed with rounded crystal corners. No glass inclusions were found.

Amphibole

Amphibole occurs only in trace amounts in the Pokai Ignimbrite. It occurs as euhedral, prismatic crystals, up to 0.8 mm long, which are often broken or fractured. In thin section, the crystals are strongly pleochroic from pale to dark green, indicating a hornblende composition. Resorption is indicated by rounded crystal margins. Due to the small size of the crystals and small amounts present, no microprobe analyses were made.

Glass chemistry

Glass from pumice samples was also analysed by microprobe. All glass analyses have been plotted in a SiO_2-K_2O variation diagram (Fig.4.14) and a comparison of representative analyses from three locations are given in Table 4.10. The glasses have a very high silica content, 78.5-80.7 vol.% (anhydrous). Uncorrected totals average 96.7 % (STD 1.4), indicating an average water content of 3.3 % H_2O. During the microprobe analysis only mineral standards were available, which probably accounts for the exceptionally high values of SiO_2 and low values in Al_2O_3, Na_2O and K_2O.[7]. Thus microprobe glass and XRF whole rock analyses are not directly comparable.

[7] Alkali elements also migrate away from the probe beam causing low Na_2O and K_2O and high SiO_2 values, and the electron beam destroys the glass structure during analysis, so results are not as reliable as for mineral analyses.

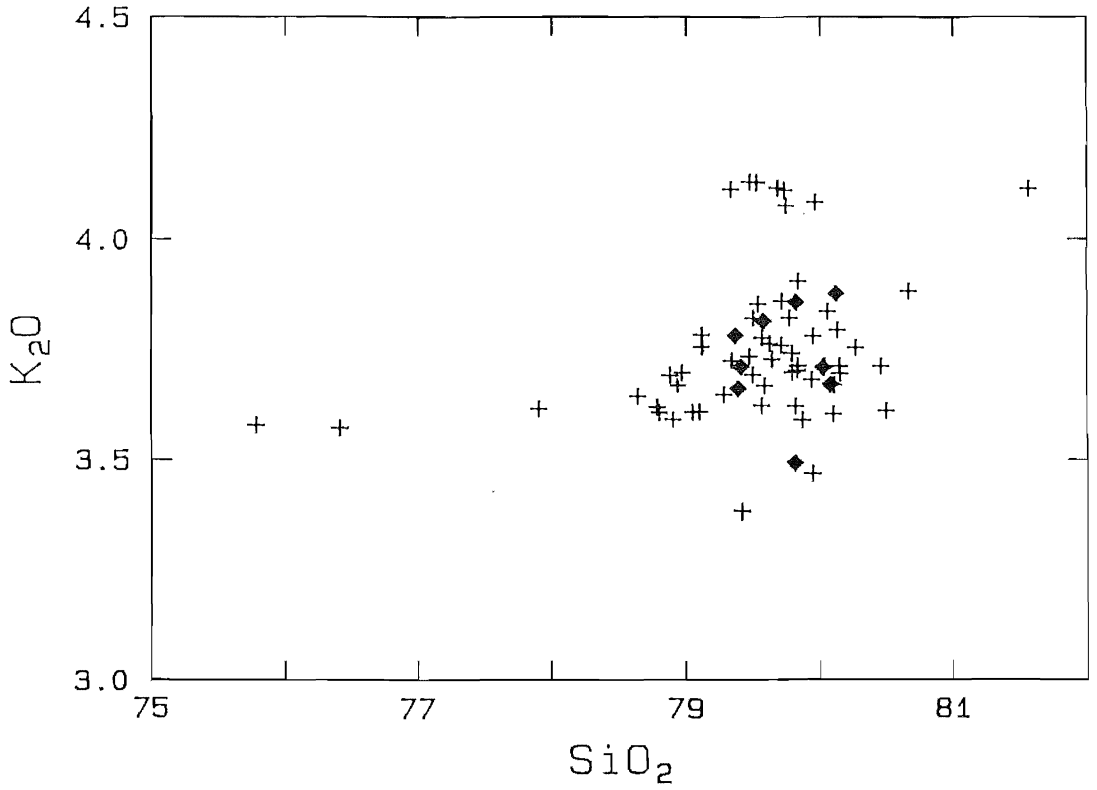

Figure 4.14. K_2O vs SiO_2 for the Pokai Ignimbrite pumice glasses from: + = Type A pumices, and ♦ = Type B pumices.

Table 4.10. Representative microprobe analyses of volcanic glass from three Pokai Ignimbrite pumice: (a) 26A/2 (Type A pumice; ref.no. 39), (b) 126/1 (Type A pumice; ref.no. 162), and (c) T19/1 (Type B pumice; ref.no. 227). An. # = analysis numbers for microprobe glass analyses listed in Appendix C, Table C.6. The data has been recalculated to 100 % anhydrous; Total = hydrous totals. Total iron as FeO_t.

Table 4.10.a.

An. #	2	3	4	5	6	Mean	STD
SiO_2	79.34	79.62	79.56	79.50	79.82	79.57	0.17
TiO_2	0.11	0.09	0.10	0.11	0.10	0.11	0.01
Al_2O_3	11.41	11.40	11.33	11.34	11.56	11.41	0.09
FeO_t	1.38	1.23	1.25	1.26	1.16	1.26	0.08
MnO	0.02	0.02	0.09	-	-	0.04	0.04
MgO	0.06	0.04	0.06	0.05	0.05	0.05	0.01
CaO	0.81	0.80	0.80	0.80	0.76	0.80	0.02
Na_2O	3.14	3.03	3.03	3.12	2.93	3.05	0.08
K_2O	3.72	3.76	3.78	3.82	3.62	3.74	0.08
Total	96.96	97.01	97.72	97.11	96.38	-	-

Table 4.10.b.

An. #	25	26	27	28	Mean	STD
SiO_2	80.13	80.14	79.83	75.78	78.97	2.13
TiO_2	0.09	0.08	0.08	0.08	0.08	0.00
Al_2O_3	11.20	11.33	11.29	16.08	12.48	2.40
FeO_t	0.99	1.02	1.03	0.85	0.97	0.08
MnO	0.05	0.03	-	-	0.04	0.02
MgO	0.04	0.04	0.04	0.04	0.04	0.00
CaO	0.62	0.65	0.67	0.64	0.64	0.02
Na_2O	3.08	3.00	3.15	2.94	3.04	0.09
K_2O	3.79	3.71	3.90	3.58	3.75	0.13
Total	95.71	91.36	94.51	96.38	-	-

Table 4.10.c.

An. #	59	60	61	62	Mean	STD
SiO_2	80.02	79.57	79.37	80.12	79.77	0.36
TiO_2	0.16	0.12	0.11	0.12	0.13	0.02
Al_2O_3	11.43	11.51	11.53	11.37	11.46	0.07
FeO_t	0.70	0.80	1.09	0.41	0.75	0.28
MnO	-	-	0.03	0.02	0.03	0.01
MgO	0.04	0.04	0.04	0.02	0.04	0.01
CaO	0.79	0.70	0.68	0.60	0.69	0.08
Na_2O	3.15	3.43	3.37	3.46	3.35	0.14
K_2O	3.71	3.81	3.78	3.88	3.79	0.07
Total	96.55	97.27	96.54	97.01	-	-

The glass analyses are relatively homogeneous and the glass compositions from Type A and Type B pumices are generally indistinguishable. However, three of the pumice samples contained a significant range in glass composition (Fig.4.14, note analyses with lower SiO_2). Glass analyses of several samples also show a range in FeO_t of ≥0.5 wt.% (Table 4.10, sample T19/1; see also Appendix C, Table C.5).

4.3. Chimp Ignimbrite

4.3.1. Petrography

Matrix.

The Chimp Ignimbrite is broadly similar in appearance to the Pokai Ignimbrite except it has lower modal pumice and is typically very crystal-poor. Most Chimp Ignimbrite outrops expose/ display only a 2-4 m thick section of non-welded ignimbrite, in which the matrix glass is relatively well preserved. Shards have cuspate and/or fibrous forms with tubular pore space. Only three outcrops of welded Chimp Ignimbrite have been found. In the welded ignimbrite a strong distortion and compression of the glass shards is evident (Fig.4.15). Some of the shards have preserved their cuspate or fibrous form, but have been strongly devitrified displaying axiolitic structure (Fig.4.16).

The ignimbrite is made of transparent, yellowish glass shards and vitric dust mixed with pumice, phenocrysts and lithics. The proportions are 65-75 vol.% glass shards, 16-30 vol.% pumice clasts and 3-6 vol.% phenocrysts (Table 4.11). Lithic content is usually low (<2 vol.%, excluding the lithic-rich segregation bodies).

Figure 4.15. Welded Chimp Ignimbrite displaying yellowish glassy matrix (mtx) composed of distorted glass shards, pumice fragments (pum), phenocrysts (Pl = plagioclase) and lithics (Li). Magnification 10x. Plane polarized light.

Figure 4.16. Strongly welded Chimp Ignimbrite matrix showing devitrified glass shards with axiolitic structure. Magnification 40x. Plane polarized light.

Figure 4.17. Welded Chimp Ignimbrite pumice with deformed glass shards and elongated vesicles (all nearly destroyed). Magnification 40x. Plane polarized light.

mix
Pl
Pl

Table 4.11. Modal proportions of Chimp Ignimbrite constituents from selected flow unit samples as vol.%. Point-counted from thin sections to approx. 1200 points. S = sample number.

S	Mtx glass	Pumice	Lithics	Phenocrysts
89/II	74.3	21.4	0.4	3.9
116a	75.8	16.8	1.6	5.8
116b	72.6	21.7	1.5	4.2

89II = Cabbage Tree Road, welded ignimbrite
116a = Downer Road, ca. 16-18 m above the base, welded ignimbrite
116b = Downer Road, ca. 16-18 m above the base, welded ignimbrite

Table 4.12. Modal proportions of phenocrysts in the Chimp Ignimbrite matrix as vol.%. S = sample number.

S	Plag	Opx	Fe-Ti	Cpx	Amph	Zr
89/II	86.2	7.4	6.4	tr	tr	-
116a	82.8	10.3	6.9	tr	tr	tr
116b	85.8	7.1	7.1	-	tr	-

Plag = plagioclase
Opx = orthopyroxene
Fe-Ti = Fe-Ti oxides
Cpx = clinopyroxene
Amph = amphibole
Zr = zircon

89/II = Cabbage Tree Road, welded ignimbrite
116a = Downer Road, ca. 16-18 m above the base, welded ignimbrite
116b = Downer Road, ca. 16-18 m above the base, welded ignimbrite

Table 4.13. Modal proportions of glass and phenocrysts from Chimp Ignimbrite pumice. Vesicularity is given separately for each sample. Values as vol.%. Rno = reference number for samples analysed by XRF (listed in Appendix D, Tables D.2 and D.8); S = sample number; T = pumice type: A = crystal-poor, B = crystal-rich.

Rno	S	T	Glass	Phenocrysts	Vesicularity
233	**11C/1**	**A**	97.7	2.3	55.5
236	**33/1**	**A**	99.8	0.2	45.9
-	**37 pum a**	**A**	100	tr	40.9
-	**37 pum b**	**B**	92.0	8.0	37.4

11C/1 = Te Whetu, 0.5 m above base, non-welded
33/1 = Pokai Road, ca. 2 m below top, total thickness unknown, non-welded
37 pum a = Panda Road, non-welded
37 pum b = Panda Road, non-welded

Plagioclase is the dominant phenocryst phase and makes up ca. 85 vol.% of crystals within the matrix (Table 4.12). Orthopyroxene and Fe-Ti oxides are more abundant than in the Pokai Ignimbrite, typically between 7-10 vol.% and 6-7 vol.%, respectively (cf: Pokai Ignimbrite: 0.6-8 and 2-4 vol.%, respectively). Amphibole, clinopyroxene, quartz and biotite are less abundant, and zircon, apatite and titanite occur in trace amounts.

Pumice.

In the non-welded Chimp Ignimbrite the pumice texture is very similar to that of the Pokai Ignimbrite; spherical to ellipsoidal vesicles with unbroken or only slightly distorted glassy vesicle walls. Vesicularity varies from 35-55 vol.% (Table 4.13). In the welded Chimp Ignimbrite pumice the glass shards are strongly deformed (Fig.4.17), and vitroclastic texture is partly destroyed. The degree of devitrification is somewhat higher than in the Pokai Ignimbrite.

Two types of pumice occur in the Chimp Ignimbrite (see chapter 3.1). Type A pumice has a very low abundance of phenocrysts, (<2 vol.%), whereas type B pumice has a phenocryst content of up to 8 vol.% phenocrysts (Table 4.13). Plagioclase is the dominant phenocryst making >95 vol.% of phenocrysts in type A pumice (Table 4.14). Orthopyroxene and Fe-Ti oxides occur in small amounts up to 2-3 vol.%, with trace amounts of amphibole, clinopyroxene, biotite and quartz. Type B pumice contains approximately 82 vol.% plagioclase, 10 vol.% orthopyroxene, 4 vol.% Fe-Ti oxides, 2 vol.% clinopyroxene and 2 vol.% amphibole (Table 4.14). Both pumice types contain trace amounts of zircon, apatite and titanite.

Table 4.14. Modal proportions of phenocrysts in Chimp Ignimbrite pumice as vol.%. Rno = reference number for samples analysed by XRF (listed in Appendix D, Tables D.2 and D.8); S = sample number.

Rno	S	Plag	Opx	F-T	Qz	Cpx	Amp	Zr	Apt	B
236	33/1	96.3	3.7	tr	-	-	-	-	-	tr
239	33/4	96.4	tr	1.8	-	1.3	0.5	-	-	-
253	146/1	99.6	tr	0.4	tr	-	-	-	-	-
249	93/1	81.6	11.9	4.4	-	1.4	0.6	tr	0.1	-

Plag = plagioclase
Opx = orthopyroxene
F-T = Fe-Ti oxides
Qz = quartz
Cpx = clinopyroxene
Amp = amphibole
Zr = zircon
Apt = apatite
B = biotite

33/1 (Type A) = Pokai Road
33/4 (Type A) = Pokai Road
146/1 (Type A) = Redwoods Road
93/1 (Type B) = Moorhouse Road

Table 4.15. Representative microprobe analyses of plagioclase phenocrysts from Chimp Ignimbrite pumice. An. # = analysis numbers for plagioclase microprobe analyses, listed in Appendix C, Table C.8. r = plagioclase rim, c = core. Total iron as FeO_t.

An. #	4 (r)	5 (c)	20 (r)	21 (c)	16 (r)	15 (c)
SiO_2	59.95	59.61	61.80	61.48	58.18	59.88
TiO_2	-	-	0.03	-	-	-
Al_2O_3	24.57	24.73	23.36	23.43	25.38	24.41
FeO_t	0.24	0.26	0.20	0.16	0.37	0.21
MnO	-	-	-	-	-	-
MgO	-	-	-	-	0.03	-
CaO	7.79	8.09	6.09	6.37	9.20	8.11
Na_2O	7.08	7.03	8.02	7.76	6.52	7.06
K_2O	0.37	0.29	0.50	0.81	0.32	0.35
Ab	60.9	60.1	68.5	65.7	55.2	60.0
An	37.0	38.2	28.7	29.8	43.1	38.1
Or	2.1	1.6	2.8	4.5	1.7	1.9

4 & 5: host pumice 33/1 (Type A; ref.no. 236)
20 & 21: host pumice 146/1 (Type A; ref.no. 253)
16 & 15: host pumice 93/1 (Type B; ref.no. 249)

4.3.2. Mineralogy and glass chemistry

Plagioclase

Plagioclase (0.5-2 mm long crystals) occurs as euhedral to subhedral phenocrysts, often with rounded crystal margins indicating resorption. Glass inclusions and tiny Fe-Ti oxide grains sometimes appear in the plagioclase cores. In the ignimbrite matrix plagioclase phenocrysts with strongly resorbed cores occur; cores have mottled appearance and are characterised by glass inclusions and patchy extinction (Fig.4.18).

Plagioclase composition varies between An_{29}-An_{43}, and is somewhat more calcic than the plagioclases in the Pokai Ignimbrite. Microprobe analyses from representative samples are given in Table 4.15 and are plotted on the An-Ab-Or diagram in Figure 4.19. Results from the plagioclase liquidus geothermometer from representative samples are shown in Table 4.16. Results from all analyses are given in Appendix C, Table C.12. A range of water pressures 0, 0.5 and 1 kB was used. The crystallisation temperatures vary from ca. 650-860°C at 0.5 kb. Table 4.17 shows the mean plagioclase An-compositions and crystallisation temperatures with standard deviations from different localities. The calculations indicate a lower equilibrium temperature for the Chimp Ignimbrite than for the Pokai Ignimbrite.

Orthopyroxene

Orthopyroxene occurs as euhedral, 0.3-1 mm long prisms, commonly with inclusions of Fe-Ti oxides. The crystal margins are usually rounded indicating resorption. Alteration to

Figure 4.18. Rounded plagioclase phenocrysts with strongly resorbed cores (partly replaced by matrix glass) in the Chimp Ignimbrite matrix. Pl = plagioclase. Magnification 40x. Polarized light.

Figure 4.20. Rounded, resorbed orthopyroxene phenocryst in the Chimp Ignimbrite matrix. Alteration along the margins and fractures to biotite and/or iddingsite. Opx = orthopyroxene; Mt = magnetite/ilmenite. Magnification 16x. Plane polarized light.

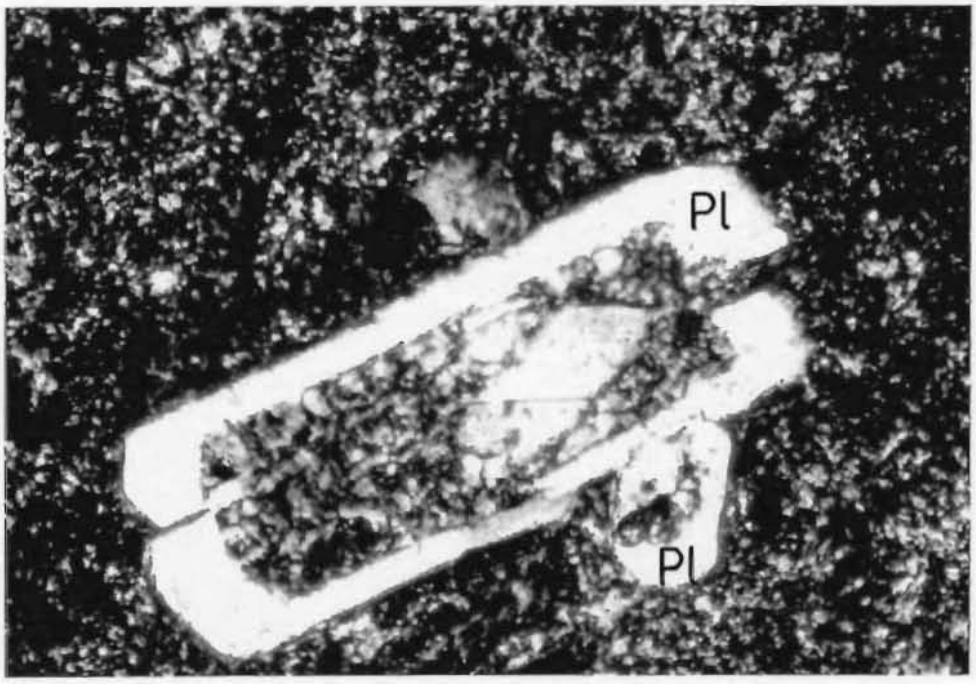
Pl
Pl

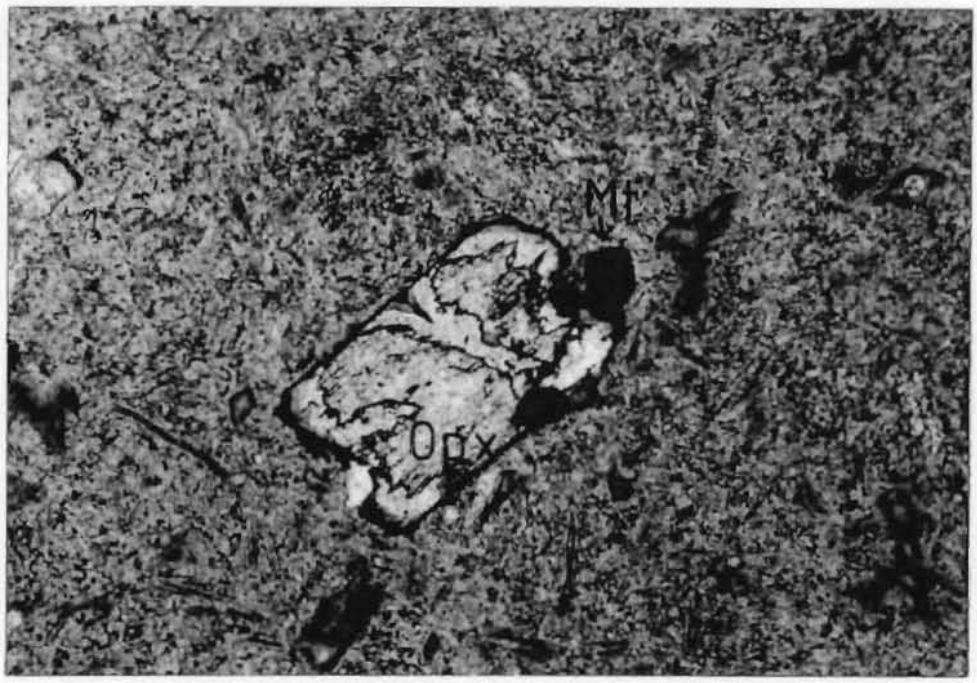
Mt
Opx

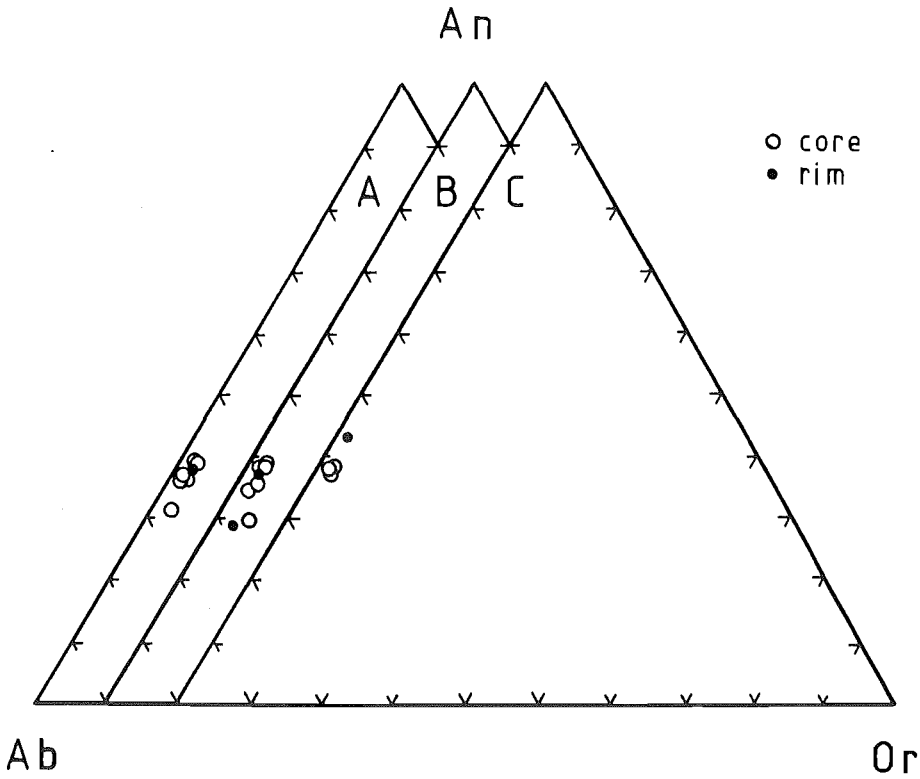

Figure 4.19. Representative plagioclase compositions from the Chimp Ignimbrite pumices from microprobe data plotted on the Ab-An-Or system.

A. Plagioclase phenocryst cores and rim, 33/1 (ref.no. 236), Pokai Road.

B. Plagioclase phenocryst cores snd rims, 146/1 (ref.no. 253), Redwoods Road.

C. Plagioclase phenocryst coes and rim, 93/1 (ref.no. 249), Moorhouse Road.

Table 4.16. Whole rock analyses for Table 4.15 plagioclase host pumices and corresponding temperature estimates at 0, 0.5 and 1 kb total water pressures using plagioclase liquidus geothermometer (based on the method of Kudo & Weill, 1970, with refinements by Mathez, 1973). Total iron as FeO_t.

	1	2	3
SiO_2	74.20	75.31	72.14
TiO_2	0.20	0.21	0.39
Al_2O_3	14.67	13.79	15.44
FeO_t	2.10	1.92	2.43
MnO	0.09	0.07	0.07
MgO	0.22	0.08	0.49
CaO	1.13	1.87	1.14
Na_2O	3.97	3.41	4.07
K_2O	3.39	4.04	3.06
P_2O_5	0.04	0.04	0.04

P H_2O	4 (r)	5 (c)	20 (r)	21 (c)	16 (r)	15 (c)
0 kb	792°C	803°C	658°C	637°C	814°C	773°C
0.5 kb	709°C	739°C	858°C	851°C	770°C	671°C
1 kb	981°C	993°C	789°C	812°C	991°C	947°C

1 = 33/1 (Type A; ref.no. 236) for plagioclase analyses 4 and 5
2 = 146/1 (Type A; ref.no. 253) for plagioclase analyses 20 and 21
3 = 93/1 (Type B; ref.no. 249) for plagioclase analyses 16 and 15

Table 4.17. Mean An compositions and mean equilibrium temperatures of plagioclase phenocrysts from the Chimp Ignibmrite pumices. Rno = reference number for samples analysed by XRF (listed in Appendix D, Tables D.2 and D.8); S = sample number; T = pumice type; Locality = sample locality; No = total number of plagioclase analyses included in mean; An = mean An composition; STD = standard deviation; 0, 0.5 & 1 kB = mean equilibrium temperature at 0, 0.5 & 1 kb water pressure, respectively.

Rno	S	T	Locality	No	An	STD
236	33/1	A	Pokai Road	10	36.8	2.1
239	33/4	A	Pokai Road	3	37.9	0.6
253	146/1	A	Redwoods Road	8	35.1	3.9
249	93/1	B	Moorhouse Road	4	39.2	2.5

Rno	S	0 kb	STD	0.5 kb	STD	1 kb	STD
236	33/1	789°C	21	721°C	28	978°C	22
239	33/4	770°C	7	727°C	14	967°C	6
253	146/1	698°C	39	806°C	34	887°C	57
249	93/1	782°C	21	692°C	53	957°C	23

Table 4.18. Microprobe analyses of orthopyroxene phenocrysts from the Chimp Ignimbrite pumice. Analysis # = analysis numbers for orthopyroxene microprobe analyses, listed in Appendix C, Table C.9. Total iron as FeO_t.

Analysis #	1	2	3
SiO_2	50.43	51.50	52.43
TiO_2	0.07	0.09	0.11
Al_2O_3	0.34	0.32	0.50
FeO_t	29.98	27.70	22.87
MnO	1.84	1.32	1.76
MgO	16.46	17.85	21.35
CaO	0.87	1.14	0.91
Na_2O	-	0.08	0.07
K_2O	-	-	-
Mg #	49.5	53.5	62.5

1: host pumice 33/1 (Type A pumice; ref.no. 236)
3 & 4: host pumice 93/1 (Type B pumice; ref.no. 249)

biotite and/or iddingsite (Shelley 1992, pers.comm.) commonly occurs around the crystal margins and along fracture zones, especially in the matrix phenocrysts (Fig.4.20).

Only two samples contained orthopyroxene large enough for microprobe analyses. These orthopyroxenes range from low-Ca enstatites to ferrosilite in composition, En_{48}-En_{61} (nomenclature of Morimoto at al.,1988). Microprobe analyses of orthopyroxene from the two samples are given in Table 4.18 and are plotted on the pyroxene quadrilateral in Figure 4.21.

Clinopyroxene.

Euhedral, prismatic, 0.8-1 mm long pyroxene crystals occur from trace amounts up to 1.4 vol.% in Chimp Ignimbrite pumice. Only one sample contained two phenocrysts large enough to be analysed by microprobe. Both pyroxenes plot as augites on the pyroxene quadrilateral (Fig.2.21). Analyses are listed in Table 4.19 with another clinopyroxene analysis from TVZ rhyolite (Waimihia rhyolite, Blake et al., 1992) for comparison.

Fe-Ti oxides

Titanomagnetite, found both as individual, 0.1-0.2 mm octahedral grains and as inclusions in orthopyroxenes, is present in all samples examined. Ilmenite was identified in only one Chimp Ignimbrite sample. Titanomagnetite and ilmenite microprobe analyses are given in Table 4.20. A temperature estimate using the titanomagnetite-ilmenite pair gives a value of 805°C with a corresponding log(10) fO_2 of -13.6.

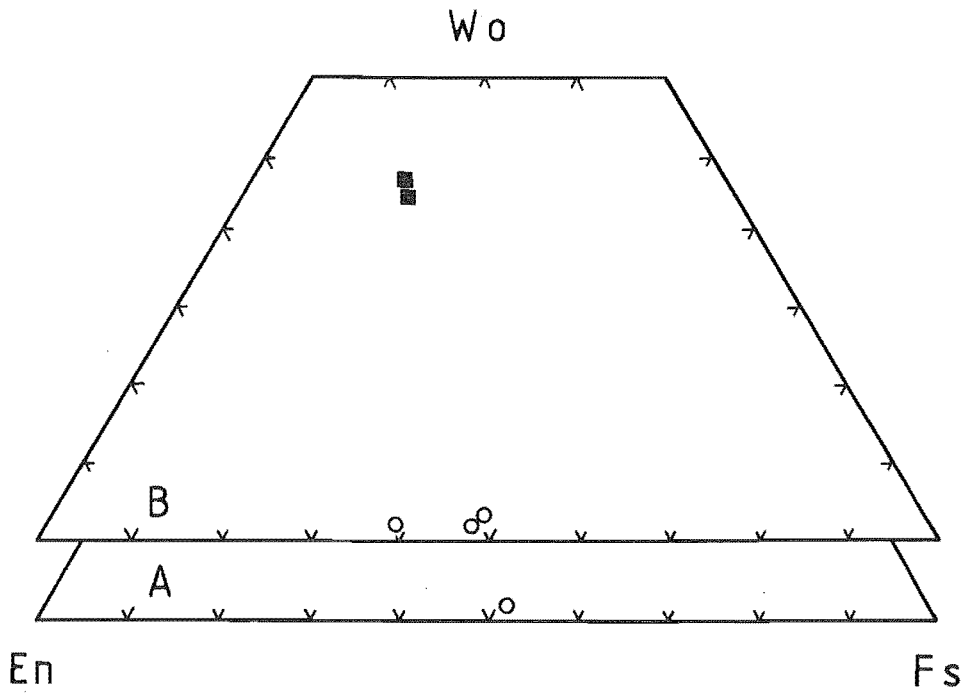

Figure 4.21. Pyroxene compositions from the Chimp Ignimbrite pumice from microprobe data plotted on the pyroxene quadrilateral.

A. Orthopyroxene phenocryst core, 33/1 (ref.no. 236), Pokai Road.

B. Ortho- (o) and clino- (■)pyroxene cores, 93/1 (ref.no. 249), Moorhouse Road.

Table 4.19. Microprobe analyses of the two pyroxene phenocrysts from Chimp Ignimbrite pumice 93/1 compared with a clinopyroxene analysis from a TVZ rhyolite. Analysis # = analysis numbers for the clinopyroxene microprobe analyses, listed in Appendix C, Table C.9. Total iron as FeO_t. The values are shown as original values.

Analysis #	1	2	Cpx
SiO_2	51.78	52.62	51.32
TiO_2	0.34	0.19	-
Al_2O_3	1.50	0.73	1.03
FeO_t	10.90	11.70	13.82
MnO	0.40	0.72	0.56
MgO	12.86	13.20	12.47
CaO	22.77	22.30	19.20
K_2O	-	-	-
Total	100.97	101.77	98.39
Mg #	67.8	66.8	61.6

1 & 2: host pumice 93/1 (Type B pumice; ref.no. 249)
Cpx = representative microprobe analysis of clinopyroxene from Waimihia rhyolite, TVZ (Blake et al. 1992: Table 2, sample 1B)

Amphibole

Small, greenish-black, primatic grains, 0.6-1.2 mm long, are occasionally found in the Chimp Ignimbrite. They occur from trace amounts up to 2.1 vol.%. Microprobe analysis was not possible because of the scarcity and small size of the crystals, however, the greenish-black colour and strong pleochroism indicate a hornblende composition.

Glass chemistry

Microprobe analyses of volcanic glass from two representative samples are given in Table 4.21. All glass analyses are plotted on a SiO_2-K_2O variation diagram in Figure 4.23. The glasses are uniform in composition with a SiO_2 content between 77.4-78.1 % (anhydrous), clearly lower than that of Pokai Ignimbrite glass. The uncorrected totals average 96.8 % (STD 0.8) indicating an average water content of 3.2 % H_2O.

Table 4.20. Microprobe analyses of titanomagnetite and ilmenite from Chimp Ignimbrite pumice and temperature estimate using the titanomagnetite-ilmenite pair (based on the method of Buddington & Lindsley 1964, with refinements by Andersen and Lindsley 1985). Analysis # = analysis numbers for titanomagnetite (tm) and ilmenite (il) microprobe analyses, listed in Appendix C, Table C.10. Total iron as FeO_t.

Analysis #	tm 9	il 1
SiO_2	0.08	0.06
TiO_2	11.66	47.64
Al_2O_3	1.56	0.09
FeO_t	85.36	48.38
MnO	0.71	1.15
MgO	0.52	1.21
CaO	0.02	0.08
Na_2O	0.07	0.14
K_2O	-	-
Temp	805°C	
Log(10)fO_2	-13.6	

9 & 1: host pumice 146/1 (Type A pumice; ref.no. 253)

Table 4.21. Representative microprobe analyses of volcanic glass from two Chimp Ignimbrite pumice: (a) 33/1 (Type A pumice; ref.no. 236), and (b) 93/1 (Type B pumice; ref.no. 249). An. # = analysis numbers for microprobe glass analyses, listed in Appendix C, Table C.11. The data has been recalculated to 100 % anhydrous; Total = hydrous totals. Total iron as FeO_t.

Table 4.21.a.

An. #	1	2	3	4	Mean	STD
SiO_2	77.92	77.93	77.85	78.12	77.96	0.12
TiO_2	0.18	0.17	0.17	0.17	0.17	0.01
Al_2O_3	12.36	12.30	12.39	12.16	12.30	0.10
FeO_t	1.63	1.56	1.68	1.71	1.65	0.07
MnO	-	0.05	0.06	-	0.03	0.03
MgO	0.14	0.13	0.13	0.13	0.13	0.00
CaO	1.16	1.17	1.15	1.16	1.16	0.01
Na_2O	2.98	3.06	2.98	3.09	3.03	0.06
K_2O	3.62	3.63	3.59	3.45	3.57	0.08
Total	97.70	96.92	96.75	96.36	-	-

Table 4.21.b.

An. #	8	9	Mean	STD
SiO_2	77.79	77.80	77.79	0.01
TiO_2	0.25	0.20	0.22	0.04
Al_2O_3	12.31	12.19	12.25	0.08
FeO_t	1.48	1.41	1.44	0.05
MnO	0.04	0.04	0.04	0.00
MgO	0.19	0.19	0.19	0.00
CaO	1.39	1.37	1.38	0.01
Na_2O	3.03	3.24	3.13	0.15
K_2O	3.53	3.57	3.55	0.03
Total	96.75	96.07	-	-

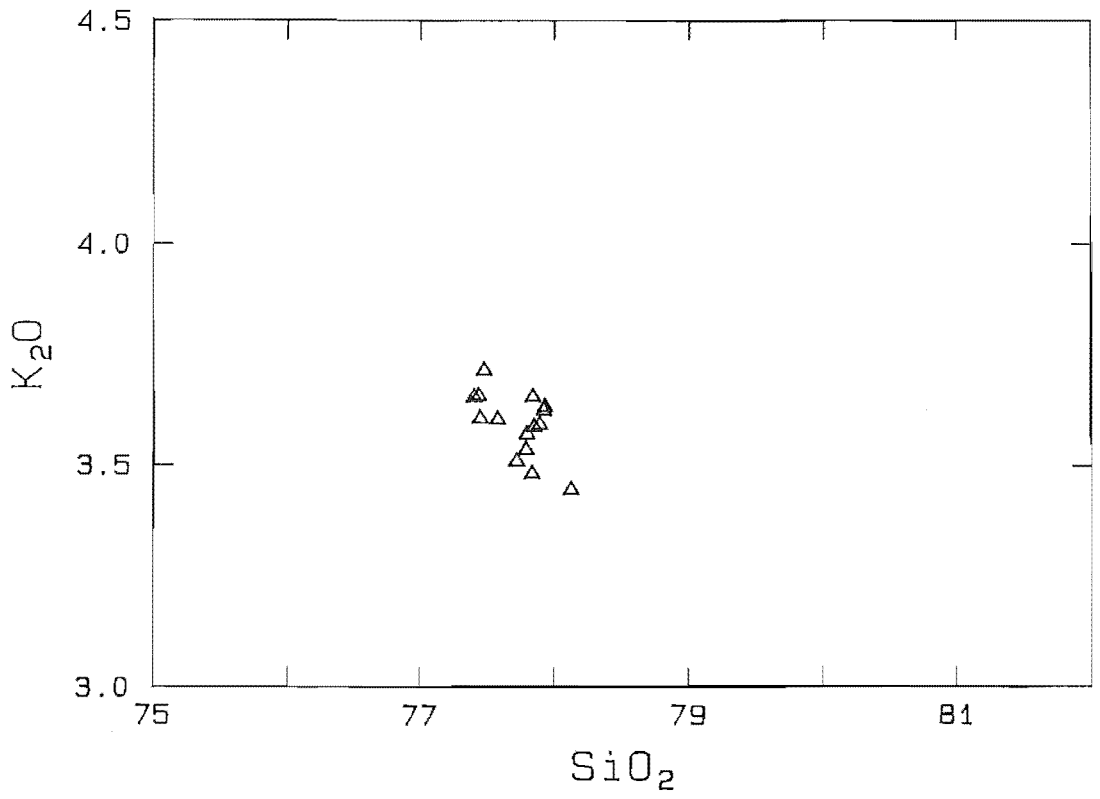

Figure 4.23. K_2O vs SiO_2 for the Chimp Ignibmrite pumice glasses.

5. GEOCHEMISTRY OF THE POKAI IGNIMBRITE

5.1. Introduction

In this chapter major and trace element data for Pokai Ignimbrite are presented. 224 XRF samples were processed for 10 major and 16 trace elements. All analyses have totals in the range 98.5-101 % for the major oxides. A further eight samples were analysed for major elements only. The data from these eight samples have been used only in plots against topographic height (see section 5.5). Except for 153b2 (ref.no.[8] 215), which is a combination of three small pumices, the analysed samples are single pumices from ignimbrite flow units and air-fall deposits. Apart from five analyses from the air-fall unit at Pokai Road (provided by S.D. Weaver, ref.nos. 63-67) all samples were prepared by the author using the method given in Appendix D.

Major and trace element analyses and CIPW norms are presented in Appendix D (Table D.3) with estimates of precision and lower limits of detection for University of Canterbury XRF analyses (Table D.1). Loss on ignition (LOI), which gives a general indication of the degree of hydrothermal alteration or weathering, is usually between 2-4 %, although samples from some of the uppermost flow units have LOI-values of 4-5 %. All analyses have been recalculated to a 100 % anhydrous basis before plotting on variation diagrams.

[8] Reference numbers for all XRF analyses are given in Appendix D, Table D.2.

5.2. General chemistry

The Pokai Ignimbrite is rhyolitic in composition, only nine analyses plot in the dacitic field on the total alkali-silica diagram (Fig.5.1.a). Most pumices are medium-K rhyolites (Fig.5.1.b). The ignimbrite is similar to other TVZ rhyolites in having a relatively high Na_2O/K_2O ratio (generally >1).

5.3. Pumice types

5.3.1. Variation between types

Two broad pumice varieties have been distinguished on the basis of their field characteristics and petrographic compositions; crystal-poor (Type A) and crystal-rich (Type B) pumices, the latter also being slightly richer in mafic minerals. In flow units where the crystal-rich pumice type predominates the ignimbrite matrix is also crystal-rich. Geochemical analyses have revealed a wide variation in the whole-pumice chemistry, SiO_2 content ranges from 68.6-77.3 wt.% and Sr from 32-186 ppm. The most notable feature is the distinct chemistry of the crystal-rich pumices, which have higher TiO_2, MgO, CaO, Zr and especially Sr contents than the crystal-poor pumices. On the basis of Sr content (Fig.5.2) the crystal-poor pumice group can be further divided into two subgroups.

Three compositional pumice types can thus be recognised:
Type 1a: high to medium SiO_2, low Sr (<70 ppm) rhyolite with low crystal content (0.5-3.5 vol.%).
Type 1b: high to low SiO_2, medium Sr (70-100 ppm) rhyolite-dacite with low crystal content (0.5-3.5 vol.%).

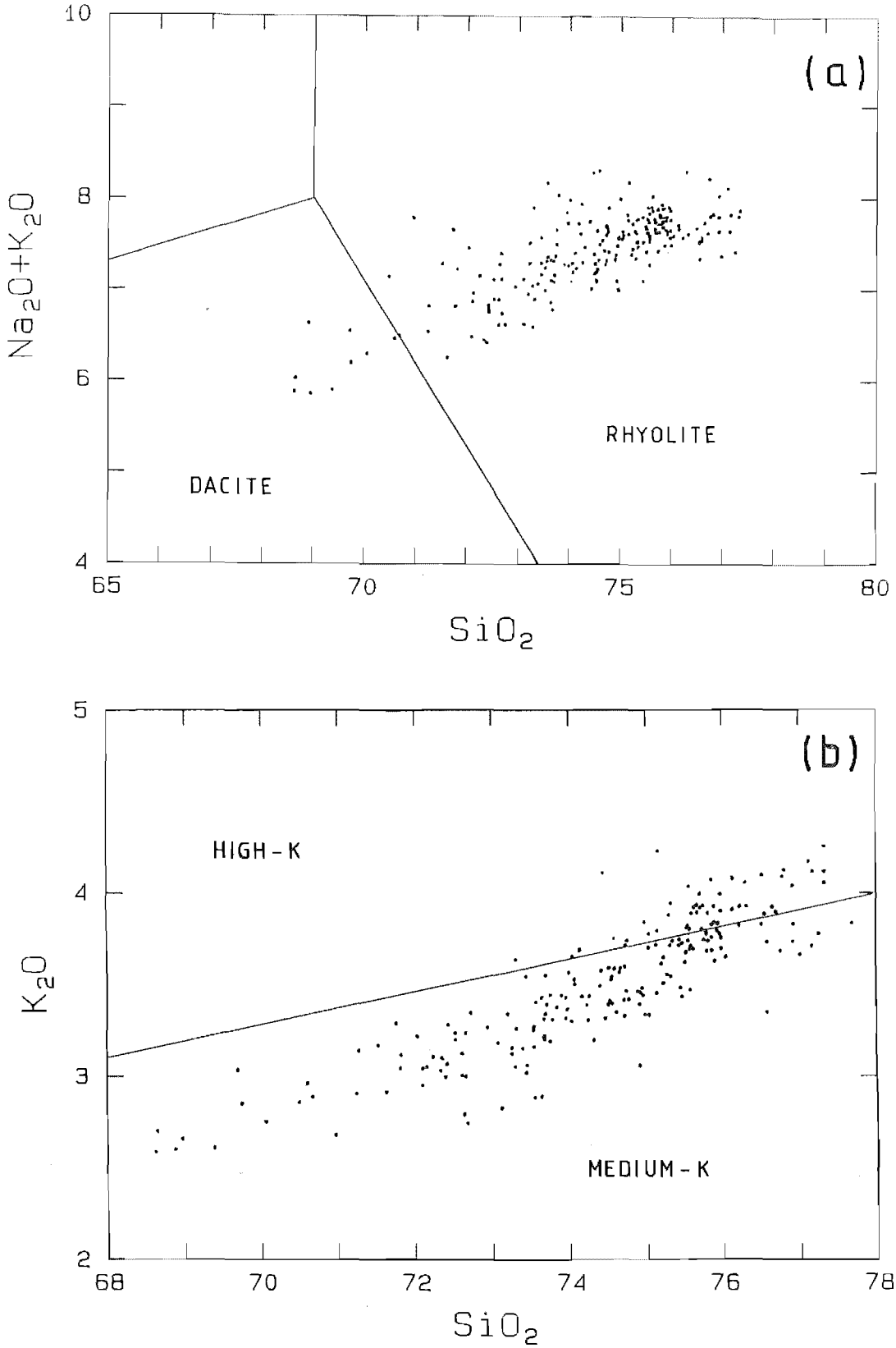

Figure 5.1. (a) Total alkali vs SiO_2, and (b) K_2O vs SiO_2 variation diagrams for the Pokai Ignimbrite. The lines defining the rhyolite - dacite and medium-K - high-K fields are from Le Maitre (1989).

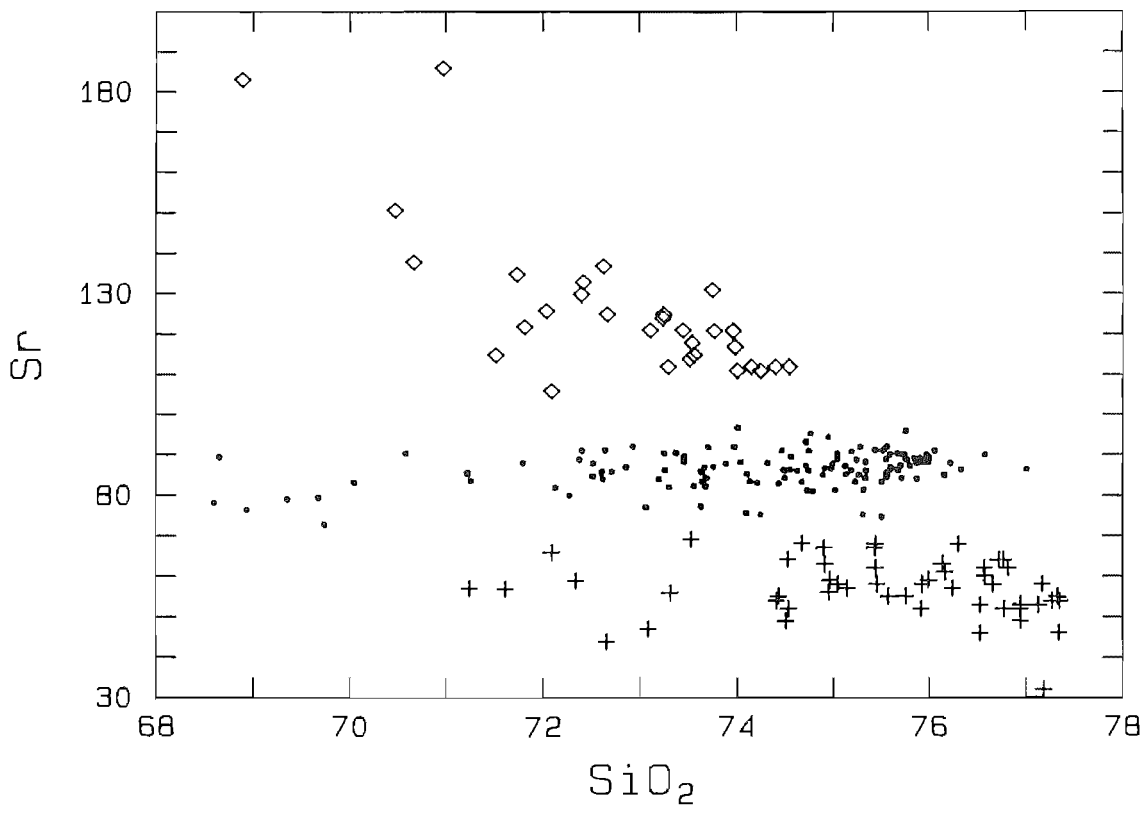

Figure 5.2. Grouping of Pokai Ignimbrite pumices defined by different Sr concentrations:

+ = Type 1a pumice (Sr <70 ppm)
● = Type 1b pumice (Sr 70-100 ppm)
◇ = Type 2 pumice (Sr >100 ppm)

Type 2: medium to low SiO_2, high Sr (>100 ppm) rhyolite-dacite with high crystal content (6-12 vol.%).

The compositional ranges, CIPW norms, means and standard deviations of the three pumice types are given in Appendix D and all analyses are plotted on variation diagrams SiO_2 vs selected major and trace elements in Figure 5.3.

Type 1a, with up to 77.35 % SiO_2, also has high Rb and relatively high K_2O contents, whereas it is low in TiO_2, FeO_t, MgO, CaO, Zr; and Sr. Type 1a is common in the basal and middle flow units at Harry Johnson and Tikorangi Roads, SW of Matahana Basin. Occasionally it occurs in the NW of the study area, at Tapapa Valley. Five out of 15 analysed air-fall pumices are of Type 1a (a list of all pumices analysed combined with the sampling locality and the compositional type is given in Appendix D, Table D.2). Type 1b shows wide chemical variation with TiO_2, FeO_t, CaO, MgO and Zr having concentrations between Types 1a and 2. Of all samples analysed 62.9 %, including seven air-fall pumices, belong to this type. Type 1b pumice predominates at Harry Johnson, Chamois, Rauna, Len, Galaxy and Pokai Roads, and in Haunui Valley and lower Tapapa Valley flow units.

Both types 1a and 1b include a number of low SiO_2, high Al_2O_3 pumices (Fig.5.3), these are also lower in K_2O, Na_2O and Rb, whereas they are slightly higher in FeO_t and Zr. This variation may be due to hydrothermal alteration, as these pumices also have high LOI values, although the feldspars appear unaltered in thin section. The low SiO_2 types predominate in the topmost flow units, especially in the western study area, at Mohina Road and at Te Whetu.

Figure 5.3. Selected major element variation diagrams for the Pokai Ignimbrite pumice. The values are in wt.%.

+ = Type 1a pumice
● = Type 1b pumice
◇ = Type 2 pumice

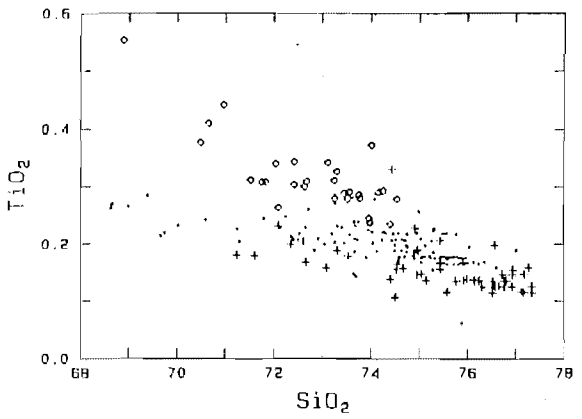
TiO2
SiO2
0.0
0.2
0.4
0.6
68
70
72
74
76
78

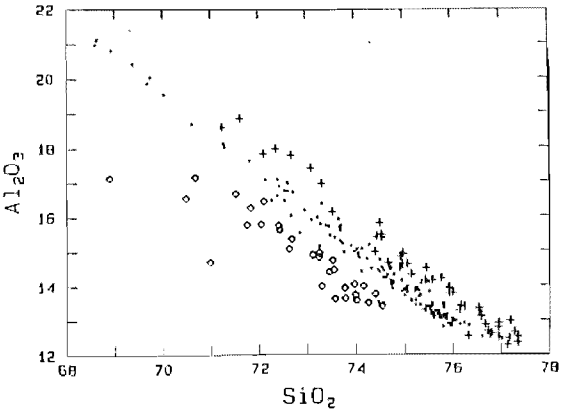
Al2O3
SiO2
12
14
16
18
20
22
68
70
72
74
76
78

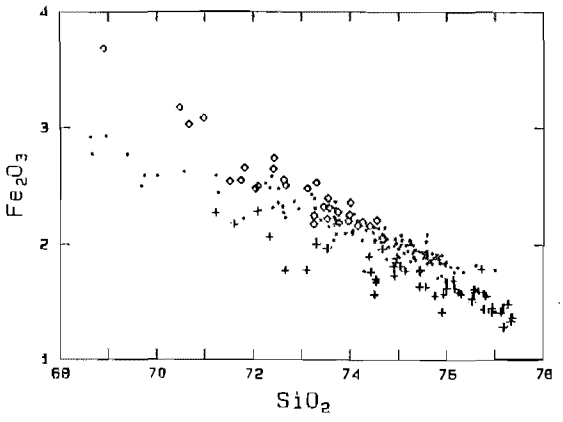
Fe2O3
SiO2
1
2
3
4
68
70
72
74
76
78

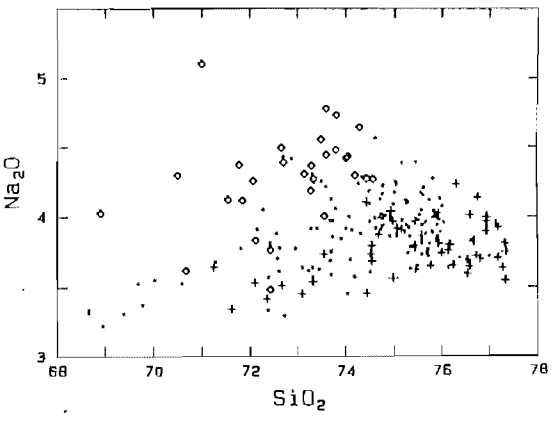
Na2O
SiO2
3
4
5
68
70
72
74
76
78

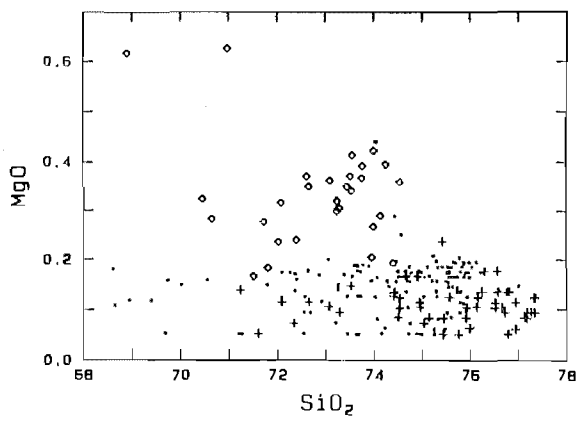
MgO
SiO2
0.0
0.2
0.4
0.6
68
70
72
74
76
78

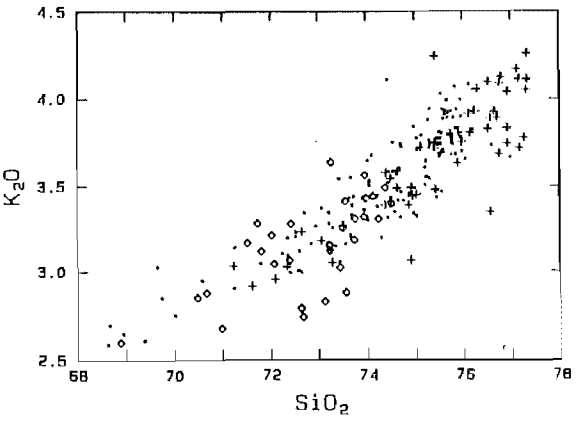
K2O
SiO2
2.5
3.0
3.5
4.0
4.5
68
70
72
74
76
78

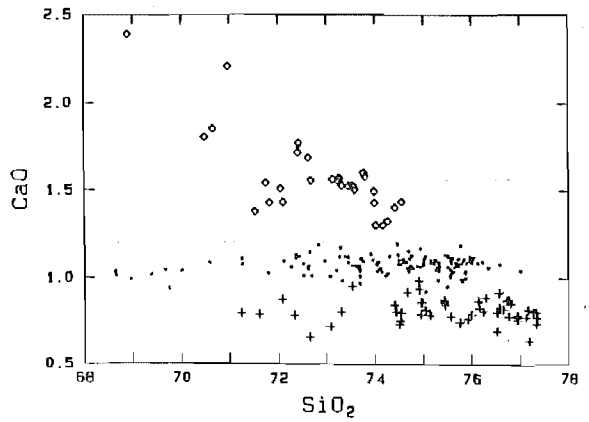
CaO
SiO2
0.5
1.0
1.5
2.0
2.5
68
70
72
74
76
78

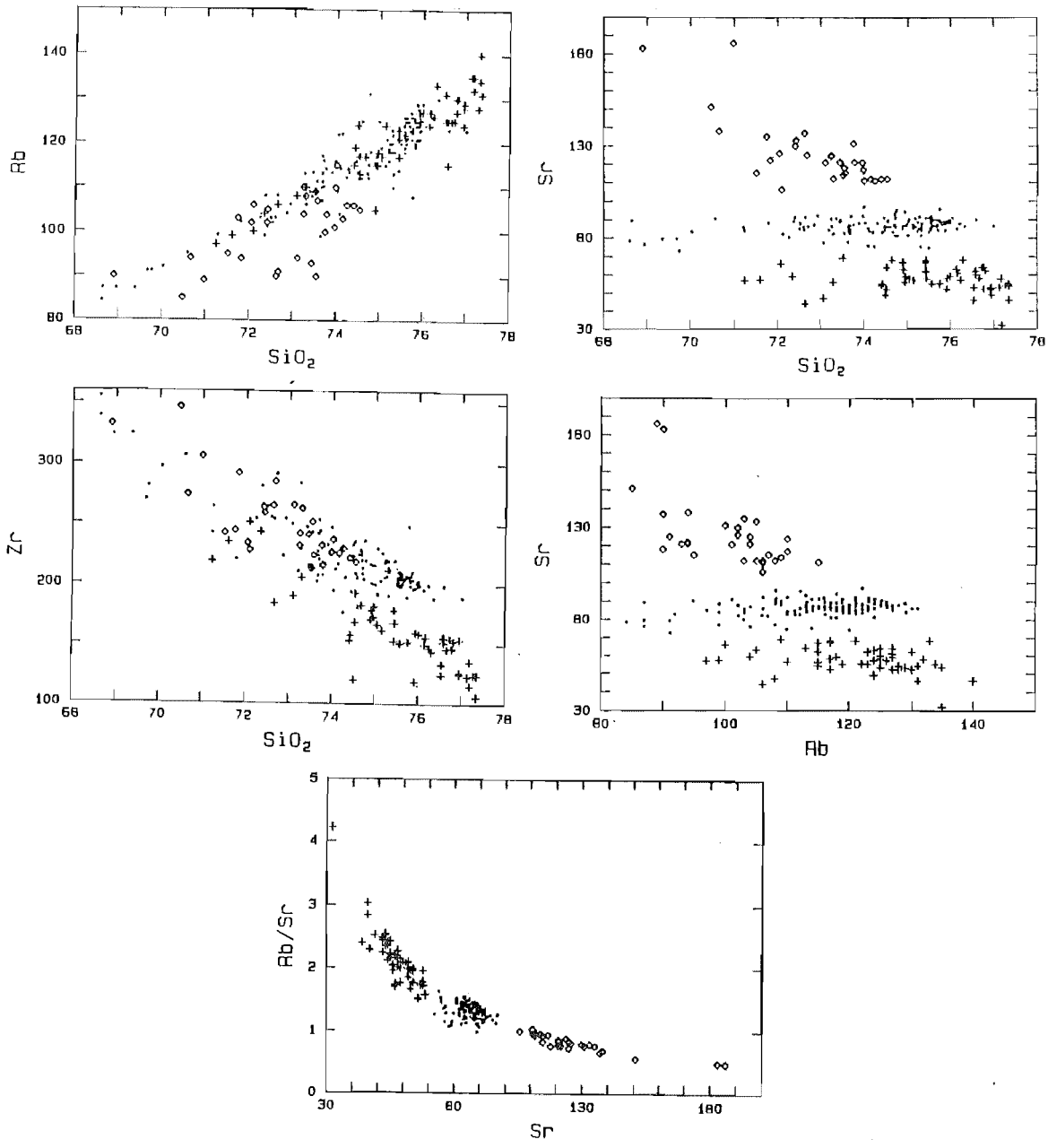

Figure 5.3. cont. Selected trace element variation diagrams for the Pokai Ignimbrite. SiO_2 in wt.%, trace element values in ppm.

+ = Type 1a pumice
● = Type 1b pumice
◇ = Type 2 pumice

Type 2 pumices are similar to the low SiO_2 Type 1b pumices with high FeO_t and Zr, and medium to low SiO_2 and low Rb contents, but differ from the other two types in having higher TiO_2, MgO, CaO, Na_2O and Sr contents. Type 2 is commonly found to the NW in Tapapa Valley and at Leslie Road and to the SW at Barron and McCracken Roads; three air-fall pumices from Glass Road are also Type 2.

5.3.2. Variation of silica and alumina within types

The Harker diagrams (Fig.5.3) reveal a wide chemical variation within the pumice types, especially in the Al_2O_3 and SiO_2 contents (in Type 1b SiO_2 ranges from 68.6-74.4 wt.% and Al_2O_3 from 12.41-21.08 wt.%). The high Al_2O_3, low SiO_2 pumices also have slightly lower Na_2O, K_2O and Rb, and higher FeO_t contents, whereas some components, such as TiO_2, CaO and Sr remain nearly constant within the pumice types. A number of these pumices, both in Types 1a and 1b, come from the uppermost part of the ignimbrite, which usually shows a much stronger red-brown colouring both in the matrix and pumices than the lower part of the ignimbrite. Though the feldspars appear unaltered, these pumices may have been secondarily altered (possibly by hydrothermal alteration and oxidation), and components such as SiO_2, K_2O and Rb have been removed, and Al_2O_3 and FeO_t correspondingly enriched.

To check whether differences within types were due to alteration (clay mineralisation), all samples with Al_2O_3 >15.00 wt.% (a total of 70 samples) were analysed by X-ray Diffraction (XRD). Two samples with low Al_2O_3 contents (13.5-14.5 wt.%) were used as reference samples. The results are

given in Appendix D (Table D.5). 40 high Al_2O_3 samples (57 %) contained kaolinite and 13 (19 %) traces of kaolinite; most of these samples were also low in SiO_2.

Post-depositional alteration (clay mineralisation) thus seems to account for much of the variation within types, predominantly the enrichment of Al_2O_3 and depletion of SiO_2. Based on the XRD-results all of the altered samples have been excluded from the following discussion. New compositional ranges, CIPW norms, means and standard deviations of the three pumice types are thus given in Tables 5.1 and 5.2, and the data for samples which do not contain kaolinite plotted on a variation diagram SiO2 vs Sr is given in Figure 5.4.

In some of the low SiO_2, high Al_2O_3 samples no clay minerals were present, indicating that some of the variation within types represents an original compositional difference. Variation in SiO_2 could be due to variation in modal quartz. About 30% of the studied samples contain quartz, though its occurrence does not seem to be related to any particular location. Most of the quartz grains have rounded crystal corners suggesting magmatic resorption.

To see if the concentrations of modal quartz and variation in SiO_2 content can be correlated, modal quartz of 41 representative samples were plotted against SiO_2 (Fig.5.5). The diagram shows that the high SiO_2 samples both in Types 1a and 1b have the highest modal quartz content, and thus low plagioclase/quartz ratio, whereas the low SiO_2 samples in Type 1b contain no modal quartz. Quartz occurs also in the crystal-rich Type 2 pumices, but its concentration is relatively low (max. 5 vol.%), and the plagioclase/quartz ratio is high.

Table 5.1. Compositional ranges, means and standard deviations for the three pumice types of the Pokai Ignimbrite, excluding all the altered (kaolinitised) samples. No. = number of samples; % = percentage of all unaltered samples analysed.

	Type 1a	Mean	STD	Type 1b	Mean	STD
SiO_2	74.41-77.35	76.16	0.85	69.68-77.01	75.05	1.06
TiO_2	0.11-0.23	0.14	0.03	0.06-0.60	0.19	0.05
Al_2O_3	12.27-14.98	13.46	0.85	12.41-19.87	13.87	1.10
FeO_t	1.29-1.96	1.60	0.17	1.58-2.58	1.98	0.18
MnO	0.04-0.10	0.06	0.02	0.03-0.12	0.07	0.02
MgO	0.05-0.18	0.11	0.04	0.05-0.44	0.15	0.06
CaO	0.63-0.99	0.82	0.07	0.92-1.20	1.08	0.05
Na_2O	3.54-4.23	3.85	0.17	3.45-4.56	3.94	0.20
K_2O	3.06-4.26	3.79	0.27	3.03-4.11	3.66	0.24
P_2O_5	0.01-0.04	0.02	0.02	0.01-0.06	0.02	0.02
V	3-8	6	1.3	3-9	6	1.4
Cr	3-5	3	0.6	3-5	4	0.6
Ni	3-4	3	0.2	3-5	3	0.6
Zn	32-71	48	8.1	38-131	54	10.0
Zr	106-183	148	19.8	177-269	209	26.4
Nb	8-13	11	1.2	9-14	11	1.0
Ba	687-1010	826	71.6	642-924	782	53.2
La	21-37	28	3.3	19-37	27	2.9
Ce	54-92	67	8.1	51-98	65	7.0
Nd	40-63	51	4.8	38-60	49	4.3
Ga	8-18	15	2.4	9-21	15	2.3
Pb	17-27	22	6.9	17-49	23	3.4
Rb	105-140	125	6.9	91-130	119	6.8
Sr	32-68	57	7.0	74-97	87	4.1
Th	11-29	16	2.0	6-23	14	2.4
Y	20-37	29	3.3	18-37	26	3.2
No.	41			108		
%	24.1 %			63.5 %		

Table 5.1 cont.

	Type 2	Mean	STD
SiO_2	70.97-74.55	73.36	0.93
TiO_2	0.23-0.44	0.30	0.05
Al_2O_3	13.40-15.78	14.35	0.76
FeO_t	2.16-3.09	2.37	0.23
MnO	0.06-0.11	0.08	0.01
MgO	0.19-0.63	0.34	0.10
CaO	1.30-2.20	1.54	0.19
Na_2O	3.49-5.11	4.40	0.31
K_2O	2.68-3.64	3.23	0.26
P_2O_5	0.01-0.10	0.03	0.02
V	7-12	9	1.4
Cr	3-5	4	0.7
Ni	3-5	3	0.6
Zn	42-68	55	7.4
Zr	213-306	240	22.2
Nb	10-13	11	0.9
Ba	633-827	737	50.4
La	20-32	26	2.8
Ce	51-78	65	7.0
Nd	38-54	50	4.0
Ga	13-19	16	1.3
Pb	15-26	20	3.2
Rb	89-115	102	7.3
Sr	111-186	123	16.5
Th	5-21	12	3.4
Y	20-31	26	3.5
No.	21		
%	12.4 %		

Table 5.2. CIPW compositional ranges, means and standard deviations for the three pumice types of the Pokai Ignimbrite, excluding all the altered (kaolinitised) samples. Total number of samples 170. No. = number of samples of each type; % = percentage of all unaltered samples analysed.

	Type 1a	Mean	STD	Type 1b	Mean	STD
Q	33.88-39.60	37.23	1.20	30.80-38.76	35.44	1.20
or	18.09-25.16	22.37	1.63	17.88-24.27	21.60	1.41
ab	29.23-35.79	32.57	1.46	29.18-38.56	33.35	1.72
an	3.07-4.82	3.88	0.35	4.44-5.74	5.19	0.25
C	0.00-4.46	1.60	1.06	0.00-8.98	1.53	1.41
di	0.00-0.96	0.03	0.13	0.00-0.36	0.004	0.03
hy	0.45-0.96	0.70	0.12	0.21-1.59	0.87	0.17
mt	0.98-1.50	1.22	0.13	1.21-1.97	1.51	0.14
il	0.21-0.63	0.27	0.05	0.12-1.14	0.36	0.09
hem	-	-	-	0.00-0.11	0.001	0.01
ap	0.02-0.26	0.05	0.04	0.02-0.14	0.05	0.02

	Type 2	Mean	STD
Q	25.55-35.30	31.52	1.96
or	15.82-21.50	19.09	1.54
ab	29.49-43.21	37.22	2.63
an	5.64-9.32	7.21	0.85
C	0.00-3.18	0.98	1.00
di	0.00-1.30	0.18	0.42
hy	0.87-1.65	1.23	0.21
mt	1.65-2.35	1.81	0.18
il	0.44-0.84	0.58	0.09
hem	-	-	-
ap	0.02-0.24	0.07	0.05

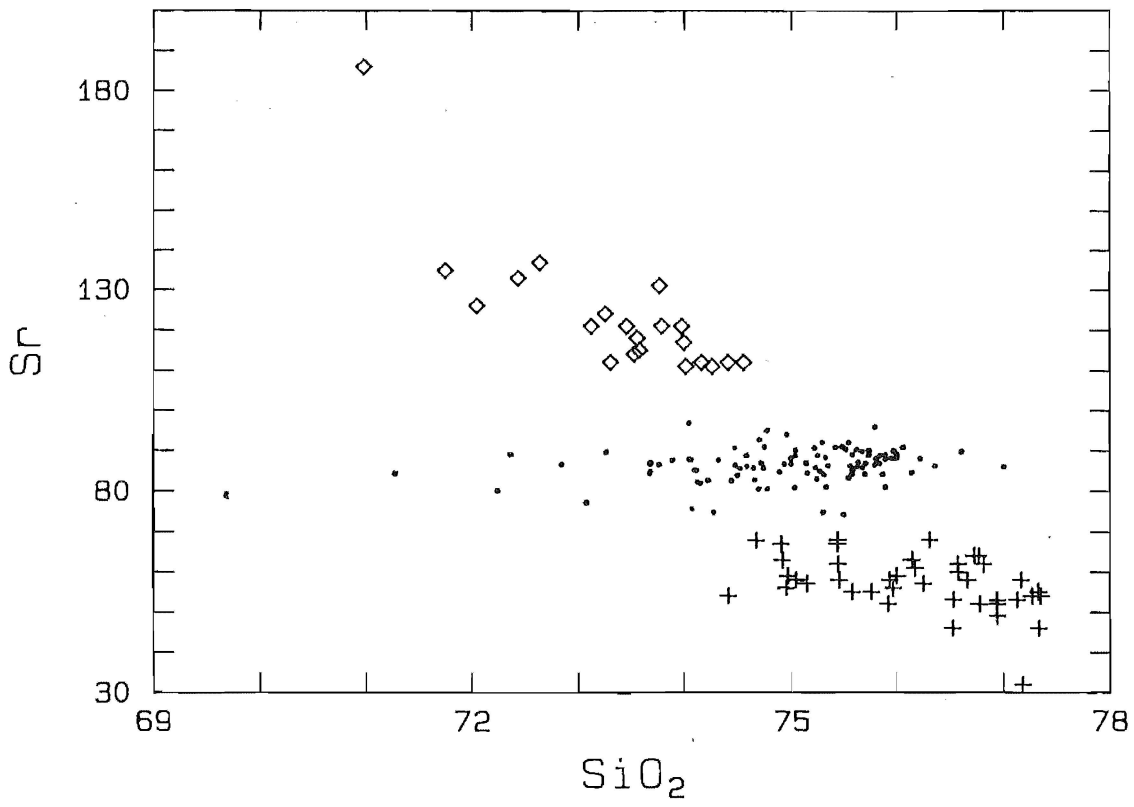

Figure 5.4. Sr vs SiO_2 for the Pokai Ignimbrite, excluding all the altered (kaolinitised) samples.

+ = Type 1a pumice (Sr <70 ppm)
● = Type 1b pumice (Sr 70-100 ppm)
◇ = Type 2 pumice (Sr >100 ppm)

Figure 5.5. Modal quartz (vol.%) vs SiO_2 (wt.%) in representative Pokai Ignimbrite pumices.

+ = Type 1a pumice
● = Type 1b pumice
◇ = Type 2 pumice

Figure 5.6. Modal proportions (vol.%) of mafic minerals (pyroxene + Fe-Ti oxides) vs SiO_2 in representative Pokai Ignimbrite pumices.

+ = Type 1a pumice
● = Type 1b pumice
◇ = Type 2 pumice

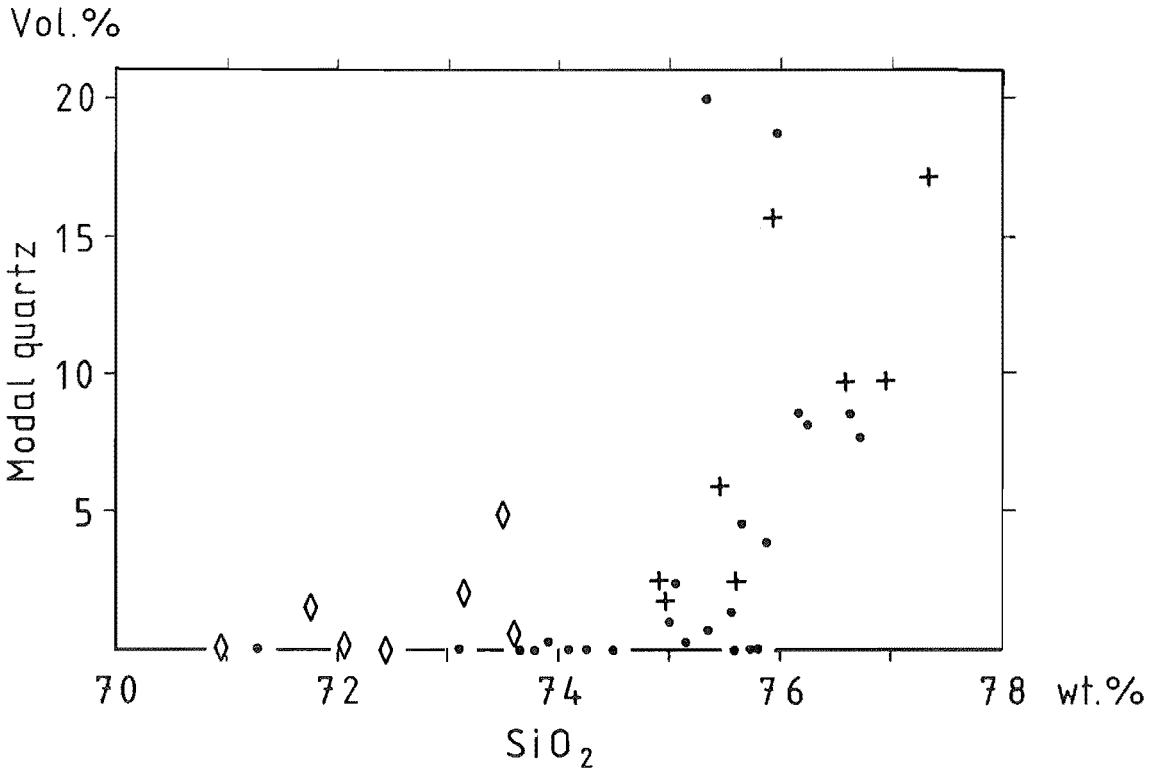
Vol.%
20
15
10
5
Modal quartz
70
72
74
76
78
wt.%
SiO2

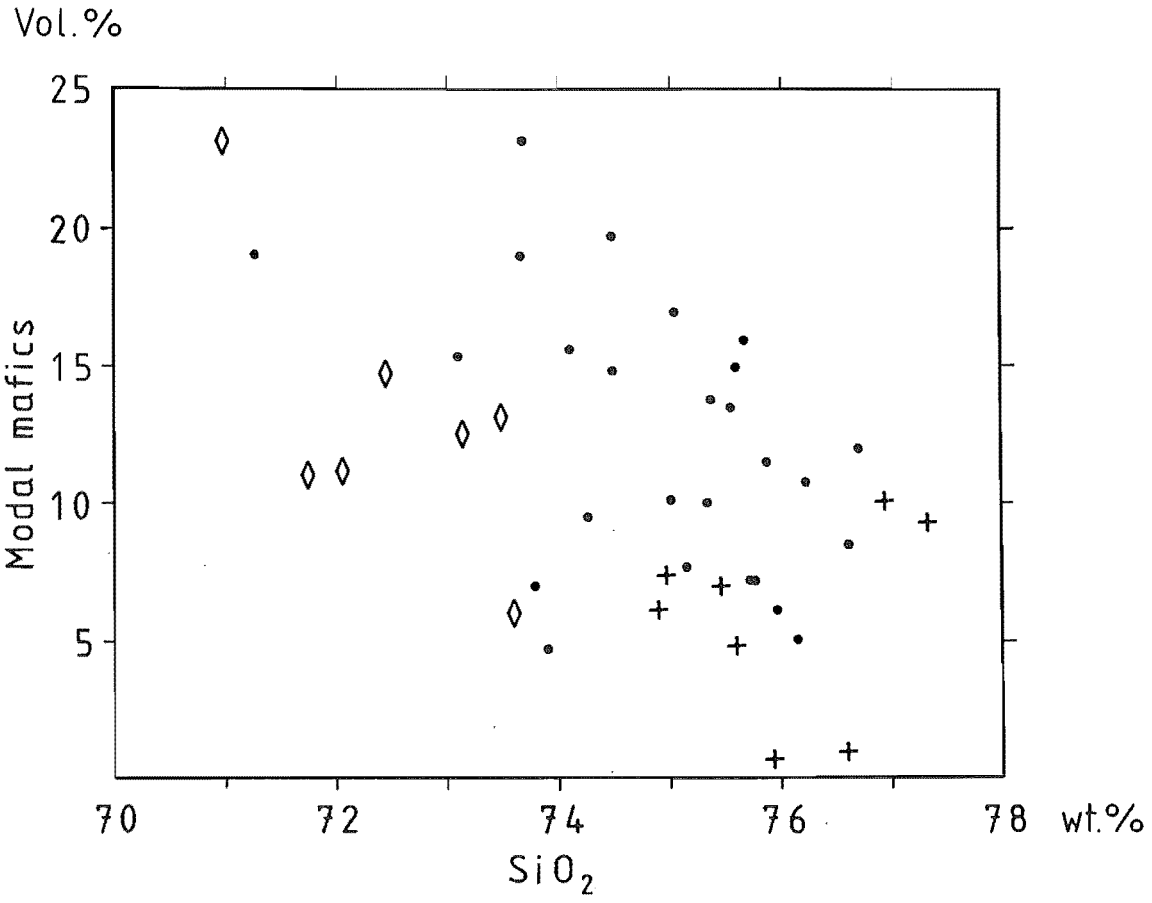
Vol.%
25
20
15
10
5
Modal mafics
70
72
74
76
78
wt.%
SiO2

Variation in mafic minerals accounts for some of the variation within the pumice types (Fig.5.6). Type 1a and the high SiO_2 Type 1b pumices do seem to have an overall lower content of mafics, whereas the medium and low SiO_2 Type 1b pumices have mafic contents up to 15-20 vol.% of all phenocrysts. One low SiO_2, high Sr (186 ppm) sample contain >20 vol.% mafics. Both types 1b and 2 low SiO_2 pumices also contain clinopyroxene.

There is therefore a strong positive correlation with the high SiO_2 pumices and the abundance of modal quartz, suggesting that the trends in the SiO_2 and Al_2O_3 contents are mainly controlled by the abundance of quartz, and thus by the plagioclase/quartz ratio. The negative correlation of FeO_t with increasing SiO_2 within each type is probably due to the inverse variation between the concentrations of ferromagnesian and felsic minerals. Some elements, such as CaO and Sr seem to be "buffered" in each type. This could be explained by the fact that the modal proportions of plagioclase remain relatively constant within each pumice type irrespective of the variation in the modal quartz content.

The compositional fields and the average composition of each pumice type are plotted on an ACF diagram in Figure 5.7. The figure also illustrates the compositional fields of the average TVZ rhyolitic lavas (including domes) and ignimbrites, andesites-dacites, and the fields of the North Island Eastern basement (Torlesse) and Western basement (Waipapa) greywackes and argillites. The composition of the crystal-poor Type 1a ranges from metaluminous to peraluminous, with a peraluminous average composition, whereas Type 1b ranges from weakly metaluminous to strongly peraluminous, with a peraluminous average composition. Type 2 is metaluminous to mildly

Figure 5.7.

(a) The compositional fields and the average compositions of the Pokai Ignimbrite pumice types plotted on an ACF diagram. The fields of TVZ rhyolitic lavas and ignimbrites are also shown. The data for the rhyolitic lavas and ignimbrites include 28 and 47 analyses, respectively, from published and unpublished records (Bellamy, 1991; Briggs et al., 1992; Cole, 1979b; Houghton & Weaver, unpublished data; Karhunen, unpublished data); a complete list of all analyses used is given in Appendix D (Tables D.6 and D.7). The MA-PA line marks the boundary line between metaluminous (MA) and peraluminous (PA) fields. The boundary between I- and S-type granites, as defined by Chappell and White (1974) lies slightly above this join (1 % normative C).


= Pokai Ignimbrite Type 1a with the average composition.


= Pokai Ignimbrite Type 1b with the average composition.


= Pokai Ignimbrite Type 2 with the average composition.


= TVZ rhyolitic lavas with the average composition.


= TVZ rhyolitic ignimbrites with the average composition.

(b) The compositional fields of the Pokai Ignimbrite pumice types, TVZ andesites-dacites (Conrad et al., 1988) and the North Island sedimentary basement rocks (Conrad et al., 1988; Reid, 1982), and the average TVZ basement compositions (Graham & Cole, 1991).

Pokai Ignimbrite fields as above


= Eastern basement (Torlesse) metagreywacke with the average bulk rock composition.


= Western basement (Waipapa) metagreywacke with the average bulk rock composition.


= TVZ andesites and dacites.

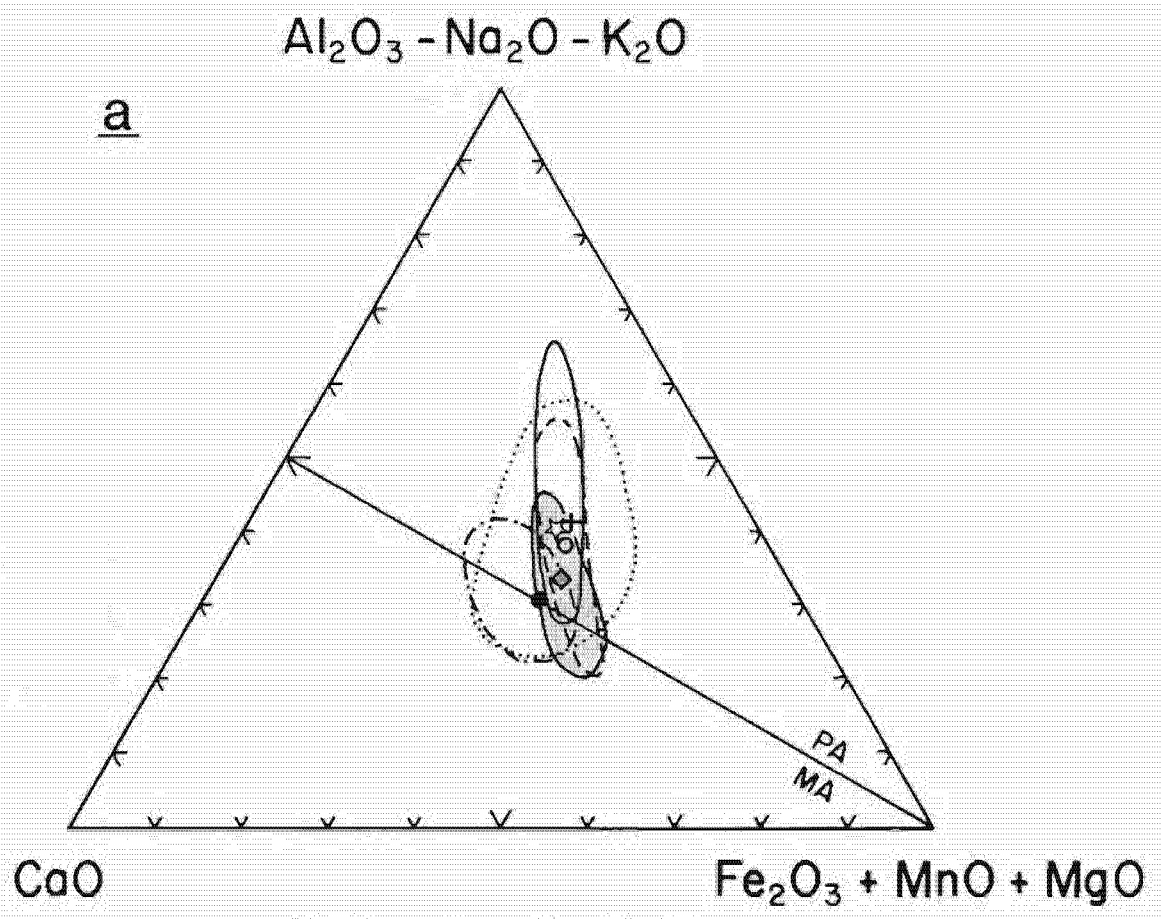
Al2O3 - Na2O - K2O
a
PA
MA
CaO
Fe2O3 + MnO + MgO

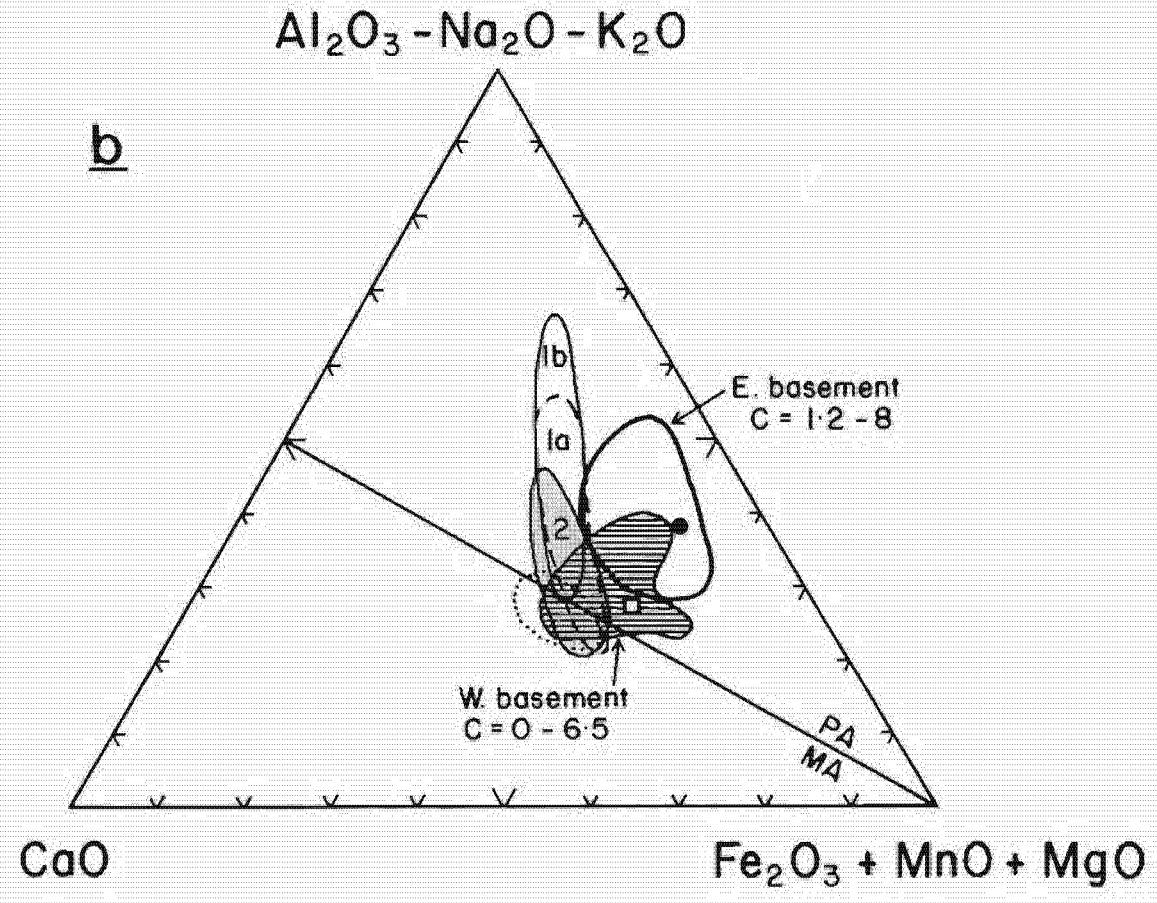
Al2O3 - Na2O - K2O
b
Ib
Ia
2
E. basement
C = 1·2 - 8
W. basement
C = 0 - 6·5
PA
MA
CaO
Fe2O3 + MnO + MgO

peraluminous, with a mildly peraluminous average composition.

It has been calculated that most TVZ rhyolites are metaluminous to mildly peraluminous, generally 'I-type' (by definition of Chappell and White, 1974) in composition (Ewart 1969; Conrad et al. 1988), however, most of the analyses are of rhyolitic lavas. As shown in Figure 5.7 most of the TVZ rhyolitic lavas are metaluminous to mildly peraluminous, whereas the rhyolitic ignimbrites have a more peraluminous average composition. The average Pokai Ignimbrite compositions thus coincide within the range of other TVZ rhyolitic ignimbrites.

5.3. CIPW norms

Although modal quartz occurs in ca. 30 % of the samples, all samples are SiO_2 oversaturated having normative quartz in the range 25 to 40 % (Table 5.2). Plagioclase, orthopyroxene, magnetite, ilmenite and apatite are calculated normative phases and these occur also as phenocryst phases. Normative diopside (i.e metaluminous) is rare. Most samples include normative corundum (i.e. they are peraluminous), the average C content ranges from 1 to 1.6 % in the distinct pumice types, but C contents as high as 6-8 % do occur.

The compositional fields for each pumice type are shown on standard An-Ab-Or and Q-Ab-Or triangular diagrams in Figure 5.8. The diagrams also show the average fields of the TVZ ignimbrites and average compositions of the North Island basement sediments. In terms of the An-Ab-Or system (Fig.5.8.a), all the pumice types project in the plagioclase field. There is also a systematic increase in normative An

Figure 5.8. Normative (CIPW) quartz and feldspar compositional fields of the Pokai Ignimbrite pumice types plotted on the (a) An-Ab-Or and (b) Q-Ab-Or triangular diagrams. The compositional field of TVZ rhyolitic ignimbrites (same data used as in Fig.5.7; Appendix D, Table D.7) and average compositions of North Island sedimentary basement rocks (Graham & Cole, 1991; Reid 1982, 1983) are also shown.
Heavy solid curve in plot (a) represents the quartz-saturated two feldspar boundary curve and in plot (b) the quartz-feldspar (horizontal line) and two-feldspar (vertical line) boundary curves. The piercing point defines the minimum melting composition for $(Q\text{-}Ab\text{-}Or)_{97}An_3$-system at 1 kb water vapour pressure (James & Hamilton, 1969).

 = Pokai Ignimbrite Type 1a.

 = Pokai Ignimbrite Type 1b.

 = Pokai Ignimbrite Type 2.

 = TVZ rhyolitic ignimbrites.

○ = Eastern basement (Torlesse) metagreywackes.

□ = Western basement (Waipapa) metagreywackes.

X / Y = experimental TVZ greywacke and argillite compositions, respectively.

★ = Kawerau Geothermal Area greywacke composition (borehole material only).

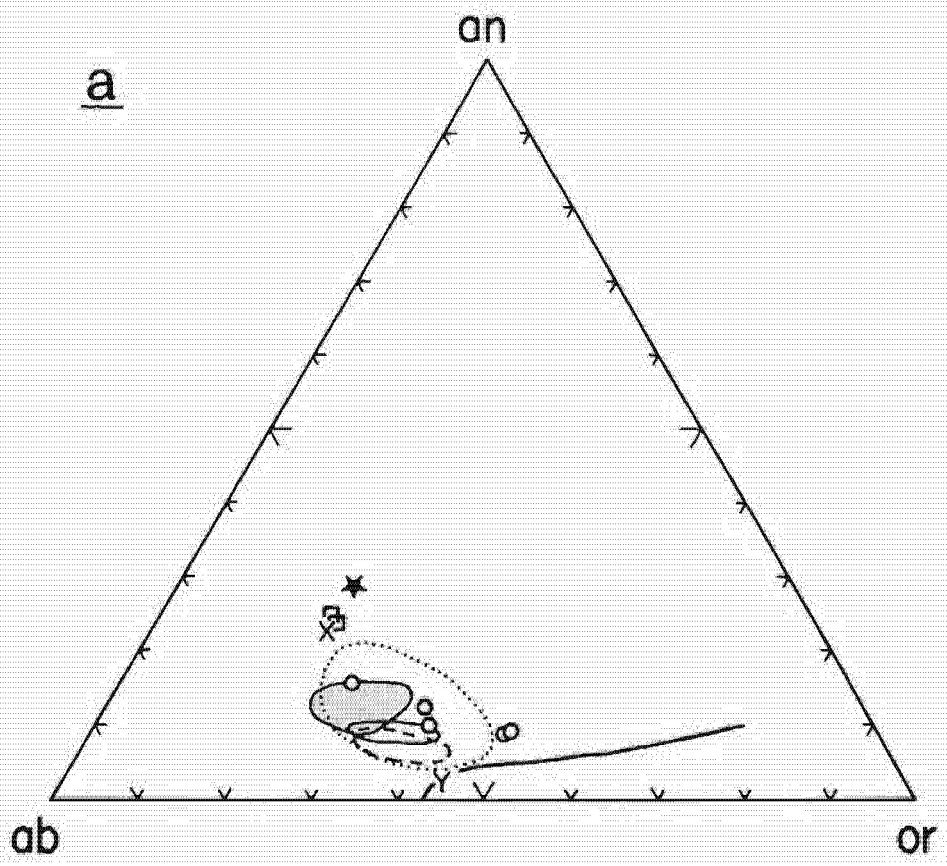
a
an
ab
or

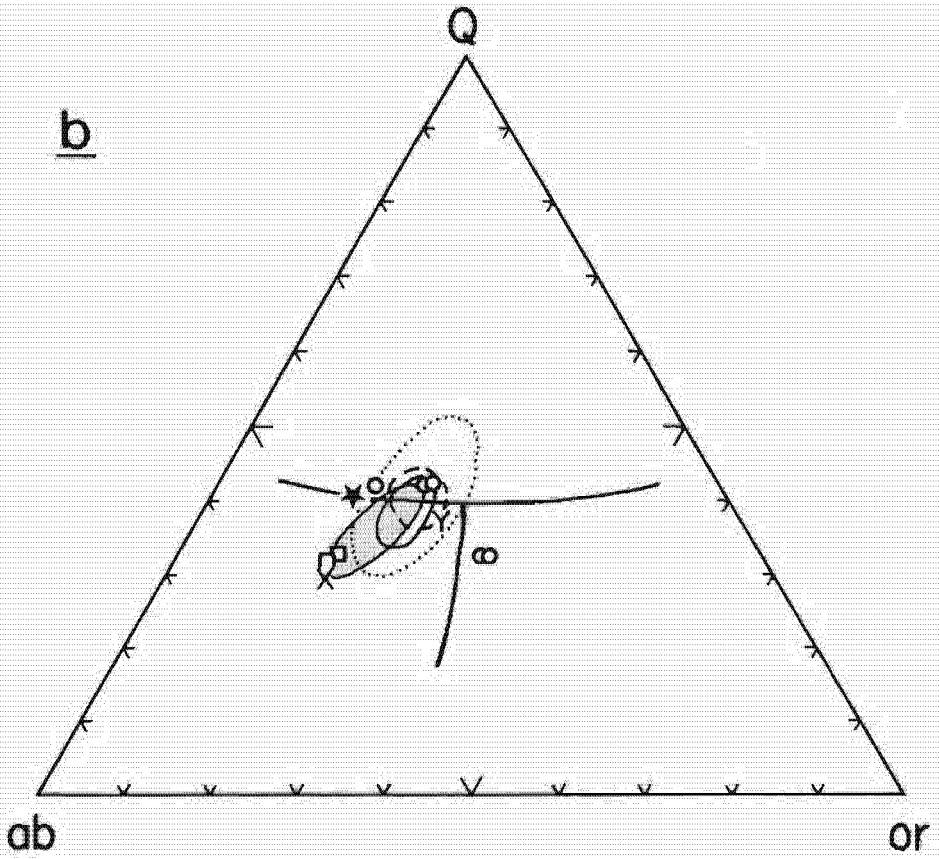
b
Q
ab
or

from Types 1a through 1b to Type 2.

In the Q-Ab-Or system (Fig.5.8.b), the pumice types plot in overlapping fields across the quartz-feldspar cotectic boundary line but not on the minimum melting point. Types 1a and 1b fall in the average compositional field of the TVZ ignimbrites, whereas Type 2 shows an enrichment of normative Ab and a depletion of Q. It is noted that several of the North Island greywacke and argillite compositions lie near the Type 2 compositional field.

5.4. Major and trace element chemistry

SiO_2 versus major oxides.

TiO_2 and FeO_t (Fig.5.9.a & b) decrease with increasing SiO_2, from Type 2 to Type 1a, which has the lowest TiO_2 and FeO_t values. Type 1a also has the lowest MgO and CaO contents (Fig.5.9.c & d). The scatter of Na_2O (Fig.5.9.e) is possibly due to the high mobility of sodium with Type 2 having the highest Na_2O content. Al_2O_3 (Fig.5.9.f) shows a strong negative correlation with increasing SiO_2. Each pumice group follows a slightly different trend corresponding to different Al/Si ratios. The trends are consistent with the variations in modal plagioclase/quartz ratios within each type. K_2O (Fig.5.9.g) shows a strong positive correlation with SiO_2.

SiO_2 versus trace elements.

Most trace-elements analysed have relatively constant concentrations in all pumice types. The only trace-elements that show significant chemical variation are Zr, Rb and Sr. A positive trend with increasing SiO_2 is shown by Rb

Figure 5.9. Selected major element variation diagrams for the Pokai Ignimbrite pumice, excluding all the altered (kaolinitised) samples. Total iron as Fe_2O_3.

+ = Type 1a pumice
● = Type 1b pumice
◇ = Type 2 pumice

(a) TiO_2 vs SiO_2
(b) Fe_2O_3 vs SiO_2
(c) MgO vs SiO_2
(d) CaO vs SiO_2
(e) Al_2O_3 vs SiO_2
(f) Na_2O vs SiO_2
(g) K_2O vs SiO_2

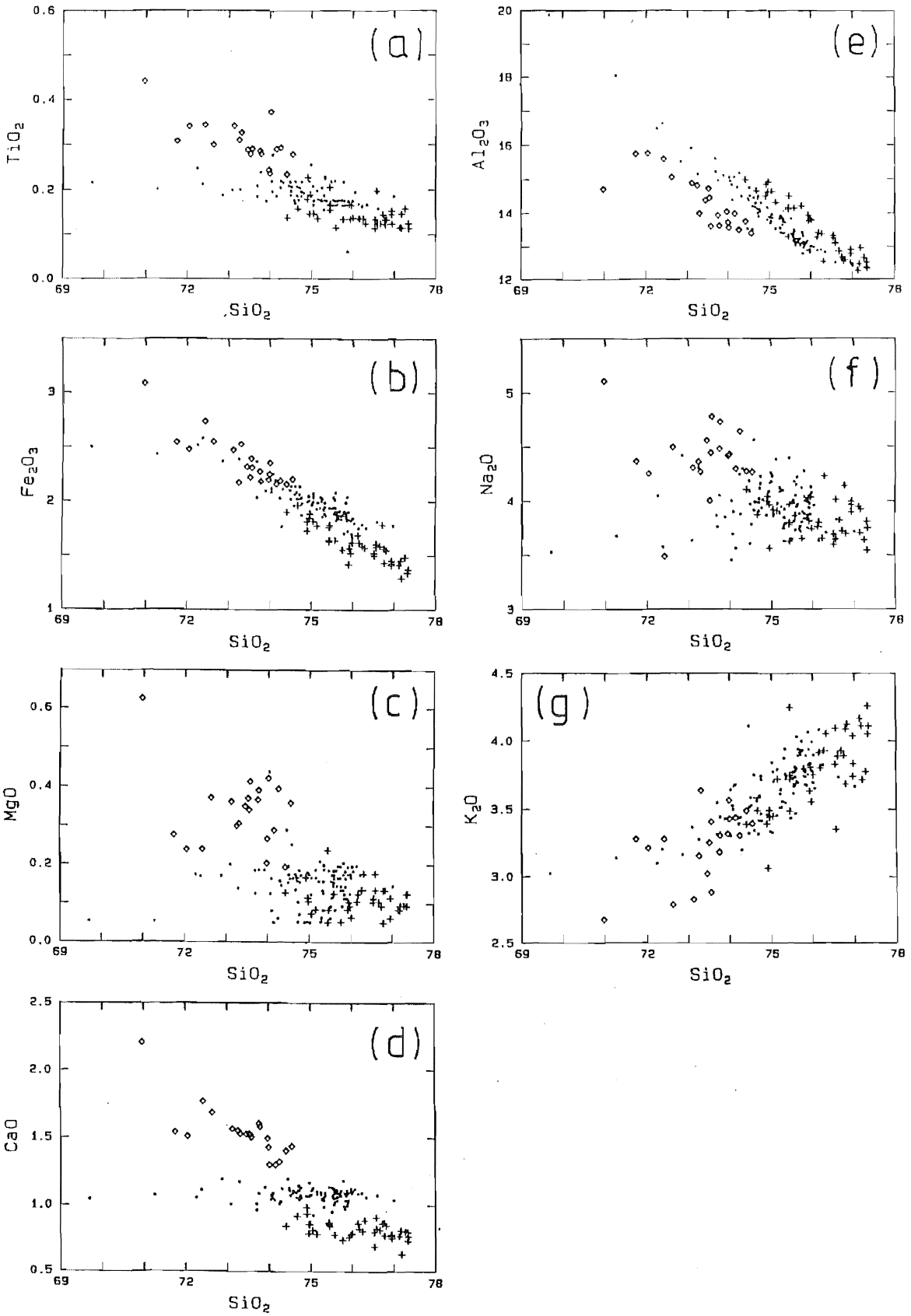
(a)
TiO_2
0.0
0.2
0.4
0.6
69
72
75
78
SiO_2
(e)
Al_2O_3
12
14
16
18
20
69
72
75
78
SiO_2
(b)
Fe_2O_3
1
2
3
69
72
75
78
SiO_2
(f)
Na_2O
3
4
5
69
72
75
78
SiO_2
(c)
MgO
0.0
0.2
0.4
0.6
69
72
75
78
SiO_2
(g)
K_2O
2.5
3.0
3.5
4.0
4.5
69
72
75
78
SiO_2
(d)
CaO
0.5
1.0
1.5
2.0
2.5
69
72
75
78
SiO_2

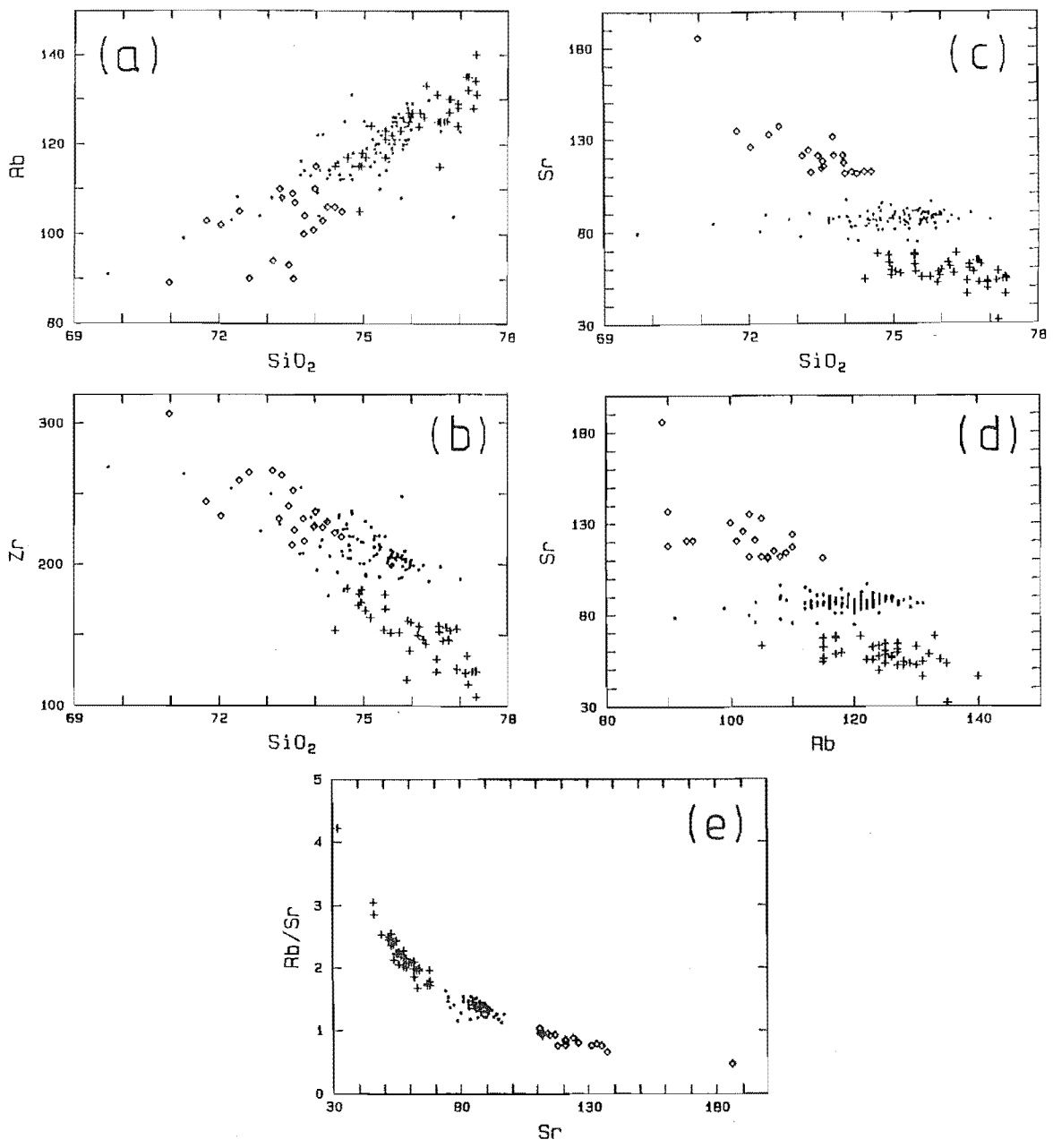

Figure 5.10. Selected trace element variation diagrams for the Pokai Ignimbrite pumice, excluding all the altered (kaolinitised) samples.

+ = Type 1a pumice
● = Type 1b pumice
◇ = Type 2 pumice

(a) Rb vs SiO_2
(b) Zr vs SiO_2
(c) Sr vs SiO_2
(d) Sr vs Rb
(e) Rb/Sr vs Sr

(Fig.5.10.a), following more or less a trend from Type 1a, with the highest values, through types 1b and 2. Zr (Fig.5.10.b) has a negative correlation with SiO_2. There is a clear compositional gap (11 ppm) in the Sr content between Types 2 and 1b as well as a slight compositional gap (4 ppm) between Types 1b and 1a (Fig.5.10.c). Note that the geochemical behaviour of Sr corresponds closely to CaO as would be expected.

Rb and Sr.

As most SiO_2-rich igneous rocks have much higher Rb/Sr ratio than SiO_2-poor igneous rocks, this ratio can be used as an index of differentiation (Halliday et al. 1991). This is because Rb is more incompatible than Sr in magmatic systems. The Rb versus Sr and Sr versus Rb/Sr graphs (Figs.5.10.d & e) divide the Pokai Ignimbrite pumice into three relatively well defined groups; Type 2 having the highest Sr content and Type 1a the lowest, whereas Type 1b pumices fall in the middle. The Rb/Sr ratio is thus lowest in Type 2 pumices and highest in Type 1a pumices.

5.5. Lateral and vertical variation in geochemistry

In order to examine possible lateral variation in the geochemistry, distribution maps for each pumice types were plotted, and these are shown in Figure 5.11. Pumice types 1a and 1b have relatively similar lateral distributions, whereas Type 2 has a more restricted distribution; no Type 2 pumices were analysed from the central western part of the study area. Figure 5.12 shows the elevation of Pokai Ignimbrite outcrops recorded along an E-W cross-section from the Kapenga caldera

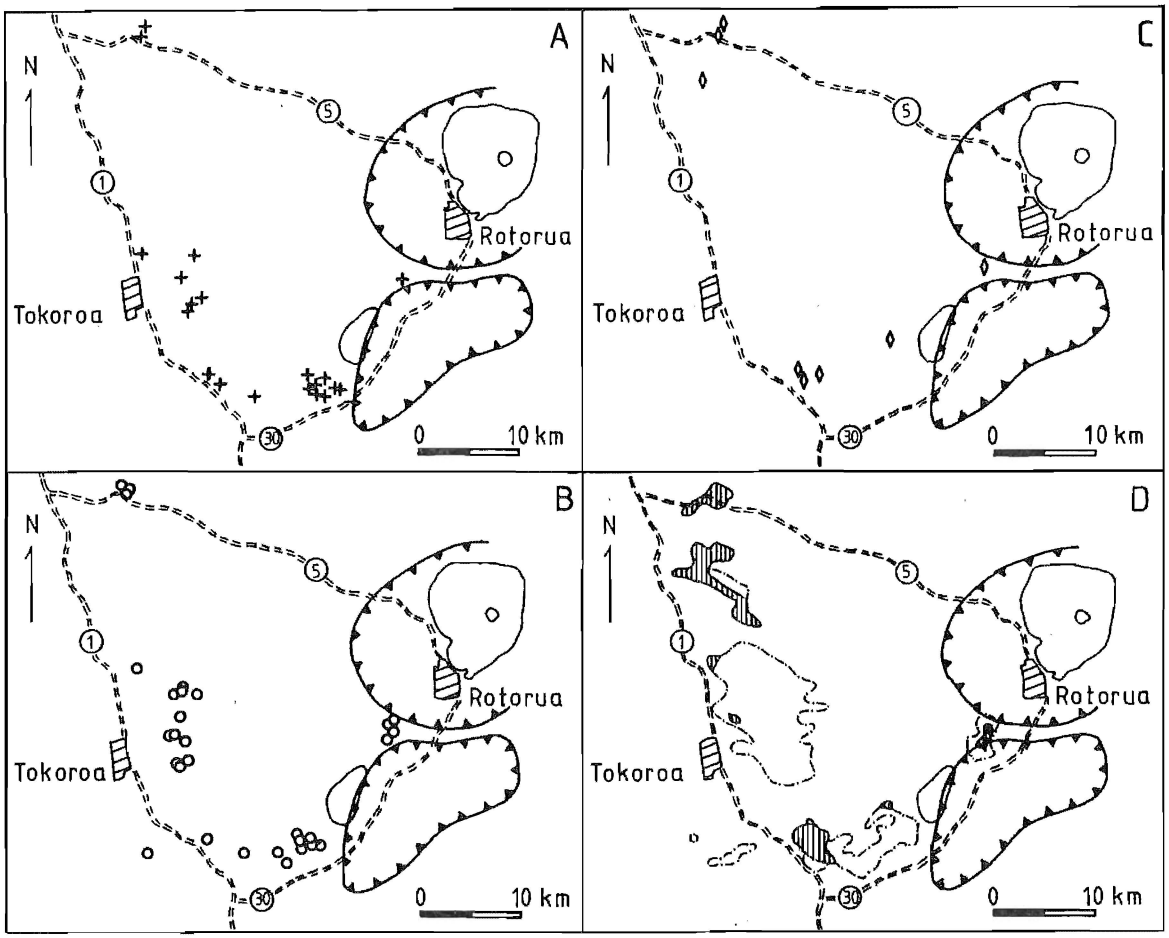

Figure 5.11. The areal distribution of the Pokai Ignimbrite pumice types: Map (A) Type 1a pumices (+), Map (B) Type 1b pumices (o), and Map (C) Type 2 pumices (◇). Each point marks a location with one or more pumices analysed that correspond to the indicated compositional type. The dashed lines mark the main outcrop areas of Pokai Ignimbrite.
Map (D): Total extension of the crystal-rich flow units (lined areas) from field mapping.
The circular cross-hatched lines mark the volcanic centres of Rotorua (E) and Kapenga (SE), respectively.

Figure 5.12. Ignimbrite stratigraphy in the southern Mamaku Plateau showing the distribution of the crystal-poor and crystal-rich Pokai Ignimbrite flow units and the occurrence of the different pumice types. Each mark indicates predominance (≥50 %) of that pumice type at each locality.

margin to Highway 1, respectively. The distribution of the crystal-rich and crystal-poor deposits are shown, and it is evident that the crystal-rich flow units (abundant in Type 2 pumice) clearly predominate in the SW and their stratigraphic position suggests that they lie above the crystal-poor (Types 1a and 1b pumice) flow units. Though the crystal-rich pumices predominate at localities 97, 98 and 108, it should be noted that rare crystal-poor types also occur in these flow units (see Appendix D, Table D.2, ref.nos. 145-158).

Significant geochemical variation in five vertical sections is plotted against stratigraphic height in Figures 5.13-5.17. SiO_2, TiO_2, FeO_t, CaO, K_2O and Sr were chosen as examples.

Only at the Pokai Road section (Fig.5.13) is the base of the ignimbrite exposed and the height of each sampling site is given as the distance from the base. The Pokai Road diagram also includes data from the Galaxy Road locality (situated only 900 m SW from the Pokai Road section); i.e. pumice analyses from the air-fall unit A (70, ref.nos. 130-134), equivalent to the Pokai Road air-fall pumice samples marked SWf (ref.nos. 63-67). Only Types 1a and 1b pumices occur at the Pokai Road section. Type 1a pumices seem be slightly more abundant in the lower part of the section than higher up. The difference in geochemistry of the two pumice types is clear, Type 1a is higher in SiO_2 and K_2O and lower in TiO_2, FeO_t, CaO and Sr. Both pumice types show a curved trend from low SiO_2 and K_2O values at the base towards higher concentrations in the middle and again lower SiO_2 and K_2O concentrations towards the top. TiO_2 and FeO_t also show curved trends with low concentrations at the base and top and higher concentrations in the middle of the section.

Large format diagram too large to be scanned.

Source archive thesis

Figure 5.13. Pokai Road section (GR 682268, field nos. 33 & R, with data from Galaxy Road, GR 673264, field no. 70) showing the variation of SiO_2, TiO_2, FeO_t, CaO, K_2O and Sr in Pokai types 1a and 1b pumices against stratigraphic height. Major element values in wt.%, Sr in ppm. M.a.s.l. = metres above sea level. k = samples containing kaolinite.

+ = Type 1a
• = Type 1b

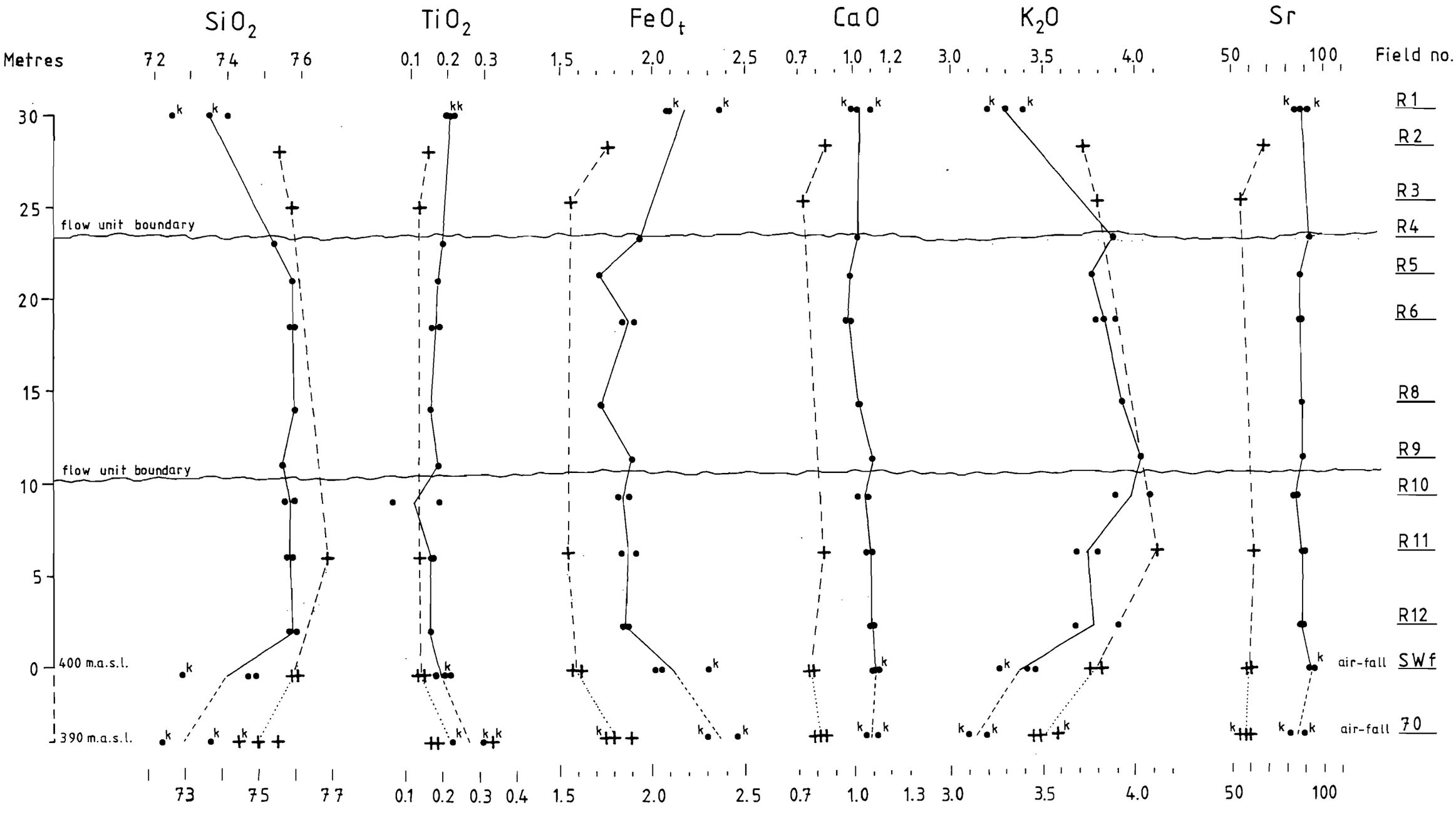

Figure 5.14. Rauna Road section (GR 739177, field no. P) showing the variation of SiO_2, TiO_2, FeO_t, CaO, K_2O and Sr in Pokai types 1a and 1b pumices against stratigraphic height. Major element values in wt.%, Sr in ppm. M.a.s.l. = metres above sea level.

+ = Type 1a
• = Type 1b

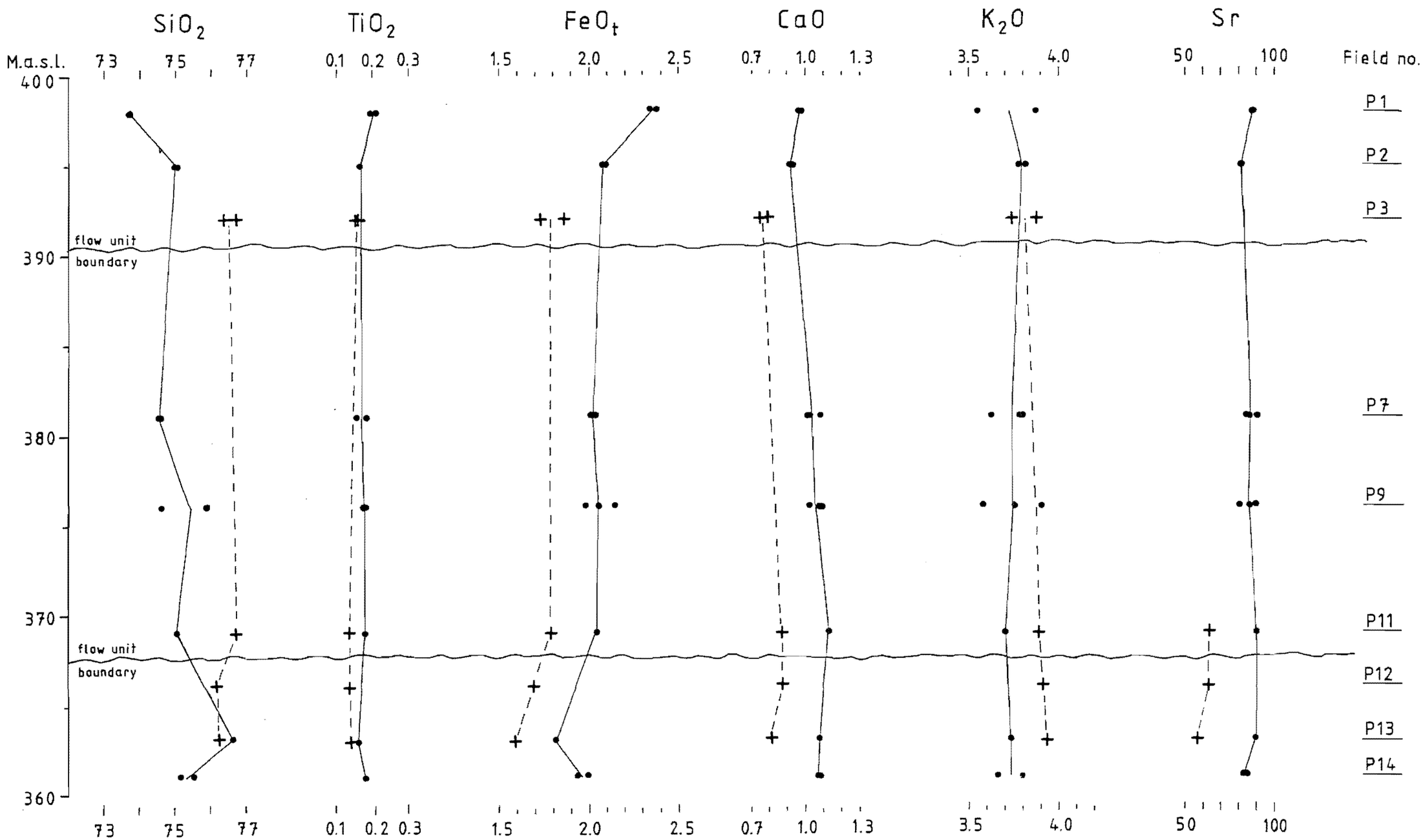

Figure 5.15. Chamois Road section (GR 803189, field nos. 48 & HJ) showing the variation of SiO_2, TiO_2, FeO_t, CaO, K_2O and Sr in Pokai types 1a and 1b pumices against stratigraphic height. Major element values in wt.%, Sr in ppm. M.a.s.l. = metres above sea level.

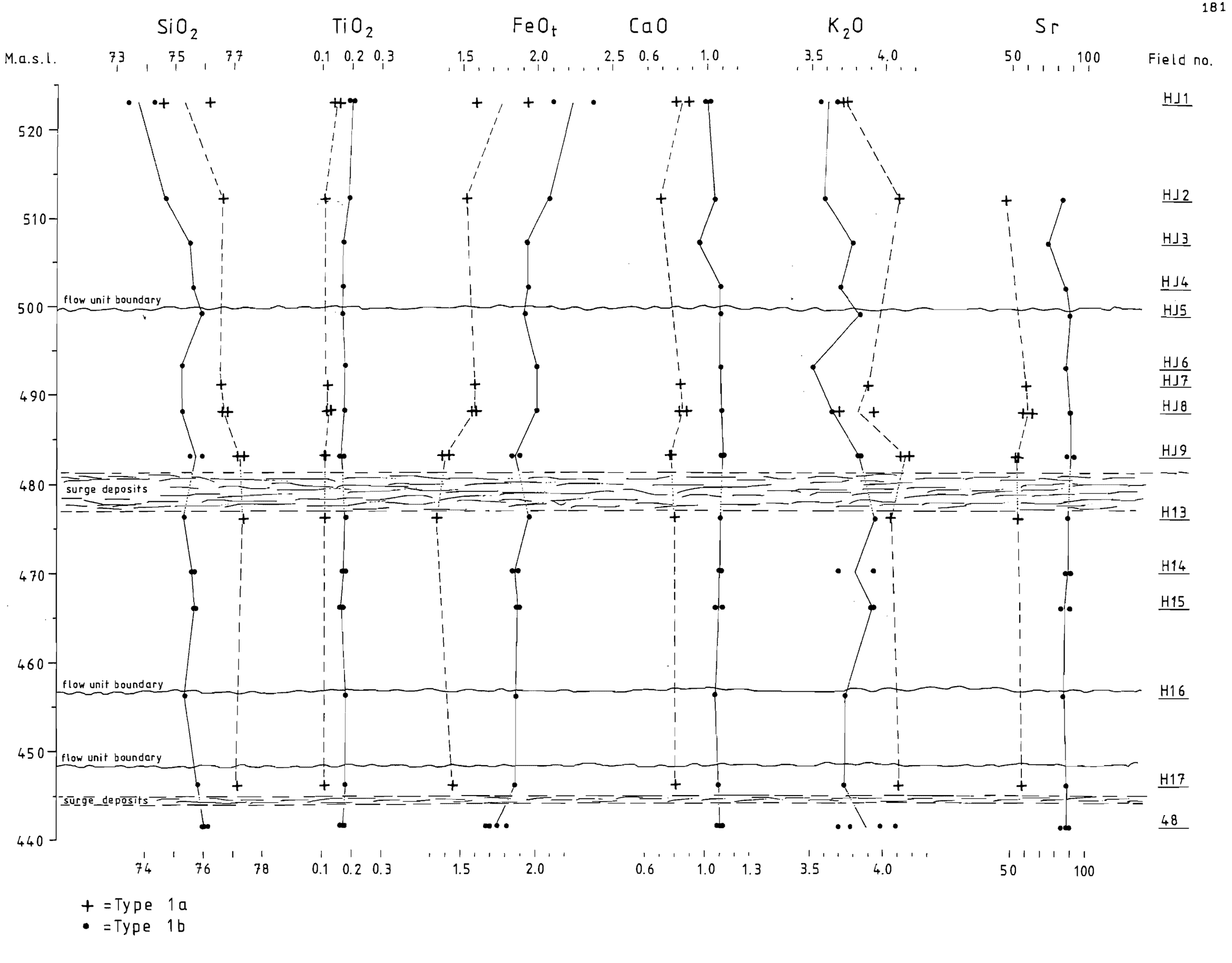
SiO2
TiO2
FeOt
CaO
K2O
Sr
M.a.s.l.
73 75 77
0.1 0.2 0.3
1.5 2.0 2.5
0.6 1.0
3.5 4.0
50 100
Field no.
520
510
500
490
480
470
460
450
440
flow unit boundary
surge deposits
flow unit boundary
flow unit boundary
surge deposits
HJ1
HJ2
HJ3
HJ4
HJ5
HJ6
HJ7
HJ8
HJ9
H13
H14
H15
H16
H17
48
74 76 78
0.1 0.2 0.3
1.5 2.0
0.6 1.0 1.3
3.5 4.0
50 100
+ =Type 1a
• =Type 1b

At localities where the base of the ignimbrite is not exposed the distances between each sampling site are quoted as the topographic height (m.a.s.l.). Trace element data are missing from one site at both Rauna and Chamois Road localities (Figs.5.14 & 5.15); as these were highly welded zones where the pumices were too small to provide enough material for trace element analyses. At Rauna Road section (Fig.5.14) a slight trend towards less evolved compositions can be seen upwards through the stratigraphy; SiO_2 content drops from 75-76.5 to <74 % and K_2O from 3.7-3.9 to 3.5 %, and FeO_t increases from 1.6-2 to >2.3 %.

Chamois Road section (> 83 m, Fig.5.15) shows unexpectedly small variation with the stratigraphy, with Type 1a and 1b pumice occurring throughout the section. Even at the top of the section (at ca. 78 m) the lowest SiO_2 value is >73 %. However, a slight change to less evolved compositions is seen in the individual pumice types, i.e. Type 1a pumices become somewhat lower in SiO_2 and K_2O and higher in FeO_t contents upwards through a flow unit (see the flow unit marked HJ9-HJ6 in Fig.5.15). SiO_2 and K_2O contents, in both pumice types 1a and 1b, are also somewhat lower at the top of the section, whereas FeO_t increases slightly. Several features (see chapter 2) indicate that this section is one of the closest to the Pokai Ignimbrite source and it is probable that most of these flow units consist of relatively homogeneous material, ejected during the early stages of the eruption.

At localities further to the west and northwest the ignimbrite has fewer and thinner flow units, so the exposed vertical sections probably include units which represent both early and late eruptive phases. Tapapa Valley section (Fig.5.16) has a

Figure 5.16. Tapapa Valley section (GR 611540-613538, field nos. 170 & T) showing the variation of SiO_2, TiO_2, FeO_t, CaO, K_2O and Sr in Pokai types 1a, 1b and 2 pumices against stratigraphic height. Major element values in wt.%, Sr in ppm. M.a.s.l. = metres above sea level. k = samples containing kaolinite.

Large format diagram too large to be scanned.

Source archive thesis

Figure 5.17. Haunui Valley section, Pylon line (GR 886294, field nos. 132 & V) showing the variation of SiO_2, TiO_2, FeO_t, CaO, K_2O and Sr in Pokai types 1a and 1b pumices against stratigraphic height. Major element values in wt.%, Sr in ppm. M.a.s.l. = metres above sea level. k = samples containing kaolinite.

+ = Type 1a
• = Type 1b

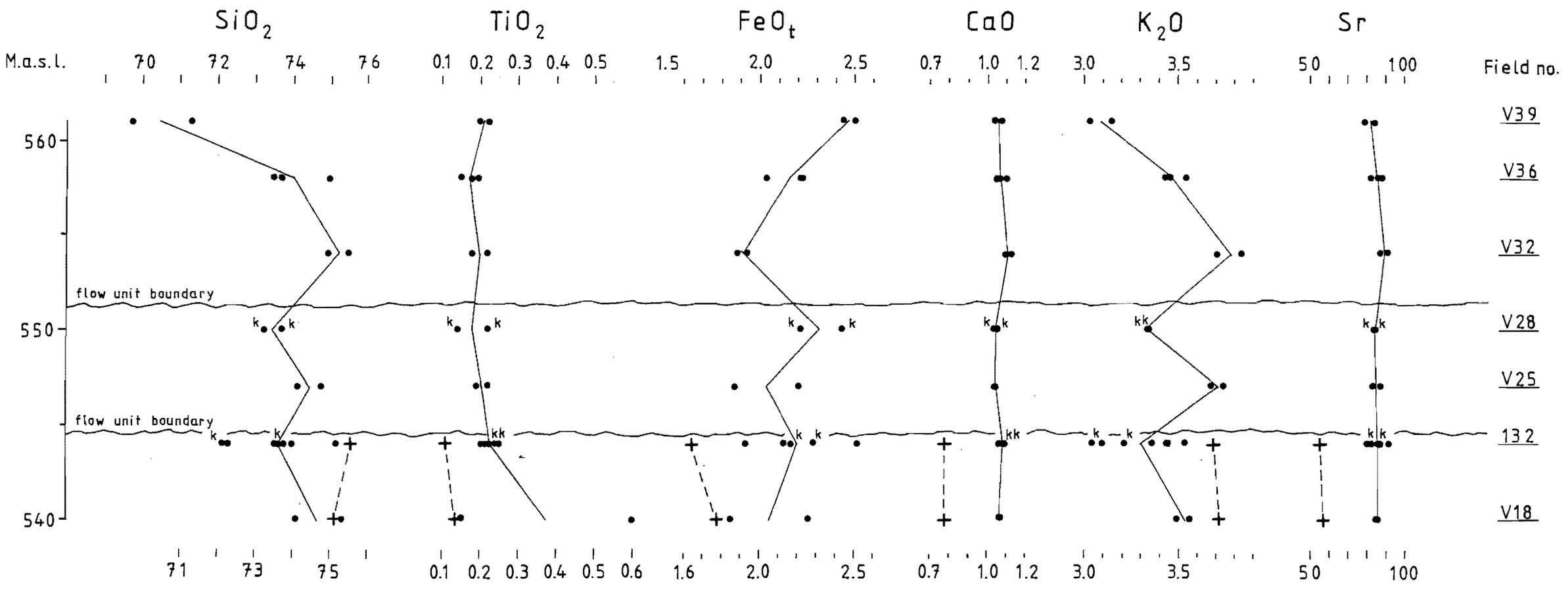

high SiO_2 base (Types 1a and 1b pumices) and a low SiO_2 top (Type 2 pumices predominating, respectively), with an overall increase of TiO_2, FeO_t, CaO and Sr in the individual Type 2 pumices upwards through the flow units.

The Haunui Valley section (Fig.5.17) is >20 m high; the base of the Pokai is not exposed. The colour (red-brown matrix and orange pumices) and welded nature of the ignimbrite suggest that the exposed section represents only an upper part of a possibly much thicker deposit. Type 1a pumice occurs only at the base of the section, Type 1b dominating most of the section. In Type 1b pumices SiO_2 and K_2O decrease and TiO_2, FeO_t and CaO increase upwards through the section. The trends are very similar to the trends at the top of the Pokai Road section (Fig.5.13).

Though one particular site often includes pumices of different composition, some variation is evident in the individual pumice types which become slightly less evolved upwards through a flow unit. The distribution and the stratigraphic position of the crystal-poor Types 1a and 1b pumices suggest that they were erupted nearly simultaneously, Type 1a possibly dominating during the early ignimbrite-building phases, whereas the crystal-rich pumices represent a later phase. The fact that chemically distinct pumices occur together in a single outcrop suggests that the magma body was zoned before the eruption and that at some stage before or during the eruption some mixing occurred.

6. GEOCHEMISTRY OF THE CHIMP IGNIMBRITE

6.1. Introduction

In this chapter major and trace element data of the Chimp Ignimbrite are presented. 23 XRF samples were processed for 10 major and 16 trace elements. All these have totals within 98.5-101 % for the major elements. All analysed samples are single pumices from ignimbrite flow units, and were prepared by the author using the method given in Appendix D. Major and trace element analyses and CIPW norms of all samples are given in Appendix D (Table D.8).

Pumices which had >15 % Al_2O_3 were checked for kaolinite alteration by XRD (see Appendix D, Table D.4). Four of the seven samples run were found to contain kaolinite, and have been excluded from the following discussion.

All analyses have been re-calculated to a 100 % anhydrous basis before plotting on variation diagrams. Loss on ignition (LOI) is typically ca. 3 % in the Chimp pumices.

6.2. General chemistry

The mean composition and standard deviations of the Chimp Ignimbrite pumice data is given in Table 6.1. The ignimbrite is rhyolitic (Fig.6.1.a) with most pumices plotting within the medium-K compositional field (Fig.6.1.b). All the pumices have Na_2O/K_2O ratio >1.

The compositional field and the average composition of the Chimp Ignimbrite is plotted on an ACF diagram in Fig.6.2. The figure also shows the compositional fields of other TVZ

Table 6.1. Compositional ranges, means and standard deviations of the Chimp Ignimbrite, excluding all the altered (kaolinitised) samples (4 of a total 23).

	Chimp	Mean	STD
SiO_2	72.14-75.60	74.68	0.78
TiO_2	0.14-0.39	0.23	0.06
Al_2O_3	13.18-15.44	14.16	0.66
FeO_t	1.89-2.43	2.02	0.13
MnO	0.05-0.10	0.07	0.01
MgO	0.06-0.49	0.18	0.11
CaO	1.12-1.87	1.22	0.19
Na_2O	3.41-4.29	3.89	0.22
K_2O	3.00-4.04	3.52	0.24
P_2O_5	0.01-0.04	0.03	0.01
V	3-11	6	2.3
Cr	3-5	4	0.7
Ni	3-4	3	0.4
Zn	37-71	53	8.0
Zr	200-298	228	19.6
Nb	9-14	11	1.4
Ba	774-975	825	42.9
La	18-30	25	2.9
Ce	48-73	59	7.3
Nd	41-54	47	4.1
Ga	11-18	15	1.8
Pb	12-23	20	2.3
Rb	101-119	109	5.7
Sr	87-147	97	15.3
Th	5-16	13	2.4
Y	17-30	24	3.3

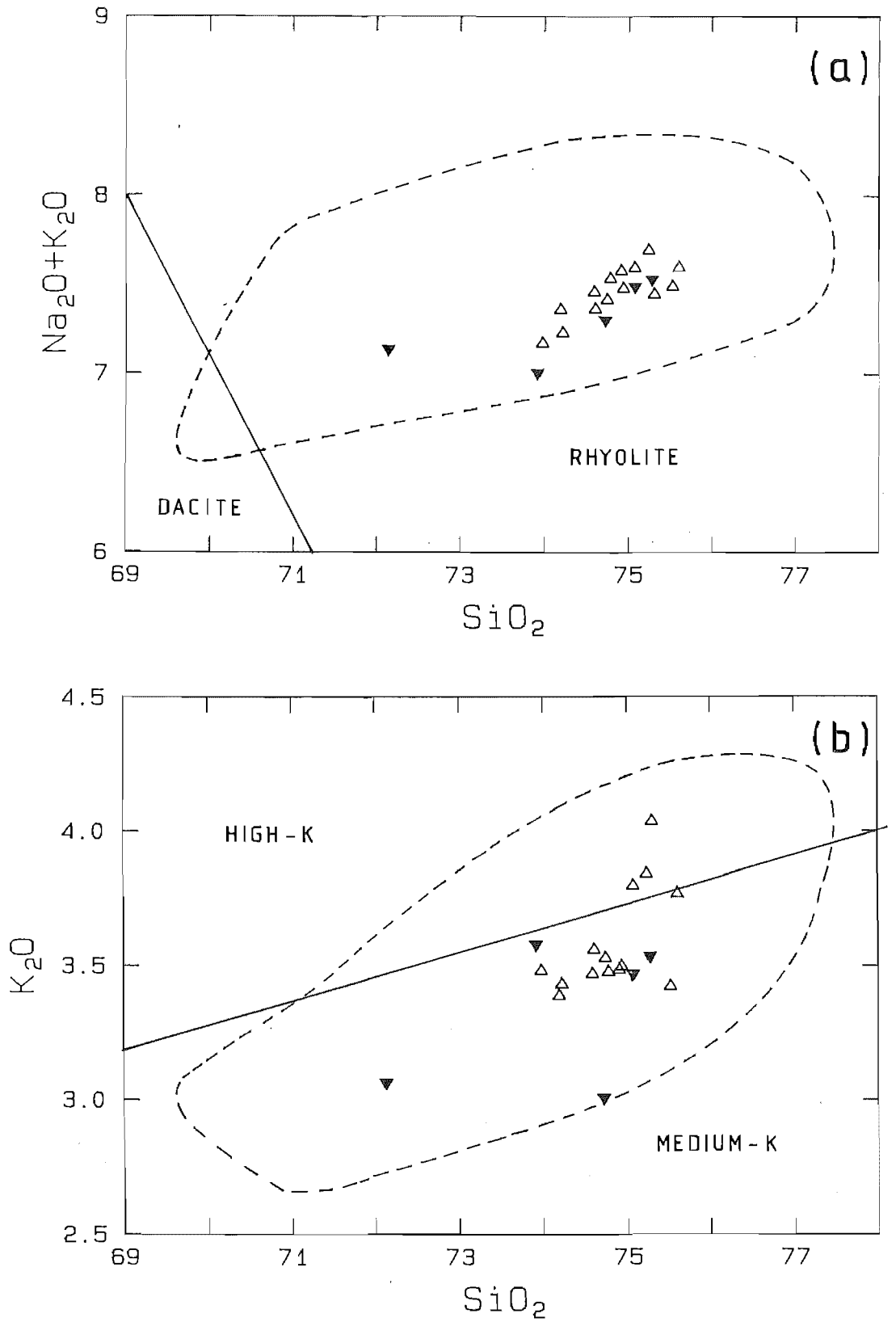

Figure 6.1. (a) Total alkali vs SiO_2, and (b) K_2O vs SiO_2 variation diagrams for Chimp Ignimbrite. The lines defining the rhyolite - dacite and medium-K - high-K fields are from Le Maitre (1989). Δ = crystal-poor pumice; ▼ = crystal-rich pumice. The dashed line shows the compositional field for Pokai Ignimbrite.

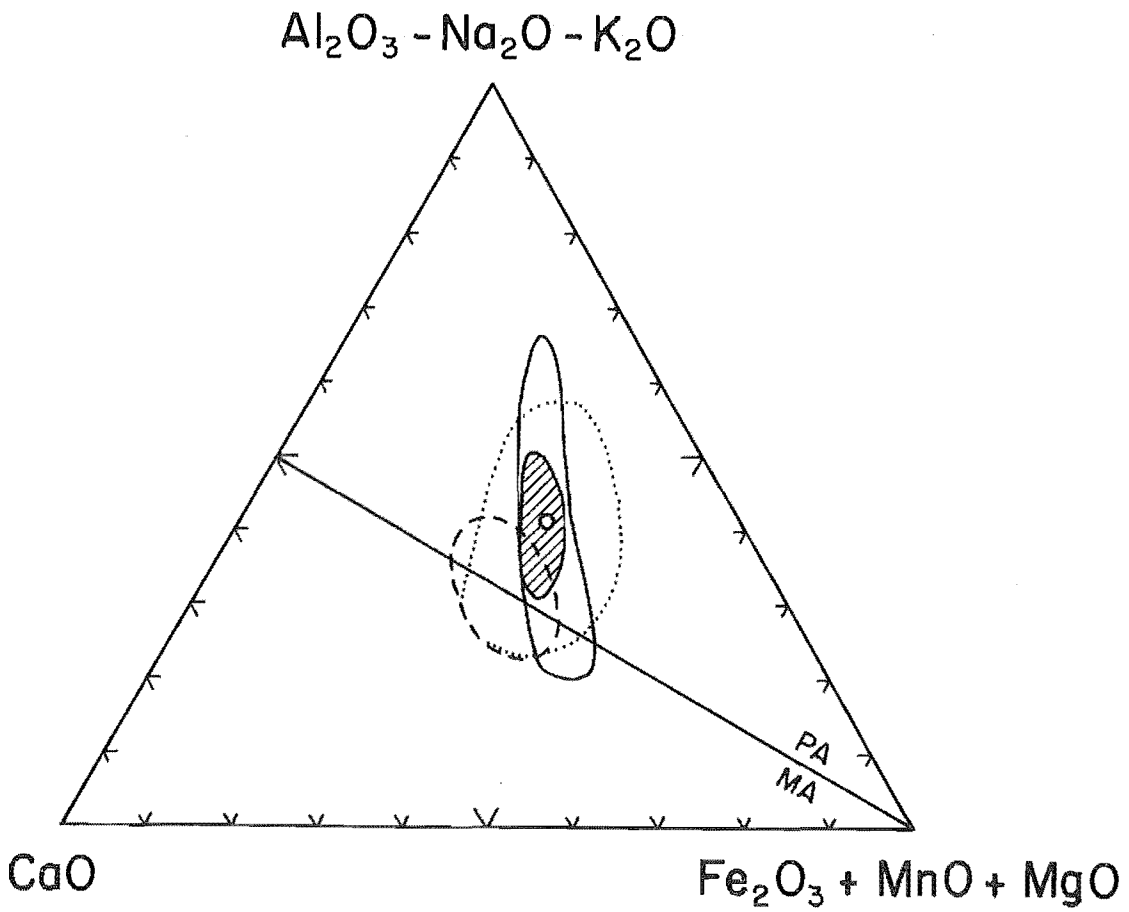

Figure 6.2. The compositional field and the average composition of the Chimp Ignimbrite pumices plotted on an ACF diagram. The fields of TVZ rhyolitic lavas and ignimbrites and of Pokai Ignimbrite are also shown. The data for the rhyolitic lavas and ignimbrites include 28 and 47 analyses, respectively, from published and unpublished records (Bellamy, 1991; Briggs et al., 1992; Cole, 1979b Houghton & Weaver, unpublished data; Karhunen, unpublished data); a complete list of all analyses used is given in Appendix D (Tables D.6 and D.7). The MA-PA line marks the boundary line between metaluminous (MA) and peraluminous (PA) fields. The boundary between I- and S-type granites, as defined by Chappell and White (1974) lies slightly above this join (1 % normative C).

= Chimp Ignimbrite with the average composition

= Pokai Ignimbrite

= TVZ rhyolitic lavas

= TVZ rhyolitic ignimbrites

rhyolitic lavas and ignimbrites, and the Pokai Ignimbrite field. Chimp Ignimbrite data plots close to the Pokai Type 1b field, except that the Chimp Ignimbrite is only mildly peraluminous to peraluminous, whereas Pokai Type 1b composition ranges from mildly to strongly peraluminous. It is also similar to other TVZ ignimbrites (see Fig.6.2).

6.3. CIPW norms

The CIPW norms and standard deviations of Chimp Ignimbrite data are given in Table 6.2. Normative quartz ranges from 32-37 %, though modal quartz is rare. Feldspar, orthopyroxene, magnetite, ilmenite and apatite are calculated normative phases and occur as phenocrysts. All samples include normative C (i.e. they are peraluminous); the average C content is 1.8 %, slightly higher than the average C contents of any of the Pokai Ignimbrite types (see Table 5.2). However, the Chimp Ignimbrite has a much narrower range in normative C.

The compositional fields for the Chimp Ignimbrite are shown on An-Ab-Or and Q-Ab-Or triangular diagrams in Fig.6.3. The diagrams also show the fields of the Pokai Ignimbrite and other TVZ ignimbrites, and the average compositions of the North Island basement sediments. The Chimp Ignimbrite projects in the plagioclase field in the An-Ab-Or system (Fig.6.3.a) and plots across the quartz-feldspar boundary line in the Q-Ab-Or system (Fig.6.3.b), coinciding within the compositional fields of the Pokai Ignimbrite and other TVZ rhyolitic ignimbrites.

Table 6.2. CIPW compositional ranges, means and standard deviations for the Chimp Ignimbrite, excluding all the altered samples (4 of a total 23).

	Chimp	Mean	STD
Q	31.96-37.37	35.55	1.12
or	17.75-23.85	20.78	1.42
ab	28.85-36.34	32.95	1.86
an	5.31-9.00	5.88	0.91
C	0.30-3.38	1.80	0.86
hy	0.60-1.56	0.91	0.25
mt	1.44-1.85	1.54	0.10
il	0.27-0.74	0.43	0.11
ap	0.02-0.10	0.06	0.03

Fig.6.3. Normative (CIPW) quartz and feldspar compositional fields of the Chimp Ignimbrite pumices plotted in the on the (a) An-Ab-Or and (b) Q-Ab-Or triangular diagrams. The compositional fields of TVZ rhyolitic ignimbrites (same data used as in Fig.6.2; Appendix D, Table D.7), the Pokai Ignimbrite and the average compositions of North Island sedimentary basement rocks (Graham & Cole, 1991; Reid, 1982, 1983) are also shown.
Heavy solid curve in plot (a) represents the quartz-saturated two feldspar boundary curve and in plot (b) the quartz-feldspar (horizontal line) and two-feldspar (vertical line) boundary curves. The piercing point defines the minimum melting composition for $(Q\text{-}Ab\text{-}Or)_{97}An_3$-system at 1 kb water vapour pressure (James & Hamilton, 1969).

= Chimp Ignimbrite

= Pokai Ignimbrite

= TVZ rhyolitic ignimbrites

O = Eastern basement (Torlesse) metagreywackes

□ = Western basement (Waipapa) metagreywackes

X / Y = experimental TVZ greywacke and argillite compositions, respectively

★ = Kawerau Geothermal Area greywacke composition (borehole material only)

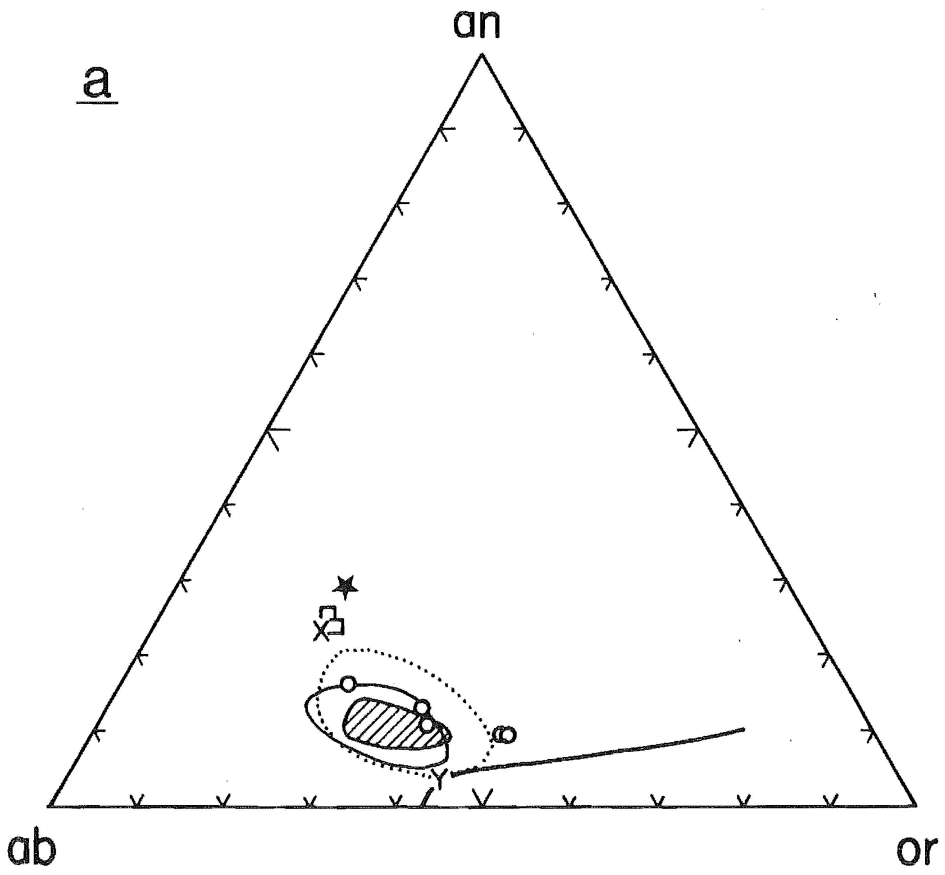
a
an
ab
or

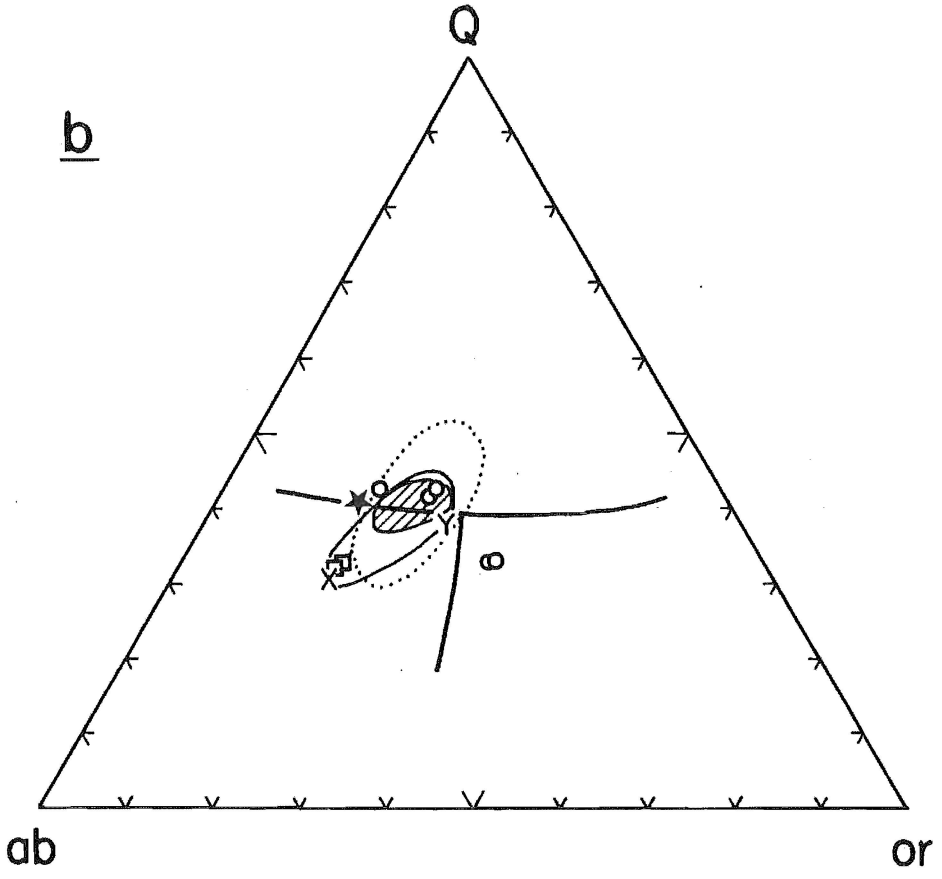
b
Q
ab
or

6.4. Major and trace element chemistry

Chimp Ignimbrite pumices have been divided into two types; crystal-poor (Type A) and crystal-rich (Type B) pumices, in much the same way as the Pokai Ignimbrite. The overall crystal content in the Chimp Ignimbrite is however lower than that in the Pokai Ignimbrite; the crystal-poor Chimp Ignimbrite pumices having phenocryst contents ranging from trace amounts to ca. 1 vol.%, while the crystal-poor Pokai pumices have 0.5-3.5 vol.% phenocrysts. The 'crystal-rich' Chimp Ignimbrite pumices have a phenocryst content of max. 8 vol.%, whereas in the crystal-rich Pokai pumices the phenocryst contents range from 6-12 vol.%.

The Chimp Ignimbrite has a relatively narrow range of major and trace element compositions compared to the Pokai Ignimbrite. The SiO_2 content ranges from 72.1-75.6 wt.% (average 74.7 %, Table 6.1), whereas the Pokai Ignimbrite ranges from 68.7-77.3 wt.% SiO_2 (Table 5.1). Selected major and trace element data plotted against SiO_2, and Sr vs Rb and Rb/Sr vs Sr diagrams are shown in Fig. 6.4.

In the Harker variation diagrams Sr vs Rb and Rb/Sr vs Sr the Chimp Ignimbrite plots in two broad groups; a low-Sr and a high-Sr group; more or less coinciding with Pokai Types 1b and 2, respectively. In general Type A pumices have lower Sr than Type B. There is an overall decrease in TiO_2, Al_2O_3, FeO_t and Zr, and an increase of K_2O and Rb with increasing SiO_2, although the differences between the crystal-poor and crystal-rich pumices are not as well marked as in the Pokai pumice types. Both MgO and Na_2O show a wide scatter in their concentrations. In most samples CaO and Sr contents are

Figure 6.4. Selected major element variation diagrams for the Chimp Ignimbrite pumice, excluding all the altered (kaolinitised) samples. Total iron as Fe_2O_3. The dashed lines mark the compositional fields of the Pokai Ignimbrite.

Δ = Type A pumice
▼ = Type B pumice

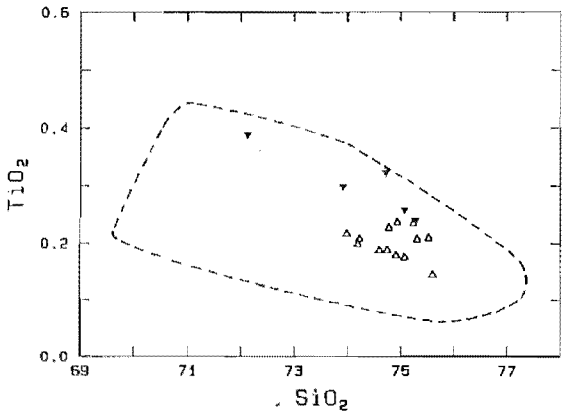
TiO2
0.6
0.4
0.2
0.0
69
71
73
75
77
SiO2

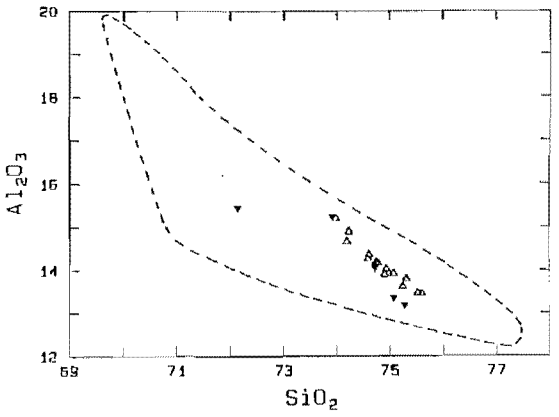
Al2O3
20
18
16
14
12
69
71
73
75
77
SiO2

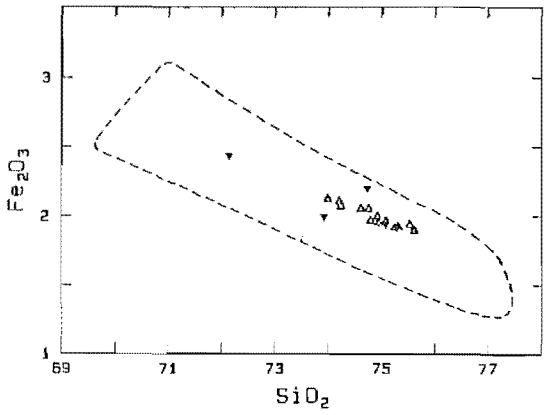
Fe2O3
3
2
1
69
71
73
75
77
SiO2

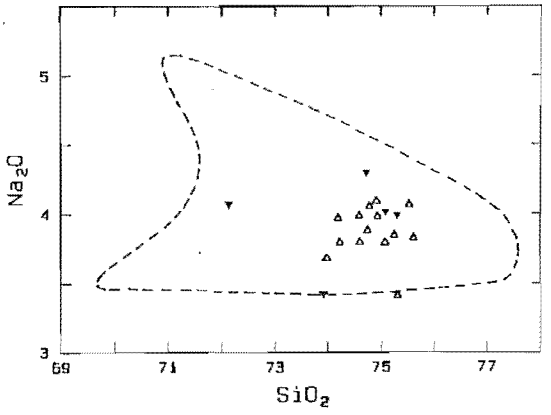
Na2O
5
4
3
69
71
73
75
77
SiO2

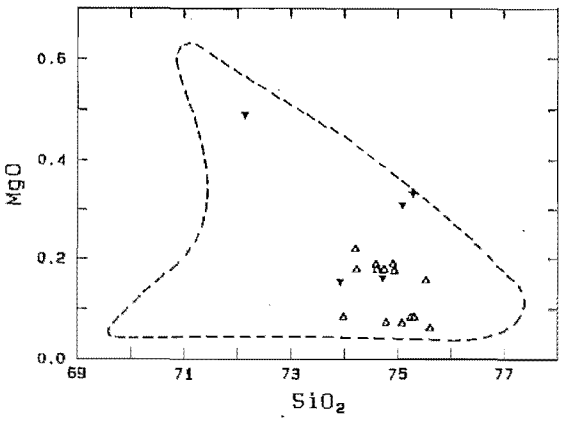
MgO
0.6
0.4
0.2
0.0
69
71
73
75
77
SiO2

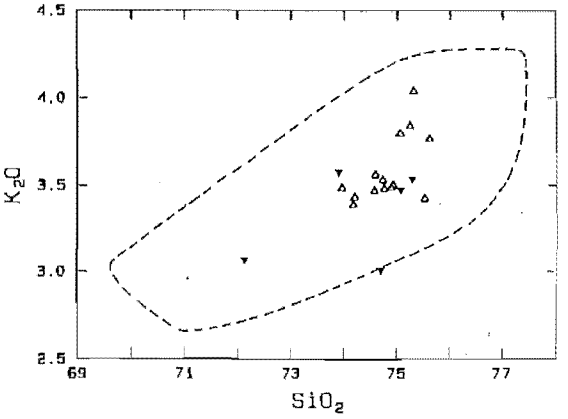
K2O
4.5
4.0
3.5
3.0
2.5
69
71
73
75
77
SiO2

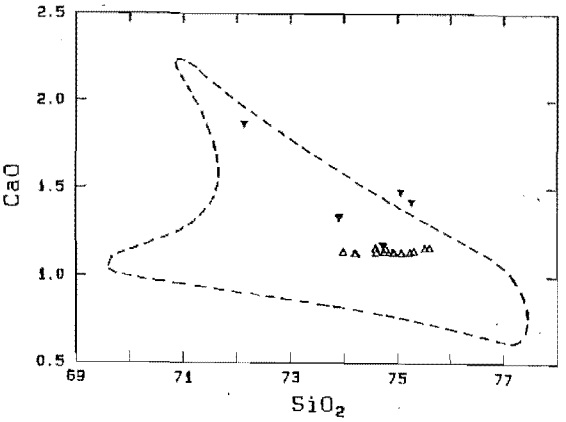
CaO
2.5
2.0
1.5
1.0
0.5
69
71
73
75
77
SiO2

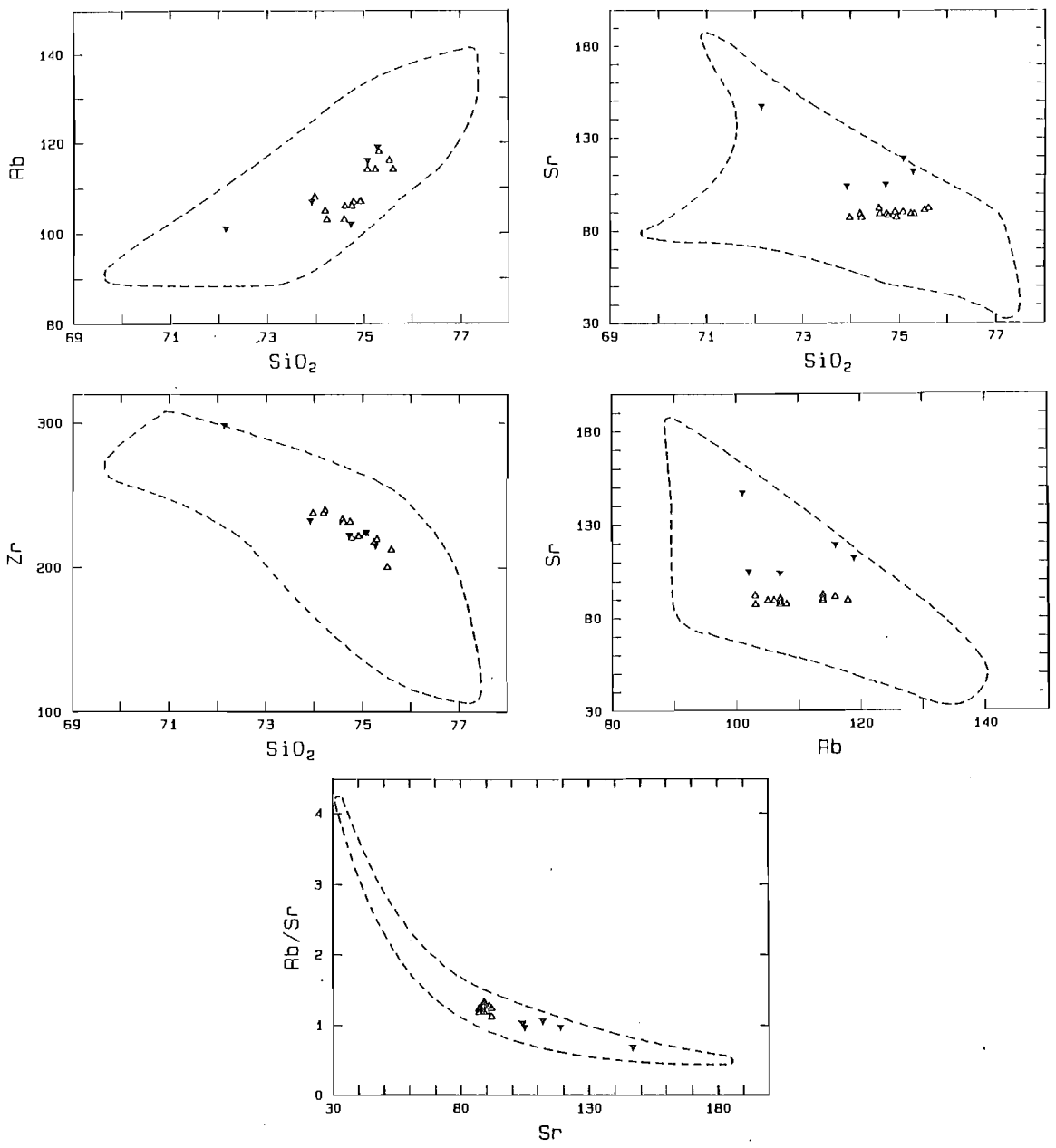

Figure 6.3. cont. Selected trace element variation diagrams for the Chimp Ignimbrite pumice, excluding all the altered (kaolinitised) samples. The dashed lines mark the compositional fields of Pokai Ignimbrite.

Δ = Type A pumice
▼ = Type B pumice

constant, but in a few samples there is a marked increase in their concentrations.

Overall, Chimp Ignimbrite pumices fall within the field of Pokai Type 1b pumices. Type B pumices with higher TiO_2, Al_2O_3, FeO_t, CaO and Sr contents fall within the Pokai Type 2 field.

7. PETROGENESIS

7.1. Introduction

In this chapter, petrographic, mineralogical and geochemical data for the Pokai and Chimp ignimbrites are discussed. As the two ignimbrites have rather similar mineralogy and geochemistry and because data for the younger, Pokai Ignimbrite are much more extensive than those of the Chimp Ignimbrite, the petrogenesis of the Pokai Ignimbrite is the main emphasis in this chapter.

7.2. Water content in the magma reservoir

The dominant volatile constituent in silicic systems, water, is inferred to vary considerably in concentration and may thus exert a strong control not only on the eruptive style but also on the type and abundance of phenocrysts (Hildreth, 1981; Rutherford, 1985). Microprobe glass analyses (chapters 4.2.2 and 4.3.2) indicate an average water content in the Pokai and Chimp pumices of 3.3 and 3.2 wt.% H_2O, respectively. Pre-eruptive water content in silicic magmas can also be estimated by comparison with appropriate experimental phase equilibria. Estimates of water content in the pre-eruptive magma reservoir, based on P_{total}= 200 MPa (2 kb; Naney, 1983), are given in Table 7.1.

Pokai Ignimbrite.

In Naney's (1983) experiments alkali feldspar always accompanies quartz; however, no modal alkali feldspar occurs in the Pokai mineral assemblage. K_2O content in the Pokai

Table 7.1. Estimated water contents in the Pokai (a) and Chimp (b) Ignimbrites by comparison with experimental studies (Naney, 1983) on synthetic granite. Temperature estimates are based on the Fe-Ti oxide equilibrium temperatures and/or the plagioclase liquidus geothermometer (Tables 4.9 for the Pokai, and 4.16 and 4.20 for the Chimp Ignimbrites, respectively).

(a) Pokai Ignimbrite

S	T	Mineral assemblage*	Fe-Ti temperature		Wt.% H_2O
			Min	Max	
1	1a	+qz(+amph)	740°C	849°C	0.5-3.1
2	1a	+qz(+amph)	741°C	833°C	0.6-3.1
3	1b	+qz	797°C	837°C	0.5-1.7
4	1b	(+qz)	790°C	1030°C	<1.8
5	2	+qz(+cpx)	793°C	823°C	0.8-1.5
6	2	(+qz)	810°C	981°C	<1.2

S = sample:
1 = T2/2 (ref.no. 219) 2 = T2/3 (ref.no. 220) 3 = 66/1 (ref.no. 128)
4 = 132/3 (ref.no. 181) 5 = 108/1 (ref.no. 153) 6 = T19/1 (ref.no.227)
T = pumice type
* Minerals in addition to ubiquitous plag+opx+Fe-Ti oxides; mineral phases in parentheses occur only in trace amounts.

(b) Chimp Ignimbrite

S	Mineral assemblage*	Temperature			Wt.% H_2O
		Plag min	Plag max	Fe-Ti	
1	(+opx+bio)	674°C	759°C	-	3-5
2	+opx+cpx+amph(+bio)	651°C	770°C	-	2.2-3.6
3	(+opx+qz)	777°C	858°C	-	<2.1
		-	-	805°C	<1.4

S = sample:
1 = 33/1 (ref.no. 236) 2 = 93/1 (ref.no. 249) 3 = 146/1 (ref.no. 253)
* Minerals in addition to ubiquitous plag+Fe-Ti oxides; mineral phases in parentheses occur only in trace amounts.

samples (an average of 3.66 wt.% in Type 1a) is much lower than that of Naney's experimental material (6.1 wt.% K_2O in the synthetic granite composition), so the absence of modal alkali feldspar is probably due to the low bulk K_2O composition. It should be noted therefore, that due to this contrast with the experimental magma composition, the results for the Pokai magma must be indicative only. However, the results can be used in estimating the relative water contents between the different pumice types.

The range of the Fe-Ti oxide equilibrium temperatures in the Pokai Ignimbrite varies considerably in individual samples, in Type 1a sample T2/2 (76.95 wt.% SiO_2, 6 % modal quartz) it ranges from 740-849°C (see Appendix C.7). A multiple phenocryst population was present in the liquid, suggesting that some of the Fe-Ti oxides were not in equilibrium with their surrounding liquid at the time of the eruption. Because the Fe-Ti oxide compositions are very sensitive to changes in temperature and oxygen fugacity of the surrounding liquid, any thermal disturbance would cause the phenocryst compositions to re-equilibrate to the new conditions (Schuraytz et al., 1989).

During mixing or convection, magma batches of different composition comingle. If the mixing occurs suddenly and is of a relatively short duration, the phenocrysts entering a new thermal system may not have time to equilibrate to the new conditions. This kind of sudden mixing may occur immediately prior to eruption and phenocrysts from different parts of the magma chamber thus reflect the conditions of their original magmatic environment. Plagioclase and orthopyroxene phenocrysts also show polymodal compositional ranges within individual pumices (see Figs.4.8 and 4.11).

Distinct chemical zones must have been present in the Pokai magma body (chapter 5.5). Because pumices from all compositional types contain polymodal phenocryst populations, some mixing among the compositional types is inferred to have occurred prior to the eruption. However, the mixing was not sufficient to obscure the primary compositional differences between Types 1a, 1b and 2.

On the basis of the previous discussion it is suggested that the minimum Fe-Ti oxide temperatures (740-760°C) calculated for Type 1a pumices (high SiO_2 and high modal quartz contents) represent the temperature conditions at the top of the Pokai magma chamber. The experimental results of Naney (1983) on synthetic granite as reference material gives a water content of 2.6-3.1 wt.% H_2O for the high-silica Type 1a magma. In both Types 1b and 2 a temperature range of 800-830°C predominates suggesting a lower water content, of 0.8-1.5 wt.% H_2O. The estimates of water contents in silicic liquids in Naney's (1983) experiments are based on a water pressure of 2 kb, whereas the water pressure in the Pokai magma chamber was probably lower, from 0.5 to 1 kb, prior to the eruption (see chapter 4.2.2). In general, the solubility of H_2O in silicate melts increases with pressure, so that at lower water pressures more liquid-phase H_2O would be present than in melts with higher pressures. Thus the H_2O contents in the Pokai magma chamber may have been somewhat higher than assumed above.

Modal amphibole (hornblende) has been found in 14 (of 77 examined) samples, of all pumice types, and ranging from trace amounts to 0.8 %. Burnham (1979) has shown that at 0.5 kb the minimum H_2O content of the melt required for crystallisation

of hornblende from magmas of granitic composition is ca. 3 wt.% H_2O. Similar constraints apply to magmatic crystallisation of biotite. Because Burnham's (1979) experiments, much like Naney's (1983) are based on high K_2O liquids, the comparisons should therefore be regarded as indicative only. The lack of biotite in the Pokai Ignimbrite may be due to the relatively low K_2O content in the magma. However, biotite has been found in the Chimp Ignimbrite, which has very similar K_2O concentration to the Pokai Ignimbrite, thus indicating that the occurrence of biotite may not be solely related to the abundance of K_2O. The rarity and small size of amphibole in the Pokai Ignimbrite suggest that the amphibole was near its stability limit, so a water content of ca. 3.5 wt.% H_2O in the upper levels of the magma chamber seems reasonable, whereas deeper in the magma column the water content was probably lower.

Chimp Ignimbrite.

In the Chimp Ignimbrite the water content estimates range from <1.4-5 wt.% H_2O; the highest value is based on the plagioclase liquidus temperature for a sample with biotite present (Table 7.1.b). The overall magma temperature seem to have been lower in the Chimp magma chamber, between 650-750°C in the uppermost part, than that in the Pokai magma. The lower temperature of the Chimp magma may have been due to higher water contents as the presence of water generally lowers the melting temperature of the magma (Burnham, 1979). Occurrence of both biotite and amphibole support the suggestion that the water content was somewhat higher in the Chimp magma, possibly ca. 4 wt.% H_2O.

7.3. Causes of variation between the pumice types

Features suggesting fractional crystallisation has occurred in the Pokai Ignimbrite magma include: a) the increasing SiO_2, K_2O and Rb contents with decreasing Al_2O_3, FeO_t, CaO, Zr and Sr from Type 2 to Types 1b and 1a (see Fig.5.9), and b) the different crystal content in pumice Types 1a-b and Type 2.

Crystallisation of feldspars will cause Rb to concentrate in the melt, and Sr and Ba to become depleted in the melt. Consequently the most fractionated, SiO_2 rich rock compositions should also have the highest Rb/Sr ratios. The abundance of Rb, Sr and Ba together with the Rb/Sr ratio can therefore be used as an indicator of degree of fractionation. The quasi-linear negative trend on the Rb/Sr concentrations (Fig.5.10.e) thus suggests fractionation between the pumice types, and together with decreasing concentrations of CaO in Types 1a and 1b, strongly indicate fractionation of plagioclase. Though Ba varies from 600 to 1300 ppm, there is no clear trend between the different pumice types, indicating that no K-feldspar or biotite crystallised; consistent with the absence of these phases in the Pokai Ignimbrite.

Decrease in TiO_2, FeO_t and MgO in Types 1b and 1a may be accounted for by fractionation of orthopyroxene and Fe-Ti oxides, both found as modal phases. Zircon is present in about half of the thin sections examined (all types) and the decrease in Zr with increasing SiO_2 indicates a further separation of zircon from the liquid as the differentiation proceeded.

To evaluate whether the pumice Types 1a, 1b and 2 are related to each other by fractional crystallisation, least squares

modelling was used. The crystal-rich Type 2 composition was chosen as a possible parent magma for Types 1a and 1b. It has a generally low SiO_2 content, and other compositional features, like the highest TiO_2, FeO_t, CaO, Zr and Sr contents indicate that it represents the least evolved Pokai magma.

All mineral phases and compositions used in the calculations are from observed (analysed) phenocrysts and whole rock analyses. Minerals used in the fractionation models are plagioclase (80-95 % of all phenocrysts), orthopyroxene (1-8 %) and ilmenite (0.5-2 %).

In the fractionation models iron was calculated as total FeO and MnO and P_2O_5 were omitted because of the relatively poor analytical precision of these components. All data were then normalised to 100 % anhydrous (due to the exclusion of MnO and P_2O_5 the major element data in the fractionation models differs slightly from the data listed in Appendix D). Fractional crystallisation models were calculated only for those trace elements that showed large or moderate variation in the system and were not the major component of any trace mineral present in the pumices. Though Zr shows great variation, it was not chosen, because zircon occurs only as an accessory mineral. The mineral/liquid distribution coefficients in silicic systems for the trace elements used are given in Table 7.2. The results of the crystallisation models are considered acceptable if the sums of the squares of the residuals (s) are <1, good if <0.2 and excellent if <0.1, and the calculated trace element abundances are within 20 % of the observed abundances.

Two steps were tested using the fractional crystallisation

Table 7.2. Mineral/liquid distribution coefficients for rhyolitic rocks (unpublished compilation by A. Ewart, University of Queensland) used in the FC model for the Pokai Ignimbrite.

	Plag	Opx	Ilm
Rb	0.10	0.09	0.01
Ba	0.6	0.02	0.01
Sr	6	0.05	0.01

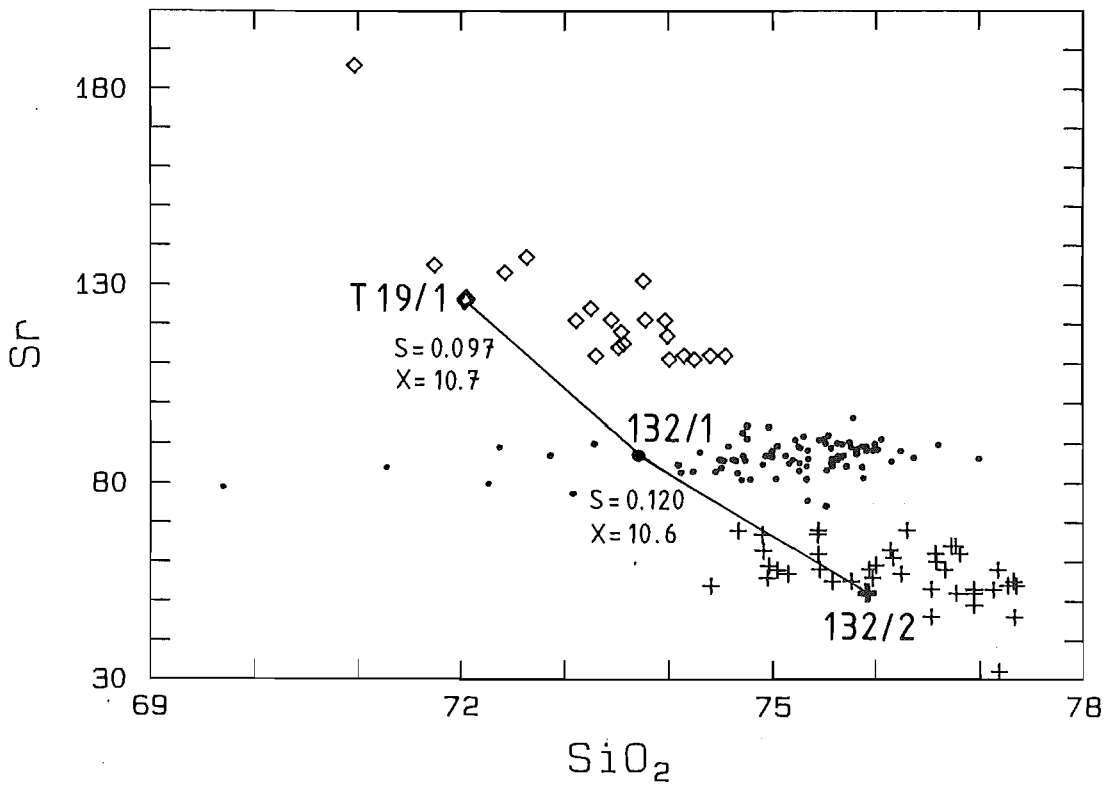

Figure 7.1. Fractionation of Type 2 (sample T19/1) → Type 1b (132/1) → Type 1a (132/2) shown as variation in Sr vs SiO_2 values.

+ = Type 1a pumice
● = Type 1b pumice
◇ = Type 2 pumice
S = sum of squares of residuals
X = crystals removed (%)

model:

Step 1 involves fractionating the crystal-rich Type 2 to produce the crystal-poor Type 1b.

Step 2 involves fractionating Type 1b to produce Type 1a.

The best fit model is shown in Table 7.3 and discussed below. To visualise the model, SiO_2/Sr fractionation paths for the end-members used are shown in Fig.7.1.

In Step 1, Type 2 sample T19/1 (72.04 % SiO_2) was used for the parent magma and Type 1b sample 132/1 (73.77 % SiO_2) was used for the daughter magma. Three mineral phases, plagioclase (An_{30}), orthopyroxene and ilmenite, were subtracted from the parent rock to obtain the calculated daughter magma. The results of this calculation are given in Table.7.3.a. Plagioclase was the main fractionating phase (9.6 %) with orthopyroxene (0.7 %) and ilmenite (0.4 %) also extracted. The residuals from this calculation are small (S = 0.097) and the mineral phases removed are consistent with the modal proportions of each phase. The trace element abundances also fall within the accepted values.

In Step 2 Type 1b sample 132/1 (73.77 % SiO_2) was used for the parent magma and Type 1a sample 132/2 (75.58 % SiO_2) as the daughter magma. Again three mineral phases, plagioclase (An_{31}), orthopyroxene and ilmenite, were subtracted from the proposed parent magma to obtain the daughter magma. The results are given in Table 7.3.b. The residuals are relatively small (S = 0.120), and the results are acceptable, though the realistic mineral proportions in the fractionating phases (in terms of modal proportions) are lower than the total calculated mineral proportions. The weight modes of minerals

Table 7.3. Results of the least squares and Rayleigh fractionation modelling (fractional crystallisation, FC; based on the method of Bryan et al., 1969) for the Pokai Ignimbrite magma types. Mineral/liquid distribution coefficients used are given in Table 7.2. The original mineral and bulk rock (whole pumice) analyses are given in Appendices C and D (Tables C.1, C.2 and C.4, and D.3, respectively.

FC-Step 1 (a): from low SiO_2 Type 2 rhyolite to medium SiO_2 Type 1b rhyolite.

FC-Step 2 (b): from medium SiO_2 Type 1b rhyolite to high SiO_2 Type 1a rhyolite.

(a) FC-Step 1
The parent magma is T19/1 (Type 2, ref.no.227)
The daughter magma is 132/1 (Type 1b, ref.no. 179)

Coef	% minerals	
-0.109	90.3	plagioclase (120)
-0.007	6.1	orthopyroxene (77)
-0.004	3.6	ilmenite (25)
1.120		

	SiO_2	TiO_2	Al_2O_3	FeO_t	MgO	CaO	Na_2O	K_2O
T19/1	72.33	0.34	15.84	2.24	0.24	1.51	4.27	3.22
132/1								
Obs	73.98	0.24	15.01	1.96	0.19	1.10	4.07	3.45
Calc	73.95	0.17	15.19	2.02	0.16	0.97	3.90	3.56
Dif	0.03	0.07	-0.17	-0.07	0.03	0.13	0.16	-0.11

S = 0.097 F = 89 % X = 10.7 %

	K_d	Parent	Daughter	Calculated	Residuals	Difference
Rb	0.10	102	114	113	1	1 %
Ba	0.53	725	786	761	25	3 %
Sr	5.42	127	87	77	11	13 %

(b) FC-Step 2
The parent magma is 132/1 (Type 1b, ref.no. 179)
The daughter magma is 132/2 (Type 1a, ref.no. 180)

Coef	% minerals	
-0.104	87.3	plagioclase (77)
-0.011	9.1	orthopyroxene (47)
-0.004	3.7	ilmenite (14)
1.119		

	SiO_2	TiO_2	Al_2O_3	FeO_t	MgO	CaO	Na_2O	K_2O
132/1	73.98	0.24	15.01	1.96	0.19	1.10	4.07	3.70
132/2								
Obs	75.75	0.11	14.18	1.48	0.12	0.78	3.87	3.70
Calc	75.71	0.05	14.37	1.55	0.09	0.56	3.77	3.81
Dif	0.04	0.07	-0.19	-0.07	0.04	0.22	0.11	-0.11

S = 0.120 F = 89 % X = 10.6 %

	K_d	Parent	Daughter	Calculated	Residuals	Difference
Rb	0.10	114	122	127	-4	3 %
Ba	0.51	786	777	826	-49	6 %
Sr	5.24	87	55	54	1	2 %

S = sum of squares of residuals
F = relative mass of magma remaining (%)
X = crystals removed (%)

fractionated were plagioclase 9.2 %, orthopyroxene 1 % and ilmenite 0.4 %. Again the trace elements show acceptable values.

The results of the fractionation model show that a low/medium SiO_2, high Sr Type 2 magma could yield a melt of the composition of medium SiO_2, medium Sr Type 1b and further a high SiO_2, low Sr Type 1a rhyolite by simple fractional crystallisation, initially involving removal of plagioclase, and in smaller amounts orthopyroxene and ilmenite.

Chemical variation within the Chimp Ignimbrite pumices suggests that some differentiation took place in the Chimp magma chamber before the eruption. The occurrence of two different pumices in a single outcrop (i.e. samples 93/1 and 93/4, ref.nos.249 and 252, Appendix D, Table D.8) indicates that the magma chamber was zonated before the eruption and that some mixing then took place either before or during the eruption. The compositional gaps in the concentrations of CaO, Zr, Rb and Sr (Fig.6.3) may be due to incomplete sampling as the number of samples, particularly of the crystal-rich, high Sr pumices is small. The data should therefore be considered with caution.

The variation in pumice chemistry is probably due to differences in modal mineralogy. Most of the very crystal-poor pumices (<1 vol.% phenocrysts, low TiO_2, FeO_t, MgO, CaO and Sr) contain plagioclase with only trace amounts of mafic minerals. With increasing crystal-content, and increasing TiO_2, FeO_t, MgO, CaO and Sr concentrations, the proportions of mafic minerals also increase. Although these features suggest

crystal fractionation the data are considered to be insufficient for reliable fractional crystallisation modelling between the different Chimp pumices.

7.4. Origin of the TVZ magmas

Rhyolites are by far the most common volcanic rocks exposed in the TVZ (16,000 km^2; Reid, 1983). Andesites and dacites make up only a small proportion of the volcanic rocks (2.1 %; Cole, 1979). Most of these occur at the southwestern end of the zone, i.e. Tongariro Volcanic Centre, although increasing amounts have been discovered subsurface further north, on the eastern side of TVZ (Browne et al., 1992). Associated with the rhyolites there have been minor basaltic eruptions, but these make only <1 % of all TVZ eruptives (Wilson et al., 1984).

Mesozoic greywackes and argillites are exposed on both sides of TVZ and probably also form the basement beneath (Reid & Cole, 1983). The basement rocks have been divided into a 'western basement', or Waipapa terrane metasediments, with an overall mildly peraluminous composition, and an 'eastern basement', or Torlesse terrane metasediments (Blattner & Reid, 1982; Reid, 1983), which is strongly peraluminous (see Fig.5.7, chapter 5.3.2).

The TVZ basalts are porphyritic (5-20 % phenocrysts of olivine, plagioclase and occasionally clinopyroxene), high-alumina basalts which are similar to many MORB's (Gamble et al., 1990). Petrologic studies indicate that the high-alumina basalts are most probably parental to more evolved, low-alumina basalts by processes such as crystal fractionation, involving olivine and plagioclase (Gamble et al., 1990). It

has also been shown that the majority of TVZ mafic and intermediate volcanic rocks are generated from the low-alumina basaltic magmas by fractional crystallisation combined with crustal assimilation (Graham & Hackett, 1987; Graham & Cole, 1991; Graham et al., 1992). Metasedimentary xenoliths, identified as being of lower crustal origin, have been found both in the andesitic and dacitic lavas in Ruapehu and White Island (Graham & Hackett, 1987; Graham & Cole, 1991), strongly supporting the suggestion of assimilation of crustal material. Further evidence indicating the presence of a contaminant is the higher Sr and lower Nd isotope ratios and greater LILE contents of the andesites than that expected by fractional crystallisation of a basaltic magma alone (Graham & Hackett, 1987).

The most likely crustal contaminants would be the subvolcanic metasedimentary basement. Of the two possible basement lithologies, the chemically more evolved and the more radiogenic Torlesse Supergroup has generally been the favoured choice over Waipapa metasediments to produce andesites, since the proportion of contaminant required in most petrogenetic models is then much lower (Graham & Hackett, 1987). Moreover, the metamorphic xenoliths found in Ruapehu and White Island lavas, have been identified as being of low-grade Torlesse terrane greywacke (Graham & Hackett, 1987; Graham & Cole, 1991).

According to Ewart (1969) and Ewart and Stipp (1968) the sedimentary rocks exposed in the TVZ represent the low-grade equivalents of deep-level metasedimentary basement rocks which melted to produce the voluminous rhyolitic magmas in the TVZ. However, on the basis of O, Sr and Nd isotope studies, Perfit

et al. (1981) and Blattner and Reid (1982) have suggested that the parental magmas to TVZ basalts, andesites and rhyolites were derived from a subcrustal or oceanic crust igneous source by differentiation or partial melting, i.e. from below the Torlesse terrane basement, but were contaminated by these sediments.

Conrad et al. (1988) have studied the melting relations of two proposed crustal source compositions for the TVZ rhyolites. They used glasses of intermediate composition (65 wt.% SiO_2) as starting material, representing a peraluminous 'S-type' greywacke and a metaluminous 'I-type' dacite. The experimental results indicate that the mainly Di-normative TVZ rhyolitic magmas are probably derived from igneous sources below the metasedimentary basement and are generated either by melting of strongly Di-normative lower crust or by fractionation of arc-related mafic and/or intermediate magmas. Conrad et al. (1988) also suggest a possibly involvement of contamination by shallower crustal material.

Graham et al. (1992) studied the origin of TVZ volcanic rocks in the light of Pb isotope and U/Pb data, with particular emphasis on the rhyolitic ignimbrites and lavas. They showed that in most of the studied samples, Pb isotope ratios of the silicic volcanics were very uniform and remarkably similar to some of the TVZ andesites found along the eastern margin of the TVZ. These andesites underlie the rhyolitic rocks and rest in part on the metasedimentary basement (Browne et al., 1992). The results of Graham et al.'s (1992) studies indicate that the voluminous ignimbrites and rhyolites could have been generated by melting of the early-formed andesites with minor crustal assimilation.

The origin of TVZ rhyolitic magmas by melting of the subvolcanic metasedimentary basement has now been largely rejected for the following reasons:

1. The TVZ rhyolites are generally of 'I-type' character with normative C contents reaching <1.4 %, slightly above the I/S boundary of Chappell and White (1974) (Conrad et al., 1988). The metaluminous to mildly peraluminous, dominantly Di-normative magmas, are unlikely to have equilibrated with peraluminous phases (C-normative) equivalent to the TVZ basement sediments.

2. The radiogenic Pb isotope composition of Torlesse metasediments and the high Sr and O isotope values in both TVZ basement rocks are in contrast with the much lower values for the rhyolites (Blattner & Reid, 1982; Graham et al., 1992).

7.5. Differentiation from mafic-intermediate magmas

In order to examine the possible relationship of the studied rhyolitic ignimbrites to the TVZ mafic-intermediate magmas least squares petrogenetic models involving fractional crystallisation (FC) and fractional crystallisation combined with crustal contamination (AFC) were used [based on the methods of Bryan et al. (1969) and DePaolo (1981), respectively].

As possible parental magmas, three basic-intermediate lava compositions from Ruapehu and related vents were chosen. Two samples represent Graham and Hackett's (1987) Ruapehu Type 1 lavas (1954 Ngauruhoe basic andesite and Wahianoa acid andesite). Phenocryst contents in both lavas range from 15-40 %, and include plagioclase, clinopyroxene, orthopyroxene,

olivine and Fe-Ti oxides. Both lavas were most probably generated by crystal fractionation of basic parents (high-alumina basalts) combined with crustal contamination. The third sample represents Graham and Hackett's (1987) Ruapehu Type 5 lava (Ohakune acid andesite), which may have generated by crystal fractionation alone from a basaltic parent magma. The Ohakune andesite contains ca. 10 % phenocrysts, plagioclase, clinopyroxene, orthopyroxene, olivine and Fe-Ti oxides. The bulk rock chemistry of the proposed parent magmas and the mineral compositions used for the FC and AFC models are given in Appendix E (Tables E.1 and E.2, respectively).

As possible contaminants in the first two AFC models two metasedimentary basement compositions were used, these are the Torlesse (Graham & Hackett, 1987), and Waipapa metagreywacke (Graham & Cole, 1991) compositions. In the third model a meta-igneous granulite (MIG) composition was used as a possible contaminant. These granulite xenoliths have been found in lavas from Mount Ruapehu, and represent either hydrothermally altered fragments of oceanic crust or igneous rocks of unknown origin altered in lower crust (Graham et al., 1990). Whole rock and trace element compositions used in the AFC models are given in Appendix E (Table E.3). In all models, iron was calculated as total FeO, and MnO and P_2O_5 were omitted due to the relatively poor analytical precision of these components. All data were then normalised to 100 % anhydrous (due to the exclusion of MnO and P_2O_5 the major element data shown in the models differs slightly from the data listed in Appendix E.

7.5.1. Fractional crystallisation

In the FC-Models 1-3 Pokai Ignimbrite Type 2 composition (sample T19/1, 72.3 % SiO2) was used as the fractionated phase (daughter magma) and Wahianoa, Ngauruhoe and Ohakune andesites, respectively, as the proposed parent magmas (Tables 7.4.a-c). As seen from Tables 7.4.b and 7.4.c (unacceptably high sums of the squares of residuals), Ngauruhoe and Ohakune andesites are not suitable as parental magmas to the Pokai Ignimbrite, and have not been used in any further petrogenetic modelling.

The Wahianoa acid andesite (Ruapehu Type 1 lava; Table 7.4.a) produces an acceptable sum of the squares of residuals (S = 0.178) for the major elements, though the observed values for TiO_2, Na_2O and K_2O are somewhat too high. The FC-Model 1 involves 49.2 % crystallisation of the andesitic magma; the weight modes of mineral phases subtracted from the parent magma are plagioclase 33.5 %, clinopyroxene 6.1 %, orthopyroxene 6 % and titanomagnetite 3.6 %. To confirm the results of the major element modelling trace-element concentrations were calculated using published K_d values (Table 7.5). The calculated trace element abundances (Fig.7.4.a) can be considered acceptable since the calculated values, except for Cr are within 20 % of measured values.

In FC-Model 4 the average Chimp composition (see Table 6.1) was used as the possible daughter magma and the Wahianoa acid andesite as the parent magma. The results are shown in Table 7.6. The sums of the squares of residuals (S = 0.099) give a slightly better fit than that for the Pokai Type 2 composition, though the observed values for TiO_2 and K_2O are

Table 7.4. Results of the least squares and Rayleigh fractionation modelling (fractional crystallisation, FC; based on the method of Bryan et al. 1969). Mineral/liquid distribution coefficients used are given in Table 7.5. The original bulk rock and mineral analyses of the andesitic parent compositions used are given in Appendix E (Tables E.1 and E.2, respectively).

FC-Model 1 (a): from Wahianoa acid andesite to low SiO_2 Pokai Type 2 rhyolite.

FC-Model 2 (b): from Ngauruhoe basic andesite to low SiO_2 Pokai Type 2 rhyolite.

FC-Model 3 (c): from Ohakune acid andesite to low SiO_2 Pokai Type 2 rhyolite.

S = sum of squares of residuals
F = relative mass of magma remaining (%)
X = crystals removed (%)

(a) FC-Model 1
The parent magma is WAH (Wahianoa acid andesite, 14867)
The daughter magma is T19/1 (Pokai Type 2, ref.no. 227)

Coef	% minerals	
-0.665	68.1	plagioclase
-0.119	12.2	orthopyroxene
-0.120	12.3	clinopyroxene
-0.071	7.3	titanomagnetite
1.969		

	SiO_2	TiO_2	Al_2O3	FeO_t	MgO	CaO	Na_2O	K_2O
WAH	61.36	0.73	17.87	6.21	2.58	6.02	3.62	1.61
T19/1								
Obs	72.33	0.34	15.84	2.24	0.24	1.51	4.27	3.22
Calc	72.35	0.17	15.87	2.27	0.18	1.48	3.95	3.02
Dif	-0.02	0.17	-0.03	-0.04	0.06	0.03	0.32	0.20

S = 0.178 F = 51 % X = 49.2 %

	K_d	Parent	Daughter	Calculated	Residuals	Difference
Rb	0.14	57	102	102	1	1 %
Ba	0.11	395	725	720	5	1 %
Sr	2.19	252	127	112	14	11 %
Zr	0.08	121	235	226	9	4 %
Nb	0.14	5	10	9	1	10 %
Ni	3.46	17	3	3	0	-
Cr	2.83	10	4	3	1	25 %
V	5.39	176	8	9	-1	13 %

(b) FC-Model 2
The parent magma is NGAUR (Ngauruhoe basic andesite, 29250)
The daughter magma is T19/1 (Pokai Type 2, ref.no. 227)

Coef	% minerals	
-0.686	54.3	plagioclase
-0.287	22.8	orthopyroxene
-0.201	15.9	clinopyroxene
-0.088	7.0	olivine
2.376		

	SiO_2	TiO_2	Al_2O_3	FeO_t	MgO	CaO	Na_2O	K_2O
NGAUR	56.38	0.76	16.68	8.30	5.26	8.33	3.15	1.14
T19/1								
Obs	72.33	0.34	15.84	2.24	0.24	1.51	4.27	3.22
Calc	70.23	1.69	17.18	10.90	-1.83	5.32	5.35	2.63
Dif	2.11	-1.35	-1.34	-8.66	2.07	-3.80	-1.08	0.59

S = 103.329 F = 42 % X = 57.9 %

	K_d	Parent	Daughter	Calculated	Residuals	Difference
Rb	0.12	38	102	82	21	21 %
Ba	0.10	215	725	470	255	35 %
Sr	1.76	248	127	128	-2	2 %
Zr	0.07	95	235	213	22	9 %
Nb	0.10	2	10	4	6	60 %
Ni	8.37	29	3	0	3	100 %
Cr	5.57	100	4	2	2	50 %
V	3.60	221	8	23	-15	>100 %

(c) FC-Model 3
The parent magma is OHAKU (Ohakune basic andesite, 14798)
The daughter magma is T19/1 (Pokai Type 2, ref.no. 227)

Coef	% minerals	
0.833	0	plagioclase
2.677	0	orthopyroxene
-0.350	16.6	clinopyroxene
-1.424	83.4	olivine
-0.775		

	SiO_2	TiO_2	Al_2O_3	FeO_t	MgO	CaO	Na_2O	K_2O
OHAKU	57.43	0.54	14.66	8.06	7.15	9.15	2.35	0.67
T19/1								
Obs	72.33	0.34	15.84	2.24	0.24	1.51	4.27	3.22
Calc	71.58	-0.11	16.76	6.97	-0.36	2.50	-0.17	-0.53
Dif	0.75	0.46	-0.92	-4.73	0.60	-0.99	4.44	3.75

S = 59.061 Trace element abundances not calculated

S = sum of squares of residuals
F = relative mass of magma remaining (%)
X = crystals removed (%)

Table 7.5. Mineral/liquid distribution coefficients for andesitic melts used in the FC, AFC and PM models. All values are from Gill (1981).

	Plag	Cpx	Opx	Oliv	Magn
Rb	0.2	0.02	0.02	0.01	0.01
Sr	3.2	0.08	0.03	0.01	0.01
Ba	0.16	0.02	0.02	0.01	0.01
Zr	0.01	0.25	0.1	0.01	0.4
Nb	0.025	0.3	0.35	0.01	1
Ni	0.01	7	14	58	12
Cr	0.01	10	7	34	10
V	0.01	18	7.2	0.08	63

Table 7.6. Results of the least squares and Rayleigh fractionation (fractional crystallisation, FC;based on the method of Bryan et al., 1969). Mineral/liquid distribution coefficients used are given in Table 7.5. The original bulk rock and mineral analyses of the andesitic parent used are given in Appendix E (Tables E.1 and E.2, respectively).

FC-Model 4: from Wahianoa acid andesite to medium SiO_2 Chimp rhyolite.
The parent magma is WAH (Wahianoa acid andesite, 14867)
The daughter is Chimp (average Chimp rhyolite, see Table 6.1)

Coef	% minerals	
-0.852	72.1	plagioclase
-0.168	14.2	orthopyroxene
-0.072	6.1	clinopyroxene
-0.090	7.6	titanomagnetite
2.176		

	SiO_2	TiO_2	Al_2O_3	FeO_t	MgO	CaO	Na_2O	K_2O
WAH	61.36	0.73	17.87	6.21	2.58	6.02	3.62	1.61
Chimp								
Obs	74.91	0.23	14.20	1.82	0.18	1.22	3.90	3.53
Calc	74.92	0.03	14.20	1.87	0.13	1.20	3.83	3.31
Dif	-0.01	0.21	0.00	-0.04	0.05	0.03	0.07	0.22

S = 0.099 F = 46 % X = 54.1 %

	K_d	Parent	Daughter	Calculated	Residuals	Difference
Rb	0.15	57	109	110	-1	1 %
Ba	0.12	395	827	783	44	5 %
Sr	2.32	252	97	90	7	7 %
Zr	0.07	121	229	250	-21	9 %
Nb	0.15	5	11	10	1	9 %
Ni	3.33	17	3	3	0	-
Cr	2.37	10	4	4	0	-
V	4.76	176	6	9	-3	50 %

S = sum of squares of residuals
F = relative mass of magma remaining (%)
X = crystals removed (%)

too high. The model involves 54.1 % crystallisation of the andesitic parent magma; plagioclase being the main fractionating phase (39 %). Other minerals subtracted were orthopyroxene (7.7 %), clinopyroxene (3.3 %) and titanomagnetite (4.1 %). Except for Cr, the calculated trace element abundances fall within acceptable values.

7.5.2. Assimilation and fractional crystallisation

In the AFC-Model 1 Pokai Type 2 composition (sample T19/1) was used as the fractionated phase, Wahianoa acid andesite as a parent magma and an average Torlesse metagreywacke composition as the contaminant. The results are given in Table 7.7.a. This model involves 49 % crystallisation of the parent magma, whereas only 4 % of material was added by assimilation of the wallrock. The weight modes of mineral phases subtracted from the parent magma are plagioclase 33.1 %, clinopyroxene 6.3 %, orthopyroxene 5.9 % and titanomagnetite 3.6 %. The sum of the squares of residuals is relatively small (S = 0.152); though the residuals for TiO_2 and Na_2O are somewhat too high. Except for Cr, the calculated trace element abundances are within acceptable values.

The AFC-Model 1 is almost identical to the FC model involving fractionation of Pokai Type 2 from a parent andesite, only the residuals for K_2O give a better fit in the AFC model. Also the proportions of mineral phases subtracted from the parent magma are similar to those obtained in the crystal fractionation model with the same daughter and parent compositions. The low amount of the assimilant (4 % contamination by Torlesse) indicates that crustal assimilation was not a dominant process

Table 7.7.a. Results of the least squares and Rayleigh fractionation modelling (assimilation and fractional crystallisation, AFC; based on the method of DePaolo, 1981). Mineral/liquid distribution coefficients used are given in Table 7.5. The original bulk rock and mineral analyses of the andesitic parent and of the contaminant rock used are given in Appendix E (Tables E.1, E.2 and E.3, respectively).

AFC-Model 1
The parent magma is WAH (Wahianoa acid andesite, 14867)
The contaminant is Torlesse metagreywacke
The daughter magma is T19/1 (Pokai Type 2, ref.no. 227)

Coef	% minerals	
-0.604	67.6	plagioclase
-0.108	12.1	orthopyroxene
-0.115	12.9	clinopyroxene
-0.067	7.4	titanomagnetite
1.816		

	SiO_2	TiO_2	Al_2O_3	FeO_t	MgO	CaO	Na_2O	K_2O
WAH	61.36	0.73	17.87	6.21	2.58	6.02	3.62	1.61
T19/1								
Obs	72.33	0.34	15.84	2.24	0.24	1.51	4.27	3.22
Calc	72.34	0.18	15.88	2.27	0.19	1.49	3.93	3.18
Dif	-0.01	0.16	-0.04	-0.03	0.04	0.02	0.34	0.05

S = 0.152 M_a = 4 % M_c = 49 % r = 0.008 F = 55 %

	K_d	Parent	Daughter	Calculated	Residuals	Difference
Rb	0.14	57	102	114	-12	12 %
Ba	0.11	395	725	739	-14	2 %
Sr	2.18	252	127	114	12	9 %
Zr	0.08	121	235	223	12	5 %
Nb	0.14	5	10	8	2	20 %
Ni	3.49	17	3	3	0	-
Cr	2.89	10	4	3	1	25 %
V	5.52	176	8	9	-1	13 %

S = sum of squares of residuals
M_a = assimilation rate, i.e. total mass of material assimilated (%)
M_c = fractionation rate, i.e. crystals removed (%)
$r = M_a/M_c$
F = relative mass of magma remaining

during the evolution of the magma. The low M_a/M_c ratio (assimilation rate/crystallisation rate, i.e. r = 0.08) suggests that the wallrock must have been relatively cool (the system operated near the surface), i.e. heat loss was extensive inhibiting assimilation and favouring crystallisation (DePaolo, 1981). Taylor (1980) has calculated that assimilation of 1 g of cool wallrock (at 150°C) into a magma at 1150°C could be thermally balanced by crystallisation of 3.25 g of crystals, which gives an approximate upper limit of r = 0.3 (1/3.25). The value of r = 0.08 determined here is well within the upper limit. The results thus show that ca. 50 % crystallisation, involving plagioclase, orthopyroxene, clinopyroxene and titanomagnetite, of a Ruapehu-type acid andesite (Wahianoa), combined with smaller amounts of wallrock assimilation (Torlesse) could yield a melt similar to Pokai Type 2 rhyolite.

In the AFC-Model 2 Pokai Type 2 composition (sample T19/1) was used as the daughter magma, Wahianoa acid andesite as a parent magma and an average Waipapa metagreywacke composition as the contaminant. The results are given in Table 7.7.b. The sum of squares of residual is small (S = 0.045), only the observed residual for K_2O is somewhat to high. In this model the ratio M_a/M_c is ca. 1 (r = 1.05), which is analogous to zone refining (DePaolo 1981). That is, the material assimilated (M_a = 78 %) is balanced by an approximately equivalent mass of crystals fractionated (M_c = 74 %), so the mass of the magma (F) remains constant. For this model to apply, the initial wallrock temperature must have been high, approaching that of the magma at a depth of 30-40 km (DePaolo, 1981).

Following Taylor's (1980) calculations, DePaolo (1981) has

Table 7.7.b. Results of the least squares and Rayleigh fractionation modelling (assimilation and fractional crystallisation, AFC; based on the method of DePaolo, 1981). Mineral/liquid distribution coefficients used are given in Table 7.5. The original bulk rock and mineral analyses of the andesitic parent and of the contaminant rock used are given in Appendix E (Tables E.1, E.2 and E.3, respectively).

AFC-Model 2
The parent magma is WAH (Wahianoa acid andesite, 14867)
The contaminant is Waipapa metagreywacke
The daughter magma is T19/1 (Pokai Type 2, ref.no. 227)

Coef	% minerals	
-0.480	67.3	plagioclase
-0.132	18.5	orthopyroxene
-0.047	6.5	clinopyroxene
-0.055	7.7	titanomagnetite
0.962		

	SiO_2	TiO_2	Al_2O_3	FeO_t	MgO	CaO	Na_2O	K_2O
WAH	61.36	0.73	17.87	6.21	2.58	6.02	3.62	1.61
T19/1								
Obs	72.33	0.34	15.84	2.24	0.24	1.51	4.27	3.22
Calc	72.34	0.27	15.82	2.25	0.21	1.50	4.30	3.03
Dif	-0.01	0.07	0.01	-0.01	0.03	0.02	-0.03	0.20

S = 0.045 M_a = 78 % M_c = 74 % r = 1.05 F = 1.04

	K_d	Parent	Daughter	Calculated	Residuals	Difference
Rb	0.14	57	102	94	8	8 %
Ba	0.11	395	725	726	-1	1 %
Sr	2.17	252	127	237	-110	87 %
Zr	0.07	121	235	233	2	1 %
Nb	0.16	5	10	4	6	60 %
Ni	3.97	17	3	5	-2	67 %
Cr	2.72	10	4	16	-12	>100 %
V	5.10	176	8	31	-23	>100 %

S = sum of squares of residuals
M_a = assimilation rate, i.e. total mass of material assimilated (%)
M_c = fractionation rate, i.e. crystals removed (%)
$r = M_a/M_c$
F = relative mass of magma remaining

shown that if the country rock was initially at 1000°C (lower crust in regions of active volcanism and high heat flow), assimilation of 1 g of wallrock into a magma at 1150°C could be thermally balanced by ca. 1 g of crystallisation. The case were $M_a = M_c$ ($r = 1$), does not, however, usually apply over any large fraction of the history of a magma chamber (DePaolo, 1981); also due to the high temperatures crystallisation would be suppressed. Thus a combination of 78 % assimilation of the Waipapa basement with simultaneous 74 % crystallisation of the andesitic parent magma gives an anomalously high assimilation/crystallisation rate. The calculated concentration of Sr is also unacceptable high.

In the AFC-Model 3, a meta-igneous granulite composition was used as the contaminant and Pokai Type 2 composition (sample T19/1) and the Wahianoa acid andesite as daughter and parent magmas, respectively (Table 7.7.c). The sum of the squares of residuals is relatively small ($S = 0.122$), but as the total mass of material assimilated ($M_a = -16$ %) is a negative value (r is also negative), this means that no assimilation occurred and the model may be rejected without further consideration.

AFC-Model 4 shows the results of assimilation-fractional crystallisation of Wahianoa acid andesite, contaminated by Torlesse metagreywacke to produce a rhyolite similar to an average Chimp composition (Table 7.8). As would be expected, the results are quite similar to the equivalent modelling with the Pokai rhyolite (Table 7.7.a), though the major oxides give a slightly better fit, and the sum of squares of residuals ($S = 0.051$) for the Chimp AFC model is smaller. This model involves 54 % crystallisation of the parent andesite combined

Table 7.7.c. Results of the least squares and Rayleigh fractionation modelling (assimilation and fractional crystallisation, AFC; based on the method of DePaolo, 1981). Mineral/liquid distribution coefficients used are given in Table 7.5. The original bulk rock and mineral analyses of the andesitic parent and of the contaminant rock used are given in Appendix E (Tables E1, E.2 and E.3, respectively).

AFC-Model 3
The parent magma is WAH (Wahianoa acid andesite, 14867)
The contaminant is MIG (meta-igneous granulite)
The daughter is T19/1 (Pokai Type 2, ref.no. 227)

Coef	% minerals	
-0.526	72.7	plagioclase
-0.046	6.3	orthopyroxene
-0.083	11.5	clinopyroxene
-0.069	9.5	titanomagnetite
2.039		

	SiO_2	TiO_2	Al_2O_3	FeO_t	MgO	CaO	Na_2O	K_2O
WAH	61.36	0.73	17.87	6.21	2.58	6.02	3.62	1.61
T19/1								
Obs	72.33	0.34	15.84	2.24	0.24	1.51	4.27	3.22
Calc	72.34	0.07	15.85	2.30	0.18	1.49	4.16	3.06
Dif	-0.01	0.28	-0.01	-0.06	0.06	0.03	0.11	0.16

S = 0.122 M_a = -16 % M_c = 35 % r = -0.44 F = 49 %

	K_d	Parent	Daughter	Calculated	Residuals	Difference
Rb	0.15	57	102	104	-2	2 %
Ba	0.12	395	725	715	9	1 %
Sr	2.34	252	127	103	23	18 %
Zr	0.08	121	235	220	15	6 %
Nb	0.14	5	10	10	0	-
Ni	2.84	17	3	-11	14	>100 %
Cr	2.55	10	4	-57	61	>100 %
V	5.80	176	8	-1	9	>100 %

S = sum of squares of residuals
M_a = assimilation rate, i.e. total mass of material assimilated (%)
M_c = fractionation rate, i.e. crystals removed (%)
$r = M_a/M_c$
F = relative mass of magma remaining

Table 7.8. Results of the least squares and Rayleigh fractionation modelling (assimilation and fractional crystallisation, AFC; based on the method of DePaolo, 1981). Mineral/liquid distribution coefficients used are given in Table 7.5. The original bulk rock and mineral analyses of the andesitic parent and of the contaminant used are given in Appendix E (Tables E.1, E.2 and E.3, respectively).

AFC-Model 4: from Wahianoa acid andesite to medium SiO_2 Chimp rhyolite, contaminated by Torlesse metagreywacke.
The parent magma is WAH (Wahianoa acid andesite, 14867)
The contaminant is Torlesse metagreywacke
The daughter is Chimp (average Chimp rhyolite, see Table 6.1)

Coef	% minerals	
-0.770	71.9	plagioclase
-0.152	14.2	orthopyroxene
-0.065	6.1	clinopyroxene
-0.083	7.8	titanomagnetite
1.967		

	SiO_2	TiO_2	Al_2O_3	FeO_t	MgO	CaO	Na_2O	K_2O
WAH	61.36	0.73	17.87	6.21	2.58	6.02	3.62	1.61
Chimp								
Obs	74.91	0.23	14.20	1.82	0.18	1.22	3.90	3.53
Calc	74.91	0.04	14.22	1.86	0.15	1.21	3.80	3.53
Dif	0.00	0.19	-0.02	-0.04	0.03	0.01	0.11	0.00

S = 0.051 M_a = 5 % M_c = 54 % r = 0.09 F = 51 %

	K_d	Parent	Daughter	Calculated	Residuals	Difference
Rb	0.15	57	109	126	-17	16 %
Ba	0.12	395	827	806	21	3 %
Sr	2.31	252	97	92	5	5 %
Zr	0.07	121	229	245	-17	7 %
Nb	0.15	5	11	9	2	18 %
Ni	3.36	17	3	3	0	-
Cr	2.39	10	4	4	0	-
V	4.83	176	6	10	-4	67 %

S = sum of squares of residuals
M_a = assimilation rate, i.e. total mass of material assimilated (%)
M_c = fractionation rate, i.e. crystals removed (%)
$r = M_a/M_c$
F = relative mass of magma remaining (%)

by 5 % contamination of the Torlesse basement. The weight modes of minerals extracted from the parent magma were 38.8 % plagioclase, 7.7 % orthopyroxene, 3.3 % clinopyroxene and 4.2 % titanomagnetite. Except for V, the trace element abundances are also within acceptable values.

The value for crystallisation rate, i.e. crystals removed, is somewhat higher than that in the equivalent Pokai AFC model, also the mass of assimilant is a slightly higher value in the AFC model for the Chimp rhyolite. The relatively similar mineralogy and geochemistry of the two ignimbrites strongly suggest that they are genetically related to each other. The results from the least squares calculations indicate that the two magmas could have been generated from the same parent magma which was similar to Wahianoa acid andesite.

7.6. Partial melting

Reid (1983) considered that the voluminous rhyolitic rocks of TVZ were generated by 35 % partial melting of the crustal rocks, equivalent to the Torlesse metasediments. The origin of TVZ rhyolites by partial melting of the sedimentary basement rocks has mainly been rejected due to the overall metaluminous (to mildly peraluminous) composition of the rhyolitic rocks (Conrad et al., 1988). However, as shown above (see chapter 5.3.2 and Fig.5.7) most of the TVZ rhyolitic ignimbrites have a more peraluminous composition than the rhyolitic lavas.

A partial melting (PM) model (based on the method of Langmuir et al., 1977) was used to assess a possible origin for the Pokai rhyolite by partial melting of crustal rocks. Two models were used, involving different source materials, namely the

Torlesse and Waipapa basement metasediments.

The starting mineralogy of the PM model is based on the observed modal mineralogy of exposed greywackes (Reid, 1983; Reid & Cole, 1983). The original modal mineralogy used in the model, together with the proportions in which the minerals enter the melt, are given in Table 7.9. Distribution coefficients used in melting of greywacke are shown in Table 7.10. The average compositions of the two basement rock types used in the PM modelling, i.e. the Torlesse and Waipapa metasediments are given in Appendix E (Table E.4).

Results of 40 %, 50 % and 60 % partial melting of the Torlesse basement for the trace elements Rb, Sr, Ba, Cr, V, Ce and Nd are given in Table 7.11.a, together with the average Pokai Type 2 compositions. Only the Sr content is consistent with partial melting in the model involving 50 % melting. The Ba and Nd values are too high, and Rb, Cr, V and Ce values too low in this model.

The results of 20 %, 30 % and 40 % partial melting of the Waipapa basement for the elements of Rb, Sr, Ba, Cr, V, Ce and Nd are given in Table 7.11.b. At 40 % melting the values of Rb and Ce are consistent with partial melting, but Sr, Cr and V are too low, whereas Ba and Nd are too high.

To check whether the Chimp rhyolite was related to the crustal rocks, the same PM models described above were used and the results were compared to the average Chimp composition. Due to relatively similar geochemistry of the two ignimbrites, the results were, as would be expected, very similar. Using different distribution coefficients (within acceptable values)

Table 7.9. The modal mineralogy of the source rock (metasedimentary basement; Reid, 1983) and the proportions in which the minerals enter the melt (Reid & Cole, 1983) used in the PM model. The same values are used for both the Torlesse and Waipapa basement models.

	Original proportion %	Proportion in melt %
Quartz	28	33
Plagioclase	37	45
K-feldspar	11	0
Clinopyroxene	5	5
Orthopyroxene	7	5
Magnetite	2	2
Biotite	7	7
Cordierite	2	3
Apatite	0.4	0.5
Total	99.4	100.5

Table 7.10. Distribution coefficients (Kd) used in melting of greywacke. K_d's for all cordierite values are from Reid (1983), others from Hanson (1978). A value of 8 for Sr/Plagioclase was used, which is higher than the typical value in the order of 4; the $K_d$value for Sr/Plagioclase could be as high as 30 for granitic melts (Hanson, 1978).

	Plag	Kfs	Cpx	Opx	Mt	Bio	Cord	Ap
Rb	0.048	0.66	0.032	0.003	-	3.26	-	-
Sr	8.0	3.87	0.52	0.00	-	0.12	1.3	-
Ba	0.16	4.0	0.13	0.003	-	4.0	0.62	-
Cr	0.01	-	60	30	80	7	0.63	-
V	0.01	-	10	6	60	-	0.63	-
Ce	0.3	0.04	0.51	0.33	0.8	0.32	0.37	34.7
Nd	0.21	0.03	1.11	0.22	-	0.29	0.3	57.1

Plag = plagioclase
Kfs = alkali feldpsar
Cpx = clinopyroxene
Opx = orthopyroxene
Mt = magnetite
Bio = biotite
Cord = cordierite
Ap = apatite

Table 7.11.

(a) Partial melting of the average Torlesse basement. The K_d values used are given in Table 9.10. Initial concentration I (Torlesse metasediment; Reid, 1983) with 40 %, 50 % and 60 % melting compositions compared with the average Pokai Type 2 composition.

	I	40 %	50 %	60 %	Type 2
Rb	91	147	131	118	102
Sr	266	112	126	144	123
Ba	633	604	570	540	737
Cr	46	9	10	11	4
V	73	19	22	25	9
Ce	53	90	82	75	65
Nd	24	39	36	33	50

(b) Partial melting of the average Waipapa basement. The K_d values used are given in Table 7.10. Initial concentration I (Waipapa metasediment; Reid, 1983) with 20 %, 30 % and 40 % melting compositions compared to the average Pokai Type 2 composition.

	I	20 %	30 %	40 %	Type 2
Rb	65	138	119	105	102
Sr	459	158	174	193	123
Ba	549	595	557	524	737
Cr	42	6	7	8	4
V	122	26	28	32	9
Ce	38	81	72	65	65
Nd	18	35	32	29	50

for PM modelling does not give any better fit for either of the ignimbrites. Thus the results do not support the origin of the Pokai, or the Chimp rhyolitic magmas as direct partial melts of the basement sediments.

8. DISCUSSION AND CONCLUSIONS

8.1. General geology

The Pokai and Chimp ignimbrites are exposed in an area west from the Kapenga Volcanic Centre in northwestern TVZ. The Pokai Ignimbrite has a minimum *in situ* volume of ca. 40 km^3 (equivalent to ca. 33 km^3 DRE), whereas the older Chimp Ignimbrite has a minimum *in situ* volume of only ca. 7 km^3 (ca. 5 km^3 DRE). Stratigraphically the ignimbrites lie between the Whakamaru Ignimbrites (330 ka) and the Mamaku Ignimbrite (140 ka). The Pokai and Chimp ignimbrites are separated by two paleosols and a number of tephra units, mineralogically very similar to the Pokai Ignimbrite, suggesting an origin from the same magma source. Both ignimbrites were preceded by plinian activity.

The Chimp Ignimbrite is relatively pumice- and crystal-poor (1-2 vol.% phenocrysts), though pumices with a phenocryst contents of 6-8 vol.% occur. The exposed flow units are relatively thin, from 4-6 m. Welded Chimp Ignimbrite is rare.

The Pokai Ignimbrite represents a multiple flow unit ignimbrite, with single flow units usually ranging from 6-30 m. Thick deposits (>20 m thick) are usually welded in the upper middle part of the deposit. The ignimbrite flow units usually include a fine-grained layer 2a underlying a pumice-rich layer 2b. Ground deposits, i.e. layer 1 deposits, are rare. The distribution of the flow units were partly topographically controlled, and the flow units show characteristics of both valley-ponded ignimbrite (VPI) and ignimbrite veneer deposit (IVD), the latter type always

occurring on the top of the VPI.

Field evidence suggest a source area for the Pokai Ignimbrite to be towards east from the study area, i.e. in Kapenga Volcanic Centre. There is not enough field evidence to point any definite source for the Chimp Ignimbrite. However, since the two ignimbrites are mineralogically and geochemically very similar, it is likely that the two ignimbrites originate from the same volcanic centre, i.e Kapenga.

Two pumice types occur in the Pokai Ignimbrite; a crystal-poor type (2-3 % phenocrysts) and a crystal-rich type (6-12 % phenocrysts). The crystal-poor type occurs throughout the ignimbrite, whereas the crystal-rich type predominates at the uppermost flow units. Plagioclase is the dominant phenocryst in all pumices, with minor amounts of orthopyroxene, Fe-Ti oxides and quartz, which occurs in ca. 30 % of the pumices. As most TVZ rhyolitic eruptives have traditionally considered to be relatively homogeneous, Pokai Ignimbrite shows a significant geochemical variation. On the basis of the mineralogical and geochemical data three pumice types can be recognised:

Type 1a: crystal-poor, high SiO_2, low Sr rhyolite.
Type 1b: crystal-poor, high to low SiO_2, medium Sr rhyolite.
Type 2: crystal-rich, medium to low SiO_2, high Sr rhyolite.
Variation in the SiO_2 content within each type is largely due to the modal quartz abundance within each pumice.

8.2. Origin of the Pokai magma

It has been suggested by several authors that large silicic magma bodies can be generated by fractional crystallisation of

more basic magmas, in some cases accompanied by crustal interaction. Lanphere et al. (1980) and Cameron et al. (1980) have suggested an origin by crystal fractionation from basaltic andesite magma for the eruptives of one of the world's largest rhyolite province, Sierra Madre Occidental in Mexico. According to Berman (1981) the voluminous rhyolite tuffs of Coquihalla in British Columbia are derived similarly. Fractional crystallisation, sometimes combined with crustal contamination, is believed to have played a significant role in the generation of silicic volcanic rocks in major volcanic fields in the western United States (i.e. San Juan volcanic field, SW Colorado; Lipman et al., 1978) and in Chile (Thorpe et al., 1979).

TVZ andesites are geochemically very similar to worldwide calc-alkaline series continental arc lavas, and were probably generated by similar processes, i.e. by differentiation of mantle derived basaltic magmas (Gamble et al., 1990; Graham et al., 1992). It has been demonstrated (Graham & Hackett, 1987), that most TVZ andesites, especially those similar to Ruapehu Type 1 lavas can be generated from low alumina basalt by AFC. Graham and Hackett (1987) have also concluded, that there are at least two basaltic magma types involved in the genesis of Ruapehu andesites, and that they are produced in the mantle wedge below TVZ by anatexis of the asthenosphere and/or the subcontinental lithosphere.

It has been shown, that most TVZ mafic-intermediate volcanic rocks have undergone varying degrees of crustal contamination prior to eruption (Graham & Hackett, 1987; Graham et al., 1988, 1992). The most likely crustal contaminants of TVZ volcanics are the subvolcanic metasedimentary basement rocks.

A number of previously published theories have favoured partial melting of subvolcanic crustal metasediments as the most likely mechanism to explain the origin of the voluminous TVZ rhyolites and ignimbrites (Ewart, 1969; Ewart & Stipp, 1968; Reid, 1983). There does exist a local crustal source within TVZ which has many of the suitable chemical and isotopic characteristics. The partial melting model, however, fails to explain the relatively low ^{18}O isotope values of the silicic volcanic rocks compared with those of the metasediments (Graham et al., 1992).

The least squares and Rayleigh calculations provide evidence that the Pokai, and Chimp ignimbrites could be products of fractional crystallisation of TVZ andesitic magmas, themselves derived from more primitive basaltic magmas. Small amounts of crustal contamination is likely to accompany the fractionation processes. It is thus suggested that the Pokai, and the Chimp rhyolitic magmas were derived from parental magmas similar to Ruapehu Type 1 andesite (Wahianoa acid andesite) by AFC, with Torlesse metasediment as the contaminant.

8.3. Evolution of the magma reservoir

The following features of the Pokai Ignimbrite must be consistent with any proposed model concerning the evolution of the magma and the eruption mechanism:

(1) Pumice fragments of different compositions occur in a single cooling unit, in a single location.

(2) Occurrence of all three pumice types in the pre-ignimbrite air-fall deposits.

(3) The vertical distribution of chemically distinct pumices,

i.e. the less evolved, more crystal-rich Type 2 predominates in the uppermost flow units.

(4) Polymodal phenocryst populations (i.e. disequilibrium phenocrysts) occur within individual pumice fragments.

Detailed geochemical and petrological studies of silicic and intermediate magmas provide evidence of compositional zoning in every large and most small magma chambers, and nearly all compositionally zoned eruptions are pyroclastic in nature (Baker & McBirney, 1985; Hildreth, 1979, 1981; Smith, 1979). Usually, but not always, the pyroclastic units show a progression from most evolved ejecta at the base to less evolved, and often phenocryst-rich ejecta at the top. Examples of reversed compositional sequences have been recorded (Ekren et al., 1980), and mixing of material from separate compositional levels of the chamber immediately prior to or during the eruption is not uncommon (Vogel et al., 1989; Schuraytz et al., 1989).

Both the Pokai and Chimp ignimbrites show heterogeneous pumice compositions indicating compositionally zoned magma chambers. As different pumice types commonly occur together at the same Pokai locality, different compositions must have co-existed within the magma chamber, although probably in discrete levels. The least squares and Rayleigh calculations suggest that the main process which produced the geochemical zonation in the Pokai magma chamber is fractional crystallisation.

Fractionation by crystal growth and large scale gravitational settling in silicic magmas has been largely discounted because of the high magma viscosity and yeild strenght (Hildreth, 1979; McBirney & Noyes, 1979; Valentine, 1992). It is now

widely considered that compositional zonation in large silicic magma chambers is produced by side-wall crystallisation and boundary (liquid) fractionation (Baker & McBirney, 1985; Storey et al., 1989).

This mechanism involves separation of crystals from melt by convection of fluid away from sites of crystallisation. This general process is termed convective fractionation (Sparks et al., 1984), and involves processes ranging from boundary layer convection to buoyant plumes of fluid rising above a crystal mush. The main effect of convective fractionation is to emplace large quantities of crystal-poor, less dense, evolved magma at high levels in a magma chamber, while leaving the crystals behind (Valentine, 1992).

Fractionation is likely to take place by accretion of crystals onto the cooler walls, as well as on the roof zone of the initial magma chamber. Crystallisation along the walls removes dense components from the liquid, leaving the residual melt less dense than either the crystallising mush at the wall or the adjacent unaffected magma (Mahood & Cornejo, 1992). This high silica melt would then migrate to the upper part of the chamber where it accumulates displacing denser magma. Simultaneously the roof zone crystals would be 'pushed' downwards by the ascending less dense liquid entering from the sides of the chamber and by the melt separated from the roof zone crystal mush.

Successive ascending liquids may then enter a zoned column at a level appropriate to their density. If thermal gradients are present in the chamber, convection may occur in this zoned column at discrete layers (Mahood & Cornejo, 1992). Transfer

of the less dense melt components upwards in the magma chamber by convection and diffusion would inhibit convection on a large scale and preserve the layering (Hildreth, 1979; Rice, 1981). Convection within each layer will disturb the thermal equilibrium and the phenocryst will tend to equilibrate with the new conditions. If the convection is sluggish and the thermal regime changes gradually, zoned phenocrysts may result. Both normally and reversely zoned plagioclase, and normally zoned orthopyroxene phenocrysts occur in all Pokai pumice types. However, the plagioclase geothermometry indicates temperature variations of no more than ca. 50°C within individual plagioclase phenocrysts, indicating only small scale convection, i.e. within the appropriate compositional layer.

The geochemical data combined with results on temperature estimates and estimated water content imposed by mineralogical data, can be used to construct a schematic model of the stratified Pokai magma chamber as it might have existed immediately prior to the eruption (Fig.8.1). The relative amounts of different magma types erupted do not necessarily reflect their relative abundance in the pre-eruptive magma body. It is thus inferred that prior to the eruption, the Pokai magma chamber was compositionally zoned from a cool (ca. 750°C), crystal-poor, high SiO_2 rhyolitic top to hotter (800-850°C), more crystal-rich, medium to low SiO_2 rhyolite at the deeper levels (Fig.8.1).

Cooling and crystallisation along the walls of the magma reservoir, probably combined with episodic additions of heat from below by intrusions of hotter, more primitive magma would promote development of convection in the stratified layers.

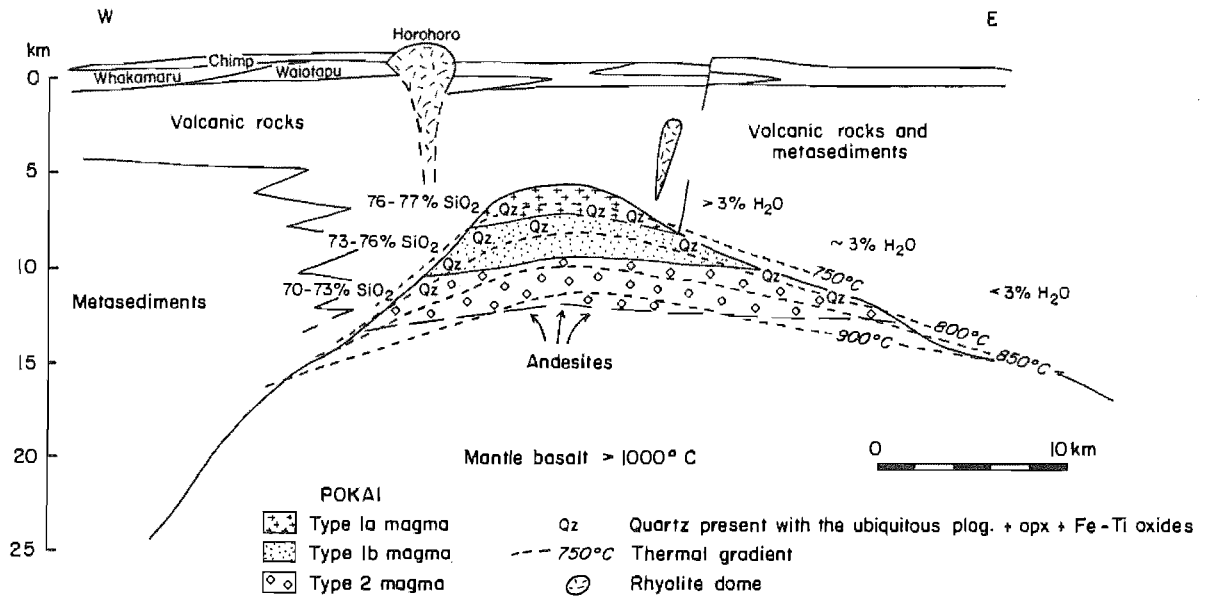

Fig.8.1. Interpretive schematic representation of the Pokai magma chamber and the surrounding stratigraphy prior to the eruption.
A pre-Pokai caldera structure could have been present at the time, formed during eruptions of older ignimbrites; it is inferred that the Kapenga area has been active from 560 to 50 ka (Wilson et al., 1984).

Injections of larger amounts of basaltic or andesitic magma could also lead to mixing of more evolved magmas with less evolved magmas. Such mixing could create explosive eruptions in the upper, more silicic part of the magma chamber (Eichelberger, 1975; Sparks et al., 1977).

It seems likely that some mixing occurred immediately prior to or during the eruption, causing the marked pumice heterogeneity, though the mixing was insufficient to destroy the original layering in the magma chamber. Violent mixing could combine separate adjacent zones of magma, which then could erupt simultaneously and form highly heterogeneous deposits.

8.2. Eruption of the Pokai magma

Eruption of magma during deposition of the Pokai Ignimbrite is illustrated in Fig.8.2 and serves as an interpretive model of processes that took place in the magma chamber and during the accumulation of the ignimbrite. The eruption of the Pokai Ignimbrite is consistent with magma evacuation models involving successive tapping of the magma chamber, each cycle drawing magma from progressively deeper levels (Blake & Ivey, 1986; Spera et al., 1986; Vogel et al., 1987).

The first magma out of the Pokai chamber, which formed the pre-ignimbrite air-fall deposits, was heterogeneous mixture of all compositional types, indicating simultaneous tapping from all three magma zones (Fig.8.2.a). The polymodal phenocryst populations in some air-fall pumices further suggest mixing between the three magma types just prior or during the eruption. During initial column collapse, several thin flow

Figure 8.2. Interpretation of the Pokai eruptive sequence schematically illustrating the tapping of the magma chamber. Key as in Figure 8.1.

(a) Initial plinian phase, in which magma from layers 1a, 1b and 2 are drawn up simultaneously. Eruption possibly from a central vent in the Kapenga area.

(b) Initial collapse of eruption column producing a series of thin ignimbrite flows and surge deposits. Magma from layers 1a and 1b is tapped simultaneously (the blackened areas on the surface indicate Pokai Ignimbrite deposits).

(c) Wholesale collapse of eruption column leading to development of massive ignimbrite flow units. Concurrent tapping of layers 1a and 1b; layer 1b magma predominating.

(d) Possible caldera collapse and generation of new vent sites. Concurrent tapping of layers 1a, 1b and 2, with layer 2 magma comprising the bulk of erupted material, as layers 1a and 1b have been exhausted.

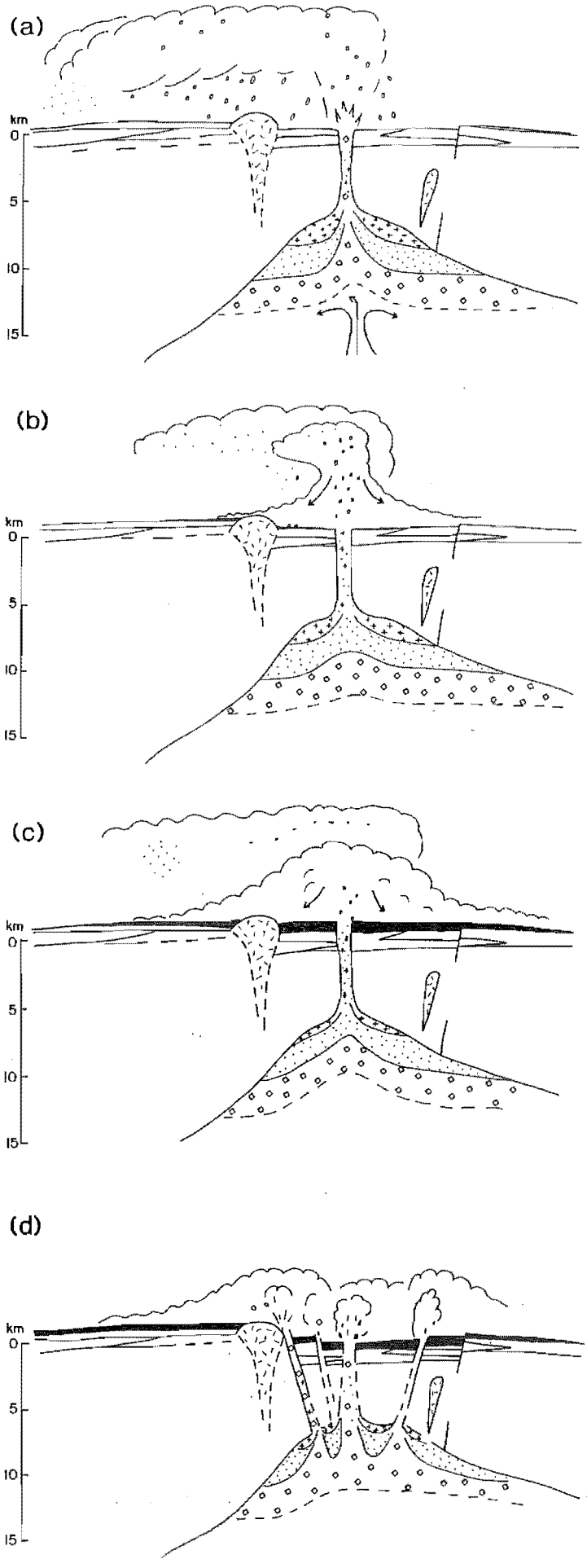
(a)
km
0
5
10
15
(b)
km
0
5
10
15
(c)
km
0
5
10
15
(d)
km
0
5
10
15

units and surge deposits accumulated (Fig.8.2.b). Only layers 1a and 1b were tapped.

As the eruption progressed widespread collapse of the eruption column took place and massive ignimbrite flow units were deposited (Fig.8.2.c). Magma continued to evacuate simultaneously from layers 1a and 1b, and was mixed either in the conduit or during the collapse of the eruption column. However, more and more of Type 1b magma was tapped, probably because most of layer 1a was erupted. There were only minor contributions from the crystal-rich layer 2 magma in this phase.

Towards the end of the eruption deeper parts of the magma chamber were evacuated (Fig.8.2.d) with Type 2 magma predominating. The volume of magma released may have been sufficient to create underpressure in the magma chamber and this could have lead to caldera collapse. The new caldera structure would have partly superimposed on an older caldera, possibly formed during eruptions of the Paeroa and/or Waiotapu ignimbrites, inferred to originate from the Kapenga area (Wilson et al., 1984). Appearance of lithic lag breccias in the eruption sequence usually marks episodes of caldera collapse (Self et al., 1986), thus the lithic breccia found in Haunui Valley (see chapter 2.7) could represent a caldera collapse deposit.

ACKNOWLEDGEMENTS

First of all I wish to thank my supervisors Professor J.W. Cole and Associate Professor S.D. Weaver, Geology Department, University of Canterbury, Christchurch, for their invaluable advice, assistance and encouragement during this study.

I also thank Dr. Y. Kawachi for use of the Jeol 8600 Superprobe microanalysor at the Geology Department, University of Otago, Dunedin, and the staff at the former DSIR Geology Division in Rotorua (now at Institute of Geological & Nuclear Sciences, Wairakei) for their help during my field work. Access to my field area in Kinleith Forests was kindly provided by NZ Forest Products Ltd, Tokoroa. I would also like to thank the Finnish family Reinikkala, in Tokoroa, for providing accommodation for me and my K9 during the field work. The Finnish sauna was highly appreciated.

Study at the University of Canterbury was made possible by scholarships, awarded by the Rotary International (Pedersöre Rotary Club as the sponsoring club), 1990, and by the Academy of Finland (Natural Science Research Council), 1991-93.

Thanks go also to the University of Canterbury Geology department staff and to S. Brown, C. Brown, A. Downing, J. Higgins, K. Holder, D. Jones, L. Leonard, J. Mawson, R. Spiers, K. Swanson and M. Wright who provided various help during the course of this study. My special thanks go to A. Nicholas for keeping my spirits up on rainy days.

I also thank all the Geology Department post-graduate students, especially S. Brown, B. Hobden and R. Smith for all their help and advice; and for helping to improve my English.

Finally, I wish to thank my parents for all their support, encouragement and understanding ♥

REFERENCES

Andersen, D.J. and Lindsley, D.H., 1985. New (and final!) models for the Titanomagnetite/ilmenite geothermometer and oxygen barometer. EOS 18: 416.

Bacon, C.R., 1983. Eruptive history of Mount Mazama and Crater Lake caldera, Cascade Range, U.S.A. In Aramaki, S. and Kushiro, I (eds). Arc Volcanism. J. Volcanol. Geotherm. Res., 18: 57-115.

Baker, B.H. and McBirney, A.R., 1985. Liquid fractionation. Part III: Geochemistry of zoned magmas and the compositional effects of liquid fractionation. In Baker, B.H. and McBirney, A.R (eds). Processes in Magma Chamber. J. Volcanol. Geotherm. Res., 24: 55-81.

Bellamy, S., 1991. Some studies of the Te Wairoa ignimbrites and the associated volcanic geology of the southwestern Okataina Volcanic Zone. Unpublished M.Sc. thesis, lodged in the Library, University of Waikato, Hamilton, New Zealand.

Berman, R.G., 1981. Differentiation of calc-alkaline magmas: Evidence from the Coquihalla volcanic complex, British Columbia. J. Volcanol. Geotherm. Res., 9: 151-179.

Blake, S. and Ivey, G.N., 1986. Magma-mixing and the dynamics of withdrawal from stratified reservoirs. J. Volcanol. Geotherm. Res., 27: 153-178.

Blake, S., Wilson, C.J.N., Smith, I.E.M. and Walker, G.P.L., 1992. Petrology and dynamics of the Waimihia mixed magma eruption, Taupo Volcano, New Zealand. J. Geol. Soc. London, 149:193-207.

Blattner, P. and Reid, F., 1982. The origin of lavas and ignimbrites of the Taupo Volcanic Zone, New Zealand, in the light of oxygen isotope data. Geochim. Cosmochim. Acta, 46: 1417-1429.

Booth, B., Croasdale, R. and Walker, G.P.L., 1978. A quantitative study of five thousand years of volcanism on Sao Miguel, Azores. Phil. Trans. R. Soc. London, A, 288: 271-319.

Briggs, N.D., 1973. Investigations of New Zealand pyroclastic flow deposits. Unpublished Ph.D. thesis, lodged in the Library, Victoria University of Wellington, New Zealand.

Briggs, R.M., Gifford, M.G., Moyle, A.R., Taylor, S.R., Norman, M.D., Houghton, B.F. and Wilson, C.J.N., 1993. Geochemical zoning and eruptive mixing in Mangakino ignimbrites, Taupo Volcanic Zone, New Zealand. J. Volcanol. Geotherm. Res., in press.

Browne, P.R.L., Graham, I.J., Parker, R.J. and Wood, C.P., 1992. Subsurface andesite lavas and plutonic rocks in the Rotokawa and Ngatamariki geothermal systems, Taupo Volcanic Zone, New Zealand. J. Volcanol. Geotherm. Res., 51: 199-215.

Bryan, W.B., Finger, L.W. and Chayes, F., 1969. Estimating proportions in petrographic mixing equations by least squares approximation. Science, 163: 926-927.

Buddington, A.F. and Lindsley, D.H., 1964. Iron-titanium oxide minerals and synthetic equivalents. J. Petrol., 5: 310-357.

Burnham, C.W., 1979. Importance of volatile constituents. In Yoder, H.D. (ed). Evolution of Igneous Rocks. Fiftieth Anniversary Perspectives. Princeton University Press, Princeton, New Jersey. pp. 439-482.

Cameron, M., Bagby, W.C. and Cameron, K.L., 1980. Petrogenesis of voluminous mid-Tertiary ignimbrites of the Sierra Madre Occidental, Chihuahua, Mexico. Contrib. Mineral. Petrol., 74: 271-284.

Carmichael, I.S.E., Turner, F.J. and Verhoogen, J., 1974. Igneous Petrology. McGraw-Hill, New York. 739 p.

Cas, R.A.F. and Wright, J.V., 1987. Volcanic Successions. Modern and ancient. Allen & Unwin, London. 528 p.

Chappell, B.W. and White, A.J.R. 1974. Two contrasting granite types. Pac. Geol., 8: 173-174.

Cole, J.W., 1979. Structure, petrology and genesis of Cenozoic volcanism, Taupo Volcanic Zone, New Zealand - a review. N.Z. J. Geol. Geophys., 22: 631-657.

-------1979b. Chemical analyses of lavas and ignimbrites of the Taupo Volcanic Zone. Publications of Geology Department of Victoria University of Wellington, no. 13. 31 p.

-------1981. Genesis of lavas of the Taupo Volcanic Zone, North Island, New Zealand. J. Volcanol. Geotherm. Res., 10: 317-337.

-------1986. Distribution and tectonic setting of late Cenozoic volcanism in New Zealand. In Smith, I.E.M., (ed). Late Cenozoic Volcanism in New Zealand. Roy. Soc. N.Z. Bull., 23: 7-20.

-------1990. Structural control and origin of volcanism in the Taupo volcanic zone, New Zealand. Bull. Volcanol., 52: 445-459.

Cole, J.W. and Lewis, K.B., 1981. Evolution of the Taupo-Hikurangi subduction system. Tectonophysics, 72: 1-21.

Conrad, W.K., Nicholls, I.A. and Wall, V.J., 1988. Water-saturated and -undersaturated melting of metaluminous and peraluminous crustal compositions at 10 kb: Evidence for the origin of silicic magmas in the Taupo Volcanic Zone, New Zealand, and other occurrences. J. Petrol., 29: 765-803.

De Paolo, D.J., 1981. Trace element and isotopic effects of combined wallrock assimilation and fractional crystallization. Earth Planet. Sci. Lett., 53: 189-202.

Druitt, T.H. and Sparks, R.S.J., 1982. A proximal ignimbrite breccia facies on Santorini, Greece. J. Volcanol. Geotherm. Res., 13: 147-171.

Eichelberger, J.C., 1975. Origin of andesite and dacite: Evidence of mixing at Glass Mountain and other circum-Pacific volcanoes. Bull. Geol. Soc. Amer., 86: 1381-1391.

Ekren, E.B., Byers, F.M., Jr., Hardyman, R.F., Marvin, R.F. and Silberman, M.L., 1980. Stratigraphy, preliminary petrology, and some structural features of Tertiary volcanic rocks in the Gabbs Valley and Gillis Ranges, Mineral County, Nevada. U.S. Geol. Surv. Bull., 1464. 54 p.

Ewart, A., 1969. Petrochemistry and feldspar crystallisation in the silicic volcanic rocks, central North Island, New Zealand. Lithos, 2: 371-388.

Ewart, A. and Stipp, J.J., 1968. Petrogenesis of volcanic rocks of the central North Island, New Zealand, as indicated by a study of 87Sr/86Sr ratios and Sr, Rb, K, U, and Th abundances. Geochim. Cosmochim. Acta, 32: 699-735.

Ewart, A., Green, D.C., Carmichael, I.S.E. and Brown, F.H., 1971. Voluminous low temperature rhyolitic magmas in New Zealand. Contrib. Mineral. Petrol., 33: 128-144.

Fisher, R.V., 1979. Models for pyroclastic surges and flows. J. Volcanol. Geotherm. Res., 6: 305-318.

Fisher, R.V., Schmincke, H.-U. and Bogard, P.V., 1983. Origin and emplacement of a pyroclastic flow and surge unit at Laacher See, Germany. J. Volcanol. Geotherm. Res., 17: 375-392.

Francis, P.W., O'Callaghan, L., Kretzchmar, G.A., Thorpe, R.S., Sparks, R.S.J., Page, R.N., de Barrio, R.E., Gillou, G. and Gonzalez, O.E., 1983. The Cerro Galan ignimbrite. Nature 301: 51-53.

Fransen, P.J.B., 1982. Geology of the western Mamaku Plateau and variations in the Mamaku Ignimbrite. Unpublished M.Sc. thesis, lodged in the Library, University of Waikato, Hamilton, New Zealand.

Gamble, J.A., Smith, I.E.M., Graham, I.J., Kokelaar, B.P., Cole, J.W., Houghton, B.F. and Wilson, C.J.N., 1990. The petrology, phase relations and tectonic setting of basalts from the Taupo Volcanic Zone, New Zealand and Kermadec Island Arc - Havre Trough, SW Pacific. J. Volcanol. Geotherm. Res., 43: 235-270.

Gill, J.B., 1981. Orogenic Andesites and Plate Tectonics. Springer-Verlag, Berlin. 390 p.

Graham, I.J. and Cole, J.W., 1991. Petrogenesis of andesites and dacites of White Island volcano, Bay of Plenty, New Zealand, in the light of new geochemical and isotopic data. N.Z. J. Geol. Geophys., 34: 303-31.

Graham, I.J. and Hackett, W.R., 1987. Petrology of calc-alkaline lavas from Ruapehu volcano and related vents, Taupo Volcanic Zone, New Zealand. J. Petrol., 28: 531-567.

Graham, I.J., Blattner, P. and McCulloch, M.T., 1990. Meta-igneous granulite xenoliths from Mount Raupehu, New Zealand: fragments of altered oceanic crust ? Contrib. Mineral. Petrol., 105: 650-661.

Graham, I.J., Grapes, R.H. and Kifle, K., 1988. The origin and petrogenesis of vitrified metagreywacke xenoliths, Tongariro Volcanic Centre, New Zealand. J. Volcanol. Geotherm. Res., 35: 205-215.

Graham, I.J., Gulson, B.L., Hedenquist, J.W. and Mizon, K., 1992. Petrogenesis of Late Cenozoic volcanic rocks from the Taupo Volcanic Zone, New Zealand, in the light of new lead isotope data. Geochim. Cosmochim. Acta, 56: 2797-2819.

Grange, L.I., 1937. The geology of the Rotorua-Taupo Subdivision. N.Z. Geol. Surv. Bull., 37. 138 p.

Grindley, G.W., 1959. Sheet N85 - Waiotapu. Geological map of New Zealand 1:63360. Dep. of Sci. and Ind. Res., Wellington, New Zealand.

Halliday, A.N., Davidson, J.P., Hildreth, W. and Holden, P., 1991. Modelling the petrogenesis of high Rb/Sr silicic magmas. Chem. Geol., 92: 107-114.

Hanson, G.N., 1978. The application of trace elements to the petrogenesis of igneous rocks of granitic composition. Earth Planet. Sci. Lett., 38: 26-43.

Harvey, P.K., Taylor, D.M., Hendry, R.D. and Bancroft, F., 1973. An accurate fusion method for the analysis of rocks and chemically related materials by X-ray fluorescence spectrometry. X.R.S., 2: 33-44.

Healy, J., 1982. Central volcanic region. In Soons, J.M. and Selby, M.J. (eds). Landforms of New Zealand. Longman Paul, Auckland, New Zealand. pp. 161-192.

Healy, J., Schofield, J.C. and Thompson, B.N., 1964. Rotorua, geological map of New Zealand, sheet 5, scale 1:250,000. Dep. of Sci. and Ind. Res., Wellington, New Zealand.

Hedberg, H.D., ed., 1976. International stratigraphic Guide. A Guide to Stratigraphic Classification, Terminology, and Procedure. John Wiley and Sons, New York. 200p.

Hildreth, W., 1979. The Bishop Tuff: Evidence for the origin of compositional zonation in silicic magma chambers. In Chapin, C.E. and Elston, W.E. ed. Ash-Flow Tuffs. Geol. Soc. Am. Spec. Paper, 180: 43-75.

-------1981. Gradients in silicic magma chambers: Implications for lithospheric magmatism. J. Geophys. Res., 86: 10153-10192.

Houghton, B.F., 1982. Geyserland: A guide to the volcanoes and geothermal areas of Rotorua. Geol. Soc. N.Z. Guidebook 4.48 p.

Houghton, B.F., Wilson, C.J.N. and Stern, T.A., 1986. Ignimbrite stratigraphy of a 457 m deep drillhole near Tokoroa. N.Z. Geol. Surv. Record, 20: 51-55.

James, R.S. and Hamilton, D.L., 1969. Phase relations in the system $NaAlSi_3O_8$-$KAlSi_3O_8$-$CaAl_2Si_2O_8$-SiO_2 at 1 kilobar water vapour pressure. Contrib. Mineral. Petrol., 21: 111-141.

Keiller, I.G., 1987. Geology of the Southern Mamaku PLateau. Unpublished B.Sc. (Hons.) thesis, lodged in the Library, University of Otago, Dunedin, New Zealand.

Kohn, B.P., 1973. Some studies of New Zealand Quaternary pyroclastic rocks. Unpublished Ph.D. thesis, lodged in the Library, Victoria University of Wellington, New Zealand.

Kudo, A.M. and Weill, D.F., 1970. An igneous plagioclase thermometer. Contrib. Mineral. Petrol., 25: 52-65.

Langmuir, C.H., Bence, J.F., Bence, A.E., Hanson, G.N. Taylor, S.R., 1977. Petrogenesis of basalts from the Famous Area, Mid-Atlantic Ridge. Earth Planet. Sci. Lett., 36: 133-156.

Lanphere, M.A., Cameron, K.L. and Cameron, M., 1980. Sr-isotope geochemistry of voluminous rhyolitic ignimbrites and related rocks, Western Mexico. Nature, 286: 594-596.

Le Maitre, R.W. (ed), Bateman, B., Dudek, A. and Keller, J. et al., 1989. A classification of Igneous rocks and Glossary of Terms: Recommendations of the International Union of Geological Sciences Subcommission on the Systematics of Igneous Rocks. Blackwell Scientific Publications, Oxford. 193 p.

Lipman, P.W., Doe, B.R., Hedge,C.E. and Steven, R.A., 1978. Petrologic evolution of the San Juan volcanic field, southwestern Colorado: Pb and Sr isotope evidence. Geol. Soc. Am. Bull., 89: 59-82.

Mahood, G.A. and Cornejo, P.C., 1992. Evidence for ascent of differentiated liquids in a silicic magma chamber found in a granitic pluton. Trans. Roy. Soc. Edinburgh, Earth Sci., 83: 63-69

Marshall, P., 1935. Acid rocks of the Taupo-Rotorua volcanic district. Trans. Roy. Soc. N.Z., 64: 323-366.

Martin, R.C., 1961. Stratigraphy and structural outline of the Taupo Volcanic Zone. N.Z. J. Geol. Geophys., 4: 449-478.

Mathez, E.A., 1973. Refinement of the Kudo-Weill plagioclase thermometer and its application to basaltic rocks. Contrib. Mineral. Petrol., 41: 61-72.

McBirney, A.R. and Noyes, R.M., 1979. Crystallization and layering of the Skaergaard Intrusion. J. Petrol., 20: 487-554.

Morimoto, N., Fabries, J., Fergusson, A.K., Ginzburg, I.V., Ross, M., Seifert, F.A., Zussman, J., Aoki, K. and Gottardi, G., 1988. Nomenclature of pyroxenes. Min. Mag., 52: 535-550.

Murphy, L.S., 1983. The Geology of the Haunui Valley, Central North Island. Unpublished B.Sc. (Hons.) thesis, lodged in the Library, University of Otago, Dunedin, New Zealand.

Murphy, R.P., 1977. The volcanic geology of the Matahana Basin. Unpublished M.Sc. thesis, lodged in the Library, Victoria University of Wellington, New Zealand.

Murphy, R.P. and Seward, D., 1981. Stratigraphy, lithology, paleomagnetism, and fission track ages of some ignimbrite formations in the Matahana Basin, New Zealand. N.Z. J. Geol. Geophys., 24: 325-331.

Nairn, I.A., 1981. Some studies of the geology, volcanic history and geothermal resources of the Okataina volcanic centre, Taupo volcanic zone, New Zealand. Unpublished Ph.D. thesis, lodged in the Library, Victoria University of Wellington, New Zealand.

Nairn, I.A., Wood, C.P. and Bailey, R.L., 1993. Recognition of the Reporoa Caldera, Taupo Volcanic Zone; Source of the Kaingaroa Ignimbrites. In press.

Naney, M.T., 1983. Phase equilibria of rock-forming ferromagnesian silicates in granitic systems. Am. J. Sci., 283: 993-1033.

Norrish, K. and Hutton, J.T., 1969. An accurate X-ray spectrograph method for the analysis of a wide range of geological samples. Geochim. Cosmochim. Acta, 33: 431-453.

Perfit, M.R., McCulloch, M.T. and Froude, D., 1981. Sr and Nd isotopic variations in volcanic and plutonic rocks from the Aleutian Islands and the Taupo Volcanic Zone, New Zealand: Implications for island arc magma genesis (abstract). IAVCEI 1981 Symposium: Arc Volcanism 24: 292-293.

Peterson, D.W., 1979. Significance of the flattening of pumice fragments in ash-flow tuffs. In Chapin, C. E. and Elston, W. E. (eds). Ash-Flow Tuffs. Geol. Soc. Am. Spec. Paper, 180: 195-204.

Pringle, M.S., McWilliams, M., Houghton, B.F., Lanphere, M.A. and Wilson, C.J.N., 1992. $^{40}Ar/^{39}Ar$ dating of Quaternary feldspar: Examples from the Taupo Volcanic Zone, New Zealand. Geology, 20: 531-534.

Reid, F., 1982. Geochemistry of central North Island greywackes and genesis of silicic magmas. Unpublished Ph.D. thesis, lodged in the Library, Victoria University of Wellington, New Zealand.

--------1983. Origin of the rhyolitic rocks of the Taupo Volcanic Zone, New Zealand. J. Volcanol. Geotherm. Res., 15: 315-338.

Reid, F.W. and Cole, J.W.,1983. Origin of dacites of Taupo Volcanic Zone, New Zealand. In Aramaki, S. and Kushiro, I. (eds). Arc Volcanism. J. Volcanol. Geotherm. Res., 18: 191-214.

Rice, A., 1981. Convective fractionation: A mechanism to provide cryptic zoning (macrosegregation), layering, crescumulates, banded tuffs and explosive volcanism in igneous processes. J. Geophys. Res., 86: 405-417.

Rogan, A.M., 1982. A geophysical study of the Taupo Volcanic Zone, New Zealand. J. Geophys. Res., 87:4073-4088.

Ross, C.S. and Smith, R.L., 1961. Ash-Flow Tuffs: their origin, geologic relations, and identification. U.S. Geol. Surv. Prof. Paper, 366. 81 p.

Rutherford, M.J., 1985. The May 18, 1980, eruption of Mount St. Helens. I. Melt composition and experimental phase equilibria. J. Geophys. Res., 90: 2929-2947.

Schroeder, B., Thompson, G., Sulanowska, M. and Ludden, J.N., 1980. Analysis of geologic materials using an automated X-ray fluorescence system. X.R.S., 9: 198-205.

Schuraytz, B.C., Vogel, T.A. and Younker, L.W., 1989. Evidence for dynamic withdrawal from a layered magma body: The Topopah Spring Tuff, southwestern Nevada. J. Geophys. Res., 94: 5925-5942.

Self, S. and Sparks, R.S.J., 1978. Characteristics of widespread pyroclastic deposits formed by the interaction of silicic magma and water. Bull. Volcanol., 41: 196-212.

Self, S., Goff, F., Gardner, J.N., Wright, J.V. and Kite, W.M., 1986. Explosive rhyolitic volcanism in the Jemez Mountains: Vent locations, caldera development and relation to regional structure. J. Geophys. Res., 91: 1779-1798.

Smith, I.E.M., 1986. Preface. In Smith, I.E.M., ed. Late Cenozoic Volcanism in New Zealand. Roy. Soc. N.Z. Bull., 23: 6.

Smith, R.L., 1960. Ash Flows. Geol. Soc. Am. Bull.4, 71: 795-842.

-------1979. Ash-flow magmatism. In Chapin, C.E. and Elston, W.E., ed. Ash flow tuffs. Geol. Soc. Am. Spec. Paper, 180: 5-27.

Smith, R.L. and Bailey, R.A., 1968. Resurgent cauldrons. In Coats, R.R., Hay, R.L. and Anderson, C.A. (eds). Studies in volcanology (Howell Williams volume). Geol. Soc. Am. Memoirs, 116: 153-210.

Sparks, R.S.J., 1975. Stratigraphy and geology of the ignimbrites of Vulsini Volcano, Central Italy. Geol. Rundschau, 64: 497-523.

-------1976. Grain size variation in ignimbrites and implications for the transport of pyroclastic flows. Sedimentology, 23: 147-188.

Sparks, R.S.J. and Walker, G.P.L., 1973. The ground surge deposit: a third type of pyroclastic rock. Nature, Phys. Sci., 241: 62-64.

------- and -------1977. The significance of vitric-enriched air-fall ashes associated with crystal-enriched ignimbrites. J. Volcanol. Geotherm. Res., 2: 329-341.

Sparks, R.S.J., Huppert, H.E. and Turner, J.S., 1984. The fluid dynamics of evolving magma chambers. Phil. Trans. R. Soc. London, A 310: 511-534.

Sparks, R.S.J., Self, S. and Walker, G.P.L., 1973. Products of ignimbrite eruptions. Geology, 1: 115-118.

Sparks, R.S.J., Sigurdsson, H. and Wilson, L., 1977. Magma mixing: A mechanism for triggering acid explosive eruptions. Nature, 267: 315-323.

Sparks, R.S.J., Wilson, L. and Hulme, G., 1978. Theoretical modelling of the generation, movement and emplacement of pyroclastic flows by column collapse. J. Geophys. Res., 83: 1727-1739.

Spera, F.J., Yuen, D.A., Greer, J.C. and Sewell, G., 1986. Dynamics of magma withdrawal from stratified magma chambers. Geology, 14: 723-726.

Storey. M., Wolff, J.A., Norry, M.J. and Mariner, G.F., 1989. Origin of hybrid lavas from Agua de Pau volcano, Sao Miguel, Azores. In Saunders, A.D. and Norry, M.J. (eds). Magmatism in the Ocean Basins. Geol. Soc. Spec. Publ., 42: 161-180.

Sweatman, T.R. and Long, J.V.P., 1969. Quantitative Electron-probe micro-analysis of rock-forming minerals. J. Petrol., 10: 332-379.

Taylor, H.P., Jr., 1980. The effects of assimilation of country rock rocks by magmas on $^{18}O/^{16}O$ and $^{87}Sr/^{86}Sr$ systematics in igneous rocks. Ibid., 47: 243-254.

Thorpe, R.S., Francis, P.W. and Moorbath, S., 1979. Rare earth and strontium isotope evidence concerning the petrogenesis of North Chilean ignimbrites. Earth Planet. Sci. Lett., 42: 359-367.

Valentine, G.A., 1992. Magma chamber dynamics. Encyclopedia of Earth System Science, 3. Academic Press Inc. pp. 1-17.

Vogel, T.A., Noble, D.C. and Younker, L.W., 1989. Evolution of a chemically zoned magma body: Black Mountain Volcanic Center, southwestern Nevada. J. Geophys. Res., 94: 6041-6058.

Vogel, T.A., Ryerson, F.J., Noble, D.C. and Younker, L.W., 1987. Limits to magma mixing based on chemistry and mineralogy of pumice fragments erupted from a chemically zoned magma body. J. Geol., 95: 659-670.

Walcott, R.I., 1978. Present tectonics of Late Cenozoic evolution of New Zealand. Geophys. J. R. Astr. Soc., 52: 137-164.

Walker, G.P.L., 1972. Crystal concentration in ignimbrites. Contrib. Miner. Petrol., 36: 135-146.

-------1980. The Taupo pumice: product of the most powerful known (ultraplinian) eruption? J. Volcanol. Geotherm. Res., 8: 69-94.

-------1981. Volcanological applications of Pyroclastic Studies. In Self, S. and Sparks, R.S.J. (eds). Tephra Studies. NATO Advanced Study Institutes series. D. Reider Publishing Company, Dordrecht, Holland. pp. 391-403.

-------1981a. Characteristics of two phreatoplinian ashes, and their water flushed origin. J. Volcanol. Geotherm. Res., 9: 395-407.

-------1981e. Generation and dispersal of fine ash dust by volcanic eruptions. J. Volcanol. Geotherm. Res., 11: 81-92.

-------1981d. New Zealand case histories of pyroclastic studies. In Self, S. and Sparks, R.S.J. (eds). Tephra Studies. NATO Advanced Study Institutes series. D. Reider Publishing Company, Dordrecht, Holland. pp. 317-330.

-------1983. Ignimbrite types and ignimbrite problems. J. Volcanol. Geotherm. Res., 17: 65-88.

-------1985. Origin of coarse lithic breccias near ignimbrite source vents. J. Volcanol. Geotherm. Res., 25: 157-171.

Walker, G.P.L. and Croasdale, R., 1971. Two Plinian-type eruptions in the Azores. J. Geol.Soc. London, 127: 17-55.

Walker, G.P.L. and Wilson, C.J.N., 1983. Lateral variations in the Taupo ignimbrite. J. Volcanol. Geotherm. Res., 18: 117-123.

Walker, G.P.L., Heming, R.F. and Wilson, C.J.N., 1980b. Low-aspect ratio ignimbrites. Nature, 283: 286-287.

Walker, G.P.L., Wilson, C.J.N. and Froggatt, P.C., 1980a. Fines-depleted ignimbrite in New Zealand - The product of a turbulent pyroclastic flow. Geology 8: 245-249.

Wilson, C.J.N., 1980. The role of fluidisation in the emplacement of pyroclastic flows: An experimental approach. J. Volcanol. Geotherm. Res., 8: 231-249.

-------1981. Studies on the origins and emplacement of pyroclastic flows. Unpublished Ph.D. thesis, lodged in the Library, Imperial College, University of London, England. 402 p.

-------1984. The role of fluidisation in the emplacement of pyroclastic flows, 2: experimental results and their interpretation. J. Volcanol. Geotherm. Res., 20: 55-84.

-------1986. Pyroclastic flows and ignimbrites. Sci. Progress, 70: 171-207.

Wilson, C.J.N. and Walker, G.P.L., 1982. Ignimbrite depositional facies: the anatomy of a pyroclastic flow. J. Geol. Soc. London 139: 581-592.

------- and -------1985. The Taupo eruption, New Zealand. I. General aspects. Phil. Trans. R. Soc. London, A, 314: 199-228.

Wilson, C.J.N., Houghton, B.F. and Lloyd, E.F., 1986. Volcanic history and evolution of the Maroa-Taupo area, central North Island. In Smith, I.E.M., ed. Late Cenozoic volcanism in New Zealand. Roy. Soc. N.Z. Bull., 23: 194-223.

Wilson, L., Sparks, .S.J. and Walker, G.P.L., 1980. Explosive volcanic eruptions - IV. The control of magma properties and conduit geometry on eruption column behaviour. Geophys. J. R. Astr. Soc., 63: 117-148.

Wilson, C.J.N., Rogan, A.M., Smith, I.E.M., Northey, D.J., Nairn, I.A. and Houghton, B.F., 1984. Caldera Volcanoes of the Taupo Volcanic Zone, New Zealand. J. Geophys. Res., 89: 8463-8484.

Wright, J.V., 1981. The Rio Caliente ignimbrite: analysis of a compound intraplinian ignimbrite from a major late Quaternary Mexican eruption. Bull. Volcanol., 44: 189-212.

Wright, J.V. and Walker, G.P.L., 1981. Eruption, transport and deposition of ignimbrite: a case study from Mexico. J. Volcanol. Geotherm. Res., 9: 111-131.

Wright, J.V., Self, S. and Fisher, R.V., 1979. Eruption sequence of the Bandelier Tuff, Jemez Mountains, New Mexico. Eos Trans. AGU, 61: 66.

-------, ------- and -------, 1981. Towards a facies model for ignimbrite-forming eruptions. In Self,S. and Sparks, R.S.J., (eds). Tephra Studies. NATO Advanced Study Institutes series. D. Reider Publishing Company, Dordrecht, Holland. pp. 433-439.

Wright, J.V., Smith, A.L. and Self, S., 1980. A working terminology of pyroclastic deposits. J. Volcanol. Geotherm. Res., 8: 315-336.

-------, ------- and -------1981b. A terminology for pyroclastic deposits. In Self, S. and Sparks, R.S.J., (eds). Tephra Studies. NATO Advanced Study Institutes series. D. Reider Publishing Company, Dordrecht, Holland. pp. 457-463.

Appendix A

Field locations

This appendix contains general information concerning the outcrop localities and rock types used in this thesis. The localities are also shown in Map B.

Field no. & loc. = field number and locality
GR = grid reference New Zealand Topographical Map 260, 1:50.000
Outcrop type:
- VPI = valley-ponded ignimbrite
- IVD = ignimbrite veneer deposit
- Paleosol = paleosol, buried soil
- Tephra(s) = pyroclastic air-fall deposit(s)
- Sediments = reworked pyro- and epiclastic sediments

Th. = thickness.

Sample codes

Because of a limitation in the number of available characters (max. five) in the petrology computer program some of the field numbers have been abbreviated. For field locations including samples from different stratigraphic levels the locations number has been replaced by a letter; i.e. 132/18/1 (the first number is the field location number, the second indicates the relative stratigraphic height, 18 m from the base, and the third number is the pumice number) = V18/1.

Localities (and samples) with a letter prefix:
R = no. 33
P = follows no. 33
HJ (and H) = no. 48
V = no. 132
T = no. 170

Field no & loc.	GR	Outcrop type	Th.
1 & 129 Puriri Rd	660294	Pokai Ignimbrite: flow units (VPI)	≥20 m
		air-fall deposits	0.6 m
		Paleosol, tephras & sediments	3.8 m
		Whakamaru Ignibmrite	≥3 m
2 Tikorangi Rd	803187	Pokai Ignimbrite: flow units (VPI)	≥20 m
3 Tikorangi Rd	793197	Pokai Ignimbrite: flow units (VPI with IVD on the top)	≥3.5 m
4 Tikorangi Rd	789198	Pokai Ignimbrite: flow units (VPI)	≥2.5 m
5 Rahui Rd	726215	Mamaku Ignimbrite	≥3 m
6 Galaxy Rd	671266	Pokai Ignimbrite: flow units (VPI with IVD on the top)	≥25 m
7 Galaxy Rd	678286	Pokai Ignimbrite: flow unit(s)	≥12 m
8 & 76 Road J	665290	Chimp Ignimbrite: flow units	≥6 m
		air-fall deposit	0.2 m
		Paleosol & sediments	±1.3 m
		Whakamaru Ignibmrite	≥4 m
9 Puriri Rd	658296	Whakamaru Ignimbrite	≥2 m
10 Puriri Rd	651309	Whakamaru Ignimbrite	≥5 m

Field no & loc.	GR	Outcrop type	Th.
11 Te Whetu	688338	(Pokai Ignimbrite, no. 12)	
		Paleosol & sediments	±0.7 m
		Chimp Ignimbrite: flow units	±4 m
		air-fall deposit	0.1 m
		Paleosol, tephras & sediments	≥3.5 m
12 Te Whetu	689335	Mamaku Ignimbrite	≥20 m
		Pokai Ignimbrite: flow unit(s) (VPI)	≥12 m
		air-fall deposits	0.6 m
13 Sutcliffe Rd	704354	Whakamaru Ignimbrite	≥5 m
14 Downer Rd	674336	Pokai Ignimbrite: flow unit(s) (VPI)	≥30 m
15 Downer Rd	666334	Pokai Ignimbrite: flow unit (IVD)	2 m
16 Rusa Rd	812186	Rahopaka Ignimbrite	≥20 m
17 Rusa Rd	807187	Tikorangi Ignimbrite	≥3 m
18 Pukerimu Rd	774158	Rhyolitic lava (Haparangi group rhyolite dome)	
19 Pukerimu Rd	773162	Pokai Ignimbrite: flow unit (VPI)	≥4 m
20 Pukerimu Rd	774172	Pokai Ignimbrite: flow unit (VPI)	≥2 m
21 Pukerimu Rd	774175-777178	Mamaku Ignimbrite	≥12 m
		Tephras & sediments	±3 m
		Pokai Ignimbrite: flow units (VPI with IVD on the top)	≥8 m
22 Bat Rd	668292	Chimp Ignimbrite: flow unit	≥ 3 m
23 Bat Rd	667289	Pokai Ignimbrite: flow unit (VPI)	3.5 m
		air-fall deposit	0.4 m
		Tephras & sediments	≥4 m
24 Puriri Rd	669283	Whakamaru Ignimbrite	≥11 m
25 Harry Johnson Rd	807193	Pokai Ignimbrite: flow unit (IVD)	≥5 m
26A Harry Johnson Rd	810193 -808189	Pokai Ignimbrite: flow unit (VPI)	≥7 m
		Rahopaka Ignimbrite	≥30 m
27 Harry Johnson Rd	823185	Unknown ignimbrite, poss. Mamaku Ign.	≥20 m
28 Rhino Rd	803201	Pokai Ignimbrite: flow unit (VPI)	≥3 m
29 Pukerimu Rd	786205	Mamaku Ignimbrite: flow unit(s)	≥10 m
		air-fall deposits	±3 m
		Paleosol & tephras	≥4 m
30 Hippo Rd	773200	Pokai Ignimbrite: flow unit (VPI)	≥2 m
31 Tokoroa Rd	691244	Mamaku Ignimbrite	≥4 m
		Pokai Ignimbrite: flow units (VPI with IVD on the top)	≥7 m
32 Kelly Rd	682251	Pokai Ignimbrite: co-ign. ash-fall	±0.3 m
		flow units	≥3 m
33 & R[9] Pokai Rd	682268	Mamaku Ignimbrite	≥4 m

[9] The 30 m high vertical Pokai Ignimbrite outcrop was mapped and sampled by Mr M. Cook in 1988, and those samples have a field number 'R'. All the samples collected by Mr Cook have been prepared and analysed by the author of this thesis, and the data based on the analyses results and the field notes of Mr Cook have been interpreted by the author.

Field no & loc.	GR	Outcrop type	Th.
		Pokai Ignimbrite: flow units (VPI with IVD on the top	30 m
		air-fall deposits	0.3 m
		Paleosols & tephras	±7 m
		Chimp Ignimbrite: flow unit	≥4 m
P[10] Rauna Rd	739177	Pokai Ignimbrite: flow units (VPI with IVD on the top)	≥39 m
34 Hanna Rd	661275	Whakamaru Ignimbrite	≥6 m
35 Pokai Rd	687269	Mamaku Ignimbrite	≥6 m
		Tephras	≥2 m
36 Panda Rd	675277	Pokai Ignimbrite: flow unit (VPI)	≥7 m
37 Panda Rd	673277	Chimp Ignimbrite: flow unit	≥10 m
38 Galaxy Rd	685293	Pokai Ignimbrite: flow unit (VPI)	≥3 m
39 Circuit Rd	683309	Pokai Ignimbrite: flow unit (IVD)	≥4 m
40 Cabbage Tree Rd	660325	Chimp Ignimbrite: flow unit	≥2 m
41 McDowall Rd	705320	Mamaku Ignimbrite	≥20 m
		Pokai Ignimbrite: flow unit (IVD)	≥2.5 m
42 MacKney Rd	689317	Pokai Ignimbrite: flow units (VPI with IVD on the top)	≥20 m
43 Lower Crimp Rd	686325	Pokai Ignimbrite: flow unit(s) (VPI)	≥25 m
44 Lower Crimp Rd	695324	Chimp Ignimbrite: flow unit	≥5 m
45 & 106 McDowall Rd	703329	Chimp Ignimbrite: flow unit	≥7 m
		Tephras & sediments	≥3 m
46 Leslie Rd	594484	Pokai Ignimbrite: flow unit (VPI)	≥4 m
47 Leslie Rd	595484	Pokai Ignimbrite: flow unit (VPI)	±8.5 m
		air-fall deposit	0.1 m
		Chimp Ignimbrite: flow unit	≥5 m
47X Harry Johnson Rd	816188	Rahopaka Ignimbrite	≥4 m
HJ[11] Chamois Rd	803189	Pokai Ignimbrite: flow units (VPI with IVD on the top)	43 m
		surge deposits	3 m
		flow units (VPI)	32 m
48 "	"	surge deposits	±0.5 m
		flow unit (VPI)	≥4 m
49 Chamois Rd	793179	Pokai Ignimbrite: flow unit (VPI)	≥3 m
50 Galaxy Road	673261	Pokai Ignimbrite: flow units (VPI with IVD on the top)	≥6 m
51 Len Rd	732181	Pokai Ignimbrite: flow unit(s) (VPI)	≥12 m
52 Jeff Rd	634300	Pokai Ignimbrite: flow unit(s)	≥10 m

[10] This >39 m high vertical Pokai Ignimbrite outcrop was mapped and sampled by Mr M. Cook in 1988, and those samples have a field number 'P'. Other information as in Footnote 9.

[11] This >78 m high vertical Pokai Ignimbrite section above location 48 was mapped and sampled by Mr M. Cook in 1988, and those samples have a field number 'HJ' or 'H'. Other information as in Footnote 9.

Field no & loc.	GR	Outcrop type	Th.
53 Puriri Rd	648312	Chimp Ignimbrite: flow unit	≥7 m
54 Galaxy Rd	700301	Pokai Ignimbrite: flow unit (IVD)	≥2.5 m
55 Puriri Rd	653301	Tephras & sediments	±3.5 m
		Whakamaru Ignimbrite	≥1.5 m
56 Tikorangi Rd	802183	Mamaku Ignimbrite	≥15 m
57 Glass Rd	795224	Pokai Ignimbrite: air-fall deposit	≥3 m
58 Bison Rd	771204	Mamaku Ignimbrite	≥7 m
59 Bison Rd	772204	Waiotapu Ignimbrite (quarry)	≥20 m
60 Rawhiti Rd	819209	Pokai Ignimbrite: flow unit (VPI)	≥7 m
61 Rawhiti Rd	823206	Pokai Ignimbrite: flow units (VPI with IVD on the top)	≥5 m
62 Tikorangi Rd	786202	Pokai Ignibmrite: flow unit (VPI)	≥7 m
63 Warthog Rd	794194	Pokai Ignimbrite: flow unit (VPI)	≥8 m
64 Deer Rd	805196	Pokai Ignimbrite: flow unit (IVD)	≥2 m
65 Chamois Rd	787175	Pokai Ignimbrite: flow unit (VPI)	≥4 m
66 Chamois Rd	784167	Pokai Ignimbrite: flow unit (VPI)	≥8 m
67 Tikorangi Rd	802183	Pisolitic tuff (stratigr. pos. unknown)	±7 m
68 Hyena Rd	669239	Pokai Ignimbrite: flow unit (VPI)	≥3 m
69 Galaxy Rd	672257	Chimp Ignimbrite: flow unit	≥4 m
70 & 128 Galaxy Rd	673264	Pokai Ignimbrite: flow unit(s)	≥15 m
		air-fall deposits	0.9 m
71 Squirrel Rd	684263	Pokai Ignimbrite: flow unit (IVD)	≥2 m
72 Cougar Rd	640273	Pokai Ignimbrite: flow unit (IVD)	≥2.5 m
73 Cougar Rd	643273	Pokai Ignimbrite: flow unit (IVD)	≥2 m
74 Hanna Rd	661274	Pokai Ignimbrite: flow unit(s) (VPI)	≥20 m
		Whakamaru Ignimbrite	≥4 m
75 Gayford Rd	645304	Pokai Ignimbrite: flow unit (IVD)	≥2.5 m
76 (see no. 8)			
77 Puriri Rd	657296	Pokai Ignimbrite: flow unit(s)	≥15 m
78 Puriri Rd	654300	Chimp Ignimbrite: flow unit	≥3 m
79 Sutton Rd	662303	Pokai Ignimbrite: flow unit (IVD)	≥5 m
"	663303	Chimp Ignimbrite: flow unit	≥4.5 m
80 Tikorangi Rd	803185	Pokai Ignimbrite: flow unit(s) (VPI)	≥18 m
81 Nemo Rd	648305	Pokai Ignimbrite: flow unit (IVD)	≥5 m
82 Puriri Rd	651307	Chimp Ignimbrite: flow units	≥8 m
83 Mohina Rd	655314	Chimp Ignimbrite: flow unit	≥2.5 m
84 Mohina Rd	654316	Pokai Ignimbrite: flow units (VPI with IVD on the top)	≥3.5 m
85 Mohina Rd	673311	Pokai Ignimbrite: flow unit (IVD)	≥2 m
86 Galaxy Rd	674285	Pokai Ignimbrite: flow unit(s) (VPI)	≥30 m
87 Circuit Rd	675315	Pokai Ignimbrite: flow unit (IVD)	≥1 m

Field no & loc.	GR	Outcrop type	Th.
88 Cabbage Tree Rd	662328	Pokai Ignimbrite: flow unit (IVD)	≥2.7 m
89 Cabbage Tree Rd	657332	Chimp Ignimbrite: flow unit	≥3 m
90 Cabbage Tree Rd	663323	Chimp Ignimbrite: flow unit	≥2 m
91 Moorhouse Rd	625358	Pokai Ignimbrite: flow units (VPI)	≥22 m
92 Moorhouse Rd	641352	Pokai Ignimbrite: flow unit (IVD)	≥2 m
93 Moorhouse Rd	637353	Chimp Ignimbrite: flow unit	≥3.5 m
94 Ngutuwera Rd	643333	Chimp Ignimbrite: flow unit	≥2 m
95 Downer Rd	642330	Chimp Ignimbrite: flow unit	≥2 m
96 Downer Rd	642327	Chimp Ignimbrite: flow unit	≥3.5 m
97 Barron Rd	703194	Pokai Ignimbrite: flow units (VPI)	≥2.5 m
98 Barron Rd	703193	Pokai Ignimbrite: flow unit (VPI)	≥2.5 m
99 Barron Rd	698187	Pokai Ignimbrite: flow unit (VPI)	≥5 m
100 Anderson Rd	705180	Pokai Ignimbrite: flow unit (VPI)	≥4.5 m
101 Elk Rd	722187	Pokai Ignimbrite: flow unit (VPI)	≥2 m
102 Elk Rd	714182	Pokai Ignimbrite: flow unit (VPI)	≥2.5 m
103 Bull Rd	713198	Pokai Ignimbrite: flow unit (VPI)	≥1.5 m
104 McDowall Rd	716321	Mamaku Ignimbrite	≥8 m
		Tephras & paleosol	±0.4 m
		Pokai Ignimbrite: flow units (VPI with IVD on the top)	≥5 m
105 McDowall Rd	706323	Pokai Ignimbrite: flow unit	≥7 m
106 (see no. 45)			
107 Hughes Rd	706337	Pokai Ignimbrite: flow unit (IVD)	≥2 m
108 McCracken Rd	723187	Pokai Ignimbrite: flow unit (VPI)	≥6 m
109 Len Rd	737166	Pokai Ignimbrite; flow units (VPI)	≥10 m
110 Len Rd	730188	Pokai Ignimbrite: flow units (VPI with IVD on the top)	≥22 m
111 Len Rd	732180	Pokai Ignimbrite: flow unit(s)	≥18 m
112 Bob Rd	747177	Pokai Ignimbrite: flow unit (VPI)	±14 m
		surge deposits	±0.7 m
		flow unit (VPI)	≥8 m
113 Downer Rd	677337	Chimp Ignimbrite: flow unit	≥4 m
114 Downer Rd	676336	Pokai Ignimbrite: flow unit (IVD)	≥3 m
115 Downer Rd	661337	Pokai Ignimbrite: flow unit(s) (VPI)	≥30 m
116 Downer Rd	654337	Chimp Ignimbrite: flow unit	≥15 m
117 Downer Rd	646334	Pokai Ignimbrite: flow unit (VPI)	±4 m
		Paleosol, tephras & sediments	±5 m
		Chimp Ignimbrite: flow unit	8 m
		Paleosol, tephras & sediments	±5 m
		Whakamaru Ignimbrite	≥10 m

Field no & loc.	GR	Outcrop type	Th.
118 Opakau Rd	645335	Pokai Ignimbrite: flow unit (IVD)	≥2 m
119 Moorhouse Rd	622345	Chimp Ignimbrite: flow unit	≥3.5 m
120 Te Ranga Rd	632336	Chimp Ignimbrite: flow unit	≥4 m
121 Jeff Rd	636309	Pokai Ignimbrite: flow units (VPI with IVD on the top)	≥25 m
122 Jeff Rd	615312	Pokai Ignimbrite: flow unit (IVD)	≥3 m
123 Jeff Rd	636303	Pokai Ignimbrite: flow unit (IVD)	≥1.5 m
124 Jeff Rd	634305	Pokai Ignimbrite: flow unit (IVD)	≥1.5 m
125 Jeff Rd	637307	Chimp Ignimbrite: flow unit	≥2 m
126 Harry Johnson Rd	818187	Pokai Ignimbrite: flow unit (VPI)	≥3 m
127 Harry Johnson Rd	813191	Pokai Ignimbrite: flow unit (VPI)	≥5 m
128 (see no. 70)			
129 (see no.1)			
130 Puriri Rd	653302	Tephras, sediments & paleosol	±6 m
		Whakamaru Ignimbrite	≥2 m
131 Haunui Valley	885305	Pokai Ignimbrite: lithic breccia	≥4 m
132 & V Haunui Valley	886294	Mamaku Ignimbrite	≥10 m
(Pylon line)		Pokai Ignimbrite: flow units (VPI with IVD on the top)	≥45 m
133 Haunui Valley	886288	Pokai Ignimbrite: flow unit(s) (VPI)	≥35 m
134 Haunui Valley	892303	Pokai Ignimbrite: flow unit (VPI)	≥2 m
135 Haunui Valley	895310	Pokai Ignimbrite: flow unit (VPI)	≥4 m
136 Whites Rd	579516	Pokai Ignimbrite: flow unit (VPI)	4 m
		air-fall deposit	≤0.1 m
137 Whites Rd	577503	Reworked Chimp Ignimbrite	1.5 m
		Whakamaru Ignimbrite	≥1.3 m
138 Leslie Rd	610477	Chimp Ignimbrite: flow unit	≥2 m
139 Orion Rd	631436	Pokai Ignimbrite: flow unit (IVD)	≥2 m
140 Tunnel Rd	650440	Chimp Ignimbrite: flow unit	1.5 m
		air-fall deposit	0.05 m
		Paleosol, tephras & sediments (equivalent to no. 141 upper tephras & sediment)	≥2.4 m
141 Waihou Rd	635447	Tephras & sediments	±2 m
		Whakamaru Ignimbrite	≥5 m
142 Moth Rd	619452	Chimp Ignimbrite: flow unit	≥6 m
143 Te Rere Rd	612363	Pokai Ignimbrite: flow unit(s) (VPI)	≥15 m
144 Te Rere Rd	609363	Pokai Ignimbrite: flow units (VPI with IVD on the top)	≥16 m
145 Ngatira	644407	Pokai Ignimbrite: flow unit (VPI)	≥2.5 m
146 Redwoods Rd	619427	Chimp Ignimbrite: flow unit(s)	≥8 m
147 Redwoods Rd	615428	Chimp Ignimbrite: flow unit	±3 m
		Paleosol, tephras & sediments	±1.5 m
		Whakamaru Ignimbrite	≥5 m

Field no & loc.	GR	Outcrop type	Th.
148 Railway Rd	587453	Pokai Ignimbrite: flow unit (IVD)	5 m
		Whakamaru Ignimbrite	≥3 m
149 Doug Rd	581433	Chimp Ignimbrite: flow unit	≥2 m
150 Waituna Rd	597184	Marshall Ignimbrite	≥5 m
151 Waituna Rd	598182	Pokai Ignimbrite: flow units (VPI)	1.1 m
		air-fall deposits	0.4 m
		Paleosol & sediments	1.5 m
		Whakamaru Ignimbrite	≥3 m
152 Kanuka Rd	616160	Pokai Ignimbrite: flow unit(s) (VPI)	≥12 m
153 Cormorant Rd	641173	Pokai Ignimbrite: flow units (VPI)	20 m
		Paleosol & sediments	0.2 m
		Whakamaru Ignimbrite	≥6 m
154 Cormorant Rd	644172	Pokai Ignimbrite: flow unit (VPI)	≥6 m
155 Tram Rd	644164	Pokai Ignimbrite: flow units (VPI)	2.2 m
		air-fall deposits	0.4 m
		Paleosol & sediments	±1.3 m
		Chimp Ignimbrite: flow unit	1.5 m
		Tephras & sediments	±2 m
		Whakamaru Ignimbrite	≥1 m
156 Tram Rd	647168	Pokai Ignimbrite: flow unit	≥3 m
157 Mastiff Rd	538270	Whakamaru Ignimbrite (not marked	±4 m
		Marshall Ignimbrite in Map B)	≥5 m
158 Highway 5	603530	Pokai Ignimbrite: flow units (VPI)	≥6 m
159 above Waihou River	594478	Pokai Ignimbrite: flow units (VPI)	±15 m
		Chimp Ignibmrite: flow unit	≥1.5 m
160 above Waihou River	593480	Pokai Ignimbrite: flow units (VPI)	≥10 m
161 Clough Rd	720150	Pokai Ignimbrite: flow unit (VPI)	≥3.5 m
162 Leslie Rd	611478	Chimp Ignimbrite: flow unit	≥2 m
163 Tram Rd	583453	Pokai Ignimbrite: flow unit (VPI)	≥10 m
164 Railway Rd	595453	Whakamaru Ignimbrite	≥4 m
165 Moth Rd	611452	Pokai Ignimbrite: flow unit (VPI)	≥4 m
166 Wasp Rd	616454	Chimp Ignimbrite: flow unit	≥3 m
167 Kakahu Rd	636593	Unknown ignimbrite (not marked in Map B)	≥4 m
168 Haunui Valley	899303	Pokai Ignimbrite: flow unit (IVD)	≥4 m
169 Highway 30	808160	Pokai Ignimbrite: flow unit (VPI)	≥3.5 m
170 & T Tapapa Valley	611540- 613538	Pokai Ignimbrite: flow units (VPI with IVD on the top	≥25 m
171 Matahana Rd	809223	Chimp Ignimbrite: flow unit	≥2 m
172 Rawhiti Rd	815213	Pokai Ignimbrite: flow units (VPI)	≥4 m
173 Boundary Rd	688231	Chimp Ignimbrite: flow unit	≥2.5 m

Appendix B

Petrographic analyses of representative samples.

Sample = field number and rock type (see Appendix A);
Ref.no = reference number for samples analysed by XRF (listed in Appendix D, Table D.2);
Method:
binoc. = samples, i.e. air-fall material and non-welded pumices and ignimbrite matrix material studied under binocular microscope;[12]
thins. = thin sections studied under the microscope;
micr. = thin sections used for microprobe analyses, containing mostly phenocrysts, separated from pumice glass.

Devitrification (in tuffs and ignimbrites) = formation of crystals and crystal aggregates (usually feldspar and cristobalite), starting within the boundaries of the glass shards; normally too fine for individual minerals to be identifiable under the microscope (Ross & Smith, 1961).

Vapour-phase crystallisation (in tuffs and ignimbrites) = the formation of crystals takes place in open spaces under the influence of a vapour phase; crystals normally very fine grained, but also coarse grained aggregates occur (Ross & Smith, 1961).

The phenocrysts are listed in the order of abundance.

Sample: 1A/2 Whakamaru Ign. pumice Ref.no: 258 Method: binoc.

Matrix: pale grey, tubular, fibrous glass shards, high phenocryst content.
Phenocrysts:
Plagioclase, eu- to subhedral, tabular grains, max.size 2x2 mm.
Quartz, rounded grains, often broken with conchoidal fractures, max.size 3x2 mm.
Biotite, brown to black flakes, max.size 1.4x1.2 mm.
Orthopyroxene, bright green, translucent, prismatic grains, max size 0.6x0.3 mm.
Fe-Ti oxides, minute grains.

Sample: 1E/3 Pokai Ign. pumice Ref.no: 3 Method: binoc.

Matrix: pale yellow, fibrous glass shards, moderate phenocryst contents.
Phenocrysts:
Plagioclase, eu- to subhedral, tabular grains, max size 1.5x1.4 mm.
Orthopyroxene, bright green, translucent prismatic grains, max.size 1.2x0.6 mm.
Quartz, slightly rounded prisms, max.size 1.3x1 mm.
Fe-Ti oxides, minute grains.

[12] The estimated phenocryst contents for samples studied under binocular microscope correspond roughly to the following modal analyses from thin section studies:
low phenocryst content = ≤3 vol.% phenocrysts;
moderate phenocryst content = 3-6 vol.% phenocrysts;
high phenocryst content = ≥ 6 vol.% phenocrysts.

Sample: 2A/2 Pokai Ign. pumice Ref.no: 6 Method: binoc.

Matrix: pale yellow-brownish, fibrous glass shards, moderate phenocryst content.

Phenocrysts:

85 % Plagioclase, eu- to subhedral, tabular grains, max.size 1.4x0.9 mm.
13 % Orthopyroxene, bright green, translucent, prismatic grains, max.size 1.1x0.5 mm.
2 % Fe-Ti oxides, max.size 0.4x0.3 mm.

Sample: 3A/2 Pokai Ign. pumice Ref.no: 12 Method: binoc.

Matrix: orange-yellow, fibrous glass shards, moderate phenocryst content.

Phenocrysts:

84 % Plagioclase, eu- to subhedral, tabular grains, max.size 1.5x1.4.
14 % Orthopyroxene, bright green, translucent, prismatic grains, max.size 1.1x0.3.
2 % Fe-Ti oxides, max.size 0.2x0.2.

Sample: 11A Chimp, air-fall pumice Ref.no: - Method: binoc.

Matrix: small, pale yellow, transparent vitric lapilli pumice and cuspate glass shards, moderate phenocryst content.

Phenocrysts:

80 % Plagioclase, eu- to subhedral, tabular grains, max.size 1.8x1.5 mm.
18 % Orthopyroxene, bright green, translucent, prismatic grains, max.size 1.1x0.4 mm.
≥1 % Fe-Ti oxides, max.size 0.2x0.1 mm.
≤1 % Amphibole (hornblende), black, short prismatic grains, max.size 0.5x0.2 mm.

Sample: 11B Chimp, distal flow unit Ref.no: - Method: binoc.

Matrix: transparent, vitric, platy, fibrous and Y-shaped ash-sized glass shards with some small lapilli pumices and lithics. Very crystal-poor.

Phenocrysts:

92 % Plagioclase, eu- to subhedral, tabular grains, max.size 0.8x0.5 mm.
8 % Orthopyroxene, bright green, translucent prismatic grains, max.size 0.5x0.2 mm.
trace Fe-Ti oxides, max.size 0.2x0.2 mm.

Sample: 11C Chimp Ign. matrix Ref.no: - Method: binoc.

Matrix: creamy-white and transparent, vitric, fibrous, platy and needle-shaped glass shards, pumices and lithics. Very crystal-poor.

Phenocrysts:

96 % Plagioclase, eu- to subhedral, tabular grains, max.size 0.7x0.5 mm.
2 % Orthopyroxene, bright green, prismatic grains, max.size 0.4x0.3 mm.
2 % Fe-Ti oxides, max.size 0.3x0.2 mm.

Sample: 11C/2 Chimp Ign. pumice Ref.no: 234 Method: thins/binoc.

99.2 % Matrix: fibrous and Y-shaped glass shards, devitrified, irregular vesicle cavities (vesicularity 55.8 %), mostly filled with vapour-phase crystallisation products.

0.8 % Phenocrysts:

- 83.3 % Plagioclase, sub- to euhedral, tabular grains, often with rounded (resorbed) crystal corners, zoning occurs, max.size 1.3x1.1 mm.
- 12.5 % Orthopyroxene, subhedral, long prismatic grains, max.size 1.2x0.5 mm; bright green, translucent under the binoc. microscope.
- 2.1 % Amphibole (hornblende), pleochroic (green), subhedral, 6-sided prismatic grains, max.size 0.8x0.6 mm; black under the binoc. microscope.
- 2.1 % Fe-Ti oxides, euhedral grains, max.size 0.3x0.3 mm.
- trace Quartz, rounded prisms, max.size 1.3x1 mm.

Sample: 21D/1 Pokai Ign. pumice Ref.no: 31 Method: thins/binoc.

97.7 % Matrix: fibrous and cuspate glass shards, devitrified, elongated vesicle cavities (vesicularity 27.6 %), partly filled with vapour-phase crystallisation products.

2.3 % Phenocrysts:

- 94.4 % Plagioclase, eu- to subhedral, tabular grains, zoning common, max.size 2.1x1.7 mm.
- 5.6 % Orthopyroxene, sub- to euhedral, prismatic grains, max.size 1.5x0.7 mm; bright green under the binoc. microscope.
- trace Fe-Ti oxides, euhedral grains, max.size 0.5x0.5 m.

Sample: 26A/1 Pokai Ign. pumice Ref.no: 38 Method: micr.

Matrix: fibrous glass shards, moderate crystal content.

Phenocrysts:

- 95.3 % Plagioclase, eu- to subhedral, tabular grains, some have rounded crystal corners, zoning common, max.size 1.8x1.4 mm.
- 3.6 % Orthopyroxene, eu- to subhedral, prismatic grains, some with rounded crystal corners, max.size 1x0.4 mm.
- 1.1 % Fe-Ti oxides, euhedral grains, max.size 0.2x0.2 mm.
- trace Quartz, rounded grains, max.size 1.2x0.7 mm.

Sample: 26A/2 Pokai Ign. pumice Ref.no: 39 Method: micr.

Matrix: fibrous glass shards, moderate phenocryst content.

Phenocrysts:

- 91.2 % Plagioclase, eu- to subhedral, tabular grains, zoning common, max.size 1.8x1.4 mm.
- 5.1 % Orthopyroxene, eu-to subhedral, prismatic grains, max.size 1x0.4 mm.
- 2.6 % Quartz, rounded grains, max.size 1.2x0.7 mm.
- 1.1 % Fe-Ti oxides, euhedral grains, max.size 0.2x0.2 mm.
- trace Zircon, euhedral, minute grains.

Sample: R6 Pokai Ign. pumice Ref.no: - Method: thins.

97.6 % Matrix: fibrous, distorted glass shards, devitrified, collapsed vesicle cavities (vesicularity 21.8 %), mostly filled with vapour-phase crystallisation products.

2.4 % Phenocrysts:

94.4 % Plagioclase, eu- to subhedral, tabular grains, zoning common.

5.6 % Orthopyroxene, eu- to subhedral, prismatic grains.

trace Fe-Ti oxides, euhedral grains.

Sample: R12 Pokai Ign. pumice Ref.no: - Method: thins.

98.8 % Matrix: fibrous and cuspate glass shards, partially devitrified, rounded and elongated vesicles (vesicularity 45.8 %), partly filled with vapour-phase crystallisation products.

1.2 % Phenocrysts:

86.4 % Plagioclase, sub- to euhedral, tabular grains, zoning common.

13.3 % Orthopyroxene, sub- to euhedral prismatic grains.

trace Quartz, an- to subhedral, rounded grains.

trace Clinopyroxene, subhedral grains.

trace Amphibole (hornblende), pleochroic (green), subhedral grains.

trace Fe-ti oxides, euhedral grains.

trace Zircon, euhedral grains.

Sample: R12/2 Pokai Ign. pumice Ref.no: 62 Method: binoc.

Matrix: pale yellow-brown, fibrous glass shards, moderate phenocryst content.

Phenocrysts:

Plagioclase, eu- to subhedral, tabular grains, max.size 1.5x1.2 mm.
Orthopyroxene, bright green, prismatic grains, max.size 1.1x0.8 mm.
Fe-Ti oxides, minute black grains.

Sample: 33 Chimp Ign. matrix Ref.no: - Method: binoc.

Matrix: Creamy-white, cuspate and fibrous glass shards, low phenocryst content, composed mostly of plagioclase.

Phenocrysts:

Plagioclase, eu- to subhedral, tabular grains, max size 1.4x1 mm.
Orthopyroxene, bright green, translucent, prismatic grains, max.size 0.8x0.2 mm.
Quartz, rounded grains, max.size 1.2x1.1 mm.
Biotite, brown to black, translucent flakes, max.size 0.3x0.2 mm.
Fe-Ti oxides, minute black grains.

Sample: 33/1 Chimp Ign. pumice Ref.no: 236 Method: micr.

Matrix: fibrous and cuspate glass shards, very crystal-poor.

Phenocrysts:

96.3 % Plagioclase, eu- to subhedral, tabular grains often with rounded crystal margins, some zoning occurs, max.size 1.5x1.4 mm.

3.7 % Fe-Ti oxides, euhedral ≤0.2 mm grains.

trace Orthopyroxene, eu- to subhedral, prismatic grains, max.size 0.5x0.2 mm.

trace Biotite, pleochroic (greenish-brown), subhedral platy grains, max.size 0.3x0.2 mm.

Sample: 33/4 Chimp Ign. pumice Ref.no: 239 Method: micr/binoc.

Matrix: cuspate and tubular glass shards, mostly devitrified, relatively well preserved, elongated vesicles, often filled with vapour-phase crystallisation products. Very low phenocryst content.

Phenocrysts:

96.4 % Plagioclase, eu- to subhedral, tabular grains, zoning occurs, max.size 1.5x1.5 mm.

1.8 % Fe-Ti oxides, euhedral, minute grains.

1.3 % Clinopyroxene, eu- to subhedral, short prismatic grains, max.size 0.6x0.2 mm, greenish-brown under the binoc. microscope.

0.5 % Amphibole (hornblende), pleochroic (green), eu- to subhedral, blade-like grains, ±0.5 mm in size; black under the binoc. microscope.

trace Orthopyroxene, eu- to subhedral, prismatic grains, max size 0.9x0.6 mm; bright green, translucent under the binoc. microscope.

Sample: P1/1i Pokai Ign. matrix Ref.no: - Method: thins.

42.8 % Matrix: slightly welded with distorted and devitrified glass shards, some alignment of shards is evident, probably due to compression during welding, and vesicularity is low (2.4 %), also due to compression and collapse of the vesicle walls.

52.2 % Pumice: fibrous, somewhat distorted, devitrified glass shards, vesicles partly collapsed (vesicularity 14.1 %) and filled with vapour-phase crystallisation products.

3.9 % Phenocrysts:

- 78.9 % Plagioclase, eu- to subhedral, tabular grains, zoning common.
- 8.8 % Quartz, rounded grains.
- 7.0 % Orthopyroxene, eu- to subhedral, prismatic grains, often rounded crystal margins.
- 3.5 % Fe-Ti oxides, euhedral grains.
- 1.8 % Zircon, euhedral grains.

1.1 % Lithics.

Sample: P1/4i Pokai Ign. matrix Ref.no: - Method: thins.

68.6 % Matrix: welded, devitrified glass shards, the fibrous texture partly destroyed, low vesicularity (1.4 %).

22.6 % Pumice: distorted, devitrified glass shards, the fibrous texture still detectable, collapsed vesicles (vesicularity 16.5 %), mostly filled with vapour-phase crystallisation products.

5.5 % Phenocrysts:

- 87.4 % Plagioclase, eu- to subhedral, tabular grains, often with rounded crystal corners, zoning common.
- 7.6 % Orthopyroxene, eu- to subhedral, prismatic grains, resorption common along the crystal margins.
- 2.5 % Quartz, rounded grains.
- 2.5 % Fe-Ti oxides, euhedral grains.

3.3 % Lithics.

Sample: P1/5i Pokai Ign. matrix Ref.no: - Method: thins.

65.7 % Matrix: welded with cuspate and Y-shaped, though distorted and compressed (vesicularity 1 %), devitrified glass shards, development to spherulites.

23.8 % Pumice: fibrous, distorted, devitrified glass shards, flattened vesicle cavities (vesicularity 23.0 %), often filled with vapour-phase crystallisation products.

3.6 % Phenocrysts:

- 83.3 % Plagioclase, eu- to subhedral, platy and tabular grains, crystal corners often rounded (resorbed), zoning common.
- 8.3 % Quartz, rounded grains.
- 5.6 % Fe-Ti oxides, euhedral grains.
- 2.8 % Orthopyroxene, eu- to subhedral, prismatic grains, crystal margins often rounded (resorbed).
- trace Zircon, euhedral grains.

6.9 % Lithics.

Sample: P1/5 Pokai Ign. pumice Ref.no: - Method: thins.

95.2 % Matrix: see above, P1/5i Pumice.

4.8 % Phenocrysts:

- 89.6 % Plagioclase, eu- to subhedral, tabular grains, some with rounded crystal corners, zoning common.
- 6.2 % Fe-Ti oxides, euhedral grains.
- 4.2 % Orthopyroxene, eu- to subhedral, prismatic grains.

Sample: P1/10 Pokai Ign. matrix Ref.no: - Method: thins.

52.2 % Matrix: moderately welded, cuspate and fibrous, slightly distorted, devitrified glass shards, vesicularity 1.3 %.

45.3 % Pumice: fibrous and cuspate, slightly distorted, devitrified glass shards, elongated vesicles (vesicularity 26.6 %), most of them filled with vapour-phase crystallisation products.

2.2 % Phenocrysts:

- 70.0 % Plagioclase, eu- to subhedral, tabular grains, zoning common.
- 22.5 % Quartz, rounded grains.
- 5.0 % Orthopyroxene, mostly euhedral grains, resorption rare.
- 2.5 % Fe-Ti oxides, euhedral grains, often attached to the orthopyroxenes.

0.3 % Lithics.

Sample: P13/1 Pokai Ign. pumice Ref.no: 83 Method: thins/binoc.

98.8 % Matrix: fibrous, slightly distorted, partly devitrified glass shards, flattened, elongated vesicles (vesicularity 23.6 %), partly filled with vapour-phase crystallisation products.

1.2 % Phenocrysts:

- 83.0 % Plagioclase, eu- to subhedral, tabular grains, some with rounded crystal corners, zoning common.
- 8.5 % Quartz, rounded grains; under the binoc. microscope the bipyramidal form is evident, though the crystal corners are slightly rounded.
- 7.4 % Orthopyroxene, eu- to subhedral, prismatic grains; bright green under the binoc. microscope.
- 1.1 % Fe-Ti oxides, euhedral grains, often attached to the orthopyroxenes.

Sample: 37 pum a Chimp Ign. pumice Ref.no: - Method: thins/binoc.

≤100 % Matrix: pale brown, fibrous, devitrified glass shards, slightly fused together, elongated vesicles (vesicularity 40.9 %), mostly filled with vapour-phase crystallisation products.

trace Phenocrysts:

≤100 % Plagioclase, eu- to subhedral, tabular grains, max.size 0.7x0.5 mm.

trace Fe-Ti oxides, irregular clusters.

Sample: 37 pum b Chimp Ign. pumice Ref.no: - Method: thins/binoc.

92.0 % Matrix: white, cuspate and fibrous, devitrified glass shards, well preserved, nearly spherical vesicles (vesicularity 37.4 %), mostly filled with vapour-phase crystallisation products.

8.0 % Phenocrysts:

91.3 % Plagioclase, subhedral, tabular grains, resorption common with 'mottled' appearance, some zoning occurs, sometimes in glomeroporphyritic aggregates with orthopyroxene, max.size 2.1x1 mm.

5.6 % Orthopyroxene, subhedral, prismatic grains, usually with rounded crystal corners, max.size 1.5x0.5 mm; bright green under the binoc. microscope.

2.5 % Fe-Ti oxides, euhedral grains, often clustered together, max.size 0.5x0.4 mm.

0.6 % Amphibole (hornblende), pleochroic (green), an- to subhedral grains, max.size 1.2x0.4 mm; black under the binoc. microscope.

Sample: 47B Pokai Ign. pumice Ref.no: - Method: thins.

94.0 % Matrix: cuspate and fibrous glass shards, partially devitrified, well preserved rounded and elongated vesicles (vesicularity 52.0 %), partly filled with vapour-phase crystallisation products.

6.0 % Phenocrysts:

90.0 % Plagioclase, eu- to subhedral, tabular grains, crystal corners are usually rounded, zoning common, occurs also as glomeroporphyritic aggregates with orthopyroxene.

6.7 % Orthopyroxene, subhedral grains with rounded crystal corners.

3.3 % Fe-Ti oxides, euhedral grains, often attached to the orthopyroxenes.

Sample: HJ2/1 Pokai Ign. pumice Ref.no: 94 Method: thins.

98.3 % Matrix: slightly welded, fibrous, distorted, devitrified glass shards, flattened, elongated vesicles (vesicularity 32.9 %), mostly filled with vapour-phase crystallisation products.

1.7 % Phenocrysts:

94.1 % Plagioclase, eu- to subhedral, tabular grains, zoning common.

5.9 % Fe-Ti oxides, euhedral grains.

trace Orthopyroxene, eu- to subhedral, prismatic grains.

trace Amphibole (hornblende), pleochroic, subhedral, rounded, resorbed grains.

Sample: HJ2/2 Pokai Ign. pumice Ref.no: 95 Method: thins.

99.1 % Matrix: welded, distorted, devitrified glass shards, fibrous texture still visible, collapsed, elongated vesicles (vesicularity 9.7 %), mostly filled with vapour-phase crystallisation products.

0.9 % Phenocrysts:

88.9 % Plagioclase, mostly euhedral, tabular grains, zoning occurs.

11.1 % Quartz, rounded grains.

trace Fe-Ti oxides, euhedral grains.

Sample: H13/1 Pokai Ign. pumice Ref.no: 108 Method: binoc.

Matrix: pale yellow-brown, fibrous and cuspate glass shards, low phenocryst content.

Phenocrysts:

74 % Plagioclase, eu- to subhedral, tabular grains.

17 % Quartz, bipyramidal grains, although crystal corners rounded.

7 % Orthopyroxene, bright green, translucent, prismatic grains.

2 % Fe-Ti oxides, euhedral grains.

Sample: 48/3 Pokai Ign. pumice Ref.no: 119 Method: thins/binoc.

96.6 % Matrix: fibrous, somewhat distorted, devitrified glass shards, elongated, partly collapsed vesicles (vesicularity 27.8 %), mostly filled with vapour-phase crystallisation products.

3.4 % Phenocrysts:

75.1 % Plagioclase, mostly euhedral, tabular grains.

18.8 % Quartz, rounded grains; the original bipyramidal form can still be seen under the binoc. microscope.

4.7 % Orthopyroxene, mostly euhedral, prismatic grains, some have rounded crystal corners; bright green, translucent under the binoc. microscope.

1.4 % Fe-Ti oxides, euhedral grains, commonly attached to the orthopyroxenes.

trace Zircon, euhedral grains, often as inclusions in the plagioclases.

0.8 % Xenoliths.

Sample: 57/3 Pokai air-fall pumice Ref.no: 126 Method: binoc.

Matrix: creamy-white fibrous and cuspate glass shards, moderate/high phenocryst content, microxenoliths (rhyolitic) up to ca. 5 % of the matrix material.

Phenocrysts:

85 % Plagioclase, eu- to subhedral, tabular grains

9 % Orthopyroxene, bright green, translucent, long prismatic grains.

4 % Fe-Ti oxides, euhedral grains, often attached to the orthopyroxenes.

2 % Clinopyroxene, greenish-brown, translucent, short prismatic grains.

Sample: 63 Pokai Ign. matrix Ref.no: - Method: thins.

65.5 % Matrix: strongly welded, devitrified and distorted glass shards, vesicularity 0.4 %.

28.2 % Pumice: fibrous, devitrified and distorted glass shards, collapsed vesicles (vesicularity 13.4 %), partly filled with vapour-phase crystallisation products.

5.1 % Phenocrysts:

- 94.0 % Plagioclase, eu- to subhedral, tabular grains, often with rounded crystal corners, resorption around crystal margins common, zoning common.
- 3.0 % Quartz, rounded grains.
- 2.4 % Fe-Ti oxides, euhedral grains.
- 0.6 % Orthopyroxene, eu- to subhedral, prismatic grains.

1.2 % Lithics.

Sample: 66/1 Pokai Ign. pumice Ref.no: 128 Method: thins/binoc/micr.

95.7 % Matrix: yellow to orange, fibrous, partly distorted, devitrified glass shards, elongated vesicle (vesicularity 14.2 %), mostly filled with vapour-phase crystallisation products.

4.3 % Phenocrysts:

- 85.5 % Plagioclase, eu- to subhedral, tabular grains, some with rounded crystal corners, zoning common, max.size 1.3x0.8 mm.
- 6.8 % Orthopyroxene, eu- to subhedral, prismatic grains, max.size 1.2x0.4 mm; bright green, translucent under the binoc. microscope.
- 6.3 % Quartz, rounded grains, max.size 1.1x0.9 mm; under the binoc. microscope the bipyramidal form can still be detected though the crystal corners are rounded.
- 1.3 % Fe-Ti oxides, small, euhedral grains.
- 0.1 % Zircon, tiny, euhedral grains.

Sample: 70a Pokai air-fall (unit A, pumice-fall) Ref.no: - Method: binoc.

Matrix: poorly sorted from fibrous glass shards to vitric, creamy-white lapilli pumice, moderate/high abundance of both phenocrysts and lithics.

Phenocrysts:

Plagioclase, eu- to subhedral, tabular grains, max.size 2.7x1.1 mm.
Orthopyroxene, bright green, translucent, prismatic grains, max.size 2.1x0.7 mm.
Quartz, bipyramidal grains with slightly rounded crystal corners, max.size 1.8x1.2 mm.
Black obsidian, usually broken grains.
Fe-Ti oxides, tiny, euhedral grains.

Sample: 70b Pokai air-fall (Unit B, ash-fall) Ref.no: - Method: binoc.

Matrix: very fine vitric ash, usually <0.1 mm, cuspate and fibrous glass shards, some fibrous and tubular glassy clusters, up to 1.5 mm in size. Tiny pieces (<0.2 mm) of black obsidian and some microlithics (max.size 0.4x0.3 mm) are present.

Sample: 70e Pokai air-fall (Unit E, pumice-fall) Ref.no: - Method: binoc.

Matrix: poorly sorted from fine, fibrous and cuspate vitric ash to creamy-white, fibrous lapilli pumice, moderate lithic and low phenocryst contents. Black/dark grey obsidian fragments are relatively common, max.size 3.1x3 mm.

Phenocrysts:

Plagioclase, eu- to subhedral, tabular grains, max.size 2x1.5 mm.
Quartz, bipyramidal grains, slightly rounded crystal corners, max.size 1.2x0.6 mm.

Sample: 70e/1 Pokai air-fall pumice Ref.no: 135 Method: micr.

Matrix: fibrous and cuspate glass shards, moderate/high phenocryst content.

Phenocrysts:

84.7 % Plagioclase, eu- to subhedral, tabular grains, many with rounded crystal corners, zoning common, max.size 1.8x1.7 mm.
7.9 % Orthopyroxene, eu- to subhedral, prismatic grains, often with rounded crystal corners, max.size 1.3x0.4 mm.
7.1 % Fe-Ti oxides, euhedral grains.
0.3 % Zircon, euhedral grains.
trace Apatite, thin, long needles usually attached to the plagioclases.

Sample: 89/I Chimp Ign. matrix Ref.no: - Method: thins.

74.3 % Matrix: densely welded, the glass texture nearly destroyed, some Y-shaped, though severely distorted, glass shards still detectable, strongly devitrified, axiolitic texture in some glass shards well represented, no vesicle spaces.
32.4 % Pumice: strongly distorted, devitrified glass shards, collapsed vesicles (vesicularity 4.1 %), filled with vapour-phase crystallisation products.
2.7 % Phenocrysts:
66.7 % Plagioclase, eu- to subhedral, rounded grains, some have strongly resorbed cores (sieve texture), some are zoned.
22.2 % Orthopyroxene, eu- to subhedral grains, rounded crystal corners common.
11.1 % Fe-Ti oxides, euhedral grains.

Sample: 89/II Chimp Ign. matrix Ref.no: - Method: thins.

74.3 % Matrix: as in 89/I, except for vesicularity 0.3 %.
21.4 % Pumice: as in 89/I, except for vesicularity 3.5 %.
3.9 % Phenocrysts:
86.2 % Plagioclase, as in 89/I.
7.4 % Orthopyroxene, as in 89/I.
6.4 % Fe-Ti oxides, as in 89/I.
trace Clinopyroxene, subhedral, resorbed grains.
trace Amphibole (hornblende), pleochroic, short prismatic grains.
4.0 % Lithics.

Sample: 91 Pokai Ign. matrix Ref.no: - Method: thins.

69.9 % Matrix: welded, distorted, devitrified glass shards, plastic moulding against phenocrysts common, fibrous and Y-shaped glass shard texture just recognisable, pore spaces rare (vesicularity 1.9 %), vesicles filled with vapour-phase crystallisation products.

28.0 % Pumice: fibrous, distorted, devitrified glass shards, elongated, partly collapsed vesicles (vesicularity 29.1 %), mostly filled with vapour-phase crystallisation products.

2.1 % Phenocrysts:

79.2 % Plagioclase, eu- to subhedral, tabular grains, often with rounded crystal corners, zoning common.

12.5 % Orthopyroxene, eu- to subhedral, prismatic grains, often with rounded crystal corners.

8.3 % Fe-Ti oxides, euhedral grains.

trace Zircon, tiny, euhedral grains.

trace Lithics.

Sample: 93/1 Chimp Ign. pumice Ref.no: 249 Method: micr.

Matrix: fibrous glass shards, high phenocryst content.

Phenocrysts:

81.6 % Plagioclase, eu- to subhedral, tabular grains, often with rounded crystal corners, max.size 1.6x1.5 mm.

11.9 % Orthopyroxene, eu- to subhedral, prismatic grains, some with rounded crystal corners, max.size 1.1x0.4 mm.

4.4 % Fe-Ti oxides, euhedral grains, max.size 0.4x0.4 mm.

1.4 % Clinopyroxene, eu- to subhedral, prismatic grains, max.size 1.5x0.4 mm.

0.6 % Amphibole (hornblende), pleochroic (green), eu- to subhedral, prismatic grains, max.size 1.2x0.9 mm.

0.1 % Apatite, long, thin needles.

trace Zircon, tiny, euhedral grains.

Sample: 97/3 Pokai Ign. pumice Ref.no: 147 Method: micr.

Matrix: fibrous glass shards, very crystal-rich.

Phenocrysts:

85.1 % Plagioclase, eu- to subhedral, tabular grains, some with rounded crystal corners, zoning common, max.size 2.9x1.5 mm, often as glomeroporphyritic aggregates with orthopyroxenes.

8.3 % Orthopyroxene, eu- to subhedral, prismatic grains, some with rounded crystal corners, max.size 1.8x0.9 mm.

4.1 % Fe-Ti oxides, small, euhedral grains.

2.1 % Quartz, rounded grains, max.size 0.5x0.4 mm.

0.2 % Apatite, long, thin needles, usually attached the plagioclases.

0.2 % Titanite, small, euhedral grains.

trace Zircon, small, euhedral grains, usually attached to the plagioclase and orthopyroxenes.

Sample: 108/1 Pokai Ign. pumice Ref.no: 153 Method: micr.

Matrix: fibrous glass shards, very crystal-rich.
Phenocrysts:
93.4 % Plagioclase, eu- to subhedral, tabular grains, some with rounded crystal corners, zoning common, max.size 2.7x1.8 mm, often as glomeroporphyritic aggregates with orthopyroxenes.
4.8 % Orthopyroxene, eu- to subhedral, prismatic grains, some with rounded crystal corners, max.size 1.5x0.9 mm.
1.2 % Fe-Ti oxides, small, euhedral grains.
0.6 % Quartz, small, rounded grains.

Sample: 108/4 Pokai Ign. pumice Ref.no: 156 Method: binoc.

Matrix: creamy-white, fibrous and cuspate glass shards, very crystal-rich, clusters of plagioclase and pyroxenes.
Phenocrysts:
77 % Plagioclase, eu-to subhedral, tabular grains.
18 % Orthopyroxene, bright green, translucent, long, prismatic grains.
5 % Fe-Ti oxides, euhedral grains, often attached to the plagioclases and orthopyroxenes.
trace Clinopyroxene, greenish-brown, dark brown, translucent, short, prismatic grains.

Sample: 116a Chimp Ign matrix Ref.no: - Method: thins.

75.8 % Matrix: strongly welded and distorted, devitrified glass shards, the shard texture partly destroyed, no vesicle spaces.
16.8 % Pumice: strongly distorted, devitrified (spherulitic) glass shards, some of the original shard texture detectable (fibrous), no vesicle spaces.
5.8 % Phenocrysts:
82.8 % Plagioclase, eu- to subhedral, tabular grains, mostly rounded and resorbed, some are zoned.
10.3 % Orthopyroxene, eu- to subhedral, prismatic grains, often with rounded crystal corners.
6.9 % Fe-Ti oxides, euhedral grains.
trace Clinopyroxene, subhedral, rounded grains.
trace Amphibole (hornblende), pleochroic, short prismatic grains.
trace Zircon, eu- to subhedral grains.

Sample: 116b Chimp Ign. matrix Ref.no: - Method: thins.

72.6 % Matrix: as in 116a.
21.7 % Pumice: as in 116a, except for vesicularity 0.5 %.
4.2 % Phenocrysts:
85.8 % Plagioclase, as in 166a.
7.1 % Orthopyroxene, as in 116a.
7.1 % Fe-Ti oxides, as in 116a.
trace Amphibole, as in 116a.

Sample: 131A Pokai Ign. lithic breccia matrix Ref.no: - Method: thins.

65.9 % Matrix: slightly welded and distorted, devitrified glass shards, some shards show plasticity by moulding between phenocrysts and lithics, low vesicularity (2.8 %).

19.0 % Pumice: fibrous, somewhat distorted, devitrified glass shards, collapsed vesicles (vesicularity 18.1 %), vapour-phase crystallisation in the vesicles.

4.5 % Phenocrysts:

- 85.6 % Plagioclase, eu- to subhedral, tabular grains, somewhat rounded, zoning common.
- 6.3 % Quartz, rounded grains.
- 4.5 % Fe-Ti oxides, euhedral grains.
- 3.6 % Orthopyroxene, eu- to subhedral, prismatic grains, some grains have rounded crystal corners.

10.5 % Lithics.

Sample 131C1 Pokai Ign.pumice Ref.no: 174 Method: binoc.

Matrix: orange-yellow fibrous and cuspate glass shards, moderate phenocryst content. Microxenoliths common.

Phenocrysts & xenoliths:

- 75 % Plagioclase, eu- to subhedral, tabular grains.
- 8 % Orthopyroxene, bright green, mostly euhedral, prismatic grains.
- 7 % Quartz, bipyramidal, slightly rounded grains.
- 3 % Fe-Ti oxides, euhedral grains.
- 1 % Amphibole (hornblende), black, short, prismatic grains.
- 6 % Xenoliths.

Sample: 132 Pokai Ign. pumice Ref.no: - Method: thins.

96.4 % Matrix: fibrous and cuspate, somewhat distorted, devitrified glass shards, slightly collapsed, elongated vesicles (vesicularity 16.5 %), filled with vapour-phase crystallisation products.

3.6 % Phenocrysts:

- 96.2 % Plagioclase, eu- to subhedral, tabular grains, some with rounded crystal corners and resorbed margins, zoning common.
- 1.9 % Orthopyroxene, eu- to subhedral, prismatic grains, slightly rounded crystal corners.
- 1.9 % Fe-Ti oxides, euhedral grains.
- trace Quartz, small, rounded grains.

Sample: 132/1 Pokai Ign. pumice Ref.no: 179 Method: micr.

Matrix: fibrous and cuspate glass shards, moderate phenocryst content.

Phenocrysts:

93.0 % Plagioclase, eu- to subhedral, tabular grains, often with rounded crystal corners, zoning common, max.size 1.7x0.9 mm.

5.3 % Orthopyroxene, eu- to subhedral, prismatic grains, rounded crystal corners common, max.size 1.3x0.5 mm.

1.7 % Fe-Ti oxides, euhedral grains, max.size 0.2x0.2 mm.

trace Quartz, small rounded grains.

trace Zircon, very small, euhedral grains.

Sample: V18/2 Pokai Ign. pumice Ref.no: 177 Method: binoc.

Matrix: pale-yellow fibrous and cuspate glass shards, moderate phenocryst content.
Phenocrysts:
84 % Plagioclase, eu- to subhedral, tabular grains.
10 % Orthopyroxene, bright green, mostly euhedral, prismatic grains.
6 % Fe-Ti oxides, euhedral grains, often attached to the orthopyroxenes.

Sample: V39/1 Pokai Ign. pumice Ref.no: 196 Method: binoc.

Matrix: orange-yellow fibrous glass shards, moderate crystal content.
Phenocrysts:
81 % Plagioclase, eu- to subhedral, tabular grains.
14 % Orthopyroxene, bright green, translucent, long, prismatic grains.
3 % Fe-Ti oxides, euhedral grains.
2 % Clinopyroxene, greenish-brown, translucent, short, prismatic grains.

Sample: 132/2 Pokai Ign. pumice Ref.no: 180 Method: micr.

Matrix: fibrous glass shards, moderate phenocryst content.
Phenocrysts:
92.5 % Plagioclase, eu- to subhedral, tabular grains, some with rounded crystal corners, zoning common, max.size 1.2x1 mm.
4.4 % Orthopyroxene, eu- to subhedral, long prismatic grains, max.size 0.8x0.2 mm.
2.6 % Quartz, rounded grains, max.size 1x0.9 mm.
0.5 % Fe-Ti oxides, tiny, euhedral grains.
trace Zircon, very small, euhedral grains, usually attached to the plagioclases.

Sample: 133 Pokai Ign. matrix Ref.no: - Method: thins.

44.4 % Matrix: slightly welded, fibrous and cuspate, distorted glass shards, devitrified, low vesicularity (2.9 %).
46.3 % Pumice: fibrous, somewhat distorted glass shards, collapsed vesicles (vesicularity 19.4 %), partly filled with vapour-phase crystallisation products.
8.3 % Phenocrysts:
92.9 % Plagioclase, eu- to subhedral, tabular grains, some with rounded crystal corners, zoning common.
5.5 % Fe-Ti oxides, euhedral grains.
1.6 % Orthopyroxene, eu- to subhedral, prismatic grains, often with rounded crystal corners.

Sample: 133a Pokai Ign. pumice Ref.no: - Method: thins.

90.9 % Matrix: fibrous, distorted, devitrified glass shards, partly collapsed vesicles (vesicularity 32.0 %), mostly filled with vapour-phase crystallisation products.

9.1 % Phenocrysts:

- 91.2 % Plagioclase, eu- to subhedral, tabular grains, some with rounded crystal corners and slightly resorbed crystal margins, zoning common.
- 5.5 % Orthopyroxene, eu- to subhedral, prismatic grains, often with rounded crystal corners.
- 3.3 % Fe-Ti oxides, euhedral grains.
- trace Zircon, tiny, euhedral grains.

Sample: 146/1 Chimp Ign. pumice Ref.no: 253 Method: micr.

Matrix: fibrous glass shards, low phenocryst content.

Phenocrysts:

99.6 % Plagioclase, eu- to subhedral, tabular grains, max.size 1.1x1 mm.

0.4 % Fe-Ti oxides, very small, euhedral grains.

trace Orthopyroxene, small, eu- to subhedral grains.

trace Quartz, small, rounded grains.

Sample: T1/1 Pokai Ign. pumice Ref.no: 216 Method: thins/binoc.

92.2 % Matrix: creamy-white to yellowish, fibrous, cuspate and some Y-shaped, partly devitrified glass shards, well preserved, round and slightly elongated vesicle cavities (vesicularity 48.3 %), partly filled with vapour-phase crystallisation products.

7.8 % Phenocrysts:

- 70.0 % Plagioclase, eu- to subhedral, tabular grains, zoning common.
- 20.0 % Quartz, rounded grains; under the binoc. microscope the bipyramidal form is evident, crystal corners only slightly rounded.
- 8.0 % Orthopyroxene, eu- to subhedral, prismatic grains; bright green under the binoc. microscope.
- 2.0 % Fe-Ti oxides, euhedral grains.

Sample: T2/1 Pokai Ign. pumice Ref.no: 218 Method: micr.

Matrix: fibrous glass shards, moderate/high phenocryst content.

Phenocrysts:

92.7 % Plagioclase, eu- to subhedral, tabular grains, some with rounded crystal corners, zoning common, max.size 0.8x0.6 mm.

6.4 % Fe-Ti oxides, euhedral grains, often in clusters.

0.9 % Orthopyroxene, eu- to subhedral, prismatic grains, max.size 0.4x0.2 mm.

Sample: T2/2 Pokai Ign. pumice Ref.no: 219 Method: micr.

Matrix: fibrous and cuspate glass shards, moderate phenocryst content.
Phenocrysts:
80.2 % Plagioclase, eu- to subhedral, tabular grains, some with rounded crystal corners, zoning common, max.size 1.2x0.8 mm.
9.7 % Quartz, rounded grains, max.size 1.2x0.9 mm.
6.7 % Orthopyroxene, eu- to subhedral, prismatic grains, max.size 0.7x0.3 mm.
3.4 % Fe-Ti oxides, small, euhedral grains, often attached to the orthopyroxenes.
trace Amphibole (hornblende), pleochroic, an- to subhedral grains, max.size 0.5x0.2 mm.
trace Apatite, long, thin needles attached to the plagioclases.

Sample: T19/1 Pokai Ign. pumice Ref.no: 227 Method: micr.

Matrix: fibrous glass shards, very crystal-rich.
Phenocrysts:
88.5 % Plagioclase, eu- to subhedral, tabular grains, often clustered together, zoning common, max.size 2.5x1.5 mm.
9.2 % Orthopyroxene, eu- to subhedral, prismatic grains, some with rounded crystal margins, max.size 2x1 mm.
2.0 % Fe-Ti oxides, euhedral grains, often clustered into the orthopyroxenes.
0.3 % Zircon, tiny, euhedral grains.
trace Quartz, rounded grains, max.size 1.5x1.1 mm.
trace Apatite, long, thin needles, usually attached to the plagioclases.

Sample: T19/3 Pokai Ign. pumice Ref.no: 229 Method: micr.

Matrix: fibrous and cuspate glass shards, moderate phenocryst content.
Phenocrysts:
86.9 % Plagioclase, eu- to subhedral, tabular grains, some with rounded crystal corners, zoning common, max.size 2.2x1.6 mm.
5.9 % Quartz, rounded grains, max.size 1.3x1.1 mm.
4.8 % Orthopyroxene, eu- to subhedral, prismatic grains, rounded crystal corners occur commonly, max.size 1x0.8 mm.
2.3 % Fe-Ti oxides, euhedral grains, max.size 0.2x0.2 mm.
0.1 % Zircon, tiny, euhedral grains.
trace Amphibole (hornblende), pleochroic, subhedral grains, max.size 0.8x0.4 mm.

Sample: T24/1 Pokai Ign. pumice Ref.no: 231 Method: thins.

87.8 % Matrix: yellow-orange, fibrous, distorted, devitrified glass shards, mostly collapsed vesicles (vesicularity 17.4 %), mostly filled with vapour-phase crystallisation products.
12.2 % Phenocrysts:
92.8 % Plagioclase, eu- to subhedral, tabular grains, rounded crystal corners common, zoning common, forms glomeroporphyritic aggregates with orthopyroxenes and Fe-Ti oxides.
5.2 % Fe-Ti oxides, euhedral grains, often attached to the orthopyroxenes.
2.0 % Orthopyroxene, subhedral, prismatic grains, usually with rounded crystal corners and slightly resorbed margins.

Appendix C

Mineral chemistry

The mineral and pumice glass analyses were made using a JEOL 8600 Superprobe at the Geology Department, University of Otago, Dunedin, under the supervision of Dr. Kawachi. Polished thin sections were carbon-coated under vacuum and then analysed with an accelerating voltage of 15 kv and a probe current of 20 nA. A beam diameter of 1 micron was used for the mineral spot analyses and of 30 micron for the glass analyses. The standards used were mostly synthetic pure oxides plus synthetic $CaSiO_2$ for Ca, amelia albite for Na and St. Gottard adualria for K. On line data reduction (Kawachi and Trinder, unpubl. data) was by ZAF method (Sweatman and Long, 1969), however, various constants were upgraded. The lower limits of detection (in wt.%) were: SiO_2 = 0.07; TiO_2 = 0.07; Al_2O_3 = 0.05; FeO = 0.12; MnO = 0.10; MgO = 0.05; Na_2O = 0.08; and K_2O = 0.03.

Microprobe analyses

Mineral analyses are expressed in both oxide weight % and cation proportions. Total iron as FeO. Cations are calculated on the following basis:

Mineral	Number of oxygens
Plagioclase	32
Pyroxene	6
Titanomagnetite	32
Ilmenite	6

List of Tables

Table C.1. Plagioclase analyses of Pokai Ignimbrite.

r = rim
c = core

Analysis #	1	2	3	4	5	6	7	8	9	10	11
Sample	26A/1	26A/1	26A/1	26A/1	26A/1	26A/1	26A/1	26A/1	26A/1	26A/1	26A/2r
SiO_2	65.14	64.05	63.55	62.60	59.72	62.99	59.08	58.95	58.72	63.31	62.24
TiO_2	-	-	-	0.02	-	-	0.02	-	-	-	-
Al_2O_3	21.97	22.49	22.76	22.86	24.26	22.63	24.71	24.46	24.58	22.56	22.99
FeO	0.10	0.14	0.16	0.18	0.21	0.21	0.28	0.28	0.24	0.14	0.24
CaO	4.75	5.41	5.64	6.02	7.82	6.09	8.73	8.57	8.57	5.86	6.13
Na_2O	8.06	7.80	7.87	7.75	6.71	7.37	6.46	6.12	6.30	7.85	7.99
K_2O	0.54	0.44	0.44	0.49	0.30	0.47	0.24	0.31	0.27	0.47	0.49
Total	100.56	100.33	100.42	99.92	99.02	99.76	99.52	98.69	98.68	100.19	100.08
$Si+_4$	11.43	11.29	11.21	11.12	10.76	11.19	10.63	10.68	10.64	11.20	11.07
$Al+_3$	4.54	4.67	4.73	4.79	5.15	4.74	5.24	5.22	5.25	4.71	4.82
$Fe+_3$	0.01	0.02	0.02	0.03	0.03	0.03	0.04	0.04	0.04	0.02	0.04
$Ca+_2$	0.89	1.02	1.07	1.15	1.51	1.16	1.68	1.66	1.66	1.11	1.17
$Na+_1$	2.74	2.66	2.69	2.67	2.34	2.54	2.26	2.15	2.21	2.69	2.75
K	0.12	0.10	0.10	0.11	0.07	0.11	0.05	0.07	0.06	0.11	0.11
Total	19.74	19.76	19.82	19.87	19.87	19.76	19.90	19.82	19.87	19.84	19.95
An	23.76	26.98	27.64	29.16	38.50	30.45	42.13	42.81	42.23	28.39	28.97
Ab	73.01	70.43	69.82	68.00	59.73	66.75	56.48	55.36	56.18	68.88	68.29
Or	3.23	2.59	2.54	2.83	1.77	2.80	1.39	1.83	1.59	2.73	2.75

Analysis #	12	13	14	15	16	17	18	19	20	21	22
Sample	26A/2c	26A/2	26A/2c	26A/2r	26A/2	26A/2	26A/2c	26A/2	HJ7/1	HJ7/1	HJ7/1
SiO_2	58.81	58.76	62.14	62.00	62.58	64.41	57.48	61.49	62.66	63.78	64.91
TiO_2	-	-	0.04	-	-	0.06	-	-	-	-	0.02
Al_2O_3	24.88	24.55	22.94	23.23	23.08	21.63	25.28	23.62	22.88	22.99	21.85
FeO	0.29	0.21	0.24	0.15	0.17	0.07	0.27	0.22	0.16	0.15	0.10
MnO	-	-	0.04	-	-	0.02	-	-	0.05	-	-
CaO	8.39	8.28	6.16	6.23	5.90	4.59	9.27	6.68	5.86	5.59	4.58
Na_2O	6.82	6.79	7.90	7.93	8.07	8.25	6.44	7.53	7.78	7.69	8.33
K_2O	0.30	0.34	0.49	0.51	0.48	0.64	0.24	0.42	0.47	0.53	0.63
Total	99.49	98.93	99.95	100.05	100.28	99.67	98.98	99.96	99.86	100.73	100.42
$Si+_4$	10.59	10.64	11.07	11.03	11.09	11.42	10.44	10.95	11.14	11.21	11.42
$Ti+_4$	-	-	-	-	-	0.01	-	-	-	-	-
$Al+_3$	5.28	5.24	4.82	4.87	4.82	4.52	5.41	4.96	4.79	4.76	4.53
$Fe+_3$	0.04	0.03	0.04	0.02	0.03	0.01	0.04	0.03	0.02	0.02	0.01
$Mn+_2$	-	-	0.01	-	-	-	-	-	0.01	-	-
$Ca+_2$	1.62	1.61	1.17	1.19	1.12	0.87	1.80	1.27	1.12	1.05	0.86
$Na+_1$	2.38	2.38	2.73	2.73	2.77	2.84	2.27	2.60	2.68	2.62	2.84
K	0.07	0.08	0.11	0.12	0.11	0.14	0.05	0.10	0.11	0.12	0.14
Total	19.99	19.98	19.94	19.96	19.94	19.81	20.02	19.92	19.86	19.78	19.81
An	39.79	39.45	29.26	29.43	28.00	22.63	43.73	32.07	28.58	27.75	22.46
Ab	58.51	58.59	67.98	67.73	69.28	73.60	54.93	65.51	68.67	69.11	73.85
Or	1.70	1.96	2.77	2.84	2.71	3.77	1.34	2.42	2.75	3.13	3.68

Table C.1. cont.

Analysis #	23	24	25	26	27	28	29	30	31	32	33
Sample	66/1	66/1	66/1	66/1	66/1	66/1	66/1r	66/1c	66/1	66/1	70/3
SiO_2	62.52	61.93	61.68	62.64	63.68	63.12	62.43	63.48	63.71	63.34	63.42
TiO_2	0.02	-	-	0.02	-	-	-	-	-	0.03	-
Al_2O_3	23.42	23.77	23.74	23.36	22.42	22.92	23.35	22.82	22.92	22.63	21.88
FeO	0.19	0.15	0.28	0.18	0.14	0.11	0.19	0.15	0.14	0.21	0.15
MnO	-	-	-	-	-	-	-	0.02	-	-	-
CaO	6.61	7.11	7.23	6.79	5.27	5.89	6.33	6.04	5.74	6.00	5.05
Na_2O	7.55	7.42	7.15	7.43	7.96	7.61	7.84	7.77	7.90	7.61	8.23
K_2O	0.43	0.40	0.33	0.39	0.60	0.48	0.48	0.48	0.52	0.47	0.56
Total	100.74	100.78	100.41	100.81	100.07	100.13	100.62	100.76	100.93	100.29	99.29
Si^{+4}	11.03	10.94	10.94	11.05	11.27	11.17	11.04	11.18	11.19	11.20	11.31
Al^{+3}	4.87	4.95	4.96	4.85	4.68	4.78	4.87	4.74	4.74	4.71	4.60
Fe^{+3}	0.03	0.02	0.04	0.03	0.02	0.02	0.03	0.02	0.02	0.03	0.02
Ca^{+2}	1.25	1.35	1.37	1.28	1.00	1.12	1.20	1.14	1.08	1.14	0.97
Na^{+1}	2.59	2.54	2.46	2.54	2.73	2.61	2.69	2.65	2.69	2.61	2.85
K	0.10	0.09	0.08	0.09	0.14	0.11	0.11	0.11	0.12	0.11	0.13
Total	19.87	19.90	19.85	19.84	19.83	19.80	19.93	19.84	19.84	19.80	19.87
An	31.80	33.85	35.16	32.79	25.86	29.11	30.00	29.20	27.80	29.52	24.52
Ab	65.72	63.87	62.92	64.95	70.64	68.07	67.28	68.03	69.19	67.71	72.25
Or	2.48	2.28	1.92	2.26	3.51	2.81	2.72	2.77	3.01	2.77	3.23

Analysis #	34	35	36	37	38	39	40	41	42	43	44
Sample	70/3	70/3	70/3	70/3	70e/1	70e/1	70e/1	70e/1	70e/1	70e/1	85/1
SiO_2	62.83	61.84	63.73	63.69	63.21	63.54	64.01	61.37	62.51	61.57	62.32
TiO_2	-	-	-	-	0.03	-	0.05	0.02	-	0.03	-
Al_2O_3	21.93	22.66	21.82	21.89	23.15	22.69	22.51	23.15	23.04	23.43	23.21
FeO	0.18	0.18	0.10	0.13	0.20	0.20	0.20	0.20	0.21	0.21	0.28
MnO	0.02	0.02	-	-	-	-	-	-	0.02	-	-
CaO	5.56	5.95	5.09	4.90	6.15	5.82	5.80	6.71	6.29	7.07	6.21
Na_2O	7.98	7.65	8.28	8.25	7.73	7.80	7.96	7.55	7.60	7.11	7.77
K_2O	0.49	0.46	0.55	0.58	0.40	0.51	0.45	0.43	0.47	0.39	0.35
Total	98.99	98.76	99.57	99.44	100.87	100.56	100.98	99.43	100.14	99.81	100.14
Si^{+4}	11.26	11.12	11.33	11.34	11.12	11.20	11.24	10.99	11.09	10.98	11.06
Ti^{+4}	-	-	-	-	-	-	0.01	-	-	-	-
Al^{+3}	4.63	4.80	4.57	4.59	4.80	4.72	4.66	4.89	4.82	4.92	4.85
Fe^{+3}	0.03	0.03	0.01	0.02	0.03	0.03	0.03	0.03	0.03	0.03	0.04
Ca^{+2}	1.07	1.15	0.97	0.93	1.16	1.10	1.09	1.29	1.20	1.35	1.18
Na^{+1}	2.77	2.66	2.86	2.85	2.64	2.67	2.71	2.62	2.62	2.46	2.67
K	0.11	0.10	0.13	0.13	0.09	0.12	0.10	0.10	0.11	0.09	0.08
Total	19.87	19.87	19.87	19.86	19.84	19.83	19.83	19.92	19.86	19.83	19.89
An	27.01	29.27	24.53	23.87	29.83	28.32	27.95	32.15	30.51	34.65	30.04
Ab	70.16	68.05	72.29	72.76	67.86	68.70	69.43	65.41	66.76	63.06	67.96
Or	2.83	2.67	3.17	3.37	2.31	2.98	2.61	2.44	2.73	2.29	2.00

Table C.1. cont.

r = rim
c = core

Analysis #	45	46	47	48	49	50	51	52	53	54	55
Sample	85/1r	85/1	85/1	85/1	85/1	85/1r	85/1	97/3r	97/3	97/3	97/3
SiO_2	64.00	64.10	64.58	62.83	63.52	64.17	62.76	63.50	63.30	62.29	59.76
TiO_2	-	0.03	0.02	0.02	-	-	-	-	-	-	0.03
Al_2O_3	22.61	22.32	21.72	22.37	22.16	21.71	22.46	21.80	22.87	22.28	23.86
FeO	0.18	0.17	0.16	0.16	0.15	0.22	0.20	0.21	0.24	0.27	0.26
MnO	-	-	-	-	-	0.02	-	-	-	0.04	-
CaO	5.09	5.18	4.84	5.48	5.12	5.16	5.69	5.01	5.62	5.20	7.62
Na_2O	8.19	8.24	8.47	7.99	8.18	8.15	7.91	8.70	8.45	8.31	7.14
K_2O	0.44	0.54	0.59	0.49	0.55	0.53	0.49	0.56	0.52	0.49	0.31
Total	100.51	100.58	100.38	99.34	99.68	99.96	99.51	99.78	101.00	98.88	98.98
Si^{+4}	11.27	11.29	11.39	11.21	11.29	11.36	11.19	11.30	11.14	11.19	10.79
Al^{+3}	4.69	4.63	4.51	4.70	4.64	4.53	4.72	4.57	4.74	4.72	5.08
Fe^{+3}	0.03	0.03	0.02	0.02	0.02	0.03	0.03	0.03	0.04	0.04	0.04
Mn^{+2}	-	-	-	-	-	-	-	-	-	0.01	-
Ca^{+2}	0.96	0.98	0.91	1.05	0.98	0.98	1.09	0.96	1.06	1.00	1.47
Na^{+1}	2.80	2.81	2.89	2.77	2.82	2.80	2.73	3.00	2.88	2.89	2.50
K	0.10	0.12	0.13	0.11	0.13	0.12	0.11	0.13	0.12	0.11	0.07
Total	19.84	19.86	19.87	19.87	19.86	19.83	19.87	19.98	19.98	19.96	19.95
An	24.91	24.98	23.19	26.72	24.90	25.12	27.65	23.41	26.10	24.97	36.45
Ab	72.52	71.91	73.44	70.45	71.90	71.83	69.53	73.48	71.05	72.20	61.76
Or	2.57	3.11	3.37	2.83	3.20	3.06	2.82	3.12	2.86	2.83	1.78

Analysis #	56	57	58	59	60	61	62	63	64	65	66
Sample	97/3	97/3c	97/3	108/1c	108/1r	108/1	108/1	108/1	108/1c	108/1r	126/1
SiO_2	59.93	63.72	62.38	60.18	62.05	62.63	63.03	62.95	60.98	60.96	62.59
TiO_2	-	-	-	-	-	0.02	-	-	-	-	-
Al_2O_3	24.47	22.22	21.72	23.89	23.49	22.69	22.64	22.88	23.42	23.97	22.18
FeO	0.22	0.19	0.11	0.29	0.20	0.20	0.17	0.20	0.20	0.23	0.14
CaO	7.86	5.11	4.96	7.30	6.01	5.61	5.51	5.55	6.69	6.96	5.39
Na_2O	7.15	8.35	8.32	7.41	7.87	8.16	7.67	7.64	7.73	7.70	8.03
K_2O	0.34	0.48	0.57	0.33	0.44	0.50	0.42	0.54	0.40	0.35	0.45
Total	99.97	100.07	98.06	99.40	100.06	99.81	99.44	99.76	99.42	100.17	98.78
Si^{+4}	10.72	11.28	11.28	10.81	11.02	11.15	11.22	11.18	10.94	10.86	11.23
Al^{+3}	5.16	4.64	4.63	5.06	4.92	4.76	4.75	4.79	4.95	5.03	4.69
Fe^{+3}	0.03	0.03	0.02	0.04	0.03	0.03	0.03	0.03	0.03	0.04	0.02
Ca^{+2}	1.51	0.97	0.96	1.41	1.14	1.07	1.05	1.06	1.29	1.33	1.04
Na^{+1}	2.48	2.87	2.92	2.58	2.71	2.82	2.65	2.63	2.69	2.66	2.79
K	0.08	0.11	0.13	0.08	0.10	0.11	0.09	0.12	0.09	0.08	0.10
Total	19.98	19.89	19.93	19.98	19.92	19.94	19.78	19.80	19.98	19.99	19.87
An	37.09	24.58	23.96	34.59	28.92	26.75	27.69	27.76	31.65	32.66	26.34
Ab	61.01	72.68	72.74	63.55	68.56	70.39	69.79	69.05	66.13	65.39	71.05
Or	1.91	2.74	3.30	1.86	2.52	2.86	2.52	3.20	2.23	1.94	2.61

Table C.1. cont.

c = core
r = rim

Analysis #	67	68	69	70	71	72	73	74	75	76	77
Sample	126/1	126/1	126/1	126/1c	126/1r	126/1	132/1	132/1	132/1	132/1	132/1
SiO_2	63.15	62.58	65.16	62.78	63.16	64.02	62.61	61.34	60.24	61.37	62.09
TiO_2	-	-	0.02	-	-	-	0.04	-	-	0.04	0.02
Al_2O_3	21.78	22.02	21.32	22.12	21.30	21.45	22.48	23.34	23.81	22.77	23.14
FeO	0.18	0.18	0.14	0.18	0.19	0.09	0.18	0.16	0.22	0.23	0.22
MnO	-	-	-	-	-	-	0.02	-	0.03	-	-
CaO	5.24	5.23	4.14	5.45	4.91	4.48	5.99	6.63	7.35	6.15	6.24
Na_2O	8.03	8.15	8.53	8.06	8.25	8.50	7.85	7.72	7.33	7.89	7.49
K_2O	0.48	0.50	0.66	0.51	0.52	0.54	0.51	0.45	0.41	0.51	0.47
Total	98.86	98.66	99.97	99.10	98.33	99.08	99.68	99.64	99.39	98.96	99.67
Si^{+4}	11.31	11.25	11.50	11.24	11.37	11.42	11.16	10.97	10.83	11.05	11.07
Al^{+3}	4.60	4.66	4.44	4.67	4.52	4.52	4.72	4.92	5.04	4.83	4.86
Fe^{+3}	0.03	0.03	0.02	0.03	0.03	0.01	0.03	0.02	0.03	0.04	0.03
Ca^{+2}	1.00	1.01	0.78	1.04	0.95	0.86	1.14	1.27	1.41	1.18	1.19
Na^{+1}	2.79	2.84	2.92	2.80	2.88	2.94	2.71	2.68	2.56	2.75	2.59
K	0.11	0.12	0.15	0.12	0.12	0.12	0.12	0.10	0.09	0.12	0.11
Total	19.84	19.90	19.81	19.89	19.87	19.86	19.89	19.96	19.97	19.97	19.85
An	25.75	25.44	20.33	26.38	23.98	21.83	28.80	31.36	34.81	29.22	30.66
Ab	71.45	71.64	75.80	70.67	73.00	75.01	68.26	66.11	62.89	67.89	66.61
Or	2.80	2.92	3.87	2.95	3.02	3.16	2.94	2.53	2.30	2.89	2.73

Analysis #	78	79	80	81	82	83	84	85	86	87	88
Sample	132/1c	132/1r	132/2r	132/2	132/2r	132/2c	132/2	132/2	132/3	132/3	132/3r
SiO_2	63.28	61.73	62.79	61.03	62.70	64.23	62.59	62.60	60.85	62.05	61.30
TiO_2	-	-	0.03	-	-	-	-	-	-	0.02	-
Al_2O_3	22.99	22.80	22.28	22.80	22.74	22.06	22.04	22.23	23.31	22.82	22.74
FeO	0.12	0.21	0.14	0.25	0.18	0.20	0.17	0.16	0.23	0.18	0.24
MnO	-	-	-	-	-	-	-	-	-	0.03	-
CaO	5.90	6.21	5.37	6.07	5.63	4.82	5.08	5.37	6.91	6.00	6.39
Na_2O	7.91	7.97	8.24	7.73	8.04	7.90	8.10	8.19	7.27	8.03	7.61
K_2O	0.53	0.49	0.56	0.54	0.58	0.70	0.61	0.63	0.45	0.52	0.45
Total	100.73	99.41	99.41	98.42	99.87	99.91	98.59	99.18	99.02	99.65	98.73
Si^{+4}	11.15	11.06	11.21	11.04	11.15	11.36	11.26	11.21	10.95	11.08	11.05
Al^{+3}	4.77	4.81	4.69	4.86	4.77	4.60	4.67	4.69	4.94	4.80	4.83
Fe^{+3}	0.02	0.03	0.02	0.04	0.03	0.03	0.03	0.02	0.04	0.03	0.04
Ca^{+2}	1.11	1.19	1.03	1.18	1.07	0.91	0.98	1.03	1.33	1.15	1.23
Na^{+1}	2.70	2.77	2.85	2.71	2.77	2.71	2.82	2.84	2.54	2.78	2.66
K	0.12	0.11	0.13	0.12	0.13	0.16	0.14	0.14	0.10	0.12	0.10
Total	19.88	19.98	19.93	19.95	19.92	19.77	19.89	19.94	19.90	19.96	19.92
An	28.31	29.26	25.62	29.32	26.98	24.18	24.80	25.64	33.54	28.38	30.87
Ab	68.64	67.99	71.17	67.59	69.72	71.67	71.63	70.76	63.88	68.69	66.56
Or	3.05	2.75	3.21	3.09	3.30	4.15	3.57	3.59	2.58	2.92	2.57

Table C.1. cont.

c = core
r = rim
a → e and A → D = rim → core analyses of two plagioclases, respectively.

Analysis #	89	90	91	92	93	94	95	96	97	98	99
Sample	132/3c	132/3	132/3	132/3r	132/3c	153/1	153/1	153/1	T2/1a	T2/1b	T2/1c
SiO_2	60.73	62.25	61.52	61.60	63.94	61.69	62.04	62.42	60.80	61.77	62.84
TiO_2	-	-	-	-	-	0.02	-	-	-	0.04	-
Al_2O_3	22.57	22.90	22.77	22.88	21.91	23.18	23.29	23.05	24.29	24.22	23.29
FeO	0.22	0.20	0.15	0.20	0.14	0.14	0.22	0.17	0.29	0.22	0.21
CaO	6.47	6.11	6.26	6.19	4.61	6.32	6.29	5.89	7.49	7.12	6.24
Na_2O	7.83	7.98	7.94	7.75	8.46	8.11	7.81	8.22	6.90	6.94	7.79
K_2O	0.43	0.47	0.45	0.50	0.61	0.50	0.49	0.51	0.28	0.33	0.35
Total	98.25	99.91	99.09	99.12	99.67	99.96	100.14	100.26	100.05	100.64	100.72
Si^{+4}	11.02	11.08	11.05	11.06	11.35	11.00	11.03	11.08	10.83	10.91	11.08
Al^{+3}	4.83	4.80	4.82	4.84	4.59	4.87	4.88	4.82	5.10	5.04	4.84
Fe^{+3}	0.03	0.03	0.02	0.03	0.02	0.02	0.03	0.03	0.04	0.03	0.03
Ca^{+2}	1.26	1.17	1.21	1.19	0.88	1.21	1.20	1.12	1.43	1.35	1.18
Na^{+1}	2.75	2.75	2.77	2.70	2.91	2.81	2.69	2.83	2.38	2.38	2.66
K	0.10	0.11	0.10	0.12	0.14	0.11	0.11	0.12	0.06	0.08	0.08
Total	19.99	19.94	19.97	19.93	19.88	20.02	19.93	19.99	19.85	19.79	19.87
An	30.58	28.98	29.58	29.76	22.33	29.27	29.96	27.55	36.87	35.46	30.05
Ab	66.98	68.40	67.88	67.38	74.14	67.98	67.25	69.59	61.50	62.56	67.92
Or	2.44	2.63	2.54	2.87	3.53	2.75	2.79	2.87	1.63	1.97	2.03

Analysis #	100	101	102	103	104	105	106	107	108	109	110
Sample	T2/1d	T2/1e	T2/1A	T2/1B	T2/1C	T2/1D	T2/1	T2/1	T2/1	T2/1	T2/1
SiO_2	62.89	61.82	61.82	62.70	62.21	62.62	63.20	59.66	61.74	61.97	63.34
TiO_2	-	-	0.02	-	0.03	-	-	0.04	-	0.04	0.03
Al_2O_3	23.43	22.77	23.93	23.47	23.80	23.61	23.18	24.79	23.41	22.69	22.68
FeO	0.21	0.20	0.18	0.19	0.16	0.19	0.11	0.11	0.22	0.10	0.14
MnO	0.03	-	-	-	-	0.02	-	-	-	-	-
MgO	-	-	-	-	-	-	-	-	-	0.02	-
CaO	6.22	6.35	6.94	6.55	6.73	6.48	6.05	8.48	6.44	6.34	5.61
Na_2O	7.55	7.46	7.42	7.64	7.03	7.60	7.81	6.38	7.61	7.37	7.86
K_2O	0.36	0.34	0.30	0.31	0.35	0.34	0.37	0.24	0.35	0.34	0.43
Total	100.69	98.94	100.61	100.86	100.31	100.86	100.72	99.70	99.77	98.87	100.09
Si^{+4}	11.08	11.09	10.93	11.05	11.00	11.03	11.13	10.68	11.00	11.12	11.21
Ti^{+4}	-	-	-	-	-	-	-	-	-	0.01	-
Al^{+3}	4.87	4.82	4.99	4.87	4.96	4.90	4.81	5.23	4.92	4.80	4.73
Fe^{+3}	0.03	0.03	0.03	0.03	0.02	0.03	0.02	0.02	0.03	0.01	0.02
Ca^{+2}	1.17	1.22	1.32	1.24	1.27	1.22	1.14	1.63	1.23	1.22	1.06
Na^{+1}	2.58	2.60	2.54	2.61	2.41	2.59	2.66	2.21	2.63	2.57	2.70
K	0.08	0.08	0.07	0.07	0.08	0.08	0.08	0.05	0.08	0.08	0.10
Total	19.82	19.83	19.88	19.86	19.76	19.85	19.84	19.83	19.89	19.80	19.82
An	30.62	31.36	33.51	31.56	33.87	31.42	29.34	41.79	31.22	31.55	27.58
Ab	67.25	66.67	64.76	66.65	64.03	66.64	68.49	56.83	66.78	66.41	69.89
Or	2.13	1.97	1.74	1.79	2.10	1.94	2.16	1.38	2.00	2.03	2.54

Table C.1. cont.

r = rim
c = core

Analysis #	111	112	113	114	115	116	117	118	119	120	121
Sample	T2/1	T2/1	T2/1	T2/2	T2/2	T2/2	T2/2	T2/2	T2/2	T19/1	T19/1r
SiO_2	63.99	63.31	62.61	63.64	62.16	62.96	63.82	62.99	57.88	61.29	62.05
TiO_2	-	-	0.04	-	-	-	-	-	-	-	0.03
Al_2O_3	22.70	23.37	23.58	22.32	22.66	22.52	21.65	22.13	25.44	23.36	22.98
FeO	0.12	0.15	0.16	0.14	0.15	0.17	0.18	0.12	0.12	0.16	0.20
MnO	-	0.03	-	-	0.03	-	-	-	-	0.03	-
CaO	5.28	6.04	6.51	4.82	5.22	5.24	4.30	4.80	9.09	6.55	5.83
Na_2O	8.08	7.70	7.56	8.52	8.41	8.45	8.71	8.64	6.50	8.05	8.37
K_2O	0.44	0.41	0.35	0.65	0.62	0.57	0.73	0.67	0.28	0.45	0.50
Total	100.61	101.01	100.81	100.09	99.25	99.91	99.39	99.35	99.31	99.89	99.96
Si^{+4}	11.25	11.11	11.03	11.27	11.13	11.19	11.37	11.25	10.46	10.95	11.05
Ti^{+4}	-	-	0.01	-	-	-	-	-	-	-	-
Al^{+3}	4.70	4.84	4.90	4.66	4.78	4.72	4.55	4.66	5.42	4.92	4.82
Fe^{+3}	0.02	0.02	0.02	0.02	0.02	0.03	0.03	0.02	0.02	0.02	0.03
Ca^{+2}	1.00	1.13	1.23	0.92	1.00	1.00	0.82	0.92	1.76	1.25	1.11
Na^{+1}	2.76	2.62	2.58	2.93	2.92	2.91	3.01	2.99	2.28	2.79	2.89
K	0.10	0.09	0.08	0.15	0.14	0.13	0.17	0.15	0.07	0.10	0.11
Total	19.82	19.82	19.85	19.94	20.01	19.97	19.94	19.99	20.00	20.04	20.03
An	25.84	29.52	31.58	22.94	24.63	24.71	20.54	22.62	42.87	30.25	27.04
Ab	71.61	68.10	66.37	73.39	71.86	72.10	75.28	73.61	55.53	67.29	70.22
Or	2.55	2.38	2.05	3.66	3.50	3.19	4.18	3.77	1.60	2.45	2.75

Analysis #	122	123	124	125	126	127	128	129	130	131	132
Sample	T19/1r	T19/1c	T19/1	T19/1r	T19/1c	T19/1r	T19/3	T19/3	T19/3	T19/3	T19/3r
SiO_2	63.53	62.75	63.01	63.00	62.82	62.81	64.89	65.39	64.13	64.03	65.00
TiO_2	-	-	0.02	0.03	-	-	-	-	0.03	-	0.03
Al_2O_3	22.35	22.38	22.68	22.56	22.62	23.14	21.90	21.82	21.02	21.94	21.34
FeO	0.21	0.26	0.19	0.20	0.18	0.15	0.12	0.14	0.19	0.12	0.19
MnO	-	-	-	0.02	-	0.02	-	-	-	-	-
CaO	5.12	5.44	5.54	5.32	5.58	5.80	3.99	3.53	3.96	4.26	3.67
Na_2O	8.73	8.48	8.36	8.14	8.48	8.32	8.83	8.66	8.65	8.57	8.91
K_2O	0.54	0.53	0.53	0.53	0.52	0.50	0.83	0.78	0.85	0.67	0.92
Total	100.48	99.84	100.33	99.80	100.20	100.74	100.56	100.32	98.83	99.59	100.06
Si^{+4}	11.23	11.18	11.16	11.20	11.15	11.09	11.41	11.49	11.48	11.37	11.48
Al^{+3}	4.66	4.70	4.73	4.72	4.73	4.82	4.54	4.52	4.43	4.59	4.45
Fe^{+3}	0.03	0.04	0.03	0.03	0.03	0.02	0.02	0.02	0.03	0.02	0.03
Ca^{+2}	0.97	1.04	1.05	1.01	1.06	1.10	0.75	0.67	0.76	0.81	0.69
Na^{+1}	2.99	2.93	2.87	2.81	2.92	2.85	3.01	2.95	3.00	2.95	3.05
K	0.12	0.12	0.12	0.12	0.12	0.11	0.19	0.17	0.19	0.15	0.21
Total	20.00	20.00	19.97	19.90	20.00	19.99	19.92	19.82	19.90	19.89	19.92
An	23.75	25.39	26.01	25.74	25.90	27.02	19.05	17.55	19.22	20.73	17.58
Ab	73.25	71.68	71.02	71.20	71.23	70.19	76.23	77.83	75.88	75.39	77.17
Or	2.99	2.93	2.96	3.06	2.88	2.79	4.73	4.62	4.90	3.89	5.25

Table C.2. Orthopyroxene analyses of Pokai Ignimbrite pumices.

c = core
r = rim

Analysis #	1	2	3	4	5	6	7	8	9	10	11
Sample	26A/1	26A/1	26A/1	26A/1	26A/2c	26A/2r	26A/2	26A/2	66/1	66/1	66/1
SiO_2	49.62	50.41	50.13	49.46	49.97	48.69	49.13	48.39	50.12	50.75	50.96
TiO_2	0.09	0.11	0.09	0.14	0.11	0.14	0.10	0.13	0.13	0.11	0.17
Al_2O_3	0.25	0.35	0.21	0.33	0.32	0.22	0.18	0.24	0.24	0.19	0.44
FeO	36.33	32.73	35.71	35.45	29.98	37.06	36.49	37.49	35.88	33.27	30.63
MnO	1.69	1.66	1.67	1.71	2.21	1.65	1.83	1.83	1.97	1.79	2.00
MgO	10.88	13.08	11.36	10.91	15.69	10.68	11.47	9.94	10.82	13.17	14.36
CaO	1.15	1.40	1.17	1.37	1.12	1.14	1.25	1.47	1.20	1.22	1.36
Na_2O	-	-	-	-	-	-	-	-	0.05	0.07	0.11
K_2O	-	-	-	-	-	-	-	0.01	-	-	-
Total	100.01	99.74	100.34	99.37	99.40	99.58	100.45	99.50	100.41	100.57	100.03
SiIV	2.00	2.00	2.00	2.00	1.97	1.98	1.98	1.98	2.00	2.00	2.00
AlIV	-	-	-	-	0.01	0.01	0.01	0.01	-	-	-
AlVI	0.01	0.01	0.01	0.01	-	-	-	-	0.01	0.01	0.02
Ti	-	-	-	-	-	-	-	-	-	-	0.01
Fe^{2+}	1.22	1.08	1.19	1.20	0.99	1.26	1.23	1.28	1.20	1.10	1.00
Mn	0.06	0.06	0.06	0.06	0.07	0.06	0.06	0.06	0.07	0.06	0.07
Mg	0.65	0.77	0.68	0.66	0.92	0.65	0.69	0.61	0.65	0.77	0.84
Ca	0.05	0.06	0.05	0.06	0.05	0.05	0.05	0.06	0.05	0.05	0.06
Na	-	-	-	-	-	-	-	-	-	0.01	0.01
Total	3.99	3.99	3.99	3.99	4.02	4.01	4.02	4.01	3.99	4.00	3.99
Wo	2.5	3.0	2.5	3.0	2.3	2.5	2.7	3.2	2.6	2.6	2.9
En	32.9	39.2	34.2	33.3	45.4	32.1	33.9	30.1	32.9	39.0	42.7
Fs	64.6	57.8	63.2	63.7	52.3	65.4	63.5	66.7	64.5	58.4	54.4
mg	34.8	41.6	36.2	35.4	48.3	34.0	35.9	32.1	35.0	41.4	45.5
Fe	0.66	0.60	0.65	0.66	0.53	0.67	0.65	0.69	0.66	0.60	0.56
F/F+M	0.778	0.724	0.767	0.773	0.672	0.784	0.770	0.798	0.778	0.727	0.694

Table C.2. cont.

Analysis #	12	13	14	15	16	17	18	19	20	21	22
Sample	66/1	66/1	66/1	66/1	66/1	70/3	70/3	70e/1	70e/1	70e/1	70e/1
SiO_2	49.86	51.42	50.22	50.13	49.73	49.40	49.24	51.26	52.75	53.10	53.65
TiO_2	0.08	0.29	0.13	0.11	0.10	0.13	0.06	0.15	0.15	0.26	0.17
Al_2O_3	0.22	1.06	0.25	0.27	0.21	0.18	0.24	0.42	0.64	0.85	1.03
FeO	34.96	28.54	35.76	35.26	35.92	35.28	34.72	31.73	27.01	23.44	21.97
MnO	1.80	1.29	1.73	1.68	1.73	1.79	1.57	1.60	1.13	0.96	0.50
MgO	11.97	16.24	11.60	11.84	11.00	10.88	11.23	13.90	17.72	20.10	21.25
CaO	1.15	1.51	1.13	1.14	1.05	1.24	1.05	1.32	1.46	1.37	1.58
Na_2O	0.09	0.07	0.08	0.09	0.10	-	0.02	0.04	0.06	0.05	0.06
Total	100.13	100.42	100.90	100.52	99.84	98.90	98.13	100.42	100.92	100.13	100.21
SiIV	1.99	1.98	2.00	1.99	2.00	2.00	2.01	2.00	2.00	1.99	1.99
AlIV	0.01	0.02	-	0.01	-	-	-	-	-	0.01	0.01
AlVI	-	0.03	0.01	0.01	0.01	0.01	0.01	0.02	0.03	0.03	0.04
Ti	-	0.01	-	-	-	-	-	-	-	0.01	-
Fe^{2+}	1.17	0.92	1.19	1.17	1.21	1.20	1.18	1.04	0.86	0.74	0.68
Mn	0.06	0.04	0.06	0.06	0.06	0.06	0.05	0.05	0.04	0.03	0.02
Mg	0.71	0.93	0.69	0.70	0.66	0.66	0.68	0.81	1.00	1.12	1.18
Ca	0.05	0.06	0.05	0.05	0.05	0.05	0.05	0.06	0.06	0.06	0.06
Na	0.01	0.01	0.01	0.01	0.01	-	-	-	-	-	-
Total	4.00	3.99	4.00	4.00	3.99	3.99	3.99	3.98	3.99	3.98	3.98
Wo	2.5	3.2	2.4	2.5	2.3	2.7	2.3	2.8	3.0	2.8	3.2
En	35.8	47.7	34.7	35.5	33.4	33.4	34.7	41.4	51.3	57.8	60.7
Fs	61.7	49.1	62.9	62.1	64.3	63.9	63.0	55.8	45.7	39.4	36.0
mg	37.9	50.4	36.6	37.4	35.3	35.5	36.6	43.9	53.9	60.9	63.3
Fe	0.63	0.51	0.64	0.64	0.66	0.66	0.64	0.57	0.47	0.40	0.37
F/F+M	0.754	0.647	0.764	0.757	0.774	0.773	0.764	0.706	0.614	0.548	0.514

Table C.2. cont.

c = core
r = rim

Analysis #	23	24	25	26	27	28	29	30	31	32	33
Sample	70e/1	70e/1	85/1	85/1	85/1c	85/1r	85/1	85/1	85/1	97/3	97/3
SiO_2	50.20	51.53	48.47	49.02	50.37	49.11	48.88	48.35	49.24	49.50	49.65
TiO_2	0.13	0.09	0.09	0.07	0.09	0.08	0.14	0.09	0.08	0.08	0.09
Al_2O_3	0.25	0.22	0.19	0.23	0.19	0.19	0.20	0.24	0.24	0.20	0.20
FeO	36.39	30.68	36.63	35.90	32.33	36.12	35.82	36.65	35.66	30.87	32.55
MnO	1.90	2.47	2.06	1.95	1.74	2.02	1.96	1.92	1.98	2.14	2.05
MgO	10.72	14.69	9.70	10.52	13.17	10.25	10.27	9.94	10.74	14.68	13.69
CaO	1.17	1.08	1.13	0.96	1.11	1.00	1.16	1.07	1.00	1.15	1.16
Na_2O	0.07	0.07	0.04	-	-	-	-	-	-	0.16	0.10
Total	100.83	100.83	98.31	98.65	99.00	98.77	98.43	98.26	98.94	98.78	99.49
SiIV	2.00	2.00	2.00	2.00	2.01	2.01	2.00	1.99	2.00	1.98	1.98
AlIV	-	-	-	-	-	-	-	0.01	-	0.01	0.01
AlVI	0.01	0.01	0.01	0.01	0.01	0.01	0.01	0.01	0.01	-	-
Fe_2+	1.21	1.00	1.26	1.23	1.08	1.23	1.23	1.26	1.21	1.03	1.09
Mn	0.06	0.08	0.07	0.07	0.06	0.07	0.07	0.07	0.07	0.07	0.07
Mg	0.64	0.85	0.60	0.64	0.78	0.62	0.63	0.61	0.65	0.87	0.81
Ca	0.05	0.04	0.05	0.04	0.05	0.04	0.05	0.05	0.04	0.05	0.05
Na	0.01	0.01	-	-	-	-	-	-	-	0.01	0.01
Total	3.99	3.99	4.00	3.99	3.99	3.99	3.99	4.00	3.99	4.02	4.02
Wo	2.5	2.3	2.5	2.1	2.4	2.2	2.6	2.4	2.2	2.4	2.5
En	32.4	43.1	30.1	32.4	39.8	31.7	31.8	30.7	33.0	43.1	40.3
Fs	65.0	54.6	67.4	65.5	57.8	66.1	65.6	66.9	64.8	54.4	57.2
mg	34.4	46.0	32.1	34.3	42.0	33.6	33.8	32.6	34.9	45.9	42.9
Fe	0.67	0.56	0.69	0.67	0.59	0.68	0.67	0.68	0.66	0.56	0.59
F/F+M	0.781	0.693	0.800	0.783	0.721	0.788	0.786	0.795	0.778	0.692	0.717

Table C.2. cont.

c = core
r = rim

Analysis #	34	35	36	37	38	39	40	41	42	43	44
Sample	97/3r	97/3	97/3	97/3	108/1	108/1c	108/1r	108/1	108/1	108/1	108/1
SiO_2	48.99	49.22	50.06	50.77	51.48	50.16	50.39	50.25	49.87	49.86	50.35
TiO_2	0.07	0.09	0.07	0.11	0.14	0.11	0.10	0.08	0.10	0.09	0.11
Al_2O_3	0.19	0.16	0.12	0.32	0.36	0.37	0.25	0.21	0.23	0.22	0.15
FeO	32.43	32.45	31.68	30.28	28.35	30.30	31.40	30.62	31.21	30.99	32.61
MnO	1.92	2.22	2.13	1.79	1.43	1.77	1.96	2.10	1.95	2.11	2.08
MgO	13.60	13.32	14.04	16.10	17.22	15.68	15.05	15.35	14.38	14.14	14.34
CaO	1.20	1.22	0.99	1.09	1.26	1.26	1.12	1.16	1.16	1.18	1.17
Na_2O	0.12	0.10	0.05	0.03	-	-	-	0.04	-	-	-
K_2O	0.01	0.02	-	-	-	-	-	-	-	-	-
Total	98.53	98.80	99.14	100.49	100.24	99.65	100.27	99.81	98.90	98.59	100.81
SiIV	1.97	1.98	1.99	1.97	1.98	1.97	1.98	1.98	1.99	1.99	1.98
AlIV	0.01	0.01	0.01	0.01	0.02	0.02	0.01	0.01	0.01	0.01	0.01
Fe_2^+	1.09	1.09	1.05	0.98	0.91	1.00	1.03	1.01	1.04	1.03	1.07
Mn	0.07	0.08	0.07	0.06	0.05	0.06	0.07	0.07	0.07	0.07	0.07
Mg	0.82	0.80	0.83	0.93	0.99	0.92	0.88	0.90	0.85	0.84	0.84
Ca	0.05	0.05	0.04	0.05	0.05	0.05	0.05	0.05	0.05	0.05	0.05
Na	0.01	0.01	-	-	-	-	-	-	-	-	-
Total	4.02	4.02	4.00	4.02	4.00	4.02	4.01	4.02	4.01	4.00	4.02
Wo	2.6	2.6	2.1	2.2	2.6	2.6	2.3	2.4	2.5	2.5	2.4
En	40.3	39.6	41.6	46.1	49.4	45.3	43.5	44.4	42.5	42.1	41.4
Fs	57.1	57.8	56.3	51.6	48.0	52.1	54.2	53.2	55.0	55.4	56.2
mg	42.8	42.3	44.1	48.6	52.0	48.0	46.1	47.2	45.1	44.8	44.0
Fe	0.59	0.59	0.57	0.53	0.49	0.53	0.55	0.54	0.56	0.57	0.58
F/F+M	0.716	0.722	0.707	0.666	0.634	0.672	0.689	0.681	0.698	0.701	0.708

Table C.2. cont.

r = rim
c = core

Analysis #	45	46	47	48	49	50	51	52	53	54	55
Sample	108/1	132/1	132/1	132/1	132/1	132/2r	132/2c	132/2	132/2	132/2	132/3
SiO_2	50.00	49.38	49.02	49.22	49.21	48.00	48.38	48.08	47.86	48.17	48.80
TiO_2	0.09	0.10	0.11	0.14	0.12	0.09	0.07	0.11	0.14	0.08	0.11
Al_2O_3	0.17	0.23	0.27	0.34	0.26	0.19	0.25	0.24	0.35	0.23	0.25
FeO	32.27	35.79	36.45	34.11	34.94	37.76	36.27	36.68	37.23	37.16	36.58
MnO	2.14	1.84	1.49	1.40	1.77	1.95	1.60	1.86	1.84	1.84	1.93
MgO	13.68	11.58	11.01	13.43	12.94	10.20	11.25	10.66	9.74	10.85	11.34
CaO	1.19	1.07	1.25	1.40	1.10	1.20	1.20	1.18	1.30	1.16	1.24
Na_2O	0.05	-	-	-	-	-	-	0.02	0.02	-	-
Total	99.59	99.99	99.60	100.04	100.34	99.39	99.02	98.83	98.48	99.49	100.25
SiIV	1.99	1.99	1.98	1.96	1.97	1.97	1.97	1.97	1.98	1.97	1.97
AlIV	0.01	0.01	0.01	0.02	0.01	0.01	0.01	0.01	0.02	0.01	0.01
Fe^{2+}	1.07	1.20	1.23	1.14	1.17	1.30	1.24	1.26	1.29	1.27	1.23
Mn	0.07	0.06	0.05	0.05	0.06	0.07	0.06	0.06	0.06	0.06	0.07
Mg	0.81	0.69	0.66	0.80	0.77	0.62	0.68	0.65	0.60	0.66	0.68
Ca	0.05	0.05	0.05	0.06	0.05	0.05	0.05	0.05	0.06	0.05	0.05
Total	4.01	4.01	4.01	4.03	4.03	4.02	4.02	4.02	4.01	4.02	4.02
Wo	2.5	2.3	2.7	2.9	2.3	2.6	2.6	2.6	2.9	2.5	2.6
En	40.4	34.6	33.2	39.1	37.7	30.6	33.7	32.2	29.9	32.3	33.5
Fs	57.1	63.1	64.1	58.0	60.0	66.8	63.7	65.3	67.3	65.2	63.9
mg	43.0	36.6	35.0	41.2	39.8	32.5	35.6	34.1	31.8	34.2	35.6
Fe	0.58	0.65	0.66	0.60	0.61	0.69	0.65	0.67	0.69	0.67	0.66
F/F+M	0.716	0.765	0.775	0.726	0.739	0.796	0.771	0.783	0.800	0.782	0.773

Table C.2. cont.

Analysis #	56	57	58	59	60	61	62	63	64	65	66
Sample	I32/3	I32/3	I32/3	I32/3	I32/3	I53/1	I53/1	I53/1	I53/1	T2/1	T2/1
SiO_2	48.72	48.84	47.68	49.86	49.47	49.16	49.62	49.65	48.41	51.08	52.89
TiO_2	0.09	0.11	0.09	0.12	0.09	0.14	0.06	0.11	0.12	0.17	0.13
Al_2O_3	0.22	0.26	0.22	0.37	0.28	0.27	0.21	0.21	0.35	0.42	0.34
FeO	37.37	36.37	37.18	30.09	32.37	36.83	35.27	36.29	34.70	29.27	25.41
MnO	1.82	1.70	1.75	2.01	1.99	1.71	1.91	1.72	1.64	1.75	1.37
MgO	10.13	11.38	10.64	14.73	13.70	11.53	11.77	11.48	12.29	15.57	18.64
CaO	1.18	1.25	1.20	1.13	1.20	1.36	1.24	1.29	1.25	1.14	1.11
Na_2O	0.03	-	0.02	0.03	-	-	-	-	-	-	-
Total	99.56	99.91	98.78	98.34	99.10	101.00	100.08	100.75	98.76	99.40	99.89
SiIV	1.99	1.97	1.96	1.99	1.98	1.97	1.99	1.98	1.97	2.00	2.01
AlIV	0.01	0.01	0.01	0.01	0.01	0.01	0.01	0.01	0.02	-	-
AlVI	-	-	-	-	-	-	-	-	-	0.02	0.02
Fe_{2+}	1.27	1.23	1.28	1.00	1.08	1.23	1.18	1.21	1.18	0.96	0.81
Mn	0.06	0.06	0.06	0.07	0.07	0.06	0.06	0.06	0.06	0.06	0.04
Mg	0.62	0.69	0.65	0.87	0.82	0.69	0.70	0.68	0.74	0.91	1.06
Ca	0.05	0.05	0.05	0.05	0.05	0.06	0.05	0.06	0.05	0.05	0.05
Total	4.01	4.02	4.03	4.00	4.01	4.02	4.00	4.01	4.02	3.99	3.98
Wo	2.6	2.7	2.6	2.4	2.5	2.9	2.7	2.7	2.7	2.4	2.3
En	30.7	33.8	31.9	43.9	40.5	33.8	35.1	34.0	36.6	46.1	54.1
Fs	66.7	63.5	65.5	53.7	57.0	63.4	62.2	63.2	60.7	51.5	43.6
ag	32.6	35.8	33.8	46.6	43.0	35.8	37.3	36.1	38.7	48.7	56.7
Fe	0.68	0.65	0.67	0.55	0.58	0.65	0.64	0.65	0.62	0.53	0.45
F/F+M	0.795	0.770	0.785	0.685	0.715	0.770	0.760	0.768	0.747	0.666	0.590

Table C.2. cont.

r = rim
c = core

Analysis #	67	68	69	70	71	72	73	74	75	76	77
Sample	T2/2	T2/2	T2/2	T2/2	T2/2	T2/2	T19/1r	T19/1c	T19/1r	T19/1	T19/1
SiO_2	50.70	49.72	49.95	50.46	48.81	49.97	49.72	51.08	50.54	50.38	49.61
TiO_2	0.17	0.06	0.11	0.13	0.13	0.09	0.09	0.11	0.26	0.14	0.12
Al_2O_3	0.40	0.15	0.34	0.41	0.20	0.14	0.22	0.39	0.96	0.30	0.22
FeO	29.72	34.01	33.38	31.52	33.93	33.86	32.94	27.08	27.52	28.61	32.42
MnO	1.68	2.12	1.88	1.81	2.07	1.99	2.14	1.48	1.62	1.91	2.10
MgO	15.78	13.15	14.02	14.74	13.17	13.34	13.75	18.31	16.97	16.29	13.99
CaO	1.19	0.96	1.09	1.24	1.14	0.94	1.20	0.98	1.32	1.27	1.04
Na_2O	-	-	-	-	-	-	0.14	0.09	0.09	0.11	0.11
K_2O	-	-	-	0.02	-	-	-	-	-	-	-
Total	99.64	100.17	100.77	100.33	99.45	100.33	100.20	99.52	99.28	99.01	99.61
SiIV	1.98	1.98	1.97	1.98	1.96	1.98	1.97	1.97	1.96	1.98	1.97
AlIV	0.02	0.01	0.02	0.02	0.01	0.01	0.01	0.02	0.04	0.01	0.01
AlVI	-	-	-	-	-	-	-	-	0.01	-	-
Fe^{2+}	0.97	1.13	1.10	1.03	1.14	1.12	1.09	0.87	0.89	0.94	1.08
Mn	0.06	0.07	0.06	0.06	0.07	0.07	0.07	0.05	0.05	0.06	0.07
Mg	0.92	0.78	0.82	0.86	0.79	0.79	0.81	1.05	0.98	0.95	0.83
Ca	0.05	0.04	0.05	0.05	0.05	0.04	0.05	0.04	0.05	0.05	0.04
Na	-	-	-	-	-	-	0.01	0.01	0.01	0.01	0.01
Total	4.00	4.01	4.02	4.01	4.03	4.01	4.03	4.02	4.01	4.01	4.02
Wo	2.5	2.0	2.3	2.6	2.4	2.0	2.5	2.0	2.8	2.7	2.2
En	46.1	38.5	40.5	42.9	38.5	39.1	40.1	52.2	49.5	47.4	41.0
Fs	51.5	59.4	57.2	54.5	59.1	59.0	57.4	45.7	47.7	49.9	56.8
mg	48.6	40.8	42.8	45.5	40.9	41.2	42.7	54.6	52.4	50.4	43.5
Fe	0.53	0.61	0.58	0.56	0.61	0.61	0.59	0.47	0.49	0.51	0.58
F/F+M	0.666	0.733	0.716	0.693	0.732	0.729	0.718	0.609	0.632	0.652	0.712

Table C.2. cont.

c = core
r = rim

Analysis #	78	79	80	81	82	83	84	85	86
Sample	T19/1	T19/1	T19/3c	T19/3r	T19/3	T19/3	T19/3	T19/3	T19/3
SiO_2	49.40	49.98	49.71	49.74	49.57	49.95	49.37	49.48	49.83
TiO_2	0.08	0.12	0.15	0.12	0.08	0.09	0.10	0.09	0.09
Al_2O_3	0.20	0.21	0.33	0.17	0.15	0.17	0.17	0.58	0.20
FeO	32.39	32.98	30.71	33.58	33.87	32.36	31.91	33.40	32.50
MnO	2.04	2.12	2.07	2.39	2.51	2.18	2.30	2.33	2.10
MgO	13.90	13.64	14.56	13.04	12.99	13.53	13.23	13.26	13.73
CaO	1.07	1.18	1.16	1.00	0.89	1.10	0.96	0.96	1.05
Na_2O	0.11	0.13	-	-	-	-	-	0.02	-
K_2O	0.02	-	-	-	-	-	-	-	-
Total	99.21	100.36	98.69	100.04	100.06	99.38	98.04	100.12	99.50
SiIV	1.97	1.98	1.98	1.98	1.98	1.99	1.99	1.97	1.98
AlIV	0.01	0.01	0.02	0.01	0.01	0.01	0.01	0.03	0.01
Fe^{2+}	1.08	1.09	1.02	1.12	1.13	1.08	1.08	1.11	1.08
Mn	0.07	0.07	0.07	0.08	0.08	0.07	0.08	0.08	0.07
Mg	0.83	0.80	0.86	0.77	0.77	0.80	0.80	0.79	0.81
Ca	0.05	0.05	0.05	0.04	0.04	0.05	0.04	0.04	0.04
Na	0.01	0.01	-	-	-	-	-	-	-
Total	4.02	4.02	4.01	4.01	4.02	4.00	4.00	4.02	4.01
Wo	2.3	2.5	2.5	2.1	1.9	2.3	2.1	2.0	2.2
En	40.9	39.9	43.1	38.4	38.1	40.1	39.9	39.0	40.5
Fs	56.9	57.6	54.5	59.5	60.0	57.5	58.0	59.0	57.3
mg	43.3	42.5	45.8	40.9	40.6	42.7	42.5	41.4	43.0
Fe	0.58	0.59	0.56	0.61	0.61	0.59	0.59	0.60	0.59
F/F+M	0.712	0.720	0.692	0.734	0.737	0.719	0.721	0.729	0.716

Table C.3. Titanomagnetite analyses of Pokai Ignimbrite pumices.

Analysis #	1	2	3	4	5	6	7	8	9	10	11
Sample	26A/1	26A/1	26A/1	26A/1	26A/1	26A/1	26A/2	26A/2	26A/2	26A/2	66/1
SiO_2	0.09	0.09	0.10	0.09	0.09	0.06	0.08	0.07	0.05	0.11	0.09
TiO_2	10.86	13.43	14.00	12.45	13.25	13.45	13.60	13.34	13.46	13.29	13.11
Al_2O_3	1.25	1.13	1.32	1.22	1.17	1.15	1.06	0.99	0.95	1.02	1.13
FeO	80.10	78.12	76.56	77.52	78.39	78.53	79.89	80.53	80.51	80.78	78.25
MnO	0.59	0.70	0.66	0.69	0.70	0.78	0.66	0.76	0.83	0.84	0.78
MgO	0.27	0.42	0.44	0.36	0.43	0.41	0.34	0.37	0.35	0.33	0.42
CaO	0.02	-	0.03	0.02	-	-	-	0.01	-	0.03	-
Na_2O	-	-	-	-	-	-	-	-	-	-	0.09
K_2O	-	-	0.01	-	-	-	-	-	-	-	-
Total	93.18	93.89	93.12	92.35	94.03	94.38	95.63	96.07	96.15	96.40	93.87
Si	0.03	0.03	0.04	0.03	0.03	0.02	0.03	0.02	0.02	0.04	0.03
Ti	3.02	3.63	3.79	3.44	3.58	3.63	3.62	3.55	3.58	3.52	3.56
Al	0.55	0.48	0.56	0.53	0.50	0.48	0.44	0.41	0.40	0.43	0.48
Fe^{+2}	24.74	23.51	23.05	23.83	23.58	23.52	23.66	23.81	23.79	23.81	23.60
Mn	0.18	0.21	0.20	0.22	0.21	0.23	0.20	0.23	0.25	0.25	0.24
Mg	0.15	0.22	0.24	0.20	0.23	0.22	0.18	0.20	0.18	0.17	0.22
Ca	0.01	-	0.01	0.01	-	-	-	0.01	-	0.01	-
Na	-	-	-	-	-	-	-	-	-	-	0.06
K	-	-	0.01	-	-	-	-	-	-	-	-
Total	28.68	28.09	27.89	28.26	28.14	28.11	28.13	28.22	28.21	28.23	28.20

Analysis #	12	13	14	15	16	17	18	19	20	21	22
Sample	66/1	66/1	66/1	66/1	66/1	66/1	66/1	70/3	70e/1	70e/1	70e/1
SiO_2	0.08	0.77	0.06	0.07	0.11	0.07	0.10	0.06	0.13	0.05	0.05
TiO_2	13.60	13.34	13.34	13.65	13.56	13.97	13.84	13.37	13.73	15.58	13.32
Al_2O_3	1.10	1.37	1.19	1.09	1.20	1.14	1.17	1.06	1.10	1.12	1.10
FeO	79.77	76.66	80.11	79.50	79.35	78.47	78.36	78.00	79.42	79.10	79.48
MnO	0.73	0.74	0.76	0.75	0.74	0.58	0.71	0.73	0.78	0.84	0.82
MgO	0.43	0.39	0.35	0.42	0.34	0.44	0.40	0.40	0.37	0.36	0.39
CaO	-	-	0.03	-	-	-	-	-	0.01	0.02	0.13
Na_2O	0.07	-	0.04	0.07	-	0.05	0.05	-	-	0.03	-
Total	95.78	93.27	95.88	95.55	95.30	94.72	94.63	93.62	95.54	97.10	95.29
Si	0.03	0.28	0.02	0.02	0.04	0.03	0.04	0.02	0.05	0.02	0.02
Ti	3.61	3.59	3.55	3.63	3.62	3.74	3.71	3.63	3.65	4.03	3.56
Al	0.46	0.58	0.49	0.46	0.50	0.48	0.49	0.45	0.46	0.46	0.46
Fe^{+2}	23.56	22.96	23.68	23.53	23.53	23.34	23.34	23.57	23.48	22.77	23.64
Mn	0.22	0.22	0.23	0.22	0.22	0.17	0.21	0.22	0.23	0.25	0.25
Mg	0.23	0.21	0.18	0.22	0.18	0.23	0.21	0.22	0.20	0.18	0.21
Ca	-	-	0.01	-	-	-	-	-	0.01	0.01	0.05
Na	0.05	-	0.03	0.05	-	0.03	0.03	-	-	0.02	-
Total	28.15	27.84	28.20	28.14	28.09	28.01	28.03	28.12	28.07	27.73	28.19

Table C.3. cont.

Analysis #	23	24	25	26	27	28	29	30	31	32	33
Sample	70e/1	70e/1	70e/1	85/1	85/1	85/1	97/3	97/3	97/3	97/3	108/1
SiO_2	0.10	0.07	0.13	0.09	0.10	0.07	0.07	0.08	0.10	0.05	0.09
TiO_2	13.56	13.76	13.54	10.57	7.21	12.44	11.44	11.33	11.45	14.77	10.69
Al_2O_3	1.12	1.18	1.13	1.13	1.16	0.70	0.99	0.92	0.97	0.94	1.02
FeO	79.64	79.16	79.69	79.69	82.48	78.08	82.83	82.08	81.03	81.86	81.54
MnO	0.69	0.58	0.68	0.75	0.59	0.66	0.83	0.81	0.80	1.09	0.79
MgO	0.40	0.40	0.40	0.24	0.23	0.27	0.46	0.47	0.50	0.61	0.57
CaO	-	-	0.02	-	-	-	-	-	-	0.02	-
Na_2O	0.06	-	0.04	-	-	-	-	0.06	-	-	-
K_2O	-	0.01	-	-	-	-	-	-	-	-	-
Total	95.57	95.16	95.63	92.47	91.77	92.22	96.62	95.75	94.85	99.34	94.70
Si	0.04	0.02	0.05	0.04	0.04	0.03	0.03	0.03	0.04	0.02	0.03
Ti	3.61	3.67	3.60	2.97	2.09	3.47	3.07	3.07	3.12	3.77	2.93
Al	0.47	0.49	0.47	0.50	0.53	0.31	0.41	0.39	0.41	0.38	0.44
Fe^{+2}	23.57	23.49	23.57	24.88	26.62	24.20	24.70	24.71	24.55	23.23	24.87
Mn	0.21	0.17	0.20	0.24	0.19	0.21	0.25	0.25	0.25	0.31	0.24
Mg	0.21	0.21	0.21	0.14	0.13	0.15	0.24	0.25	0.27	0.31	0.31
Ca	-	-	0.01	-	-	-	-	-	-	0.01	-
Na	0.04	-	0.03	-	-	-	-	0.04	-	-	-
K	-	0.01	-	-	-	-	-	-	-	-	-
Total	28.14	28.06	28.13	28.75	29.60	28.35	28.70	28.73	28.64	28.02	28.82

Analysis #	34	35	36	37	38	39	40	41	42	43	44
Sample	108/1	108/1	126/1	132/1	132/1	132/1	132/1	132/2	132/2	132/3	132/3
SiO_2	0.08	0.10	0.07	0.10	0.10	0.23	0.05	0.08	0.09	0.06	0.66
TiO_2	11.21	11.38	12.17	13.32	13.28	13.77	13.71	17.28	11.22	11.48	16.25
Al_2O_3	0.91	0.94	0.98	1.21	1.24	1.25	1.16	0.84	1.06	1.26	1.01
FeO	81.32	82.33	76.66	79.86	78.85	76.53	80.38	75.65	81.72	82.41	76.03
MnO	0.74	0.72	0.67	0.75	0.83	0.82	0.72	0.80	0.88	0.65	0.92
MgO	0.42	0.47	0.31	0.46	0.46	0.40	0.45	0.34	0.27	0.36	0.40
CaO	0.01	0.01	-	-	-	0.03	-	-	-	-	0.10
K_2O	-	-	-	-	-	-	-	-	-	-	0.03
Total	94.69	95.95	90.86	95.70	94.76	93.03	96.47	94.99	95.24	96.22	95.40
Si	0.03	0.04	0.03	0.04	0.04	0.08	0.02	0.03	0.03	0.02	0.23
Ti	3.07	3.07	3.43	3.54	3.58	3.73	3.62	4.51	3.05	3.08	4.22
Al	0.39	0.40	0.43	0.50	0.52	0.53	0.48	0.34	0.45	0.53	0.41
Fe^{+2}	24.76	24.71	24.05	23.62	23.65	23.09	23.57	21.98	24.74	24.61	21.97
Mn	0.23	0.22	0.21	0.22	0.25	0.25	0.22	0.24	0.27	0.20	0.27
Mg	0.23	0.25	0.17	0.24	0.25	0.22	0.23	0.18	0.14	0.19	0.20
Ca	0.01	0.01	-	-	-	0.01	-	-	-	-	0.04
K	-	-	-	-	-	-	-	-	-	-	0.01
Total	28.71	28.69	28.32	28.17	28.29	27.92	28.13	27.28	28.69	28.63	27.35

Table C.3. cont.

Analysis #	45	46	47	47	49	50	51	52	53	54	55
Sample	132/3	132/3	153/1	153/1	153/1	T2/2	T2/2	T2/2	T2/2	T2/2	T19/1
SiO_2	0.06	0.03	0.05	0.06	0.12	0.07	0.06	0.09	0.09	0.07	0.10
TiO_2	12.40	22.64	7.20	16.34	13.31	6.80	12.60	12.83	11.06	13.55	11.36
Al_2O_3	1.26	0.88	1.47	1.07	1.29	1.02	0.97	0.76	0.84	0.80	1.01
FeO	81.19	71.67	84.76	77.32	82.08	86.13	85.79	80.71	82.18	77.00	81.56
MnO	0.75	0.92	0.61	0.69	0.71	0.60	0.69	0.99	0.81	0.85	0.89
MgO	0.34	0.54	0.30	0.48	0.40	0.32	0.27	0.40	0.38	0.42	0.48
CaO	-	-	-	-	-	-	0.01	0.02	0.01	0.01	-
Na_2O	-	-	-	-	-	-	-	-	-	-	0.09
K_2O	-	-	0.01	-	-	-	-	-	-	-	-
Total	96.00	96.68	94.40	95.96	97.91	94.94	100.39	95.80	95.37	92.70	95.49
Si	0.02	0.01	0.02	0.02	0.04	0.03	0.02	0.03	0.03	0.03	0.04
Ti	3.31	5.61	2.03	4.25	3.47	1.92	3.24	3.44	3.02	3.72	3.08
Al	0.53	0.34	0.65	0.44	0.53	0.45	0.39	0.32	0.36	0.34	0.43
Fe^{+2}	24.13	19.73	26.57	22.35	23.78	27.06	24.55	24.06	24.91	23.50	24.57
Mn	0.23	0.26	0.19	0.20	0.21	0.19	0.20	0.30	0.25	0.26	0.27
Mg	0.18	0.26	0.17	0.25	0.21	0.18	0.14	0.21	0.21	0.23	0.26
Ca	-	-	-	-	-	-	0.01	0.01	-	0.01	-
Na	-	-	-	-	-	-	-	-	-	-	0.06
K	-	-	0.01	-	-	-	-	-	-	-	-
Total	28.40	26.21	29.63	27.51	28.23	29.83	28.54	28.37	28.77	28.08	28.70

Analysis #	56	57	58	59	60	61	62	63	64
Sample	T19/1	19/1	T19/1	T19/3	T19/3	T19/3	T19/3	T19/3	T19/3
SiO_2	0.05	0.21	0.08	0.15	0.05	0.07	0.06	0.07	0.09
TiO_2	19.13	10.64	10.32	6.92	7.34	30.31	10.45	10.03	12.37
Al_2O_3	0.83	0.91	0.94	0.96	0.94	0.37	0.84	0.85	0.82
FeO	75.16	83.21	84.04	85.92	84.43	62.76	82.26	83.57	79.57
MnO	1.16	0.85	0.85	0.71	0.76	1.64	0.94	0.84	0.89
MgO	0.53	0.38	0.45	0.32	0.31	0.71	0.35	0.38	0.40
CaO	-	-	-	-	-	0.02	-	0.01	-
Na_2O	0.14	0.12	0.09	-	-	-	-	-	-
Total	97.00	96.32	96.77	94.98	93.83	95.88	94.90	95.75	94.14
Si	0.02	0.08	0.03	0.06	0.02	0.02	0.02	0.03	0.03
Ti	4.84	2.88	2.79	1.95	2.09	7.20	2.88	2.75	3.38
Al	0.33	0.39	0.40	0.42	0.42	0.14	0.36	0.37	0.35
Fe^{+2}	21.15	25.01	25.24	26.94	26.74	16.57	25.17	25.43	24.16
Mn	0.33	0.26	0.26	0.22	0.24	0.44	0.29	0.26	0.28
Mg	0.27	0.20	0.24	0.18	0.17	0.34	0.19	0.20	0.22
Ca	-	-	-	-	-	0.01	-	0.01	-
Na	0.09	0.09	0.07	-	-	-	-	-	-
Total	27.02	28.90	29.02	29.78	29.68	24.71	28.91	29.04	28.42

Table C.4. Ilmenite analyses of Pokai Ignimbrite pumices.

Analysis #	1	2	3	4	5	6	7	8	9	10	11
Sample	26A/2	66/1	66/1	66/1	70e/1	85/1	97/3	97/3	108/1	108/1	108/1
SiO_2	0.02	0.03	0.04	0.03	0.03	0.06	-	-	0.05	-	-
TiO_2	48.39	47.65	47.78	48.13	48.04	36.10	47.33	47.01	47.16	47.77	47.31
Al_2O_3	0.08	0.09	0.09	0.04	0.07	0.38	0.07	0.08	0.08	0.07	0.07
FeO	47.80	48.51	47.48	47.67	48.20	56.90	49.11	49.07	48.86	48.82	49.12
MnO	1.13	1.08	1.20	1.11	1.16	1.37	1.34	1.43	1.15	1.44	1.38
MgO	0.85	0.87	0.88	0.87	0.78	0.64	1.02	1.00	1.22	0.99	1.10
CaO	0.01	0.02	0.01	-	-	-	-	0.03	0.03	0.01	-
Na_2O	-	0.10	0.08	0.07	0.05	-	-	0.09	-	-	-
Total	98.28	98.35	97.56	97.92	98.33	95.45	98.87	98.71	98.55	99.10	98.98
Ti	1.90	1.87	1.89	1.89	1.89	1.55	1.86	1.85	1.85	1.87	1.85
Al	0.01	0.01	0.01	-	-	0.03	0.01	0.01	0.01	-	0.01
Fe^{+2}	2.08	2.12	2.09	2.09	2.10	2.72	2.14	2.15	2.13	2.12	2.14
Mn	0.05	0.05	0.05	0.05	0.05	0.07	0.06	0.06	0.05	0.06	0.06
Mg	0.07	0.07	0.07	0.07	0.06	0.05	0.08	0.08	0.09	0.08	0.09
Na	-	0.01	0.01	0.01	0.01	-	-	0.01	-	-	-
Total	4.10	4.13	4.11	4.11	4.11	4.43	4.14	4.15	4.14	4.13	4.14

Analysis #	12	13	14	15	16	17	18	19	20	21	22
Sample	108/1	126/1	132/1	132/2	132/2	132/3	132/3	153/1	T2/1	T2/1	T2/1
SiO_2	0.03	-	0.03	0.03	0.04	0.03	0.09	0.03	0.04	0.04	0.03
TiO_2	47.84	46.70	47.97	48.04	48.26	48.10	47.51	46.90	46.87	47.35	47.32
Al_2O_3	0.09	0.08	0.08	0.07	0.08	0.07	0.05	0.03	0.05	-	0.03
FeO	47.96	46.64	48.06	48.54	47.39	48.51	48.21	49.68	46.87	45.94	46.72
MnO	1.44	1.16	1.20	1.15	1.30	1.22	1.19	1.20	1.63	1.64	1.57
MgO	1.18	0.72	0.86	0.64	0.72	0.83	0.78	0.93	0.57	0.72	0.60
CaO	-	0.01	-	-	0.03	-	0.03	0.33	0.01	0.10	0.01
Total	98.54	95.31	98.20	98.47	97.82	98.76	97.86	99.10	96.04	95.79	96.28
Si	-	-	-	-	-	-	0.01	-	-	-	-
Ti	1.87	1.89	1.88	1.89	1.90	1.88	1.88	1.84	1.89	1.90	1.90
Al	0.01	0.01	0.01	-	0.01	-	-	-	-	-	-
Fe^{+2}	2.09	2.10	2.10	2.12	2.07	2.11	2.12	2.17	2.10	2.05	2.08
Mn	0.06	0.05	0.05	0.05	0.06	0.05	0.05	0.05	0.07	0.07	0.07
Mg	0.09	0.06	0.07	0.05	0.06	0.06	0.06	0.07	0.05	0.06	0.05
Ca	-	-	-	-	-	-	-	0.02	-	0.01	-
Total	4.12	4.11	4.11	4.11	4.10	4.11	4.12	4.16	4.11	4.09	4.10

Table C.4. cont.

Analysis #	23	24	25	26	27	28	29
Sample	T2/1	T2/2	T19/1	T19/1	T19/1	T19/3	T19/3
SiO_2	1.81	-	0.05	-	-	0.03	0.05
TiO_2	45.52	47.23	47.39	47.46	47.28	47.23	47.43
Al_2O_3	0.33	0.06	0.07	0.06	0.06	0.06	0.07
FeO	44.12	48.25	49.85	49.96	49.61	48.36	48.91
MnO	1.08	1.50	1.33	1.34	1.49	1.73	1.52
MgO	0.54	0.92	1.03	1.02	1.04	0.75	0.94
CaO	0.07	-	0.02	-	-	0.02	0.03
Na_2O	-	-	0.09	0.11	0.09	-	-
K_2O	0.03	-	-	-	-	-	-
Total	93.50	97.96	99.83	99.95	99.57	98.18	98.95
Si	0.10	-	-	-	-	-	-
Ti	1.84	1.87	1.84	1.85	1.85	1.87	1.86
Al	0.02	-	-	-	-	-	0.01
Fe^{+2}	1.99	2.12	2.16	2.16	2.15	2.12	2.13
Mn	0.05	0.07	0.06	0.06	0.06	0.08	0.07
Mg	0.04	0.07	0.08	0.08	0.08	0.06	0.07
Na	-	-	0.01	0.01	0.01	-	-
Total	4.05	4.13	4.16	4.16	4.16	4.13	4.14

Table C.5. Pumice glass analyses of Pokai Ignimbrite.

Analysis #	1	2	3	4	5	6	7	8	9	10	11
Sample	26A/1	26A/2	26A/2	26A/2	26A/2	26A/2	66/1	66/1	66/1	70/3	70e/1
SiO_2	74.00	76.93	77.24	77.75	77.20	76.93	77.28	77.90	75.86	76.42	78.42
TiO_2	0.09	0.11	0.09	0.10	0.11	0.10	0.13	0.11	0.16	0.12	0.13
Al_2O_3	10.71	11.06	11.06	11.07	11.01	11.14	11.95	11.15	12.63	10.69	11.04
FeO	1.04	1.34	1.19	1.22	1.22	1.12	1.25	1.22	1.48	1.15	1.38
MnO	0.03	0.02	0.02	0.09	-	-	-	0.04	-	0.06	0.03
MgO	0.04	0.06	0.04	0.06	0.05	0.05	0.06	0.07	0.09	0.04	0.06
CaO	0.82	0.79	0.78	0.78	0.78	0.73	0.82	0.88	0.81	0.67	0.74
Na_2O	2.84	3.04	2.94	2.96	3.03	2.82	3.05	2.65	2.82	2.75	2.69
K_2O	3.41	3.61	3.65	3.69	3.71	3.49	3.55	3.61	3.52	3.50	3.61
Total	92.98	96.96	97.01	97.72	97.11	96.38	98.09	97.63	97.37	95.40	98.10

Analysis #	12	13	14	15	16	17	18	19	20	21	22
Sample	70e/1	70e/1	70e/1	70e/1	70e/1	70e/1	85/1	85/1	97/3	97/3	108/1
SiO_2	78.08	78.10	78.27	78.12	77.89	77.63	78.29	78.28	74.20	74.50	76.77
TiO_2	0.09	0.13	0.09	0.12	0.13	0.08	0.11	0.09	0.14	0.13	0.11
Al_2O_3	10.92	11.28	11.25	11.28	11.20	11.19	10.83	10.92	10.61	10.74	11.17
FeO	1.42	1.34	1.18	1.30	1.45	1.19	0.88	0.63	1.12	1.11	1.21
MnO	0.03	0.03	0.05	-	-	-	-	0.05	0.03	0.05	-
MgO	0.06	0.05	0.05	0.05	0.06	0.06	-	0.02	0.05	0.06	0.07
CaO	0.83	0.83	0.83	0.84	0.85	0.83	0.66	0.63	0.65	0.64	0.76
Na_2O	2.51	2.52	2.70	2.62	2.77	2.65	3.11	3.06	2.46	2.86	3.07
K_2O	3.62	3.51	3.63	3.39	3.66	3.61	3.66	3.61	3.40	3.26	3.54
Total	97.56	97.79	98.05	97.72	98.01	97.24	97.54	97.29	92.66	93.35	96.70

Analysis #	23	24	25	26	27	28	29	30	31	32	33
Sample	108/1	108/1	126/1	126/1	126/1	126/1	132/1	132/1	132/1	132/1	132/1
SiO_2	75.96	76.63	76.69	73.22	75.45	73.04	76.17	76.01	77.08	77.40	77.31
TiO_2	0.12	0.14	0.09	0.07	0.08	0.08	0.14	0.13	0.10	0.12	0.14
Al_2O_3	11.04	11.33	10.72	10.35	10.67	15.50	11.46	11.25	11.50	11.45	11.44
FeO	0.77	0.93	0.95	0.93	0.97	0.82	1.27	0.26	1.41	0.94	1.03
MnO	-	0.06	0.05	0.03	-	-	0.05	0.03	0.05	-	0.05
MgO	0.06	0.05	0.04	0.04	0.04	0.04	0.07	-	0.07	0.03	0.06
CaO	0.75	0.68	0.59	0.59	0.63	0.62	1.01	0.87	1.03	0.90	0.91
Na_2O	2.80	3.10	2.95	2.74	2.98	2.83	3.16	3.10	2.82	3.22	2.70
K_2O	3.67	3.58	3.63	3.39	3.69	3.45	3.53	3.64	3.58	3.56	3.52
Total	95.17	96.50	95.71	91.36	94.51	96.38	96.86	95.29	97.64	97.62	97.16

Table C.5. cont.

Analysis #	34	35	36	37	38	39	40	41	42	43	44
Sample	132/1	132/1	132/2	132/3	132/3	132/3	132/3	132/3	132/3	153/1	153/1
SiO_2	76.69	76.92	76.57	76.01	76.51	77.23	76.46	76.49	76.29	77.51	77.76
TiO_2	0.13	0.11	0.08	0.14	0.12	0.20	0.13	0.10	0.13	0.10	0.14
Al_2O_3	11.33	11.44	10.98	11.18	11.26	14.27	11.21	11.35	10.88	11.72	11.63
FeO	1.36	1.22	1.02	1.28	1.25	1.60	1.44	1.34	1.52	0.68	0.59
MnO	0.04	-	0.05	0.03	0.04	0.07	-	-	0.05	-	0.03
MgO	0.08	0.07	0.06	0.07	0.06	0.07	0.07	0.06	0.06	0.04	0.02
CaO	1.00	0.89	0.90	0.99	0.92	0.93	0.93	0.92	0.82	0.89	0.90
Na_2O	3.18	3.14	2.90	3.17	3.07	3.09	3.00	3.13	3.06	3.35	2.93
K_2O	3.51	3.51	3.71	3.46	3.49	3.61	3.58	3.58	3.25	3.68	3.64
Total	97.32	97.30	96.27	96.33	96.72	101.07	96.82	96.97	96.06	97.97	97.64

Analysis #	45	46	47	48	49	50	51	52	53	54	55
Sample	153/1	T2/1	T2/1	T2/1	T2/1	T2/1	T2/1	T2/1	T2/1	T2/1	T2/2
SiO_2	77.81	77.38	78.57	77.39	78.50	78.27	77.93	78.48	78.09	78.09	77.60
TiO_2	0.15	0.12	0.10	0.10	0.09	0.09	0.13	0.11	0.12	0.09	0.09
Al_2O_3	11.72	10.99	11.23	11.07	11.17	11.21	11.13	11.21	11.02	11.08	10.97
FeO	0.82	1.36	0.20	0.75	0.88	1.35	1.41	0.95	1.30	0.89	0.83
MnO	-	0.04	-	0.05	0.07	0.06	0.04	0.06	0.02	0.06	0.06
MgO	0.02	0.04	-	0.04	0.03	0.05	0.04	0.02	0.07	-	0.04
CaO	0.89	0.60	0.64	0.72	0.76	0.75	0.77	0.76	0.78	0.77	0.56
Na_2O	3.22	2.90	2.89	2.55	2.80	2.65	2.96	2.86	2.43	3.21	3.18
K_2O	3.72	3.65	3.78	3.47	3.76	3.67	3.62	3.53	3.60	3.78	4.00
Total	98.35	97.08	97.41	96.14	98.06	98.10	98.03	97.98	97.43	97.97	97.33

Analysis #	56	57	58	59	60	61	62	63	64	65	66
Sample	T2/2	T2/2	T2/2	T19/1	T19/1	T19/1	T19/1	T19/3	T19/3	T19/3	T19/3
SiO_2	75.71	77.39	77.11	77.26	77.40	76.62	77.72	76.82	76.74	75.72	76.03
TiO_2	0.09	0.10	0.10	0.15	0.12	0.11	0.12	0.08	0.07	0.07	0.09
Al_2O_3	10.88	11.19	10.98	11.04	11.20	11.13	11.03	11.19	9.05	11.03	11.12
FeO	0.68	0.89	0.97	0.68	0.78	1.05	0.40	0.69	0.68	0.86	1.03
MnO	0.05	-	-	-	-	0.03	0.02	-	-	0.06	0.03
MgO	0.02	0.03	0.04	0.04	0.04	0.04	0.02	0.04	0.03	0.03	0.05
CaO	0.47	0.54	0.55	0.76	0.68	0.66	0.58	0.49	0.47	0.56	0.49
Na_2O	3.21	3.22	3.01	3.04	3.34	3.25	3.36	3.15	3.18	2.96	3.06
K_2O	3.91	4.02	3.94	3.58	3.71	3.65	3.76	3.63	3.87	3.93	3.94
Total	95.02	97.38	96.70	96.55	97.27	96.54	97.01	96.09	94.09	95.22	95.84

Table C.5. cont.

Analysis #	67
Sample	T19/3
SiO_2	77.39
TiO_2	0.11
Al_2O_3	11.15
FeO	0.60
CaO	0.45
Na_2O	3.14
K_2O	3.95
Total	96.79

Table C.6. Ab-An-Or compositions of plagioclase phenocrysts in the Pokai Ignimbrite pumices with temperature estimates at 0, 0.5 and 1 kb total pressures using plagioclase liquidus geothermometer (Kudo and Weill, 1971; Mathez, 1973).

Sno. = sample number, i.e. host pumice
Pumice type = crystal-poor: 1a and 1b; crystal-rich: 2 (see also Appendix D; Table D.2)
S_{Pl} = analysis number for plagioclase microprobe analyses
$_{k}$ = kaolinitised sample (85/1), possibly of Type 1a

Sno.	Pumice type	S_{Pl}	Ab	An	Or	0 kb	0.5 kb	1 kb
26A/1	1b	1	73.0	23.8	3.2	623°C	813°C	825°C
		2	70.4	27.0	2.6	690°C	782°C	876°C
		3	69.8	27.6	2.6	700°C	776°C	885°C
		4	68.0	29.2	2.8	722°C	756°C	906°C
		5	59.8	38.5	1.8	817°C	772°C	1003°C
		6	66.7	30.5	2.8	739°C	738°C	922°C
		7	56.5	42.2	1.4	847°C	825°C	1035°C
		8	55.3	42.8	1.8	851°C	833°C	1040°C
		9	56.2	42.2	1.6	847°C	825°C	1035°C
		10	68.9	28.4	2.4	711°C	766°C	896°C
26A/2	1a	11	68.3	29.0	2.8	715°C	784°C	910°C
		12	58.6	39.5	1.9	827°C	789°C	1021°C
		13	58.5	39.8	1.7	830°C	794°C	1024°C
		14	67.9	29.3	2.8	719°C	780°C	914°C
		15	67.7	29.4	2.9	720°C	779°C	915°C
		16	69.3	28.0	2.7	699°C	795°C	896°C
		17	73.6	22.6	3.8	630°C	845°C	802°C
		18	54.9	43.7	1.3	861°C	848°C	1057°C
		19	65.5	32.1	2.4	755°C	740°C	947°C
HJ7/1	1a	20	68.7	28.6	2.7	643°C	862°C	853°C
		21	69.1	27.8	3.1	662°C	868°C	838°C
		22	73.9	22.4	3.7	735°C	904°C	754°C
66/1	1b	23	65.7	31.8	2.5	673°C	872°C	824°C
		24	63.9	33.8	2.3	628°C	859°C	859°C
		25	62.9	35.2	1.9	638°C	849°C	880°C
		26	65.0	32.8	2.2	654°C	866°C	843°C
		27	70.6	25.8	3.5	740°C	908°C	772°C
		28	68.1	29.1	2.8	708°C	889°C	759°C
		29	67.3	30.0	2.7	698°C	884°C	785°C
		30	68.0	29.2	2.8	707°C	888°C	762°C
		31	69.2	27.8	3.0	722°C	897°C	688°C
		32	67.7	29.5	2.8	704°C	887°C	771°C
70/3	1a	33	72.3	24.5	3.2	675°C	801°C	870°C
(air-fall)		34	70.2	27.0	2.8	717°C	773°C	907°C
		35	68.1	29.3	2.7	748°C	739°C	936°C
		36	72.3	24.6	3.2	677°C	800°C	872°C
		37	72.8	23.9	3.4	662°C	808°C	861°C
70e/1	1b	38	67.9	29.8	2.3	635°C	854°C	834°C
(air-fall)		39	68.7	28.3	3.0	666°C	864°C	805°C
		40	69.5	28.0	2.6	671°C	866°C	798°C
		41	65.4	32.1	2.5	643°C	837°C	871°C
		42	66.8	30.5	2.7	612°C	849°C	846°C
		43	63.1	34.7	2.3	696°C	815°C	771°C

Table C.6. cont.

Sno.	Pumice type	S_{Pl}	Ab	An	Or	0 kb	0.5 kb	1 kb
85/1[k]	(1a)	44	68.0	30.0	2.0	876°C	873°C	1051°C
		45	72.5	24.9	2.6	833°C	809°C	1003°C
		46	71.9	25.0	3.1	834°C	810°C	1004°C
		47	73.4	23.2	3.4	817°C	782°C	984°C
		48	70.5	26.7	2.8	849°C	833°C	1021°C
		49	71.9	24.9	3.2	833°C	809°C	1003°C
		50	71.8	25.1	3.1	835°C	812°C	1005°C
		51	69.5	27.6	2.8	857°C	845°C	1029°C
97/3	2	52	73.5	23.4	3.1	635°C	838°C	746°C
		53	71.0	26.1	2.9	595°C	818°C	808°C
		54	72.2	25.0	2.8	594°C	826°C	786°C
		55	61.8	36.4	1.8	762°C	692°C	944°C
		56	61.0	37.1	1.9	769°C	672°C	951°C
		57	72.7	24.6	2.7	608°C	829°C	777°C
		58	72.8	24.0	3.3	623°C	833°C	762°C
108/1	2	59	63.5	34.6	1.9	699°C	805°C	900°C
		60	68.6	28.9	2.5	634°C	713°C	944°C
		61	70.4	26.8	2.8	672°C	864°C	766°C
		62	72.2	25.0	1.8	762°C	858°C	789°C
		63	69.1	27.7	3.2	658°C	858°C	789°C
		64	66.1	31.6	2.3	641°C	830°C	859°C
		65	65.4	32.7	2.0	666°C	821°C	875°C
126/1	1a	66	71.0	26.3	2.6	696°C	815°C	905°C
		67	71.4	25.8	2.8	686°C	820°C	897°C
		68	71.7	25.4	2.9	677°C	825°C	891°C
		69	75.8	20.3	3.9	678°C	870°C	783°C
		70	70.7	26.4	2.9	698°C	814°C	906°C
		71	73.0	24.0	3.0	639°C	838°C	867°C
		72	75.0	21.8	3.1	646°C	858°C	823°C
132/1	1b	73	68.3	28.8	2.9	728°C	757°C	913°C
		74	66.1	31.4	2.5	759°C	713°C	944°C
		75	62.9	34.8	2.3	794°C	715°C	979°C
		76	67.9	29.2	2.9	733°C	752°C	918°C
		77	66.6	30.7	2.7	751°C	727°C	936°C
		78	68.7	28.3	3.0	721°C	764°C	907°C
		79	68.0	29.3	2.7	735°C	750°C	919°C
132/2	1a	80	71.2	25.6	3.2	683°C	816°C	891°C
		81	67.6	29.3	3.1	743°C	771°C	942°C
		82	69.7	27.0	3.3	708°C	800°C	912°C
		83	71.7	24.2	4.2	649°C	830°C	868°C
		84	71.6	24.8	3.5	665°C	824°C	878°C
		85	70.8	25.6	3.6	683°C	816°C	891°C
132/3	1b	86	63.9	33.5	2.6	718°C	802°C	924°C
		87	68.7	28.4	2.9	594°C	847°C	851°C
		88	66.5	30.9	2.6	674°C	827°C	890°C
		89	67.0	30.6	2.4	667°C	829°C	885°C
		90	68.4	28.9	2.7	616°C	844°C	859°C
		91	67.9	29.6	2.5	642°C	838°C	870°C
		92	67.4	29.7	2.9	645°C	837°C	872°C
		93	74.2	22.3	3.5	716°C	890°C	726°C

Table C.6. cont.

Sno.	Pumice type	S_{Pl}	Ab	An	Or	0 kb	0.5 kb	1 kb
153/1	1b	94	68.0	29.3	2.8	743°C	749°C	933°C
		95	67.3	29.9	2.8	751°C	739°C	940°C
		96	69.6	27.6	2.8	721°C	773°C	911°C
T2/1	1b	97	61.5	36.9	1.6	709°C	808°C	916°C
		98	62.6	35.5	2.0	687°C	820°C	899°C
		99	67.9	30.1	2.0	656°C	861°C	815°C
		100	67.3	30.6	2.1	646°C	858°C	825°C
		101	66.7	31.4	2.0	626°C	852°C	839°C
		102	64.8	33.5	1.7	645°C	837°C	872°C
		103	66.6	31.6	1.8	620°C	851°C	742°C
		104	64.0	33.9	2.4	655°C	834°C	878°C
		105	66.6	31.4	2.0	626°C	852°C	839°C
		106	68.5	29.3	2.1	670°C	866°C	799°C
		107	56.8	41.8	1.4	768°C	746°C	970°C
		108	66.8	31.2	2.0	632°C	854°C	836°C
		109	66.3	31.7	2.0	616°C	850°C	844°C
		110	69.9	27.6	2.5	693°C	877°C	755°C
		111	71.6	25.8	2.6	713°C	888°C	712°C
		112	68.1	29.5	2.4	667°C	865°C	803°C
		113	66.4	31.6	2.0	620°C	851°C	842°C
T2/2	1a	114	73.4	22.9	3.7	748°C	917°C	760°C
		115	71.9	24.6	3.5	730°C	906°C	753°C
		116	72.1	24.7	3.2	729°C	905°C	758°C
		117	75.3	20.5	4.2	770°C	931°C	819°C
		118	73.6	22.6	3.8	751°C	919°C	770°C
		119	55.5	42.9	1.6	821°C	758°C	1034°C
T19/1	2	120	67.3	30.2	2.5	745°C	696°C	917°C
		121	70.2	27.0	2.8	706°C	746°C	878°C
		122	73.3	23.7	3.0	652°C	782°C	828°C
		123	71.7	25.4	2.9	682°C	765°C	855°C
		124	71.0	26.0	3.0	691°C	758°C	864°C
		125	71.2	25.7	3.1	687°C	762°C	860°C
		126	71.2	25.9	2.9	690°C	759°C	863°C
		127	70.2	27.0	2.8	706°C	746°C	878°C
T19/3	1a	128	76.2	19.0	4.7	708°C	882°C	725°C
		129	77.9	17.5	4.6	725°C	893°C	772°C
		130	75.9	19.2	4.9	705°C	881°C	715°C
		131	75.4	20.7	3.9	685°C	870°C	740°C
		132	77.2	17.6	5.2	724°C	892°C	769°C

Table C.7. Temperature estimates for the Pokai Ignimbrite using titanomagnetite-ilmenite pairs (based on the method of Buddington and Lindsley 1964).

Sno. = sample number, i.e. host pumice;
Pumice type = crystal-poor: 1a and 1b; crystal-rich: 2 (see also Appendix D; Table D.2).
S_{Tm}/S_{Il} = analysis numbers for titanomagnetite and ilmenite microprobe analyses, respectively.
[k] = kaolinitised sample (85/1), possibly of Type 1a.

Sno.	Pumice type	S_{Mt}	S_{Il}	Temperature	Log (10) fO_2
26A/2	1a	8	1	793°C	-14.4
		9	1	794°C	-14.4
		10	1	792°C	-14.4
66/1	1b	12	2	829°C	-13.4
		13	2	837°C	-13.3
		14	2	825°C	-13.5
		15	2	830°C	-13.4
		12	3	808°C	-14.0
		13	3	815°C	-13.9
		14	3	804°C	-14.1
		15	3	809°C	-14.0
		12	4	801°C	-14.2
		13	4	808°C	-14.1
		14	4	797°C	-14.3
		15	4	802°C	-14.2
70e/1 (air-fall)	1b	20	5	815°C	-13.9
		21	5	839°C	-13.5
		22	5	807°C	-14.0
		23	5	812°C	-13.9
		24	5	817°C	-13.8
		25	5	812°C	-13.9
85/1[k]	(1a)	27	6	863°C	-10.9
97/3	2	29	7	819°C	-13.2
		30	7	819°C	-13.2
		31	7	823°C	-13.1
		32	7	865°C	-12.5
		29	8	824°C	-13.0
		30	8	824°C	-13.0
		31	8	828°C	-13.0
		32	8	871°C	-12.4
108/1	2	33	9	812°C	-13.3
		34	9	820°C	-13.2
		35	9	821°C	-13.1
		33	10	801°C	-13.6
		34	10	809°C	-13.5
		35	10	810°C	-13.5
		33	11	814°C	-13.2
		34	11	823°C	-13.1
		35	11	823°C	-13.1
		33	12	793°C	-13.9
		34	12	800°C	-13.8
		35	12	801°C	-13.8

Table C.7. cont.

Sno.	Pumice type	Magnetite	Ilmenite	Temperature	Log (10) fO_2
126/1	1a	36	13	796°C	-14.2
132/1	1b	37	14	812°C	-13.9
		38	14	813°C	-13.9
		39	14	825°C	-13.7
		40	14	815°C	-13.8
132/2	1a	41	15	876°C	-12.9
		42	15	780°C	-14.4
		41	16	846°C	-13.7
		42	16	758°C	-15.1
132/3	1b	43	17	790°C	-14.1
		44	17	872°C	-12.9
		45	17	803°C	-13.9
		46	17	1026°C	-10.7
		43	18	793°C	-14.1
		44	18	874°C	-12.8
		45	18	805°C	-13.9
		46	18	1030°C	-10.6
153/1	1b	47	19	764°C	-13.8
		48	19	919°C	-11.7
		49	19	857°C	-12.5
T2/2	1a	50	24	740°C	-14.5
		51	24	819°C	-13.4
		52	24	829°C	-13.2
		53	24	804°C	-12.9
		54	24	849°C	-12.9
T19/1	2	55	25	828°C	-12.9
		56	25	977°C	-10.9
		57	25	816°C	-13.1
		58	25	809°C	-13.2
		55	26	829°C	-12.9
		56	26	979°C	-10.8
		57	26	817°C	-13.1
		58	26	810°C	-13.2
		55	27	830°C	-12.9
		56	27	981°C	-10.8
		57	27	818°C	-13.1
		58	27	811°C	-13.2
T19/3	1a	59	28	741°C	-14.5
		60	28	749°C	-14.4
		62	28	795°C	-13.7
		63	28	788°C	-13.8
		64	28	826°C	-13.3
		59	29	747°C	-14.3
		60	29	755°C	-14.2
		62	29	801°C	-13.5
		63	29	794°C	-13.6
		64	29	833°C	-13.1

Table C.8. Plagioclase analyses of Chimp Ignimbrite pumices.

r = rim
c = core

Analysis #	1	2	3	4	5	6	7	8	9	10	11
Sample	33/1	33/1	33/1	33/1r	33/1c	33/1	33/1	33/1	33/1	33/1	33/4
SiO_2	59.65	58.86	60.20	59.83	59.71	59.16	60.17	59.26	59.99	61.50	60.19
TiO_2	-	0.03	0.02	-	-	-	0.03	-	-	-	-
Al_2O_3	23.72	24.41	23.93	24.52	24.77	24.54	24.08	24.88	24.47	23.56	24.63
FeO	0.18	0.25	0.30	0.24	0.26	0.25	0.28	0.27	0.26	0.20	0.27
MnO	-	-	-	-	-	-	-	-	-	-	0.02
CaO	7.74	8.05	7.59	7.77	8.10	7.94	7.56	7.62	7.82	6.55	8.09
Na_2O	7.11	6.78	7.08	7.07	7.04	6.94	7.18	6.71	7.04	7.60	7.20
K_2O	0.37	0.30	0.38	0.37	0.29	0.38	0.33	0.29	0.36	0.49	0.33
Total	98.77	98.68	99.50	99.80	100.17	99.21	99.63	99.03	99.94	99.90	100.73
Si^{+4}	10.80	10.67	10.81	10.72	10.67	10.67	10.79	10.68	10.73	10.96	10.70
Al^{+3}	5.06	5.22	5.06	5.18	5.22	5.22	5.09	5.28	5.16	4.95	5.16
Fe^{+3}	0.03	0.04	0.05	0.04	0.04	0.04	0.04	0.04	0.04	0.03	0.04
Ca^{+2}	1.50	1.56	1.46	1.49	1.55	1.53	1.45	1.47	1.50	1.25	1.54
Na^{+1}	2.49	2.38	2.46	2.46	2.44	2.43	2.50	2.35	2.44	2.63	2.48
K	0.09	0.07	0.09	0.09	0.06	0.09	0.07	0.07	0.08	0.11	0.07
Total	19.97	19.94	19.93	19.96	19.98	19.98	19.95	19.89	19.95	19.93	20.00
An	36.77	38.94	36.42	36.97	38.25	37.91	36.10	37.89	37.26	31.38	37.60
Ab	61.12	59.34	61.43	60.92	60.14	59.95	62.05	60.37	60.70	65.81	60.59
Or	2.12	1.72	2.15	2.11	1.61	2.14	1.85	1.74	2.04	2.81	1.81

Analysis #	12	13	14	15	16	17	18	19	20	21	22
Sample	33/4	33/4	93/1	93/1c	93/1r	93/1	146/1	146/1	146/1r	146/1c	146/1
SiO_2	60.08	59.96	59.64	60.42	58.56	59.80	59.60	59.63	61.40	61.62	60.34
TiO_2	-	-	-	-	-	-	0.03	-	0.03	-	-
Al_2O_3	24.81	24.90	24.25	24.63	25.55	24.31	24.36	24.00	23.21	23.48	23.69
FeO	0.30	0.21	0.29	0.21	0.37	0.28	0.20	0.20	0.20	0.16	0.20
MnO	0.03	-	-	-	0.03	-	-	-	-	-	-
MgO	-	-	-	-	-	-	-	-	-	-	0.02
CaO	8.01	8.23	8.04	8.18	9.26	8.21	7.97	7.77	6.05	6.38	7.09
Na_2O	7.13	7.01	7.12	7.12	6.56	7.04	7.09	6.68	7.97	7.78	7.48
K_2O	0.37	0.34	0.39	0.35	0.32	0.39	0.33	0.38	0.50	0.81	0.40
Total	100.73	100.65	99.73	100.91	100.65	100.03	99.58	98.66	99.36	100.23	99.22
Si^{+4}	10.68	10.66	10.71	10.72	10.46	10.71	10.71	10.79	11.00	10.97	10.86
Al^{+3}	5.20	5.22	5.13	5.15	5.38	5.13	5.16	5.12	4.90	4.93	5.02
Fe^{+3}	0.04	0.03	0.04	0.03	0.05	0.04	0.03	0.03	0.03	0.02	0.03
Ca^{+2}	1.52	1.57	1.55	1.55	1.77	1.58	1.53	1.51	1.16	1.22	1.37
Na^{+1}	2.46	2.42	2.48	2.45	2.27	2.44	2.47	2.34	2.77	2.68	2.61
K	0.08	0.08	0.09	0.08	0.07	0.09	0.08	0.09	0.12	0.18	0.09
Total	19.99	19.97	20.01	19.97	20.02	19.99	19.98	19.87	19.98	20.00	19.98
An	37.50	38.62	37.57	38.07	43.07	38.35	37.58	38.27	28.72	29.79	33.60
Ab	60.43	59.51	60.25	59.97	55.18	59.48	60.56	59.49	68.44	65.72	64.13
Or	2.07	1.87	2.18	1.96	1.75	2.18	1.87	2.24	2.84	4.49	2.27

Table C.8. cont.

r = rim

Analysis #	23	24	25
Sample	146/1r	146/1	146/1
SiO_2	59.68	59.57	60.23
Al_2O_3	23.79	23.98	24.30
FeO	0.24	0.19	0.24
CaO	7.90	7.78	7.57
Na_2O	7.16	6.49	7.03
K_2O	0.35	0.37	0.42
Total	99.12	98.38	99.79
Si^{+4}	10.77	10.80	10.78
Al^{+3}	5.06	5.12	5.13
Fe^{+3}	0.04	0.03	0.04
Ca^{+2}	1.53	1.51	1.45
Na^{+1}	2.51	2.28	2.44
K	0.08	0.09	0.10
Total	19.99	19.83	19.93
An	37.16	38.95	36.39
Ab	60.90	58.82	61.19
Or	1.95	2.23	2.42

Table C.9. Pyroxene analyses of Chimp Ignimbrite pumices.

Orthopyroxene

Analysis #	1	2	3	4
Sample	33/1	93/1	93/1	93/1
SiO_2	50.32	51.60	51.74	51.77
TiO_2	0.07	0.15	0.09	0.11
Al_2O_3	0.34	0.47	0.32	0.49
FeO	29.92	28.88	27.83	22.58
MnO	1.84	1.32	1.33	1.74
MgO	16.43	17.34	17.93	21.08
CaO	0.87	1.21	1.15	0.90
Na_2O	-	0.07	0.08	0.07
Total	99.79	101.04	100.47	98.74
SiIV	1.97	1.98	1.98	1.97
AlIV	0.02	0.02	0.01	0.02
Fe^{2+}	0.98	0.92	0.89	0.72
Mn	0.06	0.04	0.04	0.06
Mg	0.96	0.99	1.02	1.20
Ca	0.04	0.05	0.05	0.04
Na	-	0.01	0.01	0.01
Total	4.02	4.01	4.01	4.01
Wo	1.8	2.5	2.4	1.8
En	47.1	49.3	51.0	59.6
Fs	51.1	48.2	46.6	38.6
mg	49.5	51.7	53.5	62.5
Fe	0.52	0.49	0.48	0.39
F/F+M	0.659	0.635	0.619	0.536

Clinopyroxene

Analysis #	1	2
Sample	93/1	93/1
SiO_2	51.78	52.62
TiO_2	0.34	0.19
Al_2O_3	1.50	0.73
FeO	10.90	11.70
MnO	0.40	0.72
MgO	12.86	13.20
CaO	22.77	22.30
Na_2O	0.42	0.32
Total	100.97	101.78
SiIV	1.94	1.96
AlIV	0.06	0.03
AlVI	0.01	-
Ti	0.01	0.01
Fe^{2+}	0.34	0.36
Mn	0.01	0.02
Mg	0.72	0.73
Ca	0.91	0.89
Na	0.03	0.02
Total	4.03	4.03
Wo	46.0	44.3
En	36.2	36.5
Fs	17.8	19.3
mg	67.8	66.8
Fe	0.33	0.35
F/F+M	0.468	0.485

Table C.10. Titanomagnetite and ilmenite analyses of Chimp Ignimbrite pumices.

Titanomagnetite

Analysis #	1	2	3	4	5	6	7	8	9
Sample	33/1	33/1	33/1	33/1	33/4	93/1	93/1	93/1	146/1
SiO_2	0.06	0.04	0.09	0.08	0.08	0.05	0.08	0.04	0.08
TiO_2	11.41	11.05	11.21	10.83	10.98	8.87	11.21	7.40	11.14
Al_2O_3	1.49	1.47	1.43	1.43	1.45	1.64	1.64	1.54	1.49
FeO	80.90	81.30	79.71	80.69	80.65	85.06	82.82	83.96	81.54
MnO	0.67	0.77	0.75	0.75	0.53	0.61	0.68	0.82	0.68
MgO	0.66	0.66	0.58	0.62	0.64	1.08	1.28	1.12	0.50
CaO	-	-	0.01	0.01	-	0.03	-	-	0.02
Na_2O	-	-	-	-	-	0.04	-	0.05	0.07
K_2O	-	-	-	-	-	-	0.01	-	-
Total	95.19	95.29	93.78	94.41	94.33	97.38	97.72	94.93	95.52
Si	0.02	0.02	0.03	0.03	0.03	0.02	0.03	0.01	0.03
Ti	3.08	2.99	3.08	2.96	3.00	2.38	2.94	2.06	3.01
Al	0.63	0.62	0.62	0.61	0.62	0.69	0.67	0.67	0.63
Fe^{+2}	24.29	24.47	24.31	24.53	24.50	25.39	24.18	25.96	24.47
Mn	0.20	0.24	0.23	0.23	0.16	0.19	0.20	0.26	0.21
Mg	0.35	0.35	0.32	0.34	0.35	0.57	0.66	0.62	0.27
Ca	-	-	0.01	0.01	-	0.01	-	-	0.01
Na	-	-	-	-	-	0.03	-	0.03	0.05
K	-	-	-	-	-	-	0.01	-	-
Total	28.58	28.68	28.58	28.70	28.66	29.27	28.70	29.61	28.67

Ilmenite

Analysis #	1
Sample	146/1
SiO_2	0.06
TiO_2	47.64
Al_2O_3	0.09
FeO	48.38
MnO	1.15
MgO	1.21
CaO	0.08
Na_2O	0.14
Total	98.75
Ti	1.86
Al	0.01
Fe^{+2}	2.10
Mn	0.05
Mg	0.09
Ca	0.01
Na	0.01
Total	4.14

Table C.11. Pumice glass analyses of Chimp Ignimbrite.

Analysis #	1	2	3	4	5	6	7	8	9	10	11
Sample	33/1	33/1	33/1	33/1	33/4	33/4	33/4	93/1	93/1	146/1	146/1
SiO_2	76.13	75.53	75.32	75.28	75.97	76.26	74.89	75.26	74.74	75.01	75.16
TiO_2	0.18	0.16	0.16	0.16	0.16	0.17	0.14	0.24	0.19	0.15	0.16
Al_2O_3	12.08	11.92	11.99	11.72	12.23	12.22	12.13	11.91	11.71	11.80	11.76
FeO	1.59	1.51	1.63	1.65	1.69	1.62	1.43	1.43	1.35	1.36	1.65
MnO	-	0.05	0.06	-	0.05	0.05	0.04	0.04	0.04	0.05	0.07
MgO	0.14	0.13	0.13	0.13	0.12	0.10	0.11	0.18	0.18	0.13	0.13
CaO	1.13	1.13	1.11	1.12	1.18	1.09	1.17	1.34	1.32	1.19	1.10
Na_2O	2.91	2.97	2.88	2.98	2.92	3.06	3.15	2.93	3.11	3.15	3.00
K_2O	3.54	3.52	3.47	3.32	3.43	3.41	3.48	3.42	3.43	3.46	3.53
Total	97.70	96.92	96.75	96.36	97.75	97.98	96.54	96.75	96.07	96.30	96.56

Analysis #	12	13	14	15
Sample	146/1	146/1	146/1	146/1
SiO_2	75.42	73.45	74.88	74.98
TiO_2	0.20	0.18	0.13	0.17
Al_2O_3	11.86	12.19	11.91	12.04
FeO	1.67	1.17	1.75	1.63
MnO	0.09	0.05	0.05	0.03
MgO	0.13	0.10	0.12	0.11
CaO	1.14	1.10	1.16	1.12
Na_2O	3.37	3.18	3.06	3.21
K_2O	3.56	3.42	3.59	3.54
Total	97.44	94.84	96.65	96.83

Table C.12. Ab-An-Or compositions of plagioclase phenocrysts in the Chimp Ignimbrite pumices with temperature estimates at 0, 0.5 and 1 kb total pressures using plagioclase liquidus geothermometer (Kudo and Weill, 1971; Mathez, 1973).

Sno. = sample number, i.e. host pumice;
Pumice type = crystal-poor: A; crystal-rich: B (see also Appendix D; Table D.2).
S_{Pl} = analysis number for plagioclase microprobe analyses.

Sno	Pumice type	S_{Pl}	Ab	An	Or	0 kb	0.5 kb	1 kb
33/1	A	1	61.1	36.8	2.1	790°C	702°C	979°C
		2	59.3	38.9	1.7	809°C	754°C	999°C
		3	61.4	36.4	2.2	786°C	688°C	975°C
		4	60.9	37.0	2.1	792°C	709°C	981°C
		5	60.1	38.2	1.6	803°C	739°C	993°C
		6	59.9	37.9	2.2	800°C	732°C	990°C
		7	62.0	36.1	1.9	783°C	674°C	972°C
		8	60.4	37.9	1.7	800°C	732°C	990°C
		9	60.7	37.3	2.0	795°C	717°C	984°C
		10	65.8	31.4	2.8	732°C	759°C	921°C
33/4	A	11	60.6	37.6	1.8	767°C	734°C	964°C
		12	60.4	37.5	2.1	766°C	736°C	963°C
		13	59.5	38.6	1.9	778°C	711°C	974°C
93/1	B	14	60.2	37.6	2.2	768°C	651°C	942°C
		15	60.0	38.1	1.9	773°C	671°C	947°C
		16	55.2	43.0	1.8	814°C	770°C	991°C
		17	59.5	38.3	2.2	775°C	678°C	949°C
146/1	A	18	60.5	37.6	1.9	724°C	785°C	923°C
		19	59.5	38.3	2.2	733°C	777°C	931°C
		20	68.5	28.7	2.8	658°C	858°C	789°C
		21	65.7	29.8	4.5	637°C	851°C	812°C
		22	64.1	33.7	2.3	664°C	822°C	874°C
		23	60.9	37.1	2.0	718°C	791°C	917°C
		24	58.8	39.0	2.2	741°C	769°C	938°C
		25	61.2	36.4	2.4	708°C	798°C	909°C

Appendix D

Major element analyses and CIPW norms.

For major and trace element analyses the pumice samples were first carefully washed and ovendried at 120°C overnight. The samples were then crushed and transferred to a tungsten carbide swing mill and ground into approximately B.S. 240 mesh.
Fused glass beads for major element analyses were prepared using the general methods of Norrish and Hutton (1969), with modifications after Harvey et al. (1973) and Schroeder et al. (1980). Approximately 0.30 g of rock powder and 1.61 g flux (Lithium tetraborate, Lithium carbonate and Lanthanum oxide mix) plus a few grains of oxidant (NH_4NO_3) were used. The mixture was then fused in Pt/Au crucibles in an electric furnace at 1000°C for 20 minutes for each sample. After determination of loss on ignition (LOI), each melt was poured into an aluminium platten and pressed to form a bead.

Trace element concentrations were measured from 30 mm diameter pressed powder pellets (made by the methods of Norrish and Hutton, 1969) using ca. 6 g of rock powder mixed with 10-12 drops of polyvinyl alcohol binder.

X-ray Fluorescence

Major and trace element concentrations were determined at the University of Canterbury geochemistry laboratory using Philips PW 1400 X-ray spectrometer. The operation of the XRF was carried out by Mr. S. Brown. Major elements were analysed using Sc and Cr tubes, and trace elements using Au and Mo tubes. The detection limits for the University of Canterbury XRF-analyses are given in Table D.1.

Total iron is given as Fe_2O_3. CIPW norms have been calculated assuming an arbitrary iron oxide ratio of
$Fe_2O_3 = 1.0\ FeO$.

X-ray Diffraction

The presence of kaolinite in some samples was confirmed by X-ray diffraction on powdered rock samples, using a Philips PW 1540 manual diffractometer. The operation of the XRD was carried out by Mrs. C. Brown.

List of Tables

Table D.1. X-ray fluorescence detection limits (DL) and calibrated standard deviations (STD) for major and trace element determinations at the University of Canterbury (Weaver et al. 1990). Oxides in wt.%, trace elements in ppm.

	DL	STD
SiO_2	0.2	0.210
TiO_2	0.01	0.004
Al_2O_3	0.2	0.078
FeO_t	0.01	0.036
MnO	0.01	0.018
MgO	0.05	0.020
CaO	0.01	0.005
Na_2O	0.1	0.074
K_2O	0.01	0.033
P_2O_5	0.01	0.007
V	3	1.1
Cr	3	0.8
Ni	3	1.1
Zn	3	4.7
Zr	2	10
Nb	2	1.0
Ba	20	n.d.
La	5	2.5
Ce	5	3.1
Nd	10	1.3
Ga	2	0.9
Pb	1	1.7
Rb	1	1.6
Sr	1	0.5
Th	1	0.7
Y	1	2.7

Table D.2. List of all Pokai Ignimbrite pumices analysed by XRF. At localities where a stratigraphic section is exposed the elevation from the basement is given; if the actual basement is not exposed (confirmed by air-fall deposits), the minimum elevation is given, shown by >.

Rno = reference number
* = air-fall pumice (all other pumices are from ignimbrite flow units).
k = samples containing kaolinite.
m = samples with major analyses only.
GR = grid reference (New Zealand Topographical Map 260, 1:50000).
T = the compositional pumice type: crystal-poor, low to medium Sr = 1a and 1b, respectively; crystal-rich, high Sr = 2; for samples containing kaolinite or with major analyses only the pumice type is given in parenthesis and should be regarded as indicative only.
Lab no. = the geochemistry laboratory number, Geology Department, University of Canterbury.

Rno	Sample no. and locality	GR	T	Lab no.
1	1E/1 Puriri Rd	660294	1b	21906
2	1E/2 "	"	1b	21926
3	1E/3 "	"	1a	21927
4	1E/4 "	"	1b	21928
5	2A/1 Tikorangi Rd	803187	1b	21907
6	2A/2 "	"	1b	21929
7	2A/3 "	"	1b	21930
8	2A/4 "	"	1b	21931
9	2B/1^{k} "	"	(1a)	21908
10	2B/2^{k} "	"	(1a)	21932
11	3A/1 Tikorangi Rd	793197	1a	21909
12	3A/2 "	"	1b	21933
13	3B/1 "	"	1a	21910
14	3B/2 "	"	1b	21934
15	3B/3 "	"	1b	21935
16	3B/4 "	"	1b	21936
17	3B/5 "	"	1a	21937
18	3B/6 "	"	1b	21938
19	4/1 Tikorangi Rd	789198	1a	21911
20	4/2^{k} "	"	(1a)	21939
21	4/3 "	"	1a	21940
22	6B Galaxy Rd	671266	1b	21899

Table D.2. cont.

Rno	Sample no. and locality	GR	T	Lab no.
23	7 Galaxy Rd	678286	1b	21900
24	12A/1[k] Te Whetu	689335	(1b)	21903
25	12A/2[k] "	"	(1b)	21947
26	14 Downer Rd	674336	1b	21904
27	15/1[k] Downer Rd	666334	(1b)	21905
28	15/2[k] "	"	(1b)	21949
29	15/3[k] "	"	(1b)	21950
30	15/4[k] "	"	(1b)	21951
31	21D/1 Pukerimu Rd	777178	1b	21952
32	21D/2 "	"	1b	21953
33	21D/3 "	"	1b	21954
34	21D/4 "	"	1b	21955
35	*23D/1[k] Bat Rd	667289	(1b)	23158
36	23E/1 "	"	1b	22497
37	23E/2[k] "	"	(1b)	22498
38	26A/1 Harry Johnson Rd	810193	1b	22401
39	26A/2 "	"	1a	22402
40	26A/3 "	"	1b	22403
41	26A/4 "	"	1a	22404
42	26A/5 "	"	1a	22405
43	26A/6 "	"	1b	22406
44	R1/1[k] Pokai Rd 30 m	682268	(1b)	21887
45	R1/2[k] " 30 m	"	(1b)	21916
46	R1/3 " 30 m	"	1b	21917
47	R2/1 " 28 m	"	1a	21888
48	R3/1 " 25 m	"	1a	21889
49	R4/1 " 23 m	"	1b	21890
50	R5/1 " 21 m	"	1b	21891
51	R6/1 " 18.5 m	"	1b	21892
52	R6/2 " 18.5 m	"	1b	21918
53	R6/3 " 18.5 m	"	1b	21919

Table D.2. cont.

Rno	Sample no. and locality			GR	T	Lab no.
54	R8/1	"	14 m	"	1b	21894
55	R9/1	"	11 m	"	1b	21895
56	R10/1	"	9 m	"	1b	21896
57	R10/2	"	9 m	"	1b	21920
58	R11/1	"	6 m	"	1b	21897
59	R11/2	"	6 m	"	1a	21921
60	R11/3	"	6 m	"	1b	21922
61	R12/1	"	2 m	"	1b	21898
62	R12/2	"	2 m	"	1b	21923
63	*SWf1	"	0.2 m	"	1b	21059
64	*SWf3	"	0.2 m	"	1a	21061
65	*SWf4	"	0.2 m	"	1a	21062
66	*SWf7	"	0.2 m	"	1b	21065
67	*SWf9[k13]	"	0.2 m	"	(1b)	21067
68	P1/1[m]	Rauna Rd	>38 m	739177	(1b)	22109
69	P1/2	"	>38 m	"	1b	22110
70	P2/1	"	>35 m	"	1b	22111
71	P2/2[m]	"	>35 m	"	(1b)	22112
72	P3/1[m]	"	>30 m	"	(1a)	22114
73	P3/2[m]	"	>30 m	"	(1a)	22115
74	P7/1	"	>21 m	"	1b	22119
75	P7/2	"	>21 m	"	1b	22120
76	P7/3	"	>21 m	"	1b	22121
77	P9/1	"	>16 m	"	1b	22122
78	P9/2	"	>16 m	"	1b	22123
79	P9/3	"	>16 m	"	1b	22124
80	P11/1	"	>9 m	"	1a	22125
81	P11/2	"	>9 m	"	1b	22126
82	P12/1	"	>6 m	"	1a	22127

[13] Sample SWf9 was not available for XRD analysis, but the Al_2O_3 content of 16.18 % (anhydrous) indicates presence of kaolinite; this sample has thus been deleted from the main geochemical data together with the other kaolinite-bearing samples.

Table D.2. cont.

Rno	Sample no. and locality		GR	T	Lab no.
83	P13/1	Rauna Rd >3 m	739177	1b	22128
84	P13/2	" >3 m	"	1a	22129
85	P14/1	" road level	"	1b	22130
86	P14/2	" road level	"	1b	22131
87	46/1	Leslie Rd	595484	2	22412
88	46/2	"	"	2	22413
89	46/3	"	"	2	22414
90	HJ1/1[m]	Chamois Rd >82 m	801188	(1b)	21970
91	HJ1/2[m]	" >82 m	"	(1a)	21971
92	HJ1/3[m]	" >82 m	"	(1b)	21972
93	HJ1/4[m]	" >82 m	"	(1a)	21973
94	HJ2/1	" >72 m	"	1b	21956
95	HJ2/2	" >72 m	"	1a	21957
96	HJ3/1	" >65 m	"	1b	21958
97	HJ4/1	" >61 m	"	1b	21959
98	HJ5/1	" >57 m	"	1b	21960
99	HJ6/1	" >52 m	"	1b	21961
100	HJ7/1	" >49 m	"	1a	21962
101	HJ8/1	" >46 m	"	1a	21963
102	HJ8/2	" >46 m	"	1b	21964
103	HJ8/3	" >46 m	"	1a	21965
104	HJ9/1	" >42 m	"	1a	21966
105	HJ9/2	" >42 m	"	1b	21967
106	HJ9/3	" >42 m	"	1a	21968
107	HJ9/4	" >42 m	"	1b	21969
108	H13/1	" >34 m	"	1a	21974
109	H13/2	" >34 m	"	1b	21975
110	H14/1	" >30 m	"	1b	21976
111	H14/2	" >30 m	"	1b	21977
112	H15/1	" >25 m	"	1b	21978

Table D.2. cont.

Rno	Sample no. and locality	GR	T	Lab no.
113	H15/2 Chamois Rd >25 m	801188	(1b)	21979
114	H16/1 " >16 m	"	1b	21980
115	H17/1 " >6 m	"	1b	21981
116	H17/2 " >6 m	"	1a	21982
117	48/1 " road level	"	1b	21983
118	48/2 " road level	"	1b	21984
119	48/3 " road level	"	1b	21985
120	48/4 " road level	"	1b	21986
121	50A/1[k] Galaxy Rd	673261	(1a)	22415
122	50A/2[k] "	"	(1a)	22416
123	50A/3[k] "	"	(1a)	22417
124	*57/1[k] Glass Rd	795224	(2)	23160
125	*57/2[k] "	"	(2)	23161
126	*57/3 "	"	2	23162
127	62/3 Tikorangi Rd	786202	1a	22420
128	66/1 Chamois Rd	784167	1b	22422
129	66/2 "	"	1b	22423
130	*70/1[k] Galaxy Rd	673264	(1b)	22424
131	*70/2 "	"	1a	22425
132	*70/3 "	"	1a	22426
133	*70/4[k] "	"	(1a)	22427
134	*70/5[k] "	"	(1b)	22428
135	*70e/1 "	"	1b	22429
136	85/1[k] Mohina Rd	673311	(1a)	22430
137	85/2[k] "	"	(1b)	22431
138	85/3[k] "	"	(1b)	22432
139	85/4[k] "	"	(1b)	22433
140	85/5[k] "	"	(1a)	22434
141	85/6[k] "	"	(1b)	22435
142	91/1 Moorhouse Rd	625358	1b	22436

Table D.2. cont.

Rno	Sample no. and locality	GR	T	Lab no.
143	91/2 Moorhouse Rd	625358	1b	22437
144	91/3[k] "	"	(1b)	22438
145	97/1 Barron Rd	703194	1a	22445
146	97/2 "	"	2	22446
147	97/3 "	"	2	22447
148	97/4 "	"	1a	22448
149	98/1[k] Barron Rd	703193	(1b)	22449
150	98/2[k] "	"	(2)	22450
151	98/3 "	"	1a	22451
152	98/4 "	"	2	22452
153	108/1 McCracken Rd	723187	2	22453
154	108/2 "	"	2	22454
155	108/3 "	"	2	22455
156	108/4 "	"	2	22456
157	108/5 "	"	2	22457
158	108/6 "	"	2	22458
159	122/2[k] Jeff Rd	615312	(1a)	22460
160	122/3[k] "	"	(1b)	22461
161	122/4[k] "	"	(1b)	22462
162	126/1 Harry Johnson Rd	818187	1a	22463
163	126/2 "	"	1a	22464
164	126/3[k] "	"	(1a)	22465
165	126/4[k] "	"	(1b)	22466
166	126/5[k] "	"	(1b)	22467
167	126/6[k] "	"	(1a)	22468
168	127/1[k] Harry Johnson Rd	813191	(1b)	22469
169	127/2 "	"	1a	22470
170	127/3 "	"	1b	22471
171	127/4 "	"	1b	22472
172	127/5 "	"	1a	22473

Table D.2. cont.

Rno	Sample no. and locality	GR	T	Lab no.
173	127/6 Harry Johnson Rd	813191	1b	22474
174	131C1 Haunui Valley	885305	1b	22475
175	131C2 "	"	1b	22476
176	V18/1 " Pylon line >18 m	886294	1b	23177
177	V18/2 " >18 m	"	1b	23178
178	V18/3 " >18 m	"	1a	23179
179	132/1 " >22 m	"	1b	22477
180	132/2 " >22 m	"	1a	22478
181	132/3 " >22 m	"	1b	22479
182	132/4[k] " >22 m	"	(1b)	22480
183	132/5[k] " >22 m	"	(1b)	22481
184	132/6 " >22 m	"	1b	22482
185	132/7 " >22 m	"	1b	22483
186	132/8[k] " >22 m	"	(1b)	22484
187	V25/1 " >25 m	"	1b	23180
188	V25/2 " >25 m	"	1b	23181
189	V28/1[k] " >28 m	"	(1b)	23182
190	V28/2[k] " >28 m	"	(1b)	23183
191	V32/1 " >32 m	"	1b	23184
192	V32/2 " >32 m	"	1b	23185
193	V36/1[k] " >36 m	"	(1b)	23186
194	V36/2 " >36 m	"	1b	23187
195	V36/3[k] " >36 m	"	(1b)	23188
196	V39/1 " >39 m	"	1b	23189
197	V39/2 " >39 m	"	1b	23190
198	134/1[k] Haunui Valley	892303	(2)	22485
199	134/2 "	"	2	22486
200	134/3 "	"	2	22487
201	134/4 "	"	1b	22488
202	134/5[k] "	"	(2)	22489

Table D.2. cont.

Rno	Sample no. and locality	GR	T	Lab no.
203	134/6 Haunui Valley	892303	2	22490
204	135/1 Haunui Valley	895310	1b	22491
205	135/2 "	"	1b	22492
206	135/3 "	"	1b	22493
207	135/4[k] "	"	(1b)	22494
208	135/5 "	"	1b	22495
209	135/6 "	"	1b	22496
210	153/1 Cormorant Rd	642173	1b	23171
211	153/2 "	"	1b	23172
212	153/3 "	"	1b	23173
213	153/4[k] "	"	(1b)	23174
214	153b1 "	"	1b	23175
215	153b2 "	"	1b	23176
216	T1/1 Tapapa Valley track level	611540	1b	23191
217	T1/2 " track level	613538	1b	23192
218	T2/1 " >2 m	"	1b	23193
219	T2/2 " >2 m	"	1a	23194
220	T2/3 " >2 m	"	1a	23195
221	T7/1 " >7 m	"	2	23196
222	T7/2 " >7 m	"	2	23197
223	T11/1 " >11 m	"	2	23198
224	T11/2 " >11 m	"	2	23199
225	T15/1 " >15 m	612536	1a	23200
226	T15/2 " >15 m	"	1b	23201
227	T19/1 " >19 m	"	2	23202
228	T19/2[k] " >19 m	"	(2)	23203
229	T19/3 " >19 m	"	1a	23204
230	T19/4 " >19 m	"	2	23205
231	T24/1[k] " >24 m	"	(2)	23206
232	T24/2[k] " >24 m	"	(2)	23207

Table D.2. cont. List of all Chimp Ignimbrite pumices analysed by XRF.

Rno = reference number
k = samples containing kaolinite.
m = samples with major analyses only.
GR = grid reference (New Zealand Topographical Map 260, 1:50,000).
T = pumice type: crystal-poor = A; crystal-rich = B.
Lab no. = the geochemistry laboratory number, Geology Department, University of Canterbury.

Rno	Sample no. and locality	GR	T	Lab no.
233	11C/1 Te Whetu	688338	B	21901
234	11C/2 "	"	B	21946
235	11D^{m} "	"	A	21902
236	33/1 Pokai Rd	682268	A	22104
237	33/2 "	"	A	22105
238	33/3 "	"	A	22106
239	33/4 "	"	A	22107
240	33/5 "	"	A	22108
241	45A/1^{k} McDowall Rd	703329	A	22407
242	45B/1 "	703330	A	22409
243	45B/2 "	"	A	22410
244	45B/3 "	"	B	22411
245	76/1^{k} Road J (off Puriri Rd)	665290	A	23163
246	76/2 "	"	A	23164
247	76/3 "	"	B	23165
248	76/4 "	"	A	23166
249	93/1 Moorhouse Rd	637353	B	22440
250	93/2^{k} "	"	A	22441
251	93/3^{k} "	"	A	22442
252	93/4 "	"	A	22443
253	146/1 Redwoods Rd	619427	A	23167
254	146/2 "	"	A	23168
255	146/3 "	"	A	23169
256	146/4 "	"	A	23170

Table D.2. cont. List of all Whakamaru Ignimbrite pumices analysed by XRF; the major element analyses are given in Table D.7.

Rno = reference number
GR = grid reference (New Zealand Topographical Map 260, 1:50,000).
Lab no. = the geochemistry laboratory number, Geology Department, University of Canterbury.

Rno	Sample no. and locality	GR	Lab no.
257	1A/1 Puriri Rd	660294	21924
258	1A/2 "	"	21925
259	1A/3 "	"	21941
260	1A/4 "	"	21942
261	8 Road J (off Puriri Rd)	665290	21913
262	9/1 Puriri Rd	658296	21914
263	9/2 "	"	21944
264	9/3 "	"	21945

Table D.3. Major and trace element analyses and CIPW norms of the Pokai Ignimbrite.

Ref.no. #	1	2	3	4	5	6	7	8	9	10	11
Sample	1E/1	1E/2	1E/3	1E/4	2A/1	2A/2	2A/3	2A/4	2B/1	2B/2	3A/1
SiO_2	73.19	71.20	73.61	72.54	73.12	73.43	72.59	71.71	69.45	70.24	73.68
TiO_2	0.17	0.16	0.12	0.17	0.16	0.17	0.17	0.19	0.15	0.17	0.13
Al_2O_3	12.66	12.90	12.10	13.08	12.69	12.71	13.24	14.19	16.55	15.41	12.97
Fe_2O_3	1.85	1.87	1.52	1.87	1.77	1.86	1.92	1.95	1.69	1.88	1.57
MnO	0.08	0.08	0.07	0.10	0.09	0.07	0.06	0.06	0.08	0.06	0.08
MgO	0.14	0.24	0.17	0.15	0.16	0.16	0.12	0.17	0.10	0.14	0.12
CaO	1.03	1.06	0.86	1.06	1.08	1.05	1.00	1.04	0.68	0.91	0.80
Na_2O	3.83	4.35	4.08	3.97	3.82	3.65	3.64	3.47	3.28	3.57	3.68
K_2O	3.79	3.58	3.91	3.48	3.81	3.87	3.62	3.45	3.02	3.12	3.68
P_2O_5	0.02	0.03	0.03	0.02	0.01	0.02	0.02	0.03	0.02	0.02	0.02
LOI	3.38	2.62	3.46	3.27	2.87	3.08	3.61	3.69	5.07	4.14	3.32
Total	100.14	98.09	99.93	99.71	99.58	100.07	99.99	99.95	100.09	99.66	100.05
q	34.94	30.80	34.09	34.67	34.70	35.81	36.39	37.09	38.98	36.86	37.35
or	23.15	22.16	23.95	21.33	23.28	23.58	22.20	21.18	18.78	19.30	22.48
ab	33.49	38.56	35.79	34.83	33.42	31.84	31.96	30.50	29.21	31.63	32.19
an	5.15	5.30	3.27	5.32	5.47	5.24	5.01	5.16	3.41	4.59	3.97
C	0.45	0.01	-	0.94	0.35	0.68	1.62	3.04	7.05	4.77	1.58
di	-	-	0.79	-	-	-	-	-	-	-	-
hy	0.89	1.19	0.53	0.97	0.95	0.92	0.83	0.94	0.78	0.87	0.81
mt	1.46	1.49	1.20	1.48	1.40	1.46	1.52	1.54	1.36	1.50	1.24
il	0.33	0.32	0.24	0.33	0.31	0.33	0.33	0.37	0.30	0.34	0.26
ap	0.05	0.07	0.07	0.05	0.02	0.05	0.05	0.07	0.05	0.05	0.05
V	5	5	5	8	5	6	8	8	5	3	6
Cr	4	4	3	4	4	3	4	4	4	5	4
Ni	3	3	3	3	3	3	3	3	3	3	3
Zn	52	51	45	55	56	58	61	64	61	60	52
Zr	205	181	144	206	201	207	214	235	190	214	156
Nb	10	10	10	11	11	11	10	13	14	12	11
Ba	774	715	739	821	757	793	785	772	851	719	793
La	31	32	25	27	25	28	27	25	28	25	31
Ce	69	56	61	61	61	68	59	63	94	56	62
Nd	46	45	52	52	47	55	47	44	47	43	51
Ga	11	12	16	15	13	15	13	15	17	17	14
Pb	25	24	20	20	26	22	21	25	40	22	21
Rb	126	125	133	119	125	127	118	113	108	109	127
Sr	87	89	68	91	90	87	81	84	47	69	61
Th	14	13	15	15	15	12	12	15	22	17	14
Y	28	26	26	26	30	29	27	25	25	25	29
FeO*	1.66	1.68	1.37	1.68	1.59	1.67	1.73	1.75	1.52	1.69	1.41
F/F+M	0.926	0.880	0.894	0.922	0.913	0.916	0.937	0.914	0.941	0.926	0.926
K/Rb	249.7	237.8	244.1	242.8	253.0	253.0	254.7	253.5	232.1	237.6	240.6
K/Ba	40.7	41.6	43.9	35.2	41.8	40.5	38.3	37.1	29.5	36.0	38.5
Rb/Sr	1.45	1.40	1.96	1.31	1.39	1.46	1.46	1.35	2.30	1.58	2.08
Y/Nb	2.80	2.60	2.60	2.36	2.73	2.64	2.70	1.92	1.79	2.08	2.64

Table D.3. cont.

Ref.no. #	12	13	14	15	16	17	18	19	20	21	22
Sample	3A/2	3B/1	3B/2	3B/3	3B/4	3B/5	3B/6	4/1	4/2	4/3	6B
SiO_2	72.00	71.49	68.13	69.15	69.50	70.53	69.10	71.85	67.22	72.17	73.19
TiO_2	0.18	0.15	0.20	0.19	0.19	0.13	0.18	0.14	0.17	0.14	0.17
Al_2O_3	13.91	14.04	15.66	14.30	15.14	14.20	14.73	14.01	17.57	14.08	12.75
Fe_2O_3	1.95	1.88	2.43	2.25	2.37	1.80	2.24	1.74	2.14	1.78	1.84
MnO	0.09	0.06	0.11	0.07	0.07	0.08	0.09	0.09	0.06	0.05	0.04
MgO	0.19	0.16	0.16	0.13	0.19	0.12	0.16	0.07	0.13	0.11	0.17
CaO	1.07	0.88	1.05	1.11	0.96	0.80	1.13	0.78	0.75	0.76	1.02
Na_2O	3.84	3.71	3.36	4.07	3.46	3.89	4.19	3.75	3.44	3.82	4.04
K_2O	3.40	3.34	3.01	3.09	3.20	3.21	3.00	3.30	2.86	3.36	3.62
P_2O_5	0.03	0.03	0.03	0.02	0.02	0.03	0.03	0.01	0.02	0.02	0.02
LOI	3.75	4.20	5.13	4.18	4.76	4.61	4.55	4.19	5.53	3.75	3.02
Total	100.41	99.94	99.27	98.56	99.86	99.40	99.40	99.93	99.89	100.04	99.88
Q	35.08	36.40	36.47	32.70	36.33	35.40	32.02	36.99	36.30	36.49	34.33
or	20.79	20.62	18.90	19.35	19.89	20.01	18.69	20.37	17.91	20.62	22.09
ab	33.62	32.79	30.20	36.49	30.79	34.73	37.38	33.14	30.85	33.57	35.29
an	5.29	4.36	5.33	5.70	4.87	3.98	5.70	3.97	3.80	3.78	5.09
C	2.11	2.92	5.35	2.43	4.51	3.11	2.75	3.00	7.95	2.93	0.39
hy	1.06	0.96	1.19	0.98	1.17	0.91	1.11	0.75	0.95	0.79	0.89
mt	1.54	1.50	1.97	1.82	1.90	1.45	1.80	1.39	1.73	1.41	1.45
il	0.35	0.30	0.40	0.38	0.38	0.26	0.36	0.28	0.34	0.28	0.33
ap	0.07	0.07	0.07	0.05	0.05	0.07	0.07	0.02	0.05	0.05	0.05
V	8	6	8	9	9	8	7	6	6	5	5
Cr	5	4	5	3	3	4	4	4	4	3	4
Ni	3	3	4	3	5	3	3	3	3	3	3
Zn	58	60	69	67	64	71	71	54	67	61	51
Zr	224	183	259	228	250	153	223	167	219	173	211
Nb	10	12	12	11	12	12	9	11	14	11	12
Ba	755	722	642	680	704	687	648	815	600	823	789
La	28	30	25	27	27	27	27	30	22	37	26
Ce	75	62	70	64	67	67	69	71	47	80	62
Nd	46	43	42	42	43	45	39	48	38	48	45
Ga	13	13	19	15	17	12	18	18	17	14	14
Pb	25	23	25	23	26	21	22	23	21	24	22
Rb	115	117	108	108	108	115	104	117	97	115	124
Sr	86	68	89	90	77	54	87	58	57	56	86
Th	17	15	17	16	20	17	17	17	19	17	13
Y	28	28	28	26	26	28	27	27	22	29	27
FeO*	1.75	1.69	2.19	2.02	2.13	1.62	2.02	1.57	1.93	1.60	1.66
F/F+M	0.907	0.916	0.935	0.942	0.921	0.934	0.929	0.959	0.939	0.938	0.909
K/Rb	245.5	237.0	231.4	237.5	246.0	231.7	239.5	234.2	244.8	242.6	242.4
K/Ba	37.4	38.4	38.9	37.7	37.7	38.8	38.4	33.6	39.6	33.9	38.1
Rb/Sr	1.34	1.72	1.21	1.20	1.40	2.13	1.20	2.02	1.70	2.05	1.44
Y/Nb	2.80	2.33	2.33	2.36	2.17	2.33	3.00	2.45	1.57	2.64	2.25

Table D.3. cont.

Ref.no. #	23	24	25	26	27	28	29	30	31	32	33
Sample	7/RAK	12A/1	12A/2	14	15/1	15/2	15/3	15/4	21D/1	21D/2	21D/3
SiO_2	72.95	68.96	69.19	72.35	66.17	67.44	69.52	66.44	73.76	73.73	73.13
TiO_2	0.16	0.19	0.20	0.18	0.22	0.23	0.20	0.21	0.17	0.16	0.17
Al_2O_3	12.67	16.15	16.12	13.66	18.48	17.86	16.02	19.07	12.71	12.80	12.69
Fe_2O_3	1.78	2.21	2.21	1.90	2.44	2.51	2.17	2.46	1.80	1.68	1.83
MnO	0.06	0.06	0.09	0.05	0.09	0.09	0.10	0.10	0.08	0.06	0.09
MgO	0.08	0.11	0.15	0.18	0.14	0.15	0.12	0.15	0.11	0.10	0.17
CaO	1.00	1.00	1.07	1.04	0.98	1.04	1.00	0.89	0.97	1.01	1.07
Na_2O	4.00	3.43	3.64	3.81	3.35	3.37	3.62	3.21	3.88	3.76	3.70
K_2O	3.75	2.85	2.86	3.60	2.60	2.82	2.99	2.71	3.72	3.82	3.90
P_2O_5	0.02	0.02	0.03	0.02	0.02	0.03	0.01	0.02	0.02	0.03	0.02
LOI	3.21	4.63	4.44	3.41	5.38	4.77	4.28	5.73	3.02	3.17	2.92
Total	99.68	99.61	100.00	100.20	99.87	100.31	100.03	100.99	100.24	100.32	99.69
Q	34.12	37.47	35.96	34.88	36.17	35.98	35.98	36.75	35.53	35.83	35.09
or	22.97	17.73	17.69	21.98	16.26	17.44	18.45	16.81	22.61	23.24	23.82
ab	35.09	30.56	32.23	33.31	30.00	29.85	31.99	28.51	33.77	32.75	32.35
an	5.01	5.09	5.35	5.20	5.01	5.20	5.11	4.50	4.82	4.96	5.35
C	0.27	5.95	5.40	1.71	8.91	7.79	5.26	9.75	0.60	0.74	0.50
hy	0.69	0.89	1.03	0.94	1.06	1.09	0.95	1.12	0.79	0.70	0.98
mt	1.41	1.77	1.76	1.50	1.97	2.00	1.73	1.97	1.41	1.32	1.44
il	0.31	0.38	0.40	0.35	0.44	0.46	0.40	0.42	0.33	0.31	0.33
ap	0.05	0.05	0.07	0.05	0.05	0.07	0.02	0.05	0.05	0.07	0.05
V	5	4	5	6	3	4	4	5	5	5	6
Cr	3	4	4	3	7	4	3	4	4	4	4
Ni	3	3	3	3	3	3	3	3	3	3	3
Zn	49	68	70	60	70	69	64	70	48	50	49
Zr	199	255	266	236	296	306	255	280	210	204	205
Nb	10	14	13	11	13	13	14	14	10	10	11
Ba	772	879	848	774	850	835	821	845	835	850	820
La	26	35	33	28	39	36	37	39	28	28	28
Ce	64	88	71	60	77	71	81	81	62	64	64
Nd	43	46	50	47	42	48	52	48	46	56	53
Ga	15	17	20	15	23	17	17	21	14	12	15
Pb	20	31	29	24	31	28	31	29	24	25	22
Rb	120	103	101	115	92	95	103	91	121	128	126
Sr	86	84	91	91	83	90	85	72	89	88	89
Th	12	18	16	17	20	19	17	22	12	14	16
Y	27	32	30	28	34	32	34	34	28	29	29
FeO*	1.60	1.99	1.99	1.71	2.20	2.26	1.95	2.21	1.62	1.51	1.65
F/F+M	0.954	0.949	0.933	0.907	0.942	0.940	0.945	0.939	0.939	0.940	0.911
K/Rb	259.4	229.7	235.1	259.9	234.6	246.4	241.0	247.2	255.2	247.8	257.0
K/Ba	40.3	26.9	28.0	38.6	25.4	28.0	30.2	26.6	37.0	37.3	39.5
Rb/Sr	1.40	1.23	1.11	1.26	1.11	1.06	1.21	1.26	1.36	1.45	1.42
Y/Nb	2.70	2.29	2.31	2.55	2.62	2.46	2.43	2.43	2.80	2.90	2.64

Table D.3. cont.

Ref.no. #	34	35	36	37	38	39	40	41	42	43	44
Sample	21D/4	23D/1	23E/1	23E/2	26A/1	26A/2	26A/3	26A/4	26A/5	26A/6	R1/1
SiO_2	73.67	66.31	71.71	69.69	71.33	71.41	72.01	74.37	74.85	72.33	70.85
TiO_2	0.06	0.21	0.21	0.19	0.17	0.17	0.20	0.13	0.12	0.21	0.20
Al_2O_3	12.66	16.88	14.00	14.68	14.61	13.83	13.71	12.96	12.12	13.34	14.62
Fe_2O_3	1.78	2.41	2.04	2.10	2.02	1.73	1.95	1.46	1.29	1.94	2.01
MnO	0.05	0.08	0.07	0.08	0.07	0.05	0.06	0.04	0.04	0.06	0.10
MgO	0.16	0.05	0.14	0.12	0.18	0.16	0.17	0.11	0.09	0.17	0.17
CaO	1.01	1.03	1.09	1.06	1.10	0.94	1.06	0.78	0.71	1.13	1.07
Na_2O	3.73	3.39	4.14	4.03	3.72	3.81	3.85	3.59	3.43	3.95	3.82
K_2O	3.95	2.70	3.08	2.90	3.31	3.23	3.44	3.72	4.12	3.36	3.26
P_2O_5	0.03	0.02	0.02	0.02	0.01	0.01	0.01	0.01	0.01	0.01	0.01
LOI	3.01	5.56	3.80	3.83	3.97	4.06	3.49	3.35	3.17	3.15	3.62
Total	100.11	98.64	100.30	98.70	100.49	99.40	99.95	100.52	99.95	99.65	99.73
Q	35.28	36.25	34.33	34.25	35.41	36.16	34.98	38.36	38.60	34.87	34.73
or	24.04	17.14	18.86	18.07	20.27	20.02	21.08	22.62	25.16	20.58	20.05
ab	32.51	30.82	36.30	35.95	32.61	33.82	33.77	31.26	29.99	34.64	33.63
an	4.96	5.35	5.47	5.41	5.59	4.82	5.38	3.92	3.57	5.74	5.46
C	0.50	7.04	1.99	3.20	3.04	2.50	1.81	1.68	0.78	1.22	3.00
hy	1.04	0.82	0.87	0.91	1.04	0.85	0.92	0.66	0.57	0.90	1.02
mt	1.40	1.97	1.61	1.69	1.60	1.38	1.54	1.15	1.02	1.53	1.59
il	0.12	0.43	0.41	0.38	0.33	0.34	0.39	0.25	0.24	0.41	0.40
ap	0.07	0.05	0.05	0.05	0.02	0.02	0.02	0.02	0.02	0.02	0.02
V	5	3	7	6	6	3	5	6	8	5	6
Cr	3	4	3	3	3	4	4	4	4	3	4
Ni	3	3	3	3	3	3	3	3	3	3	3
Zn	51	63	58	59	56	51	52	45	39	57	60
Zr	196	243	205	240	233	171	225	133	106	216	244
Nb	9	13	12	10	13	13	11	12	11	12	11
Ba	819	898	767	824	882	871	834	842	848	806	860
La	29	32	28	27	30	30	31	28	29	25	37
Ce	62	73	72	83	98	70	69	64	72	75	80
Nd	49	40	53	52	54	53	51	53	53	52	55
Ga	13	19	16	16	17	16	17	17	16	16	17
Pb	24	25	24	28	28	21	21	18	19	19	26
Rb	129	97	113	113	113	115	117	125	140	118	110
Sr	84	85	88	89	88	67	86	53	46	94	92
Th	14	18	16	18	18	18	15	18	15	13	16
Y	27	30	27	25	26	30	27	26	29	26	33
N	5	0	2	2	20	20	20	20	20	20	30
FeO*	1.60	2.17	1.84	1.89	1.82	1.56	1.75	1.31	1.16	1.75	1.81
F/F+M	0.912	0.978	0.932	0.943	0.913	0.909	0.914	0.925	0.930	0.914	0.918
K/Rb	254.2	231.1	226.3	213.1	243.2	233.2	244.1	247.1	244.3	236.4	246.0
K/Ba	40.0	25.0	33.3	29.2	31.2	30.8	34.2	36.7	40.3	34.6	31.5
Rb/Sr	1.54	1.14	1.28	1.27	1.28	1.72	1.36	2.36	3.04	1.26	1.20
Y/Nb	3.00	2.31	2.25	2.50	2.00	2.31	2.45	2.17	2.64	2.17	3.00

Table D.3. cont.

Ref.no. #	45	46	47	48	49	50	51	52	53	54	55
Sample	R1/2	R1/3	R2/1	R3/1	R4/1	R5/1	R6/1	R6/2	R6/3	R8/1	R9/1
SiO_2	69.55	70.91	73.08	73.44	72.81	73.42	73.76	73.47	72.88	73.73	73.13
TiO_2	0.21	0.19	0.15	0.13	0.18	0.17	0.17	0.17	0.17	0.16	0.17
Al_2O_3	16.08	14.44	13.66	13.78	13.22	12.91	12.71	12.73	12.57	12.80	12.69
Fe_2O_3	2.26	2.00	1.71	1.51	1.87	1.66	1.80	1.84	1.84	1.68	1.83
MnO	0.10	0.10	0.09	0.07	0.09	0.08	0.08	0.08	0.07	0.06	0.09
MgO	0.09	0.12	0.05	0.05	0.13	0.09	0.11	0.11	0.13	0.10	0.17
CaO	0.97	1.00	0.83	0.72	1.01	0.96	0.97	0.95	0.95	1.01	1.07
Na_2O	3.55	3.83	3.68	3.54	3.62	3.91	3.88	3.76	3.89	3.76	3.70
K_2O	3.07	3.16	3.60	3.68	3.75	3.65	3.72	3.77	3.64	3.82	3.90
P_2O_5	0.02	0.02	0.02	0.02	0.02	0.01	0.02	0.03	0.02	0.03	0.02
LOI	4.48	3.41	3.37	3.67	3.09	3.37	3.02	2.73	2.67	3.17	2.92
Total	100.38	99.18	100.24	100.61	99.79	100.23	100.24	99.64	98.83	100.32	99.69
Q	36.19	35.51	37.02	38.17	36.05	35.45	35.53	35.93	35.28	35.83	35.09
or	18.92	19.50	21.96	22.43	22.92	22.27	22.61	22.99	22.37	23.24	23.82
ab	31.32	33.84	32.15	30.90	31.68	34.16	33.77	32.83	34.23	32.75	32.35
an	4.88	5.04	4.12	3.55	5.05	4.85	4.82	4.66	4.77	4.96	5.35
C	5.42	3.08	2.32	2.80	1.47	0.83	0.60	0.83	0.57	0.74	0.50
hy	0.89	0.91	0.66	0.58	0.88	0.69	0.79	0.81	0.85	0.70	0.98
mt	1.80	1.59	1.35	1.19	1.47	1.31	1.41	1.45	1.46	1.32	1.44
il	0.42	0.38	0.29	0.25	0.35	0.33	0.33	0.33	0.34	0.31	0.33
ap	0.05	0.05	0.05	0.05	0.05	0.02	0.05	0.07	0.05	0.07	0.05
V	4	5	4	5	6	3	5	5	6	5	6
Cr	4	3	5	3	4	3	4	3	3	4	4
Ni	3	3	3	3	4	3	3	3	3	3	3
Zn	67	60	52	43	58	52	48	51	51	50	49
Zr	265	2	179	152	220	203	210	207	206	204	205
Nb	13	12	12	10	11	13	10	11	11	10	11
Ba	905	882	878	907	916	847	835	833	824	850	820
La	34	37	33	32	30	28	28	27	24	28	28
Ce	73	84	75	68	71	68	62	62	52	64	64
Nd	51	52	51	54	50	47	46	43	47	56	53
Ga	17	17	15	14	16	13	14	14	11	12	15
Pb	24	24	23	23	24	23	24	24	25	25	22
Rb	103	109	121	123	123	119	121	126	125	128	126
Sr	85	88	68	55	92	87	89	87	87	88	89
Th	16	18	16	18	14	16	12	15	12	14	16
Y	34	37	30	31	31	29	28	28	28	29	29
FeO*	2.03	1.80	1.54	1.36	1.68	1.49	1.62	1.66	1.66	1.51	1.65
F/F+M	0.960	0.941	0.970	0.966	0.932	0.946	0.939	0.940	0.930	0.940	0.911
K/Rb	247.4	240.7	247.0	248.4	253.1	254.6	255.2	248.4	241.8	247.8	257.0
K/Ba	28.2	29.7	34.0	33.7	34.0	35.8	37.0	37.6	36.7	37.3	39.5
Rb/Sr	1.21	1.24	1.78	2.24	1.34	1.37	1.36	1.45	1.44	1.45	1.42
Y/Nb	2.62	3.08	2.50	3.10	2.82	2.23	2.80	2.55	2.55	2.90	2.64

Table D.3. cont.

Ref.no. #	56	57	58	59	60	61	62	63	64	65	66
Sample	R10/1	R10/2	R11/1	R11/2	R11/3	R12/1	R12/2	SWf1	SWf3	SWf4	SWf7
SiO_2	73.67	73.12	73.96	74.69	73.68	73.74	73.92	72.35	73.40	72.09	71.78
TiO_2	0.06	0.17	0.16	0.13	0.16	0.16	0.16	0.19	0.13	0.13	0.17
Al_2O_3	12.66	12.71	12.47	12.26	12.66	12.65	12.65	13.47	13.30	13.07	13.88
Fe_2O_3	1.78	1.81	1.86	1.51	1.79	1.82	1.80	1.97	1.52	1.54	1.95
MnO	0.05	0.07	0.08	0.06	0.07	0.08	0.06	0.10	0.08	0.09	0.08
MgO	0.16	0.16	0.20	0.13	0.13	0.18	0.16	0.15	0.10	0.06	0.10
CaO	1.01	1.05	1.06	0.83	1.08	1.08	1.06	1.10	0.74	0.75	1.07
Na_2O	3.73	3.75	4.17	3.60	4.01	3.89	3.65	4.09	3.69	3.55	3.76
K_2O	3.95	3.76	3.59	4.01	3.69	3.58	3.79	3.35	3.68	3.56	3.28
P_2O_5	0.03	0.02	0.02	0.01	0.02	0.02	0.02	0.02	0.02	0.01	0.01
LOI	3.01	1.89	2.68	1.79	2.57	3.10	3.07	3.20	3.48	4.20	3.38
Total	100.11	98.51	100.25	99.02	99.86	100.30	100.34	99.99	100.14	99.05	99.46
Q	35.28	35.46	34.13	37.30	34.49	35.65	36.51	34.05	37.20	37.87	36.11
or	24.04	23.00	21.74	24.37	22.41	21.77	23.03	20.45	22.50	22.18	20.17
ab	32.51	32.84	36.16	31.33	34.88	33.86	31.75	35.76	32.30	31.67	33.11
an	4.96	5.26	4.82	4.17	5.37	5.38	5.27	5.50	3.66	3.85	5.46
C	0.50	0.63	-	0.53	0.16	0.47	0.68	1.20	2.02	2.15	2.31
di	-	-	0.36	-	-	-	-	-	-	-	-
hy	1.04	0.91	0.88	0.77	0.84	1.00	0.90	0.96	0.74	0.67	0.83
mt	1.40	1.43	1.45	1.18	1.40	1.43	1.41	1.55	1.20	1.24	1.55
il	0.12	0.33	0.31	0.25	0.31	0.31	0.31	0.37	0.26	0.26	0.34
ap	0.07	0.05	0.05	0.02	0.05	0.05	0.05	0.05	0.05	0.02	0.02
V	5	5	7	5	7	4	5	8	8	7	6
Cr	3	4	3	3	3	3	4	3	3	3	3
Ni	3	3	3	3	3	3	3	3	3	3	3
Zn	51	54	53	48	51	54	51	60	55	53	59
Zr	196	205	199	153	190	204	198	237	160	159	220
Nb	9	10	11	8	10	9	10	10	10	10	12
Ba	819	838	790	828	801	820	808	813	895	887	876
La	29	27	28	27	25	28	25	30	25	33	33
Ce	62	57	66	59	51	74	62	68	67	67	68
Nd	49	45	45	50	48	45	46	40	40	40	40
Ga	13	15	14	12	13	15	17	16	11	15	14
Pb	24	25	24	19	22	24	20	21	24	27	26
Rb	129	124	126	130	126	124	125	112	125	127	113
Sr	84	86	88	62	90	89	88	95	58	59	93
Th	14	12	13	14	14	13	14	13	16	14	12
Y	27	28	28	29	27	28	28	36	37	37	37
FeO*	1.60	1.63	1.67	1.36	1.61	1.64	1.62	1.77	1.37	1.39	1.75
F/F+M	0.912	0.914	0.898	0.916	0.928	0.905	0.913	0.926	0.935	0.961	0.948
K/Rb	254.2	251.7	236.5	256.1	243.1	239.7	251.7	248.3	244.4	232.7	241.0
K/Ba	40.0	37.3	37.7	40.2	38.2	36.2	38.9	34.2	34.1	33.3	31.1
Rb/Sr	1.54	1.44	1.43	2.10	1.40	1.39	1.42	1.18	2.16	2.15	1.22
Y/Nb	3.00	2.80	2.55	3.63	2.70	3.11	2.80	3.60	3.70	3.70	3.08

Table D.3. cont.

Ref.no. #	67	68	69	70	71	72	73	74	75	76	77
Sample	SW19	P1/1	P1/2	P2/1	P2/2	P3/1	P3/2	P7/1	P7/2	P7/3	P9/1
SiO_2	69.77	70.56	70.67	72.36	72.37	73.64	73.73	72.84	73.43	72.94	73.35
TiO_2	0.20	0.18	0.20	0.16	0.16	0.15	0.14	0.17	0.16	0.17	0.16
Al_2O_3	15.48	14.80	14.60	13.46	13.53	12.69	12.97	12.91	13.01	12.97	12.57
Fe_2O_3	2.20	2.24	2.27	2.00	2.02	1.65	1.80	1.96	1.96	1.95	1.92
MnO	0.09	0.04	0.07	0.06	0.08	0.03	0.04	0.04	0.08	0.06	0.05
MgO	0.11	0.09	0.12	0.12	0.12	0.05	0.08	0.11	0.15	0.14	0.12
CaO	1.05	0.92	0.93	0.89	0.88	0.76	0.72	1.04	0.98	0.99	1.04
Na_2O	3.61	3.57	3.61	3.72	3.69	3.45	3.32	3.87	3.70	3.60	3.72
K_2O	3.12	3.32	3.40	3.64	3.68	3.58	3.74	3.49	3.67	3.67	3.77
P_2O_5	0.02	0.02	0.02	0.02	0.02	0.02	0.03	0.02	0.03	0.02	0.03
LOI	3.92	3.92	3.75	3.37	3.42	3.69	3.78	2.96	3.16	3.33	3.11
Total	99.57	99.66	99.64	99.80	99.97	99.71	100.35	99.41	100.33	99.84	99.84
Q	35.75	36.33	35.74	35.79	35.78	39.63	39.67	35.68	36.39	36.73	35.91
or	19.28	20.49	20.95	22.31	22.53	22.03	22.89	21.38	22.32	22.47	23.03
ab	31.94	31.55	31.86	32.64	32.34	30.40	29.09	33.95	32.22	31.56	32.54
an	5.31	4.63	4.68	4.44	4.39	3.79	3.50	5.21	4.80	4.95	5.13
C	4.50	3.87	3.48	1.90	1.99	1.88	2.30	0.96	1.28	1.37	0.57
hy	0.92	0.82	0.93	0.88	0.92	0.53	0.69	0.78	0.97	0.89	0.82
mt	1.75	1.78	1.81	1.58	1.60	1.31	1.42	1.55	1.54	1.54	1.51
il	0.40	0.36	0.40	0.32	0.31	0.30	0.28	0.33	0.31	0.33	0.31
ap	0.05	0.05	0.05	0.05	0.05	0.05	0.07	0.05	0.07	0.05	0.07
V	6	n.a.	5	5	n.a.	n.a.	n.a.	6	7	4	6
Cr	3	n.a.	5	4	n.a.	n.a.	n.a.	3	3	3	4
Ni	3	n.a.	3	3	n.a.	n.a.	n.a.	3	3	3	3
Zn	64	n.a.	52	50	n.a.	n.a.	n.a.	49	49	47	49
Zr	254	n.a.	254	191	n.a.	n.a.	n.a.	205	198	200	191
Nb	12	n.a.	12	10	n.a.	n.a.	n.a.	11	9	9	9
Ba	934	n.a.	703	741	n.a.	n.a.	n.a.	734	756	751	777
La	30	n.a.	30	28	n.a.	n.a.	n.a.	23	28	27	26
Ce	64	n.a.	62	55	n.a.	n.a.	n.a.	54	52	58	63
Nd	40	n.a.	44	53	n.a.	n.a.	n.a.	48	45	47	49
Ga	18	n.a.	16	17	n.a.	n.a.	n.a.	13	17	11	15
Pb	23	n.a.	24	23	n.a.	n.a.	n.a.	25	22	22	23
Rb	106	n.a.	116	124	n.a.	n.a.	n.a.	116	119	122	123
Sr	92	n.a.	87	81	n.a.	n.a.	n.a.	90	84	86	87
Th	14	n.a.	14	13	n.a.	n.a.	n.a.	12	15	15	12
Y	36	n.a.	28	27	n.a.	n.a.	n.a.	26	27	27	28
FeO*	1.98	2.02	2.04	1.80	1.82	1.48	1.62	1.76	1.76	1.75	1.73
F/F+M	0.950	0.958	0.946	0.939	0.941	0.968	0.954	0.943	0.925	0.928	0.937
K/Rb	244.4	0.0	243.3	243.7	0.0	0.0	0.0	249.8	256.0	249.7	254.5
K/Ba	27.7	0.0	40.2	40.8	0.0	0.0	0.0	39.5	40.3	40.6	40.3
Rb/Sr	1.15	0.00	1.33	1.53	0.00	0.00	0.00	1.29	1.42	1.42	1.41
Y/Nb	3.00	0.00	2.33	2.70	0.00	0.00	0.00	2.36	3.00	3.00	3.11

n.a. = not analysed

Table D.3. cont.

Ref.no. #	78	79	80	81	82	83	84	85	86	87	88
Sample	P9/2	P9/3	P11/1	P11/2	P12/1	P13/1	P13/2	P14/1	P14/2	46/1	46/2
SiO_2	73.81	72.31	74.16	72.62	72.79	73.22	73.41	72.30	72.74	71.66	71.22
TiO_2	0.17	0.17	0.14	0.17	0.13	0.15	0.13	0.17	0.17	0.36	0.28
Al_2O_3	12.76	13.80	12.25	13.34	12.69	11.96	12.88	13.03	12.86	13.14	12.95
Fe_2O_3	1.99	2.07	1.73	1.97	1.62	1.74	1.53	1.91	1.87	2.28	2.10
MnO	0.09	0.08	0.06	0.08	0.08	0.10	0.10	0.08	0.08	0.09	0.08
MgO	0.14	0.16	0.09	0.16	0.10	0.13	0.13	0.16	0.15	0.41	0.38
CaO	0.99	1.06	0.84	1.09	0.83	1.03	0.78	1.04	1.02	1.26	1.27
Na_2O	3.65	3.80	3.60	3.75	3.60	3.66	3.52	3.83	3.86	4.29	4.45
K_2O	3.65	3.47	3.76	3.58	3.74	3.57	3.78	3.65	3.53	3.32	3.17
P_2O_5	0.02	0.03	0.02	0.01	0.02	0.03	0.02	0.03	0.03	0.01	0.01
LOI	3.22	3.40	3.39	3.52	3.33	3.93	4.58	4.28	3.68	3.66	2.75
Total	100.49	100.35	100.04	100.29	98.93	99.52	100.86	100.48	99.99	100.48	98.66
Q	37.08	35.31	38.00	35.45	37.07	37.35	37.84	34.75	35.53	31.55	31.07
or	22.18	21.15	22.99	21.86	23.12	22.07	23.20	22.42	21.66	20.26	19.53
ab	31.75	33.17	31.52	32.79	31.86	32.40	30.94	33.69	33.91	37.49	39.26
an	4.92	5.22	4.18	5.52	4.17	5.14	3.88	5.16	5.05	6.39	6.26
C	1.08	2.00	0.81	1.38	1.32	0.29	1.69	1.00	0.94	0.23	-
di	-	-	-	-	-	-	-	-	-	-	0.20
hy	0.96	1.02	0.73	0.99	0.78	0.91	0.86	0.97	0.93	1.43	1.33
mt	1.56	1.63	1.37	1.55	1.29	1.39	1.21	1.51	1.48	1.80	1.67
il	0.33	0.33	0.28	0.33	0.26	0.30	0.26	0.34	0.34	0.71	0.55
ap	0.05	0.07	0.05	0.02	0.05	0.07	0.05	0.07	0.07	0.02	0.02
V	5	4	5	5	5	4	5	5	5	8	7
Cr	3	4	3	5	3	3	3	3	3	4	3
Ni	3	3	3	3	3	3	3	3	3	3	3
Zn	49	52	48	52	48	49	46	55	52	58	56
Zr	202	206	155	192	150	199	147	226	205	237	230
Nb	10	10	11	11	11	9	11	11	12	11	12
Ba	758	815	797	747	798	924	781	771	793	827	722
La	25	24	24	26	26	23	25	28	25	28	28
Ce	63	56	61	65	64	58	64	72	64	67	60
Nd	45	50	50	50	51	47	50	53	46	49	51
Ga	14	13	15	11	14	14	14	17	14	15	15
Pb	23	26	23	24	20	20	20	24	25	24	26
Rb	120	117	125	119	124	123	126	121	121	115	106
Sr	81	89	64	90	63	90	57	85	83	111	111
Th	12	14	14	13	14	14	14	15	14	13	10
Y	27	25	28	25	27	25	27	26	27	31	29
FeO*	1.79	1.86	1.56	1.77	1.46	1.57	1.38	1.72	1.68	2.05	1.89
F/F+M	0.931	0.924	0.947	0.921	0.939	0.928	0.919	0.918	0.922	0.839	0.838
K/Rb	252.5	246.2	249.7	249.8	250.4	241.0	249.1	250.4	242.2	239.7	248.3
K/Ba	40.0	35.3	39.2	39.8	38.9	32.1	40.2	39.3	37.0	33.3	36.5
Rb/Sr	1.48	1.31	1.95	1.32	1.97	1.37	2.21	1.42	1.46	1.04	0.95
Y/Nb	2.70	2.50	2.55	2.27	2.45	2.78	2.45	2.36	2.25	2.82	2.42

Table D.3. cont.

Ref.no. #	89	90	91	92	93	94	95	96	97	98	99
Sample	46/3	HJ1/1	HJ1/2	HJ1/3	HJ1/4	HJ2/1	HJ2/2	HJ3/1	HJ4/1	HJ5/1	HJ6/1
SiO_2	71.83	69.39	73.66	71.02	71.18	71.62	74.02	72.80	73.51	73.87	72.03
TiO_2	0.28	0.19	0.13	0.18	0.15	0.18	0.11	0.16	0.17	0.17	0.17
Al_2O_3	13.55	15.03	12.81	14.17	14.63	13.74	12.83	13.33	12.84	12.53	13.26
Fe_2O_3	2.09	2.24	1.54	2.01	1.84	2.00	1.48	1.86	1.89	1.86	1.95
MnO	0.07	0.06	0.10	0.07	0.07	0.08	0.05	0.08	0.05	0.06	0.05
MgO	0.28	0.14	0.11	0.15	0.10	0.13	0.10	0.09	0.18	0.19	0.15
CaO	1.26	0.94	0.84	0.97	0.76	1.01	0.67	0.92	1.06	1.06	1.04
Na_2O	4.16	3.18	3.88	3.60	3.18	3.70	3.48	3.52	3.94	3.83	3.72
K_2O	3.33	3.37	3.59	3.50	3.56	3.44	3.96	3.64	3.60	3.73	3.36
P_2O_5	0.01	0.02	0.02	0.01	0.02	0.03	0.02	0.02	0.02	0.02	0.03
LOI	3.56	4.25	2.88	3.90	4.61	4.07	3.34	3.55	3.09	2.87	3.38
Total	100.42	98.81	99.56	99.58	100.10	100.00	100.06	99.97	100.35	100.19	99.14
Q	32.64	37.61	36.42	35.71	38.85	35.87	38.15	37.44	35.08	35.55	36.49
or	20.32	21.06	21.94	21.62	22.03	21.19	24.20	22.31	21.87	22.65	20.74
ab	36.34	28.46	33.96	31.84	28.18	32.64	30.45	30.89	34.28	33.30	32.87
an	6.39	4.79	4.18	4.96	3.81	5.02	3.30	4.60	5.27	5.27	5.18
C	0.86	4.75	1.10	2.84	4.41	2.26	1.70	2.05	0.60	0.32	1.76
hy	1.13	0.98	0.81	0.95	0.81	0.91	0.70	0.79	0.95	0.98	0.90
mt	1.65	1.81	1.21	1.60	1.47	1.59	1.17	1.47	1.48	1.46	1.55
il	0.55	0.38	0.26	0.36	0.30	0.36	0.22	0.32	0.33	0.33	0.34
ap	0.02	0.05	0.05	0.02	0.05	0.07	0.05	0.05	0.05	0.05	0.07
V	8	n.a.	n.a.	n.a.	n.a.	6	4	6	7	6	7
Cr	4	n.a.	n.a.	n.a.	n.a.	4	3	3	4	4	3
Ni	3	n.a.	n.a.	n.a.	n.a.	3	3	3	3	3	3
Zn	54	n.a.	n.a.	n.a.	n.a.	51	44	51	56	64	56
Zr	226	n.a.	n.a.	n.a.	n.a.	229	124	202	210	204	218
Nb	12	n.a.	n.a.	n.a.	n.a.	11	12	12	10	10	10
Ba	802	n.a.	n.a.	n.a.	n.a.	746	782	735	762	765	736
La	27	n.a.	n.a.	n.a.	n.a.	27	29	27	32	31	22
Ce	62	n.a.	n.a.	n.a.	n.a.	69	67	60	68	64	55
Nd	53	n.a.	n.a.	n.a.	n.a.	43	48	50	49	47	54
Ga	16	n.a.	n.a.	n.a.	n.a.	16	14	15	13	12	11
Pb	18	n.a.	n.a.	n.a.	n.a.	20	18	18	21	20	25
Rb	103	n.a.	n.a.	n.a.	n.a.	116	131	120	118	124	116
Sr	112	n.a.	n.a.	n.a.	n.a.	83	46	74	86	89	86
Th	15	n.a.	n.a.	n.a.	n.a.	17	17	16	15	11	13
Y	27	n.a.	n.a.	n.a.	n.a.	25	27	26	28	29	24
FeO*	1.88	2.02	1.39	1.81	1.66	1.80	1.33	1.67	1.70	1.67	1.75
F/F+M	0.874	0.937	0.931	0.926	0.945	0.935	0.933	0.951	0.907	0.901	0.923
K/Rb	268.4	0.0	0.0	0.0	0.0	246.2	251.0	251.8	253.3	249.7	240.5
K/Ba	34.5	0.0	0.0	0.0	0.0	38.3	42.0	41.1	39.2	40.5	37.9
Rb/Sr	0.92	0.00	0.00	0.00	0.00	1.40	2.85	1.62	1.37	1.39	1.35
Y/Nb	2.25	0.00	0.00	0.00	0.00	2.27	2.25	2.17	2.80	2.90	2.40

n.a. = not analysed

Table D.3. cont.

Ref.no. #	100	101	102	103	104	105	106	107	108	109	110
Sample	HJ7/1	HJ8/1	HJ8/2	HJ8/3	HJ9/1	HJ9/2	HJ9/3	HJ9/4	H13/1	H13/2	H14/1
SiO_2	73.88	74.79	72.86	73.99	75.25	73.99	73.87	73.22	75.22	72.80	73.50
TiO_2	0.12	0.13	0.17	0.12	0.11	0.16	0.11	0.16	0.11	0.17	0.17
Al_2O_3	12.66	12.28	13.01	12.42	11.99	12.56	11.75	12.87	12.03	12.97	12.87
Fe_2O_3	1.53	1.53	1.94	1.54	1.33	1.79	1.35	1.83	1.30	1.88	1.79
MnO	0.06	0.07	0.08	0.05	0.06	0.06	0.07	0.04	0.04	0.03	0.07
MgO	0.13	0.13	0.20	0.10	0.12	0.17	0.08	0.17	0.12	0.19	0.19
CaO	0.80	0.85	1.07	0.79	0.75	1.07	0.74	1.09	0.78	1.06	1.06
Na_2O	3.52	4.03	3.96	3.69	3.65	3.88	3.78	3.85	3.71	3.72	3.64
K_2O	3.75	3.59	3.53	3.79	4.00	3.73	3.99	3.69	3.94	3.81	3.82
P_2O_5	0.02	0.02	0.02	0.02	0.02	0.03	0.03	0.02	0.02	0.02	0.02
LOI	2.95	2.87	3.03	2.81	2.77	2.88	2.99	3.08	2.60	3.00	2.91
Total	99.42	100.29	99.87	99.32	100.05	100.32	98.76	100.02	99.87	99.65	100.04
Q	38.35	36.38	34.63	37.34	37.83	35.37	36.37	35.04	37.64	35.06	36.03
or	22.97	21.78	21.54	23.21	24.30	22.62	24.62	22.50	23.94	23.30	23.24
ab	30.88	35.00	34.60	32.35	31.75	33.69	33.40	33.61	32.27	32.57	31.71
an	3.98	4.19	5.35	3.93	3.69	5.25	3.46	5.44	3.84	5.31	5.28
C	1.46	0.27	0.80	0.89	0.35	0.27	-	0.63	0.30	0.88	0.89
di	-	-	-	-	-	-	0.15	-	-	-	-
hy	0.80	0.79	1.08	0.71	0.71	0.92	0.57	0.90	0.66	0.94	0.97
mt	1.21	1.20	1.53	1.22	1.04	1.40	1.08	1.44	1.02	1.48	1.41
il	0.24	0.25	0.33	0.24	0.21	0.31	0.22	0.31	0.21	0.33	0.33
ap	0.05	0.05	0.05	0.05	0.05	0.07	0.07	0.05	0.05	0.05	0.05
V	7	6	6	6	7	5	7	6	7	6	6
Cr	3	3	3	3	3	3	3	3	3	3	3
Ni	3	3	3	3	3	3	3	3	3	3	3
Zn	51	50	53	45	41	50	44	75	43	53	54
Zr	152	147	220	146	124	197	123	199	124	211	203
Nb	11	10	10	10	12	12	8	10	10	11	11
Ba	780	782	766	791	795	747	780	755	803	733	753
La	27	24	25	26	26	25	26	27	28	25	26
Ce	56	54	68	61	54	62	58	60	65	68	61
Nd	56	57	60	59	63	49	53	52	57	51	54
Ga	9	12	10	12	13	15	8	18	10	15	12
Pb	22	24	22	21	18	23	22	21	19	19	22
Rb	125	127	118	125	131	121	135	121	134	122	125
Sr	60	64	89	58	54	88	53	92	55	88	90
Th	16	16	13	14	15	14	11	13	16	14	13
Y	26	26	27	28	28	27	28	27	27	25	27
FeO*	1.38	1.38	1.75	1.39	1.20	1.61	1.21	1.65	1.17	1.69	1.61
F/F+M	0.917	0.918	0.901	0.935	0.913	0.908	0.941	0.908	0.910	0.901	0.898
K/Rb	249.1	234.7	248.4	251.7	253.5	255.9	245.4	253.2	244.1	259.3	253.7
K/Ba	39.9	38.1	38.3	39.8	41.8	41.5	42.5	40.6	40.7	43.2	42.1
Rb/Sr	2.08	1.98	1.33	2.16	2.43	1.38	2.55	1.32	2.44	1.39	1.39
Y/Nb	2.36	2.60	2.70	2.80	2.33	2.25	3.50	2.70	2.70	2.27	2.45

Table D.3. cont.

Ref.no. #	111	112	113	114	115	116	117	118	119	120	121
Sample	H14/2	H15/1	H15/2	H16/1	H17/1	H17/2	48/1	48/2	48/3	48/4	50A/1
SiO_2	73.58	73.88	73.60	73.18	73.63	74.89	73.11	73.80	73.14	73.72	68.57
TiO_2	0.17	0.16	0.17	0.17	0.17	0.11	0.16	0.17	0.16	0.16	0.22
Al_2O_3	12.69	12.78	12.86	13.33	12.71	12.10	12.33	12.62	12.35	12.53	16.98
Fe_2O_3	1.83	1.84	1.82	1.82	1.82	1.41	1.75	1.63	1.69	1.65	2.17
MnO	0.08	0.08	0.08	0.07	0.04	0.05	0.08	0.05	0.05	0.04	0.06
MgO	0.18	0.14	0.19	0.18	0.17	0.08	0.12	0.19	0.19	0.17	0.11
CaO	1.07	1.08	1.04	1.04	1.06	0.79	1.06	1.07	1.04	1.09	0.83
Na_2O	4.10	3.71	3.62	3.68	3.88	3.60	3.97	3.96	3.49	3.77	3.36
K_2O	3.59	3.83	3.81	3.63	3.63	3.99	3.64	3.59	3.92	3.87	2.81
P_2O_5	0.02	0.03	0.02	0.03	0.02	0.02	0.02	0.03	0.02	0.03	0.01
LOI	2.96	2.82	3.02	2.98	2.88	2.90	2.82	2.94	3.05	2.68	4.92
Total	100.27	100.35	100.23	100.11	100.01	99.94	99.06	100.05	99.10	99.71	100.04
Q	34.17	35.85	36.29	36.29	35.52	37.86	34.79	35.38	36.64	35.35	37.98
or	21.80	23.21	23.16	22.09	22.09	24.30	22.35	21.85	24.12	23.57	17.46
ab	35.65	32.19	31.51	32.06	33.80	31.39	34.91	34.51	30.75	32.88	29.89
an	5.32	5.29	5.17	5.11	5.28	3.90	5.27	5.26	5.24	5.37	4.26
C	0.17	0.66	0.97	1.57	0.53	0.49	-	0.36	0.54	0.24	7.28
di	-	-	-	-	-	-	0.05	-	-	-	-
hy	0.98	0.90	1.00	0.96	0.88	0.62	0.80	0.88	0.93	0.83	0.82
mt	1.43	1.44	1.43	1.43	1.43	1.11	1.39	1.28	1.34	1.30	1.74
il	0.33	0.31	0.33	0.33	0.33	0.22	0.32	0.33	0.32	0.31	0.44
ap	0.05	0.07	0.05	0.07	0.05	0.05	0.05	0.07	0.05	0.07	0.02
V	7	4	5	6	7	6	5	5	6	6	6
Cr	3	3	4	4	3	3	3	3	3	4	3
Ni	3	3	3	3	3	3	3	3	3	3	3
Zn	53	60	62	57	54	46	51	46	53	53	82
Zr	209	205	206	212	204	135	201	203	196	200	251
Nb	11	10	10	10	11	11	11	10	11	11	14
Ba	776	749	742	744	769	774	761	749	756	773	887
La	24	25	25	25	28	28	27	28	27	26	33
Ce	62	70	60	60	64	65	61	61	65	61	91
Nd	55	52	50	49	51	48	45	49	46	49	55
Ga	10	12	9	15	10	12	12	13	13	13	16
Pb	22	23	26	21	23	20	23	24	26	24	24
Rb	121	121	123	118	120	132	123	129	127	125	100
Sr	87	89	84	86	88	58	88	89	85	90	66
Th	14	11	12	16	12	14	11	14	12	12	23
Y	27	27	26	26	25	28	26	27	28	27	28
FeO*	1.65	1.66	1.64	1.64	1.64	1.27	1.57	1.47	1.52	1.48	1.95
F/F+M	0.906	0.925	0.900	0.905	0.908	0.943	0.932	0.889	0.892	0.900	0.948
K/Rb	246.3	262.8	257.2	255.4	251.1	250.9	245.7	231.0	256.3	257.0	233.3
K/Ba	38.4	42.5	42.6	40.5	39.2	42.8	39.7	39.8	43.0	41.6	26.3
Rb/Sr	1.39	1.36	1.46	1.37	1.36	2.28	1.40	1.45	1.49	1.39	1.52
Y/Nb	2.45	2.70	2.60	2.60	2.27	2.55	2.36	2.70	2.55	2.45	2.00

Table D.3. cont.

Ref.no. #	122	123	124	125	126	127	128	129	130	131	132
Sample	50A/2	50A/3	57/1	57/2	57/3	62/3	66/1	66/2	70/1	70/2	70/3
SiO_2	68.07	70.34	69.23	67.28	69.61	73.85	74.67	74.19	68.80	72.40	71.50
TiO_2	0.17	0.18	0.29	0.39	0.33	0.15	0.16	0.19	0.29	0.16	0.18
Al_2O_3	17.94	16.27	15.06	16.35	15.00	12.10	12.63	12.65	16.25	13.91	14.23
Fe_2O_3	2.07	1.92	2.53	2.88	2.63	1.42	1.76	1.76	2.36	1.71	1.80
MnO	0.05	0.04	0.07	0.06	0.08	0.09	0.05	0.06	0.05	0.05	0.06
MgO	0.05	0.09	0.23	0.27	0.23	0.09	0.17	0.18	0.13	0.08	0.10
CaO	0.75	0.77	1.64	1.76	1.70	0.77	1.07	1.09	1.07	0.81	0.82
Na_2O	3.18	3.40	3.60	3.45	3.35	3.48	3.68	3.86	3.17	3.48	3.40
K_2O	2.77	2.93	2.93	2.74	3.15	3.61	3.75	3.56	2.94	3.34	3.28
P_2O_5	0.01	0.01	0.03	0.03	0.03	0.01	0.01	0.01	0.01	0.01	0.01
LOI	5.36	4.80	4.34	4.83	3.72	4.09	2.05	2.84	5.40	3.91	4.59
Total	100.42	100.75	99.95	100.04	99.83	99.66	100.00	100.39	100.47	99.86	99.97
Q	39.00	38.97	34.58	34.05	35.30	39.60	36.95	36.24	38.34	38.93	38.89
or	17.22	18.05	18.11	17.01	19.37	22.32	22.63	21.57	18.28	20.57	20.32
ab	28.31	29.98	31.86	30.66	29.49	30.81	31.79	33.48	28.21	30.69	30.16
an	3.85	3.91	8.30	8.97	8.57	3.93	5.35	5.48	5.51	4.12	4.20
C	8.81	6.39	3.20	4.81	3.18	1.14	0.61	0.50	6.24	3.25	3.80
hy	0.69	0.70	1.16	1.20	1.14	0.67	0.88	0.88	0.80	0.65	0.72
mt	1.66	1.53	2.02	2.31	2.09	1.13	1.37	1.38	1.89	1.36	1.44
il	0.34	0.36	0.58	0.78	0.65	0.30	0.31	0.37	0.58	0.32	0.36
ap	0.02	0.02	0.07	0.07	0.07	0.02	0.02	0.02	0.02	0.02	0.02
V	5	6	10	14	11	6	7	5	6	6	6
Cr	4	3	5	5	5	4	4	4	3	3	4
Ni	3	3	3	3	3	3	3	3	3	3	3
Zn	74	62	48	55	52	47	49	51	81	56	65
Zr	235	205	264	274	259	124	199	199	281	168	182
Nb	15	14	10	10	10	11	11	11	12	13	12
Ba	934	874	789	831	811	903	789	782	1020	939	978
La	36	36	24	27	29	31	27	29	28	32	33
Ce	80	71	67	60	71	92	62	70	63	70	67
Nd	53	54	40	43	53	53	52	52	53	55	54
Ga	16	17	15	14	16	16	17	16	16	16	16
Pb	22	21	23	22	23	27	22	24	23	24	22
Rb	99	110	102	94	105	128	126	124	99	117	118
Sr	57	56	130	138	133	54	88	91	89	58	59
Th	23	18	16	14	13	17	16	15	18	19	18
Y	29	29	20	22	23	28	26	26	30	30	30
FeO*	1.86	1.73	2.28	2.59	2.37	1.28	1.58	1.58	2.12	1.54	1.62
F/F+M	0.975	0.952	0.911	0.908	0.914	0.938	0.906	0.901	0.944	0.952	0.944
K/Rb	232.3	221.1	238.5	242.0	249.1	234.1	247.1	238.3	246.5	237.0	230.8
K/Ba	24.6	27.8	30.8	27.4	32.2	33.2	39.5	37.8	23.9	29.5	27.8
Rb/Sr	1.74	1.96	0.78	0.68	0.79	2.37	1.43	1.36	1.11	2.02	2.00
Y/Nb	1.93	2.07	2.00	2.20	2.30	2.55	2.36	2.36	2.50	2.31	2.50

Table D.3. cont.

Ref.no. #	133	134	135	136	137	138	139	140	141	142	143
Sample	70/4	70/5	70e/1	85/1	85/2	85/3	85/4	85/5	85/6	91/1	91/2
SiO_2	72.19	70.35	73.03	69.09	65.41	64.80	64.86	69.25	63.75	71.17	70.65
TiO_2	0.32	0.22	0.21	0.19	0.27	0.25	0.25	0.16	0.25	0.18	0.21
Al_2O_3	14.96	15.02	13.03	17.19	19.24	19.56	19.84	16.97	19.58	15.08	14.25
Fe_2O_3	1.71	2.20	2.01	1.97	2.61	2.75	2.75	1.69	2.57	1.96	2.02
MnO	0.06	0.06	0.07	0.08	0.10	0.06	0.08	0.04	0.08	0.05	0.06
MgO	0.13	0.12	0.16	0.07	0.11	0.11	0.17	0.11	0.10	0.18	0.42
CaO	0.78	1.02	1.06	0.75	0.96	0.93	0.97	0.63	0.94	0.98	1.03
Na_2O	3.35	3.43	3.70	3.26	3.11	3.02	3.13	3.35	3.09	3.73	3.29
K_2O	3.47	3.05	3.35	2.89	2.46	2.49	2.44	3.08	2.50	3.20	3.48
P_2O_5	0.02	0.01	0.01	0.01	0.01	0.01	0.03	0.02	0.01	0.06	0.01
LOI	3.69	4.81	3.36	5.27	5.83	5.51	5.48	5.60	7.09	4.05	5.58
Total	100.68	100.29	99.99	100.77	100.11	99.49	100.00	100.90	99.96	100.64	101.00
Q	38.70	37.86	37.24	38.90	37.56	37.53	36.77	38.13	36.38	36.04	36.86
or	21.14	18.88	20.49	17.88	15.42	15.66	15.26	19.10	15.91	19.58	21.55
ab	29.23	30.40	32.40	28.89	27.91	27.19	28.02	29.75	28.15	32.68	29.18
an	3.86	5.23	5.37	3.83	4.98	4.84	4.88	3.14	4.95	4.63	5.29
C	4.46	4.45	1.46	7.71	10.33	10.89	10.96	7.37	10.88	3.98	3.38
hy	0.52	0.85	0.91	0.73	0.98	0.99	1.18	0.71	0.95	0.96	1.59
mt	1.34	1.76	1.59	1.57	2.11	2.23	2.22	1.35	2.11	1.55	1.61
il	0.63	0.44	0.41	0.38	0.54	0.51	0.50	0.32	0.51	0.35	0.42
ap	0.05	0.02	0.02	0.02	0.02	0.02	0.07	0.05	0.02	0.14	0.02
V	4	6	5	7	4	4	3	5	5	7	6
Cr	3	3	4	4	5	3	5	3	4	4	4
Ni	3	3	3	3	3	3	3	3	3	4	3
Zn	64	68	51	56	75	77	83	52	70	71	131
Zr	158	242	207	243	324	323	354	184	338	207	195
Nb	12	12	12	15	17	15	15	11	16	10	12
Ba	1009	930	809	855	848	757	827	806	1334	836	820
La	33	30	29	31	50	35	58	31	23	24	24
Ce	70	65	67	100	116	90	89	91	107	65	69
Nd	55	52	52	52	54	55	56	52	49	52	50
Ga	17	17	16	16	17	17	18	17	18	16	17
Pb	21	21	22	30	29	26	24	23	27	21	20
Rb	119	107	119	104	87	87	84	106	87	113	122
Sr	55	82	85	59	79	76	78	44	89	85	97
Th	22	16	17	29	24	22	21	23	24	14	14
Y	32	30	27	26	38	33	42	23	18	22	23
FeO*	1.54	1.98	1.81	1.77	2.35	2.47	2.47	1.52	2.31	1.76	1.82
F/F+M	0.925	0.944	0.922	0.964	0.957	0.958	0.938	0.934	0.960	0.910	0.817
K/Rb	242.1	236.6	233.7	230.7	234.7	237.6	241.2	241.2	238.6	235.1	236.8
K/Ba	28.6	27.2	34.4	28.1	24.1	27.3	24.5	31.7	15.6	31.8	35.2
Rb/Sr	2.16	1.30	1.40	1.76	1.10	1.14	1.08	2.41	0.98	1.33	1.26
Y/Nb	2.67	2.50	2.25	1.73	2.24	2.20	2.80	2.09	1.13	2.20	1.92

Table D.3. cont.

Ref.no. #	144	145	146	147	148	149	150	151	152	153	154
Sample	91/3	97/1	97/2	97/3	97/4	98/1	98/2	98/3	98/4	108/1	108/2
SiO_2	67.74	73.67	71.00	70.64	74.34	70.90	70.56	72.68	70.30	71.00	71.28
TiO_2	0.23	0.19	0.28	0.33	0.14	0.27	0.30	0.22	0.29	0.28	0.28
Al_2O_3	16.63	12.59	13.96	14.39	12.48	15.33	14.92	14.41	14.59	13.14	13.97
Fe_2O_3	2.09	1.55	2.31	2.39	1.24	1.90	2.43	1.68	2.47	2.23	2.25
MnO	0.07	0.06	0.07	0.08	0.04	0.06	0.10	0.06	0.08	0.07	0.07
MgO	0.14	0.17	0.33	0.35	0.09	0.18	0.34	0.16	0.36	0.40	0.34
CaO	0.97	0.88	1.47	1.51	0.61	1.03	1.51	0.91	1.63	1.45	1.48
Na_2O	3.57	3.86	4.29	4.16	3.78	3.83	4.26	3.92	4.35	4.61	4.42
K_2O	2.87	3.22	2.78	2.73	3.58	2.78	2.66	2.97	2.70	3.29	2.93
P_2O_5	0.04	0.01	0.04	0.03	0.01	0.01	0.01	0.01	0.02	0.03	0.02
LOI	5.51	3.72	3.01	3.83	3.00	3.08	3.31	3.81	2.75	2.77	2.94
Total	99.86	99.92	99.54	100.44	99.31	99.37	100.40	100.83	99.54	99.27	99.98
Q	35.61	38.07	32.80	33.25	38.53	36.75	32.59	37.31	31.46	29.13	31.46
or	17.98	19.78	17.02	16.70	21.97	17.06	16.19	18.09	16.49	20.15	17.84
ab	32.02	33.95	37.61	36.44	33.21	33.66	37.13	34.19	38.03	40.42	38.54
an	4.82	4.47	7.28	7.55	3.07	5.24	7.65	4.59	8.22	5.64	7.43
C	6.34	1.23	1.36	1.99	1.35	4.33	2.38	3.21	1.65	-	0.91
di	-	-	-	-	-	-	-	-	-	1.30	-
hy	0.88	0.79	1.34	1.36	0.52	0.81	1.43	0.76	1.48	0.87	1.34
mt	1.69	1.23	1.83	1.89	0.98	1.50	1.91	1.32	1.95	1.76	1.77
il	0.46	0.38	0.55	0.65	0.28	0.53	0.59	0.43	0.57	0.55	0.55
ap	0.10	0.02	0.10	0.07	0.02	0.02	0.02	0.02	0.05	0.07	0.05
V	7	8	9	8	6	5	8	5	10	9	8
Cr	4	4	4	3	3	4	4	4	4	4	4
Ni	3	3	3	3	3	3	4	3	3	3	3
Zn	174	42	62	64	39	60	73	56	68	44	51
Zr	220	156	252	266	115	202	285	179	265	224	241
Nb	13	12	12	13	12	13	13	13	11	11	10
Ba	718	799	778	746	832	964	756	991	749	633	737
La	26	29	28	28	32	29	28	30	27	25	27
Ce	62	63	78	74	78	91	80	76	67	51	60
Nd	51	52	54	51	54	53	52	52	52	50	53
Ga	16	17	14	16	16	18	17	16	17	16	17
Pb	25	22	21	17	17	19	21	21	22	15	19
Rb	102	115	90	94	135	99	91	105	90	107	93
Sr	88	62	118	121	32	77	125	63	137	115	121
Th	17	15	5	12	17	20	15	17	14	12	13
Y	23	35	31	29	36	31	29	32	27	28	30
FeO*	1.88	1.39	2.08	2.15	1.12	1.71	2.19	1.51	2.22	2.01	2.02
F/F+M	0.933	0.895	0.867	0.864	0.928	0.908	0.871	0.908	0.865	0.838	0.860
K/Rb	233.6	232.5	256.4	241.1	220.2	233.1	242.7	234.8	249.1	255.3	261.6
K/Ba	33.2	33.5	29.7	30.4	35.7	23.9	29.2	24.9	29.9	43.1	33.0
Rb/Sr	1.16	1.85	0.76	0.78	4.22	1.29	0.73	1.67	0.66	0.93	0.77
Y/Nb	1.77	2.92	2.58	2.23	3.00	2.38	2.23	2.46	2.45	2.55	3.00

Table D.3. cont.

Ref.no. #	155	156	157	158	159	160	161	162	163	164	165
Sample	108/3	108/4	108/5	108/6	122/2	122/3	122/4	126/1	126/2	126/3	126/4
SiO_2	71.40	69.22	72.30	72.71	72.58	69.77	69.88	72.76	73.62	70.37	71.28
TiO_2	0.27	0.43	0.28	0.27	0.16	0.25	0.22	0.16	0.16	0.10	0.21
Al_2O_3	13.19	14.35	13.67	13.07	14.99	16.03	15.59	13.36	13.39	14.95	14.92
Fe_2O_3	2.11	3.01	2.23	2.15	1.63	2.39	1.95	1.36	1.48	1.48	2.08
MnO	0.09	0.11	0.08	0.08	0.05	0.08	0.08	0.04	0.05	0.04	0.07
MgO	0.38	0.61	0.36	0.35	0.12	0.09	0.08	0.08	0.09	0.08	0.16
CaO	1.53	2.15	1.57	1.40	0.78	0.97	0.94	0.73	0.76	0.69	1.04
Na_2O	4.58	4.98	4.39	4.16	3.59	3.15	3.47	3.86	3.91	3.53	4.08
K_2O	3.20	2.61	3.12	3.31	3.45	3.21	3.10	3.48	3.44	3.20	3.06
P_2O_5	0.02	0.06	0.02	0.03	0.02	0.01	0.01	0.01	0.01	0.01	0.01
LOI	2.65	2.07	2.34	2.28	3.47	4.58	5.17	3.61	3.80	4.68	3.73
Total	99.42	99.60	100.36	99.81	100.84	100.53	100.49	99.45	100.71	99.13	100.64
Q	29.80	25.55	31.39	33.02	37.50	38.27	37.26	36.73	36.96	37.93	34.22
or	19.54	15.82	18.81	20.06	20.94	19.77	19.22	21.46	20.98	20.02	18.66
ab	40.05	43.21	37.90	36.09	31.20	27.78	30.80	34.08	34.14	31.63	35.63
an	6.18	9.32	7.81	6.92	3.84	4.95	4.82	3.71	3.82	3.56	5.26
C	-	-	0.27	0.17	4.09	5.87	5.08	2.02	1.94	4.71	3.13
di	1.24	0.97	-	-	-	-	-	-	-	-	-
hy	0.85	1.65	1.39	1.36	0.71	0.83	0.70	0.50	0.59	0.66	0.94
mt	1.66	2.35	1.74	1.68	1.28	1.90	1.56	1.08	1.16	1.20	1.64
il	0.53	0.84	0.54	0.53	0.31	0.49	0.44	0.32	0.31	0.20	0.41
ap	0.05	0.14	0.05	0.07	0.05	0.02	0.02	0.02	0.02	0.02	0.02
V	8	12	9	10	6	4	7	7	6	5	5
Cr	3	4	5	3	3	4	3	3	3	3	4
Ni	3	5	4	3	3	3	3	3	3	3	3
Zn	50	63	51	54	42	66	59	50	50	56	66
Zr	216	306	232	219	193	291	232	118	139	120	243
Nb	11	11	11	11	12	12	13	11	10	14	12
Ba	686	637	723	727	793	790	782	1010	900	1267	1000
La	25	24	27	25	32	41	32	29	31	29	30
Ce	62	61	58	72	71	87	106	70	87	59	92
Nd	53	51	54	52	54	53	50	51	51	51	52
Ga	17	17	17	17	16	17	17	14	16	17	16
Pb	18	16	17	17	21	24	26	24	20	21	22
Rb	104	89	100	105	113	106	106	127	126	124	111
Sr	121	186	131	112	64	86	82	52	56	49	82
Th	9	7	12	12	17	20	18	19	20	20	20
Y	29	25	29	31	30	29	28	27	29	26	27
FeO*	1.90	2.71	2.01	1.93	1.47	2.15	1.75	1.22	1.33	1.33	1.87
F/F+M	0.840	0.822	0.853	0.852	0.927	0.961	0.958	0.940	0.939	0.945	0.924
K/Rb	255.4	243.5	259.0	261.7	253.5	251.4	242.8	227.5	226.7	214.2	228.9
K/Ba	38.7	34.0	35.8	37.8	36.1	33.7	32.9	28.6	31.7	21.0	25.4
Rb/Sr	0.86	0.48	0.76	0.94	1.77	1.23	1.29	2.44	2.25	2.53	1.35
Y/Nb	2.64	2.27	2.64	2.82	2.50	2.42	2.15	2.45	2.90	1.86	2.25

Table D.3. cont.

Ref.no. #	166	167	168	169	170	171	172	173	174	175	176
Sample	126/5	126/6	127/1	127/2	127/3	127/4	127/5	127/6	131C1	131C2	V18/1
SiO_2	69.81	72.24	70.34	74.88	73.27	72.85	74.44	72.19	74.15	73.30	73.47
TiO_2	0.22	0.15	0.26	0.12	0.17	0.22	0.14	0.20	0.18	0.16	0.15
Al_2O_3	15.43	15.01	15.15	12.44	12.84	13.30	12.49	13.34	11.95	12.33	13.52
Fe_2O_3	2.14	1.65	2.22	1.37	1.89	1.89	1.38	1.92	1.71	1.69	1.81
MnO	0.08	0.05	0.05	0.04	0.06	0.05	0.05	0.05	0.04	0.04	0.06
MgO	0.17	0.10	0.14	0.11	0.18	0.15	0.11	0.16	0.14	0.13	0.06
CaO	1.10	0.73	1.07	0.75	1.10	1.03	0.73	1.07	1.00	1.02	1.03
Na_2O	4.25	3.68	3.76	3.86	4.26	3.79	3.77	4.07	3.58	3.56	4.00
K_2O	2.88	3.30	3.00	3.73	3.33	3.43	3.62	3.20	3.53	3.77	3.47
P_2O_5	0.01	0.01	0.01	0.01	0.01	0.01	0.01	0.01	0.01	0.01	0.03
LOI	3.92	4.08	4.90	3.32	3.02	4.12	3.52	3.81	3.50	3.08	2.68
Total	100.01	101.00	100.90	100.63	100.13	100.84	100.26	100.02	99.79	99.09	100.28
Q	32.51	37.48	35.74	37.25	33.90	36.29	38.04	34.89	38.76	37.11	35.33
or	17.71	20.12	18.47	22.65	20.27	20.96	22.11	19.66	21.67	23.21	21.01
ab	37.43	32.13	33.14	33.57	37.12	33.16	32.98	35.80	31.46	31.38	34.68
an	5.61	3.67	5.46	3.76	5.55	5.22	3.68	5.45	5.08	5.20	5.03
C	3.48	4.21	3.95	0.73	0.26	1.56	1.10	1.31	0.46	0.59	1.42
hy	0.99	0.69	0.82	0.65	0.97	0.79	0.64	0.86	0.75	0.75	0.66
mt	1.70	1.30	1.76	1.07	1.48	1.49	1.09	1.52	1.35	1.34	1.41
il	0.43	0.29	0.51	0.23	0.33	0.43	0.27	0.39	0.36	0.32	0.29
ap	0.02	0.02	0.02	0.02	0.02	0.02	0.02	0.02	0.02	0.02	0.07
V	5	5	6	6	6	7	5	6	7	6	3
Cr	4	5	4	3	5	4	3	3	3	3	3
Ni	3	3	3	3	3	3	3	3	3	3	3
Zn	69	57	67	40	50	54	46	55	40	39	43
Zr	254	169	283	125	220	214	126	230	189	188	207
Nb	11	13	13	12	12	12	10	11	10	11	12
Ba	845	877	764	814	789	809	854	767	727	746	771
La	27	29	26	27	29	28	30	26	24	24	25
Ce	85	89	71	78	66	66	66	71	64	64	63
Nd	51	52	51	52	52	53	52	51	51	51	48
Ga	16	16	16	16	16	17	15	16	15	15	15
Pb	23	27	22	23	23	20	22	22	23	20	25
Rb	108	117	113	128	114	113	124	116	123	130	120
Sr	91	52	86	52	91	84	49	89	86	86	85
Th	19	22	17	18	10	13	14	14	15	11	13
Y	26	27	26	28	27	28	28	24	25	24	22
FeO*	1.93	1.48	2.00	1.23	1.70	1.70	1.24	1.73	1.54	1.52	1.63
F/F+M	0.922	0.939	0.936	0.920	0.907	0.921	0.922	0.917	0.919	0.923	0.966
K/Rb	221.4	234.2	220.4	241.9	242.5	252.0	242.4	229.0	238.3	240.8	240.1
K/Ba	28.3	31.2	32.6	38.0	35.0	35.2	35.2	34.6	40.3	42.0	37.4
Rb/Sr	1.19	2.25	1.31	2.46	1.25	1.35	2.53	1.30	1.43	1.51	1.41
Y/Nb	2.36	2.08	2.00	2.33	2.25	2.33	2.80	2.18	2.50	2.18	1.83

Table D.3. cont.

Ref.no. #	177	178	179	180	181	182	183	184	185	186	187
Sample	V18/2	V18/3	132/1	132/2	132/3	132/4	132/5	132/6	132/7	132/8	V25/1
SiO_2	71.55	71.89	70.76	72.75	72.47	70.48	66.58	66.87	72.31	69.83	72.35
TiO_2	0.58	0.13	0.23	0.11	0.19	0.23	0.21	0.23	0.20	0.21	0.21
Al_2O_3	13.91	13.70	14.36	13.62	13.08	14.62	15.76	15.28	14.08	14.18	13.60
Fe_2O_3	2.18	1.70	2.08	1.58	1.86	2.08	2.11	2.33	2.07	2.05	1.81
MnO	0.06	0.09	0.05	0.04	0.04	0.06	0.05	0.05	0.05	0.05	0.05
MgO	0.08	0.08	0.18	0.12	0.18	0.17	0.16	0.16	0.16	0.15	0.07
CaO	1.02	0.75	1.05	0.75	1.06	1.01	1.01	0.98	1.05	1.04	1.02
Na_2O	3.77	3.74	3.89	3.72	4.23	3.95	3.61	3.75	3.67	3.70	4.03
K_2O	3.38	3.56	3.30	3.55	3.33	3.07	2.81	2.87	3.42	3.17	3.62
P_2O_5	0.04	0.03	0.02	0.02	0.01	0.01	0.01	0.03	0.01	0.02	0.03
LOI	3.80	3.48	4.20	3.76	3.06	4.26	7.89	7.80	3.76	4.59	2.92
Total	100.37	99.15	100.12	100.02	99.51	99.94	100.20	100.35	100.78	98.99	99.71
Q	35.72	36.19	34.24	36.98	33.61	34.65	34.92	34.12	36.27	35.56	33.76
or	20.68	21.99	20.33	21.79	20.40	18.96	17.99	18.33	20.83	19.85	22.10
ab	33.03	33.08	34.32	32.70	37.11	34.93	33.09	34.29	32.01	33.17	35.23
an	4.97	3.68	5.29	3.73	5.38	5.17	5.36	5.04	5.30	5.33	5.03
C	2.37	2.51	2.64	2.43	0.64	3.12	5.38	4.64	2.53	2.99	1.31
hy	0.21	0.78	0.92	0.77	0.89	0.92	0.95	1.00	0.91	0.88	0.57
mt	1.57	1.36	1.65	1.25	1.47	1.66	1.74	1.92	1.63	1.66	1.43
il	1.14	0.26	0.46	0.22	0.37	0.46	0.43	0.47	0.39	0.42	0.41
hem	0.11	-	-	-	-	-	-	-	-	-	-
ap	0.10	0.07	0.05	0.05	0.02	0.02	0.03	0.08	0.02	0.05	0.07
V	3	3	4	7	5	6	6	7	5	4	3
Cr	4	4	4	3	4	3	5	4	3	3	4
Ni	3	3	3	3	3	3	3	3	4	3	3
Zn	38	39	54	35	51	54	61	67	45	55	43
Zr	212	162	208	151	203	227	250	254	209	247	204
Nb	11	10	11	11	11	11	14	14	13	13	12
Ba	732	743	784	775	741	760	793	818	785	1118	718
La	20	21	27	29	29	27	25	25	27	28	19
Ce	62	57	63	69	63	70	70	64	59	79	55
Nd	45	46	51	49	51	50	51	49	51	50	43
Ga	14	16	15	16	16	18	16	17	16	15	16
Pb	24	25	21	20	22	24	20	23	19	26	25
Rb	114	124	114	122	115	117	102	103	112	116	131
Sr	85	57	87	55	87	86	82	80	86	92	86
Th	13	17	15	19	14	23	16	19	6	19	14
Y	20	20	23	25	25	23	21	23	23	22	19
FeO*	1.96	1.53	1.87	1.42	1.67	1.87	1.90	2.10	1.86	1.84	1.63
F/F+M	0.962	0.953	0.914	0.924	0.905	0.919	0.924	0.931	0.923	0.927	0.960
K/Rb	246.1	238.3	240.3	241.6	240.4	217.8	228.7	231.3	253.5	226.9	229.4
K/Ba	38.3	39.8	34.9	38.0	37.3	33.5	29.4	29.1	36.2	23.5	41.9
Rb/Sr	1.34	2.18	1.31	2.22	1.32	1.36	1.24	1.29	1.30	1.26	1.52
Y/Nb	1.82	2.00	2.09	2.27	2.27	2.09	1.50	1.64	1.77	1.69	1.58

Table D.3. cont.

Ref.no. #	188	189	190	191	192	193	194	195	196	197	198
Sample	V25/2	V28/1	V28/2	V32/1	V32/2	V36/1	V36/2	V36/3	V39/1	V39/2	134/1
SiO_2	71.52	71.23	70.75	73.26	72.67	70.09	72.28	70.23	66.98	64.71	68.49
TiO_2	0.18	0.14	0.21	0.18	0.21	0.17	0.18	0.14	0.19	0.20	0.25
Al_2O_3	14.54	15.16	15.44	13.38	12.87	15.02	13.64	14.94	16.96	18.45	15.62
Fe_2O_3	2.12	2.14	2.35	1.85	1.87	2.12	1.97	2.13	2.29	2.32	2.37
MnO	0.05	0.06	0.06	0.06	0.05	0.06	0.05	0.05	0.06	0.06	0.07
MgO	0.05	0.05	0.07	0.05	0.06	0.05	0.05	0.05	0.05	0.05	0.30
CaO	1.00	1.01	1.01	1.06	1.09	1.04	1.03	1.00	1.01	0.97	1.36
Na_2O	3.44	3.64	3.49	4.07	3.83	3.46	3.90	3.51	3.46	3.27	3.64
K_2O	3.55	3.22	3.23	3.75	3.59	3.38	3.33	3.27	2.95	2.81	2.89
P_2O_5	0.02	0.02	0.03	0.03	0.02	0.04	0.03	0.03	0.03	0.03	0.01
LOI	3.48	3.40	3.71	2.58	2.56	4.89	3.36	4.79	5.84	7.41	4.32
Total	99.95	100.07	100.35	100.27	98.82	100.32	99.82	100.14	99.82	100.28	99.32
Q	36.82	36.48	36.88	33.54	35.43	36.23	35.70	36.59	35.26	35.10	34.39
or	21.75	19.68	19.75	22.69	22.04	20.93	20.40	20.27	18.55	17.88	17.98
ab	30.17	31.86	30.56	35.25	33.67	30.68	34.21	31.15	31.15	29.79	32.42
an	5.01	5.05	4.98	5.18	5.48	5.13	5.09	5.00	5.12	4.97	7.03
C	3.39	4.03	4.59	0.79	0.78	4.06	1.89	4.07	6.72	8.98	4.27
hy	0.68	0.78	0.79	0.60	0.57	0.73	0.63	0.76	0.77	0.77	1.36
mt	1.68	1.69	1.85	1.44	1.48	1.69	1.56	1.70	1.86	1.91	1.90
il	0.35	0.28	0.41	0.35	0.41	0.34	0.35	0.28	0.38	0.41	0.50
ap	0.05	0.05	0.07	0.07	0.05	0.10	0.07	0.07	0.07	0.07	0.02
V	3	3	5	6	4	3	3	3	6	9	15
Cr	4	3	4	3	4	4	4	4	4	5	4
Ni	3	3	3	3	3	3	3	3	3	4	3
Zn	49	44	46	40	46	57	53	53	56	61	46
Zr	217	221	211	200	201	215	200	225	264	269	228
Nb	12	11	12	10	10	13	11	11	12	12	11
Ba	733	721	678	671	753	744	746	727	686	656	671
La	22	18	21	22	24	21	26	24	28	23	26
Ce	64	53	59	57	60	58	66	63	62	62	63
Nd	41	43	43	41	46	47	44	45	43	38	49
Ga	16	20	18	21	11	18	18	19	21	18	17
Pb	23	23	22	22	24	26	24	23	24	25	24
Rb	122	111	110	125	121	108	117	110	99	91	106
Sr	83	84	84	88	91	88	87	83	84	79	106
Th	14	16	13	15	13	14	13	15	18	18	18
Y	19	18	18	19	23	21	22	18	19	18	19
FeO*	1.91	1.93	2.11	1.66	1.68	1.91	1.77	1.92	2.06	2.09	2.13
F/F+M	0.975	0.975	0.969	0.972	0.967	0.975	0.973	0.975	0.977	0.977	0.880
K/Rb	241.6	240.8	243.8	249.1	246.3	259.8	236.3	246.8	247.4	256.4	226.3
K/Ba	40.2	37.1	39.6	46.4	39.6	37.7	37.1	37.3	35.7	35.6	35.8
Rb/Sr	1.47	1.32	1.31	1.42	1.33	1.23	1.34	1.33	1.18	1.15	1.00
Y/Nb	1.58	1.64	1.50	1.90	2.30	1.62	2.00	1.64	1.58	1.50	1.73

Table D.3. cont.

Ref.no. #	199	200	201	202	203	204	205	206	207	208	209
Sample	134/2	134/3	134/4	134/5	134/6	135/1	135/2	135/3	135/4	135/5	135/6
SiO_2	71.24	70.87	71.05	66.05	70.85	71.81	73.15	71.81	70.64	72.93	72.04
TiO_2	0.27	0.27	0.21	0.53	0.30	0.17	0.25	0.21	0.22	0.19	0.21
Al_2O_3	14.28	14.46	14.53	16.43	14.34	13.94	13.54	13.92	15.16	13.96	13.96
Fe_2O_3	2.15	2.17	1.69	3.53	2.10	1.95	1.92	1.98	2.12	1.93	2.03
MnO	0.07	0.06	0.04	0.08	0.06	0.06	0.06	0.06	0.07	0.06	0.07
MgO	0.36	0.31	0.15	0.59	0.29	0.15	0.17	0.16	0.16	0.17	0.15
CaO	1.48	1.52	0.98	2.29	1.50	1.00	1.05	1.06	1.08	1.03	1.10
Na_2O	3.88	4.05	3.71	3.86	4.22	3.83	4.15	3.84	3.77	3.91	3.95
K_2O	3.15	3.02	3.29	2.49	3.05	3.19	3.25	3.22	3.03	3.33	3.21
P_2O_5	0.01	0.01	0.01	0.02	0.01	0.01	0.01	0.01	0.01	0.01	0.01
LOI	3.77	3.81	4.84	3.55	3.41	3.47	3.46	3.55	3.77	3.37	3.19
Total	100.66	100.55	100.50	99.42	100.13	99.58	101.01	99.82	100.03	100.89	99.92
Q	33.79	32.94	36.00	29.32	31.90	36.16	34.78	35.80	35.69	35.68	35.15
or	19.21	18.45	20.33	15.35	18.64	19.62	19.69	19.77	18.60	20.18	19.61
ab	33.89	35.43	32.82	34.07	36.92	33.72	36.00	33.75	33.14	33.93	34.55
an	7.51	7.73	5.01	11.71	7.63	5.09	5.27	5.39	5.50	5.17	5.57
C	1.88	1.85	3.25	3.41	1.44	2.49	1.34	2.30	3.88	2.13	2.08
hy	1.37	1.23	0.72	2.06	1.11	0.92	0.81	0.89	0.94	0.92	0.89
mt	1.69	1.71	1.35	2.81	1.66	1.55	1.50	1.57	1.68	1.51	1.60
il	0.53	0.53	0.42	1.05	0.59	0.34	0.49	0.41	0.43	0.37	0.41
ap	0.02	0.02	0.02	0.05	0.02	0.02	0.02	0.02	0.02	0.02	0.02
V	12	10	6	21	10	5	6	5	5	5	7
Cr	5	3	4	5	4	3	3	3	5	3	4
Ni	3	3	3	4	3	3	3	3	3	3	3
Zn	49	47	46	64	42	57	55	55	63	57	58
Zr	213	242	177	332	232	210	216	225	248	219	233
Nb	11	10	12	11	10	10	12	11	11	11	11
Ba	740	733	766	660	675	831	831	839	888	879	839
La	32	29	27	32	27	29	30	28	30	30	30
Ce	71	62	57	70	77	76	75	82	86	70	88
Nd	51	51	52	49	49	52	53	52	51	53	53
Ga	17	15	17	16	16	16	16	16	16	15	17
Pb	20	20	21	19	19	33	19	22	23	17	22
Rb	109	104	114	90	110	117	117	112	109	118	115
Sr	114	125	75	183	124	81	87	86	90	81	91
Th	18	12	15	17	21	22	16	17	17	15	23
Y	26	21	25	20	21	30	30	29	30	25	28
FeO*	1.93	1.95	1.52	3.18	1.89	1.75	1.73	1.78	1.91	1.74	1.83
F/F+M	0.848	0.867	0.912	0.847	0.871	0.924	0.913	0.920	0.925	0.914	0.927
K/Rb	239.9	241.1	239.6	229.7	230.2	226.4	230.6	238.7	230.8	234.3	231.7
K/Ba	35.3	34.2	35.7	31.3	37.5	31.9	32.5	31.9	28.3	31.5	31.8
Rb/Sr	0.96	0.83	1.52	0.49	0.89	1.44	1.34	1.30	1.21	1.46	1.26
Y/Nb	2.36	2.10	2.08	1.82	2.10	3.00	2.50	2.64	2.73	2.27	2.55

Table D.3. cont.

Ref.no. #	210	211	212	213	214	215	216	217	218	219	220
Sample	153/1	153/2	153/3	153/4	153b1	153b2	T1/1	T1/2	T2/1	T2/2	T2/3
SiO_2	71.99	72.77	72.99	70.06	73.50	73.47	73.89	72.14	73.26	75.85	75.32
TiO_2	0.20	0.20	0.20	0.20	0.20	0.17	0.22	0.27	0.21	0.15	0.12
Al_2O_3	14.32	13.66	13.81	15.92	13.56	14.14	13.79	14.44	12.99	12.32	12.31
Fe_2O_3	1.97	2.01	2.09	2.39	1.98	1.95	1.85	2.20	1.53	1.43	1.41
MnO	0.05	0.05	0.05	0.05	0.07	0.07	0.06	0.06	0.06	0.05	0.04
MgO	0.06	0.05	0.05	0.05	0.05	0.05	0.08	0.16	0.05	0.06	0.05
CaO	0.98	1.12	1.03	1.04	1.02	1.05	0.97	1.06	1.15	0.77	0.76
Na_2O	4.11	4.01	3.92	3.75	3.85	3.79	3.56	3.60	3.77	3.94	4.06
K_2O	3.28	3.50	3.52	3.12	3.43	3.39	3.65	3.43	3.62	3.98	4.01
P_2O_5	0.02	0.02	0.03	0.02	0.02	0.02	0.03	0.03	0.03	0.02	0.02
LOI	3.23	2.10	2.08	3.67	2.73	2.43	2.14	2.96	2.12	1.79	1.86
Total	100.21	99.49	99.77	100.27	100.41	100.53	100.24	100.35	98.79	100.36	99.96
Q	34.22	34.31	35.11	34.98	36.39	36.64	37.63	36.40	36.09	36.38	35.24
or	19.99	21.24	21.29	19.09	20.75	20.42	21.99	20.81	22.13	23.86	24.16
ab	35.86	34.84	33.95	32.85	33.35	32.69	30.71	31.28	33.00	33.82	35.02
an	4.88	5.57	5.03	5.21	5.05	5.18	4.71	5.20	5.70	3.74	3.59
C	2.35	1.32	1.79	4.69	1.75	2.42	2.34	3.03	0.88	0.18	-
di	-	-	-	-	-	-	-	-	-	-	0.10
hy	0.62	0.60	0.63	0.75	0.63	0.67	0.60	0.85	0.44	0.50	0.45
mt	1.55	1.57	1.63	1.89	1.55	1.52	1.44	1.72	1.21	1.11	1.10
il	0.39	0.39	0.39	0.39	0.39	0.33	0.43	0.53	0.41	0.29	0.23
ap	0.05	0.05	0.07	0.05	0.05	0.05	0.07	0.07	0.07	0.05	0.05
V	3	3	3	3	5	6	5	7	3	5	3
Cr	4	4	4	4	4	3	4	5	4	3	3
Ni	3	3	3	3	3	3	3	3	3	3	3
Zn	55	50	47	54	57	52	43	62	61	44	35
Zr	231	204	214	265	212	217	191	238	248	154	146
Nb	12	10	9	12	10	11	11	11	12	11	10
Ba	752	784	777	713	820	874	793	820	858	809	788
La	22	29	29	30	29	25	37	31	29	28	26
Ce	65	70	72	56	65	72	70	72	64	66	68
Nd	46	50	46	49	54	48	50	48	55	58	45
Ga	14	16	13	18	16	16	16	17	17	16	17
Pb	24	24	24	24	25	27	23	26	49	21	21
Rb	112	117	117	102	120	118	110	104	108	129	130
Sr	83	87	87	88	83	85	75	76	96	53	52
Th	15	15	14	17	15	16	13	12	12	15	14
Y	21	25	22	24	25	24	33	27	31	34	31
FeO*	1.77	1.81	1.88	2.15	1.78	1.75	1.66	1.98	1.38	1.29	1.27
F/F+M	0.968	0.974	0.975	0.978	0.974	0.973	0.956	0.927	0.966	0.957	0.963
K/Rb	243.1	248.4	249.8	253.9	237.3	238.5	275.5	273.8	278.3	256.1	256.1
K/Ba	36.2	37.1	37.6	36.3	34.7	32.2	38.2	34.7	35.0	40.8	42.2
Rb/Sr	1.35	1.34	1.34	1.16	1.45	1.39	1.47	1.37	1.13	2.43	2.50
Y/Nb	1.75	2.50	2.44	2.00	2.50	2.18	3.00	2.45	2.58	3.09	3.10

Table D.3. cont.

Ref.no. #	221	222	223	224	225	226	227	228	229	230	231
Sample	T7/1	T7/2	T11/1	T11/2	T15/1	T15/2	T19/1	T19/2	T19/3	T19/4	T24/1
SiO_2	73.15	71.98	71.94	72.70	73.44	72.15	69.78	69.08	73.06	69.96	69.21
TiO_2	0.23	0.23	0.32	0.24	0.20	0.20	0.33	0.30	0.16	0.30	0.37
Al_2O_3	13.52	13.36	13.73	13.81	12.95	13.13	15.28	16.09	13.71	15.37	16.26
Fe_2O_3	2.12	2.19	2.48	2.16	1.60	1.84	2.40	2.45	1.58	2.48	3.12
MnO	0.06	0.07	0.08	0.07	0.05	0.06	0.08	0.10	0.05	0.07	0.10
MgO	0.19	0.26	0.30	0.20	0.23	0.28	0.23	0.16	0.05	0.27	0.32
CaO	1.38	1.39	1.50	1.47	0.85	1.16	1.46	1.33	0.84	1.50	1.77
Na_2O	4.20	4.30	4.19	4.34	3.86	4.05	4.12	3.98	3.66	4.26	4.22
K_2O	3.43	3.47	3.57	3.26	4.13	3.98	3.11	3.06	3.63	3.20	2.80
P_2O_5	0.03	0.03	0.03	0.03	0.40	0.06	0.07	0.04	0.11	0.10	0.03
LOI	1.51	1.89	2.11	1.85	2.24	2.46	2.90	2.89	2.96	2.83	2.18
Total	99.82	99.17	100.25	100.13	99.95	99.37	99.76	99.48	99.81	100.34	100.38
Q	32.77	31.01	30.68	31.94	34.80	31.40	31.42	32.09	37.32	30.12	30.00
or	20.62	21.08	21.50	19.60	24.98	24.27	18.98	18.72	22.15	19.39	16.85
ab	36.15	37.40	36.13	37.37	33.43	35.36	35.99	34.87	31.98	36.97	36.36
an	6.76	6.89	7.38	7.22	1.64	5.53	7.01	6.56	3.56	6.96	8.74
C	0.47	0.08	0.32	0.55	1.58	0.20	2.74	4.05	2.58	2.47	3.20
hy	0.96	1.19	1.26	1.00	0.91	1.16	1.05	0.98	0.52	1.20	1.49
mt	1.64	1.72	1.93	1.68	1.25	1.45	1.89	1.93	1.24	1.94	2.42
il	0.44	0.45	0.62	0.46	0.39	0.39	0.65	0.59	0.31	0.58	0.72
ap	0.07	0.07	0.07	0.07	0.95	0.14	0.17	0.10	0.26	0.24	0.07
V	7	8	9	8	5	7	8	8	4	8	11
Cr	5	4	5	5	5	4	4	4	4	4	6
Ni	3	3	4	5	3	3	3	3	4	3	4
Zn	43	50	60	52	32	48	62	71	40	64	62
Zr	222	227	263	226	168	194	234	242	153	244	346
Nb	10	10	11	10	10	11	10	12	12	13	12
Ba	732	754	786	757	770	805	722	787	764	733	696
La	23	22	23	22	25	27	26	21	21	20	17
Ce	59	72	64	63	75	60	61	64	62	60	74
Nd	43	44	51	51	55	56	47	41	44	38	37
Ga	19	16	13	17	18	20	16	20	18	18	21
Pb	22	23	25	22	21	24	24	23	21	22	27
Rb	106	110	108	101	123	116	102	95	117	103	85
Sr	112	117	112	121	62	83	126	115	67	135	151
Th	12	10	11	10	14	10	11	11	13	11	14
Y	28	24	22	24	28	23	22	21	27	20	16
FeO*	1.91	1.97	2.23	1.94	1.44	1.66	2.16	2.20	1.42	2.23	2.81
F/F+M	0.912	0.887	0.885	0.910	0.866	0.860	0.907	0.935	0.967	0.895	0.901
K/Rb	268.6	261.9	274.4	268.0	278.8	284.8	253.1	267.4	257.6	257.9	273.5
K/Ba	38.9	38.2	37.7	35.8	44.5	41.0	35.8	32.3	39.4	36.2	33.4
Rb/Sr	0.95	0.94	0.96	0.83	1.98	1.40	0.81	0.83	1.75	0.76	0.56
Y/Nb	2.80	2.40	2.00	2.40	2.80	2.09	2.20	1.75	2.25	1.54	1.33

Table D.3. cont.

Ref.no. #	232
Sample	T24/2
SiO_2	70.06
TiO_2	0.30
Al_2O_3	15.85
Fe_2O_3	2.59
MnO	0.10
MgO	0.18
CaO	1.39
Na_2O	4.01
K_2O	3.04
P_2O_5	0.02
LOI	2.25
Total	99.79
Q	32.44
or	18.42
ab	34.79
an	6.94
C	3.57
hy	1.07
mt	2.03
il	0.58
ap	0.05
V	7
Cr	4
Ni	3
Zn	50
Zr	232
Nb	12
Ba	705
La	19
Ce	70
Nd	38
Ga	20
Pb	25
Rb	94
Sr	122
Th	14
Y	18
FeO*	2.33
F/F+M	0.931
K/Rb	268.5
K/Ba	35.8
Rb/Sr	0.77
Y/Nb	1.50

Table D.4. Compositional ranges, means and standard deviations for the three pumice types of the Pokai Ignimbrite. No. = number of samples, % = percentage of all samples analysed.

	Type 1a	Mean	STD	Type 1b	Mean	STD
SiO_2	71.24-77.35	75.48	1.57	68.62-77.01	74.39	1.70
TiO_2	0.11-0.33	0.15	0.04	0.06-0.60	0.20	0.05
Al_2O_3	12.27-18.87	14.25	1.77	12.41-21.08	14.62	1.88
FeO_t	1.29-2.28	1.67	0.23	1.58-2.93	2.07	0.26
MnO	0.04-0.10	0.06	0.02	0.03-0.12	0.07	0.02
MgO	0.05-0.24	0.11	0.04	0.05-0.44	0.14	0.05
CaO	0.63-0.99	0.81	0.07	0.95-1.19	1.07	0.05
Na_2O	3.35-4.23	3.79	0.20	3.21-4.56	3.89	0.25
K_2O	3.03-4.26	3.66	0.36	2.58-4.11	3.52	0.34
P_2O_5	0.01-0.04	0.02	0.01	0.01-0.11	0.02	0.03
V	3-8	6	1.3	3-9	5	1.4
Cr	3-5	3	0.6	3-7	4	0.5
Ni	3-4	3	0.1	3-5	3	0.6
Zn	32-82	51	10.3	38-174	57	14.4
Zr	106-251	160	32.4	177-354	221	36.6
Nb	8-15	11	1.5	9-17	11	1.4
Ba	600-1010	837	99.3	642-1334	799	83.4
La	21-37	29	3.6	18-58	28	5.0
Ce	47-100	69	11.6	51-107	68	10.9
Nd	38-63	51	4.9	38-60	49	4.2
Ga	8-18	15	2.3	9-23	15	2.5
Pb	17-40	22	3.5	18-49	24	3.4
Rb	97-140	121	9.8	84-129	115	9.9
Sr	32-69	57	7.0	72-97	86	4.3
Th	11-29	17	3.2	6-24	15	3.0
Y	20-37	28	3.3	18-42	27	4.2
No.	53			141		
%	23.7 %			62.9 %		

Table D.4. cont.

	Type 2	Mean	STD
SiO_2	68.90-74.41	72.81	1.34
TiO_2	0.23-0.55	0.32	0.06
Al_2O_3	13.40-17.17	14.92	1.15
FeO_t	2.16-3.68	2.49	0.35
MnO	0.06-0.11	0.08	0.01
MgO	0.17-0.63	0.33	0.11
CaO	1.30-2.39	1.58	0.24
Na_2O	3.49-5.11	4.29	0.34
K_2O	2.60-3.64	3.15	0.27
P_2O_5	0.01-0.07	0.03	0.02
V	7-21	10	2.9
Cr	3-6	4	0.8
Ni	3-5	3	0.6
Zn	42-73	55	8.3
Zr	213-346	251	33.4
Nb	10-13	11	1.0
Ba	633-831	737	51.9
La	20-32	25	3.5
Ce	51-80	66	6.8
Nd	37-54	48	5.2
Ga	13-21	17	1.8
Pb	15-27	21	3.1
Rb	85-115	100	7.7
Sr	106-186	126	18.7
Th	5-21	13	3.3
Y	16-31	25	4.4
No.	30		
%	13.4 %		

Table D.4. cont. Mean CIPW normative compositions and standard deviations (STD) in the three Pokai Ignimbrite pumice types.

	Type 1a	STD	Type 1b	STD	Type 2	STD
Q	37.42	1.18	35.60	1.24	31.81	1.95
or	21.61	2.11	20.81	2.02	18.60	1.60
ab	32.04	1.71	32.91	2.09	36.31	2.84
an	3.87	0.35	5.18	0.25	7.50	1.17
C	2.65	2.30	2.51	2.47	1.71	1.49
di	0.02	0.11	0.003	0.03	0.12	0.36
hy	0.71	0.12	0.88	0.16	1.26	0.25
mt	1.27	0.18	1.58	0.20	1.90	0.27
il	0.29	0.07	0.38	0.09	0.60	0.12
hem	-	-	0.0008	0.009	-	-
ap	0.04	0.04	0.05	0.02	0.07	0.05

Table D.5. List of all Pokai Ignimbrite pumices analysed by XRD.

Rno = reference number for XRF analyses (pumices listed in Table D.2).
T = pumice type: crystal-poor, low to medium Sr = 1a and 1b, respectively; crystal-rich, high Sr = 2; for samples containing kaolinite the pumice type is given in parenthesis and should be regarded as indicative only.

Rno	Sample no.	T	Al_2O_3 %	SiO_2 %	Kaolinite
9	2B/1	(1a)	17.42	73.09	yes
10	2B/2	(1a)	16.13	73.53	yes
14	3B/2	1b	16.63	72.37	no
15	3B/3	1b	15.15	73.27	no
16	3B/4	1b	15.92	73.08	no
18	3B/6	1b	15.53	72.85	no
20	4/2	(1a)	18.62	71.24	yes
24	12A/1	(1b)	17.00	72.60	yes
25	12A/2	(1b)	16.87	72.40	yes
27	15/1	(1b)	19.56	70.03	yes
28	15/2	(1b)	18.69	70.59	yes
29	15/3	(1b)	16.73	72.61	yes
30	15/4	(1b)	20.02	69.75	yes
35	23D/1	(1b)	18.13	71.24	yes
37	23E/2	(1b)	15.47	73.46	yes
38	26A/1	1b	15.14	73.90	no
39	26A/2	1a	14.51	74.90	no
44	R1/1	(1b)	15.21	73.72	trace
45	R1/2	(1b)	16.77	72.52	trace
46	R1/3	1b	15.08	74.04	no
69	P1/2	1b	15.23	73.70	no
121	50A/1	(1a)	17.85	72.09	yes
122	50A/2	(1a)	18.87	71.61	yes
123	50A/3	(1a)	16.69	73.31	yes
124	57/1	(2)	15.75	72.41	yes

Table D.5. cont.

Rno	Sample no.	T	Al_2O_3 %	SiO_2 %	Kaolinite
125	57/2	(2)	17.17	70.66	yes
126	57/3	2	15.61	72.43	no
130	70/1	(1b)	17.09	72.37	yes
133	70/4	(1a)	15.42	74.43	trace
134	70/5	(1b)	15.73	73.68	yes
135	70e/1	1b	13.48	75.58	no
136	85/1	(1a)	18.00	72.35	yes
137	85/2	(1b)	20.41	69.38	yes
138	85/3	(1b)	20.81	68.95	yes
139	85/4	(1b)	20.99	68.62	yes
140	85/5	(1a)	17.81	72.68	yes
141	85/6	(1b)	21.08	68.64	yes
142	91/1	1b	15.61	73.68	no
144	91/3	(1b)	17.63	71.80	trace
149	98/1	(1b)	15.92	73.63	yes
150	98/2	(2)	15.37	72.67	yes
152	98/4	2	15.07	72.63	no
159	122/2	(1a)	15.39	74.54	yes
160	122/3	(1b)	16.71	72.71	yes
161	122/4	(1b)	16.36	73.31	yes
164	126/3	(1a)	15.83	74.51	yes
165	126/4	(1b)	15.40	73.55	yes
166	126/5	(1b)	16.06	72.65	yes
167	126/6	(1a)	15.49	74.54	yes
168	127/1	(1b)	15.78	73.27	yes
182	132/4	(1b)	15.28	73.66	trace
183	132/5	(1b)	17.07	72.13	trace
184	132/6	1b	16.51	72.25	no
186	132/8	(1b)	15.02	73.97	trace
188	T25/2	1b	15.07	74.14	no
189	T28/1	(1b)	15.68	73.68	trace

Table D.5. cont.

Rno	Sample no.	T	Al_2O_3 %	SiO_2 %	Kaolinite
190	V28/2	(1b)	15.98	73.21	trace
193	V36/1	(1b)	15.74	73.45	trace
195	V36/3	(1b)	15.67	73.65	trace
196	V39/1	1b	18.05	71.27	no
197	V39/2	1b	19.87	69.68	no
198	134/1	(2)	16.44	72.09	yes
200	134/3	2	14.95	73.26	no
201	134/4	1b	15.19	74.27	no
202	134/5	(2)	17.14	68.90	trace
207	135/4	(1b)	15.75	73.38	yes
213	153/4	(1b)	16.48	72.53	yes
227	T19/1	2	15.78	72.04	no
228	T19/2	(2)	16.66	71.52	yes
230	T19/4	2	15.76	71.75	no
231	T24/1	(2)	16.56	70.48	yes
232	T24/2	(2)	16.25	71.83	trace

Table D.5. cont. List of all Chimp Ignimbrite pumices analysed by XRD.

Rno	Sample no.	Al_2O_3 %	SiO_2 %	Kaolinite
241	45A/1	15.24	73.66	yes
245	76/1	16.19	73.15	yes
247	76/3	15.23	73.92	no
248	76/4	15.20	73.98	no
249	93/1	15.44	72.14	no
250	93/2	17.04	72.08	yes
251	93/3	15.08	73.96	trace

Table D.6. Whole rock analyses of TVZ rhyolitic lavas (including domes).

Sample	179	180	184	186	187	188	194	195	199	201	203
SiO_2	69.08	69.12	70.86	71.02	71.19	71.20	71.87	71.91	72.20	72.36	72.49
TiO_2	0.41	0.36	0.44	0.30	0.40	0.46	0.29	0.29	0.24	0.35	0.36
Al_2O_3	14.36	14.04	14.08	13.69	14.37	14.06	13.16	13.76	13.74	13.68	13.40
Fe_2O_3	2.85	1.46	2.37	1.07	1.61	1.90	1.38	0.69	2.25	1.03	1.25
FeO	1.18	1.80	0.58	1.48	1.27	0.70	1.20	1.32	0.50	0.87	1.32
MnO	0.08	0.07	0.07	0.05	0.07	0.06	0.08	0.07	0.06	0.09	0.07
MgO	0.82	0.88	0.54	0.66	0.71	0.20	0.37	0.53	0.16	0.72	0.44
CaO	3.23	2.94	2.29	2.19	2.86	1.90	1.70	2.14	1.55	2.32	1.95
Na_2O	4.52	3.65	4.29	4.12	4.12	4.30	4.47	3.96	4.62	4.40	4.69
K_2O	2.57	3.30	2.70	2.97	2.79	3.00	2.71	2.78	3.32	2.36	2.87
P_2O_5	0.11	0.12	0.09	0.07	0.11	0.06	0.06	0.03	0.02	0.09	0.06
LOI	0.85	2.49	0.88	2.58	0.49	1.30	2.74	2.30	0.07	0.46	0.30
Total	100.06	100.23	99.19	100.20	99.99	99.14	100.03	99.78	98.73	98.73	99.20

Sample	209	211	213	214	219	220	221	232	233	234	235
SiO_2	72.80	72.83	72.90	73.00	73.40	73.40	73.43	74.60	74.70	74.74	74.76
TiO_2	0.31	0.41	0.29	0.35	0.26	0.49	0.30	0.27	0.27	0.20	0.21
Al_2O_3	13.02	14.30	13.20	13.55	13.40	13.90	13.53	13.30	13.40	13.10	12.10
Fe_2O_3	0.94	2.88	0.70	0.80	0.08	1.30	1.12	0.90	0.55	1.31	0.23
FeO	0.77	-	1.10	0.95	1.10	0.80	1.01	0.90	1.05	0.35	0.69
MnO	0.10	0.08	0.09	0.01	0.03	0.02	0.07	0.07	0.06	0.05	0.09
MgO	0.23	0.48	0.41	0.10	0.30	0.38	0.43	0.15	0.25	0.11	0.22
CaO	1.74	1.89	1.70	1.30	1.70	1.90	1.68	1.45	1.65	1.26	0.76
Na_2O	4.22	4.44	4.10	3.80	4.00	4.00	3.45	5.05	4.80	4.47	4.12
K_2O	3.00	2.93	3.20	3.55	2.80	3.00	3.38	3.00	3.00	3.20	3.57
P_2O_5	0.04	0.05	0.06	0.10	0.07	0.06	0.03	0.03	0.01	0.02	0.01
LOI	1.58	0.67	2.22	2.20	2.29	0.67	1.25	0.36	0.16	0.82	2.26
Total	98.75	100.96	99.97	99.71	99.43	99.92	99.68	100.08	99.90	99.63	99.02

179, 180, 184, 186, 187, 194, 199, 203, 211 (Taupo Volcanic Centre); 188, 195, 213, 219, 221 (Maroa Volcanic Centre); 201, 209, 214, 232, 233, 235 (Okataina Volcanic Centre); 220, 234 (Rotorua Volcanic Centre) from Cole (1979).

Table D.6. cont.

Sample	236	238	240	244	255	256
SiO_2	75.00	75.03	75.10	75.40	78.15	78.20
TiO_2	0.23	0.17	0.23	0.26	0.10	0.11
Al_2O_3	12.30	12.50	12.99	13.00	12.09	12.71
Fe_2O_3	1.10	0.47	136.00	0.50	0.62	0.66
FeO	0.50	0.83	0.98	1.00	0.18	0.18
MnO	0.03	0.10	0.07	0.06	0.01	0.03
MgO	0.05	0.40	0.23	0.50	0.07	0.26
CaO	1.20	1.38	1.37	1.50	0.84	0.84
Na_2O	3.90	4.12	4.61	4.10	3.84	4.02
K_2O	3.40	2.82	2.91	2.80	3.66	3.66
P_2O_5	-	0.13	0.19	0.06	0.01	0.02
LOI	1.41	0.80	0.61	2.21	1.07	0.62
Total	99.12	98.75	235.29	101.39	100.64	101.31

240 (Taupo Volcanic Centre), 236 (Maroa Volcanic Centre); 238, 244, 255, 256 (Okataina Volcanic Centre) from Cole (1979).

Table D.7. Pumice clast* analyses of TVZ ignimbrites.

Sample	28247	28260	28247	28259	28271	28243	28244	28245	NGA	O/1	H32
SiO_2	75.42	76.01	75.97	75.46	74.84	75.73	75.72	75.07	71.28	71.25	73.30
TiO_2	0.14	0.18	0.20	0.20	0.21	0.20	0.19	0.20	0.33	0.32	0.32
Al_2O_3	14.71	13.24	13.15	13.55	14.25	13.25	13.49	14.24	15.35	14.55	15.49
Fe_2O_3	0.36	0.40	0.42	0.43	0.44	0.40	0.42	0.42	3.59	3.07	2.27
FeO	1.09	1.21	1.26	1.30	1.33	1.21	1.25	1.25	-	-	-
MnO	0.05	0.06	0.06	0.07	0.06	0.05	0.05	0.05	0.03	0.08	0.02
MgO	0.12	0.20	0.23	0.24	0.24	0.24	0.20	0.19	0.32	0.48	0.32
CaO	0.84	1.10	1.15	1.16	1.18	1.13	1.07	1.07	1.14	2.09	1.91
Na_2O	3.55	4.12	4.07	4.13	4.19	4.30	4.24	4.21	3.71	4.67	3.11
K_2O	3.70	3.48	3.46	3.42	3.22	3.48	3.42	3.30	4.20	3.38	3.22
P_2O_5	0.02	0.01	0.03	0.03	0.03	0.02	0.01	0.01	0.05	0.11	0.04
LOI	4.47	3.32	3.66	3.27	3.12	2.52	2.82	2.98	-	-	-
Total	104.47	103.33	103.66	103.26	103.11	102.53	102.88	102.99	100.00	100.00	100.00

28247 (Te Wairoa Ignimbrites, Unit 1); 28260, 28247, 28259 (Te Wairoa Ignimbrites, Unit 2); 28271 (Te Wairoa Ignimbrites, Unit 3); 28243, 28244, 28245 (Pokopoko Ignimbrite) from Bellamy (1991; Table IV). NGA (Ngaroma Ignimbrite, *whole rock analysis); O/1, H32 (Ongatiti Ignimbrite) from Briggs et al. (1992).

Table D.7. cont.

Sample	A4PB	SX	M5	M7	183	190	243	251	252	Mm1/1	mM110
SiO_2	73.56	77.22	72.46	75.33	70.75	71.52	75.39	76.40	76.52	73.39	73.35
TiO_2	0.29	0.23	0.46	0.29	0.34	0.34	0.14	0.13	0.12	0.17	0.17
Al_2O_3	14.22	12.95	16.56	14.55	13.90	14.46	12.89	12.55	12.48	13.77	14.72
Fe_2O_3	3.51	2.08	3.19	2.46	2.50	1.28	1.24	1.10	1.13	1.62	1.58
FeO	-	-	-	-	0.15	1.16	0.26	0.25	0.30	-	-
MnO	0.08	0.03	0.06	0.04	0.07	0.07	0.03	0.02	0.02	0.08	0.06
MgO	0.20	0.17	0.21	0.14	0.55	0.67	0.16	0.09	0.13	0.16	0.14
CaO	1.14	1.13	0.94	0.75	2.27	2.68	0.91	1.33	1.03	0.82	0.74
Na_2O	3.37	2.94	2.49	2.61	4.12	4.11	2.94	4.24	3.52	3.66	3.53
K_2O	3.60	3.22	3.61	3.81	2.95	2.56	3.69	3.38	3.88	3.15	3.07
P_2O_5	0.03	0.03	0.02	0.02	0.07	0.07	0.07	0.07	0.07	0.01	0.02
LOI	4.99	5.28	3.93	2.73	2.38	-	2.14	0.73	0.85	2.65	3.28
Total	104.99	105.28	103.93	102.73	100.05	98.92	99.86	100.29	100.05	99.48	100.66

Sample	MmU16	Oh1/1	Oh1/4	Oh1/6	Oh3/P	Oh4/5	Oh4/8	At1	At5	At7	At9
SiO_2	72.05	74.74	75.24	74.40	74.37	69.77	70.64	74.60	74.61	74.26	74.88
TiO_2	0.30	0.11	0.15	0.15	0.15	0.30	0.26	0.17	0.16	0.17	0.16
Al_2O_3	14.09	12.09	11.98	12.25	12.45	13.42	12.99	13.14	12.86	13.29	13.02
Fe_2O_3	2.43	1.20	1.42	1.40	1.43	2.37	2.16	1.64	1.56	1.70	1.72
MnO	0.06	0.04	0.05	0.04	0.04	0.07	0.08	0.07	0.09	0.05	0.08
MgO	0.18	0.11	0.18	0.17	0.15	0.51	0.38	0.13	0.13	0.14	0.15
CaO	1.33	0.57	0.76	0.81	0.81	1.79	1.48	0.75	0.83	0.77	0.81
Na_2O	4.74	3.48	3.68	3.60	3.59	4.35	4.04	4.00	4.29	4.01	4.04
K_2O	3.04	4.18	3.80	3.77	3.78	2.98	3.39	3.47	3.47	3.48	3.47
P_2O_5	0.04	0.02	0.02	0.02	0.02	0.08	0.11	0.02	0.03	0.02	0.03
LOI	0.57	3.24	3.27	2.81	3.39	3.87	4.03	2.52	2.17	2.34	1.67
Total	98.83	99.78	100.55	99.42	100.18	99.51	99.56	100.51	100.20	100.23	100.03

A4PB (Ahuroa Ignimbrite); SX, M5, M7 (Marshall Ignimbrite) from Briggs et al. (1992). 183, 190 (Whakamaru Ignimbrite); 243 (Kaingaroa Ignimbrite); 251, 252 (Matahina Ignimbrite) from Cole (1979). Mm1/1, mM110, MmU16 (Mamaku Ignimbrite); Oh1/1, Oh1/4, Oh1/6, Oh3/P, Oh4/5, Oh4/8 (Ohakuri Ignimbrite); At1, At7, At9 (Atiamuri Ignimbrite) from Houghton and Weaver (unpubl. data).

Table D.7. cont.

Sample	Mk1/1	Mk1/3	Mk2/3	pMs1	Ms1/3	Ms1/9	1A/1	1A/2	1A/3	1A/4	8
SiO_2	74.15	73.71	73.96	69.66	68.65	69.19	72.64	73.53	71.84	72.32	74.23
TiO_2	0.27	0.27	0.27	0.30	0.25	0.24	0.16	0.14	0.15	0.14	0.17
Al_2O_3	13.92	14.14	13.49	14.28	17.23	15.95	14.08	13.41	14.37	13.73	12.65
Fe_2O_3	2.16	2.21	2.16	2.40	2.69	2.54	1.51	1.39	1.64	1.46	1.47
MnO	0.06	0.06	0.07	0.07	0.07	0.10	0.05	0.06	0.09	0.06	0.02
MgO	0.27	0.26	0.28	0.33	0.13	0.15	0.22	0.21	0.23	0.20	0.25
CaO	1.17	1.20	1.25	1.85	1.04	1.06	1.13	0.84	0.89	0.89	1.08
Na_2O	4.45	4.36	4.55	3.18	3.04	3.44	3.07	3.11	3.15	2.99	3.34
K_2O	3.26	3.25	3.25	3.38	3.10	3.09	4.02	4.29	3.96	4.01	4.22
P_2O_5	0.01	0.03	0.04	0.02	0.02	0.02	0.02	0.01	0.03	0.03	0.02
LOI	0.52	0.75	0.59	3.62	4.34	3.56	3.08	1.96	3.52	3.38	2.94
Total	100.24	100.24	99.91	99.09	100.56	99.34	99.98	98.96	99.87	99.21	100.39

Sample	9/1	9/2	9/3
SiO_2	71.37	74.65	72.45
TiO_2	0.28	0.17	0.18
Al_2O_3	13.70	12.66	14.38
Fe_2O_3	2.31	1.51	1.69
MnO	0.07	0.07	0.05
MgO	0.52	0.26	0.24
CaO	2.05	1.11	1.17
Na_2O	3.87	3.20	3.19
K_2O	3.30	4.24	3.95
P_2O_5	0.03	0.02	0.02
LOI	2.23	2.06	2.58
Total	99.73	99.96	99.91

Mk1/1, Mk1/3, Mk2/3 (Mokai Ignimbrite); pMs1 (pre-Marshall Ignimbrite); Ms1/3, Ms1/9 (Marshall Ignimbrite) from Houghton and Weaver (unpubl. data). A1/1, A1/2, A1/3, A1/4, 8, 9/1, 9/2, 9/3 (Whakamaru Ignimbrite) from Karhunen (unpubl. data).

Table D.8. Major and trace element analyses and CIPW norms of the Chimp Ignimbrite.

Ref.no. #	233	234	235	236	237	238	239	240	241	242	243
Sample	11C/1	11C/2	11D	33/1	33/2	33/3	33/4	33/5	45A/1	45B/1	45B/2
SiO_2	72.62	73.13	69.81	71.23	71.63	71.81	71.57	71.87	70.17	73.05	72.61
TiO_2	0.23	0.25	0.21	0.19	0.18	0.18	0.17	0.18	0.23	0.23	0.20
Al_2O_3	12.71	13.00	15.18	14.08	13.70	13.63	13.27	13.84	14.52	13.67	12.94
Fe_2O_3	1.85	1.89	2.06	2.02	1.97	1.97	1.91	1.98	2.14	1.90	1.86
MnO	0.07	0.08	0.05	0.09	0.07	0.07	0.10	0.09	0.07	0.06	0.06
MgO	0.32	0.30	0.18	0.21	0.18	0.17	0.18	0.17	0.18	0.17	0.15
CaO	1.37	1.44	1.02	1.08	1.11	1.09	1.08	1.09	1.11	1.10	1.11
Na_2O	3.85	3.91	3.64	3.81	3.83	3.73	3.91	3.66	3.83	3.88	3.91
K_2O	3.41	3.38	3.05	3.25	3.33	3.39	3.33	3.43	3.00	3.41	3.29
P_2O_5	0.04	0.03	0.03	0.04	0.03	0.03	0.02	0.02	0.01	0.01	0.01
LOI	3.05	2.77	4.75	3.78	3.44	3.76	3.34	3.54	3.16	3.37	3.23
Total	99.52	100.18	99.98	99.78	99.47	99.83	98.88	99.87	98.42	100.85	99.37
Q	34.93	34.72	36.10	35.27	35.20	35.80	34.85	35.98	35.23	35.56	35.89
or	20.89	20.51	18.93	20.01	20.49	20.85	20.60	21.04	18.61	20.67	20.22
ab	33.77	33.97	32.34	33.58	33.75	32.85	34.63	32.15	34.02	33.68	34.41
an	6.77	7.13	5.11	5.31	5.53	5.42	5.47	5.48	5.71	5.53	5.66
C	0.30	0.37	4.31	2.53	1.93	1.99	1.38	2.26	3.13	1.66	0.99
hy	1.24	1.17	0.96	1.13	1.01	0.98	1.07	1.02	0.99	0.84	0.84
mt	1.46	1.48	1.65	1.60	1.56	1.56	1.52	1.57	1.71	1.49	1.48
il	0.45	0.49	0.42	0.38	0.36	0.36	0.34	0.35	0.46	0.45	0.40
ap	0.10	0.07	0.07	0.10	0.07	0.07	0.05	0.05	0.02	0.02	0.02
V	8	9	n.a.	6	5	6	6	7	7	7	6
Cr	4	4	n.a.	3	3	4	3	3	4	4	3
Ni	3	3	n.a.	3	3	3	3	3	3	3	4
Zn	46	43	n.a.	56	58	58	57	59	61	58	58
Zr	215	224	n.a.	237	233	231	221	231	246	221	200
Nb	9	9	n.a.	11	11	11	11	12	13	12	14
Ba	787	774	n.a.	799	812	816	820	822	901	821	813
La	21	24	n.a.	23	26	27	25	25	26	29	28
Ce	51	49	n.a.	59	59	52	58	60	84	73	73
Nd	41	47	n.a.	44	45	47	43	43	51	54	53
Ga	12	13	n.a.	14	14	13	11	12	18	15	16
Pb	20	21	n.a.	20	20	19	18	19	18	19	21
Rb	119	116	n.a.	105	103	106	107	106	104	107	116
Sr	112	119	n.a.	89	92	89	90	89	88	87	91
Th	12	11	n.a.	13	14	12	12	14	18	10	13
Y	22	22	n.a.	26	26	26	27	26	26	29	26
FeO*	1.66	1.70	1.85	1.82	1.77	1.77	1.72	1.78	1.93	1.71	1.67
F/F+M	0.844	0.856	0.914	0.901	0.911	0.916	0.910	0.917	0.917	0.912	0.920
K/Rb	237.9	241.9	0.0	257.0	268.4	265.5	258.4	268.6	239.5	264.6	235.5
K/Ba	36.0	36.3	0.0	33.8	34.0	34.5	33.7	34.6	27.6	34.5	33.6
Rb/Sr	1.06	0.97	0.00	1.18	1.12	1.19	1.19	1.19	1.18	1.23	1.27
Y/Nb	2.44	2.44	0.00	2.36	2.36	2.36	2.45	2.17	2.00	2.42	1.86

Table D.8. cont.

Ref.no. #	244	245	246	247	248	249	250	251	152	253	254
Sample	458/3	76/1	76/2	76/3	76/4	93/1	93/2	93/3	93/4	146/1	146/2
SiO_2	74.13	70.30	72.68	71.90	71.83	70.68	69.20	71.13	71.40	73.34	73.85
TiO_2	0.32	0.20	0.22	0.29	0.21	0.38	0.20	0.23	0.20	0.20	0.14
Al_2O_3	13.93	15.56	13.77	14.81	14.76	15.13	16.36	14.50	14.32	13.43	13.13
Fe_2O_3	2.18	2.17	1.91	1.94	2.06	2.38	2.25	2.03	1.99	1.87	1.85
MnO	0.06	0.07	0.07	0.05	0.06	0.07	0.08	0.07	0.07	0.07	0.07
MgO	0.16	0.06	0.07	0.15	0.08	0.48	0.23	0.17	0.17	0.08	0.06
CaO	1.17	1.07	1.12	1.30	1.10	1.83	1.05	1.08	1.08	1.11	1.13
Na_2O	4.26	3.37	3.94	3.33	3.58	3.99	3.46	3.72	3.65	3.32	3.74
K_2O	2.98	3.27	3.38	3.48	3.38	3.00	3.13	3.24	3.30	3.93	3.68
P_2O_5	0.01	0.03	0.03	0.02	0.03	0.04	0.04	0.01	0.01	0.04	0.03
LOI	0.91	3.76	2.88	3.01	2.91	2.02	4.02	4.35	4.51	2.88	2.58
Total	100.11	99.86	100.07	100.28	100.00	100.00	100.02	100.53	100.70	100.27	100.26
Q	35.35	37.08	35.20	37.14	36.52	31.96	35.77	35.71	36.15	37.37	36.18
or	17.75	20.11	20.55	21.14	20.57	18.09	19.27	19.91	20.27	23.85	22.26
ab	36.34	29.67	34.30	28.97	31.20	34.46	30.50	32.73	32.11	28.85	32.40
an	5.79	5.32	5.52	6.50	5.42	9.00	5.15	5.50	5.50	5.39	5.54
C	1.61	4.79	1.71	3.34	3.38	2.13	5.70	3.05	2.92	1.84	1.04
hy	0.75	0.73	0.63	0.68	0.70	1.56	1.23	0.92	0.95	0.67	0.71
mt	1.68	1.72	1.50	1.52	1.62	1.85	1.79	1.61	1.58	1.46	1.44
il	0.61	0.40	0.43	0.57	0.41	0.74	0.40	0.45	0.39	0.39	0.27
ap	0.02	0.07	0.07	0.05	0.07	0.09	0.10	0.02	0.02	0.10	0.07
V	8	3	3	4	5	11	6	6	7	3	3
Cr	5	4	5	4	4	4	5	4	4	5	4
Ni	4	3	3	3	3	3	3	3	3	3	3
Zn	40	54	52	37	49	48	76	67	71	50	55
Zr	222	248	220	232	237	298	278	244	239	219	212
Nb	13	13	10	9	11	10	12	12	11	9	12
Ba	790	842	849	803	833	787	1034	948	975	859	831
La	30	22	23	18	25	23	27	28	28	25	25
Ce	56	65	62	50	61	48	68	63	70	62	58
Nd	52	53	53	42	46	48	50	51	51	45	46
Ga	16	15	15	18	15	17	16	16	15	15	14
Pb	12	22	21	20	20	18	18	17	17	21	22
Rb	102	103	107	107	108	101	96	101	103	118	114
Sr	105	85	88	104	87	147	81	85	87	89	92
Th	5	15	13	16	15	14	19	18	16	14	13
Y	30	23	26	17	24	18	25	27	26	23	21
FeO*	1.96	1.95	1.72	1.75	1.85	2.14	2.02	1.83	1.79	1.68	1.66
F/F+M	0.927	0.971	0.962	0.923	0.960	0.822	0.901	0.918	0.916	0.956	0.967
K/Rb	242.5	263.6	262.3	270.0	259.8	246.6	270.7	266.3	266.0	276.5	268.0
K/Ba	31.3	32.2	33.1	36.0	33.7	31.6	25.1	28.4	28.1	38.0	36.8
Rb/Sr	0.97	1.21	1.22	1.03	1.24	0.69	1.19	1.19	1.18	1.33	1.24
Y/Nb	2.31	1.77	2.60	1.89	2.18	1.80	2.08	2.25	2.36	2.56	1.75

Table D.8. cont.

Ref.no. #	255	256
Sample	146/3	146/4
SiO_2	73.86	73.17
TiO_2	0.23	0.17
Al_2O_3	13.36	13.56
Fe_2O_3	1.88	1.91
MnO	0.06	0.06
MgO	0.08	0.07
CaO	1.11	1.10
Na_2O	3.78	3.70
K_2O	3.77	3.70
P_2O_5	0.04	0.03
LOI	2.06	2.34
Total	100.23	99.81
Q	35.53	35.79
or	22.70	22.43
ab	32.58	32.12
an	5.34	5.40
C	1.16	1.58
hy	0.60	0.69
mt	1.46	1.49
il	0.44	0.33
ap	0.09	0.07
V	3	3
Cr	4	4
Ni	3	4
Zn	54	59
Zr	217	223
Nb	12	11
Ba	836	842
La	24	23
Ce	60	60
Nd	44	43
Ga	16	16
Pb	23	21
Rb	114	114
Sr	89	90
Th	14	14
Y	24	23
FeO*	1.69	1.72
F/F+M	0.956	0.962
K/Rb	274.5	269.5
K/Ba	37.4	36.5
Rb/Sr	1.28	1.27
Y/Nb	2.00	2.09

Appendix E

Table E.1. Major and trace element concentrations of the Ruapehu and related lavas used in the FC, AFC and PM models. All analyses are from Graham & Hackett (1987; Table 4).

	Wahianoa 14867	Ngauruhoe 29250	Ohakune 14798
SiO_2	60.40	56.22	56.79
TiO_2	0.72	0.76	0.53
Al_2O_3	17.59	16.63	14.50
Fe_2O_3	1.90	2.37	2.11
FeO	4.40	6.14	6.07
MnO	0.08	0.15	0.19
MgO	2.54	5.24	7.07
CaO	5.93	8.31	9.05
Na_2O	3.56	3.14	2.32
K_2O	1.58	1.14	0.66
P_2O_5	0.13	0.17	0.07
LOI	0.35	0.19	0.73
Total	99.18	100.46	100.09
V	173	220	226
Cr	10	100	192
Ni	17	29	39
Zr	119	95	65
Nb	5	2	3
Ba	389	214	144
Rb	56	38	16
Sr	248	247	390

Table E.2. Mineral data from the Ruapehu and related lavas used in the FC and AFC models. All analyses are from Graham and Hackett (1987; Table 3).

	Wahianoa Formation acid andesite 14867			
	cpx	opx	plag	tm
SiO_2	51.67	53.39	53.41	0.10
TiO_2	0.43	0.16	-	15.74
Al_2O_3	1.05	1.31	28.28	1.65
Cr_2O_3	-	-	-	0.36
FeO	14.82	16.30	0.64	75.53
MnO	0.49	0.31	-	0.44
MgO	14.22	25.59	-	0.91
CaO	17.00	1.31	12.21	-
Na_2O	0.26	-	4.69	-
K_2O	-	-	0.21	-
Total	99.92	98.37	100.44	94.73

	Ngauruhoe 1954 basic andesite 29250			
	oliv	cpx	opx	plag
SiO_2	38.70	51.91	52.85	50.05
TiO_2	-	0.32	0.20	-
Al_2O_3	-	2.62	1.47	31.23
Cr_2O_3	-	0.22	-	-
FeO	19.40	7.59	17.74	0.60
MnO	0.22	0.14	0.43	-
MgO	42.01	16.51	24.82	0.08
CaO	0.15	19.37	1.82	14.54
Na_2O	-	0.25	-	3.02
K_2O	-	-	-	0.12
Total	100.48	98.95	99.33	99.62

	Ohakune basic andesite 14798			
	oliv	cpx	opx	plag
SiO_2	40.75	53.88	55.75	49.55
TiO_2	-	0.15	0.14	-
Al_2O_3	-	1.51	1.38	31.72
Cr_2O_3	-	0.17	0.27	-
FeO	12.48	6.43	12.00	0.82
MnO	0.17	0.26	0.21	-
MgO	47.29	17.13	29.13	0.13
CaO	0.11	20.11	1.51	15.27
Na_2O	-	0.19	-	2.37
K_2O	-	-	-	0.07
Total	100.80	99.83	100.39	99.93

cpx = clinopyroxene
opx = orthopyroxene
plag = plagioclase
tm = titanomagnetite
oliv = olivine

Table E.3. Average analyses of the Torlesse and Waipapa metasedimentary basements and the meta-igneous granulite (MIG) xenolith used in the AFC modelling. All iron as FeO_t.

	Torlesse(1)	Waipapa(2)	MIG(3)
SiO_2	70.2	64.5	54.5
TiO_2	0.5	0.7	0.7
Al_2O_3	13.4	16.7	16.5
FeO_t	3.8	5.7	8.5
MnO	-	0.1	0.2
MgO	0.5	2.5	8.1
CaO	1.2	3.4	8.8
Na_2O	3.2	4.1	2.2
K_2O	5.2	2.1	0.3
P_2O_5	-	0.2	0.1
Total	98.0	100	100
V	10	135	227
Cr	6	43	364
Ni	9	15	120
Zr	188	166	56
Ba	961	516	150
Rb	269	62	12
Sr	32	487	324

(1) Torlesse metagreywacke partial melt composition of xenolithic restite glass (Graham & Hackett, 1987); in the AFC models the Sr value has been reassessed at 100 ppm (cf. Graham & Hackett, 1987; Graham & Cole, 1991).
(2) Waipapa metagreywacke bulk rock composition (Reid, 1982; Graham, 1985a).
(3) Meta-igneous granulite bulk rock composition (Graham et al., 1990).

Table E.4. Average compositions of Torlesse and Waipapa basement rocks (Reid, 1983) used in the PM modelling. All iron as FeO_t.

	Torlesse	Waipapa
SiO_2	69.86	62.14
TiO_2	0.53	0.77
Al_2O_3	14.67	15.93
FeO_t	3.73	6.04
MnO	0.04	0.11
MgO	1.24	2.37
CaO	1.89	3.04
Na_2O	3.73	3.84
K_2O	2.47	2.12
P_2O_5	0.11	0.16
LOI	2.50	3.36
Rb	91	65
Sr	266	459
Ba	633	549
Cr	46	42
V	73	122
Ce	53	38
Nd	24	4.5